CR 73189

Available to the Public

SD 67-621-2
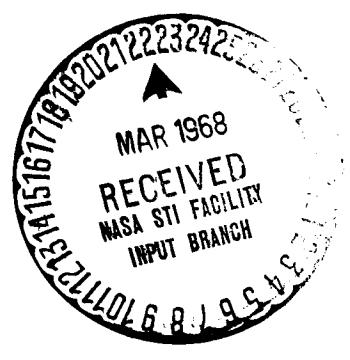
FINAL REPORT

TECHNOLOGICAL REQUIREMENTS
COMMON TO
MANNED PLANETARY MISSIONS

(Contract NAS2-3918)

MAR 1968
RECEIVED
NASA STI FACILITY
INPUT BRANCH

APPENDIX A
Mission Requirements

SPACE DIVISION
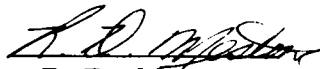NORTH AMERICAN ROCKWELL CORPORATION

SD 67-621-2

TECHNOLOGICAL REQUIREMENTS
COMMON TO MANNED PLANETARY MISSIONS
NAS2-3918

Appendix A - Mission Requirements

January 1968

Prepared by

R. D. Meston
Project Engineer

Approved by

A. Codik
Project Manager

SPACE DIVISION
NORTH AMERICAN ROCKWELL CORPORATION

FOREWORD

This report contains the final results of the studies conducted under Contract NAS2-3918, Technological Requirements Common to Manned Planetary Missions. This report consists of five volumes. The first volume (SD 67-621-1) summarizes the study results. The detailed descriptions of the study are presented in the following volumes:

Appendix A - Mission Requirements   (SD 67-621-2)

Appendix B - Environments   (SD 67-621-3)

Appendix C - Subsystem Synthesis and   (SD 67-621-4)
             Parametric Analysis

Appendix D - System Synthesis and   (SD 67-621-5)
             Parametric Analysis

CONTENTS

ILLUSTRATIONS

- x -

Figure		Page

TABLES

INTRODUCTION

The mission performance requirements for all mission objectives and mission modes considered in the study are presented. The mission objectives considered are: Mercury, Venus, Mars, Jupiter and its satellite Ganymede, and the asteroids Ceres and Vesta. The mission modes considered are direct transfers from Earth to the target body, direct returns, non-propulsive Venus swingby missions to and from Mars, propulsive swingby missions to and from Mercury, and flyby missions to Ceres, Vesta, and Jupiter. Mission opportunities which represent the extremes in the performance requirements are presented for each mission objective and mission mode considered in the study.

Results of the aerobraking technology requirements study are also presented in this report. The study defines the characteristics of the aerobraking entry corridors at Mars and Venus and the heatshield requirements for aerobraking spacecraft.

The characteristic velocity requirements for manned landings on Mercury, Mars, Ganymede, and the asteroids Ceres and Vesta are presented in the final section.

SD 67-621-2

Page XVIII IS NOT IN DOC.

PERFORMANCE REQUIREMENTS

Mission performance requirements are determined by the mission objective, mission opportunity, and mission mode being considered. In order to establish basic performance requirements for manned planetary missions during the post-1980 era, performance analyses were conducted for the following mission objectives: Mercury, Venus, Mars, Jupiter and its satellite Ganymede, and the asteroids Ceres and Vesta. Mission modes considered were: direct missions to all of the mission objectives; Ceres, Vesta, and Jupiter flyby missions; non-propulsive Venus-swingby missions to Mars; and propulsive Venus-swingby missions to Mercury. Performance data were generated to the level of detail required to define the variations in mission performance requirements during a complete cycle of opportunities. The evaluation of the mission requirements included the determination of the effects of mission opportunity, trip time, and planetary stay time.

The basic trajectory data for the direct outbound and return missions were stored on magnetic tapes and plotted automatically, using a SD-developed digital computer program. The trajectory tapes provide a permanent record of the mission requirements over a wide range of mission characteristics. These data can be repeatedly processed to determine the effects of mission parameters, such as parking orbit altitude and shape, on the mission performance requirements. For the purposes of this study, the Earth parking orbit was restricted to a circular orbit at an altitude of 300 kilometers. Only circular parking orbits were considered at the target body during the initial investigations. The analyses were extended to include elliptic planetary parking orbits about Mercury, Venus, Mars, Jupiter, and Ganymede under an amendment to the basic contract.

A limited orbit stability study was conducted for low eccentricity ($e=0.1$) orbits about Mercury, Ceres, Vesta, and Ganymede. The purpose of the study was to establish the stability characteristics prior to the generation of extensive mission performance data for the orbital and landing missions. It was determined that no significant stability problems exist for the planetary stay times considered.

MISSION OPPORTUNITIES

The selection of mission opportunities was based on data provided by the NASA at the initial coordination meeting, on gross performance scans, and on the relative positions of Earth and target body at the time of Earth departure and target body arrival. Opportunities for direct missions will occur once during each synodic period of the target body, and the performance requirements will roughly repeat once each synodic cycle. The synodic periods and cycles for the mission objectives are shown in Table 1 and are based on the planetary ephemeris data contained in Reference 1. As can be seen from the table, the frequency of mission opportunities will be a maximum for Mercury and a minimum for Mars (approximately every 116 days and 780 days, respectively).

Only a limited number of mission opportunities were investigated in detail since the objective of the mission analysis study was to determine mission opportunities representative of minimum, average, and maximum performance requirements. The selection of mission opportunities for Mars and Mercury direct missions was based on the data contained in References 2 and 3. Since extensive outbound and return mission data were not available for Jupiter, Ceres, and Vesta, gross performance analyses were made for these target bodies.

The results of the gross performance analyses for missions to Jupiter are shown in Figures 1 through 8. Figures 1 through 4 show the total incremental velocity requirements for the Earth-to-Jupiter mission phase. The trans-Jupiter requirements are defined by the sum of the incremental velocity required for escape from an Earth parking orbit at an altitude of 300 kilometers (km) and the incremental velocity required for insertion into a circular parking orbit about Jupiter at the radius of Ganymede (approximately 15 Jupiter radii). The Jupiter-to-Earth incremental velocity requirements are defined by the parking orbit escape requirements only. The Jupiter-to-Earth requirements do not include a retrobraking maneuver at Earth since only direct entry was assumed during this study. The data do not include the incremental velocity requirements for insertion into a parking orbit about Ganymede. The Jupiter mission opportunities that were selected for the direct missions correspond to Earth departures during 1985, 1987 and 1990.

The performace scans for the Ceres and Vesta did not produce obvious mission opportunities that would have the desired variations in the performance

requirements. Therefore, data were generated such that the arrival dates would occur when the target bodies would be in the vicinity of the ascending node, descending node, maximum declination, minimum declination, aphelion, and perihelion.

SD 67-621-2

Table 1. Synodic Periods and Cycles

Target Body	Synodic Period (days)	Synodic Cycles
Mercury	115.88	13 years + 2 days 33 years - 1 day
Venus	583.92	8 years - 1 day 243 years - 1/2 day
Mars	779.94	15 years + 17 days 32 years - 9 days 47 years + 8 days 79 years - 1 day
Vesta	504.17	Approximately 28 years
Ceres	466.61	14 years + 19 days 22 years + 2 days
Jupiter	398.88	Approximately 12 years
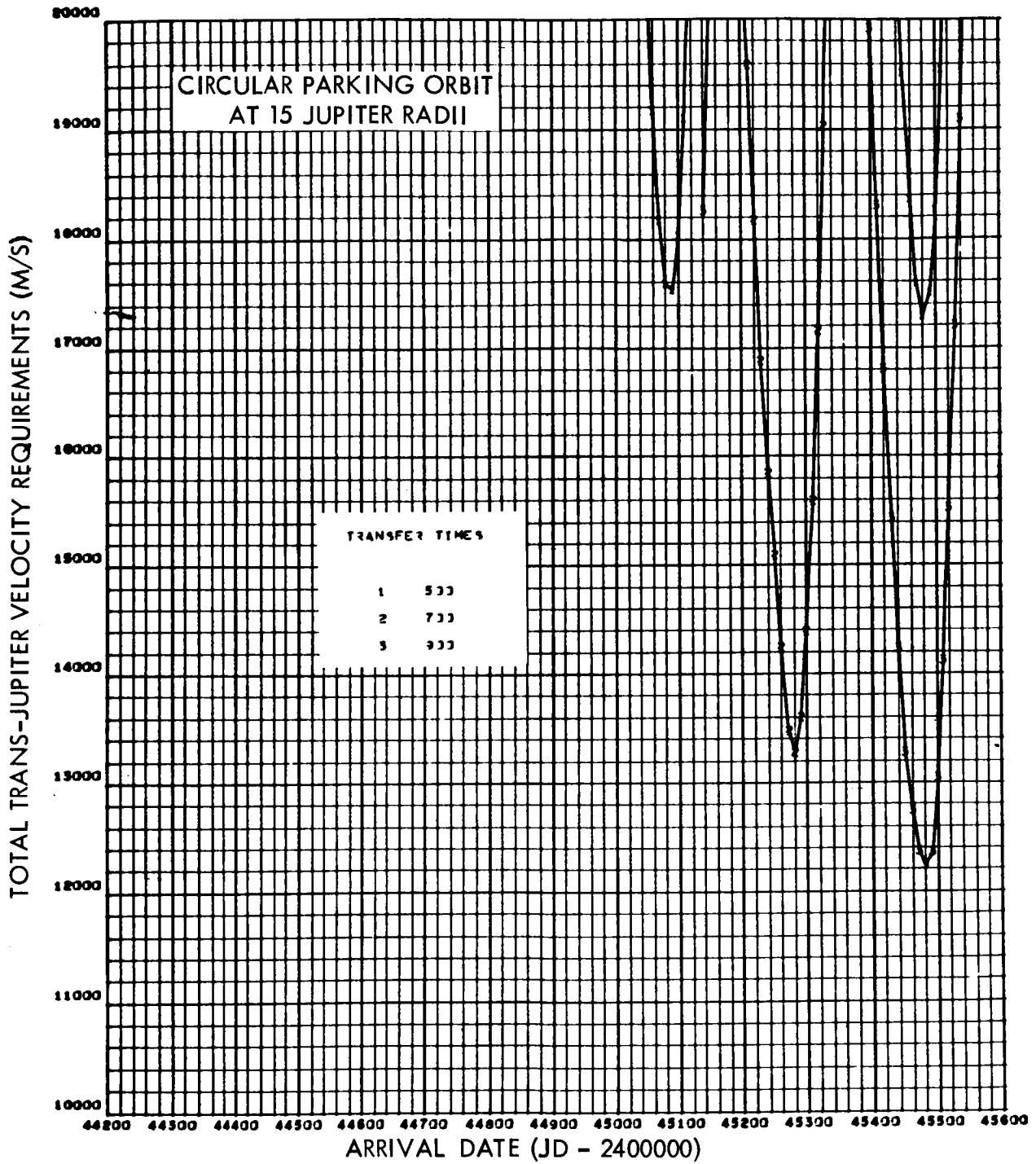
Figure 1. Earth-to-Jupiter Velocity Requirements (1982 to 1983 Arrival)

SD 67-621-2
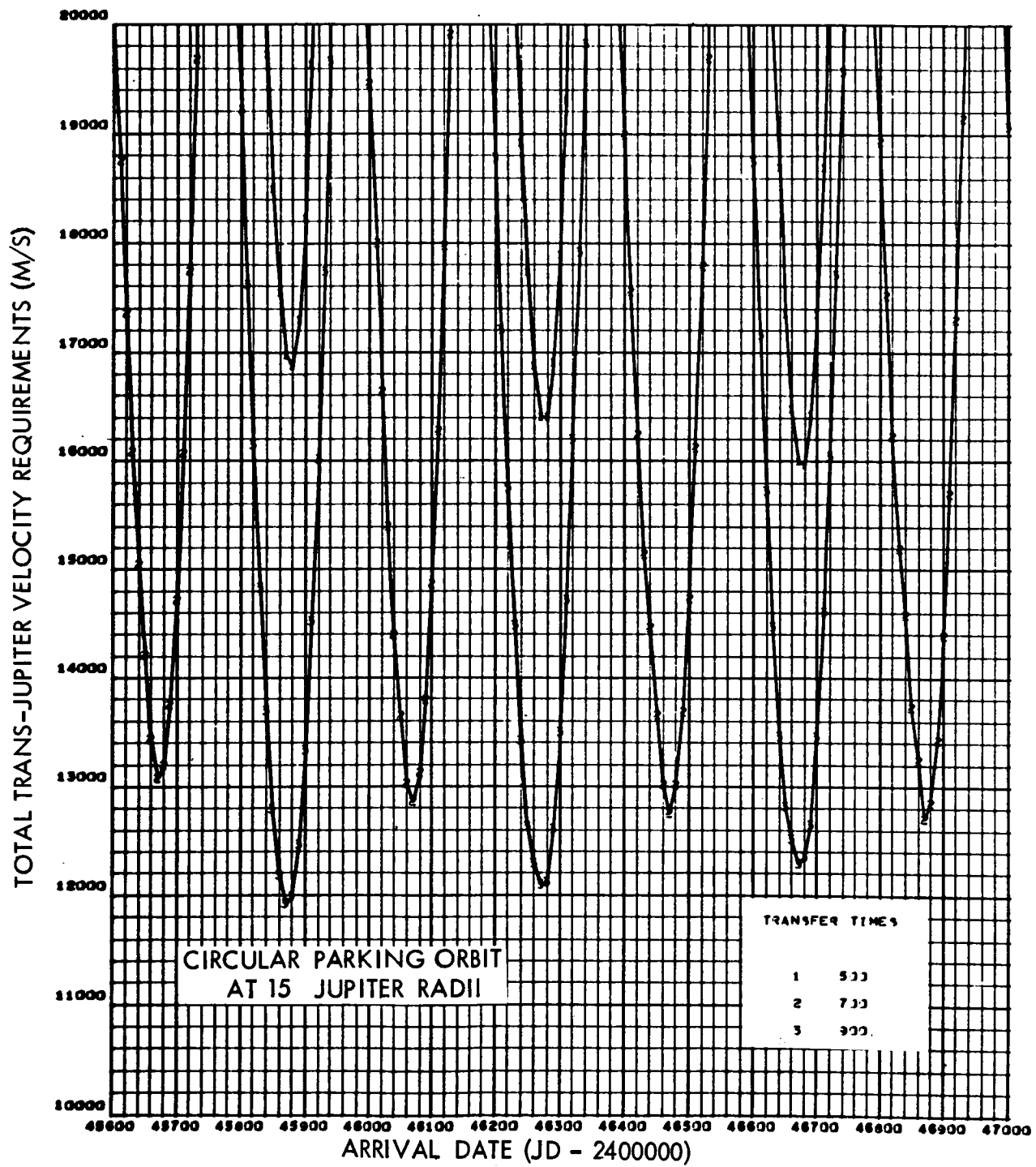
Figure 2. Earth-to-Jupiter Velocity Requirements (1983 to 1987 Arrival)
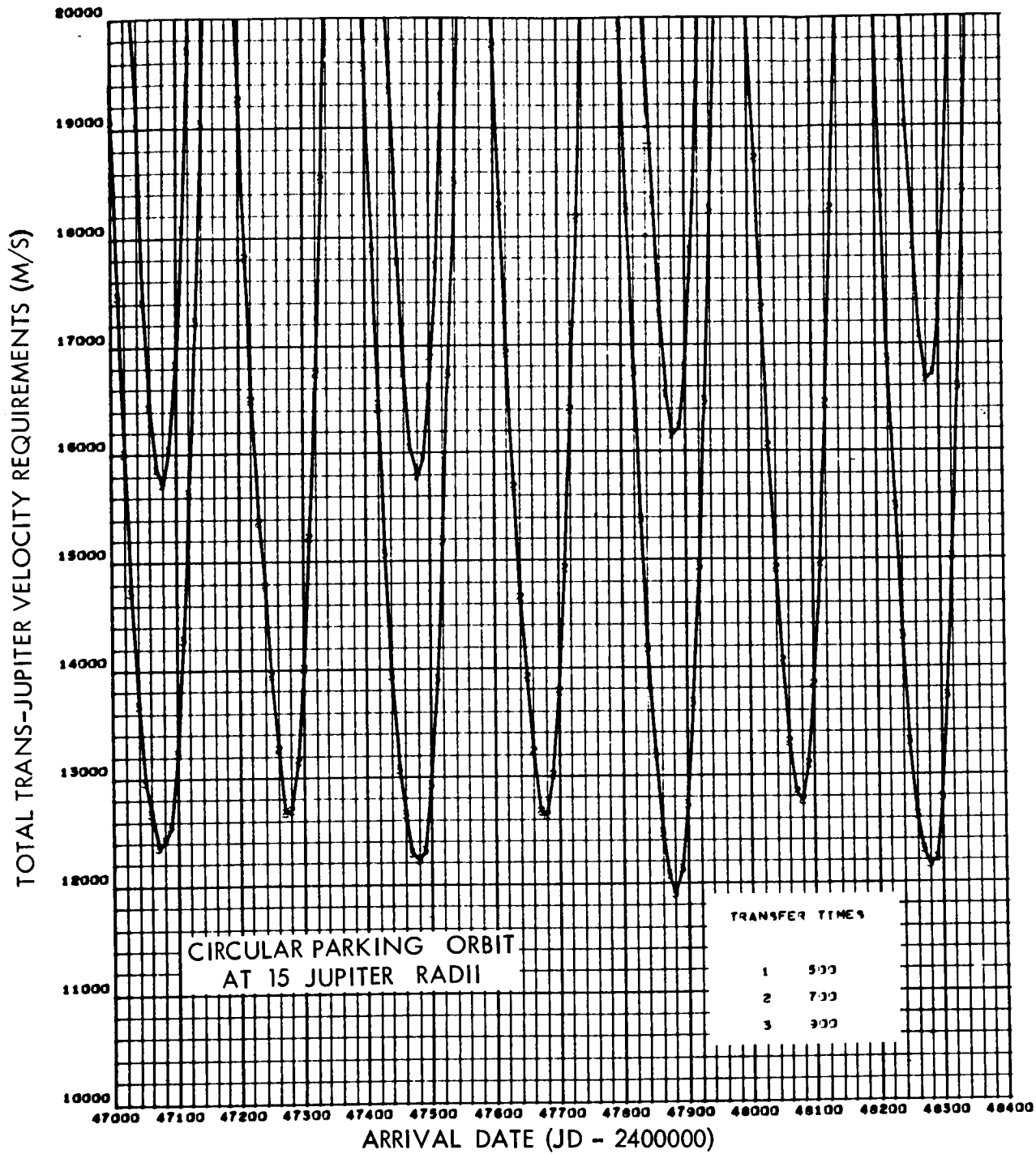
Figure 3. Earth-to-Jupiter Velocity Requirements (1987 to 1991 Arrival)

SD 67-621-2
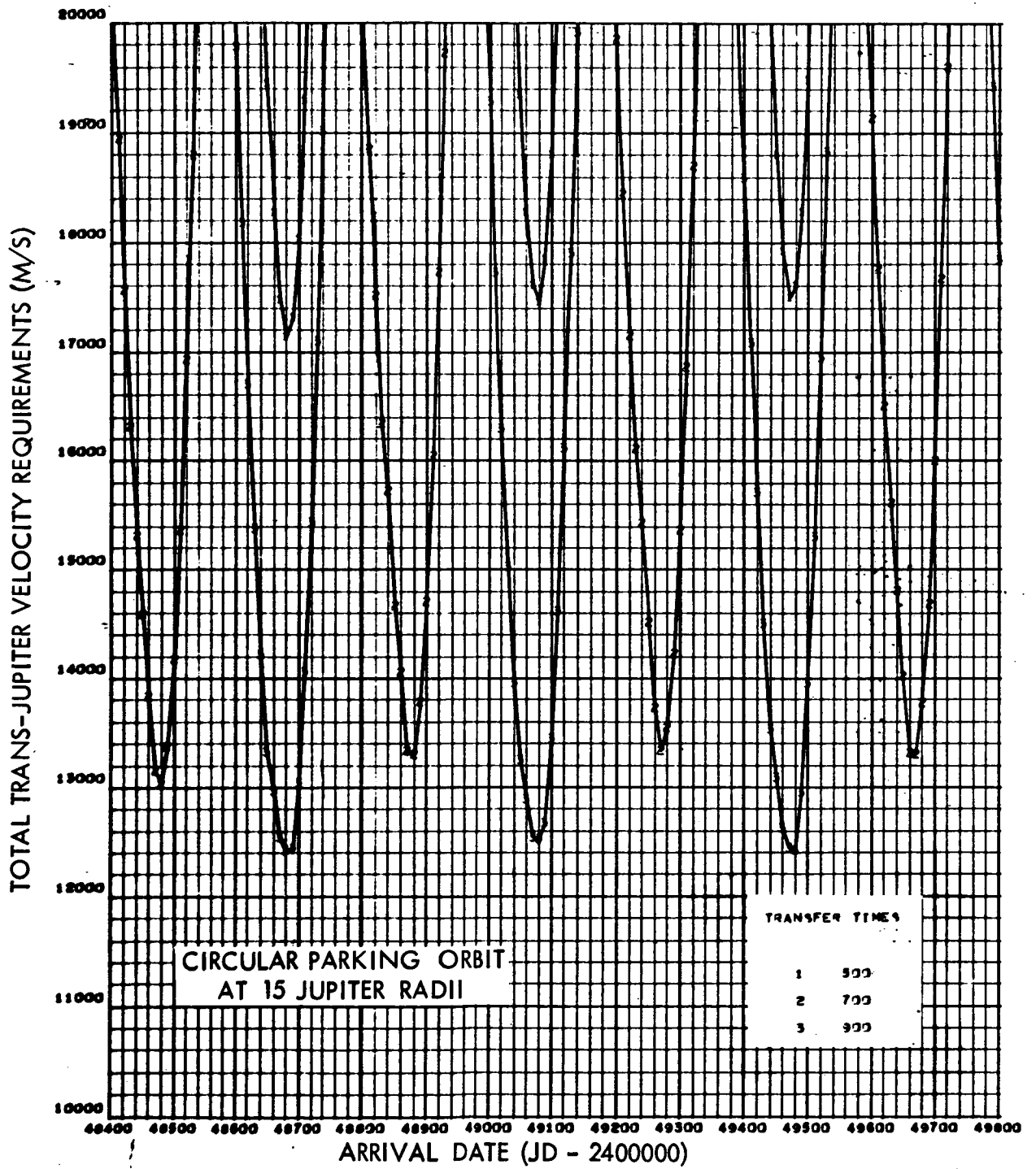
Figure 4. Earth-to-Jupiter Velocity Requirements (1991 to 1995 Arrival)
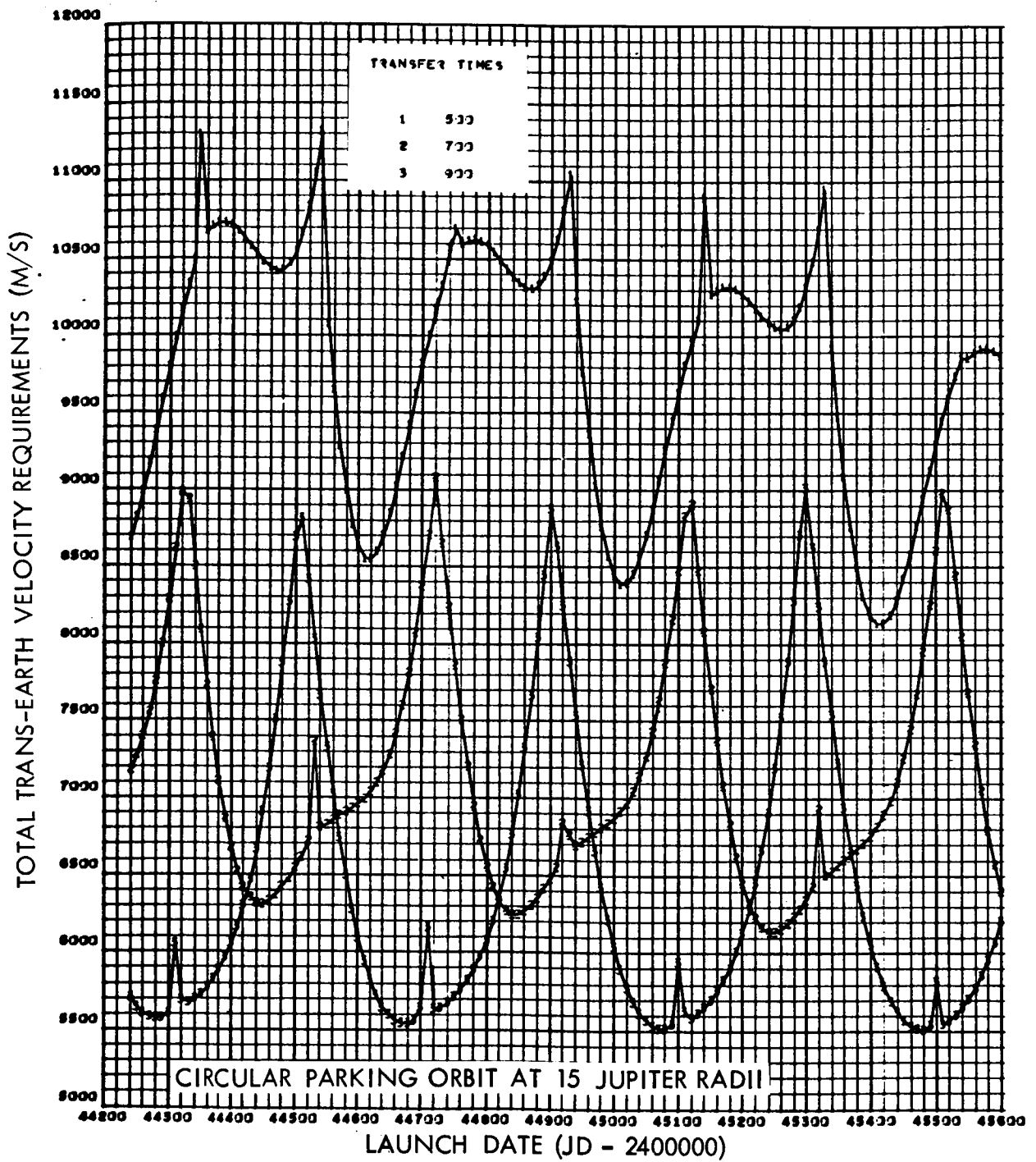
Figure 5. Jupiter-to-Earth Velocity Requirements (1980 to 1983 Departure)

- 12 -
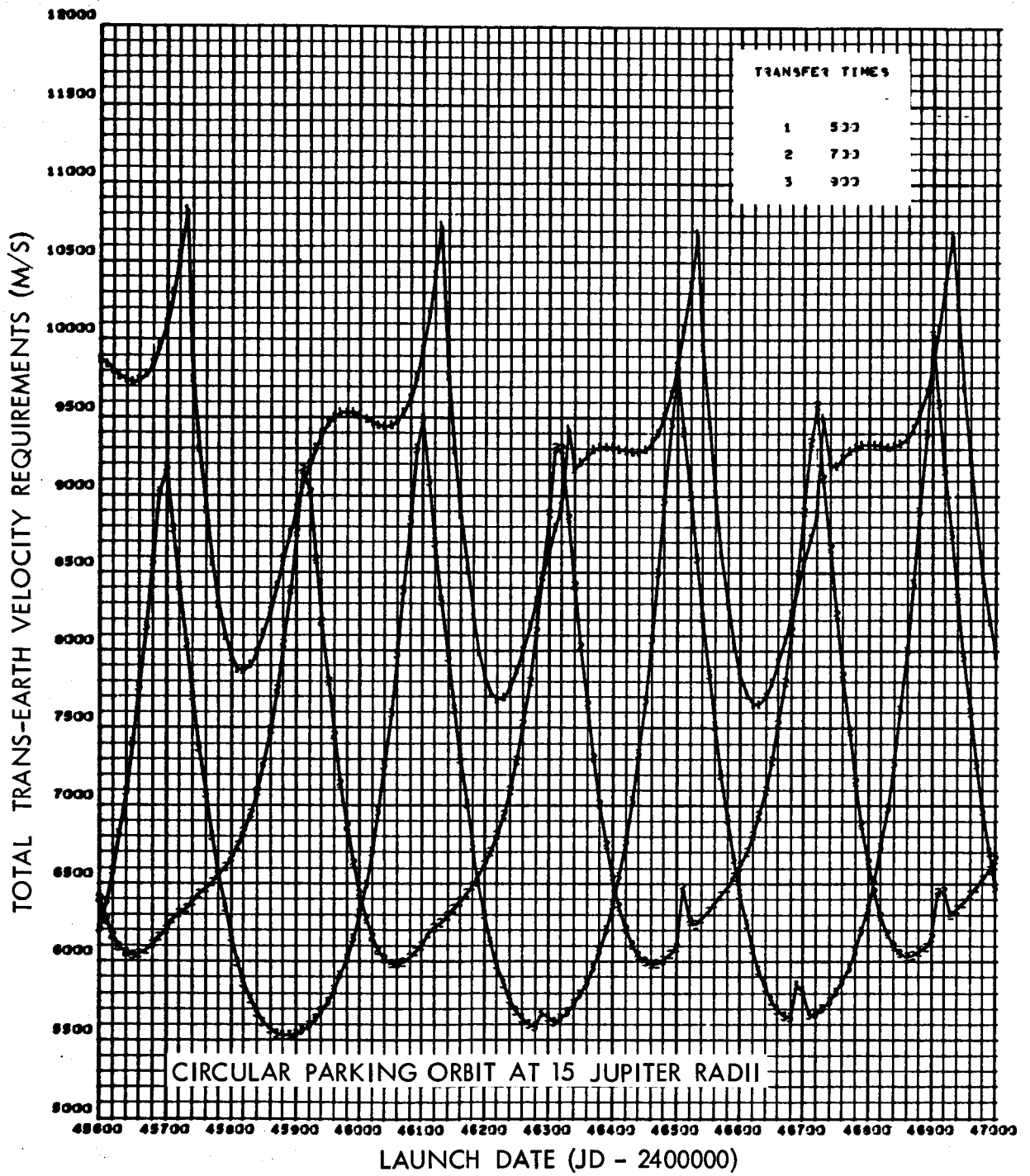
Figure 6. Jupiter-to-Earth Velocity Requirements (1983 to 1987 Departure)
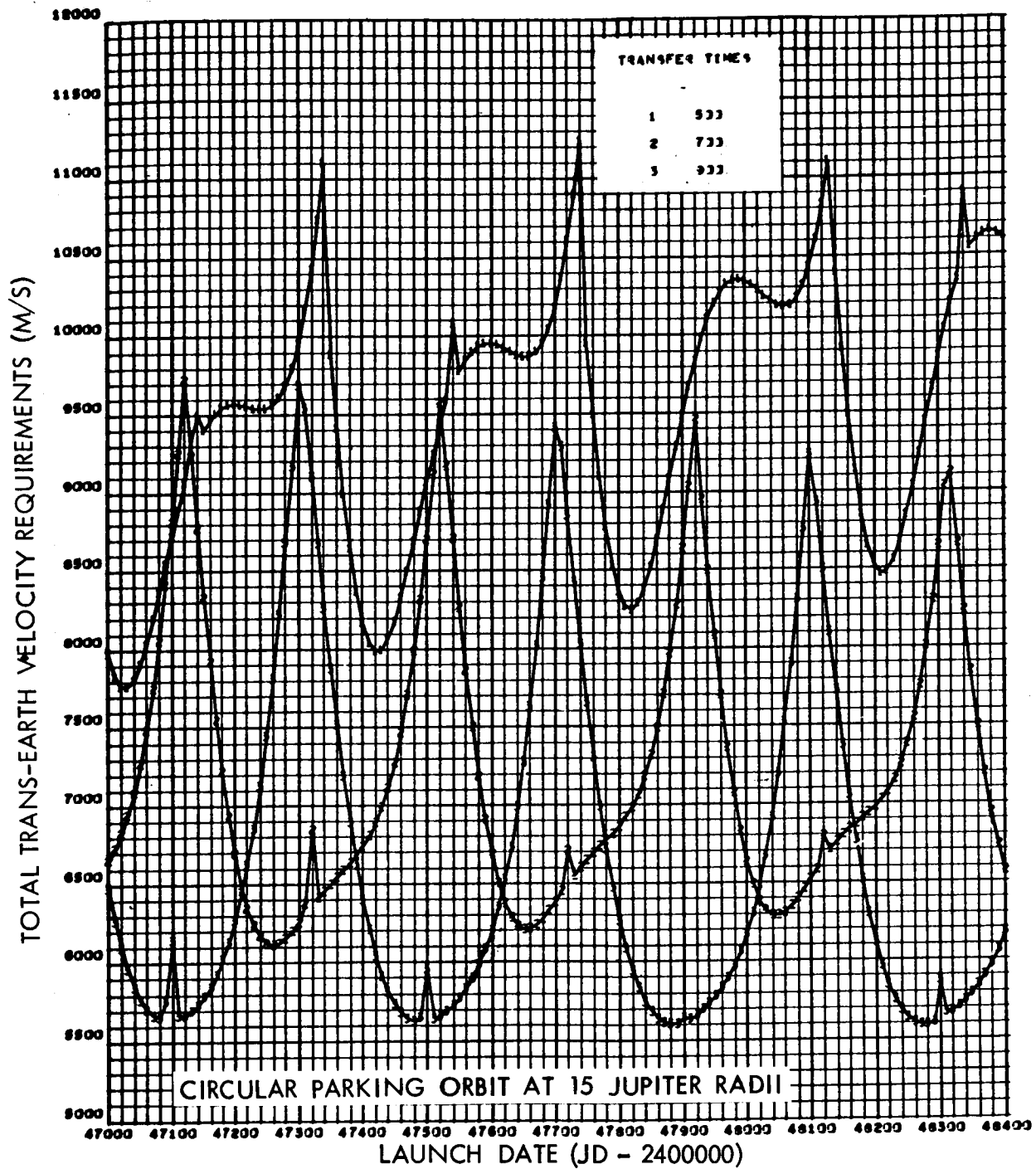
Figure 7. Jupiter-to-Earth Velocity Requirements (1987 to 1991 Departure)
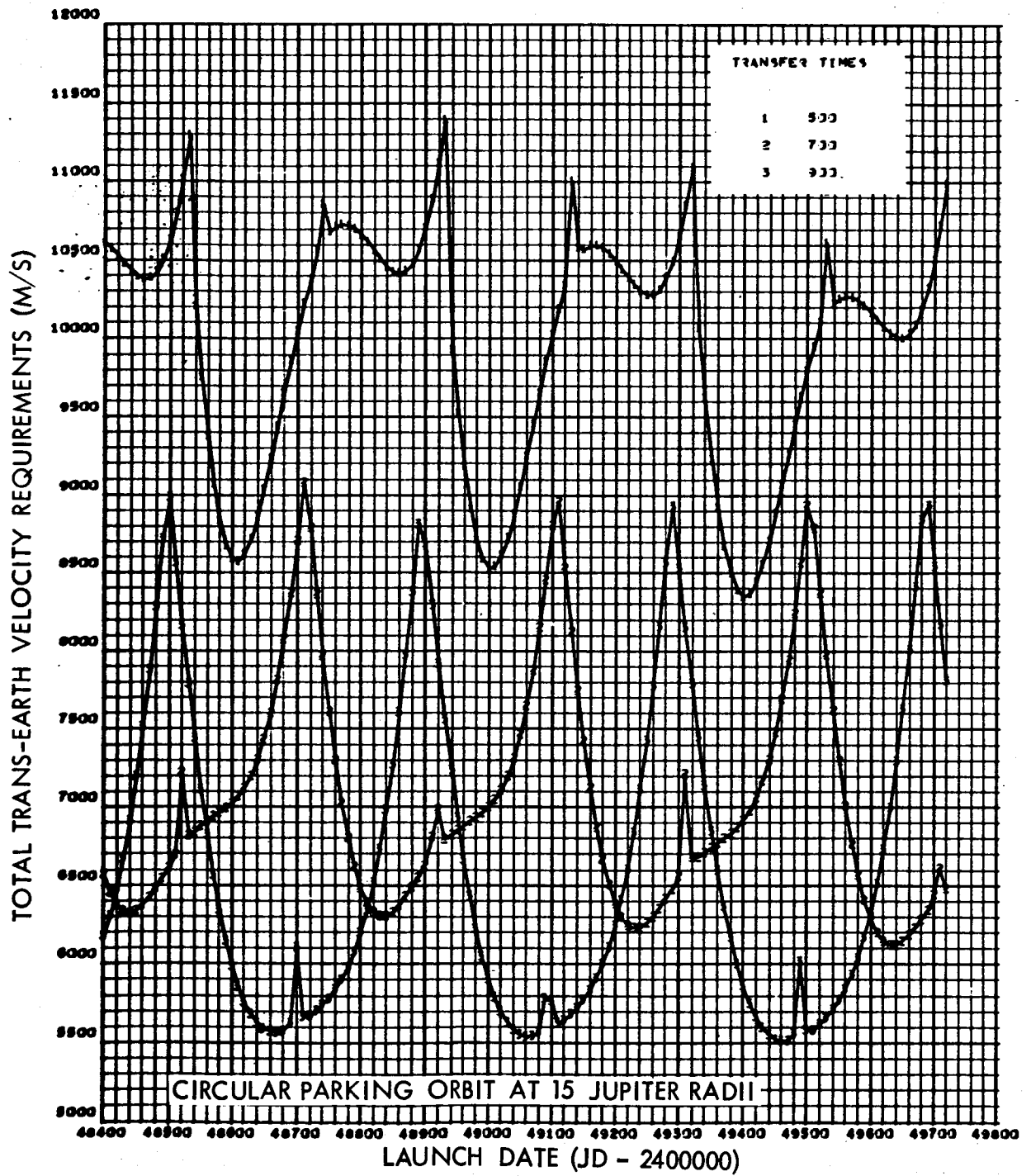
Figure 8. Jupiter-to-Earth Velocity Requirements (1991 to 1995 Departure)

SD 67-621-2

MISSION SELECTION METHODOLOGY
AND RATIONALE

Basepoint missions were selected for each of the mission opportunities considered on the basis of performance requirements only. Such an approach neglects the effects of mission duration on the mass requirements of the manned modules, and thus, the total system mass. For the flyby missions, the mission selection was based only on the Earth departure velocity require- ments. However, two methods of establishing the performance requirements for the direct and swingby missions were considered. The first method consists of selecting the combination of Earth departure date, target body arrival date, target body departure date (for a given stay time), and Earth arrival date, which minimizes the summation of the incremental velocity requirements. This approach assumes the effects of staging and propellant selection will not affect the mission selection. The second method uses a simplified approximation to account for the effects of propellant selection and staging.

In the first method, the basic trajectory data for the direct missions are generated and stored on magnetic tape. These tapes are then processed, using a SD-developed digital computer plotting program. Sample outputs from this program were shown in Figures 1 through 8 for Jupiter missions and are shown in Figures 9 through 13 for the 1990 Mars missions. Figure 9 shows the Earth departure (transplanet) velocity requirements as a function of Mars arrival date for a range of transfer times. For heliocentric transfer angles near 180 degrees, two-plane transfers are evaluated and, if beneficial, the velocity increment is included in the Earth departure velocity require- ment. These data are used to determine the velocity requirements for the Earth-to-Mars phase of an aerobraking mission. Figure 10 shows the total transplanet velocity requirements using a retrobraking maneuver at Mars. The corresponding Mars-to-Earth velocity requirements are shown in Figure 11. The data shown in Figure 11 are based only on the planetary orbit escape incremental velocity requirements since direct reentry was assumed at Earth. Retrobraking maneuvers prior to reentry which reduce the Earth reentry speed were not considered. The performance require- ments are also plotted as velocity contours as shown in Figures 12 and 13 for the Earth-to-Mars and Mars-to-Earth phases, respectively.

Desirable mission opportunities were located by overlaying trans- parencies of the contour plots. By overlaying Figures 12 and 13, it can be seen that two families of solutions exist which have low total velocity require- ments. One family of missions, the conjunction class missions, have
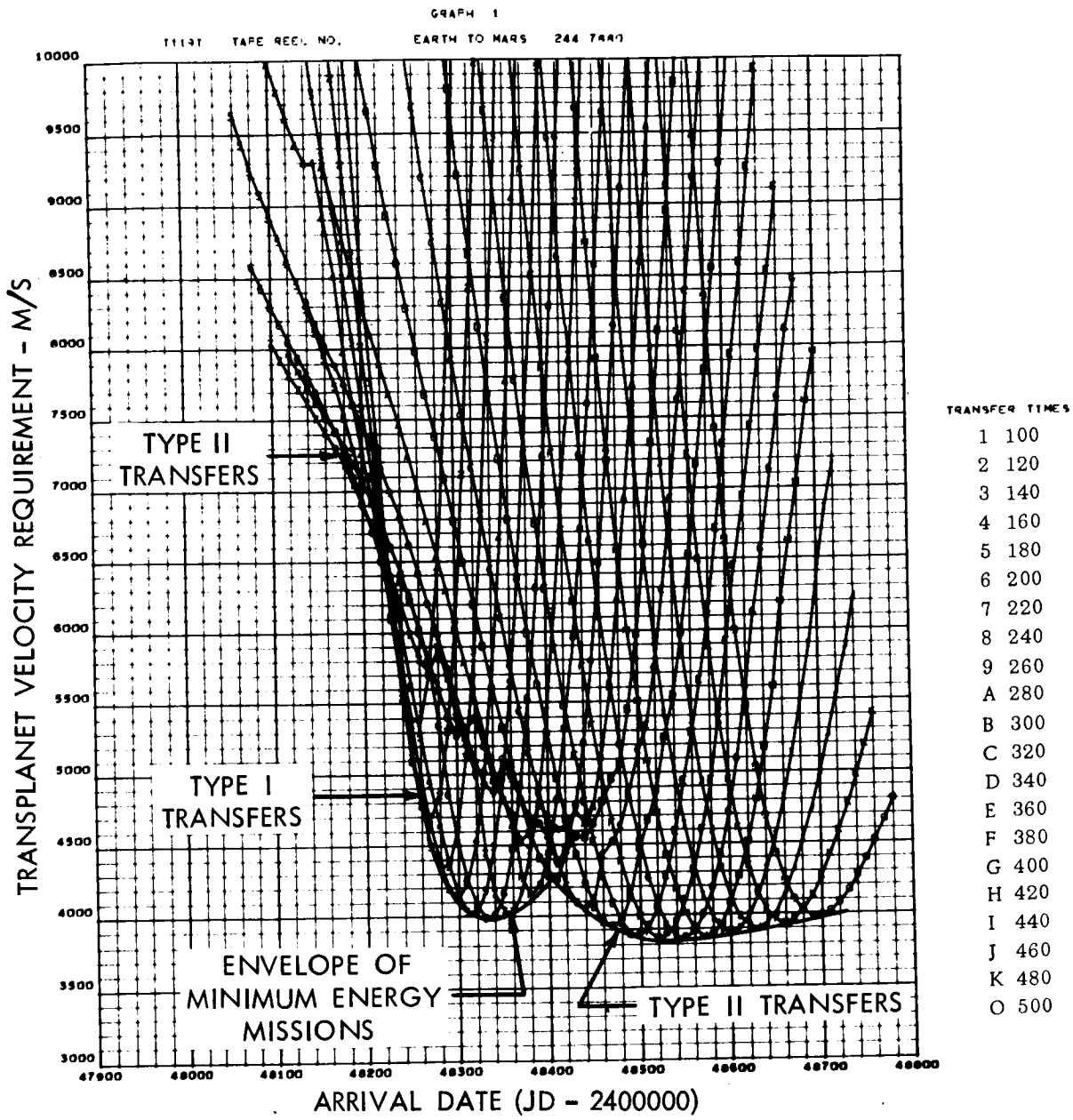
Figure 9. Transplanet Velocity Requirements (1990 Mars Opposition)

SD 67-621-2
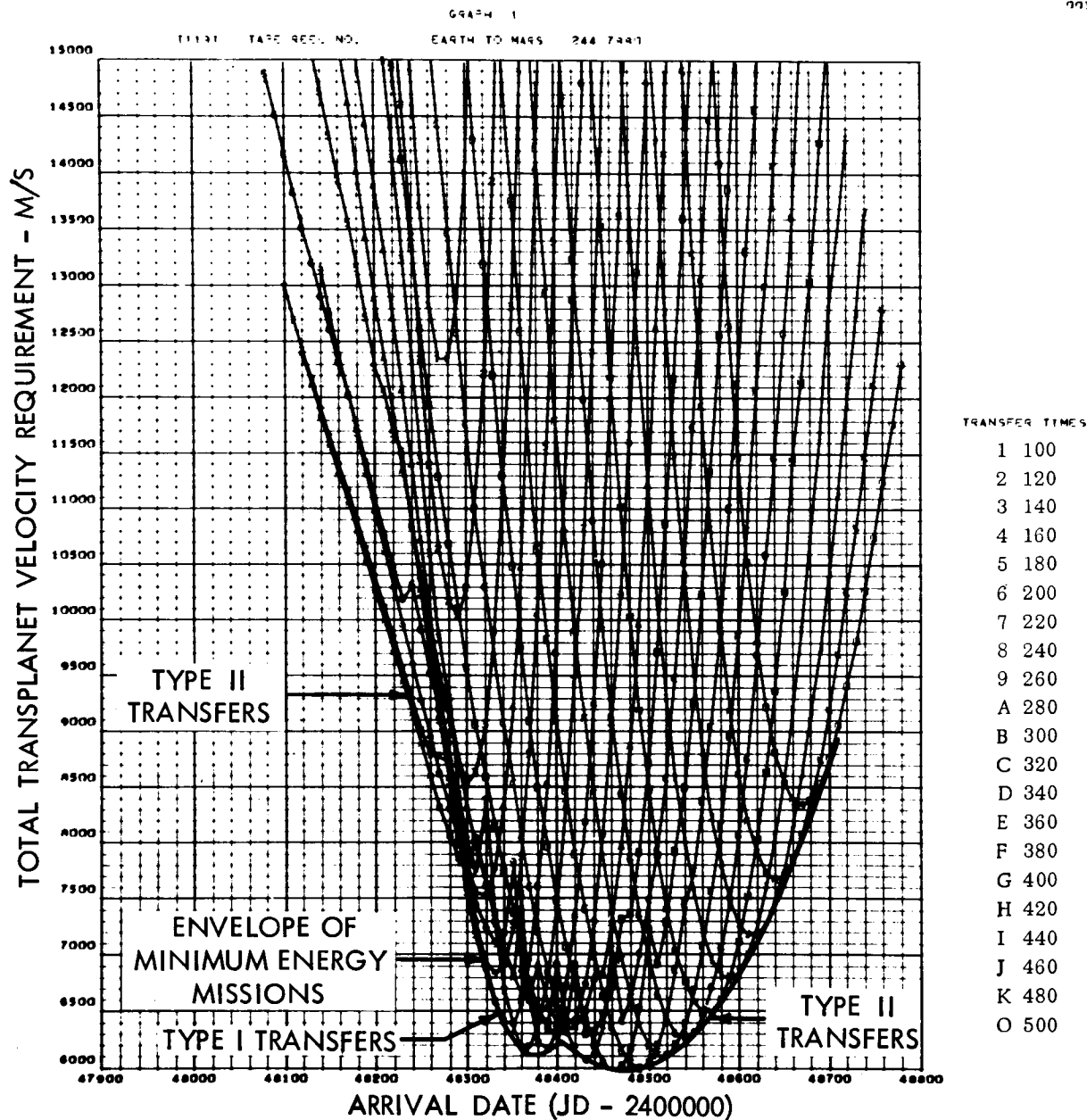
Figure 10. Total Transplanet Velocity Requirements (1990 Mars Opposition)

SD 67-621-2
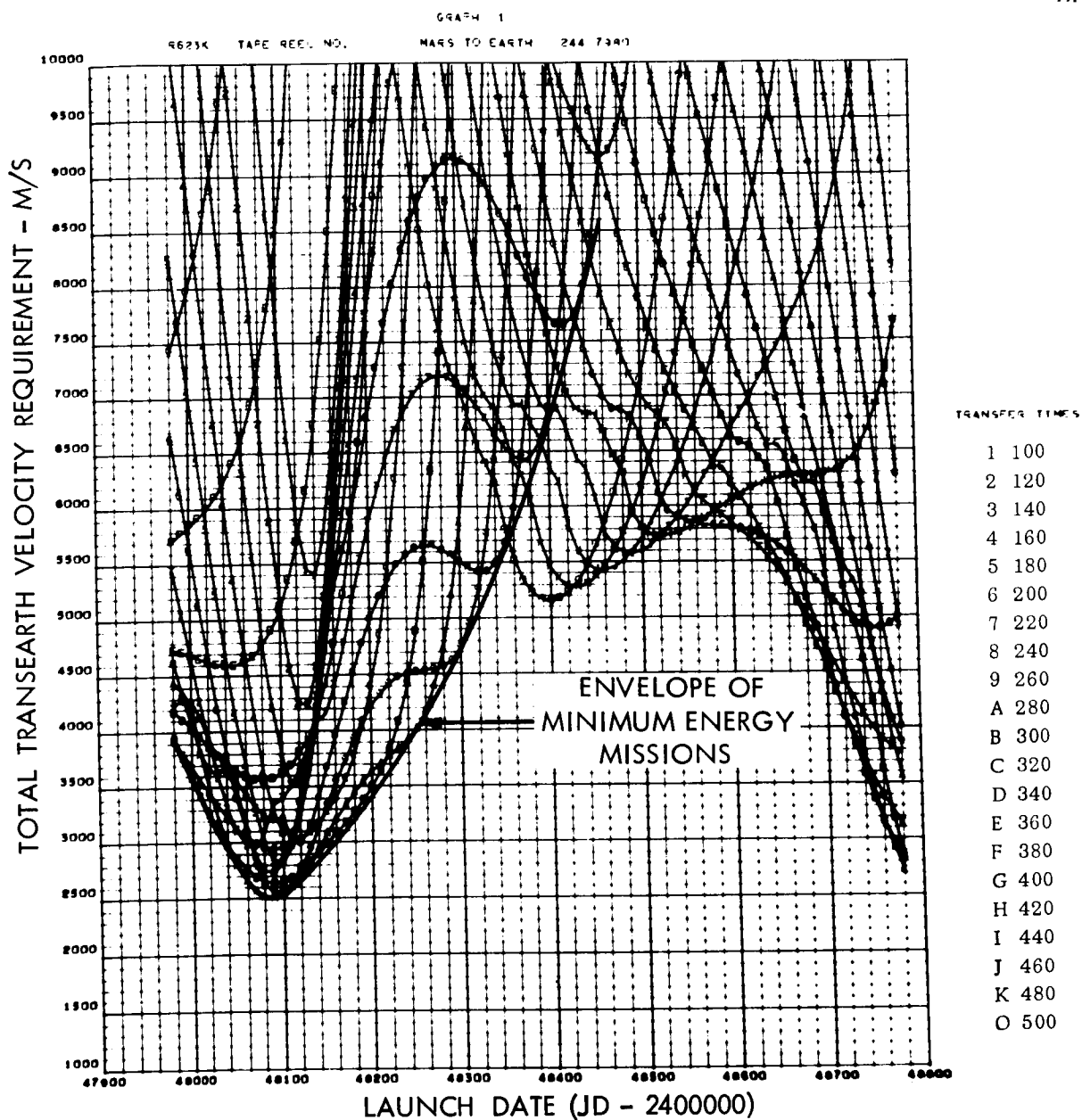
Figure 11. Total Trans-Earth Velocity Requirements (1990 Mars Opposition)

SD 67-621-2
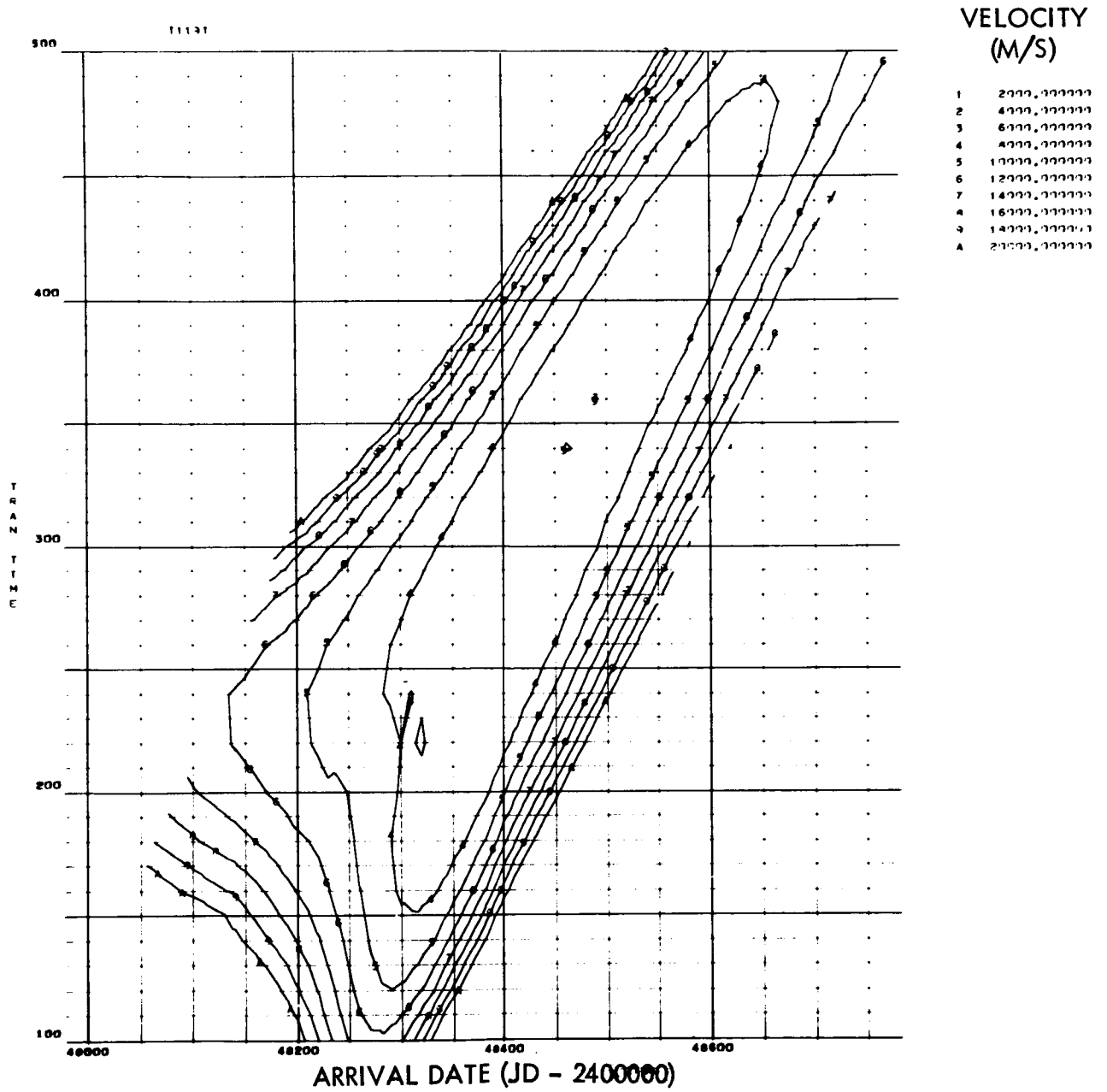
Figure 12. Total Transplanet Velocity Contours (1990 Mars Opposition)

SD 67-621-2
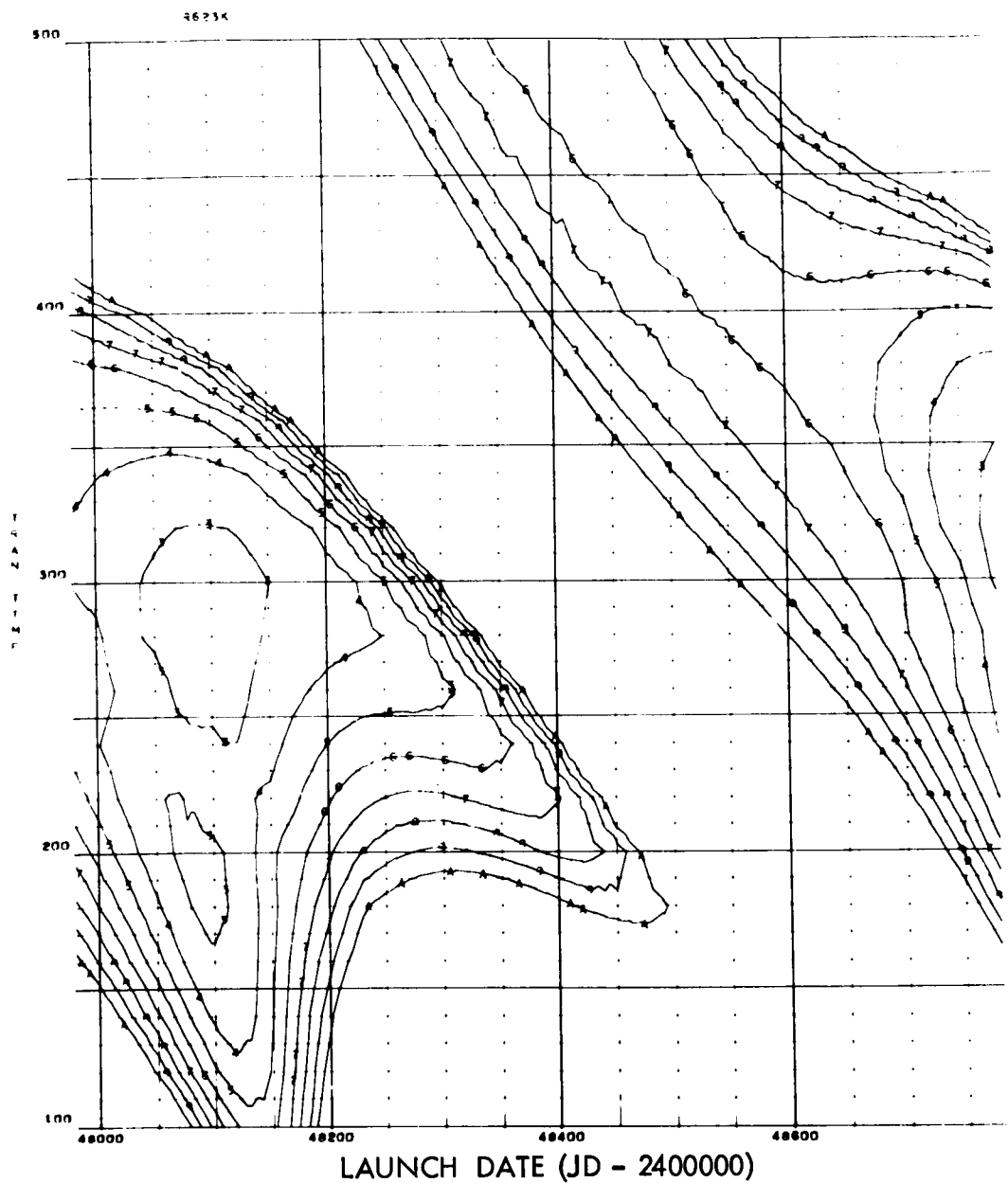
Figure 13. Total Trans-Earth Velocity Contours (1990 Mars Opposition)

SD 67-621-2

mission durations of approximately 1,000 days. The second family of missions, the opposition class missions, have higher velocity requirements but shorter mission durations. Only the opposition class missions were considered in the present study. The effects of stay time at Mars can be seen by translating the overlays horizontally while trip time effects can be seen by a vertical translation. Once desirable regions of mission opportunities are located, the basic plots of the velocity requirements (e.g., Figures 10 and 11) are used to define the mission. The mission is determined by examining the envelopes of the velocity requirements to determine the arrival date (and thus the departure date for a given stay time) which minimizes the total velocity requirements. Again, transparencies of the plots can be used to facilitate the analyses. The mission selection is performed by translating the overlays vertically (with an initial horizontal translation to account for stay time) and evaluating the requirements at the intersection of the envelopes. The trip times and the individual incremental velocity requirements can then be determined.

The second method of establishing performance requirements is based on the use of propulsion factors (initial gross mass/payload mass) to obtain an initial mass ratio. For landing missions, the initial mass in Earth orbit (W_o) is approximated by

$$W_o = \left[(W_{EM} + W_{MM}) \, P_{TEI} + W_{PEM} \right] \, P_{POI} \, P_{TPI} \qquad (1)$$

where

W_{EM} = Earth entry module mass (kilograms)

W_{MM} = mission module mass (kilograms)

W_{PEM} = planetary excursion module mass (kilograms)

P_{TEI} = trans-Earth injection propulsion factor

P_{POI} = planetary orbit insertion propulsion factor

P_{TPI} = transplanet injection propulsion factor

For simplicity, only the major propulsive maneuvers are shown. Transplanet and trans-Earth midcourse correction velocity requirements (P_{TPMCC} and P_{TEMCC}) were considered in the actual evaluations. Rewriting Equation 1,

$$\frac{W_o}{W_{EM} + W_{MM}} = \left[P_{TEI} + \left(\frac{W_{PEM}}{W_{EM} + W_{MM}} \right) \right] P_{POI} \, P_{TPI} \qquad (2)$$

- 23 -

For this application, the propulsion factors are approximated by

$$P_i \approx e^{m_i \Delta V_i}$$

where m_i is dependent upon the propellant type. The approximation for P_i is based on data similar to Figures 6.2.2-8 through 6.2.2-20 of Reference 4. Rewriting Equation 2 we have,

$$Ln \left[\frac{W_o}{W_{EM} + W_{MM}} \right] = Ln \left[e^{m_{TEI} \Delta V_{TEI}} + \frac{W_{PEM}}{W_{EM} + W_{MM}} \right]$$

$$+ (m_{POI} \Delta V_{POI} + m_{TPI} \Delta V_{TPI}) \tag{3}$$

The components of Equation 3 are plotted in a manner similar to the velocity data and are shown in Figures 14 through 16 for the 1990 Mars mission. Figure 14 shows the transplanet propulsion factors ($\ln P_{TP} = m_{TPI} \Delta V_{TPI} + m_{TPMCC} \Delta V_{TPMCC}$) for aerobraker missions assuming a value of m_{TPI} of 0.22×10^{-3} seconds/meter and a value of m_{TPMCC} of 0.28×10^{-3} second/meter. For the retrobraker missions shown in Figure 15, the transplanet propulsion factors include the planetary orbit insertion requirements (i.e., $\ln P_{TP} = m_{TPI} \Delta V_{TPI} + m_{TPMCC} \Delta V_{TPMCC} + m_{POI} \Delta V_{POI}$), assuming a value of m_{POI} of 0.22×10^{-3}. The trans-Earth component of Equation 3 is presented in Figure 16 for a value of m_{TEI} of 0.28×10^{-3} seconds/meter. The plots are used in pairs in the same manner as the velocity plots to determine missions which minimizes the mass ratio. Figures 14 and 16 are used for the aerobraker missions while Figures 15 and 16 are used for the retrobraker missions.

Summaries of the performance requirements for the 1990 Mars mission opportunity are shown in Figures 17 and 18 (as a function of stay time) for the aerobraker and retrobraker missions, respectively. The total velocity requirements shown in Figure 17 were obtained by summing the envelope of the transplanet velocity requirements of Figure 9 and the total trans-Earth velocity requirements of Figure 11. The mass ratio data of Figure 17 was obtained in a similar manner from Figures 14 and 16. The total velocity requirements and mass ratio requirements for the 1990 retrobraker mission were obtained in an analogous manner from Figures 10 and 11 and from Figures 15 and 16, respectively. The discontinuity shown in Figure 18 is due to the transition from Type II to Type I Earth-to-Mars transfers. As shown in the figures, neither the stay time nor the technique employed to establish the spacecraft performance requirements appears to have an appreciable effect on the arrival date. Since the arrival date is approximately the same for the stay times considered, the transplanet mission characteristics will be the same. The characteristics of the trans-Earth missions will
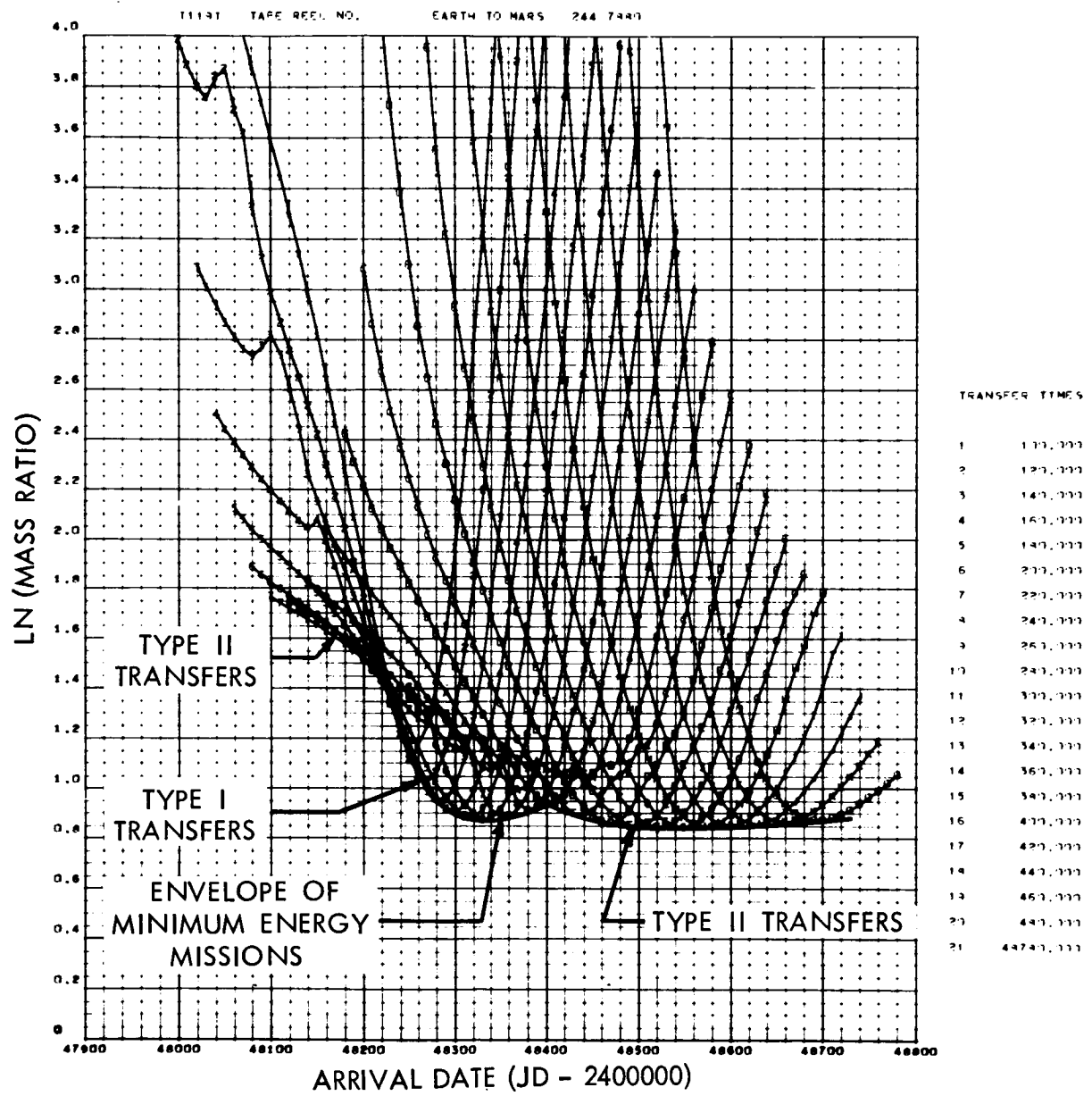
Figure 14. Transplanet Propulsion Factors (1990 Mars Opposition)
(Nuclear Injection Stage)

SD 67-621-2
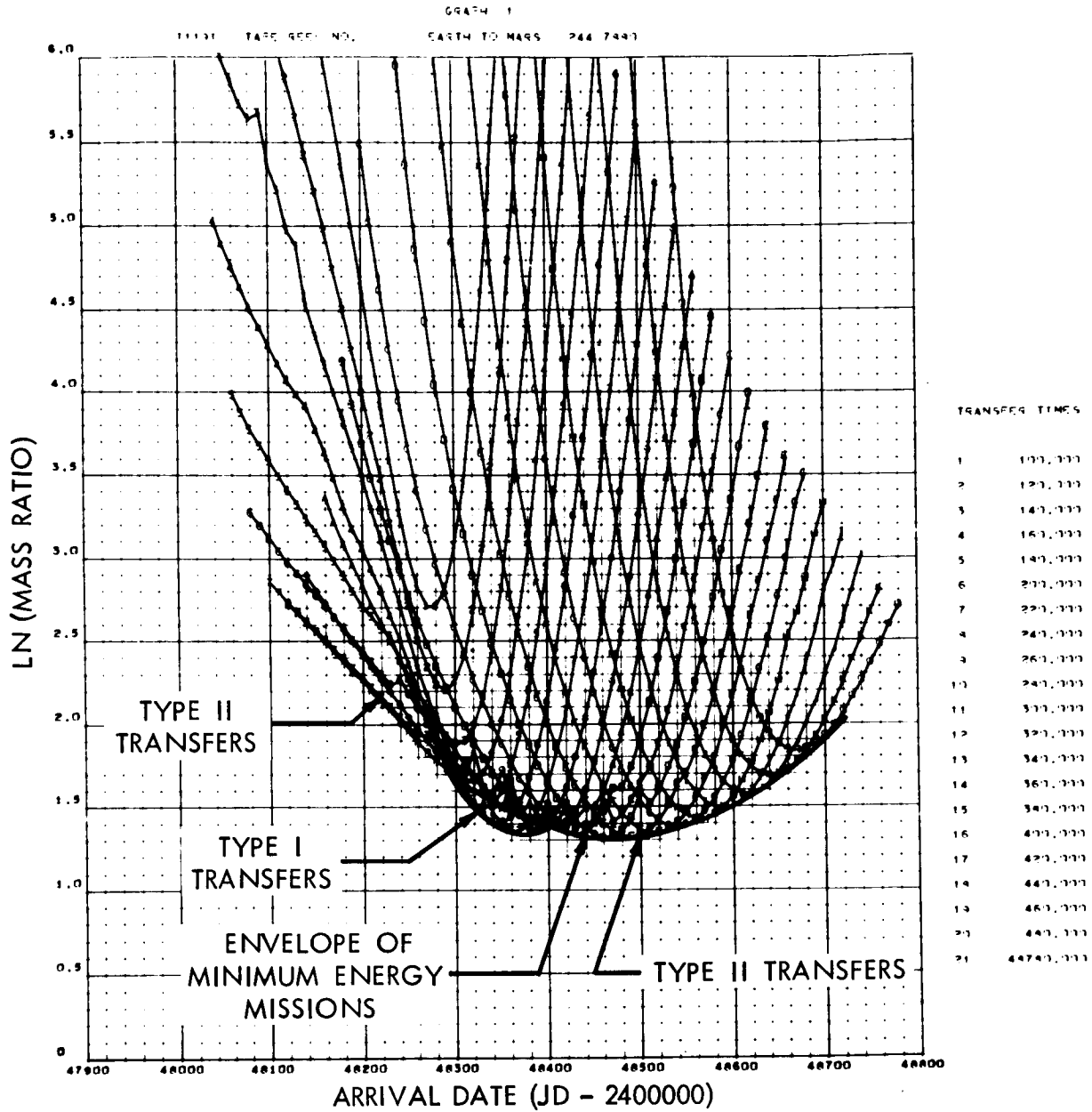
Figure 15. Total Transplanet Propulsion Factors (1990 Mars Opposition)
(Nuclear Injection Stage)

- 26 -
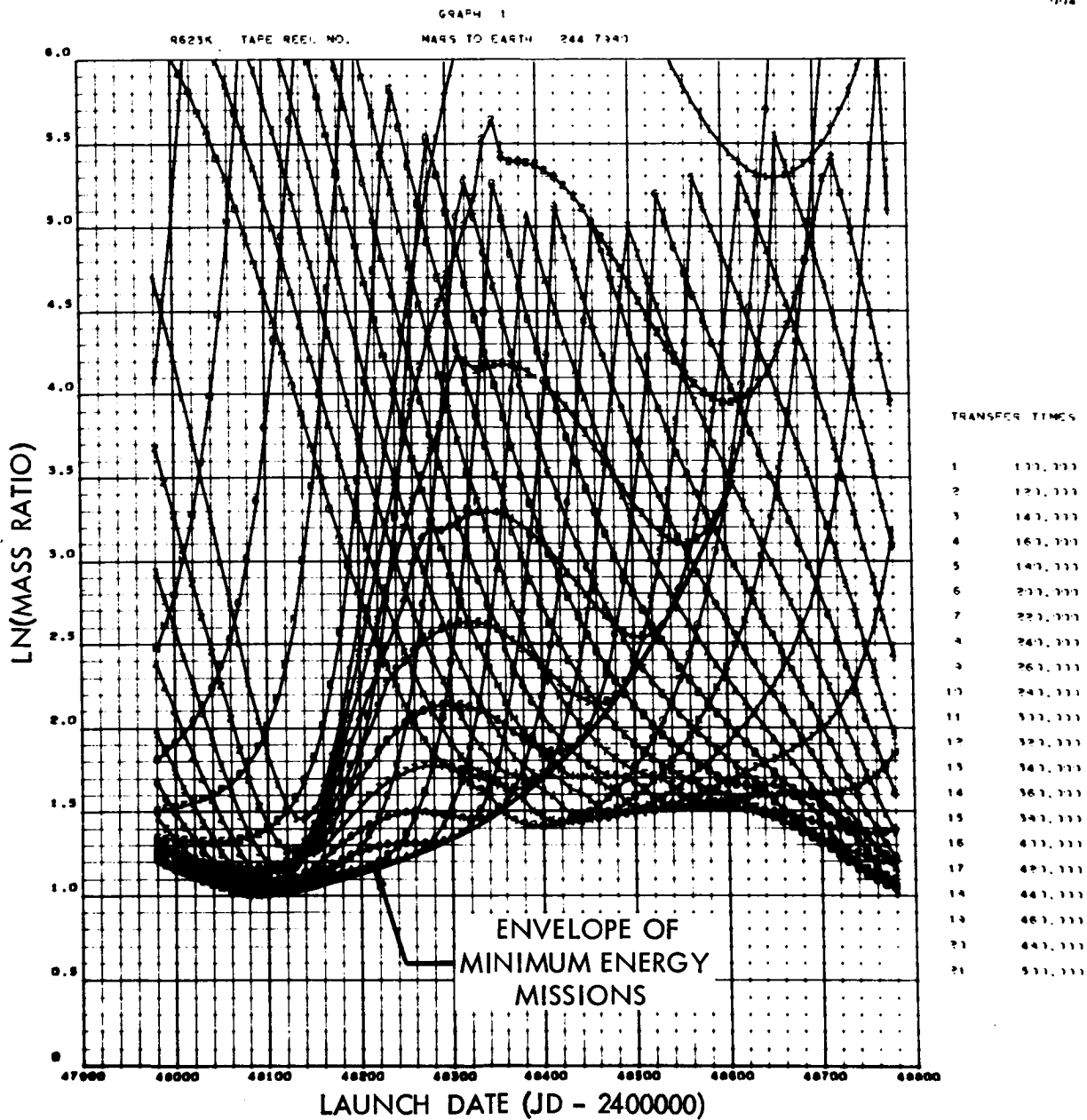
Figure 16.   Total Trans-Earth Propulsion Factors (1990 Mars Opposition)
(Chemical Injection Stage)

- 27 -

SD 67-621-2
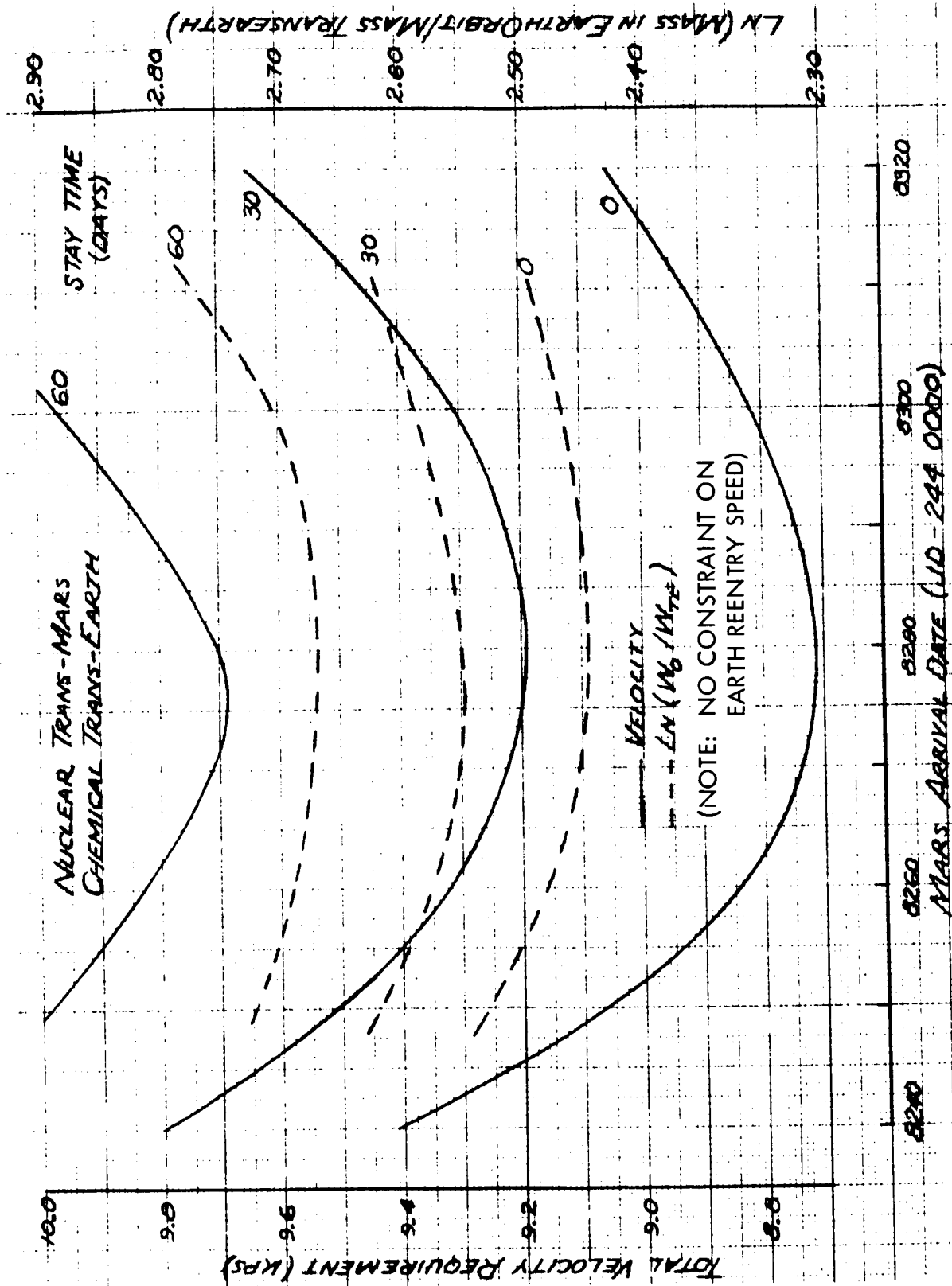
Figure 17. Total Mars Mission Requirements (1990 Aerobraker Mission)
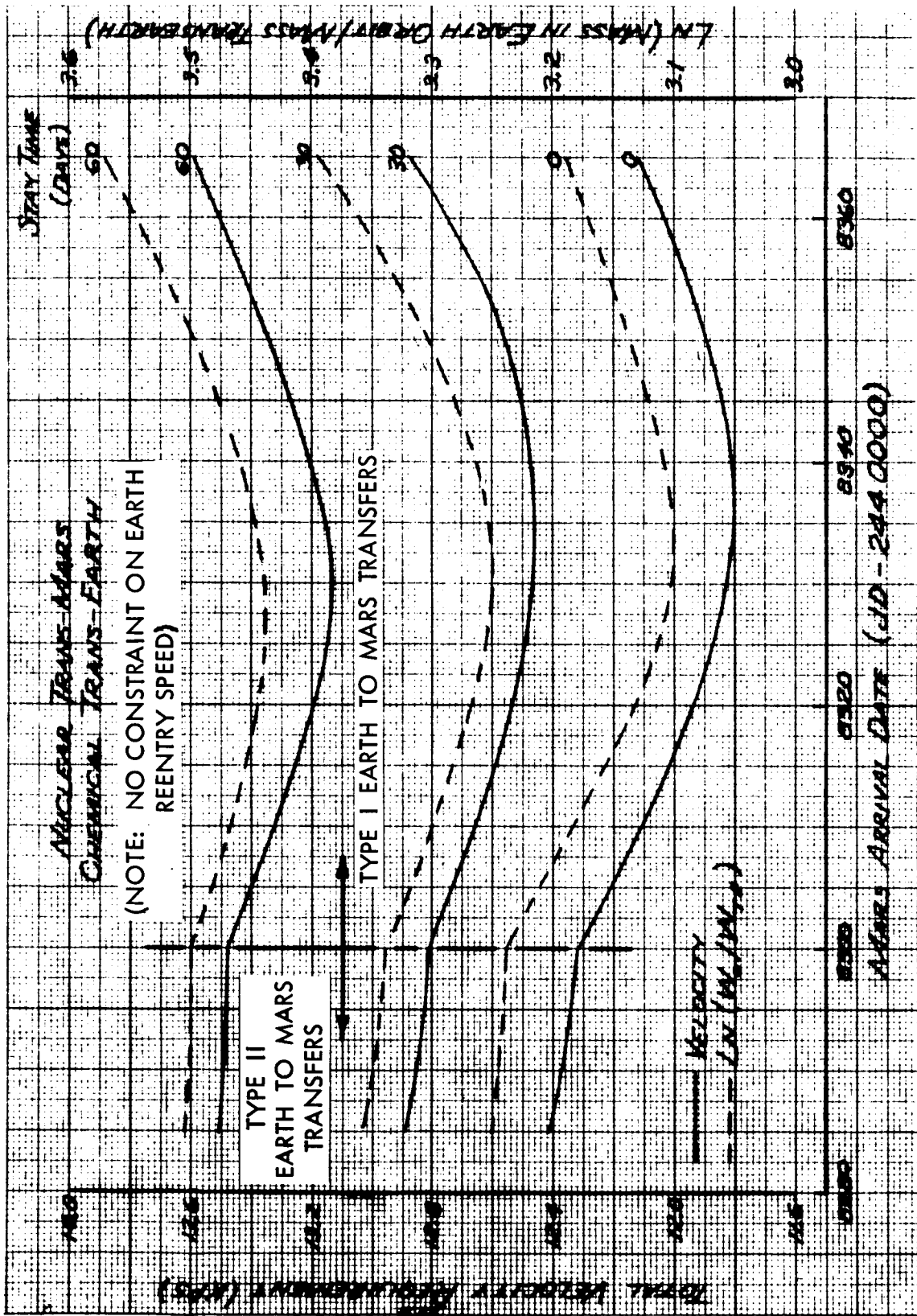
Figure 18. Total Mars Mission Requirements (1990 Retrobraker Mission)

differ since the planet departure date varies as the stay time increases. The trip times and the incremental velocity requirements for the individual maneuvers which correspond to the minimization of the total incremental velocity requirements (and thus the minimization of the initial mass in Earth orbit) can be obtained from Figures 9 through 11. For example, the total velocity requirements for the Mars 1990 retrobraker mission with a stay time of 30 days are minimized by arriving at Mars on Julian Date (JD) 244 8335 (Figure 18). The required Earth departure incremental velocity and the trans-Mars trip time are obtained from Figure 9, i.e., approximately 4 km/s and 200 days, respectively. The total trans-Mars velocity requirement is obtained from Figure 10 (6.5 km/s). Therefore, the Mars planetary orbit insertion incremental velocity requirement is approximately 2.5 km/s. The corresponding trans-Earth incremental velocity requirements are obtained from Figure 11 for a launch date of JD 244 8365 (approximately 6 km/s). The resultant total mission incremental velocity requirement is then 12.5 km/s and the total mission duration is approximately 460 days.

The missions defined by Figure 17 and 18 do not include considerations of other factors such as Earth reentry speed. During subsequent analyses, the Earth reentry speed was constrained to 19.8 km/s (65,000 ft/sec) and for some missions was achieved only at the expense of increased total incremental velocity requirements. The 19.8 km/s reentry speed constraint was imposed as an upper bound and was achieved without retrobraking prior to Earth entry.

The mass ratios were evaluated for all mission objectives and mission opportunities considered in the study. In all cases, it was found that essentially the same missions were defined by minimizing either the total velocity requirements or the mass ratio requirements for the broad spectrum of missions considered in the study. Therefore, it is concluded that a mission defined by the simple minimization of the total incremental velocity requirements will also approximate the minimum mass in Earth orbit mission for a given mission duration. This qualification is reasonable since, in general, the duration of the minimum mass mission is slightly less than the minimum total incremental velocity mission. Although the total velocity requirements would increase, the total mass in Earth orbit would decrease due to a reduction in the time dependent mass requirements (mission module mass, boil-off propellant, etc.). Of significance, however, is that once the mission duration and stay time are prescribed by the mission objective, the best particular trajectory (i.e., proper Earth departure and planet arrival dates) can be selected from trajectory considerations only without recourse to more time consuming mass calculations.

MISSION PERFORMANCE REQUIREMENTS

Extensive mission requirements data were generated for each of the mission objectives and mission modes considered in the study. The data were generated using a three-dimensional model which assumes elliptic planetary and asteroidal orbits with constant mean elements. The heliocentric transfer orbit was determined using Lambert's theorem to solve for the conic transfer between two points in a central force field in a fixed time. The inclination of the transfer conic to the ecliptic approaches 90 degrees as the difference in celestial longitude of the departure planet (at the time of departure) and the target planet (at the time of arrival) approaches 180 degrees. The required high inclination results in large velocity requirements for departure and arrival. In order to reduce the requirements, a two-plane transfer was also evaluated and employed when beneficial.

FLYBY MISSIONS

Mission-performance requirements for Ceres and Vesta flyby missions were generated for mission opportunities representative of minimum and maximum requirements. Mission times equal to an integral number of years were considered for these missions, since the trajectory perturbations due to the asteroids will be small and the transfer trajectory will depart and return tangentially to the orbit of Earth. A two-year Vesta flyby mission is possible when Vesta is near perihelion. As Vesta moves away from perihelion, two-year missions are no longer possible and three-year missions are required. Three-year missions are required at all times for Ceres flyby missions.

Mission opporturnities were estimated by computing the time and central angle in the transfer ellipse from Earth departure out to the mean radius of the asteroid. Subtracting the product of the transfer time and the mean orbital motion of the asteroid from the transfer central angle gave an estimate of the required relative position at launch. After scanning each mission opportunity from 1980 to 2000, it was determined that in May 1992 Ceres would be near its maximum celestial latitude and near aphelion at flyby. This opportunity thus appears to represent the most severe conditions during the 20-year period. During the July 1993 opportunity, Ceres is near both a node and its mean distance. This is the most favorable configuration for missions to Ceres.

The required Vesta orientation for a two-year mission occurs during the 1991 opportunity, when Vesta is in the vicinity of perihelion and at a celestial latitude of 1.5 degrees at flyby. The maximum performance requirements mission occurs during 1993, when Vesta is at a minimum celestial latitude of -7.13 degrees and at slightly greater than mean distance at the time of flyby.

A family of possible Ceres and Vesta flyby missions with various Earth-departure dates, departure velocity requirements, total mission times, flyby dates, earth-return entry velocities, and perifocal radii at the asteroids was evaluated. The resultant characteristics are shown in Figures 19 through 22,* assuming a grazing flyby at the asteroid. An increase in the flyby altitude will result in a slight increase in the velocity requirements.

For Jupiter flyby missions, it was found that missions composed of nearly symmetrical elliptical areas for the transplanet and transearth legs provided the optimum Jupiter swingby missions. This technique most effectively utilizes the turn-angle capability of Jupiter. A symmetrical mission profile requires that the Earth and Jupiter be either near opposition or near conjunction at the time of flyby. Figures 23 and 24 present Jupiter swingby missions for 500- and 700-day outbound and inbound transit times. The 700-day transit time to Jupiter requires less turn angle at Jupiter to complete the Earth return than the 500-day missions. Therefore, swingbys are obtained at high flyby altitudes for 700-day missions because the available turn angle decreases as flyby altitude increases.

DIRECT MISSIONS

Extensive mission requirements data were generated for direct outbound and inbound missions for each of the mission objectives considered in the study. The trajectory data that were generated were stored on a magnetic tape and, with the exception of Mercury missions, plotted using a digital computer plotting routine. The resultant plots are presented in sets showing the outbound and return velocity requirements for a given mission opportunity as a function of arrival or departure date, incremental velocity requirements, and trip time. The transplanet velocity requirement is the incremental velocity requirement for departure from Earth orbit plus the plane-change increment if the two-plane solution has a total requirement which is less than the single-plane solution. The total transplanet velocity requirement for retrobraker missions is the sum of the transplanet requirement and the

---

*These and subsequent figures referred to in this section are located after the text, beginning on page 61.

incremental velocity required for planetary orbit insertion. The total trans- . Earth velocity requirement is analogous to the transplanet velocity requirement.

Venus

Minimum energy Venus missions occur when Venus is in the vicinity of an inferior conjunction at the time of Venus arrival. In order to establish the range of performance requirements for Venus missions, the mission performance requirements were determined for missions occurring during three of the five inferior conjunctions which occur each synodic cycle. The basic performance requirements for the opportunities selected are shown in Figures 25 through 39. During the first opportunity (1988 inferior conjunc- tion), Venus is near the ascending node at the time of inferior conjunction. Venus is near perihelion at the time of the second opportunity (1990 inferior conjunction), and between aphelion and maximum declination at the time of inferior conjunction for the final opportunity.

Summaries of the characteristics of the missions which define the envelopes of velocity requirements are presented in Figures 40 through 42. Figure 40 shows the Earth-to-Venus velocity and trip time requirements for both the aerobraker and the retrobraker missions. The Venus-to-Earth velocity requirements, trip time, and Earth entry speed are shown in Figure 41. Where appropriate both Type I (heliocentric transfer angles less than 180°) and Type II (transfer angles greater than 180°) trajectories are shown. These data define the total mission incremental velocity require- ments, trip times, and Earth entry speed for a given arrival date and stay time. Total incremental velocity requirements are shown in Figure 42 for stay times of zero, thirty, and sixty days. The corresponding mass ratio requirements are shown in Figure 43. These data, and the similar data for the remaining opportunities (Figures 44 through 49) provide the basic data required for the selection of the baseline missions presented in the next section.

Mars

The analyses of Mars missions were limited to the opposition class missions, which have total mission durations of 400 to 550 days. The first opposition during the period of interest occurs at 25.3 February 1980 (Julian date 2444294.8) and successive oppositions occur at intervals of approximately 780 days.

The 1986- and 1993-opposition missions are representative of oppor- tunities which define the limits in the performance requirements. The 1986 opportunity is representative of the lower bound, while the 1993 opportunity

is representative of the upper bound. Basic performance requirements for the 1988 and 1990 opportunities were also generated. The 1988 opportunity was selected as being representative of the average velocity, hence initial mass, requirements.

The velocity requirements data for the 1990 opportunity were discussed under Mission Selection Methodology and Rationale. The velocity requirements plots and contour plots for the 1986, 1988 and 1993 mission opportunities are presented in Figures 50 through 64. The summary plots are presented in Figures 65 through 73. The total velocity requirements defined in Figures 72 and 73 do not assume any constraints on the Earth reentry speed. The effect of imposing a 19.8 km/s (65,000 ft/sec) reentry speed contraint is shown in Figures 74 and 75. The penalty for imposing the reentry speed constraint is approximately 1.66 km/s for a stay time of 60 days.

Ceres and Vesta

Six mission opportunities were investigated for Vesta. Total mission performance requirements and requirements summaries are presented in Figures 76 through 108. Comparable velocity requirements data are shown in Figures 109 through 141 for the five Ceres opportunities investigated.

Jupiter

The Jupiter mission associated with the minimum incremental velocity requirements results in outbound and inbound trip times on the order of 900 days. It was agreed with NASA that the resultant total mission duration of 1800 days was unnecessary since the total mission duration can be decreased to approximately 1400 days by utilizing missions which impose only slightly higher velocity requirements. The mission requirements plots for the opportunities investigated are shown in Figures 142 and 156. Mission requirements summaries for the 1985 Jupiter missions are presented in Figures 157 and 158. The resultant total velocity requirements are shown in Figure 159 for those missions which have total durations of approximately 1400 days. Similar data are presented in Figures 160 through 165 for the 1987 and 1990 opportunities. The requirements defined by Figures 159, 162, and 165 do not include the effects of an earth entry speed constraint. As can be seen from Figures 158, 161, and 164, the earth entry speed could be in excess of the 19.8 km/s constraint for the missions which are defined by the minimum total velocity requirements. The entry speed can be substantially reduced, however, by increasing the performance requirements by a slight amount. Due to the sensitivity of the Earth entry speed to trans-Earth transient time, missions which minimize the Earth entry speed can be achieved with a minor performance penalty. This can be seen by referring to Figures 158 and 161 and 164, which show the trans-Earth incremental velocity requirements as a function of Jupiter departure date for the minimum

entry velocity missions. By agreement with NASA, the minimum entry velocity criteria were adopted for the Jupiter missions. The resultant total velocity requirements are shown in Figures 166 through 168 for the three opportunities.

Ganymede

The incremental velocity requirements for establishing an orbit about Ganymede were determined for two possible mission profiles. The first profile assumes the spacecraft is injected into an orbit about Jupiter and, after a coast period to attain the proper phase angle, is injected into a transfer orbit that results in a Ganymede-centered orbit with the required perifocal radius. At the Ganymede perifocus, a third propulsive maneuver is required for injection into orbit about Ganymede. The second profile, which requires only one propulsive maneuver, is a direct injection into orbit about Ganymede from the Jupiter/Ganymede approach hyperbola. The incremental velocity requirements have been determined as a function of the Jupiter approach hyperbolic excess speed (V_∞) using a two-dimensional patched conic trajectory model.

The performance requirements for the indirect mode depend upon the radius of the final orbit about Ganymede, the Jupiter approach hyperbolic excess speed, and the radius of the initial orbit about Jupiter. For this study, the Ganymede parking-orbit radius was assumed to be equal to two Ganymede radii. The hyperbolic excess speed with respect to Jupiter depends upon the earth departure date and the earth-to-Jupiter transit time and is between 6.9 and 8.3 km/s for the missions being considered. The incremental velocity requirement for injecting into orbit about Jupiter can be minimized by selecting the parking orbit radius as a function of the hyperbolic excess speed. For the present problem, however, the total requirement is minimized by injecting into an orbit that is essentially equal to the orbit of Ganymede about Jupiter. The incremental velocity requirements for injecting into orbit about Jupiter at the radius of Ganymede and the total requirement for establishing the specified orbit about Ganymede are shown in Figure 169 as a function of the Jupiter approach V_∞. As can be seen from the figure, the additional velocity increment for establishing the orbit about Ganymede is approximately 0.36 km/s for the range of hyperbolic excess speeds being considered.

The incremental velocity requirements for the direct injection mode depend upon the Jupiter approach hyperbolic excess speed, the Ganymede parking orbit radius, and the position of Ganymede in orbit about Jupiter at the time of Ganymede encounter. The parking orbit injection requirements were determined as a function of the magnitude of the Jupiter approach hyperbolic excess velocity and the position of the spacecraft relative to the Jupiter-Ganymede line of centers at the time the spacecraft enters the sphere of influence of Ganymede. Only posigrade Jupiter approach hyperbolas were

considered, but both posigrade and retrograde Ganymede approaches were considered. The posigrade approach (to Ganymede) results in a slightly lower orbit insertion incremental velocity requirement due to the lower speed of the spacecraft relative to Ganymede at the time of entry into the sphere of influence of Ganymede. The resultant Ganymede orbit insertion requirements for the minimum energy solutions are also shown in Figure 169. For the family of missions being considered, the orbit insertion requirements are between 4.8 and 5.3 km/s and represent a savings of approximately 1.56 km/s when compared with the indirect mode. Based on results of this analysis and results of the guidance and navigation considerations presented in a subsequent section, the direct Ganymede orbit injection profile was selected as the nominal profile for weight synthesis analyses.

Mercury

The analyses of the performance requirements for missions to Mercury were limited to the examination of discrete opportunities because of the restricted mission selection flexibility. The mission flexibility constraint is imposed by excessively high velocity requirements which limit the Mercury arrival and departure dates (and thus the stay time) to discrete dates. The selection of mission opportunities representative of minimum, average, and maximum performance requirements was based on the data contained in Reference 3 and a gross mission performance requirements scan. The selected missions are presented in the Selected Basepoint Missions section.

The Mercury stay time between the arrival date and the first low energy direct return opportunity varies from 60 to 90 days. The total mission performance requirements can be decreased further by delaying the return until the absolute minimum energy opportunity occurs about 90 days later. Missions have been selected by employing both of these selection criteria.

SWINGBY MISSIONS

Mercury

The evaluation and selection of powered Venus swingby missions to Mercury is simplified by the fact that the Venus synodic period is essentially five times the Mercury synodic period, with the result that the relative planetary positions of Earth, Venus, and Mercury for initiating a successful powered-swingby mission will be repeated by successive Venus synodic periods. A limited number of powered-swingby-outbound, direct-return and direct-outbound, powered-swingby return missions were generated.[1] These were selected on purely geometric bases, and the investigation was limited to a narrow range of launch opportunities and trip-time variations. The resulting missions are summarized in Tables 2 and 3.

---

[1]An investigation was also conducted of unpowered Venus swingby missions. For the opportunities investigated, however, either the direct or powered swingby missions resulted in lower total incremental velocity requirements.

Table 2. Powered Venus Swingby to Mercury

Earth Launch (Year)	(JD*)	ΔV_1 (kps)	Earth-Venus Trip Time (days)	ΔV_2 (kps)	Arrive Venus (JD)*	ΔV_{swing} (kps)	Venus-Mercury Trip Time (days)	ΔV_3 (kps)	Arrive Mercury (JD)*	ΔV_4 (kps)	ΔV_{TTP} (kps)
1983	5475	3.74	190	0.0	5665	0.62	86	2.70	5751	7.02	14.08
1985	6070	3.83	170	0.0	6240	2.51	96	0.0	6336	6.86	13.20
1985	6200	4.58	160	0.0	6360	0.45	108	1.93	6468	6.46	13.42
1986	6650	3.87	190	0.0	6840	3.72	74	0.0	6914	4.44	12.03
1988	7210	3.96	180	0.0	7390	2.32	100	0.0	7490	7.27	14.50

Earth Launch (Year)	Arrive Mercury (JD)*	Stay Time (days)	Depart Mercury (JD)*	ΔV_{TE} (kps)	Transearth Transit Time (days)	ΔV_5 (kps)	ΔV_{TTE} (kps)	Arrive Earth (JD)*	V_{entry} (kps)	Mission Duration (days)	ΔV_{total} (kps)
1983	5751	41	5792	8.33	65	0.0	8.33	5857	17.75	382	22.41
1985	6336	50	6386	8.47	182	0.0	8.47	6568	18.68	498	21.67
1985	6468	18	6486	6.55	75	0.0	6.55	6561	16.37	361	19.97
1986	6914	42	6956	11.21	85	0.0	11.21	7041	13.91	391	23.24
1988	7490	42	7532	6.96	123	0.0	6.96	7655	15.02	445	21.46

Notes:

ΔV_1 = Transplanetary injection velocity increment

ΔV_2 = First transplanet leg plane change velocity increment

ΔV_{swing} = Velocity increment added during Venus swingby passage

ΔV_3 = Second transplanet leg plane change velocity increment

ΔV_4 = Mercury orbit insertion velocity increment

ΔV_{TTP} = Total transplanet incremental velocity requirement

ΔV_{TE} = Trans-Earth injection velocity increment

ΔV_5 = Trans-Earth leg plane change velocity increment

ΔV_{TTE} = Total Trans-Earth velocity increment requirement

V_{entry} = Earth entry speed

ΔV_{total} = Total mission incremental velocity requirement

*Julian Date - 2440000.

The search for a candidate powered Venus swingby mission to Mercury was initiated by determining the relative planet orientation required for a minimum energy transfer from Venus to Mercury combined with a low-energy Earth-Venus transit opportunity. The first opportunity investigated was the 1988 Venus inferior conjunction. By varying Earth departure date and the trip times, a local minimum energy powered-swingby transfer was established. Both single-plane and two-plane solutions were evaluated for the single leg trajectories.

During the initial investigation, it was found that over the low-energy mission opportunity interval, Mercury arrival times remained essentially constant for the minimum energy solutions as both first- and second-leg trip times (i. e. , Earth to Venus and Venus to Mercury) were varied to achieve minimum performance requirements for each launch date evaluated. This emphasises the significance of the original premise that the planetary geometric association occurring at the venus inferior conjunction represents a favorable swingby mission opporturnity. The investigation was then extended by searching for additional earlier launch opportunities, using an opportunity time increment of 584 days (Venus synodic period) for successive trials.

Comparison of the tabulated data for these missions with direct outbound-direct inbound missions with identical return legs show that in all five cases the Mercury stay times were reduced by approximately fifty percent, while total mission duration was increased by 100 to 140 days. In all five missions, the total velocity requirement was less than the compared direct mission, and four of the five swingby missions had lower total velocity requirements than any direct mission immediately adjacent to the compared missions.

The alternate mission mode (direct-outbound, swingby-return) is represented by the three cases tabulated in Table 3. Comparison with equivalent direct missions show Mercury stay times reduced by approximately fifty percent but the swingby return missions all required higher total mission velocity requirements.

Mars Outbound Venus Swingby Missions

Outbound Venus swingby missions to Mars with retrobraking and atmospheric braking and direct returns are analyzed on the basis of total mission velocity requirements for the three successive syzygistic periods of 1986, 1993, and 1999. The characteristics of these missions are summarized in Figures 170 through 175. These mission opportunities are representative of opportunities having minimum, average, and maximum velocity requirements for both the aerobraker and retrobraker mission modes.

Table 3. Powered Venus Swingby from Mercury

Earth Launch (Year)	(JD*)	ΔV_1 (kps)	Earth-Mercury Trip Time (days)	ΔV_2 (kps)	Arrive Mercury (JD)*	ΔV_3 (kps)	ΔV_{TTP} (kps)	Stay Time (days)	Depart Mercury (JD)*
1981	4710	6.75	90	0.0	4800	8.19	14.94	54	4854
1987	7008	6.36	115	0.0	7123	10.95	17.31	37	7160
1992	8752	6.83	105	0.0	8857	6.35	13.18	35	8892

Earth Launch (Year)	Depart Mercury (JD)*	ΔV_4 (kps)	Mercury-Venus Trip Time (days)	ΔV_5 (kps)	Arrive Venus (JD)	ΔV_{swing} (kps)	Venus-Earth Trip Time (days)	ΔV_6 (kps)	ΔV_{TTE} (kps)	Arrive Earth (JD)*	V_{entry} (kps)	Mission Duration (days)	ΔV_{total} (kps)
1981	4854	7.65	80	0.0	4934	1.63	160	0.0	9.28	5094	12.39	384	24.22
1987	7160	7.71	100	0.0	7260	1.43	170	0.0	9.13	7430	12.00	422	26.44
1992	8892	7.65	80	0.0	8972	1.66	160	0.0	9.31	9132	11.63	380	22.49

Notes:

ΔV_1 = Transplanetary injection velocity increment

ΔV_2 = Transplanet plane change velocity increment

ΔV_3 = Mercury orbit insertion velocity increment

ΔV_{TTP} = Total transplanet incremental velocity requirement

ΔV_4 = Trans-Earth injection velocity increment

ΔV_5 = First trans-Earth leg plane change velocity increment

ΔV_{swing} = Velocity increment added during Venus swingby passage

ΔV_6 = Second Trans-Earth leg plane change velocity increment

ΔV_{TTE} = Total Trans-Earth incremental velocity requirement

ΔV_{total} = Total mission incremental velocity requirement

*Julian Date - 2440000.

SD 67-621-2

The minimum Venus swingby altitude is 0.1 Venus radius and is a constraint for some of the 30- and 60-day stay-time missions. Earth departure and Mars retrobraker altitudes are 300 kilometers and 800 kilometers, respectively. Earth entry and Mars entry altitudes are 122 km (400,000 feet) and 305 km (1,000,000 feet), respectively.

All transfers considered are in one plane. Typical Earth-to-Venus legs are 160 days and involve a heliocentric transfer angle of 270 degrees. The Sun-Venus-Spacecraft angle at swingby perifocus is typically 120 degrees and decreases gradually to about 90 degrees as the total outbound trip time increases for any one given launch date. The Venus-Mars heliocentric transfer angles and trip times are typically 120 degrees and 140 days, respectively.

The required launch incremental velocity is relatively sensitive to launch date but remains relatively constant over a range of total outbound trip times (i.e., Mars arrival dates) for any given launch date. Therefore, the Mars-to-Earth transfer is the predominant influence on the mission opportunity selection.

Mars Inbound Venus Swingby Missions

Inbound swingbys were investigated for the 1982, 1984, 1988, and 1995 opportunities. The 1982 and 1984 opportunities were considered to represent the upper limits for reasonable aerobraker and retrobraker missions, respectively. The 1997 swingby requirements are greater than the requirements for the above opportunities for both modes; however, the requirements were considered to be excessive. Direct missions can be accomplished during the 1997 opportunity within the requirements of the limiting direct missions which were considered. The 1988 and 1995 opportunities are representative of aerobraker missions having average and minimum velocity requirements. The 1995 and 1988 retrobraker missions are representative of missions which have average and minimum requirements, respectively. Mission summaries are presented in Figures 176 through 184.

SELECTED BASEPOINT MISSIONS

Summaries of the characteristics of the basepoint missions from which missions were selected for the weight synthesis analyses are presented in Tables 4 through 19. The tables define the dates at which major mission events occur, the durations of the mission phases, the major incremental velocity requirements, and the Earth reentry speed. Table 4 defines the characteristics of the Vesta, Ceres, and Jupiter flyby missions. The characteristics of the direct missions for all mission objectives are defined in Tables 5 through 13. The Mercury and Mars missions with a Venus swingby are shown in Tables 14 through 19.

The mission opportunities were selected on the criterion of representative opportunities with minimum, maximum, and average total velocity requirements for the post-1980 era. For all cases except Mercury, stay times of zero, thirty, and sixty days have been considered. An Earth reentry speed of 19.8 kilometers per second (65,000 ft/s) was the only constraint imposed on the mission selection except for the Jupiter and Ganymede missions which were based on minimizing the reentry speed. The requirements are based on the parking orbit altitudes shown on the tables.

The direct missions were selected on the basis of minimizing the total mission incremental velocity requirements considering Type I, Type II, and two-plane transfers when necessary to reduce the requirements for transfer angles near 180 degrees. The Earth-to-target transfers for the Venus and Mars aerobraker missions and the Ganymede missions are all Type I transfers. The outbound Mars and Venus retrobraker missions and the Mercury missions include both Type I and Type II transfers. The two-plane transfer mode has been found to be advantageous only for a limited number of Earth-to-Ceres and Earth-to-Vesta missions.

The majority of the missions require Type II transfers for the target-to-Earth mission phase. The exception is Vesta which requires both Type I and Type II returns to minimize the total incremental velocity requirements. No solutions have been found which require two-plane transers for the return phase.

Table 4. Flyby Baseline Missions

Target	Depart Earth (Year)	Depart Earth (JD*)	First Leg Trip Time (days)	Arrive Target (JD*)	Second Leg Trip Time (days)	Entry Speed (kps)	Total Mission Time (days)	Total Mission ΔV (kps)
Vesta	1991	8590	430	9020	300	12.43	730	4.57
	1993	9138	245	9383	851	14.14	1096	6.32
Ceres	1993	9175	315	9490	779	13.22	1094	5.37
	1992	8745	354	9099	742	16.00	1096	8.30
Jupiter	1991	8570	708	9278	672	17.72	1380	6.80
	1985	6170	520	6690	515	15.21	1035	7.10

*Julian date -2440000

- 42 -

Table 5. Mercury Baseline Missions (Direct)

Depart Earth Year	JD*	Trip Time (days)	ΔV_1 (kps)	ΔV_2 (kps)	ΔV_3 (kps)	ΔV_{TP} (kps)	Arrive Mercury (JD*)	Stay Time (days)	Depart Mercury (JD*)	Trip Time (days)	ΔV_{TE} (kps)	Entry Speed (kps)	Total Mission Time (days)	Total Mission ΔV (kps)
1988	7344	125	7.32	0.0	9.81	17.13	7469	63	7532	123	6.96	15.02	311	24.09
1990	8022	135	8.57	0.0	6.54	15.10	8157	77	8234	157	7.83	16.96	369	22.94
1992	8752	105	6.83	0.0	6.36	13.18	8857	179	9036	80	6.51	15.59	364	19.69

Note: Circular parking orbit
Parking orbit altitude = one planetary radius

ΔV_1 = Earth departure incremental velocity
ΔV_2 = Plane change incremental velocity
ΔV_3 = Planetary orbit insertion incremental velocity
ΔV_{TP} = Total transplanetary incremental velocity
ΔV_{TE} = Planetary departure incremental velocity

*Julian date -244 0000

Table 6. Venus Aerobraker Baseline Missions

Depart Earth Year	JD*	Trip Time (days)	ΔV_1 (kps)	ΔV_2 (kps)	ΔV_{TP} (kps)	Venus Entry Speed (kps)	Arrive Venus (JD*)	Stay Time (days)	Depart Venus (JD*)	Trip Time (days)	ΔV_{TE} (kps)	Entry Speed (kps)	Total Mission Time (days)	Total Mission ΔV (kps)
1988	7240	120	3.57	0.0	3.57	11.6	7360	0	7360	275	3.87	13.7	395	7.44
	7240	110	3.75	0.0	3.75	12.2	7350	30	7380	285	3.86	14.0	425	7.61
	7240	110	3.75	0.0	3.75	12.2	7350	60	7410	310	4.08	14.3	480	7.83
1990	7840	100	3.81	0.0	3.81	11.4	7940	0	7940	280	3.74	13.6	380	7.55
	7835	100	3.81	0.0	3.81	11.8	7935	30	7965	290	3.87	14.0	420	7.68
	7830	100	3.86	0.0	3.86	12.2	7990	60	7990	310	4.17	14.5	470	8.03
1991	8415	115	3.68	0.0	3.68	10.9	8530	0	8530	270	3.76	13.5	385	7.44
	8405	110	3.78	0.0	3.78	12.0	8515	30	8545	285	3.96	13.7	425	7.74
	8425	130	3.62	0.0	3.62	10.6	8555	60	8615	345	4.19	14.9	535	7.81

Note: Circular parking orbit
Parking orbit altitude = 1000 km

ΔV_1 = Earth departure incremental velocity
ΔV_2 = Plane change incremental velocity
ΔV_{TP} = Total transplanetary incremental velocity
ΔV_{TE} = Planetary departure incremental velocity

*Julian date -244 0000

Table 7. Venus Retrobraker Baseline Missions

Depart Earth		Trip Time (days)	ΔV_1 (kps)	ΔV_2 (kps)	ΔV_3 (kps)	ΔV_{TP} (kps)	Arrive Venus (JD*)	Stay Time (days)	Depart Venus (JD*)	Trip Time (days)	ΔV_{TE} (kps)	Entry Speed (kps)	Total Mission Time (days)	Total Mission ΔV (kps)
Year	JD*													
1988	7180	200	4.15	0.0	3.48	7.63	7380	0	7380	285	3.86	14.01	485	11.49
	7170	200	4.26	0.0	3.39	7.66	7370	30	7400	300	3.97	14.19	530	11.63
	7165	200	4.32	0.0	3.37	7.70	7365	60	7425	325	4.27	14.40	585	11.97
1990	7850	100	3.90	0.0	3.57	7.47	7950	0	7950	280	3.75	13.72	380	11.22
	7850	100	3.90	0.0	3.57	7.47	7950	30	7980	300	4.06	14.27	430	11.53
	7850	115	3.97	0.0	3.30	7.27	7965	60	8025	335	4.32	15.05	510	11.58
1991	8415	130	3.64	0.0	3.23	6.87	8545	0	8545	285	3.96	13.66	415	10.83
	8415	135	3.64	0.0	3.20	6.84	8555	30	8585	325	4.20	14.36	490	11.04
	8400	135	3.64	0.0	3.20	6.84	8550	60	8610	345	4.19	14.89	540	11.02

Note: Circular parking orbit
Parking orbit altitude = 1000 km

ΔV_1 = Earth departure incremental velocity
ΔV_2 = Plane change incremental velocity
ΔV_3 = Planetary orbit insertion incremental velocity
ΔV_{TP} = Total transplanetary incremental velocity
ΔV_{TE} = Planetary departure incremental velocity

*Julian date -244 0000

SD 67-621-2

Table 8. Mars Aerobraker Baseline Missions (Direct)

Depart Earth Year	JD*	Trip Time (days)	ΔV_1 (kps)	ΔV_2 (kps)	ΔV_{TP} (kps)	Mars Entry Speed (kps)	Arrive Mars (JD*)	Stay Time (days)	Depart Mars (JD*)	Trip Time (days)	ΔV_{TE} (kps)	Entry Speed (kps)	Total Mission Time (days)	Total Mission ΔV (kps)
1986	6540	120	3.92	0.0	3.92	9.5	6660	0	6660	250	3.66	14.0	370	7.58
	6540	125	3.84	0.0	3.84	8.9	6665	30	6695	255	4.14	14.7	410	7.98
	6540	120	3.92	0.0	3.92	9.5	6660	60	6720	260	4.54	15.5	440	8.46
1988	7350	125	4.06	0.0	4.06	7.7	7475	0	7475	280	4.17	15.9	405	8.28
	7350	120	4.14	0.0	4.14	8.1	7470	30	7500	270	4.46	16.8	420	8.60
	7350	125	4.06	0.0	4.06	7.7	7475	60	7535	260	4.98	18.6	445	9.03
1993	8900	160	4.39	0.0	4.39	9.1	9060	0	9060	257	4.45	19.8	417	8.84
	8900	140	4.89	0.0	4.89	10.9	9040	30	9070	246	4.73	19.8	416	9.62
	8895	120	6.16	0.0	6.16	13.8	9015	60	9075	239	5.00	19.8	419	11.16

Note: Circular parking orbit
Parking orbit altitude = 800 km

ΔV_1 = Earth departure incremental velocity
ΔV_2 = Plane change incremental velocity
ΔV_{TP} = Total transplanetary incremental velocity
ΔV_{TE} = Planetary departure incremental velocity

*Julian date −244 0000

Table 9. Mars Retrobraker Baseline Missions (Direct)

Depart Earth		Trip Time (days)	ΔV₁ (kps)	ΔV₂ (kps)	ΔV₃ (kps)	ΔVTP (kps)	Arrive Mars (JD*)	Stay Time (days)	Depart Mars (JD*)	Trip Time (days)	ΔVTE (kps)	Entry Speed (kps)	Total Mission Time (days)	Total Mission ΔV (kps)
Year	JD*													
1986	6545	180	3.57	0.0	2.49	6.10	6725	0	6725	260	4.62	15.7	440	10.71
	6540	180	3.56	0.0	2.57	6.17	6720	30	6750	260	5.06	16.8	470	11.23
	6545	180	3.57	0.0	2.49	6.10	6725	60	6785	250	5.55	18.2	490	11.64
1988	7335	190	3.75	0.0	2.23	6.02	7525	0	7525	265	4.83	18.2	455	10.85
	7330	190	3.79	0.0	2.28	6.10	7520	30	7550	255	5.23	19.4	475	11.33
	7330	180	3.81	0.0	2.47	6.28	7510	60	7570	240	5.72	19.8	480	12.00
1993	8810	260	5.84	0.0	2.79	8.63	9070	0	9070	246	4.73	19.8	506	13.36
	8780	260	6.86	0.0	2.78	9.64	9040	30	9070	246	4.73	19.8	536	14.37
	8770	240	7.42	0.0	3.33	10.76	9010	60	9070	246	4.73	19.8	546	15.49

Note: Circular parking orbit
Parking orbit altitude = 800 km

ΔV₁ = Earth departure incremental velocity
ΔV₂ = Plane change incremental velocity
ΔV₃ = Planetary orbit insertion incremental velocity
ΔVTP = Total transplanetary incremental velocity
ΔVTE = Planetary departure incremental velocity

*Julian date -244 0000

Table 10. Vesta Baseline Missions

Depart Earth		Trip Time (days)	ΔV₁ (kps)	ΔV₂ (kps)	ΔV₃ (kps)	ΔV_TP (kps)	Arrive Vesta (JD*)	Stay Time (days)	Depart Vesta (JD*)	Trip Time (days)	ΔV_TE (kps)	Entry Speed (kps)	Total Mission Time (days)	Total Mission ΔV (kps)
Year	JD*													
1985	6070	330	4.35	0.15	5.42	9.82	6410	0	6410	390	5.05	12.34	720	14.87
	6080	320	4.32	0.0	5.25	9.58	6400	30	6430	370	4.87	12.78	720	14.44
	6080	310	4.40	0.0	5.27	9.67	6390	60	6450	350	5.01	12.89	720	14.67
1987	7035	435	6.66	0.0	5.38	12.04	7470	0	7470	290	5.32	14.62	725	17.36
	7035	425	6.74	0.0	5.42	12.15	7460	30	7490	270	5.48	14.63	725	17.63
	7035	435	6.66	0.0	5.38	12.04	7470	60	7530	345	5.72	15.91	840	17.77
1991	8605	380	4.39	1.22	5.53	11.14	8985	0	8985	375	5.11	13.378	755	16.25
	8620	345	5.96	0.0	5.18	11.14	8965	30	8995	365	5.14	13.35	740	16.28
	8620	320	5.96	0.0	5.20	11.16	8940	60	9000	365	5.24	13.54	745	16.41

Note: Circular parking orbit
Parking orbit altitude = one planetary radius

ΔV_1 = Earth departure incremental velocity
ΔV_2 = Plane change incremental velocity
ΔV_3 = Planetary orbit insertion incremental velocity
ΔV_{TP} = Total transplanetary incremental velocity
ΔV_{TE} = Planetary departure incremental velocity

*Julian date -244 0000

Table 11. Ceres Baseline Missions

Depart Earth		Trip Time (days)	ΔV_1 (kps)	ΔV_2 (kps)	ΔV_3 (kps)	ΔV_{TP} (kps)	Arrive Ceres (JD*)	Stay Time (days)	Depart Ceres (JD*)	Trip Time (days)	ΔV_{TE} (kps)	Entry Speed (kps)	Total Mission Time (days)	Total Mission ΔV (kps)
Year	JD*													
1980	4550	300	8.59	0.0	6.16	14.75	4880	0	4880	415	6.53	19.05	745	21.28
	4545	315	8.34	0.0	6.62	15.00	4860	30	4890	410	6.65	19.41	755	21.65
	4540	300	8.09	0.0	7.25	15.34	4840	60	4900	405	6.80	19.80	765	21.14
1989	7775	385	4.79	4.53	5.29	14.61	8160	0	8160	405	6.87	19.8	800	21.47
	7770	380	4.78	4.54	5.43	14.75	8150	30	8180	385	7.17	19.8	795	21.92
	7805	310	7.83	0.0	7.53	15.37	8140	60	8175	390	7.07	19.8	760	22.44
1991	8260	350	5.10	0.0	6.33	11.43	8610	0	8610	425	7.24	19.8	775	18.67
	8255	340	5.26	0.0	6.57	11.83	8595	30	8625	410	7.61	19.8	780	19.44
	8250	330	5.61	0.0	6.88	12.49	8580	60	8640	395	8.07	19.8	785	20.56

Note: Circular parking orbit
Parking orbit altitude = one planetary radius

ΔV_1 = Earth departure incremental velocity
ΔV_2 = Plane change incremental velocity
ΔV_3 = Planetary orbit insertion incremental velocity
ΔV_{TP} = Total transplanetary incremental velocity
ΔV_{TE} = Planetary departure incremental velocity

*Julian date -244 0000

Table 12. Jupiter Baseline Missions

Depart Earth Year	JD*	Trip Time (days)	ΔV_1 (kps)	ΔV_2 (kps)	ΔV_3 (kps)	ΔV_{TP} (kps)	Arrive Jupiter (JD*)	Stay Time (days)	Depart Jupiter (JD*)	Trip Time (days)	ΔV_{TE} (kps)	Entry Speed (kps)	Total Mission Time (days)	Total Mission ΔV (kps)
1985	6173	717	6.55	0.0	6.05	12.60	6890	0	6890	705	6.10	14.4	1422	18.70
	6173	702	6.55	0.0	6.13	12.68	6875	30	6905	690	6.18	14.4	1422	18.86
	6173	687	6.57	0.0	6.22	12.79	6860	60	6920	675	6.27	14.4	1422	19.06
1987	6974	711	6.54	0.0	5.99	12.53	7685	0	7685	712	6.28	14.4	1423	18.81
	6974	696	6.56	0.0	6.07	12.63	7670	30	7700	697	6.39	14.4	1423	19.02
	6974	681	6.59	0.0	6.16	12.75	7655	60	7715	683	6.51	14.4	1424	19.26
1990	8174	716	6.83	0.0	6.29	13.12	8890	0	8890	699	6.56	14.7	1415	19.68
	8174	706	6.84	0.0	6.36	13.20	8880	30	8910	680	6.74	14.7	1416	19.94
	8174	696	6.85	0.0	6.44	13.29	8870	60	8930	660	6.94	14.8	1416	20.23

Note: Circular parking orbit
Parking orbit altitude = 80 km

ΔV_1 = Earth departure incremental velocity
ΔV_2 = Plane change incremental velocity
ΔV_3 = Planetary orbit insertion incremental velocity
ΔV_{TP} = Total transplanetary incremental velocity
ΔV_{TE} = Planetary departure incremental velocity

*Julian date -244 0000

- 49 -

Table 13. Ganymede Baseline Missions

Depart Earth Year	Depart Earth JD*	Trip Time (days)	ΔV_1 (kps)	ΔV_2 (kps)	ΔV_3 (kps)	ΔV_{TP} (kps)	Arrive Ganymede (JD*)	Stay Time (days)	Depart Ganymede (JD*)	Trip Time (days)	ΔV_{TE} (kps)	Entry Speed (kps)	Total Mission Time (days)	Total Mission ΔV (kps)
1985	6173	717	6.55	0.0	4.89	11.44	6890	0	6890	705	4.94	14.4	1422	16.38
	6173	702	6.55	0.0	4.97	11.52	6875	30	6905	690	5.02	14.4	1422	16.54
	6173	687	6.57	0.0	5.06	11.63	6860	60	6920	675	5.10	14.4	1422	16.73
1987	6974	711	6.54	0.0	4.84	11.38	7685	0	7685	712	5.11	14.4	1423	16.49
	6974	696	6.56	0.0	4.91	11.47	7670	30	7700	697	5.21	14.4	1423	16.68
	6974	681	6.59	0.0	5.00	11.59	7655	60	7715	683	5.32	14.4	1424	16.91
1990	8174	716	6.83	0.0	5.12	11.95	8890	0	8890	699	5.36	14.7	1415	17.31
	8174	706	6.84	0.0	5.18	12.02	8880	30	8910	680	5.52	14.7	1416	17.54
	8174	696	6.85	0.0	5.25	12.10	8870	60	8930	660	5.69	14.8	1416	17.79

Note: Circular parking orbit
Parking orbit altitude = one Ganymede radius

ΔV_1 = Earth departure incremental velocity

ΔV_2 = Plane change incremental velocity

ΔV_3 = Planetary orbit insertion incremental velocity

ΔV_{TP} = Total transplanetary incremental velocity

ΔV_{TE} = Planetary departure incremental velocity

*Julian date - 244 0000

Table 14. Outbound Swingby - Mercury Missions

Earth Departure (Year)	(JD)*	ΔV_1 (kps)	Earth-Venus Trip Time (days)	ΔV_2 (kps)	Arrive Venus (JD)*	ΔV_{swing} (kps)	Venus-Mercury Trip Time (days)	ΔV_3 (kps)	Arrive Mercury (JD)*	ΔV_4 (kps)	ΔV_{TTP} (kps)
1985	6200	4.58	160	0.0	6360	0.45	108	1.93	6468	6.46	13.42
1986	6650	3.87	190	0.0	6840	3.72	74	0.0	6914	4.44	12.03
1988	7210	3.96	180	0.0	7390	2.32	100	0.0	7490	7.27	14.50

Earth Departure (Year)	Arrive Mercury (JD)*	Stay Time (days)	Depart Mercury (JD)*	ΔV_{TE} (kps)	ΔV_5 (kps)	Transearth Transit Time (days)	ΔV_{TTE} (kps)	Arrive Earth (JD)*	ΔV_{entry} (kps)	Mission Duration (days)	ΔV_{total} (kps)
1985	6468	18	6486	6.55	0.0	75	6.55	6561	16.37	361	19.97
1986	6914	42	6956	11.21	0.0	85	11.21	7041	13.91	391	23.24
1988	7490	42	7532	6.96	0.0	123	6.96	7655	15.02	445	21.46

Notes:

ΔV_1 = Transplanetary injection velocity increment

ΔV_2 = First transplanet leg plane change velocity increment

ΔV_{swing} = Velocity increment added during Venus swingby passage

ΔV_3 = Second transplanet leg plane change velocity increment

ΔV_4 = Mercury orbit insertion velocity increment

ΔV_{TTP} = Total transplanet incremental velocity requirement

ΔV_{TE} = Transearth injection velocity increment

ΔV_5 = Transearth leg plane change velocity increment

ΔV_{TTE} = Total Trans-Earth velocity increment requirement

ΔV_{entry} = Earth entry speed

ΔV_{total} = Total mission incremental velocity requirement

*Julian Date - 2440000.

SD 67-621-2

Table 15. Inbound Swingby - Mercury Missions

Earth Departure (Year)	ΔV_1 (kps)	Earth-Mercury Trip Time (days)	ΔV_2 (kps)	Arrive Mercury (JD)*	ΔV_3 (kps)	ΔV_{TTP} (kps)	Stay Time (days)	Depart Mercury (JD)*
1981	6.75	90	0.0	4800	8.19	14.94	54	4854
1987	6.36	115	0.0	7123	10.95	17.31	37	7160
1992	6.83	105	0.0	8857	6.35	13.18	35	8892

Earth Departure (Year)	Depart Mercury (JD)*	ΔV_4 (kps)	Mercury-Venus Trip Time (days)	ΔV_5 (kps)	Arrive Venus (JD)*	ΔV_{swing} (kps)	Venus-Earth Trip Time (days)	ΔV_6 (kps)	ΔV_{TTE} (kps)	Arrive Earth (JD)*	Ventry (kps)	Mission Duration (days)	ΔV_{total} (kps)
1981	4854	7.65	80	0.0	4934	1.63	160	0.0	9.28	5094	12.39	384	24.22
1987	7160	7.71	100	0.0	7260	1.43	170	0.0	9.13	7430	12.00	422	26.44
1992	8892	7.65	80	0.0	8972	1.66	160	0.0	9.31	9132	11.63	380	22.49

Notes:

ΔV_1 = Transplanetary injection velocity increment

ΔV_2 = Transplanet plane changes velocity increment

ΔV_3 = Mercury orbit insertion velocity increment

ΔV_{TTP} = Total transplanet incremental velocity requirement

ΔV_4 = Trans-Earth injection velocity increment

ΔV_5 = First trans-Earth leg plane change velocity increment

ΔV_{swing} = Velocity increment added during Venus swingby passage

ΔV_6 = Second Trans-Earth leg plane change velocity increment

ΔV_{TTE} = Total Trans-Earth incremental velocity requirement

ΔV_{total} = Total mission incremental velocity requirement

*Julian Date - 2440000.

Table 16. Outbound Swingby – Mars Aerobraker Missions

Mission Year	Depart Earth			Venus Swingby			Arrive Mars		Stay Time (days)	Depart Mars			Arrive Earth		Total Mission Time (days)	Total Mission ΔV (km/s)
	JD	ΔV_1 (km/s)	Δt_1 (days)	JD	h_p (VR)	Δt_2 (days)	JD	VEN (km/s)		JD	ΔV_3 (km/s)	Δt_3 (days)	JD	VEN (km/s)		
1986	6143	3.93	172	6315	0.97	160	6475	9.15	0	6475	1.94	213	6688	11.68	545	5.87
	6141	3.93	174	6315	0.82	150	6465	10.06	30	6495	1.96	202	6697	11.59	556	5.89
	6141	3.92	173	6314	0.73	146	6460	10.59	60	6520	2.12	194	6714	11.58	573	6.04
1993	8509	4.18	161	8670	1.49	155	8825	7.89	0	8825	2.24	290	9115	11.41	606	6.42
	8493	4.28	175	8668	1.45	132	8800	8.17	30	8830	2.25	287	9117	11.41	624	6.53
	8493	4.28	175	8668	1.45	132	8800	8.17	60	8860	2.55	267	9127	11.46	634	6.83
1999	10835	4.16	168	11003	0.63	157	11160	8.51	0	11160	1.98	298	11458	12.84	623	6.14
	10835	4.16	168	11003	0.63	157	11160	8.51	30	11190	2.10	288	11478	13.44	643	6.26
	10835	4.16	168	11003	0.63	157	11160	8.51	60	11220	2.29	278	11498	14.07	663	6.45

Note: Circular parking orbit
Parking orbit altitude = 800 km

JD = Julian date - 244 0000
ΔV_1 = Earth departure incremental velocity
ΔV_2 = Planetary departure incremental velocity
VEN = Entry speed
h_p = Venus swingby altitude in Venus radii

Table 17. Outbound Swingby – Mars Retrobraker Missions

Mission Year	Depart Earth JD	ΔV₁ (km/s)	Δt₁ (days)	Venus Swingby JD	hₚ (VR)	Δt₂ (days)	Arrive Mars JD	ΔV₂ (km/s)	Stay Time (days)	Depart Mars JD	ΔV₃ (km/s)	Δt₃ (days)	Arrive Earth JD	VEN (km/s)	Total Mission Time (days)	Total Mission ΔV (km/s)
1986	6155	4.01	163	6318	1.32	207	6525	3.66	0	6525	2.17	193	6718	11.60	563	9.84
	6153	3.99	164	6317	1.31	203	6520	3.72	30	6550	2.49	190	6740	11.87	587	10.20
	6153	3.99	164	6317	1.31	203	6520	3.72	60	6580	2.72	240	6820	12.94	667	10.43
1993	8512	4.20	157	8669	1.53	151	8820	4.48	0	8820	2.26	294	9114	11.41	602	10.92
	8510	4.18	158	8668	1.54	147	8815	4.49	30	8845	2.33	277	9122	11.42	612	10.98
	8509	4.17	159	8668	1.55	142	8810	4.52	60	8870	2.77	260	9130	11.50	621	11.46
1999	10840	4.18	165	11005	0.81	210	11215	3.31	0	11215	2.25	280	11495	13.98	655	9.73
	10838	4.18	167	11005	0.81	205	11210	3.35	30	11240	2.44	272	11512	14.50	674	9.95
	10838	4.18	167	11005	0.81	205	11210	3.35	60	11270	2.72	260	11530	15.00	692	10.23

JD = Julian date - 244 0000
ΔV₁ = Earth departure incremental velocity
ΔV₂ = Planetary orbit insertion incremental velocity
ΔV₃ = Planetary departure incremental velocity
VEN = Entry speed
hₚ = Venus swingby altitude in Venus radii

Note: Circular parking orbit
Parking oribt altitude = 800 km

SD 67-621-2

Table 18. Inbound Swingby - Mars Aerobraker Missions

Mission Year	Depart Earth JD	ΔV1 (km/s)	Δt1 (days)	Arrive Mars JD	VEN (km/s)	Stay Time (days)	Depart Mars JD	ΔV2 (km/s)	Δt2 (days)	Venus Swingby JD	hp (VR)	Δt3 (days)	Arrive Earth JD	VEN (km/s)	Total Mission Time (days)	Total Mission ΔV (km/s)
1982	4940	3.60	300	5240	5.73	0	5240	4.48	149	5389	1.24	160	5549	12.15	609	8.06
	4931	3.64	284	5215	5.78	30	5245	4.48	145	5390	1.26	160	5550	12.14	619	8.10
	4955	3.62	225	5180	6.78	60	5240	4.48	149	5389	1.24	160	5549	12.15	594	8.08
1988	7354	3.73	181	7535	5.61	0	7535	3.81	210	7745	0.93	160	7905	11.95	551	7.52
	7342	3.76	168	7510	6.00	30	7540	3.82	205	7745	0.97	160	7905	11.95	563	7.58
	7340	3.98	140	7480	7.16	60	7540	3.82	205	7745	0.97	160	7905	11.95	565	7.78
1995	9660	3.85	215	9875	6.95	0	9875	3.44	181	10056	0.74	158	10214	12.24	554	7.28
	9660	3.95	195	9855	7.91	30	9885	3.49	172	10057	0.75	158	10215	12.23	555	7.44
	9660	4.17	175	9835	9.21	60	9895	3.61	163	10058	0.74	159	10217	12.21	557	7.77

Note: Circular parking orbit
Parking orbit altitude = 800 km

JD = Julian date - 244 0000
ΔV1 = Earth departure incremental velocity
ΔV2 = Planetary orbit insertion incremental velocity
VEN = Entry speed
hp = Venus swingby altitude in Venus radii

Table 19. Inbound Swingby - Mars Retrobraker Missions

Mission Year	Depart Earth JD	Depart Earth ΔV₁ (km/s)	Δt₁ (days)	Arrive Mars JD	Arrive Mars ΔV₂ (km/s)	Stay Time (days)	Depart Mars JD	Depart Mars ΔV₃ (km/s)	Δt₂ (days)	Venus Swingby JD	Venus Swingby h_p (VR)	Δt₃ (days)	Arrive Earth JD	Arrive Earth V_EN (km/s)	Total Mission Time (days)	Total Mission Total (km/s)
1984	5669	4.02	266	5935	2.85	0	5935	4.25	157	6092	0.75	138	6230	12.58	561	11.12
	5643	4.57	262	5905	3.43	30	5935	4.25	157	6092	0.75	138	6230	12.58	587	12.33
	5622	5.18	263	5885	3.78	60	5945	4.64	158	6103	0.11	141	6244	12.86	622	13.58
1988	7350	3.71	190	7540	2.09	0	7540	3.82	205	7745	1.00	160	7905	11.95	555	9.62
	7344	3.75	171	7515	2.45	30	7545	3.87	200	7745	1.02	160	7905	11.95	561	10.07
	7340	3.81	160	7500	2.84	60	7560	4.20	186	7746	1.04	159	7905	11.95	565	10.85
1995	9660	3.82	240	9900	2.72	0	9900	3.71	159	10059	0.74	159	10218	12.21	558	10.22
	9660	3.82	225	9885	3.16	30	9915	4.17	145	10060	0.70	160	10220	12.19	560	11.13
	9585	5.16	270	9855	3.16	60	9915	4.17	145	10060	0.70	160	10220	12.19	635	12.48

JD   = Julian date - 244 0000
ΔV₁ = Earth departure incremental velocity
ΔV₂ = Planetary orbit insertion incremental velocity
ΔV₃ = Planetary departure incremental velocity
V_EN = Entry speed
h_p = Venus swingby altitude in Venus radii

Note: Circular parking orbit
Parking orbit altitude = 800 km

ELLIPTICAL PLANETARY ORBITS

The initial analyses of the performance requirements were based on circular planetary parking orbits only. The use of elliptical planetary parking orbits can, however, result in significant reductions in the planetary orbit insertion and planetary orbit escape incremental velocity requirements. The magnitude of the reduction is dependent upon the mass of the central body and the pericenter radius. The most significant reductions will occur when considering orbits of low pericenter altitudes about Jupiter. The effects of eccentricity will be the least significant for Vesta and Ceres because of the low mass of the asteroids.

The circular orbit restriction was imposed at the onset of this study because it was felt that elliptical orbits would inordinately complicate rendezvous operations and significantly increase launch window requirements. Analyses conducted after the initiation of the study, however, have shown that only modest performance penalties are incurred for performing off-pericenter planetary orbit insertion and escape maneuvers. Maneuvers carried out as much as 60 degrees in true anomaly from pericenter can result in increases in the incremental velocity requirements of only about 7 percent. These penalties are much less than the velocity reductions inherent in the use of elliptical orbits.

Under an amendment to the basic contract, the effects of planetary orbit eccentricity on the incremental velocity requirements were investigated for Mercury, Venus, Mars, Jupiter, and Ganymede. The planetary orbit insertion and escape incremental velocity requirements were determined for the baseline missions defined in Tables 5 through 7, 12, 13, and 16 through 19, assuming a thirty-day planetary stay time. Only the Venus swingby mission mode was investigated for Mars missions. Both aerobraking and retrobraking mission modes were investigated for Venus and Mars. For the retrobraking missions, the planetary orbit insertion assumes a cotangential incremental velocity at pericenter of the approach hyperbola. Therefore, the approach hyperbola and the resultant elliptical parking orbit are coplanar with a common pericenter radius. In all cases, a cotangential maneuver is assumed for trans-Earth injection. While it is realized that such maneuvers are not possible in practice the velocity requirements will be optimistic by a small amount (e.g., 0.5 km/s).

The resultant requirements are shown in Figure 185 through 192 for pericenter altitudes of 300 kilometers for Mercury, Mars, and Ganymede; 500 kilometers for Venus; and 0, 5, 10, and 15 Jupiter radii for Jupiter

- 57 -

orbiter missions. It should be noted that the pericenter altitudes differ from the circular orbit altitudes used in the generation of the incremental velocity requirements shown in the tables of the previous section.

ORBIT STABILITY STUDY

Prior to the generation of extensive mission data, the stability characteristics of satellites around Mercury, Ceres, Vesta, and Ganymede with various third body perturbant forces were investigated. The study determined the changes in shape, size, and orientation of these orbits. The analyses were limited to the investigation of orbits of low eccentricity (e = 0.1).

A digital computer program in which all central and perturbing bodies are assumed to be perfect, homogeneous spheres was used to generate the stability data. The disturbing forces acting on the satellite orbit are due solely to perturbing bodies. The changes in orbital elements due to each disturbing body are found from an integration of Lagrange's planetary equations over one orbit revolution. These equations assume that the positions of the disturbing bodies remain constant throughout the period of integration. The elemental changes due to each perturbing body are summed to obtain the total change in each element from which the analytical orbital parameters are computed.

The perturbations due to Sun, Earth, and Jupiter were considered for orbits about Mercury, Vesta, and Ceres. The Sun was found to be the predominant disturbing body for these cases and accounted for more than 99 percent of the variations in the orbital elements. The orbits were found to be stable for the assumed semimajor axis of two planet radii or less, eccentricity of 0.1, and stay time of 100 days. The variation in apofocal and perifocal radii for Mercury was less than one kilometer for the orbital duration considered, and the variations were negligible for orbits about Vesta and Ceres.

The disturbing bodies considered for orbits about Ganymede were Jupiter, Europa, Callisto, and Sun. The effect of Jupiter was predominant, with Europa and Callisto having about equal, but negligible, effects. The effect of the Sun was about one tenth that of Europa and Callisto.

The orbits about Ganymede resulted in significant, though not prohibitive, variations in apofocus and perifocus radii. The extent of these variations is dependent upon the initial inclination of the orbit as shown in Figures 193 through 196 for inclinations of zero and ninety degrees relative to the plane of the orbit of Ganymede about Jupiter. The initial semimajor axis is 5600 kilometers, which corresponds to a mean altitude of approximately one Ganymede radius.

For an initial inclination of zero degrees, the short-term cyclic variation in perifocus and apofocus radii is 81 kilometers during the initial orbits and decreases to 71 kilometers at the end of 100 days. The long-term variation (i.e., the difference between minimum cyclic perifocal values at 0 and 100 days) was 72 kilometers, resulting in a total variation of 143 kilometers. The eccentricity of this orbit decreased from an initial value of 0.1 to approximately 0.086 at the end of 100 days.

An orbital inclination of 90 degrees resulted in a short-term cyclic variation of 6 to 5 kilometers in the perifocus and apofocus altitudes, and a long-term change of 67 kilometers at the end of the 100 days. The resultant total variation was 73 kilometers. The orbital eccentricity increased with time from the initial value of 0.1 to 0.112 after 100 days. Although the eccentricity increases, the variation in perifocus radius is relatively small over the interval considered.

Orbits of extended duration about Mercury, Vesta, Ceres, and Ganymede appear to present no significant problems with respect to stability for semimajor axes up to two planet/asteroid radii. Variations in orbit shape for orbits about Mercury, Vesta, and Ceres are negligible. Although the disturbing body effects are more significant for orbits about Ganymede, the magnitude of the variations is such that no significant stability problems are apparent.
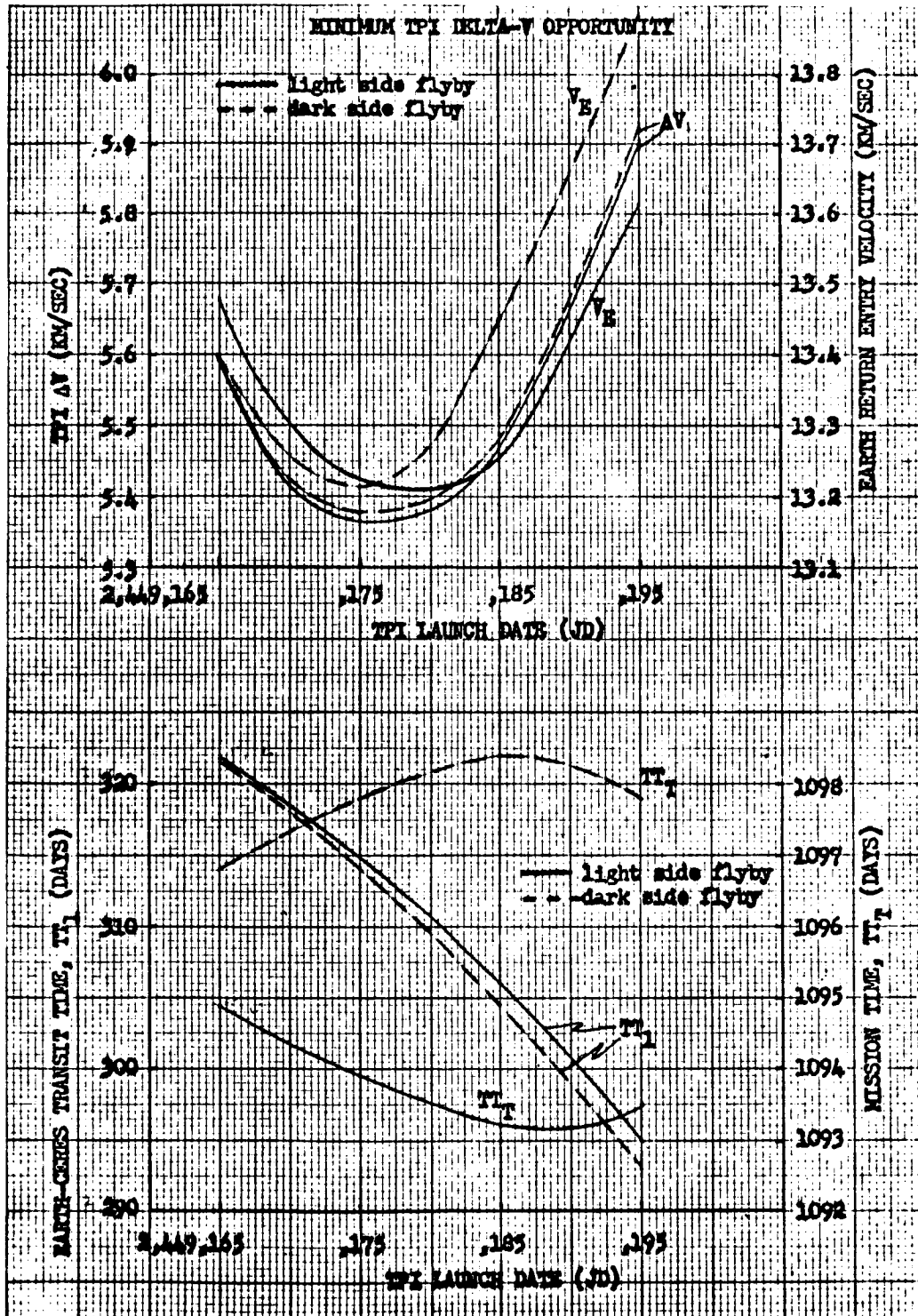
Figure 19. Ceres Minimum Velocity Flyby Mission

- 61 -
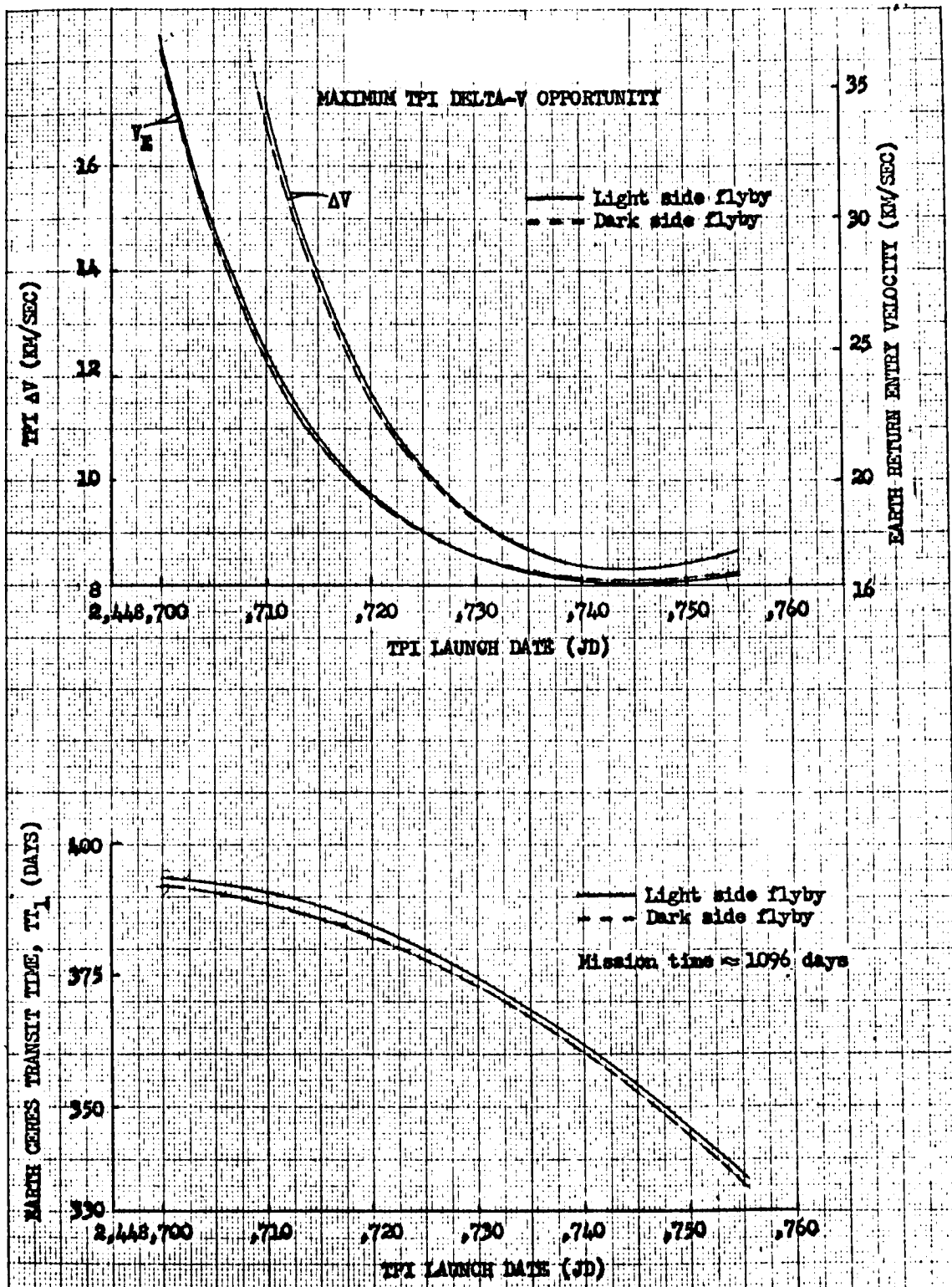
Figure 20. Ceres Maximum Velocity Flyby Mission

SD 67-621-2
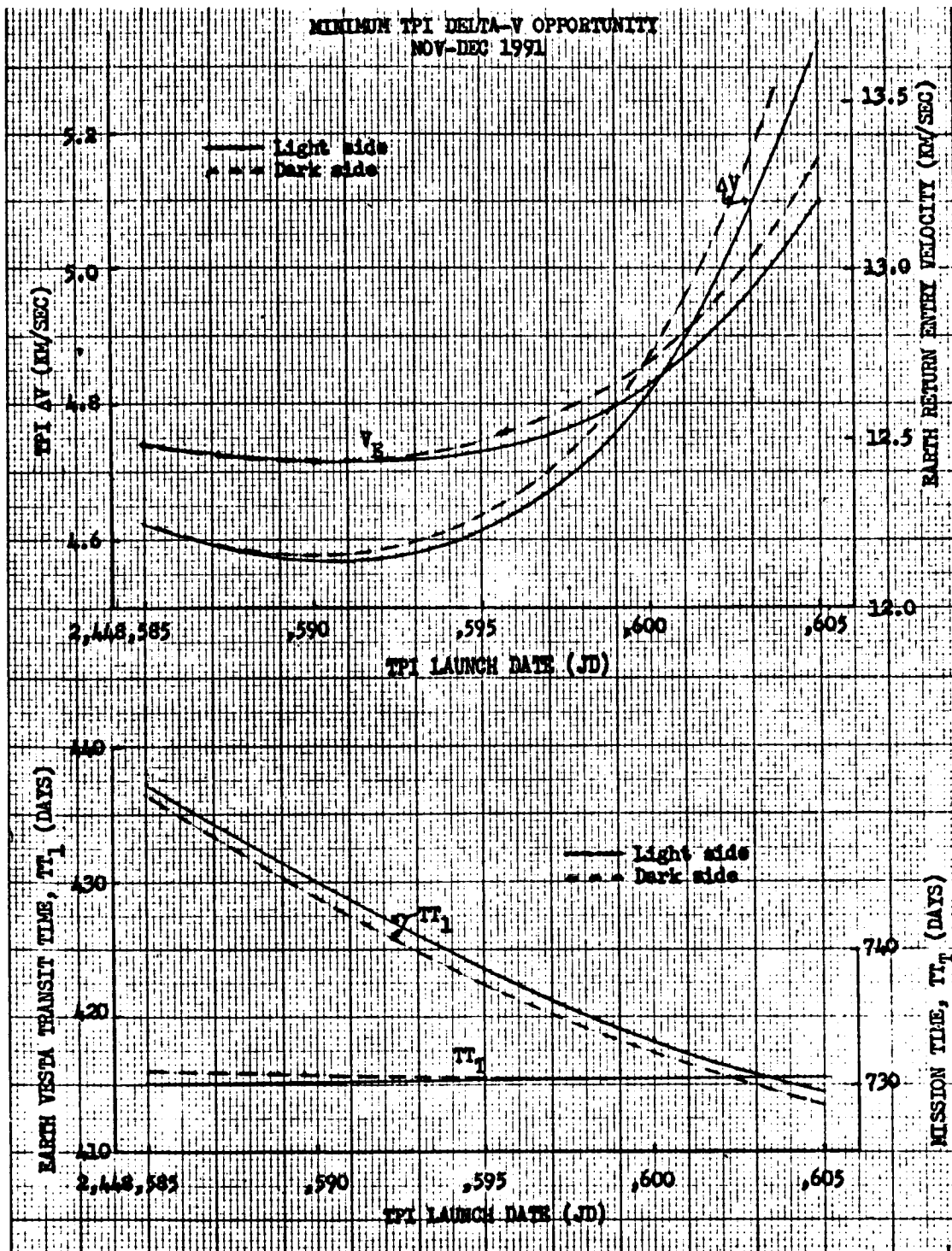
Figure 21. Vesta Minimum Velocity Flyby Mission
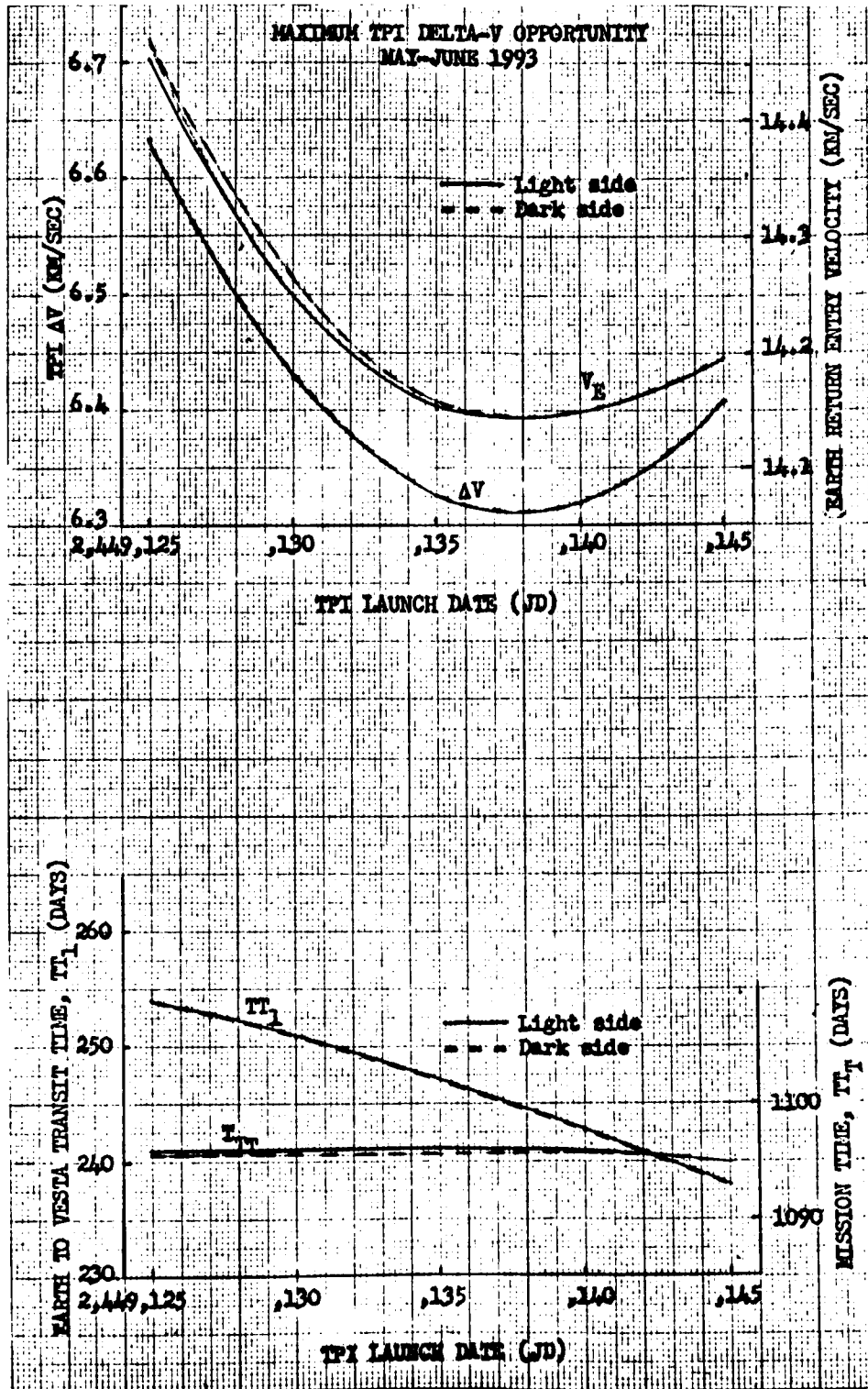
Figure 22. Vesta Maximum Velocity Flyby Mission

- 64 -
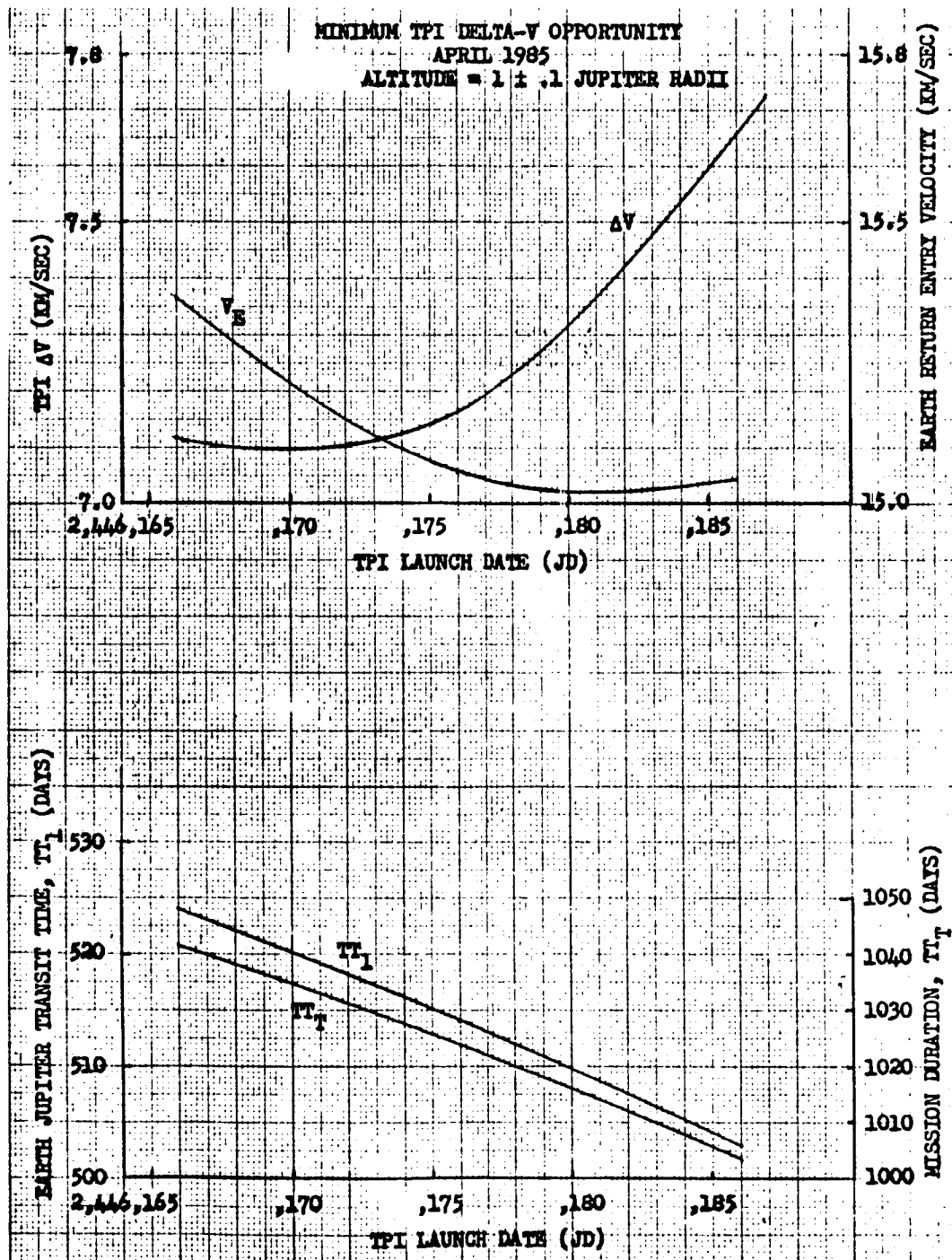
Figure 23. Jupiter Maximum Velocity Flyby Mission
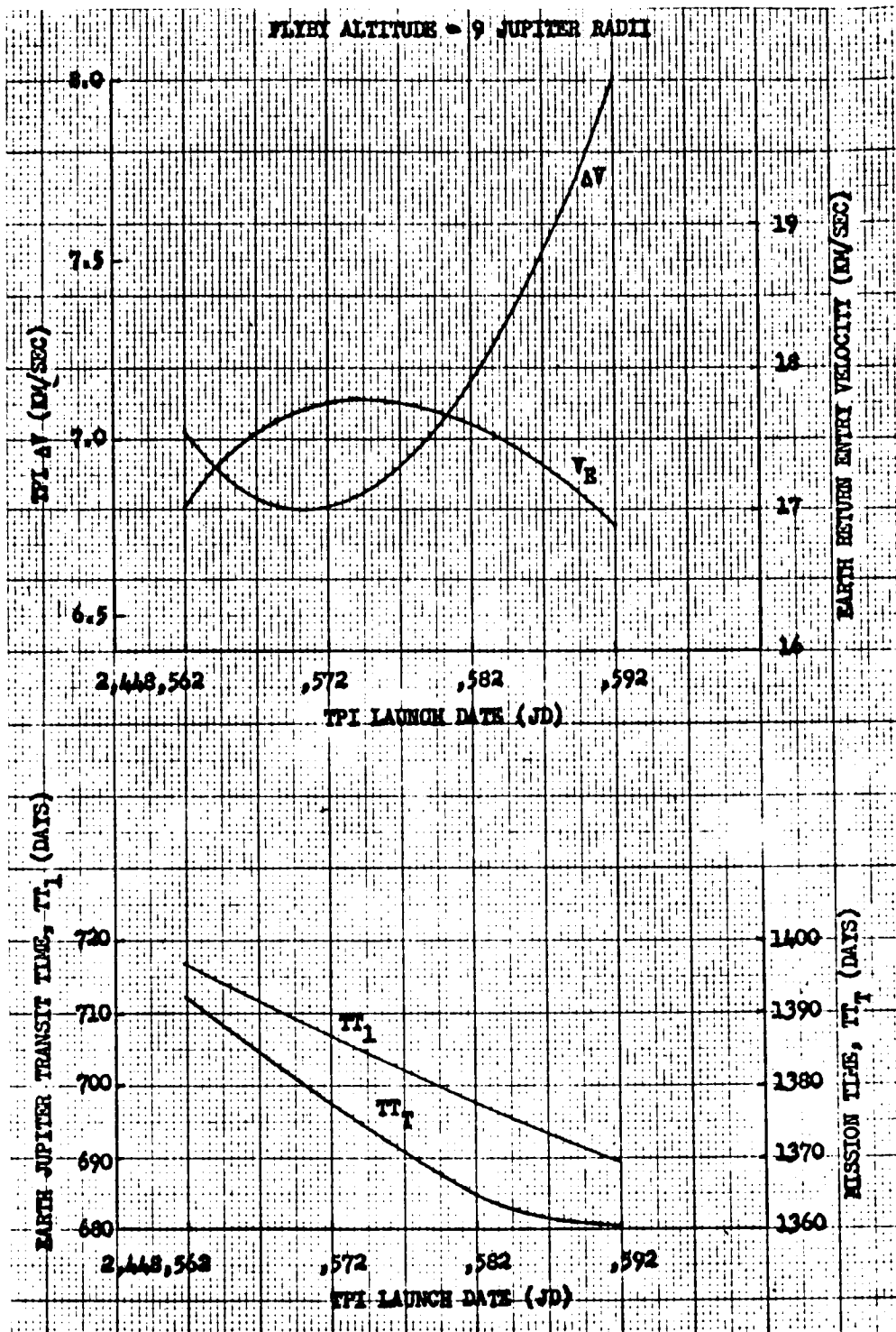
Figure 24. Jupiter Minimum Velocity Flyby Mission
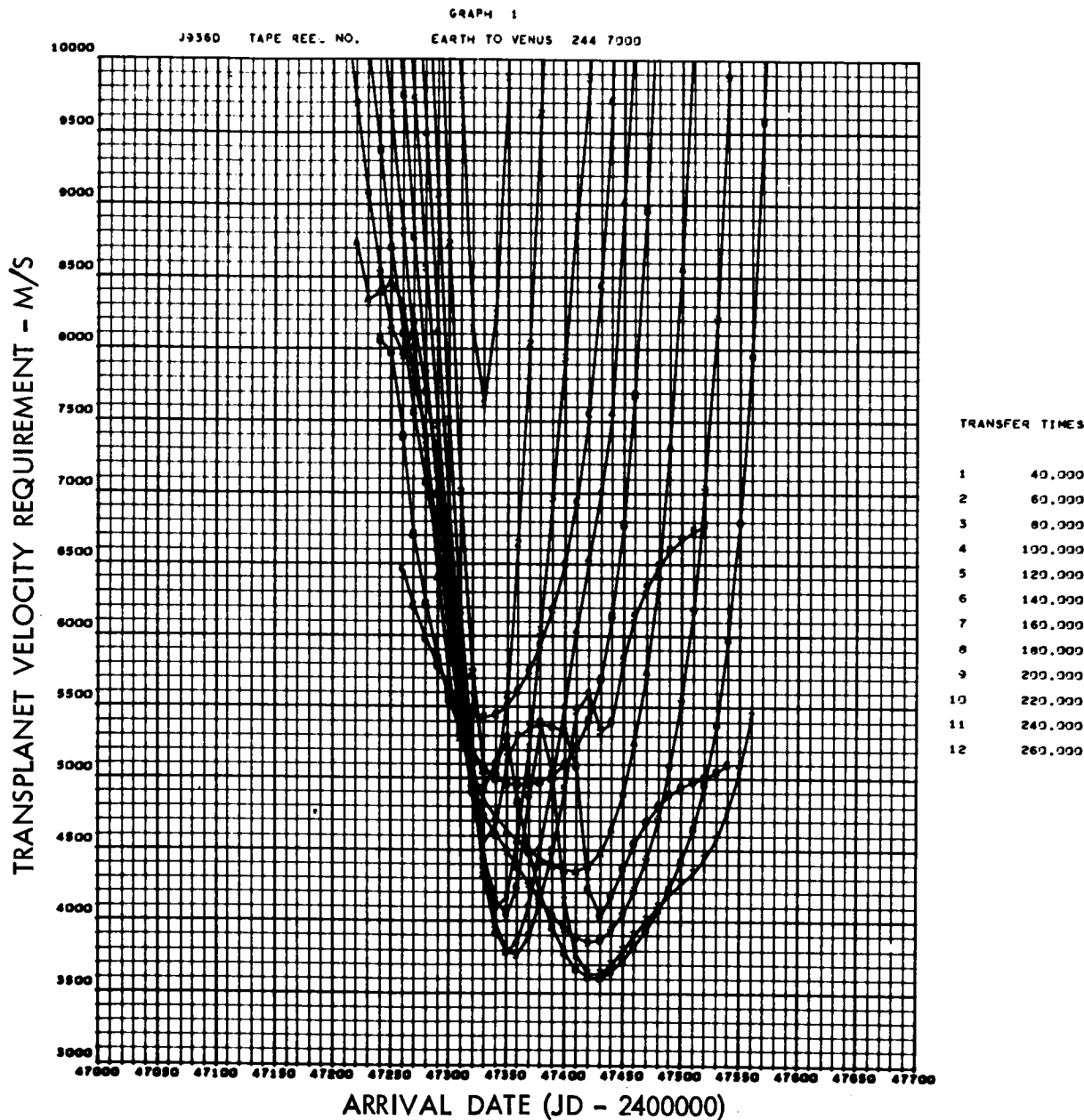
Figure 25. Transplanet Velocity Requirements (1988 Venus Conjunction)

SD 67-621-2

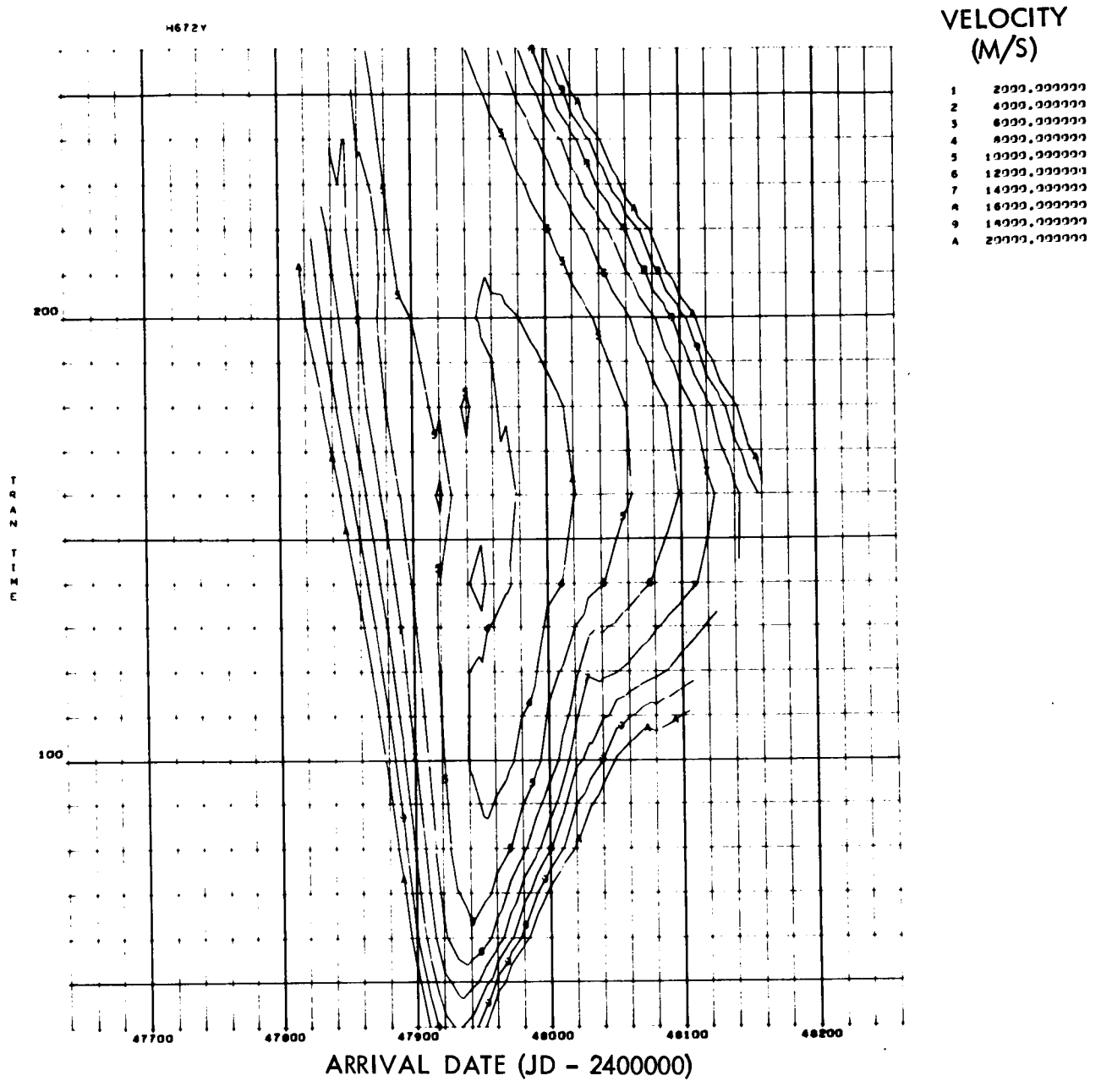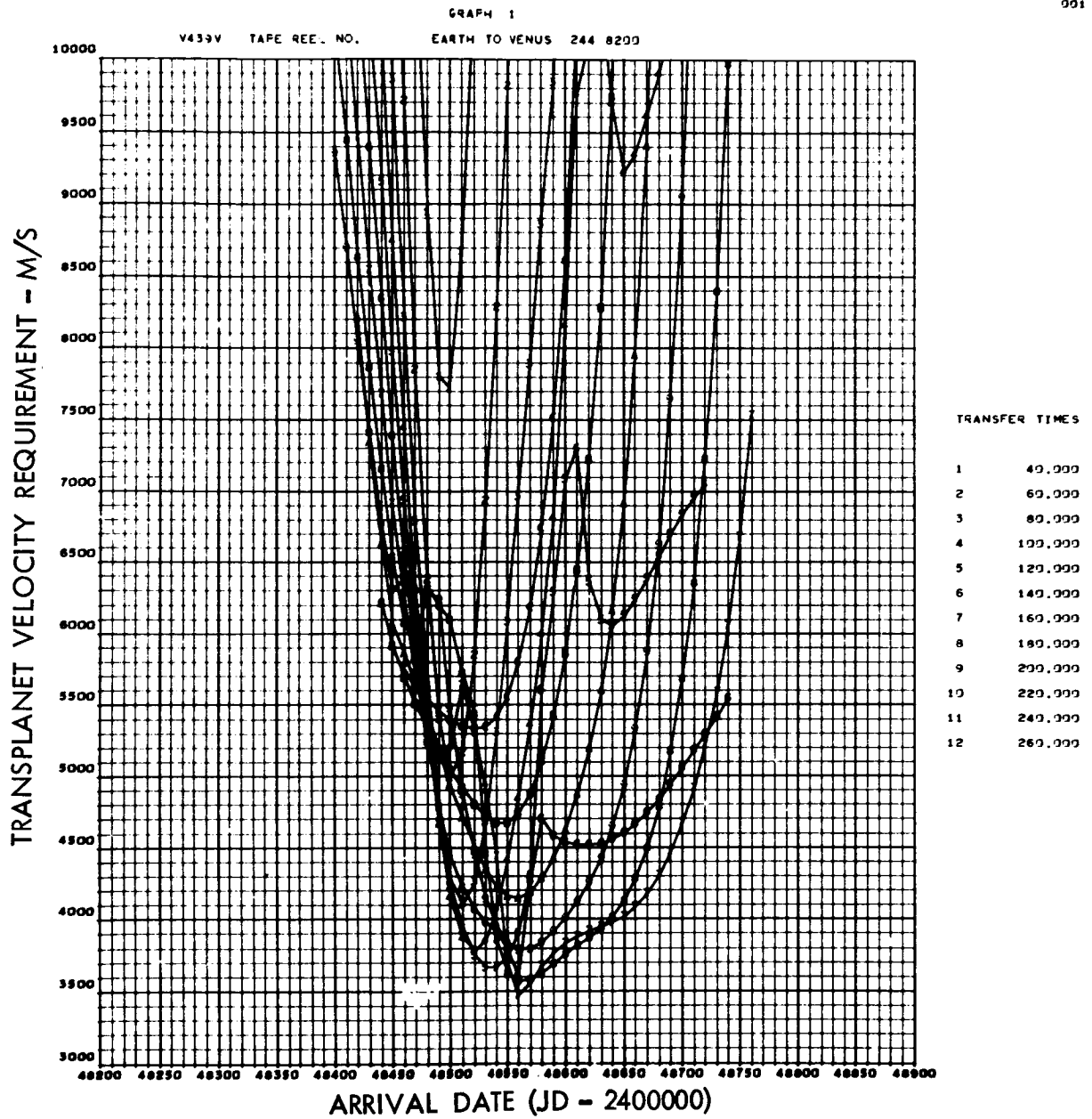Figure 26. Total Transplanet Velocity Requirements
(1988 Venus Conjunction)

- 68 -

SD 67-621-2
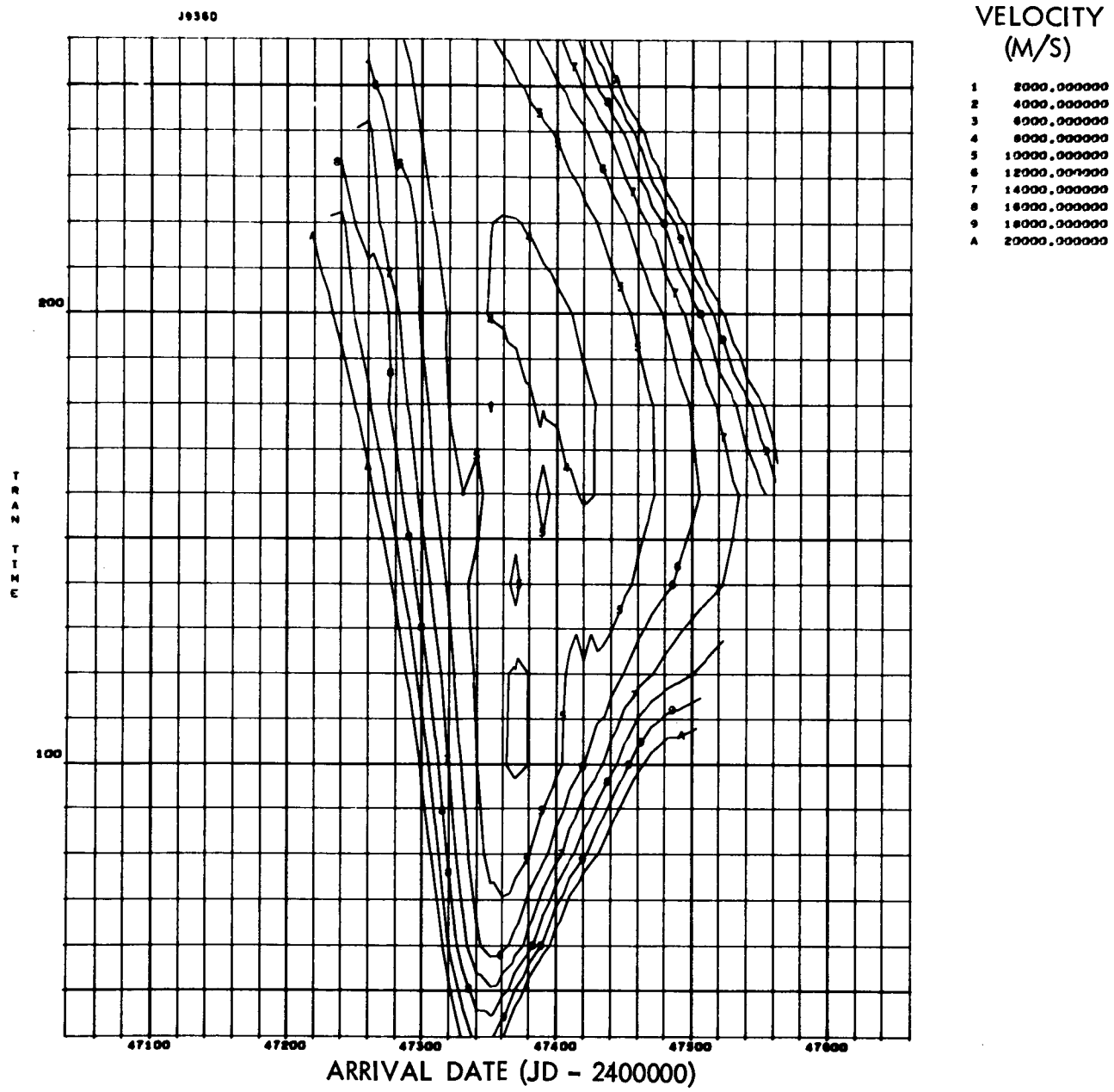
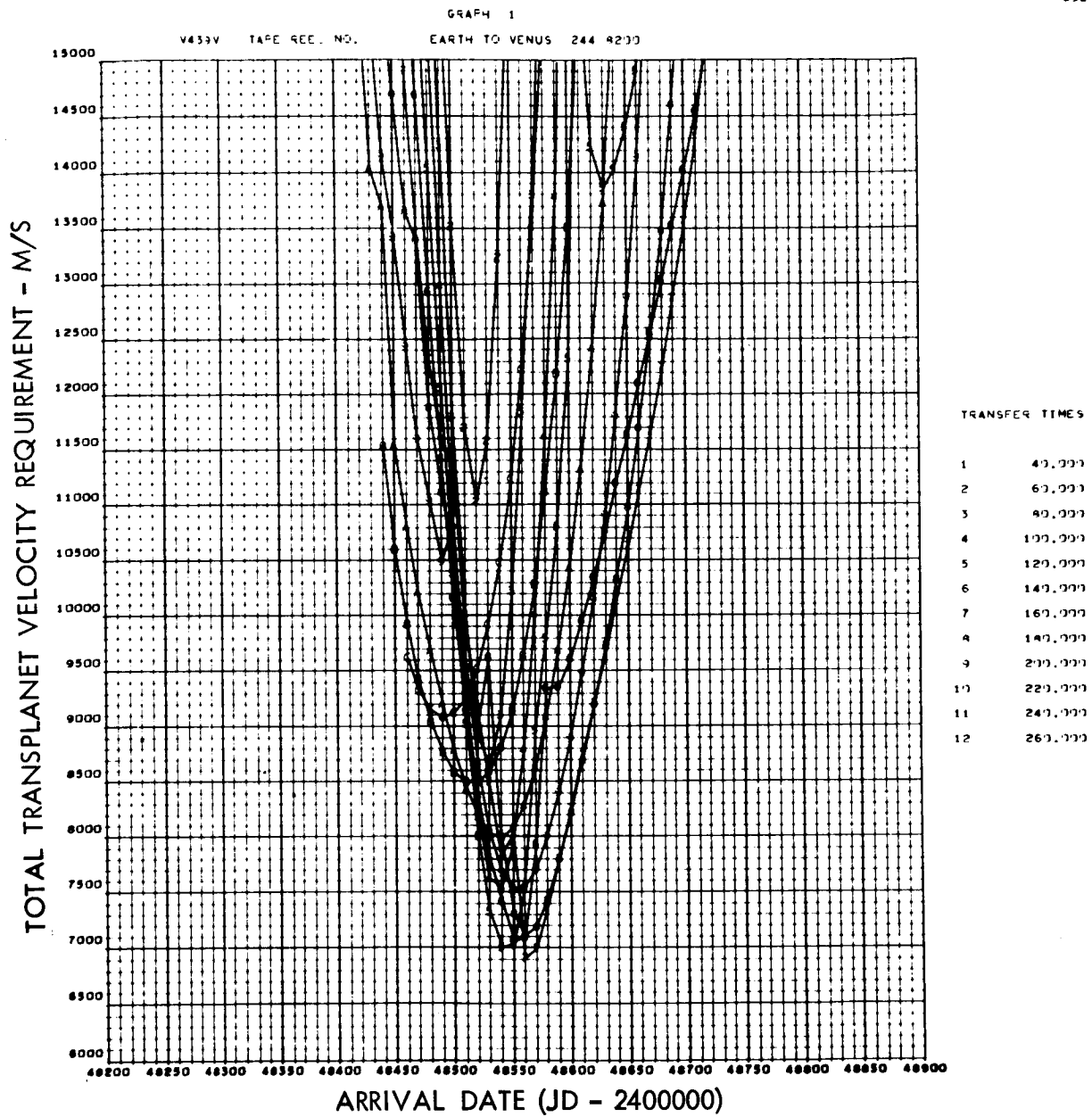Figure 27. Total Transplanet Velocity Contours (1988 Venus Conjunction)
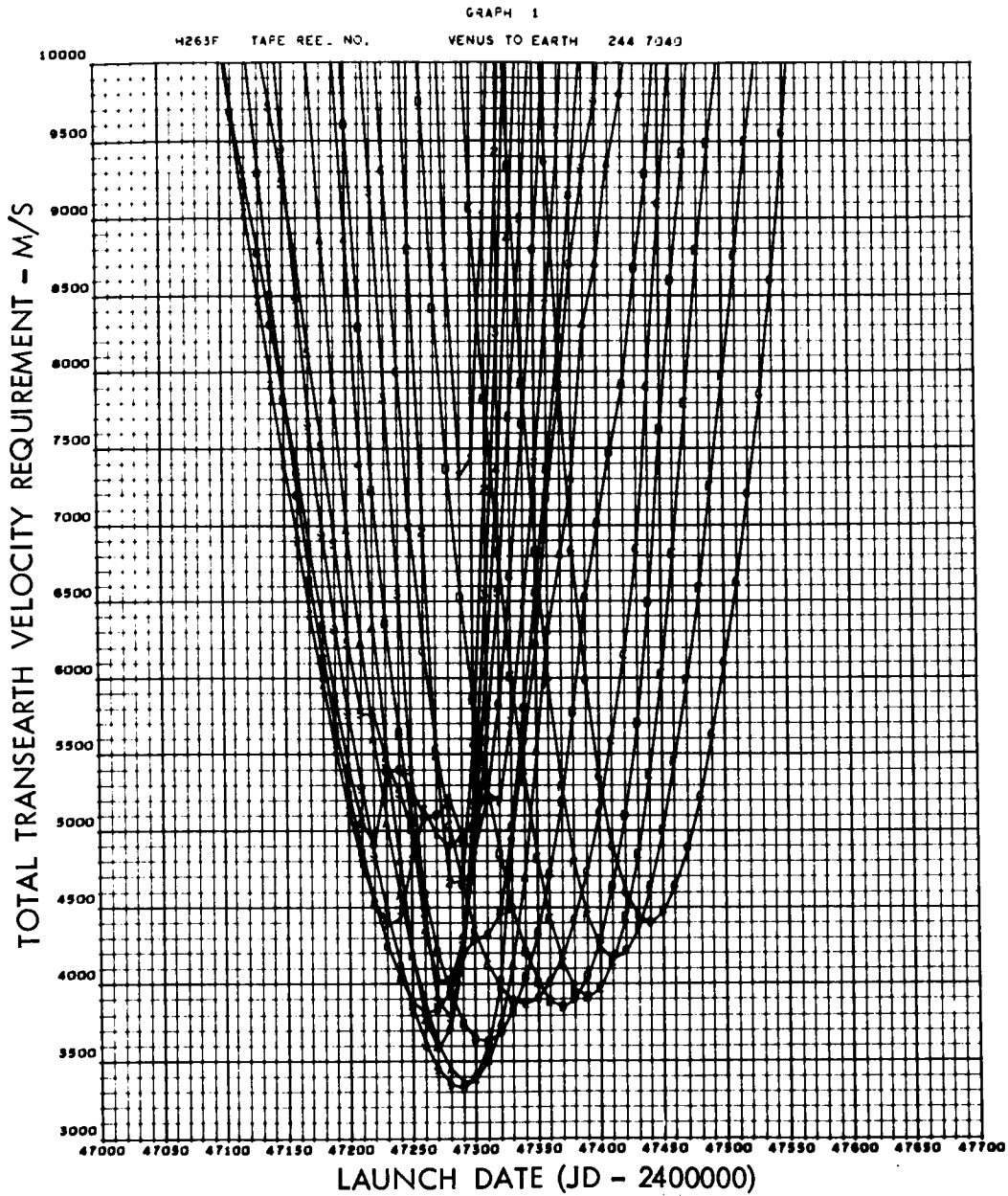
Figure 28. Total Trans-Earth Velocity Requirements
(1988 Venus Conjunction)
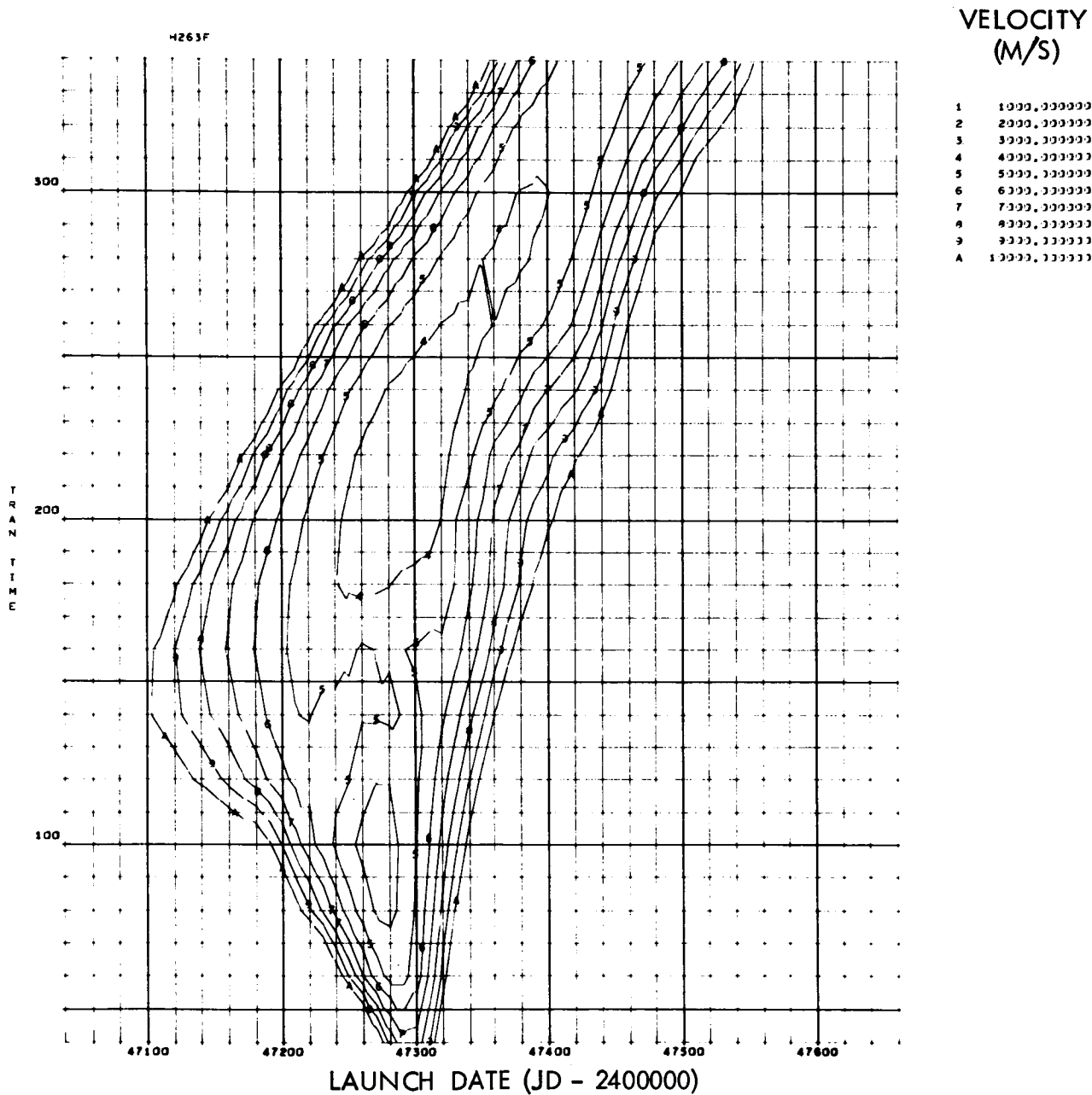
Figure 29. Total Trans-Earth Velocity Contours (1988 Venus Conjunction)
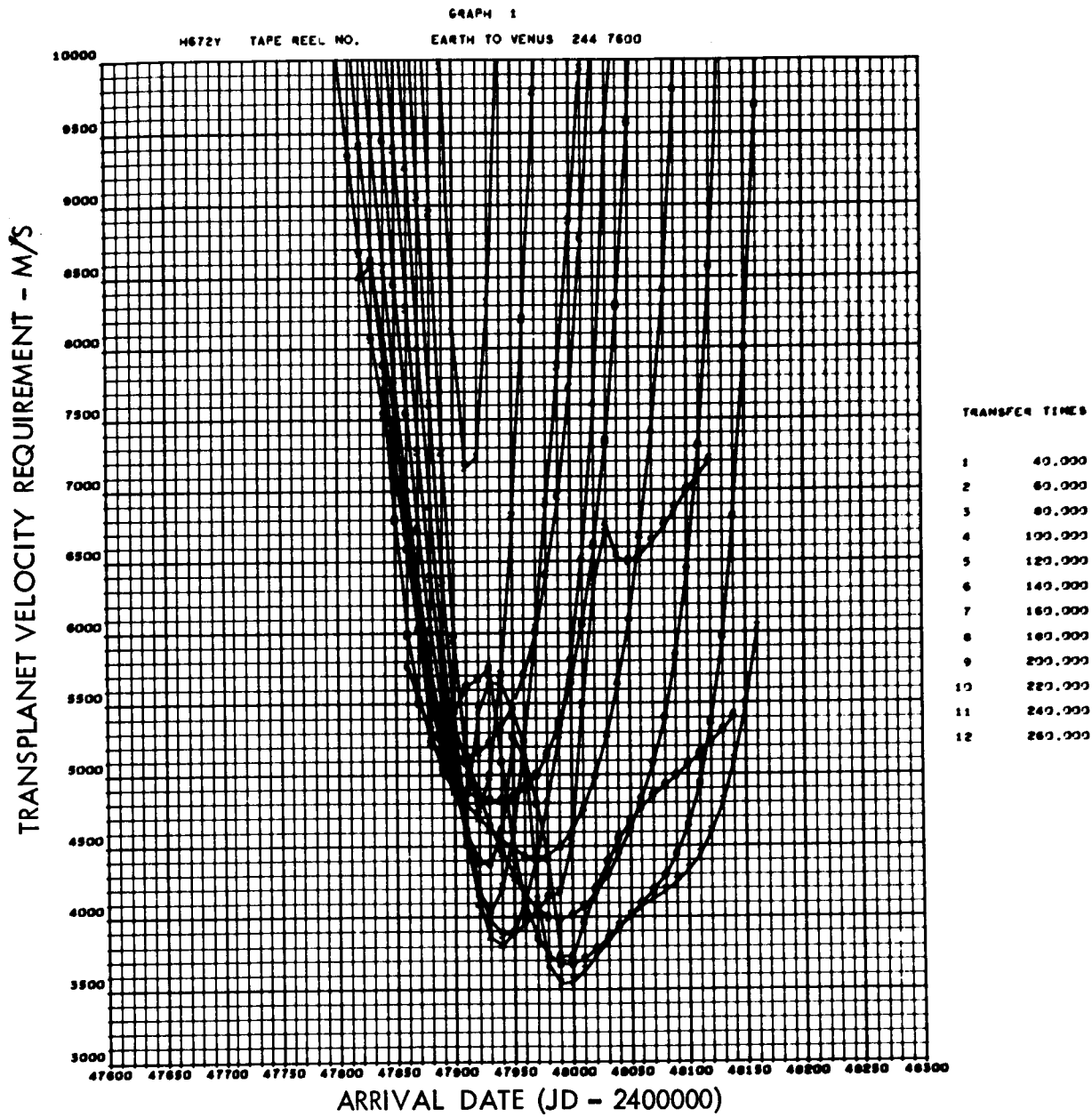
Figure 30. Transplanet Velocity Requirements (1990 Venus Conjunction)
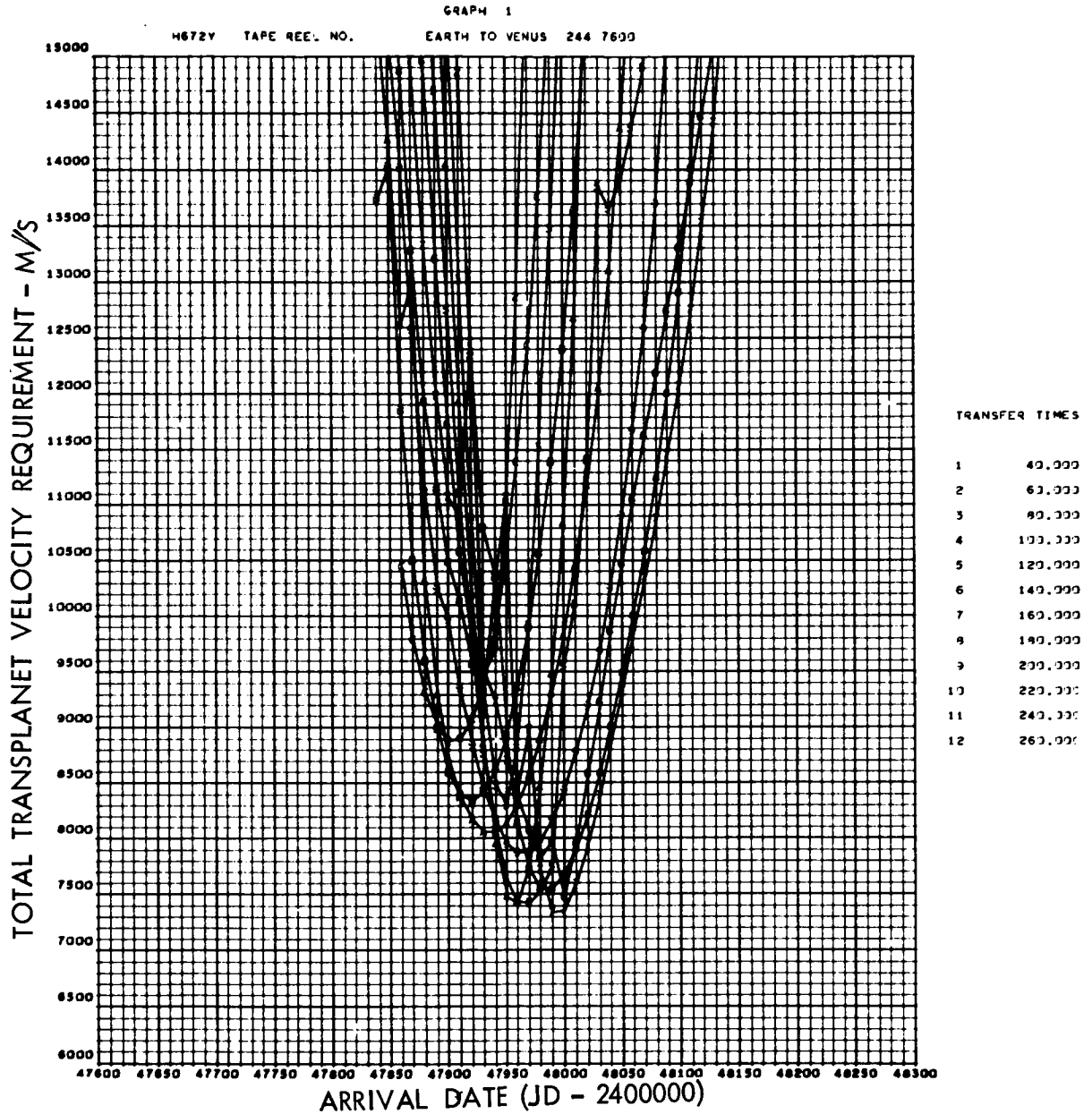
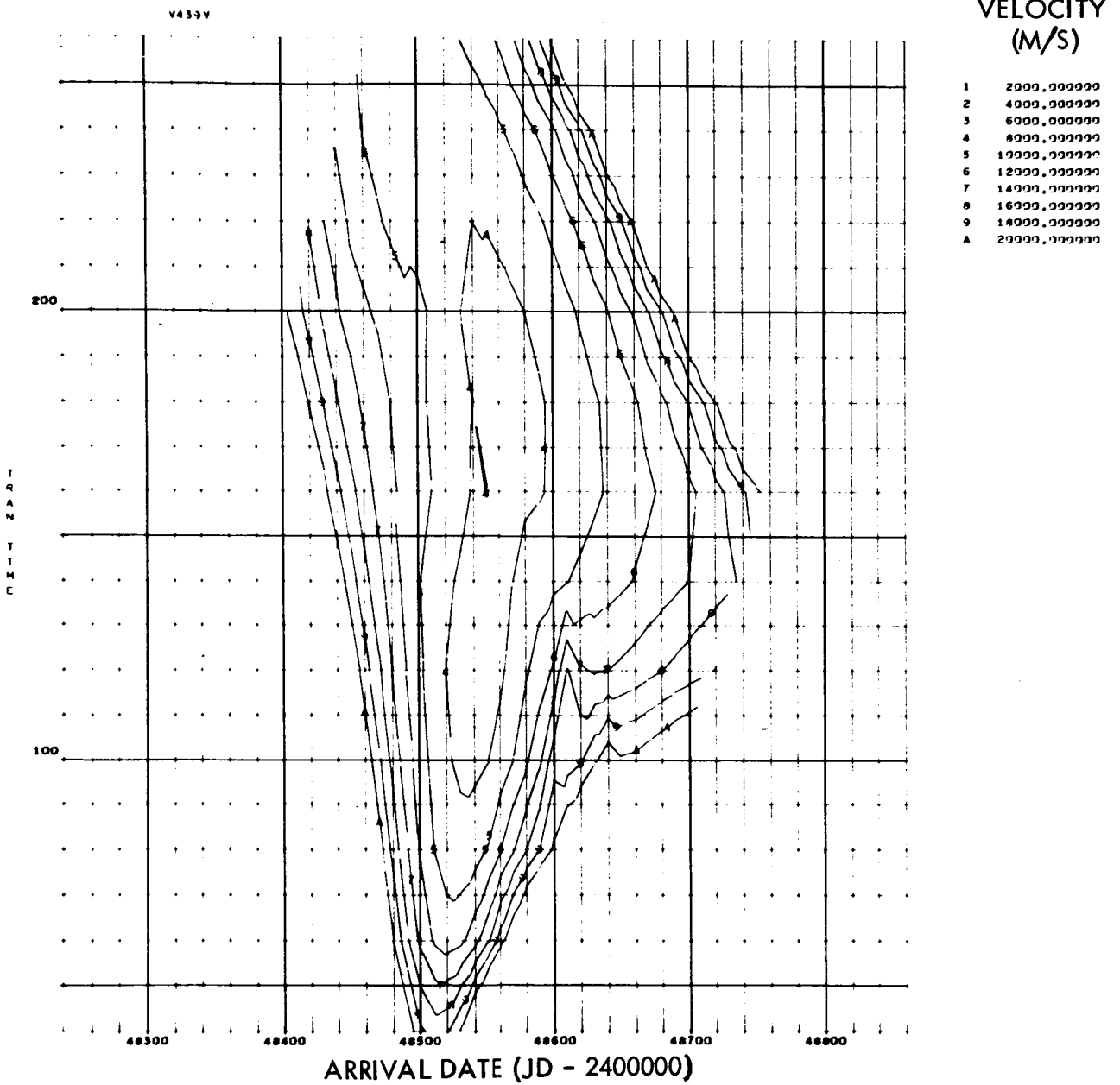Figure 31. Total Transplanet Velocity Requirements
(1990 Venus Conjunction)

Figure 32. Total Transplanet Velocity Contours (1990 Venus Conjunction)
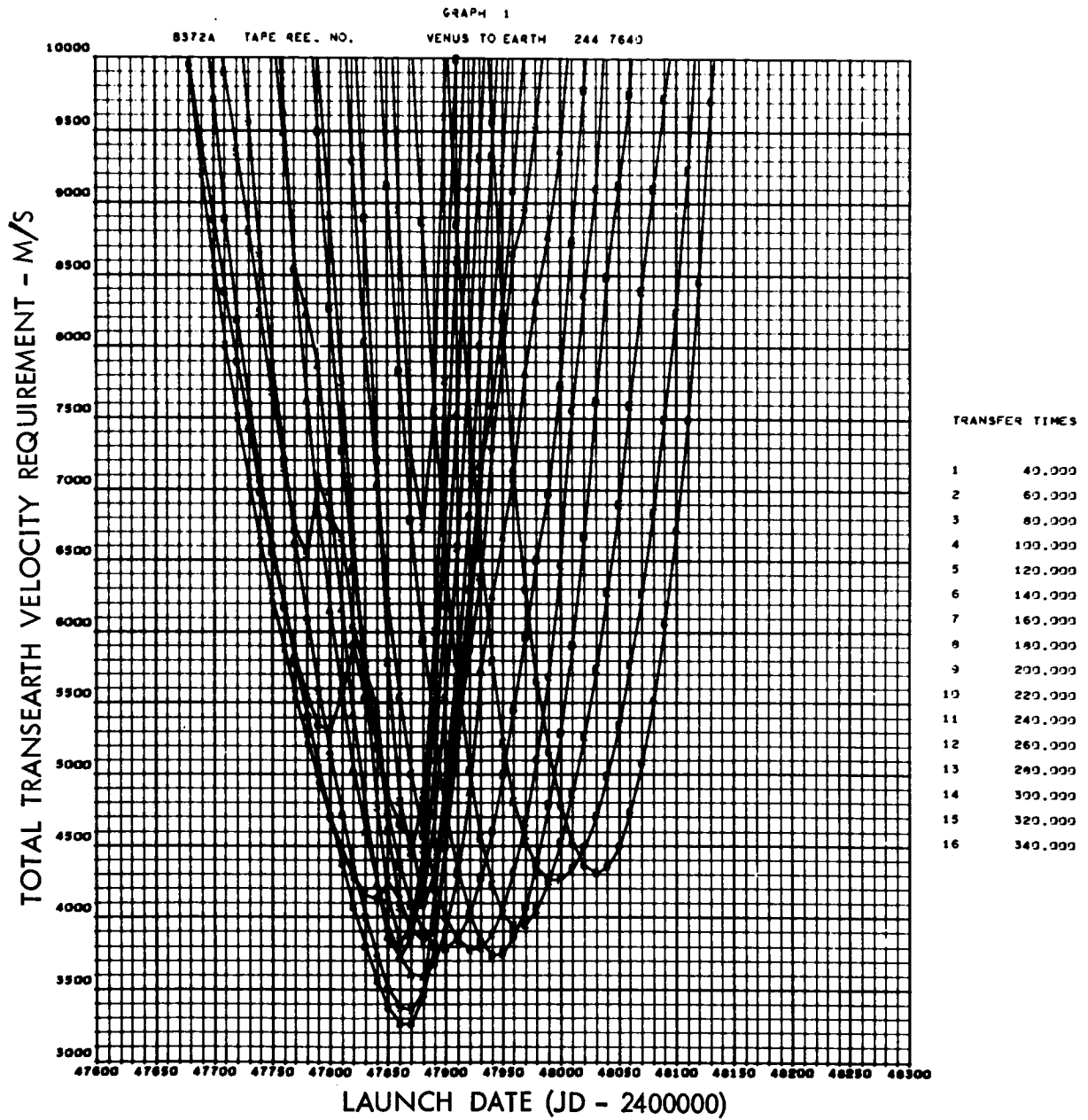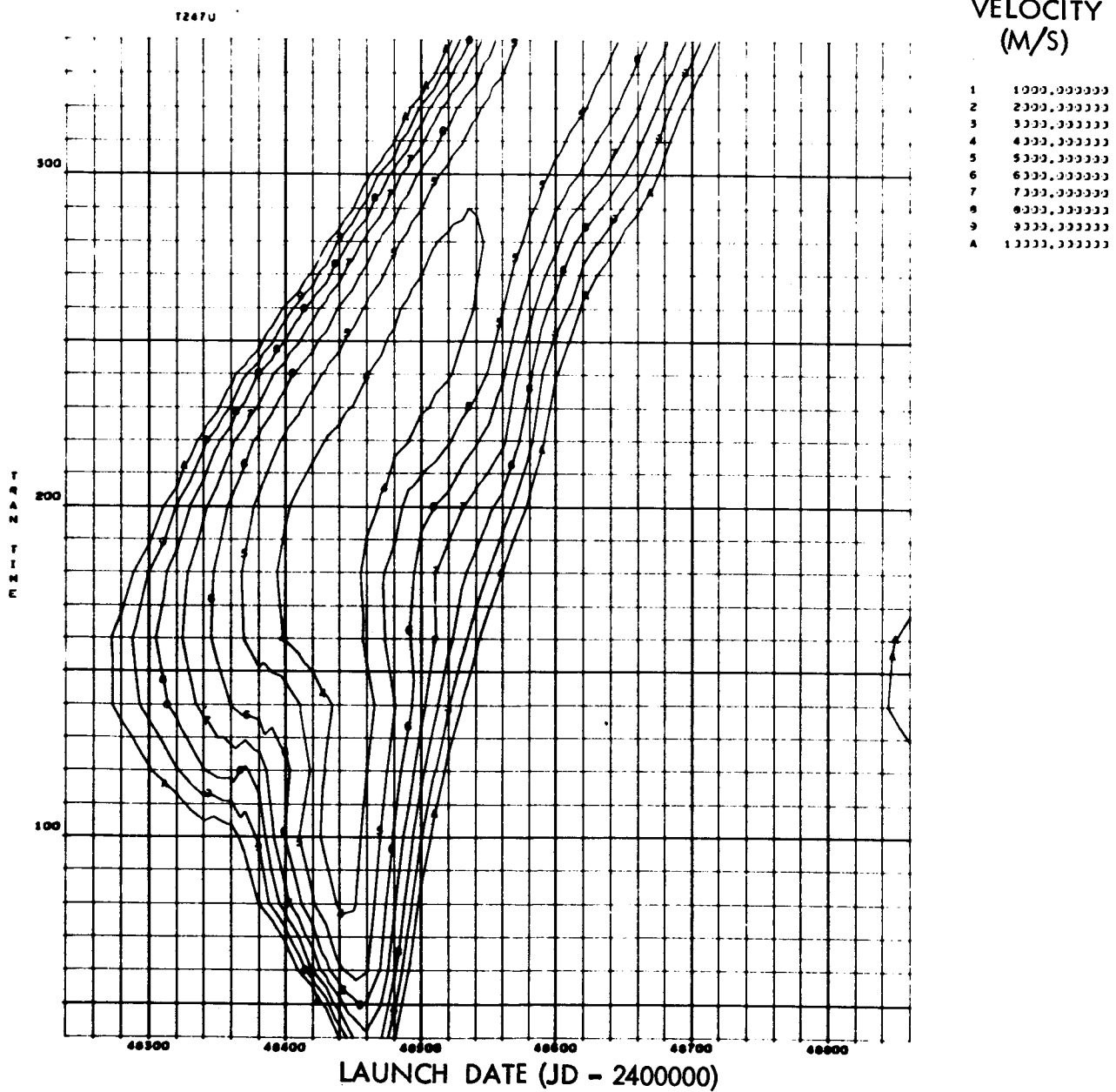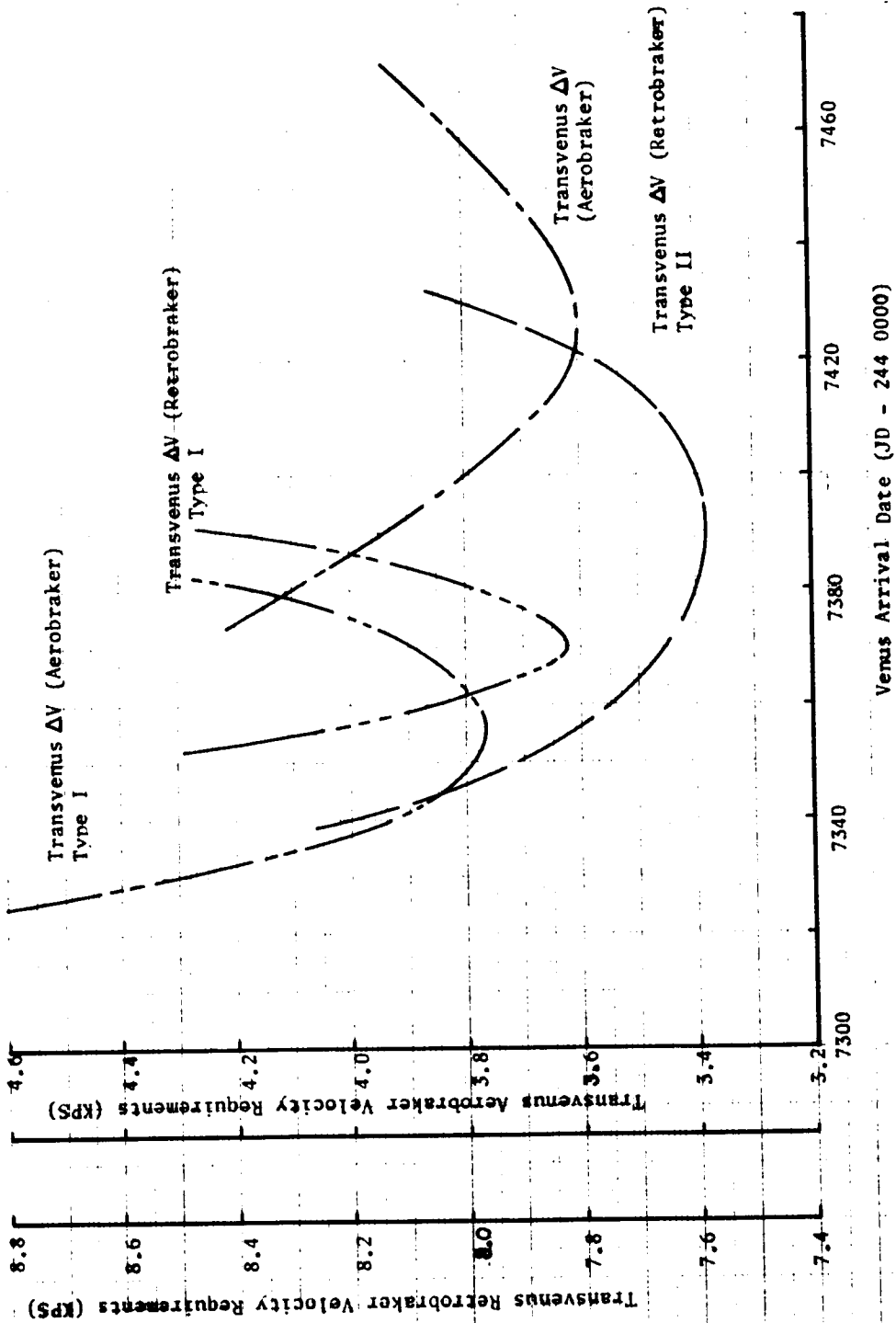
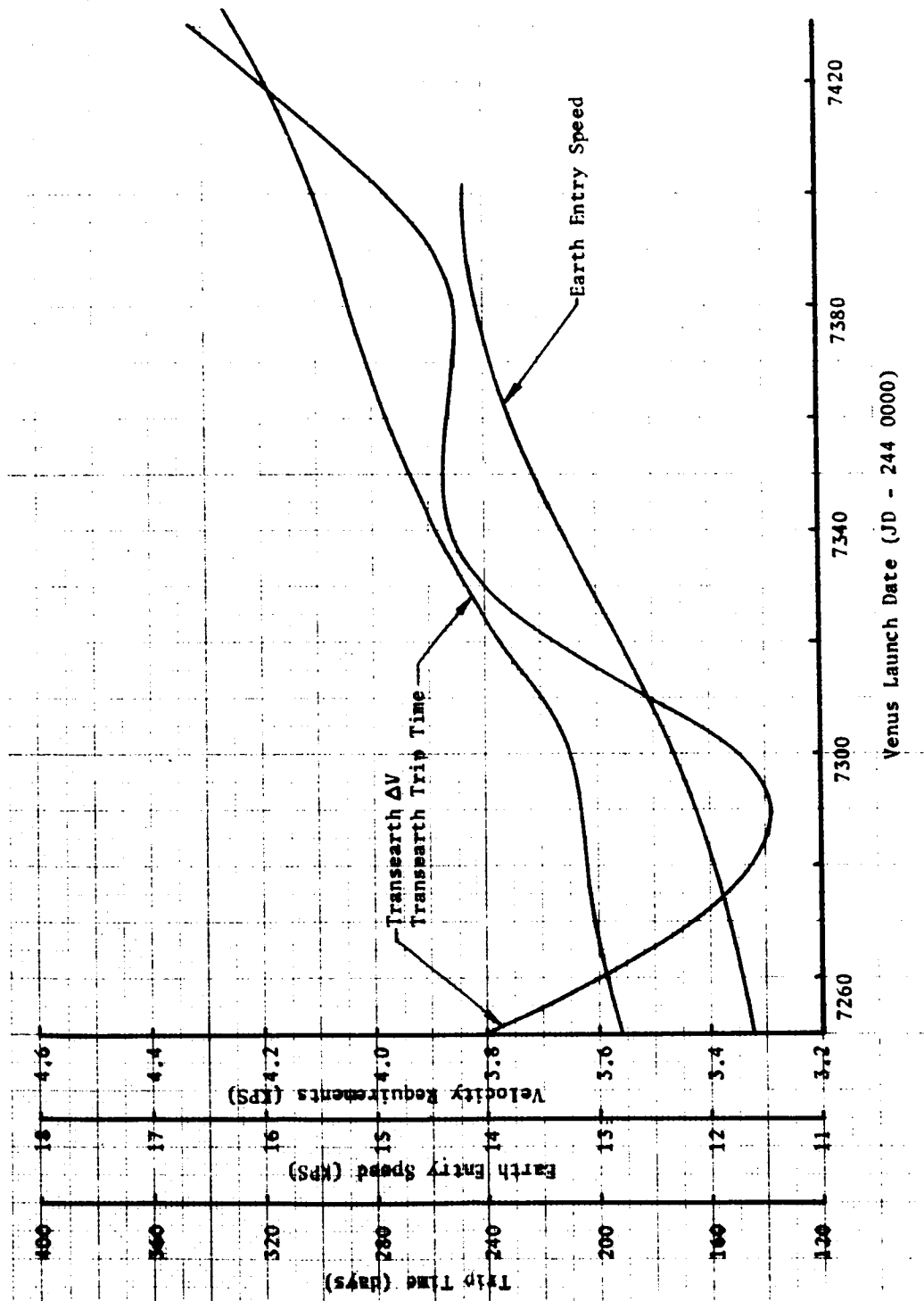Figure 33. Total Trans-Earth Velocity Requirements
(1990 Venus Conjunction)
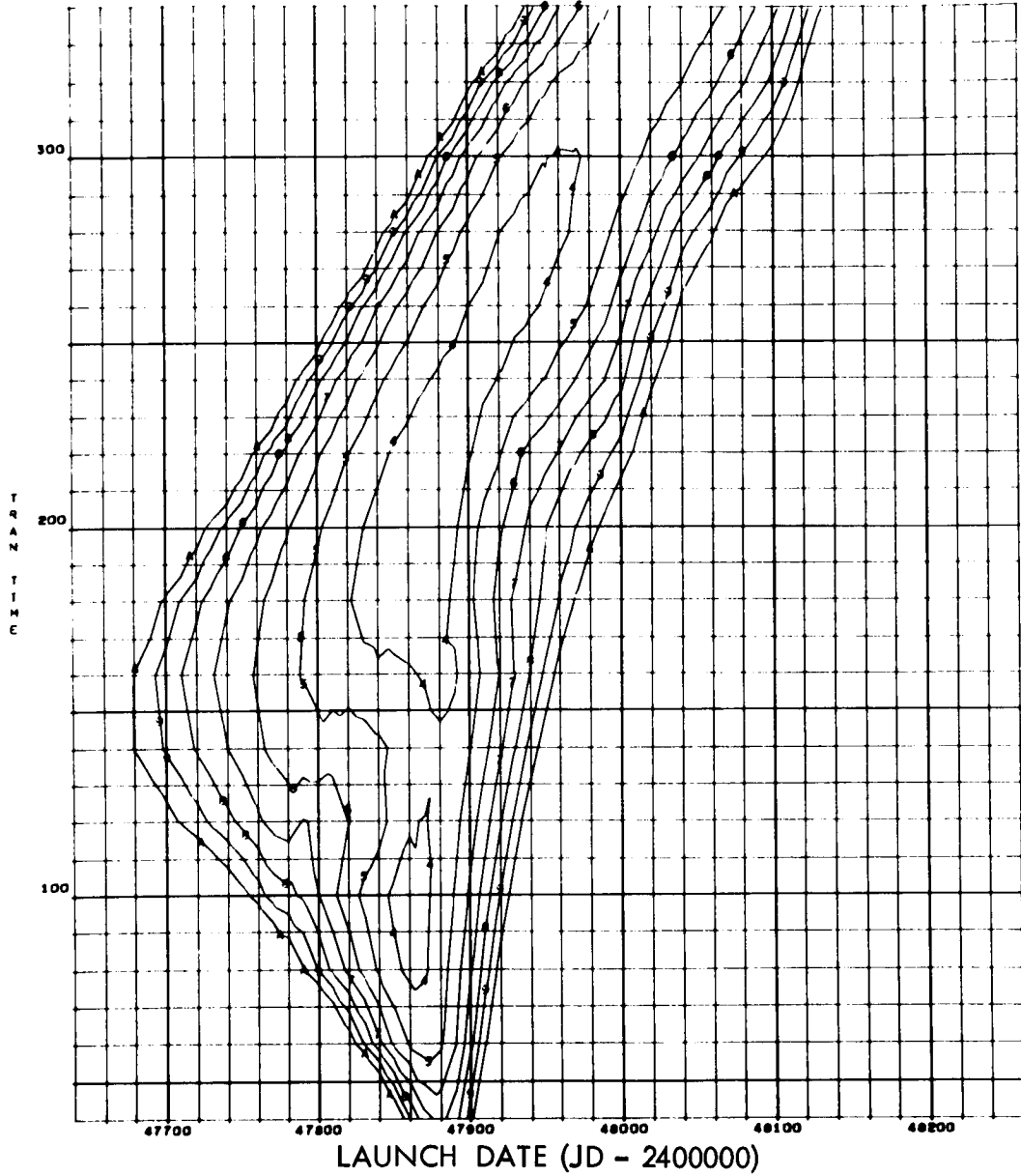
SD 67-621-2

Figure 34. Total Trans-Earth Velocity Contours
(1990 Venus Conjunction)

SD 67-621-2

GRAPH 1

V439V   TAPE REEL NO.   EARTH TO VENUS   244 8200

TRANSPLANET VELOCITY REQUIREMENT – M/S (y-axis, 3000 to 10000)

ARRIVAL DATE (JD – 2400000) (x-axis, 48200 to 48900)

TRANSFER TIMES

1	40.000
2	60.000
3	80.000
4	100.000
5	120.000
6	140.000
7	160.000
8	180.000
9	200.000
10	220.000
11	240.000
12	260.000

Figure 35. Transplanet Velocity Requirements (1991 Venus Conjunction)

- 77 -

SD 67-621-2

Figure 36. Total Transplanet Velocity Requirements (1991 Venus Conjunction)

VELOCITY
(M/S)

1	2000.000000
2	4000.000000
3	6000.000000
4	8000.000000
5	10000.000000
6	12000.000000
7	14000.000000
8	16000.000000
9	18000.000000
A	20000.000000

ARRIVAL DATE (JD - 2400000)

Figure 37. Total Transplanet Velocity Contours (1991 Venus Conjunction)

- 79 -

GRAPH 1

T247U   TAPE REE. NO.   VENUS TO EARTH   244 8240
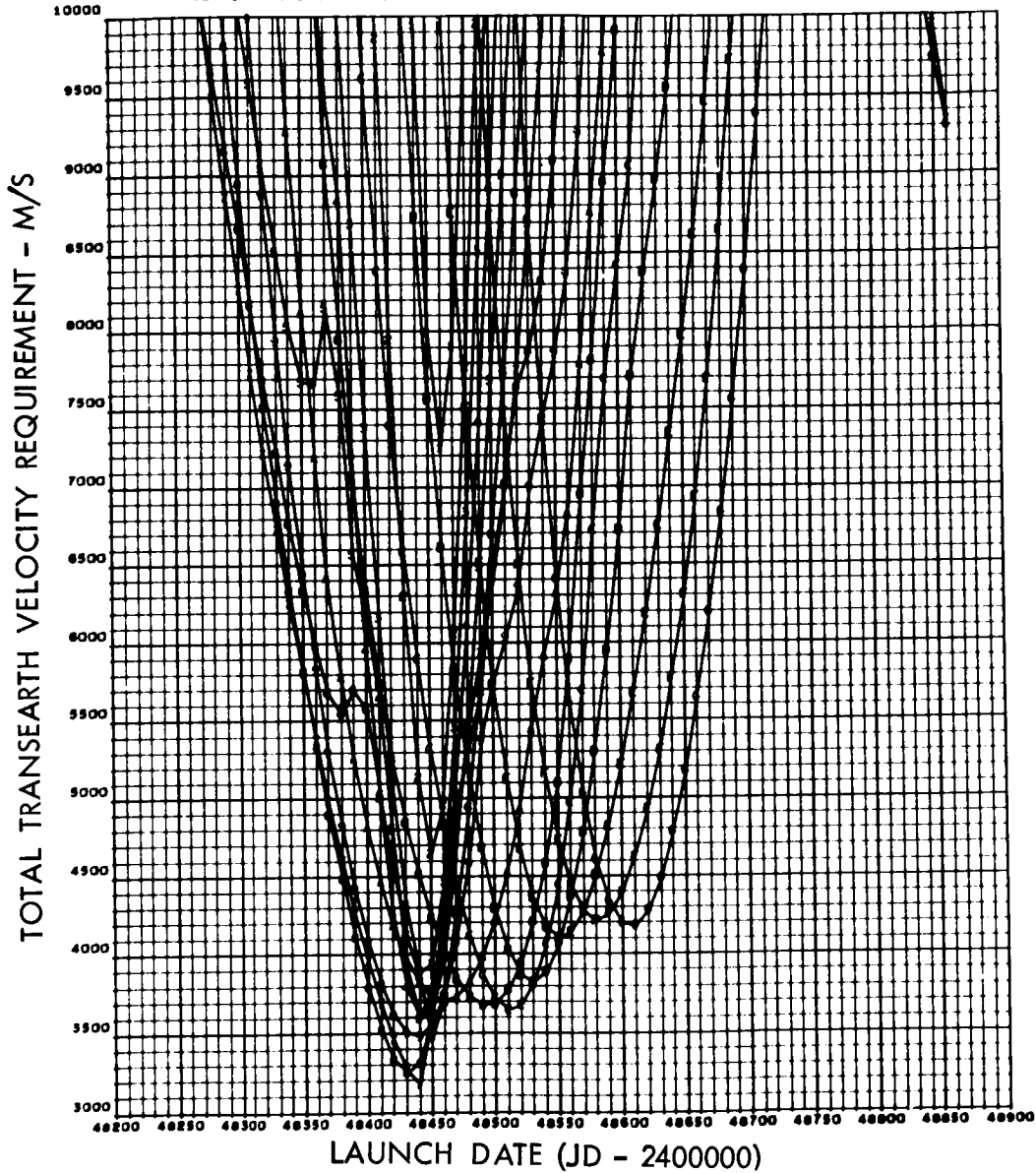
Figure 38.   Total Trans-Earth Velocity Requirements
(1991 Venus Conjunction)

ERRATA

Technological Requirements Common to Manned Planetary Missions

Final Report - Appendix A, SD67-621-2

1. Page 49 - footnote to Table 12 should read "Parking orbit altitude =
    14 Jupiter radii."

Figure 39. Total Trans-Earth Velocity Contours
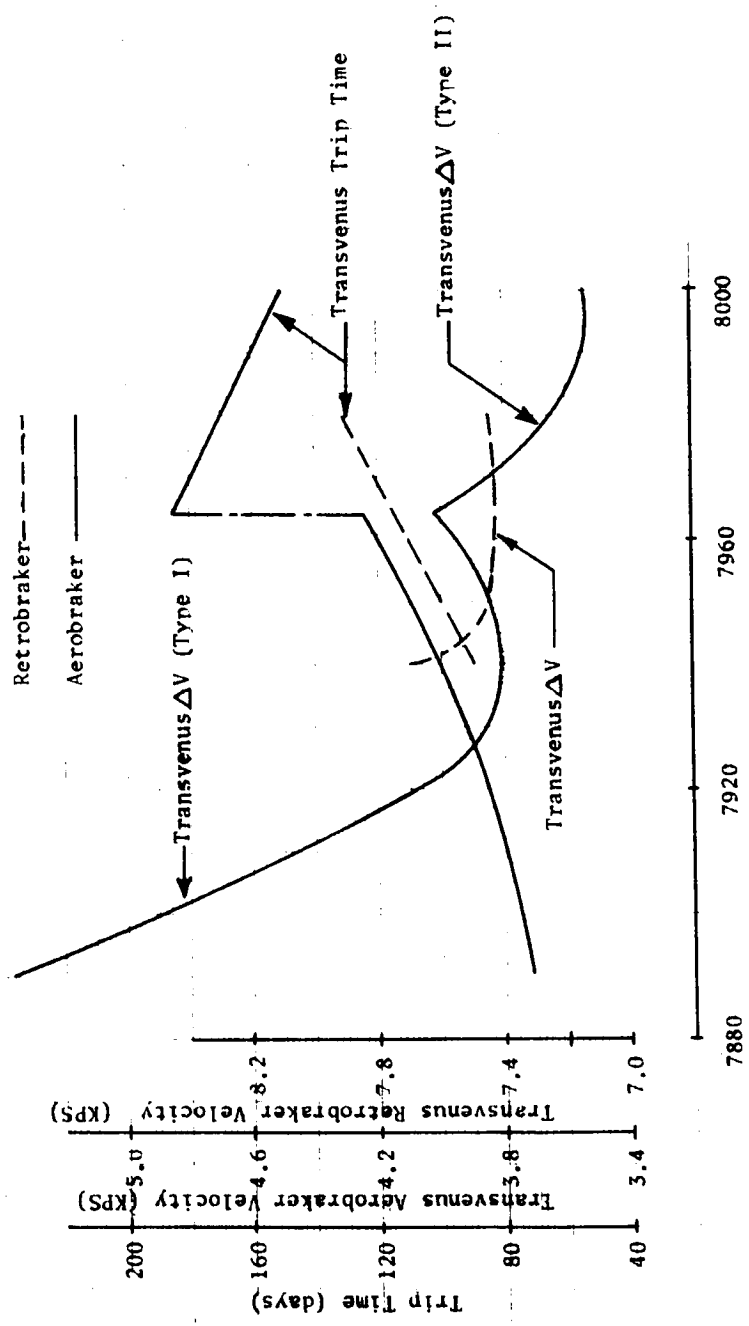(1991 Venus Conjunction)

SD 67-621-2

Figure 40. Transplanet Velocity Requirements Summary
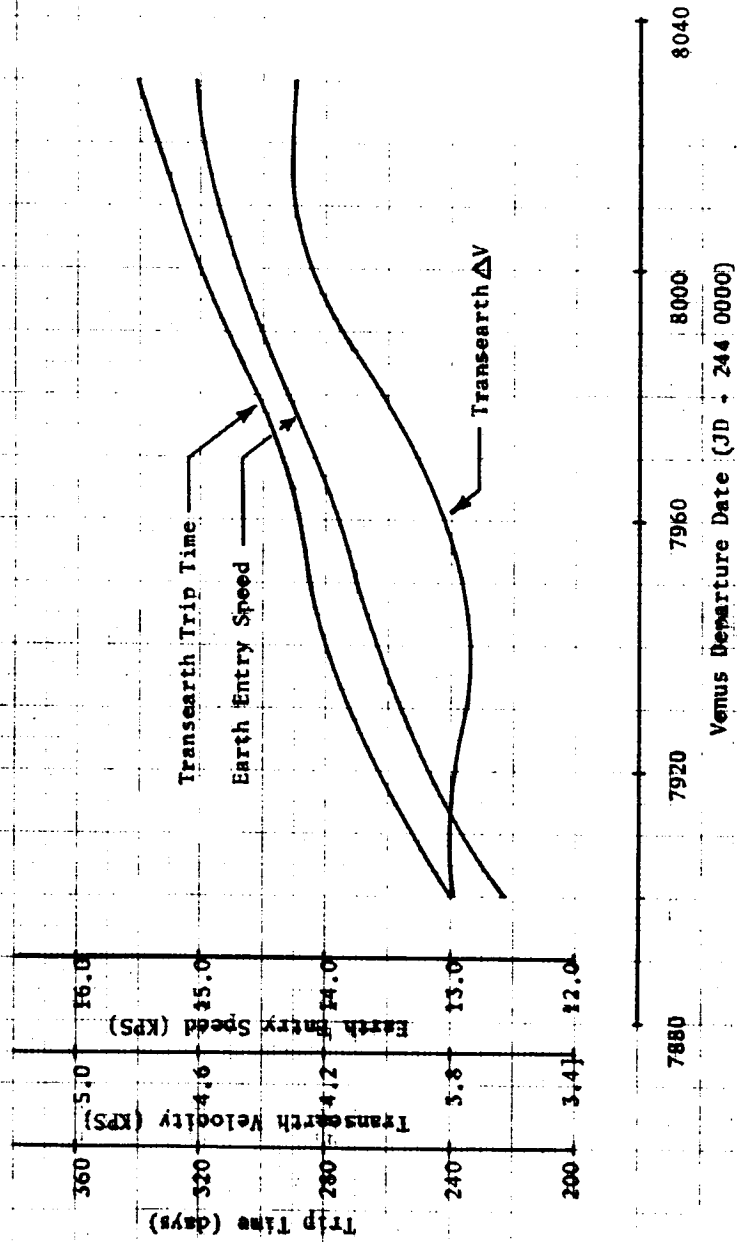(1988 Venus Conjunction)

- 82 -

Figure 41. Trans-Earth Velocity Requirements Summary
(1988 Venus Conjunction)

- 83 -
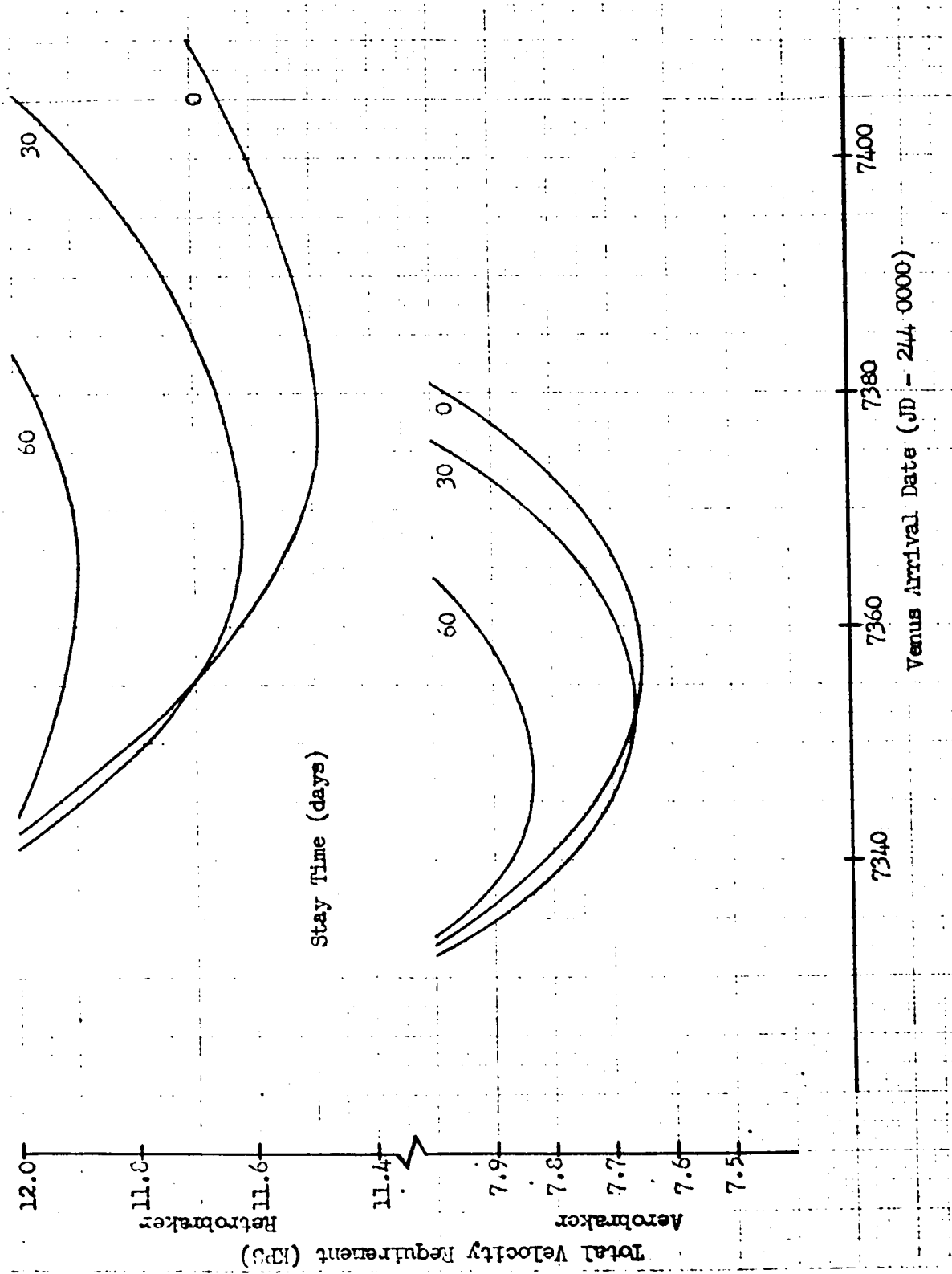
Figure 42.   Total Venus Mission Requirements (1988 Venus Conjunction)
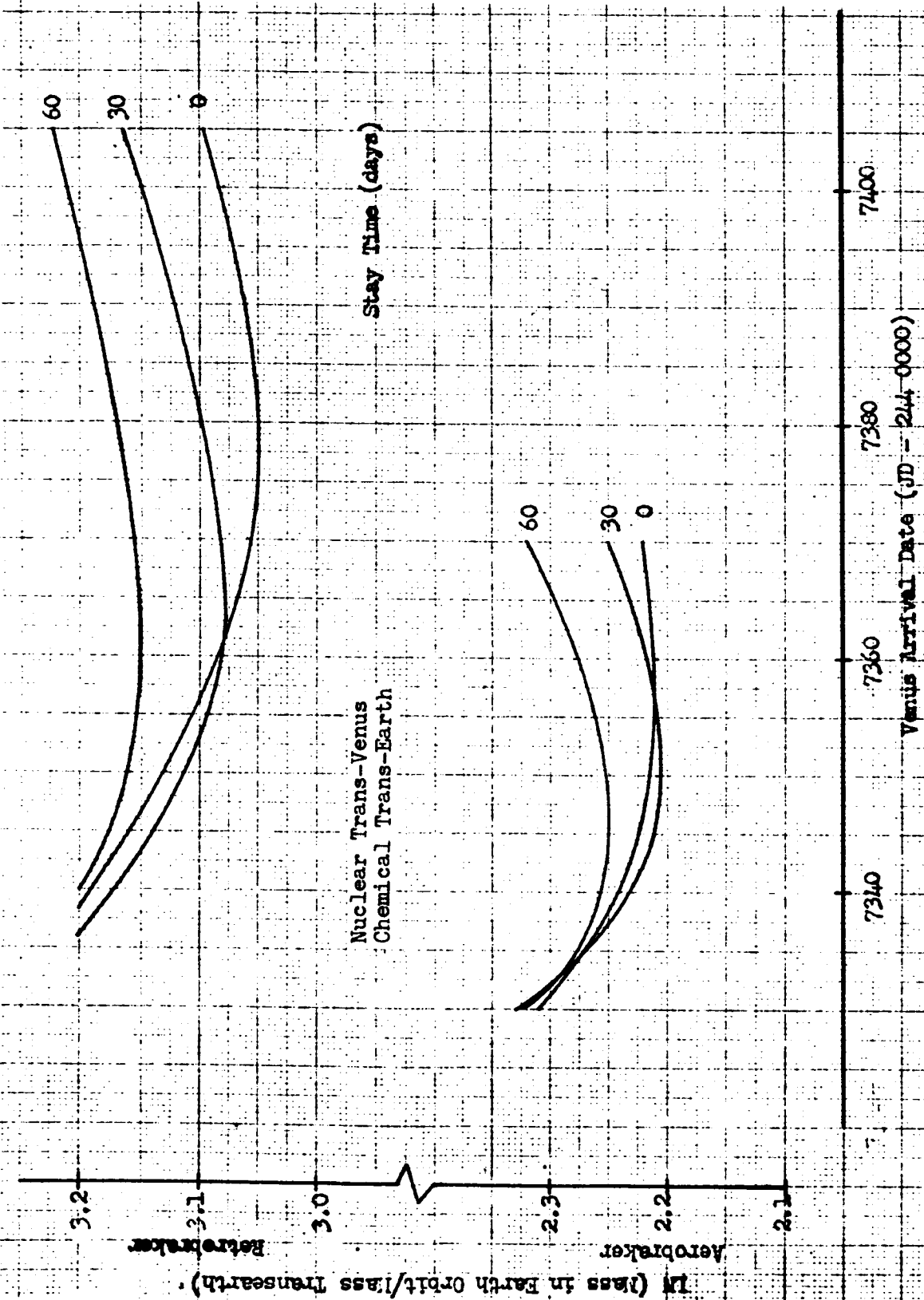
Figure 43. Venus Mass Ratio Requirements (1988 Venus Conjunction)

SD 67-621-2

Figure 44. Transplanet Velocity Requirements Summary
(1990 Venus Conjunction)

Figure 45. Trans-Earth Velocity Requirements Summary
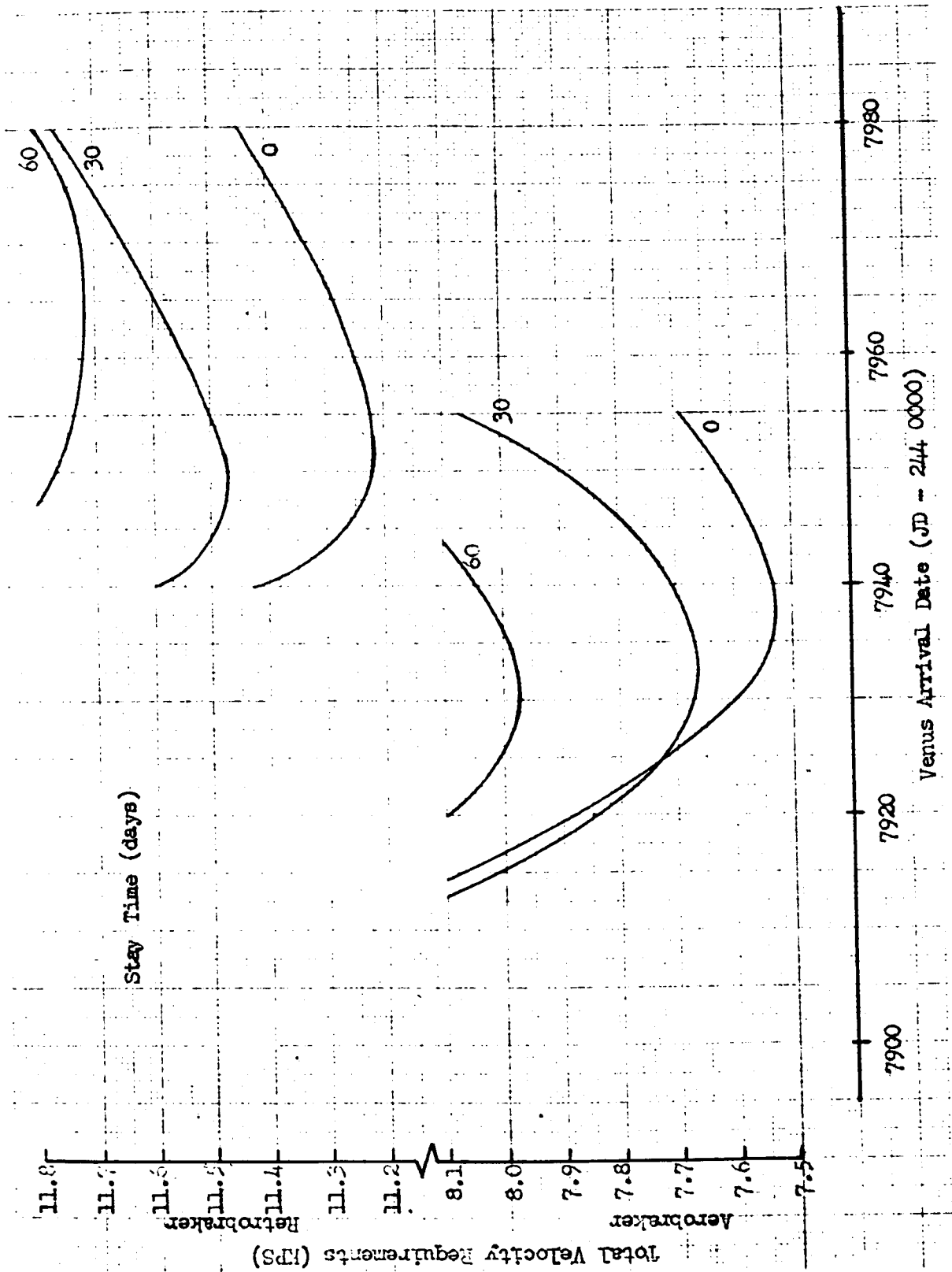(1990 Venus Conjunction)

- 87 -

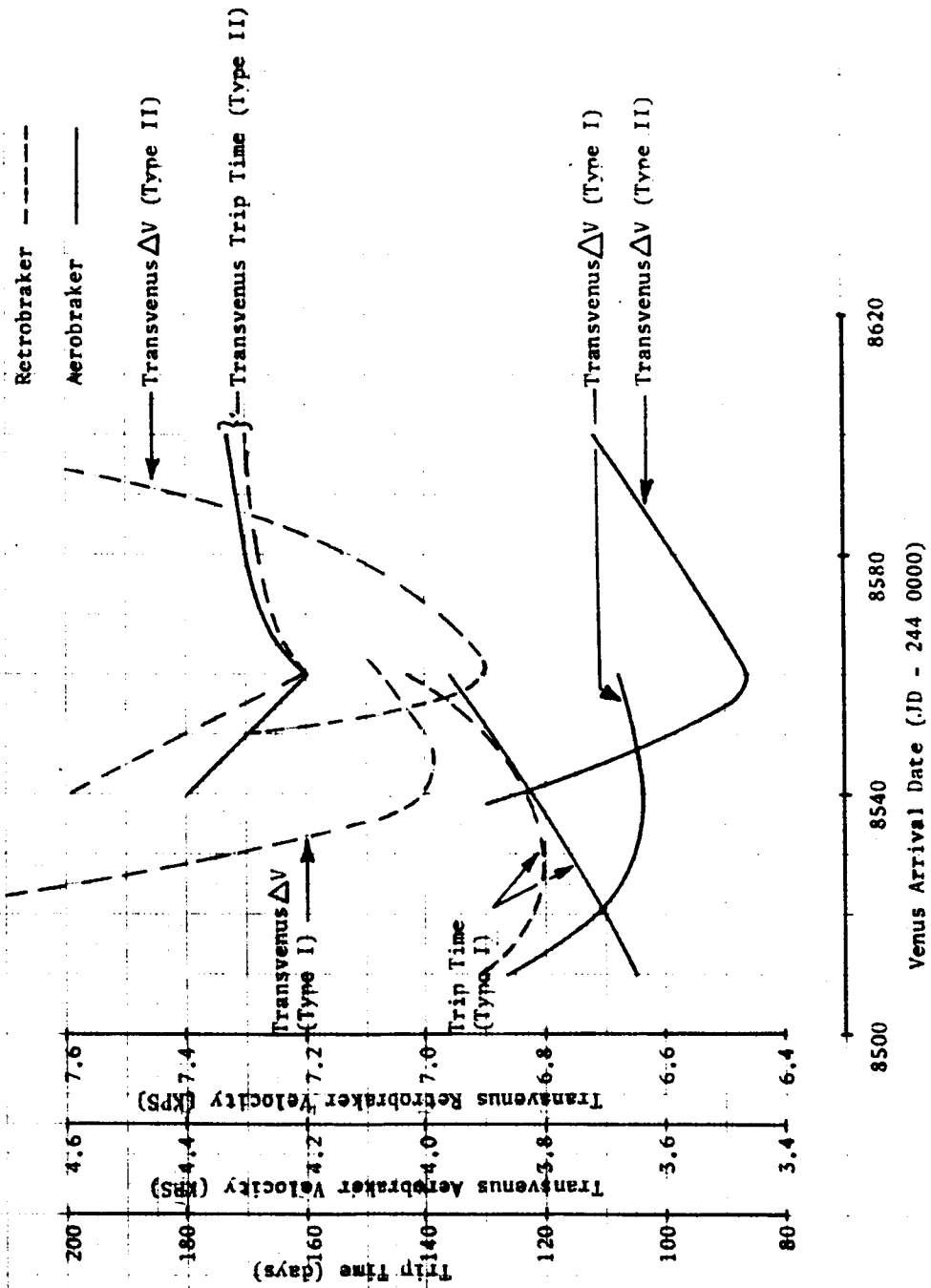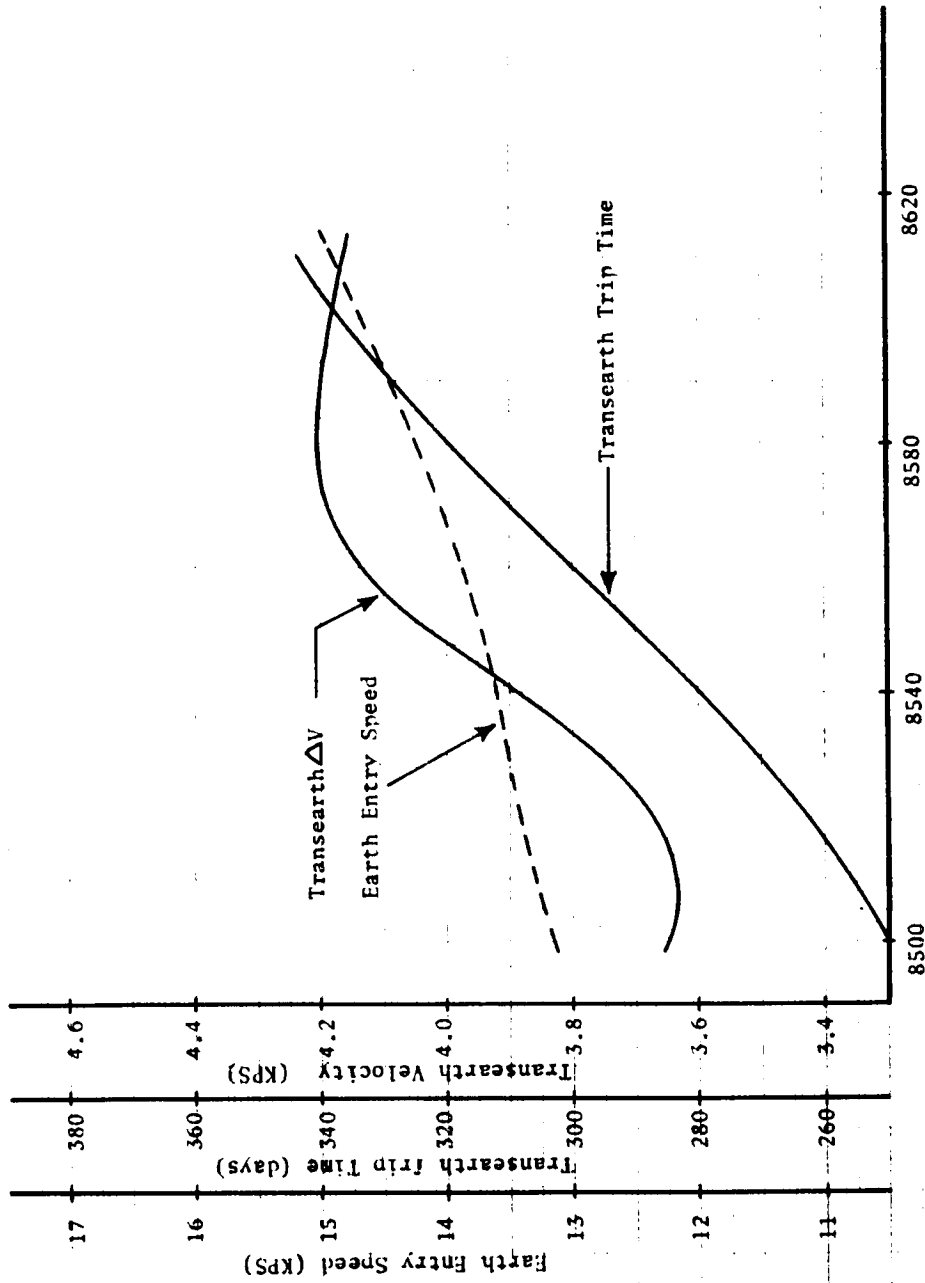Figure 46.   Total Venus Mission Requirements (1990 Venus Conjunction)

- 88 -

SD 67-621-2

Figure 47. Transplanet Velocity Requirements Summary
(1991 Venus Conjunction)

- 89 -

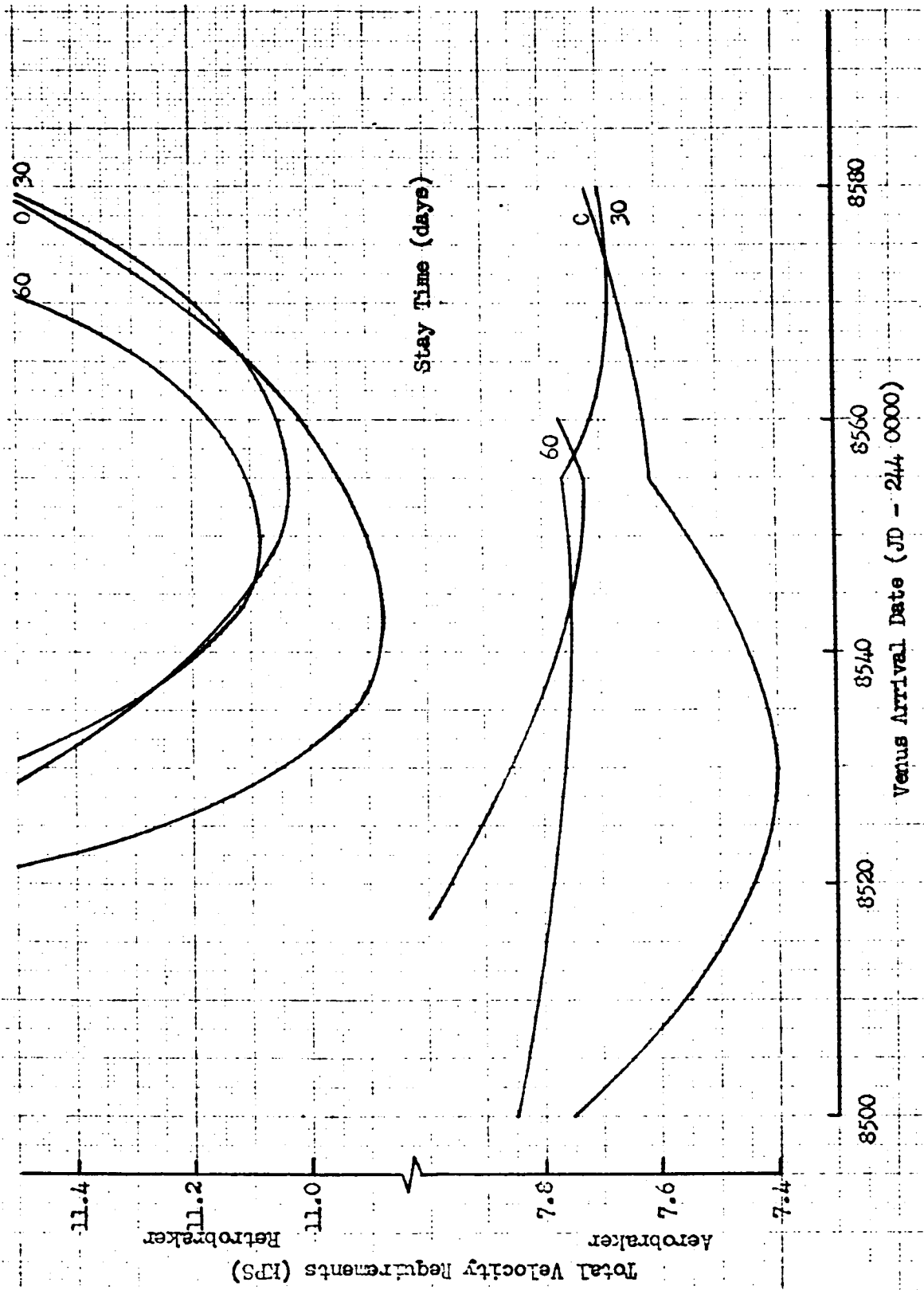Figure 48. Trans-Earth Velocity Requirements Summary
(1991 Venus Conjunction)

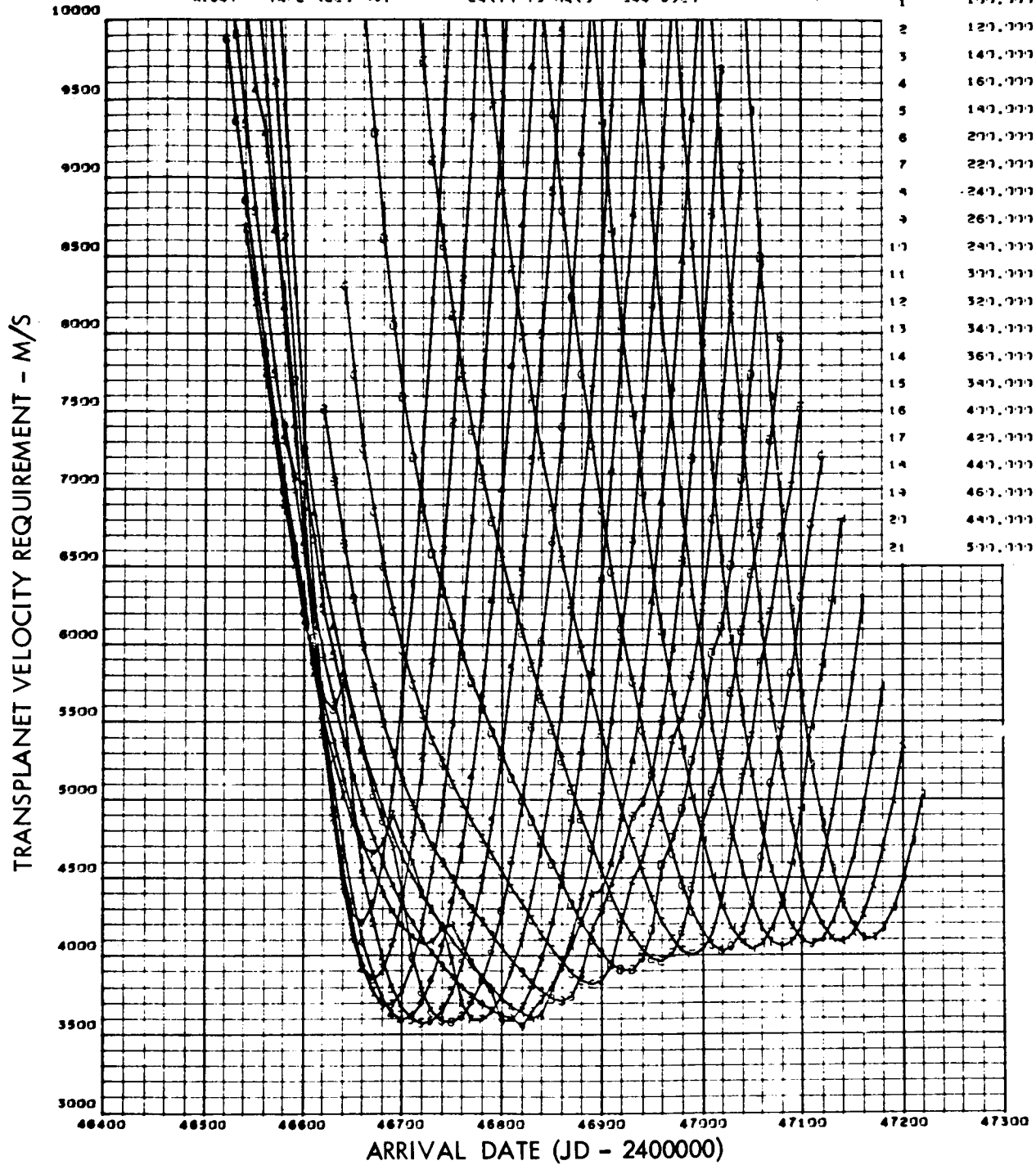Figure 49. Total Venus Mission Requirements (1991 Venus Conjunction)

- 91 -

Figure 50. Transplanet Velocity Requirements (1986 Mars Opposition)

SD 67-621-2
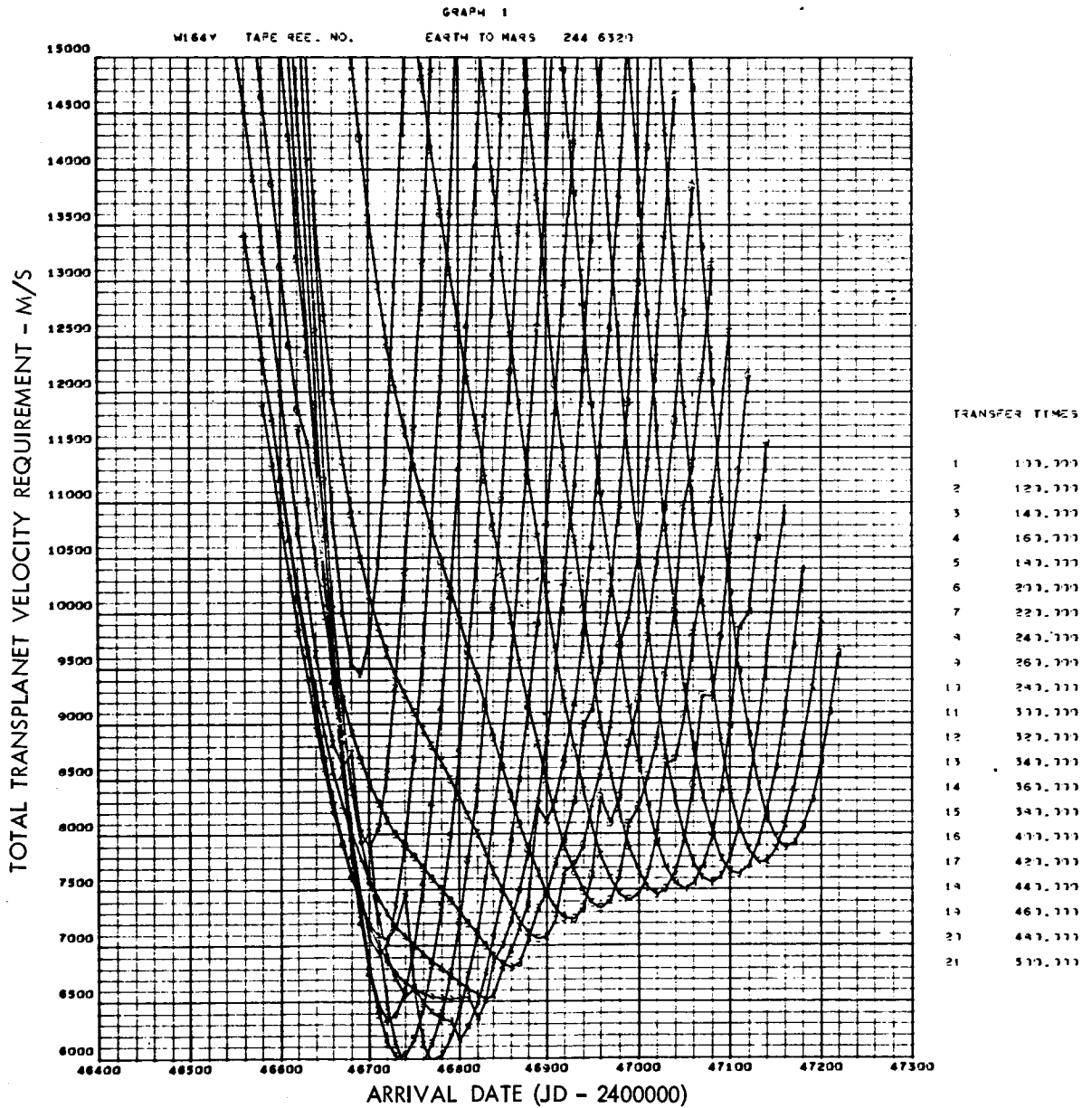
Figure 51. Total Transplanet Velocity Requirements (1986 Mars Opposition)

900

400

T
R
A
N

T
I
M
E

300

200

100

VELOCITY
(M/S)

1	2000.000000
2	4000.000000
3	6000.000000
4	8000.000000
5	10000.000000
6	12000.000000
7	14000.000000
8	16000.000000
9	18000.000000
A	20000.000000

46600   46800   47000   47200

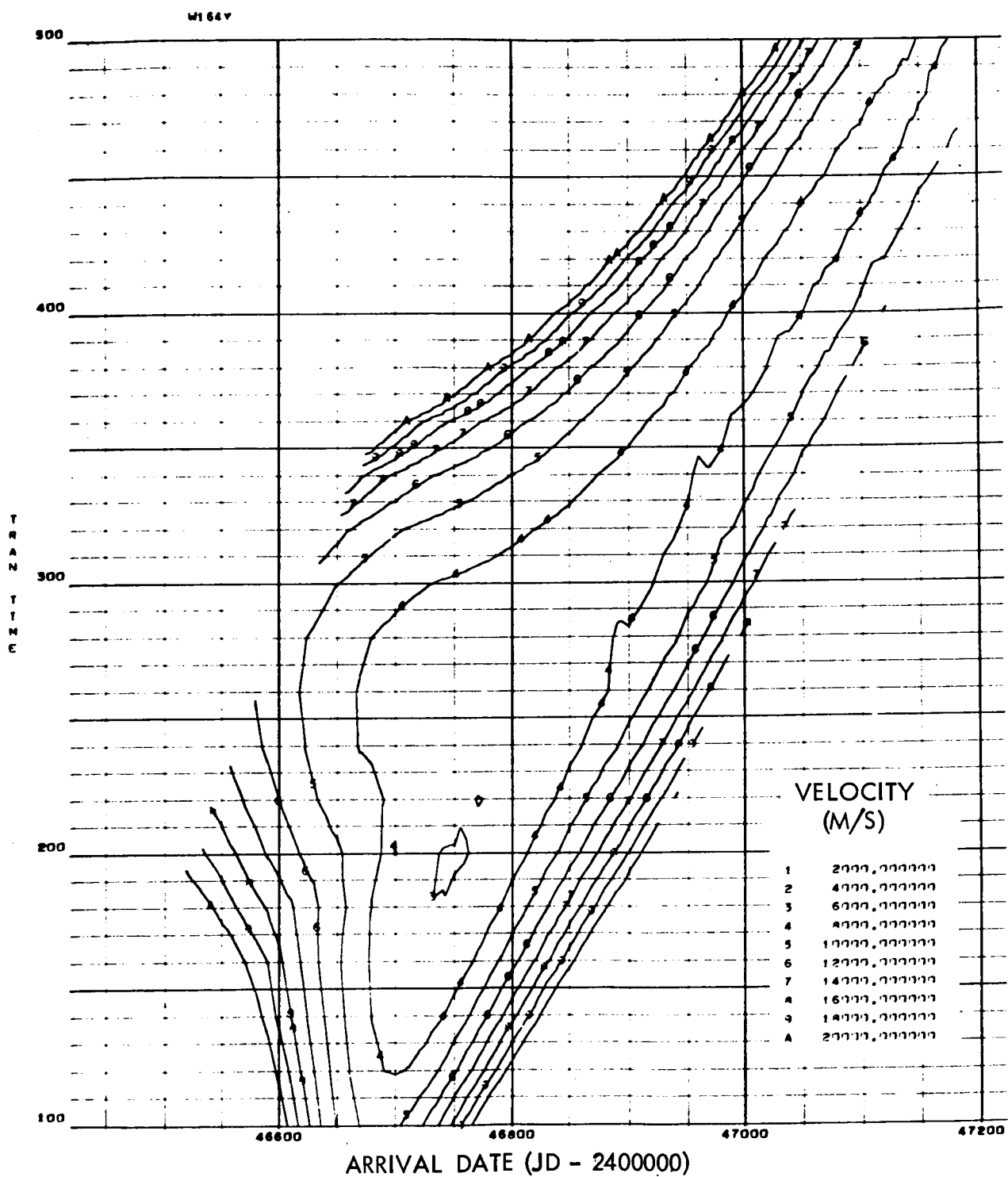ARRIVAL DATE (JD - 2400000)

Figure 52. Total Transplanet Velocity Contours (1986 Mars Opposition)

- 94 -

Figure 53. Trans-Earth Velocity Requirements (1986 Mars Opposition)

- 95 -

VELOCITY
(M/S)

1   1000.000000
2   2000.000000
3   3000.000000
4   4000.000000
5   5000.000000
6   6000.000000
7   7000.000000
8   8000.000000
9   9000.000000
A   10000.000000

LAUNCH DATE (JD - 2400000)

Figure 54. Total Trans-Earth Velocity Contours (1986 Mars Opposition)

- 96 -

SD 67-621-2

Figure 55. Transplanet Velocity Requirements (1988 Mars Opposition)

Figure 56.   Total Transplanet Velocity Requirements
(1988 Mars Opposition)

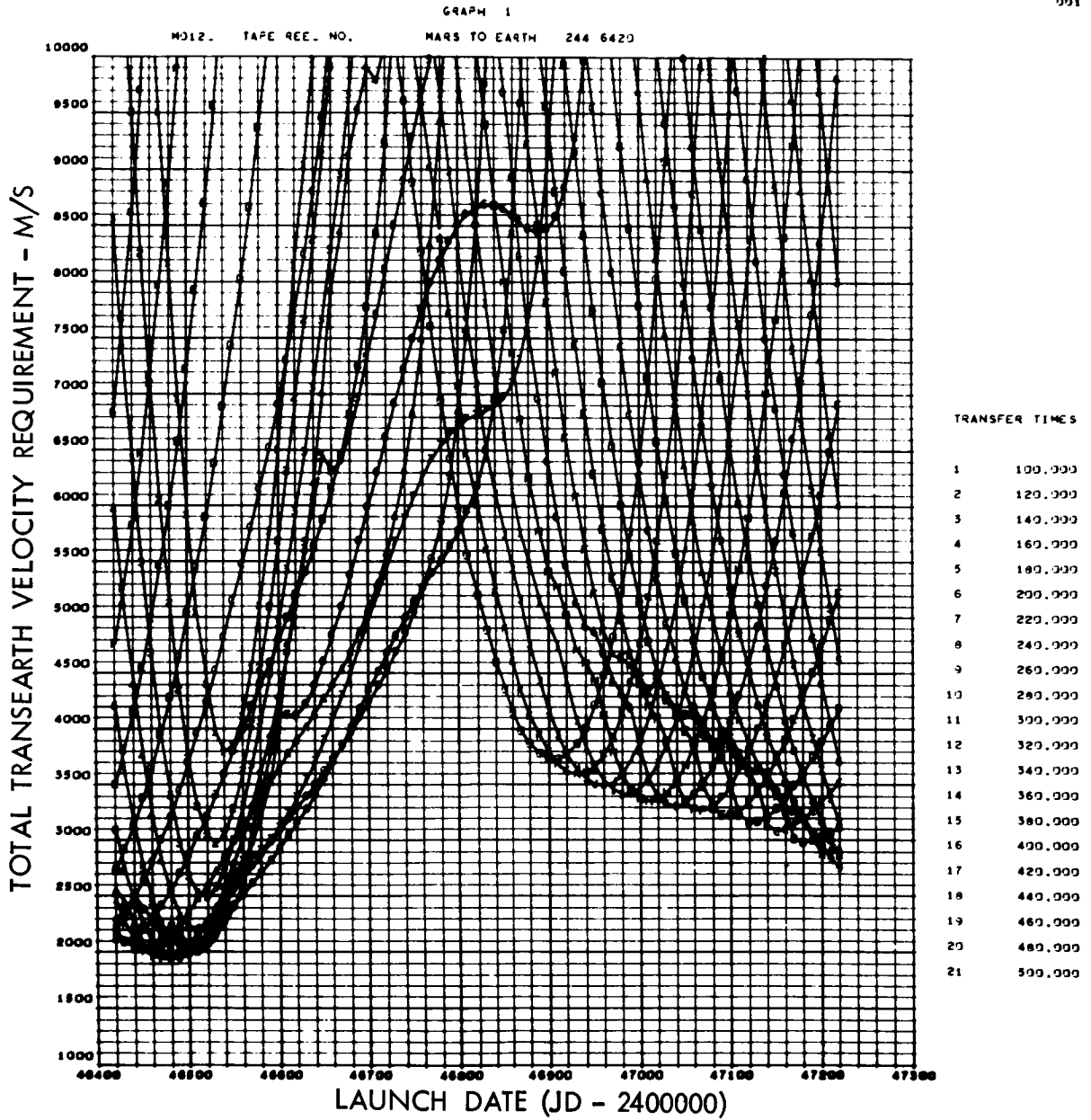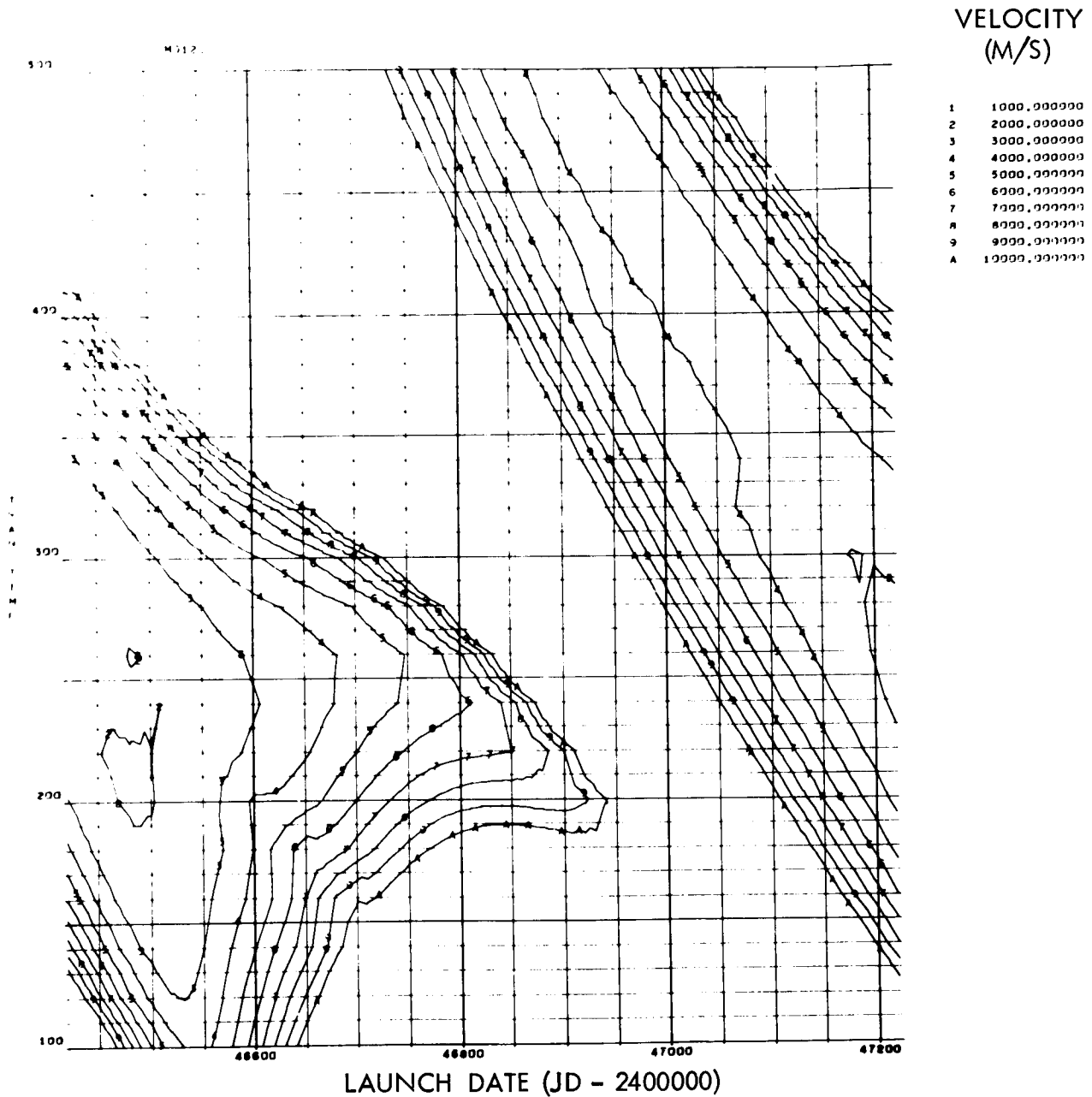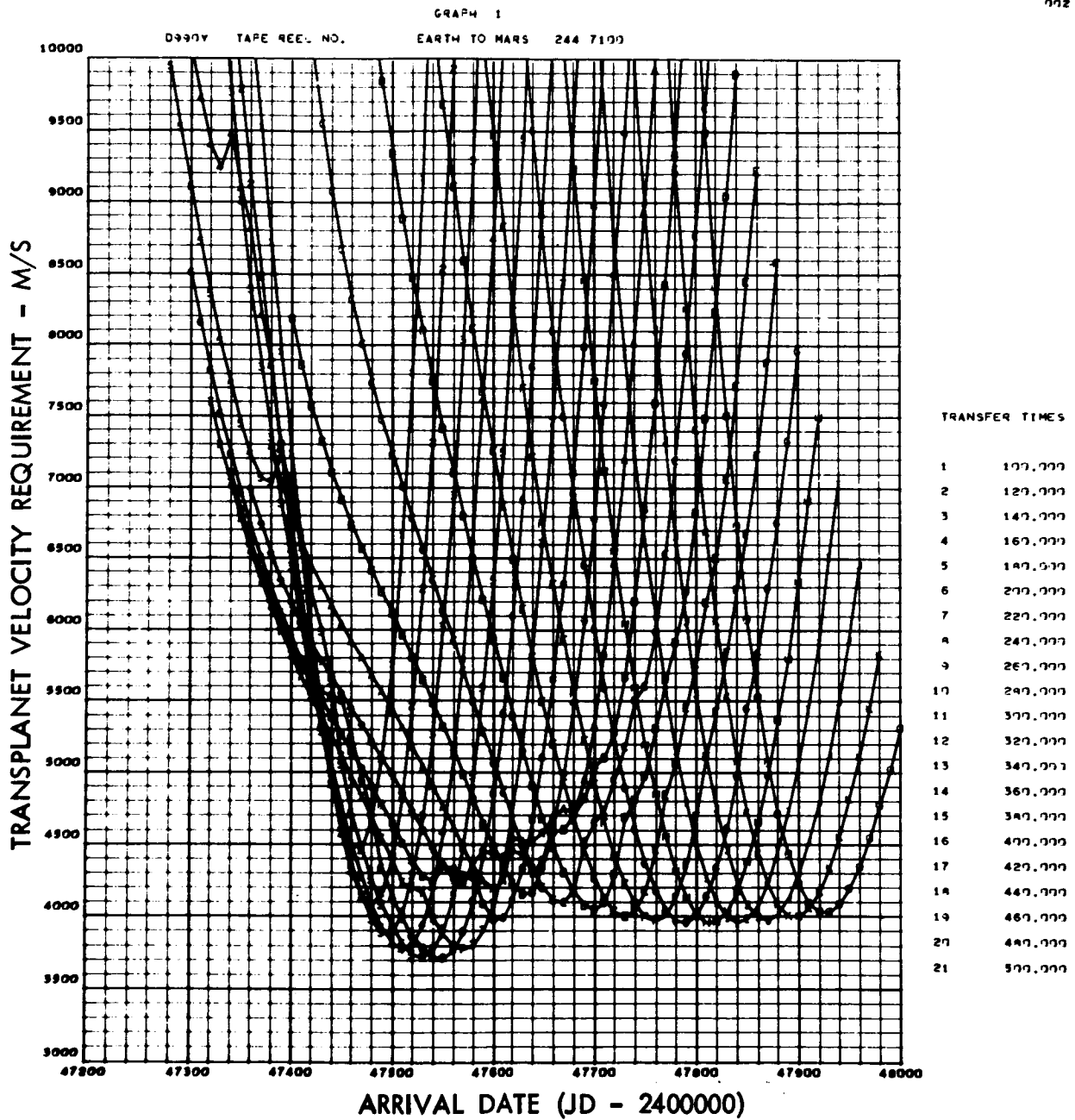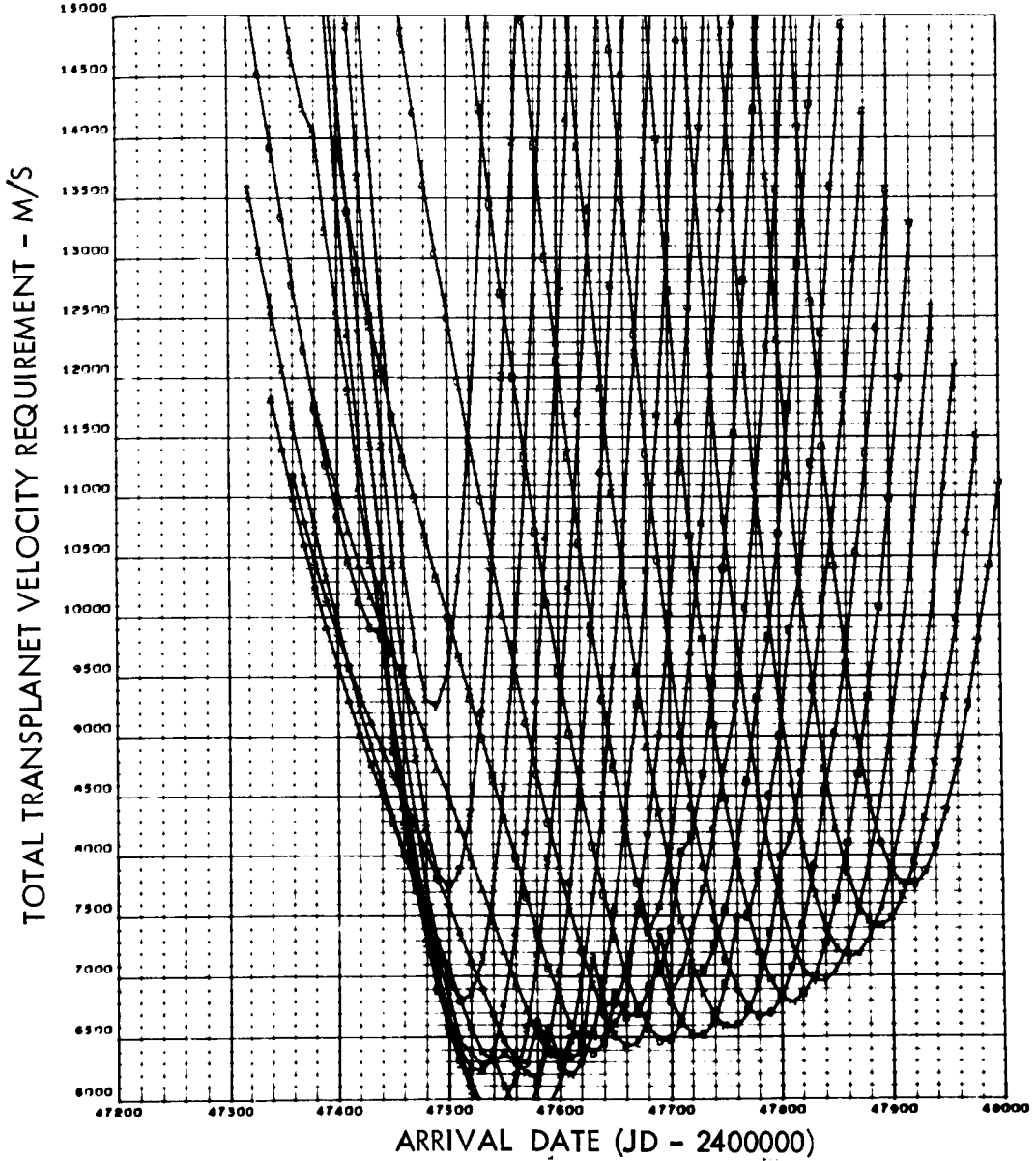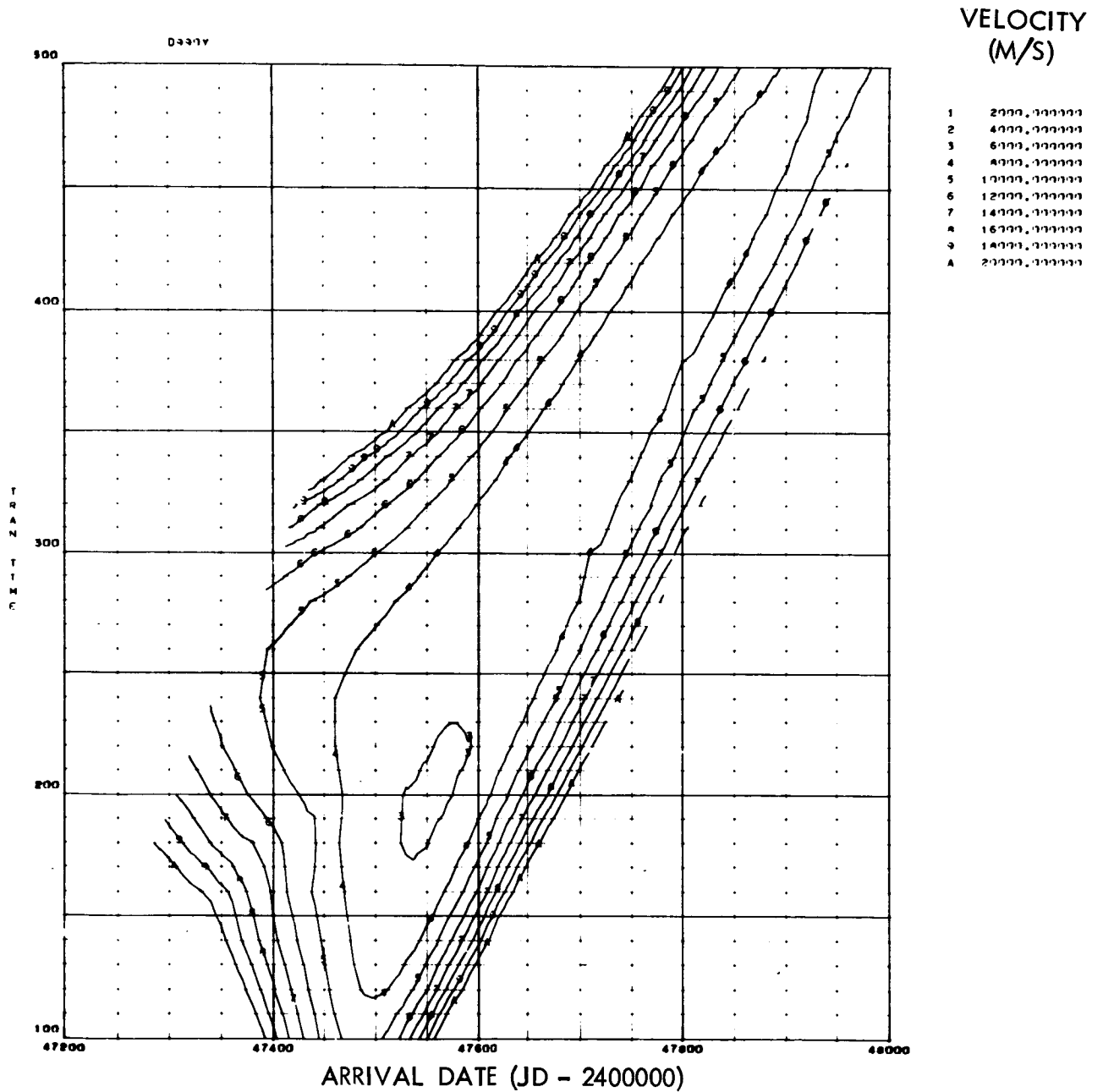Figure 57. Total Transplanet Velocity Contours
(1988 Mars Opposition)

- 99 -

SD 67-621-2
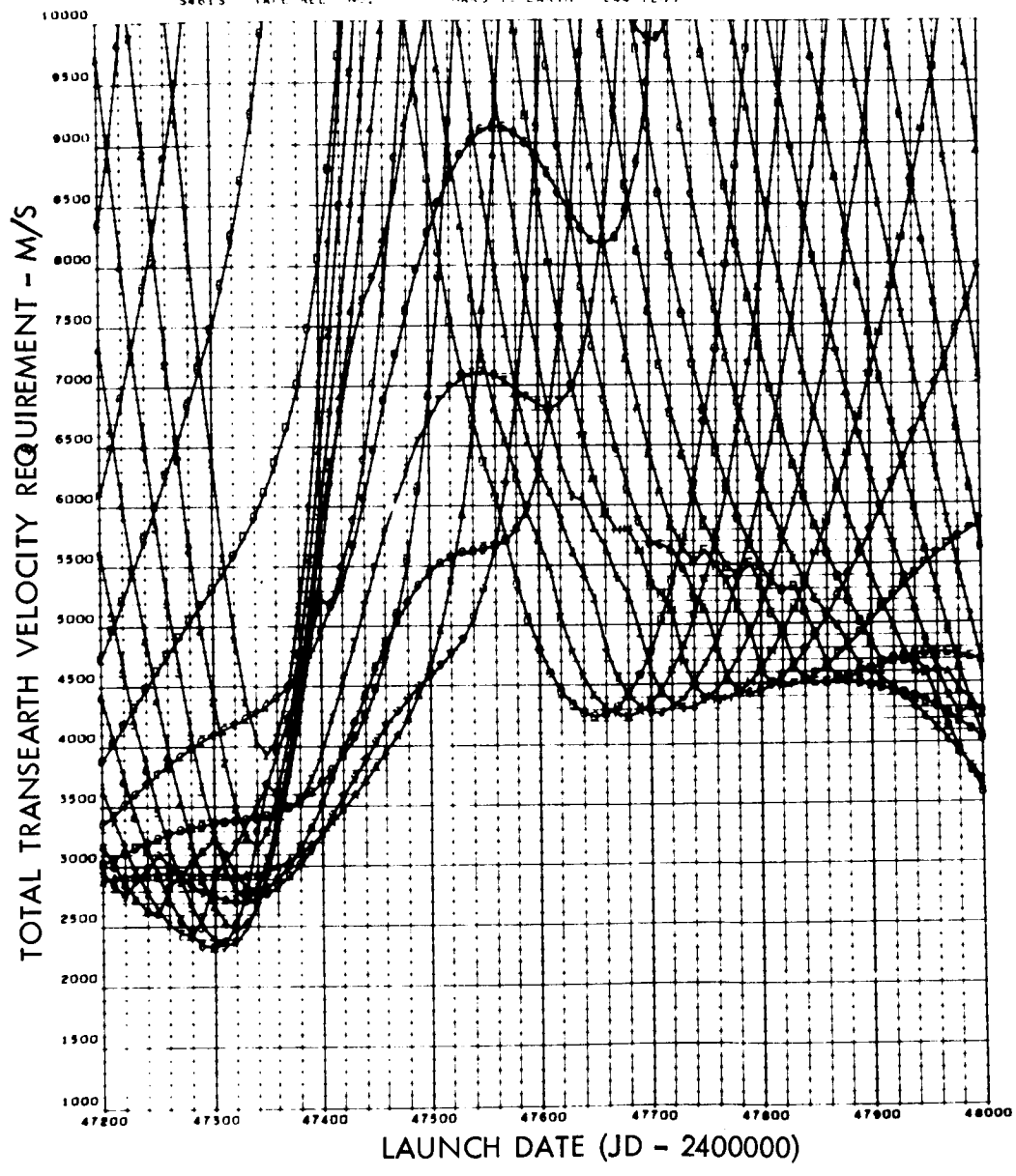
Figure 58. Total Trans-Earth Velocity Requirements
(1988 Mars Opposition)

- 100 -

SD 67-621-2

VELOCITY
(M/S)

1	1000.000000
2	2000.000000
3	3000.000000
4	4000.000000
5	5000.000000
6	6000.000000
7	7000.000000
8	8000.000000
9	9000.000000
A	10000.000000

LAUNCH DATE (JD - 2400000)

Figure 59. Total Trans-Earth Velocity Contours
(1988 Mars Opposition)

GRAPH 1

T032V   TAPE REEL NO.   EARTH TO MARS   244 8660

TRANSPLANET VELOCITY REQUIREMENT – M/S

TRANSFER TIMES

1	100.000
2	120.000
3	140.000
4	160.000
5	180.000
6	200.000
7	220.000
8	240.000
9	260.000
10	280.000
11	300.000
12	320.000
13	340.000
14	360.000
15	380.000
16	400.000
17	420.000
18	440.000
19	460.000
20	480.000
21	500.000

ARRIVAL DATE (JD – 2400000)
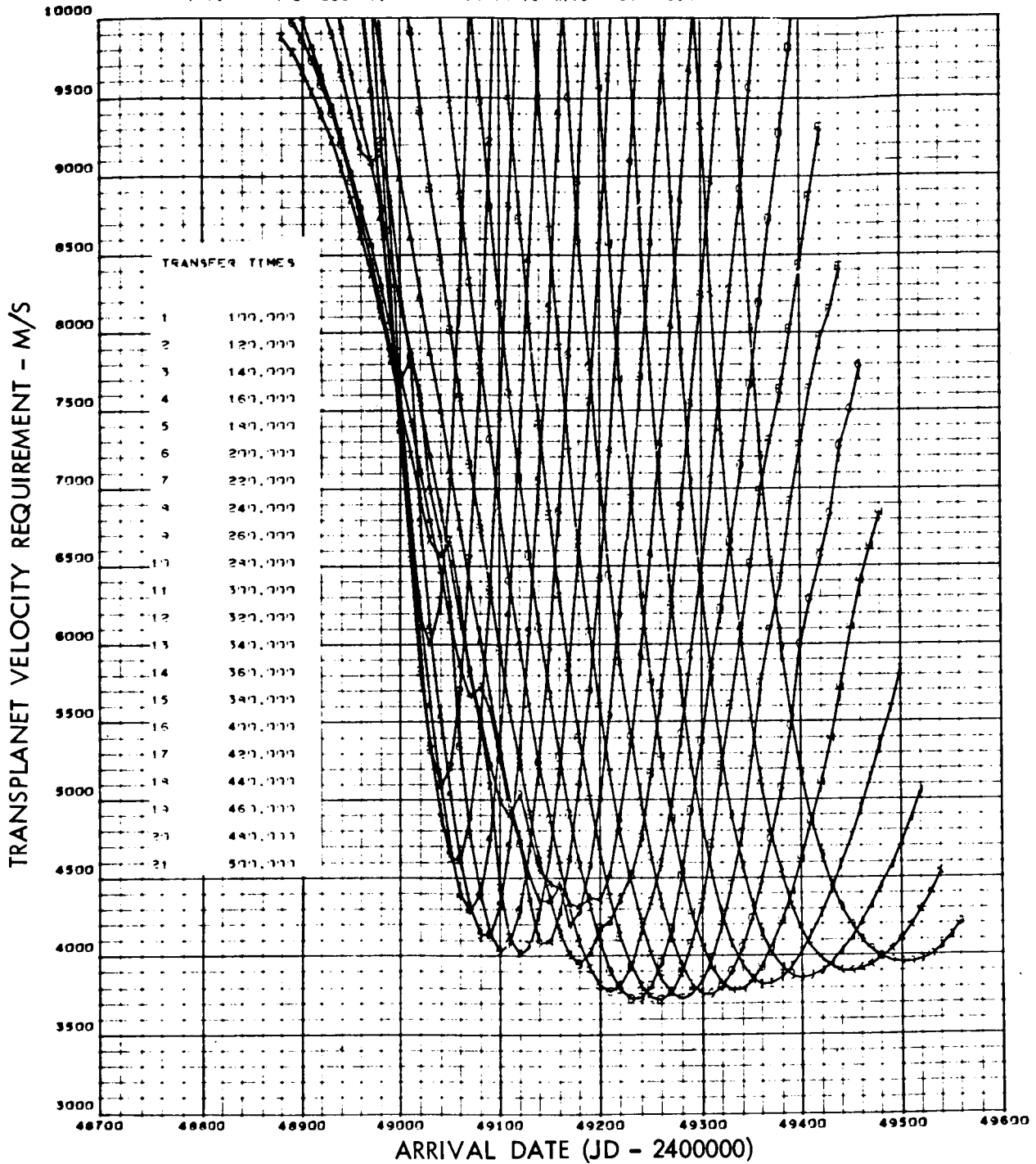
Figure 60. Transplanet Velocity Requirements
(1993 Mars Opposition)

- 102 -

SD 67-621-2

Figure 61. Total Transplanet Velocity Requirements
(1993 Mars Opposition)

- 103 -

SD 67-621-2
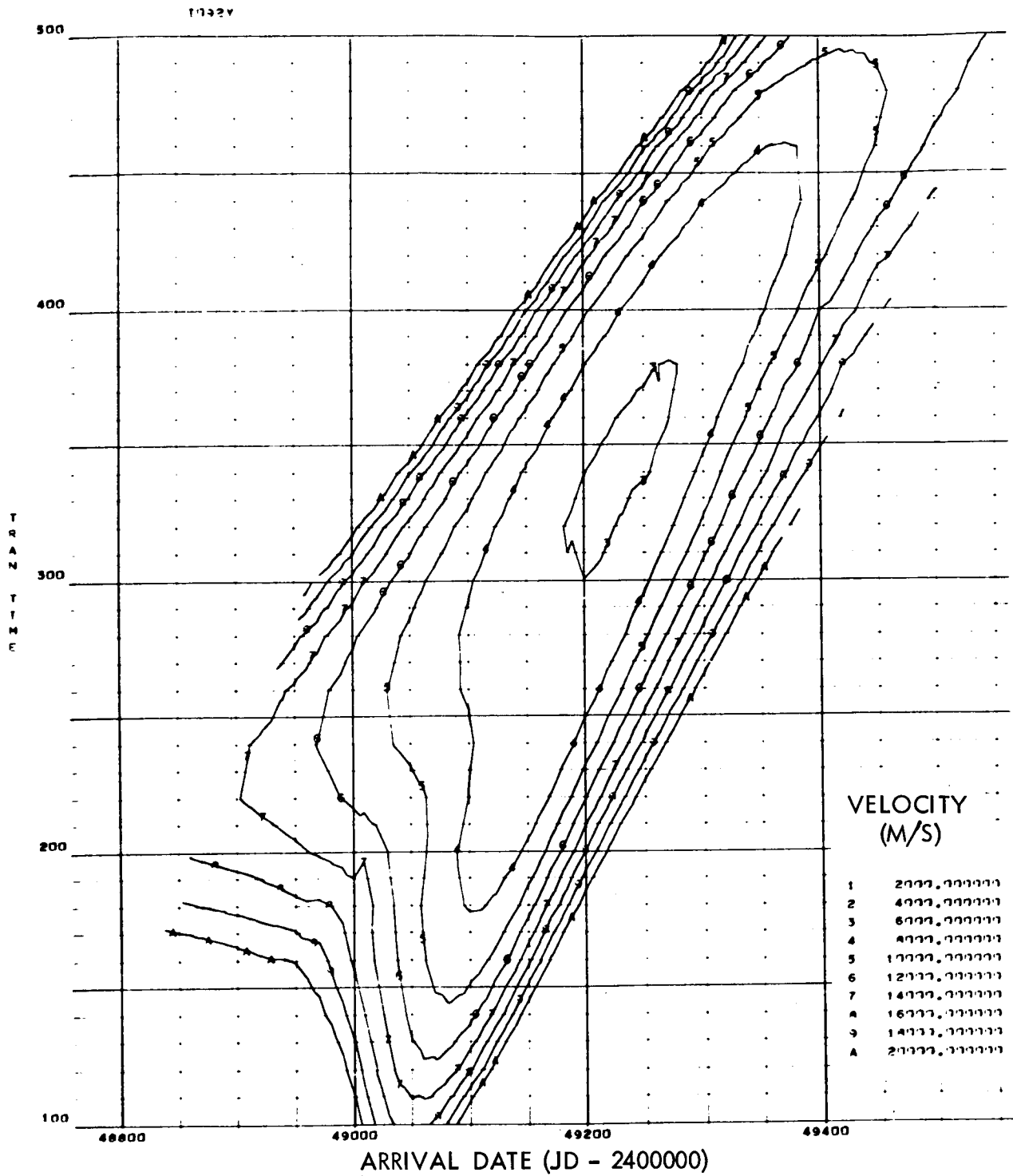
Figure 62. Total Transplanet Velocity Contours
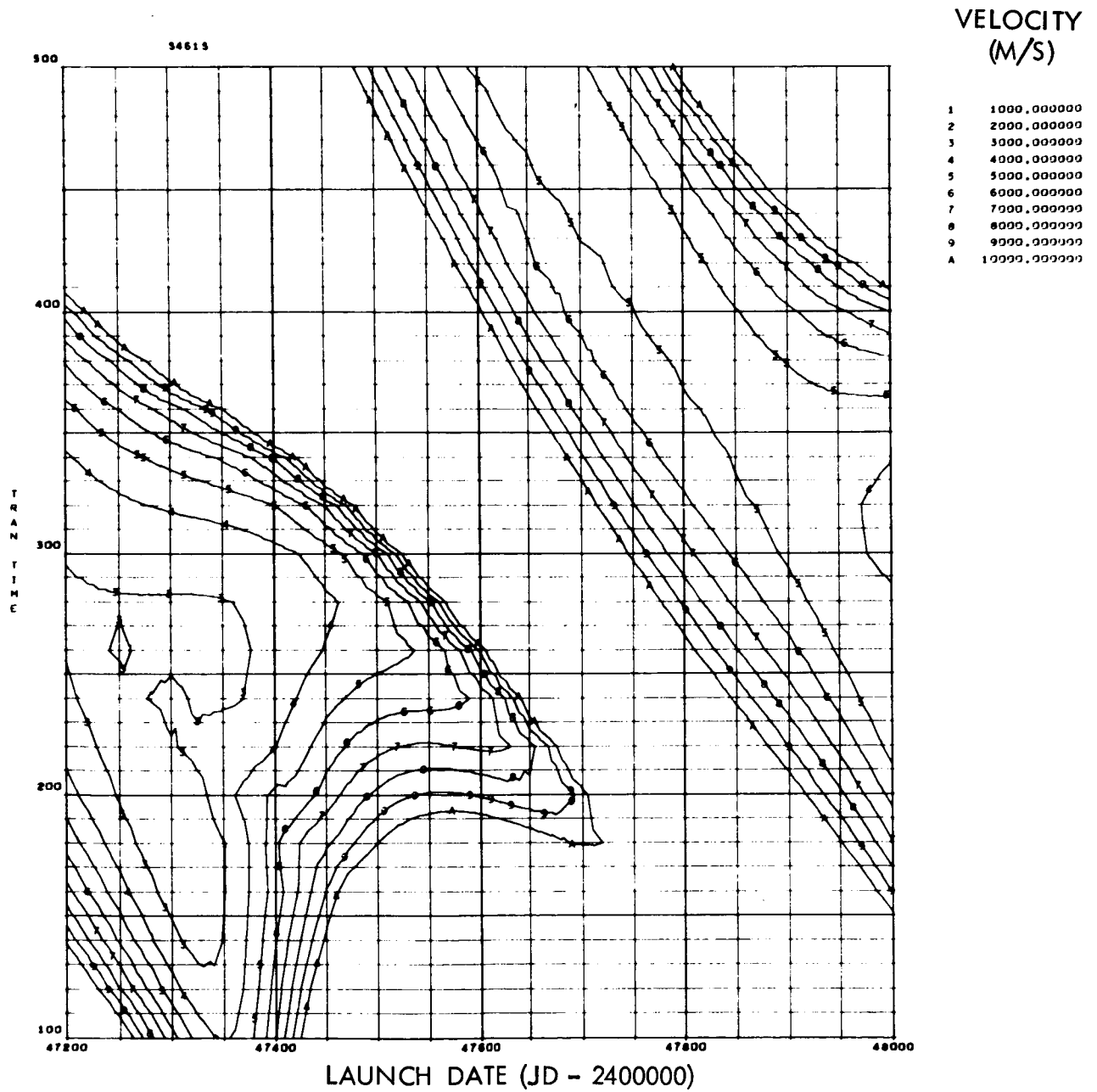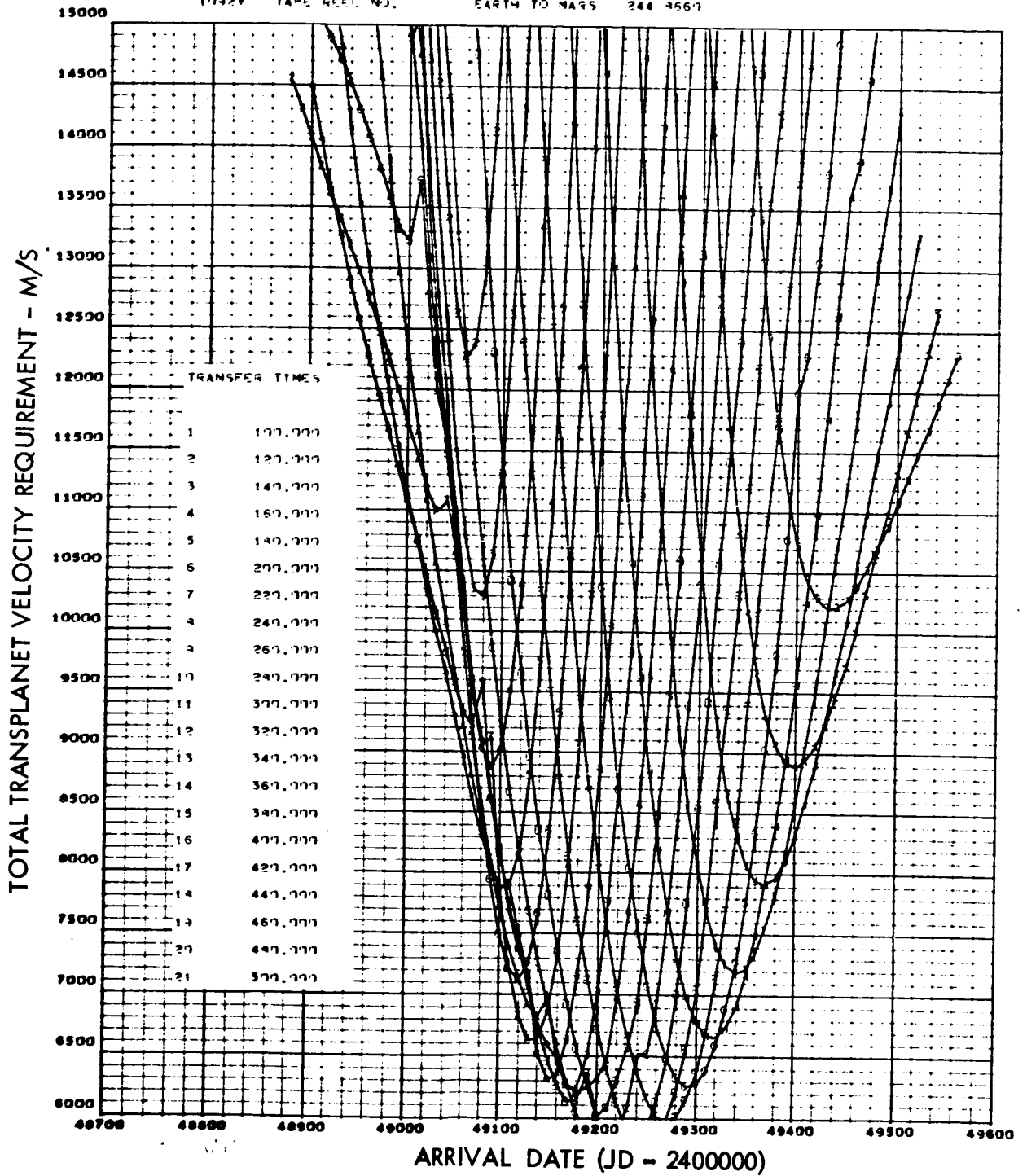(1993 Mars Opposition)

- 104 -
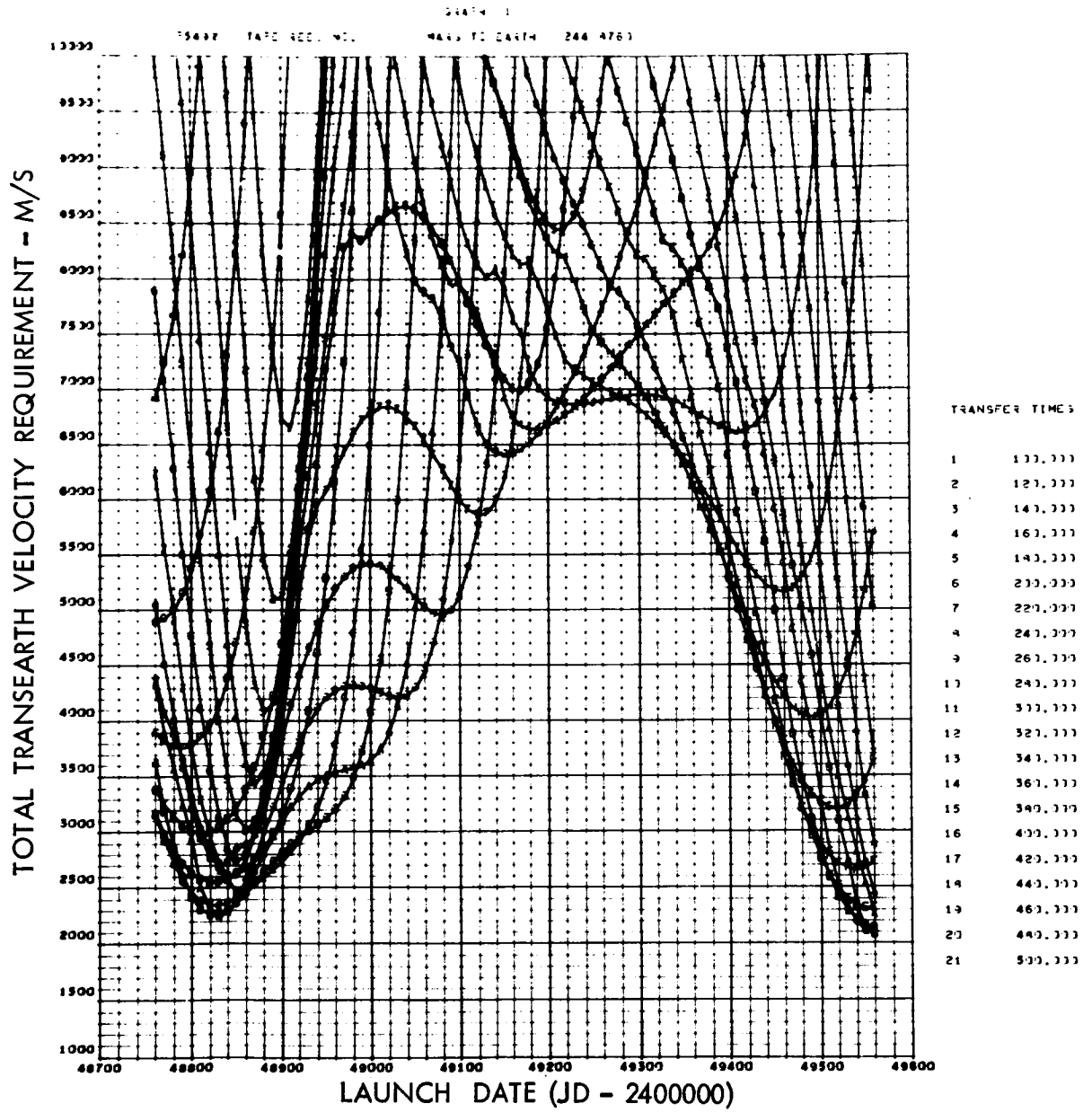
Figure 63. Total Trans-Earth Velocity Requirements
(1993 Mars Opposition)

SD 67-621-2
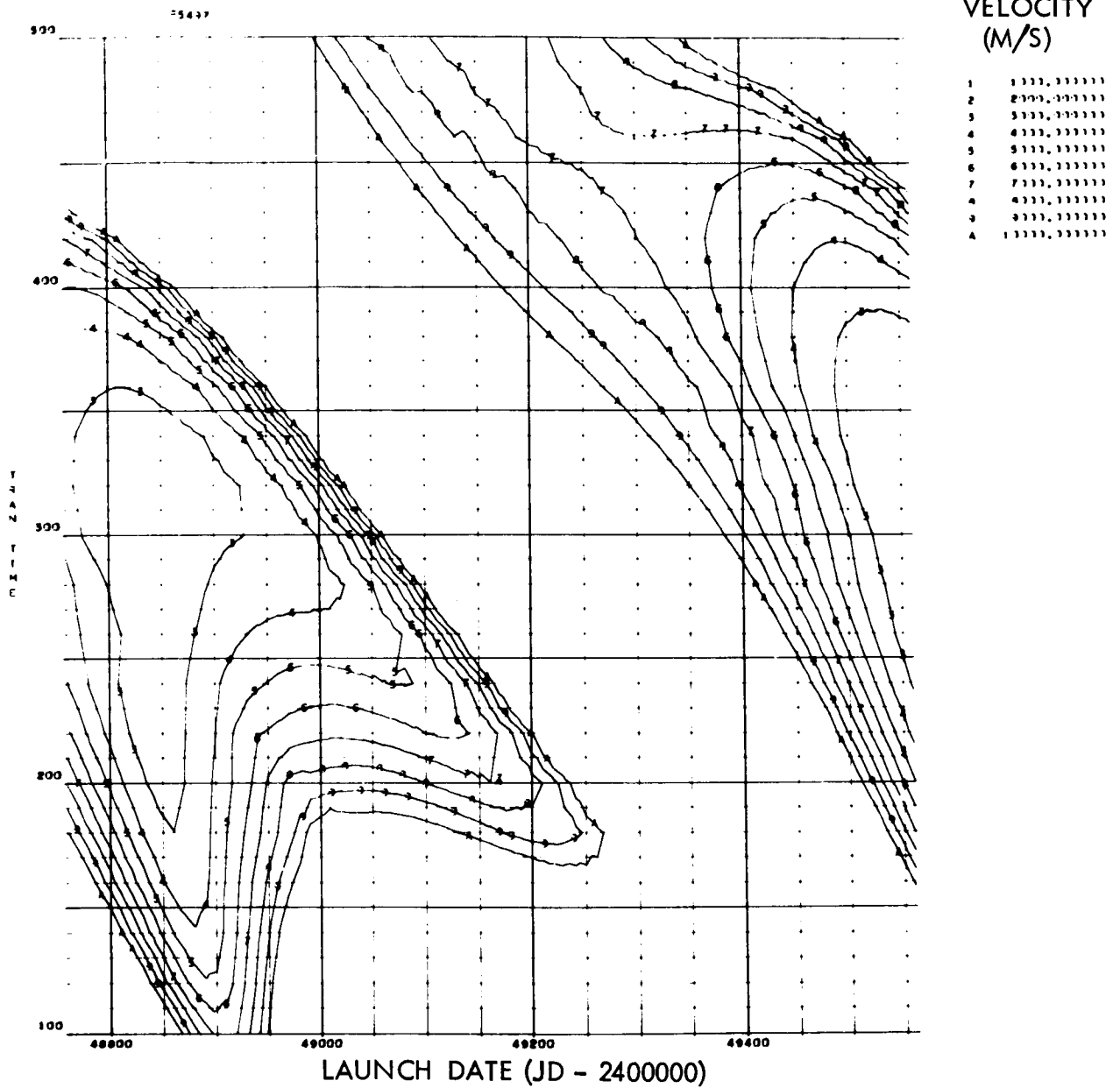
VELOCITY
(M/S)

Figure 64. Total Trans-Earth Velocity Contours
(1993 Mars Opposition)

- 106 -

SD 67-621-2

Figure 65. Velocity Requirements Summary (1986 Mars Opposition)

SD 67-621-2

Figure 66. Total Mars Aerobraker Mission Requirements:
(1986 Mars Opposition)
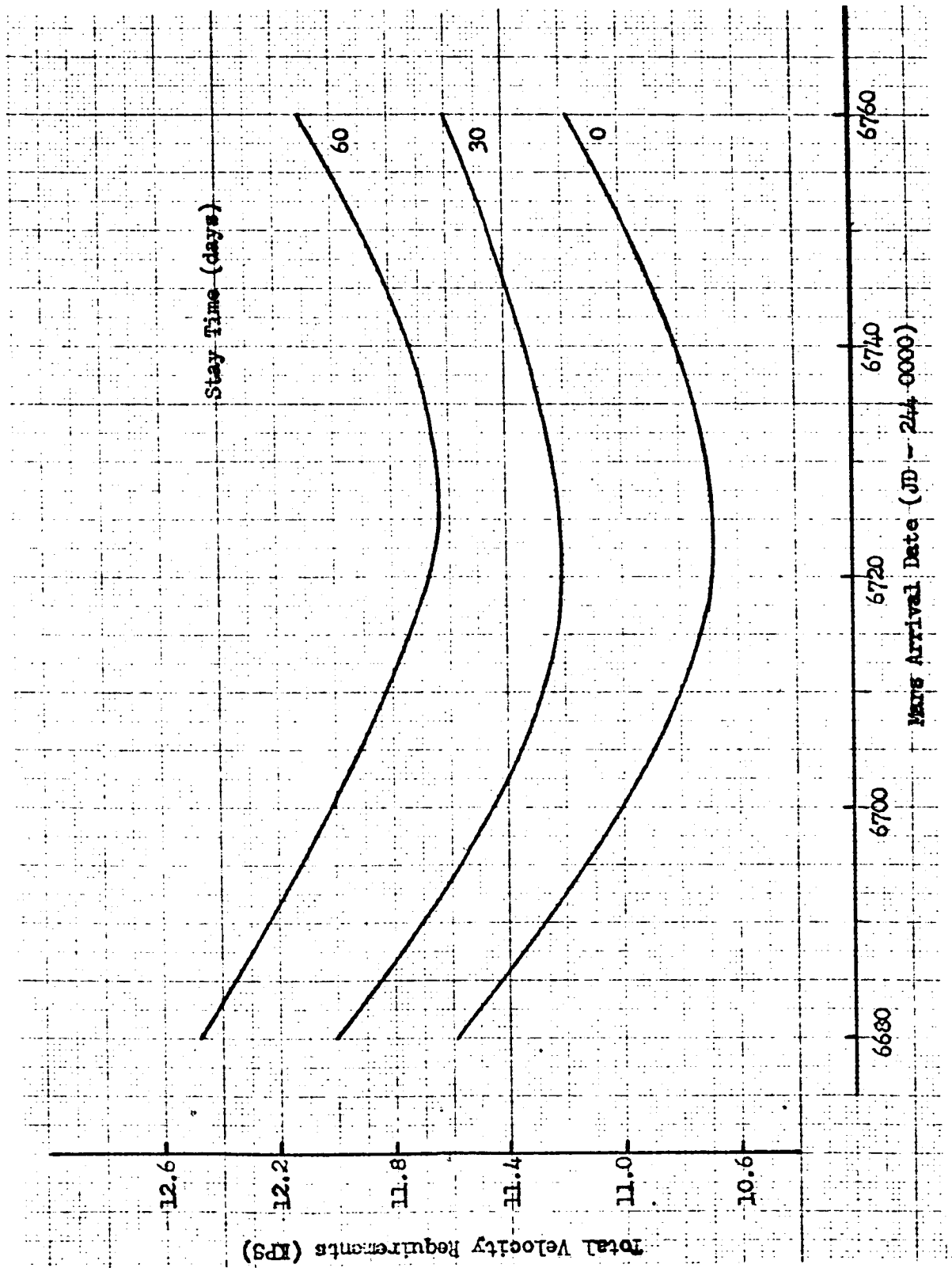
Figure 67. Total Mars Retrobraker Mission Requirements
(1986 Mars Opposition)

SD 67-621-2

Figure 68. Velocity Requirements Summary (1988 Mars Opposition)
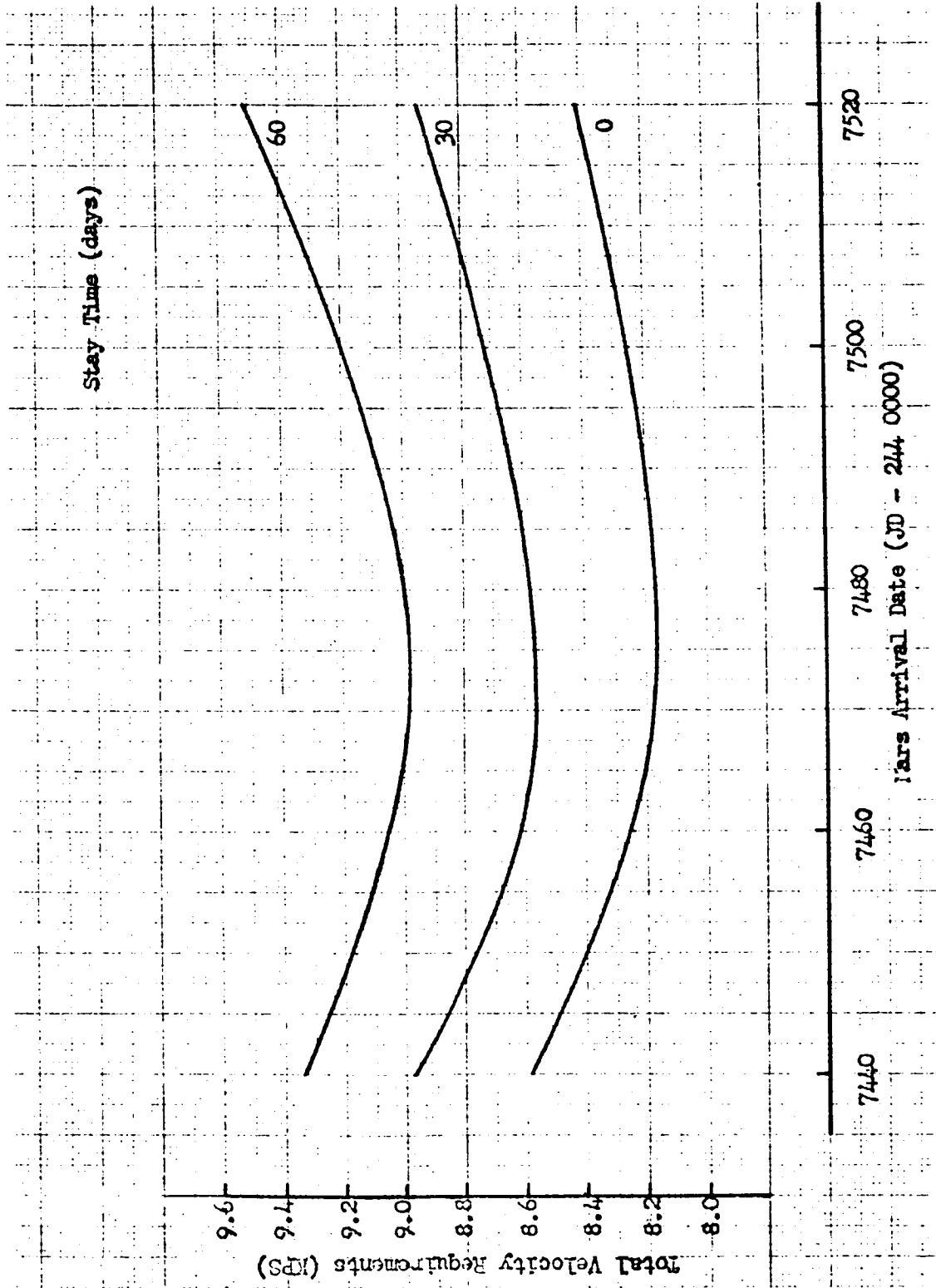
Figure 69.   Total Mars Aerobraker Mission Requirements
(1988 Mars Opposition)

SD 67-621-2
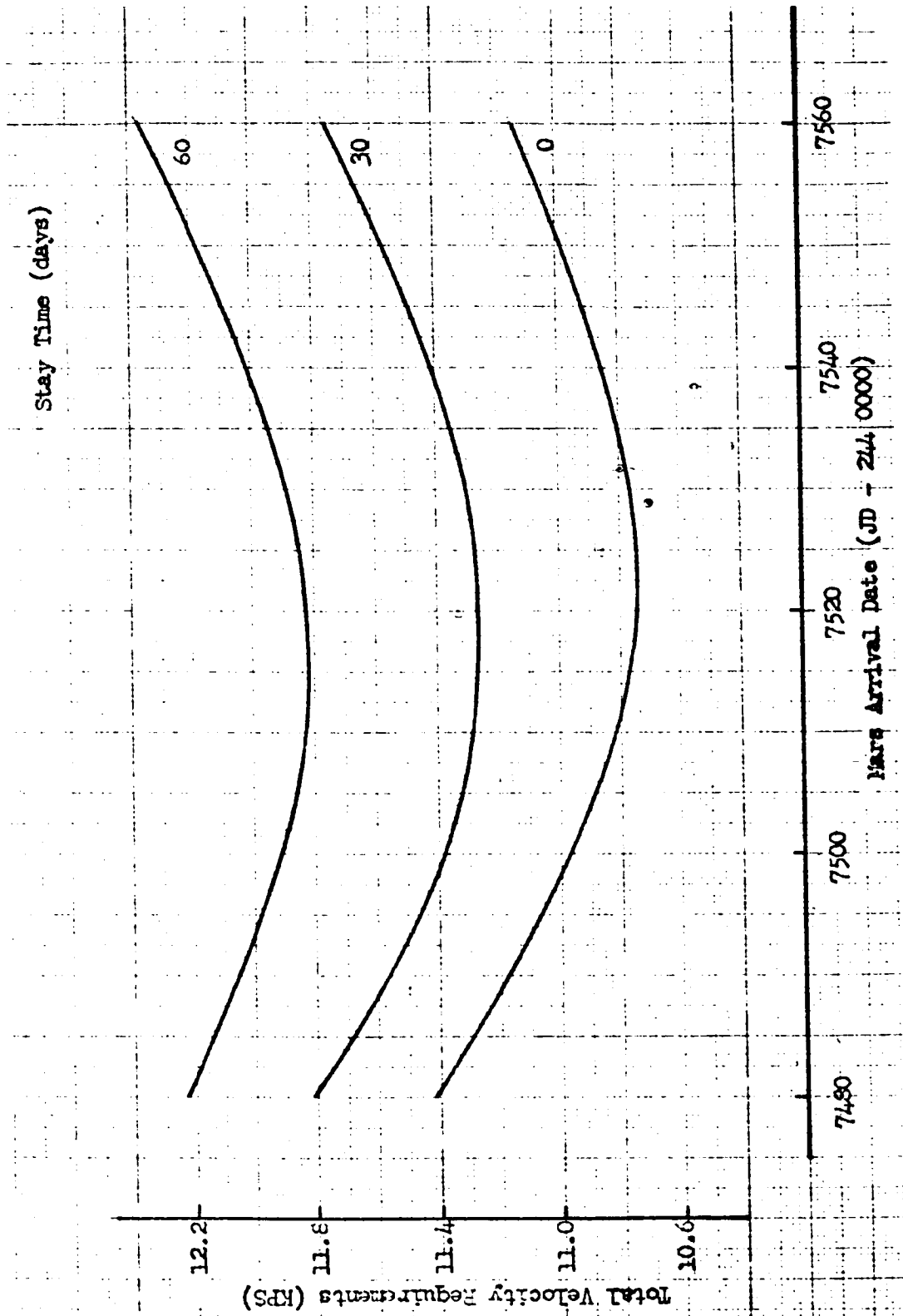
Figure 70. Total Mars Retrobraker Mission Requirements
(1988 Mars Opposition)
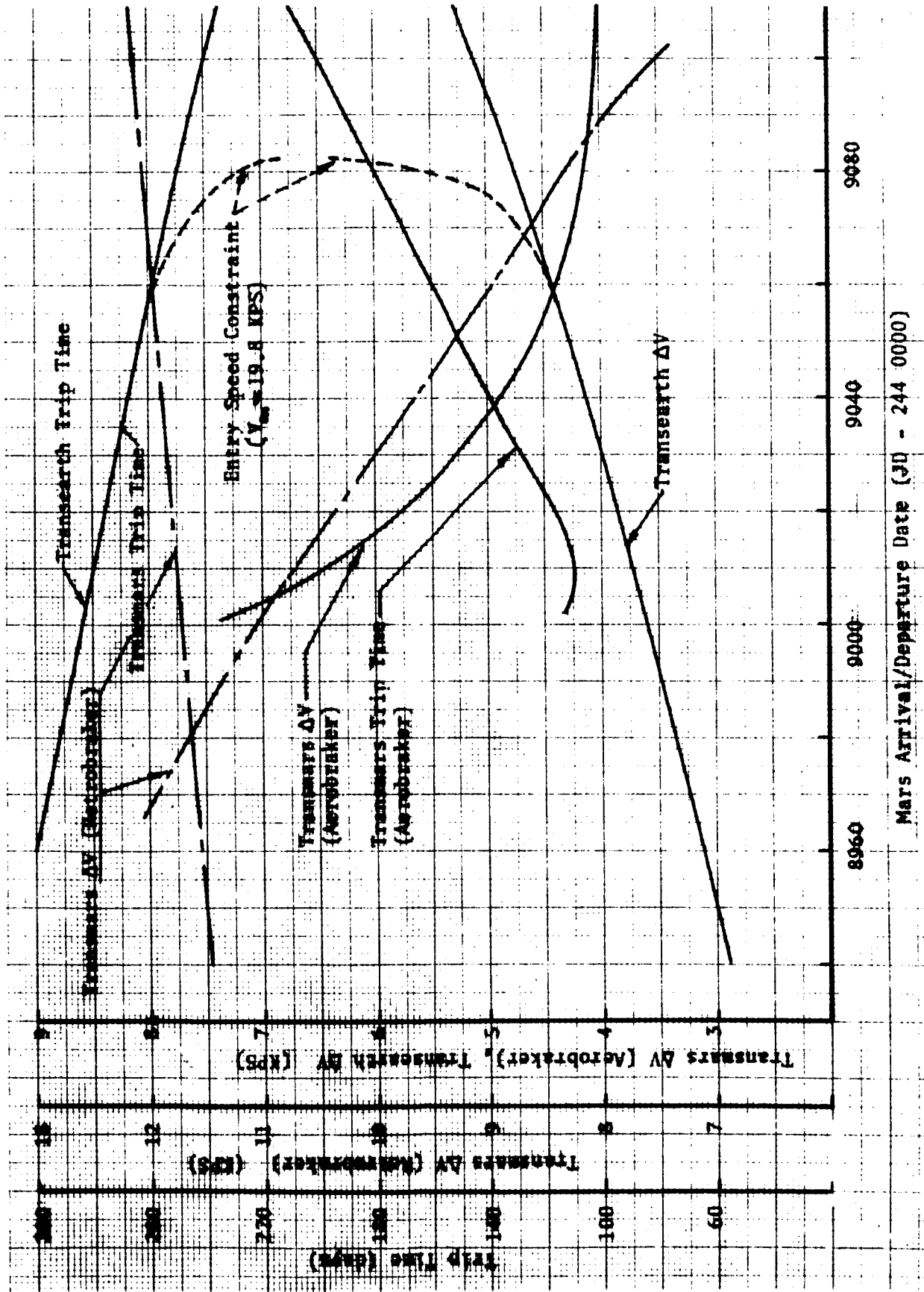
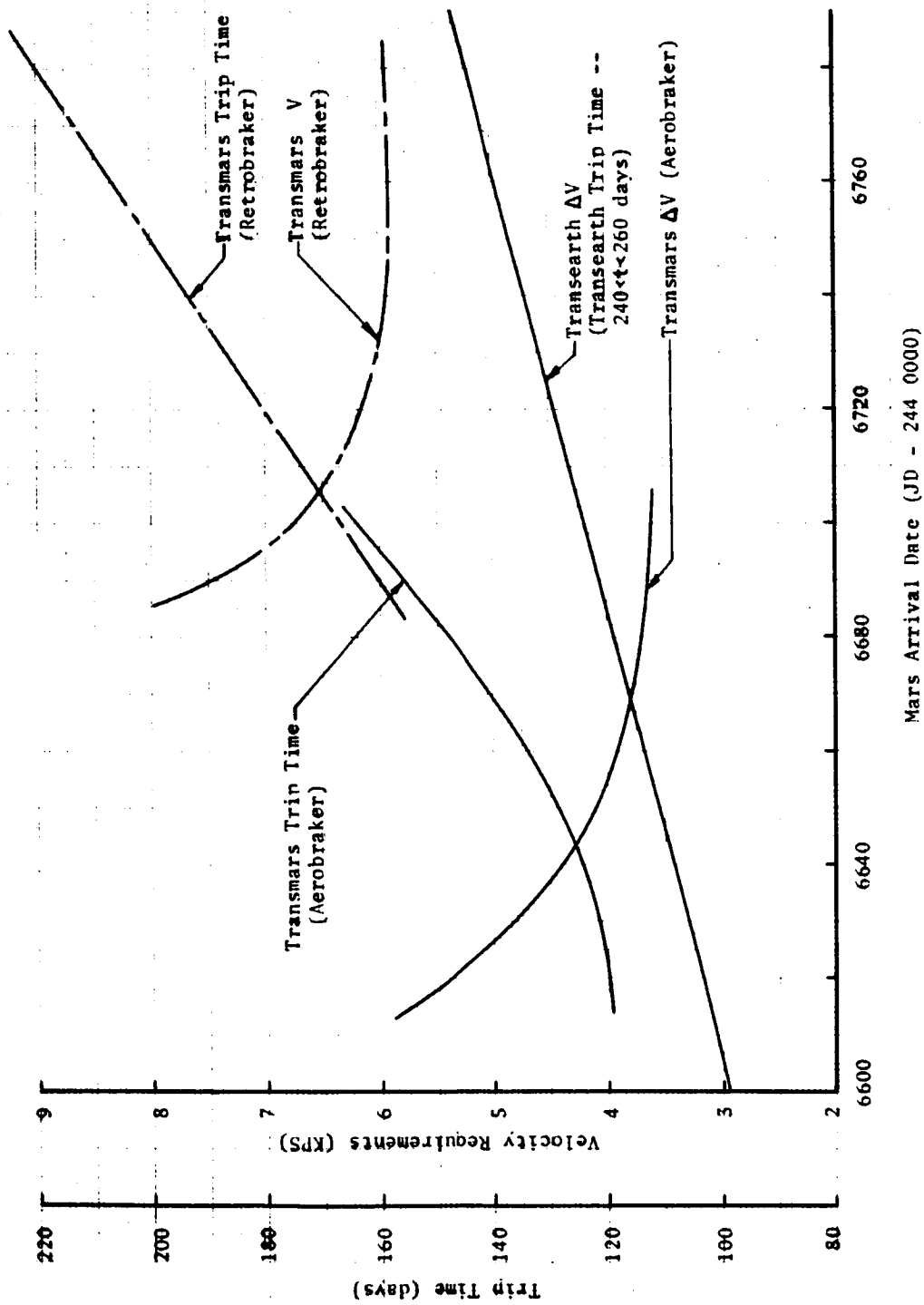Figure 71. Velocity Requirements Summary (1993 Mars Opposition)

SD 67-621-2
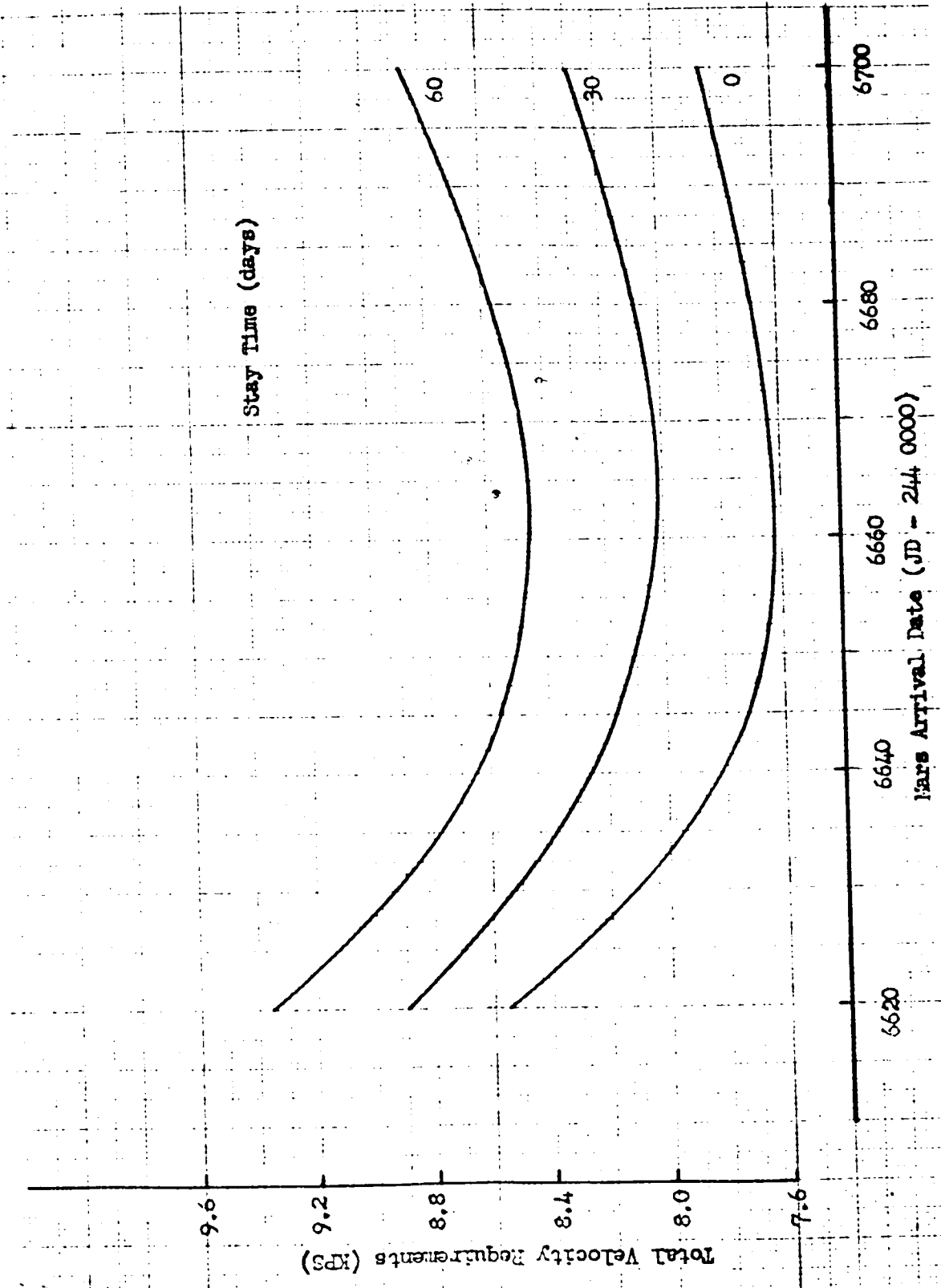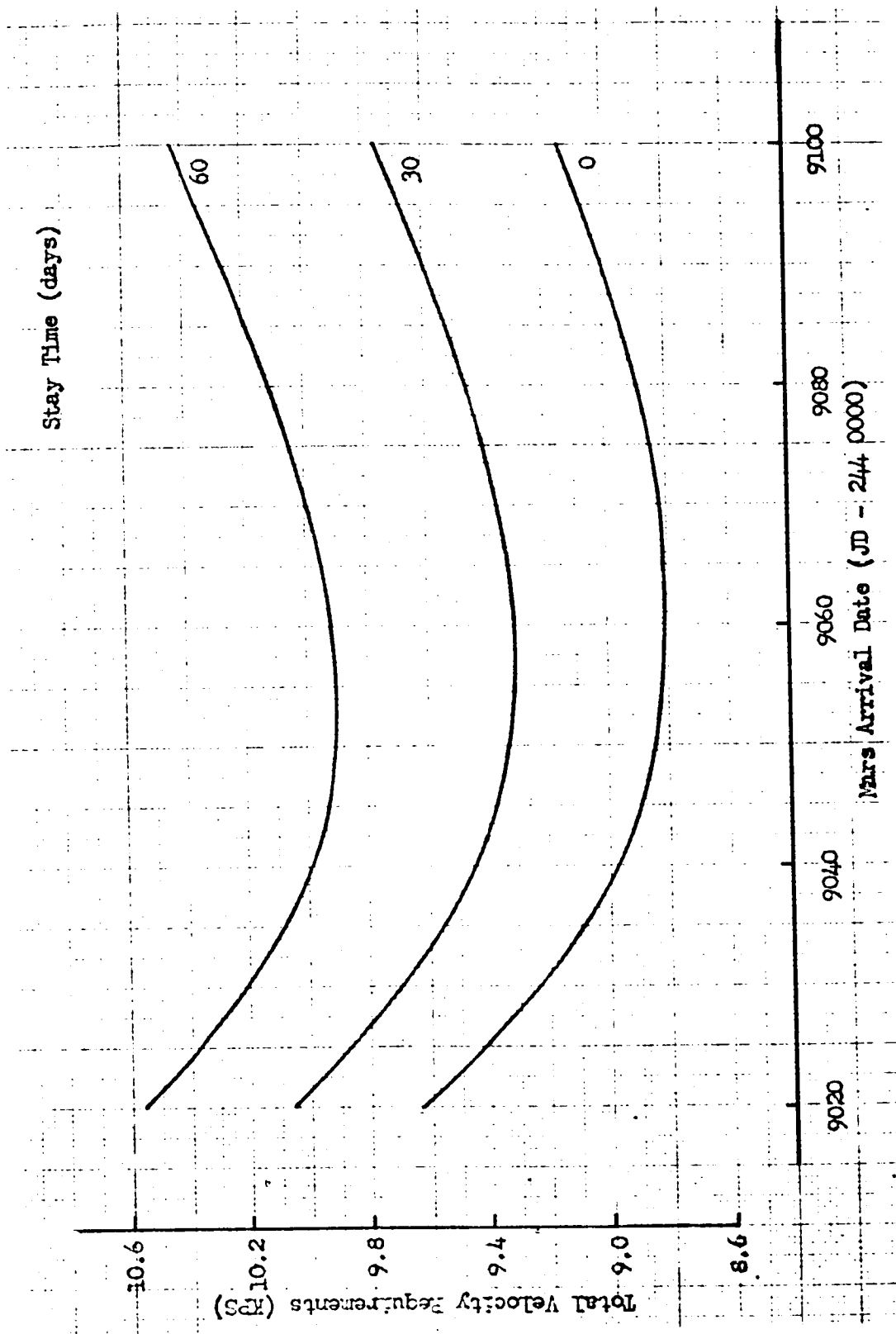
Figure 72.   Total Mars Aerobraker Mission Requirements
(1993 Mars Opposition)
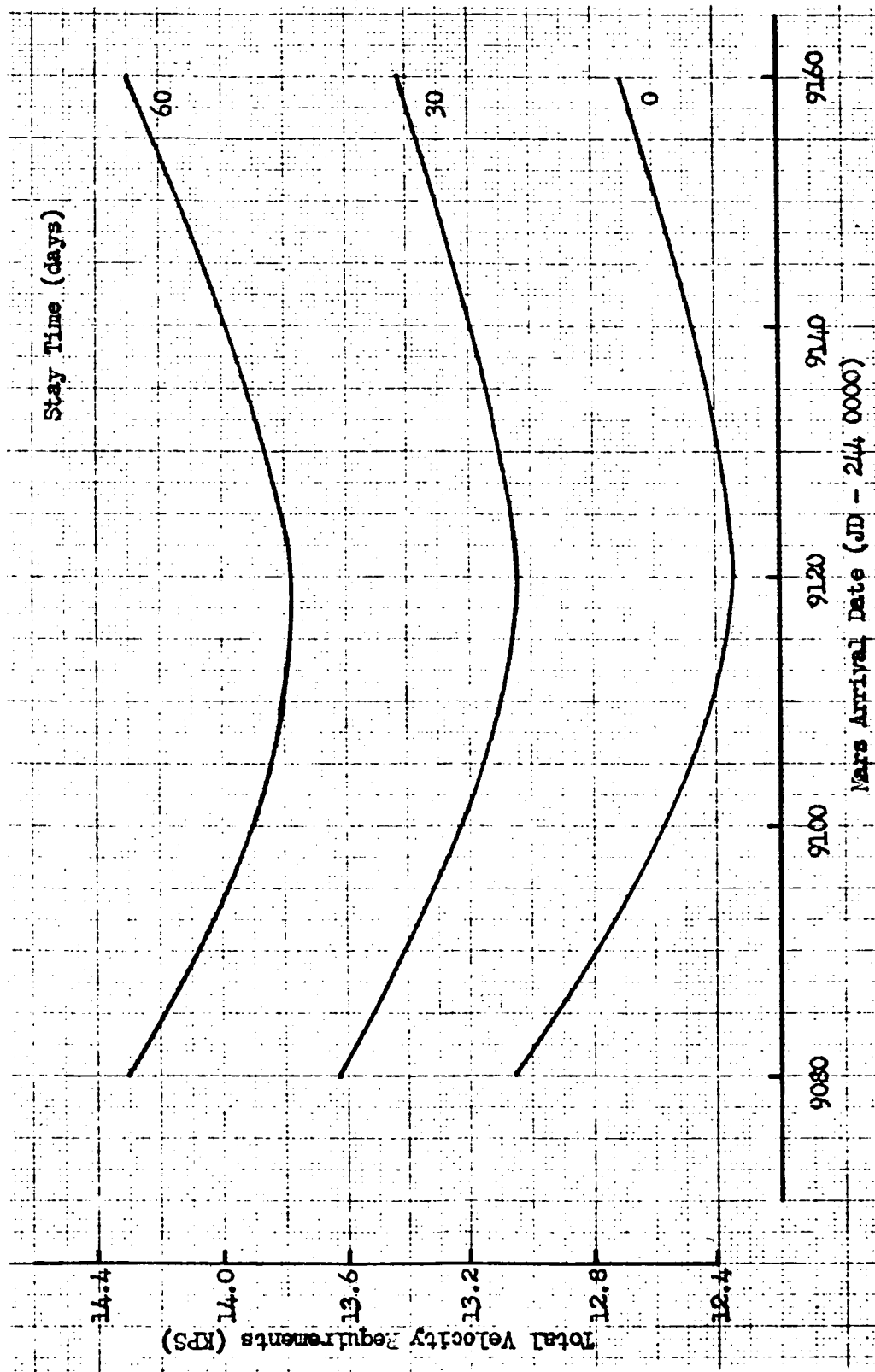
Figure 73. Total Mars Retrobraker Mission Requirements
(1993 Mars Opposition)

SD 67-621-2

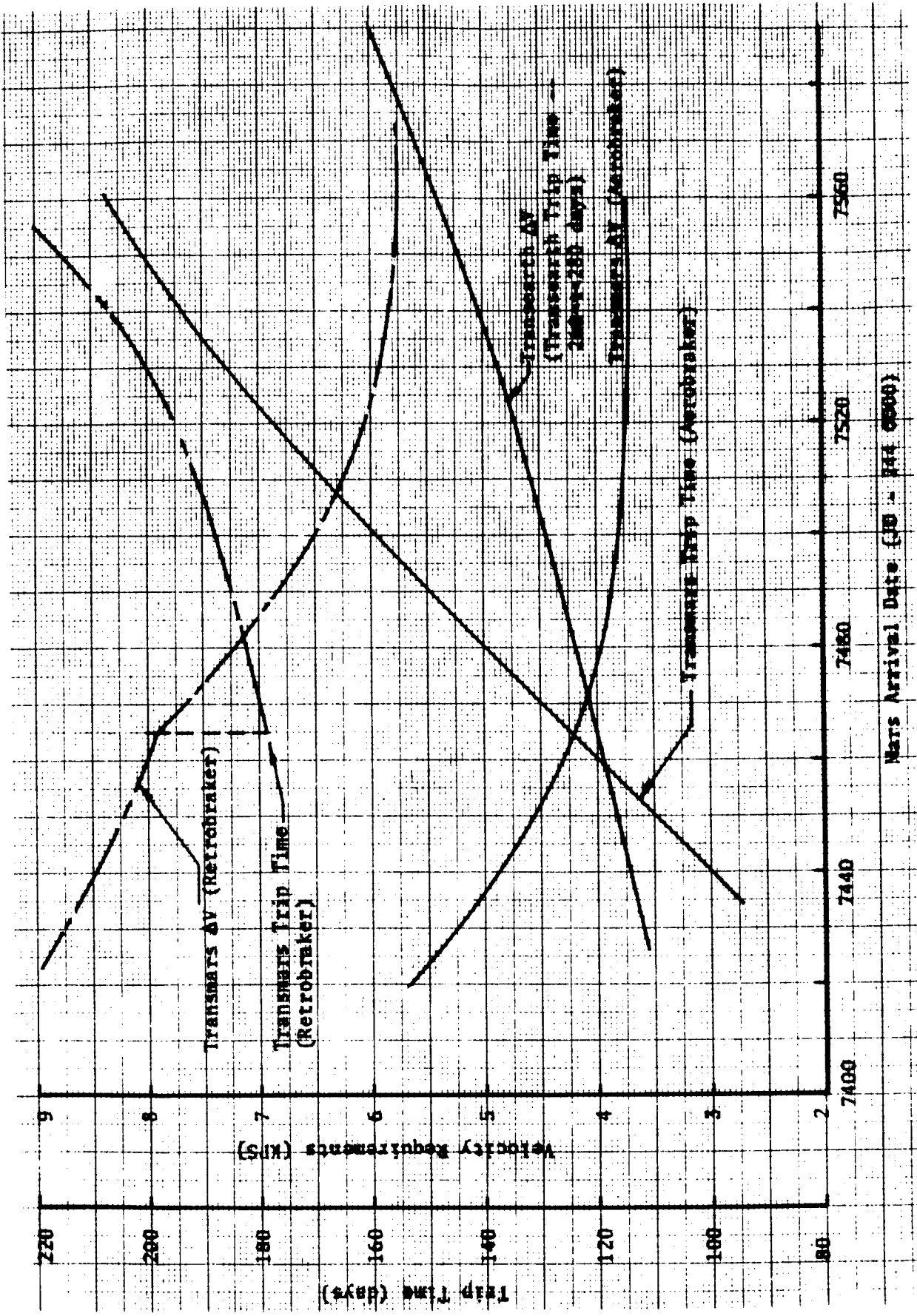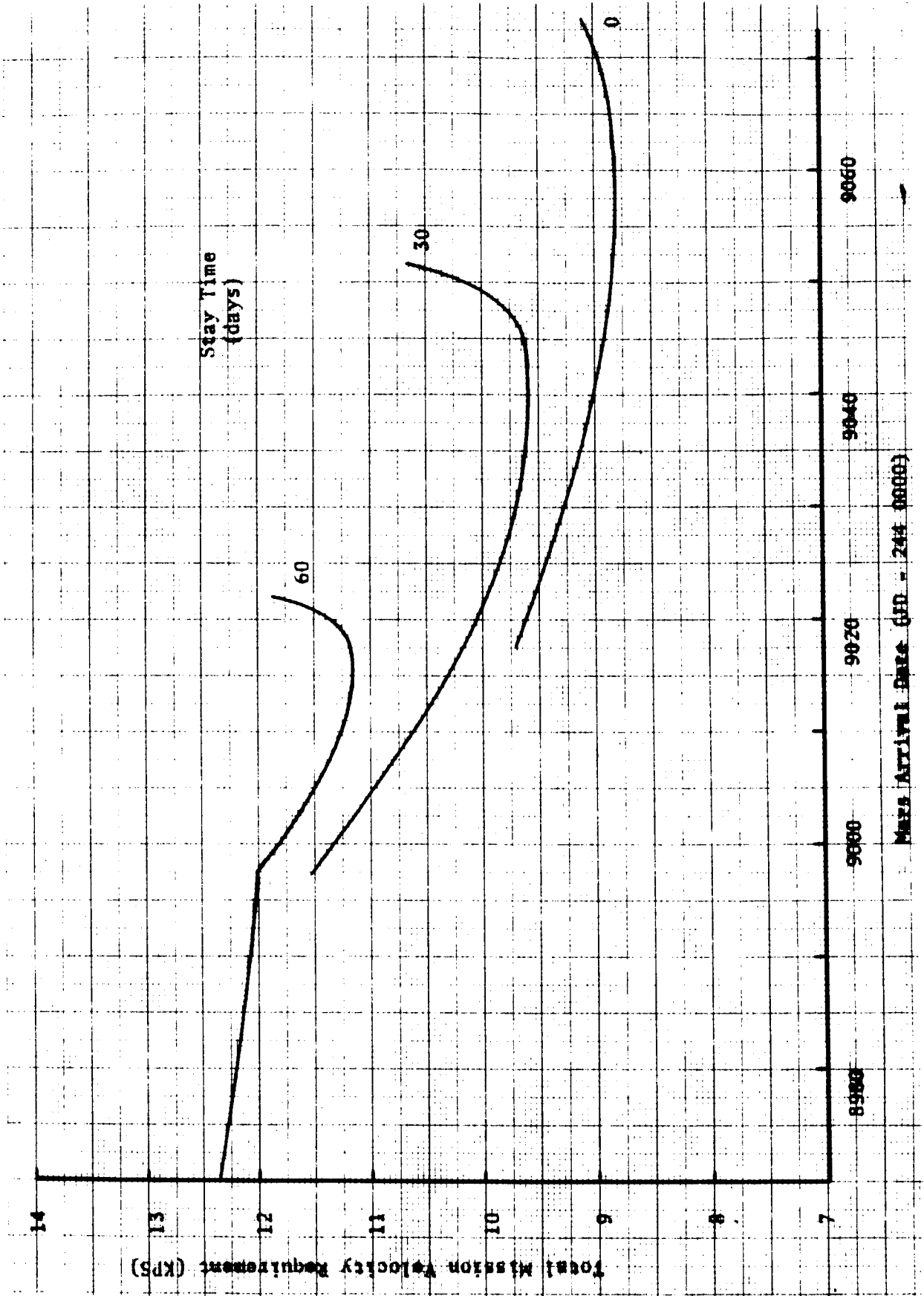Figure 74. Total Mars Aerobraker Mission Requirements (Reentry Velocity = 19.8 km/s, 1993 Mars Opposition)
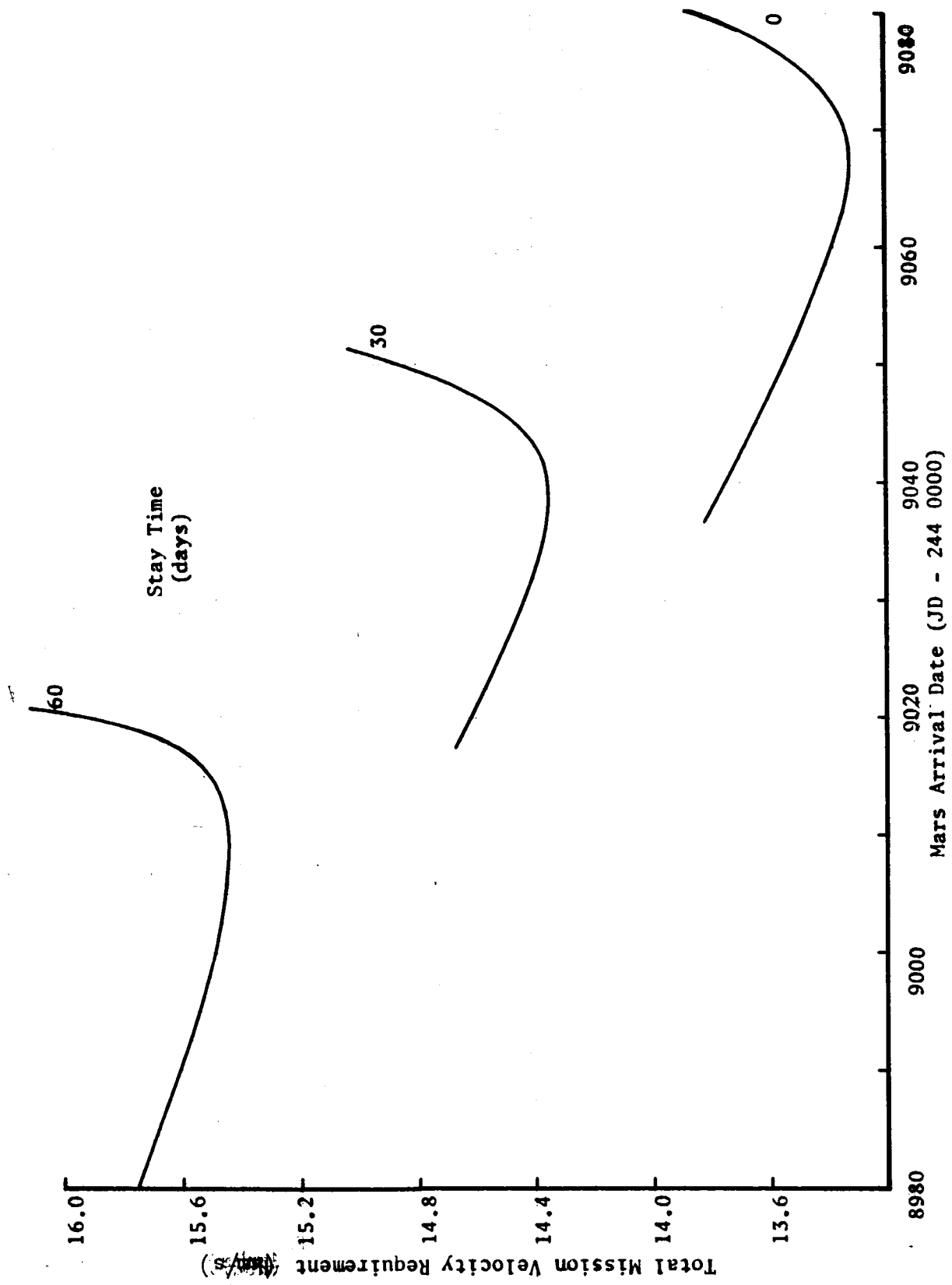
Figure 75. Total Mars Retrobraker Mission Requirements
(Reentry Velocity = 19.8 km/s, 1993 Mars Opposition)

GRAPH 1

X344V   TAPE REEL NO.   EARTH TO VESTA   244 4960
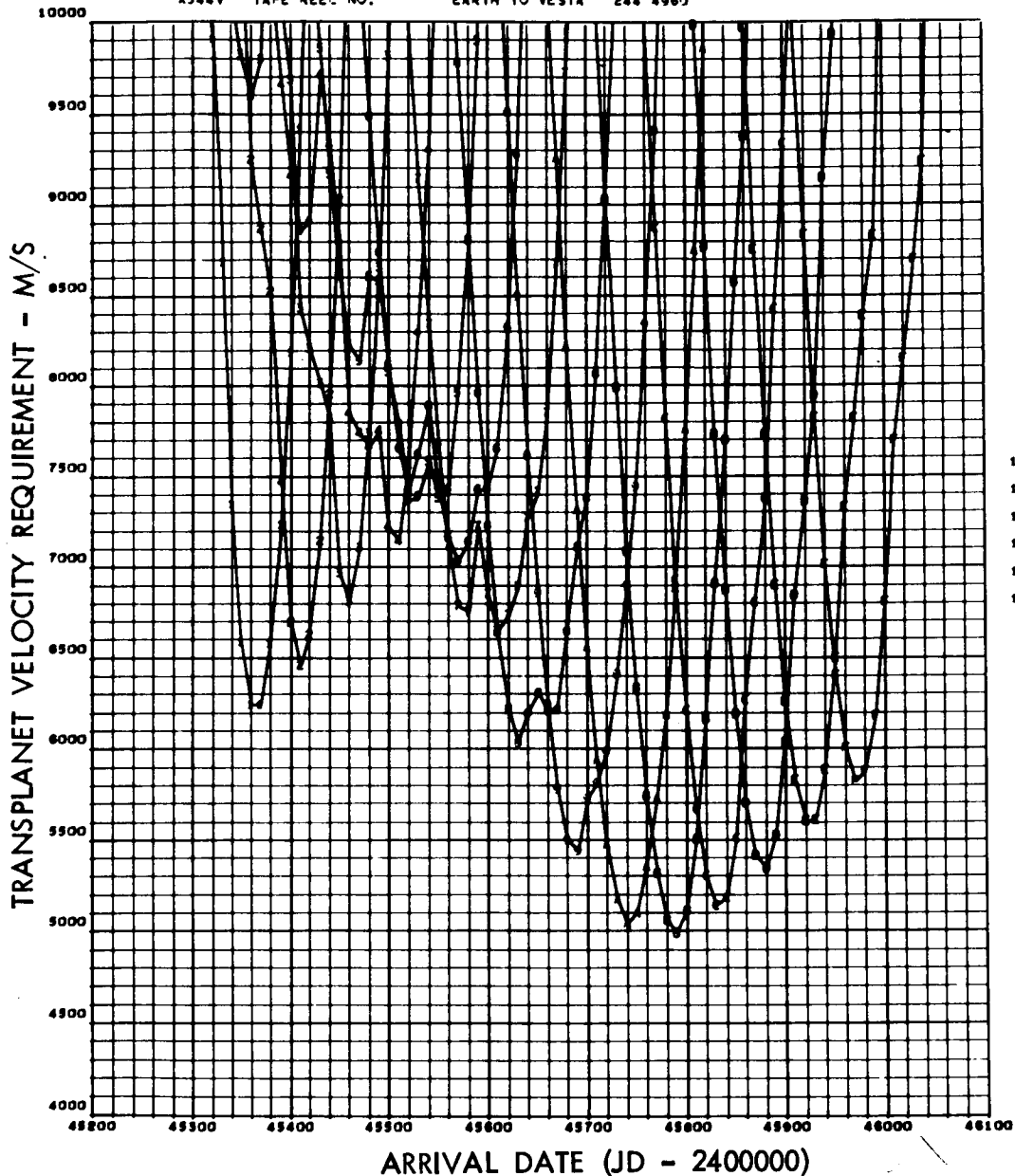
TRANSFER TIMES

1	1	260.000
2	2	300.000
3	3	340.000
4	4	340.000
5	5	420.000
6	6	460.000
7	7	500.000
8	8	540.000
9	9	590.000
10	A	620.000
11	B	660.000
12	C	700.000
13	D	740.000
14	E	740.000
15	F	820.000

WEIGHT SCALING
PROPULSION FACTORS

MAN	M	K
1	1.0000000	1.00
2	1.0000000	1.00
3	0.0000000	1.00

Figure 76. Transplanet Velocity Requirements (1983 Vesta
Opportunity)

- 118 -

SD 67-621-2
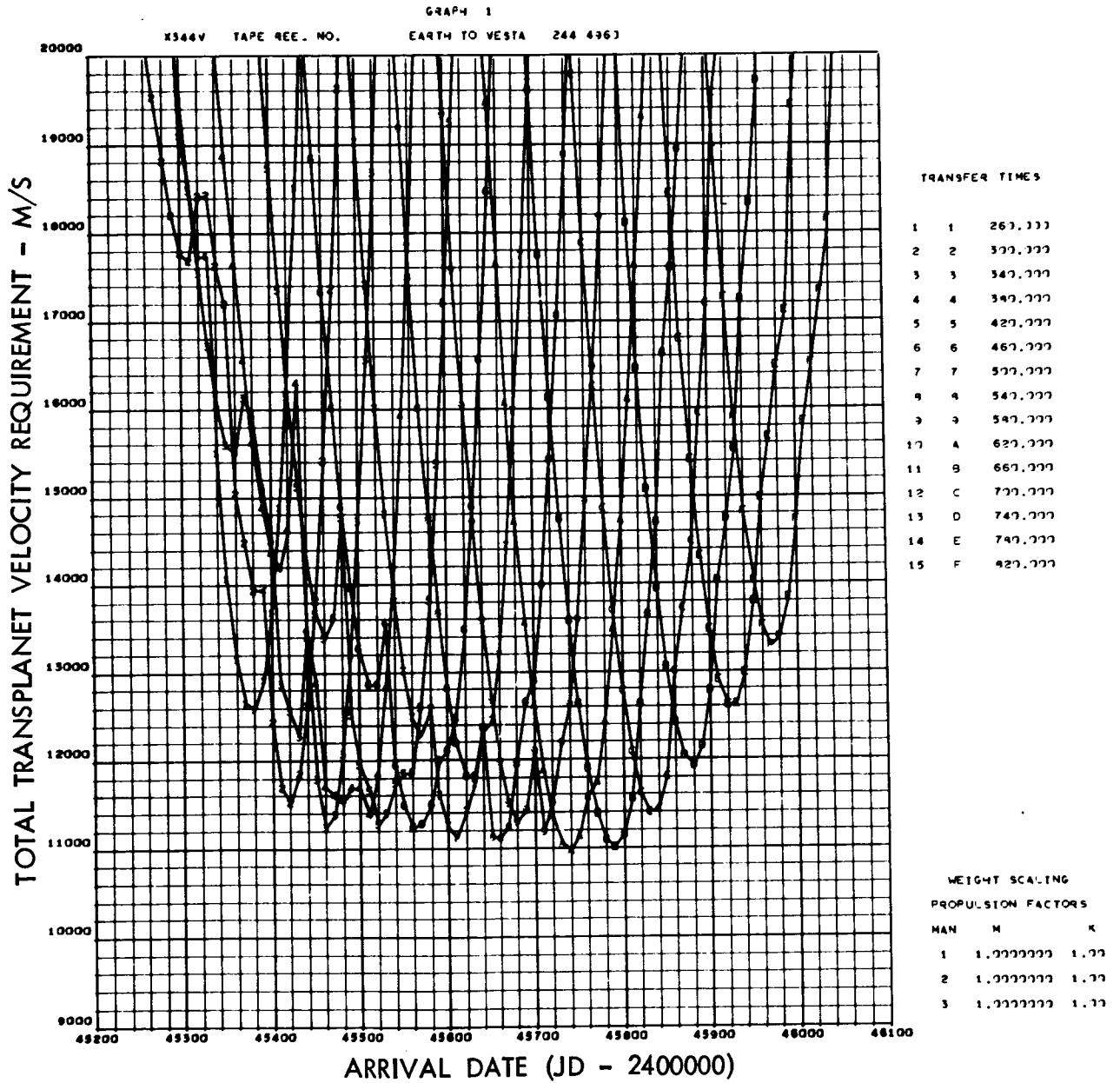
Figure 77. Total Transplanet Velocity Requirements (1983 Vesta Opportunity)

SD 67-621-2

GRAPH 1

X364C   TAPE REEL NO.   VESTA TO EARTH

TRANSFER TIMES

1	1	260.000
2	2	300.000
3	3	340.000
4	4	340.000
5	5	420.000
6	6	460.000
7	7	500.000
8	8	540.000
9	9	540.000
10	A	620.000
11	B	660.000
12	C	700.000
13	D	740.000
14	E	740.000
15	F	820.000
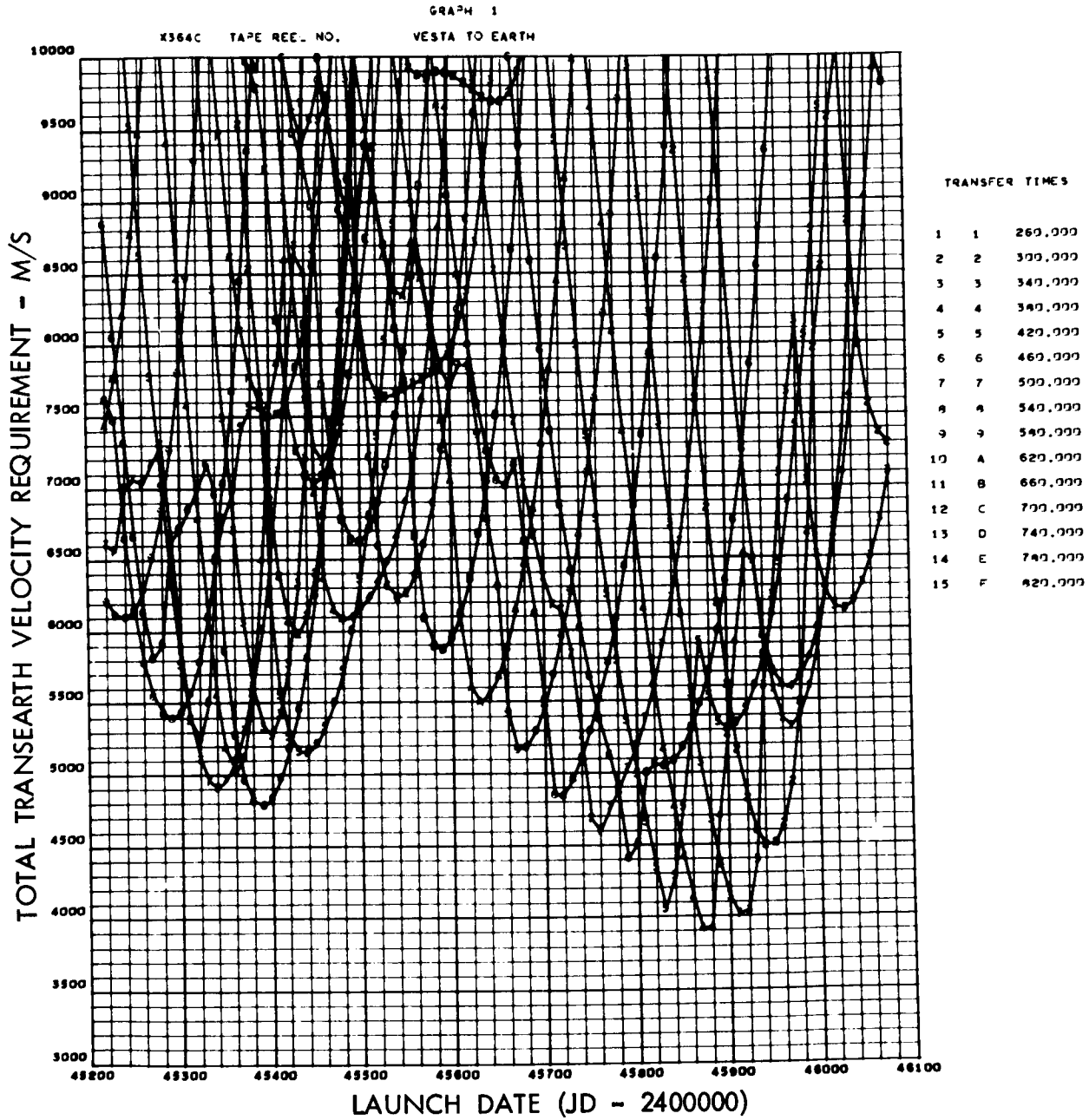
Figure 78.   Trans-Earth Velocity Requirements (1983 Vesta Opportunity)

- 120 -

SD 67-621-2
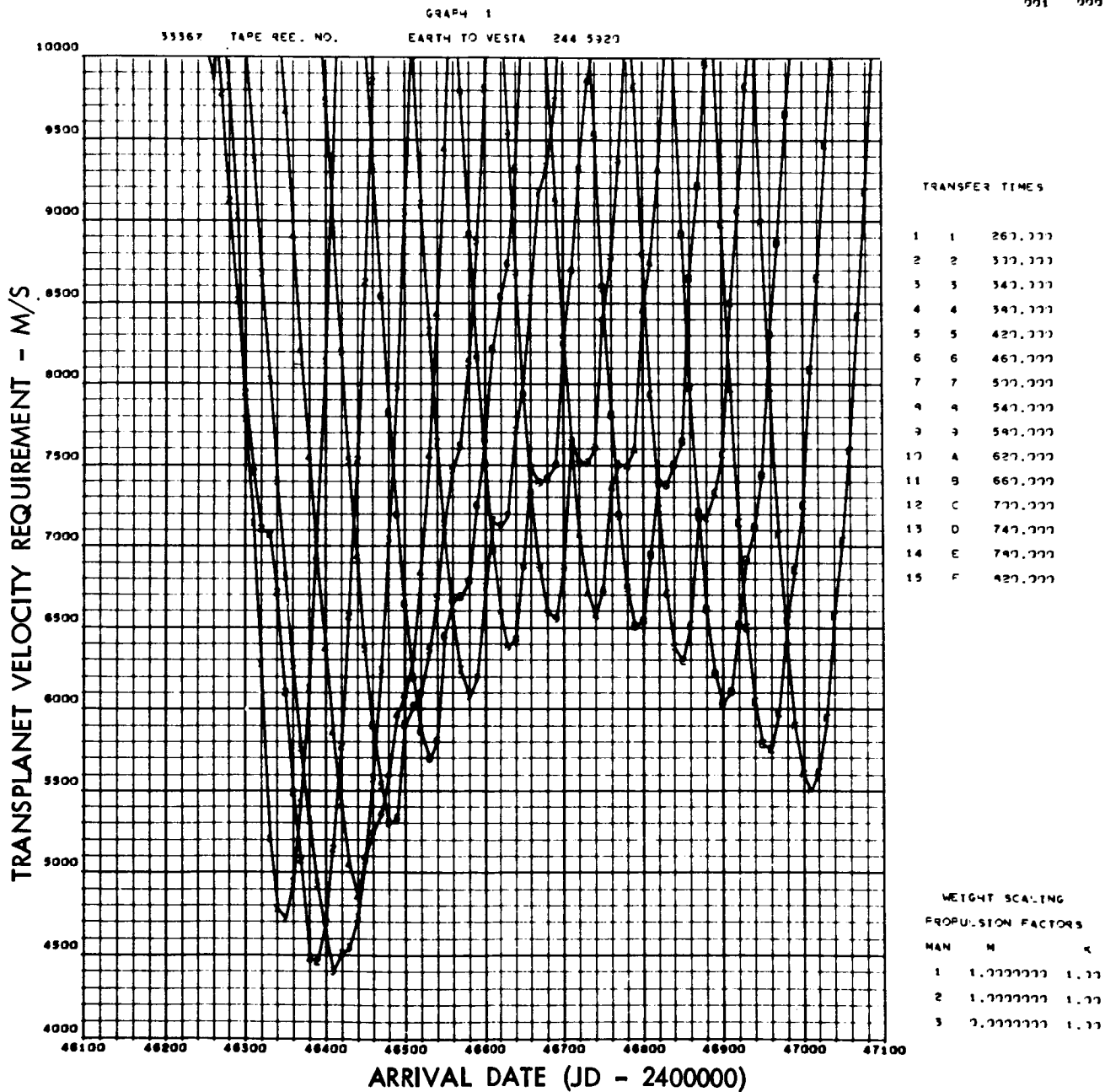
Figure 79. Transplanet Velocity Requirements (1985 Vesta Opportunity)

GRAPH 1

53367   TAPE REEL NO.   EARTH TO VESTA   244 5920
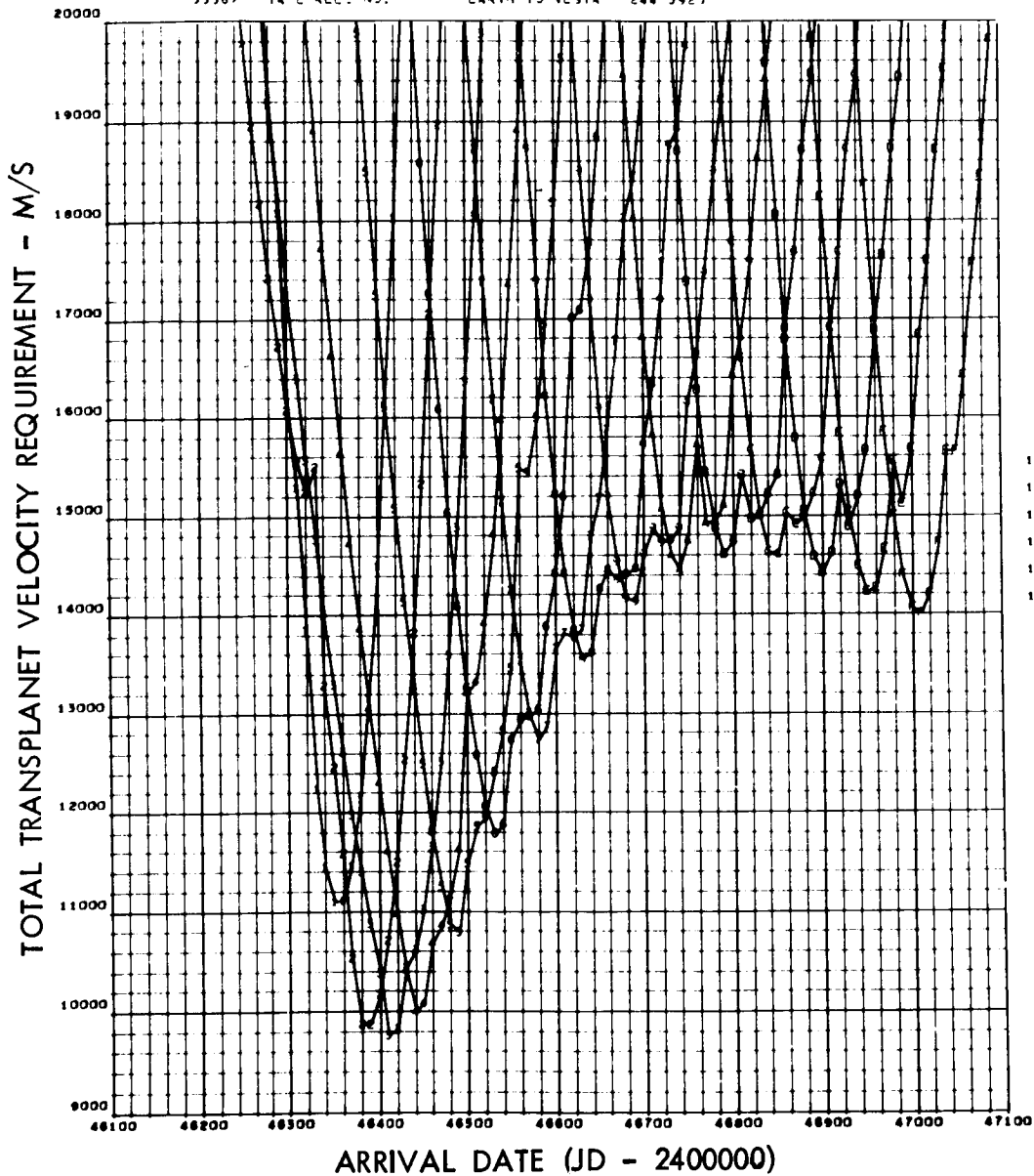
TRANSFER TIMES

1	1	261.111
2	2	311.111
3	3	341.111
4	4	391.111
5	5	421.111
6	6	461.111
7	7	511.111
8	8	541.111
9	9	591.111
11	A	621.111
11	9	661.111
12	C	711.111
13	D	741.111
14	E	741.111
15	F	821.111

WEIGHT SCALING
PROPULSION FACTORS

MAN	M	K
1	1.0000000	1.11
2	1.0000000	1.11
3	1.0000000	1.11

ARRIVAL DATE (JD - 2400000)

TOTAL TRANSPLANET VELOCITY REQUIREMENT - M/S

Figure 80.   Total Transplanet Velocity Requirements (1985 Vesta Opportunity)

- 122 -

SD 67-621-2

GRAPH 1

X364C   TAPE REEL NO.   VESTA TO EARTH

TRANSFER TIMES

1	1	260.000
2	2	300.000
3	3	340.000
4	4	380.000
5	5	420.000
6	6	460.000
7	7	500.000
8	8	540.000
9	9	580.000
10	A	620.000
11	B	660.000
12	C	700.000
13	D	740.000
14	E	780.000
15	F	820.000
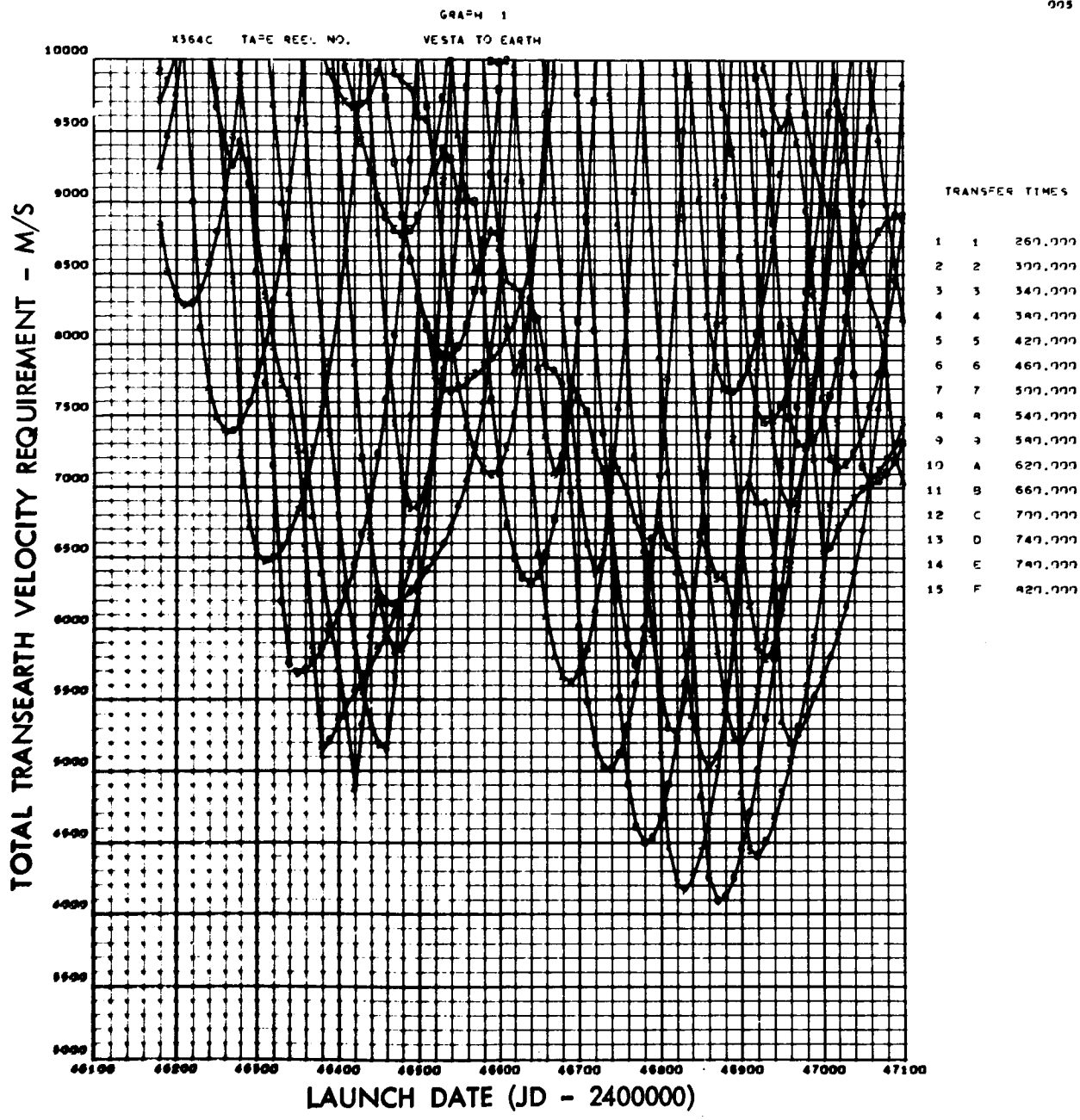
Figure 81. Total Trans-Earth Velocity Requirements (1985 Vesta
Opportunity)

- 123 -

SD 67-621-2

X364C TAPE REEL NO.   VESTA TO EARTH

VELOCITY
(M/S)

1	1000.000000
2	2000.000000
3	3000.000000
4	4000.000000
5	5000.000000
6	6000.000000
7	7000.000000
8	8000.000000
9	9000.000000
A	10000.000000

TRAN TIME

LAUNCH DATE (JD - 2400000)

Figure 82. Total Trans-Earth Velocity Contours (1985 Vesta
Opportunity)

- 124 -

GRAPH 1

3209U   TAPE REEL NO.   EARTH TO VESTA   244 6490

TRANSPLANET VELOCITY REQUIREMENT - M/S

ARRIVAL DATE (JD - 2400000)

TRANSFER TIMES

1	1	260.000
2	2	300.000
3	3	340.000
4	4	390.000
5	5	420.000
6	6	460.000
7	7	500.000
8	8	540.000
9	9	580.000
10	A	620.000
11	B	660.000
12	C	700.000
13	D	740.000
14	E	780.000
15	F	820.000

WEIGHT SCALING
PROPULSION FACTORS

MAN	M	K
1	1.0000000	1.00
2	1.0000000	1.00
3	0.0000000	1.00

Figure 83.   Transplanet Velocity Requirements (1986 Vesta
Opportunity)

- 125 -

GRAPH 1

3204U   TAPE REEL NO.   EARTH TO VESTA   244 6490

20000

TOTAL TRANSPLANET VELOCITY REQUIREMENT - M/S
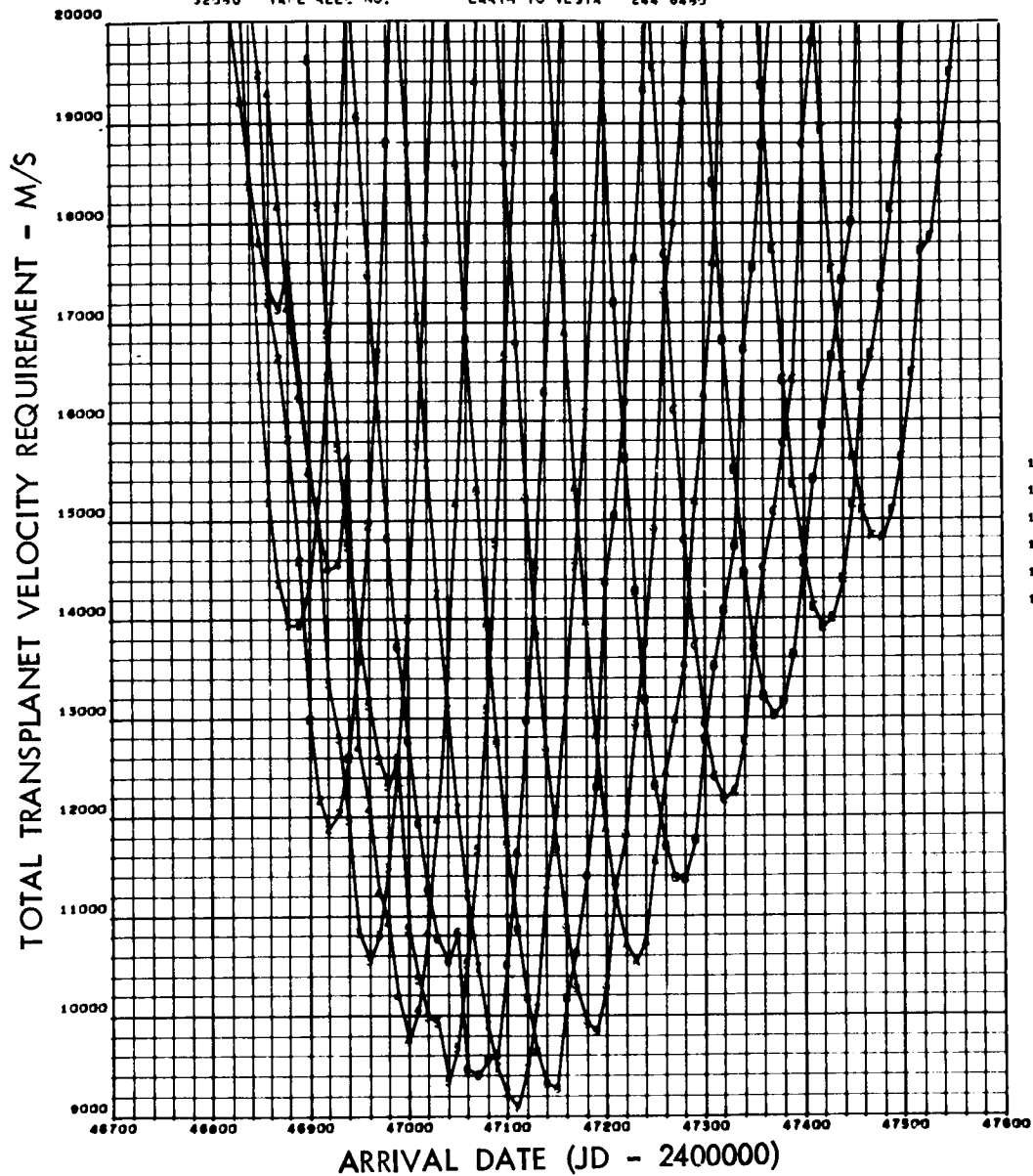
TRANSFER TIMES

1	1	260.000
2	2	300.000
3	3	340.000
4	4	390.000
5	5	420.000
6	6	460.000
7	7	500.000
9	9	540.000
9	9	590.000
10	A	620.000
11	B	660.000
12	C	700.000
13	D	740.000
14	E	790.000
15	F	920.000

WEIGHT SCALING
PROPULSION FACTORS

MAN	M	K
1	1.0000000	1.00
2	1.0000000	1.00
3	1.0000000	1.00

ARRIVAL DATE (JD - 2400000)

Figure 84. Total Transplanet Velocity Requirements (1986 Vesta
Opportunity)

- 126 -

SD 67-621-2
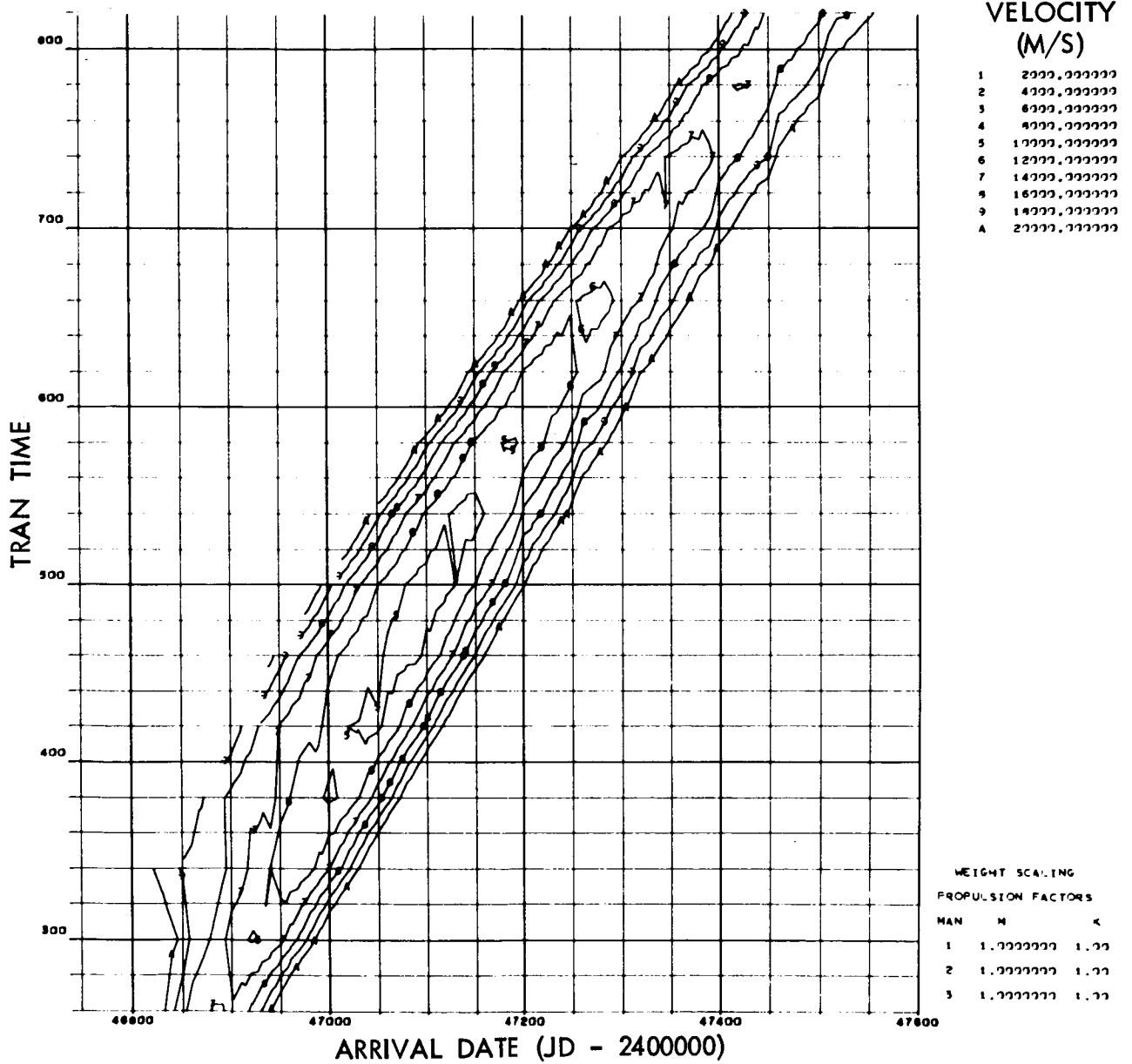
Figure 85. Total Transplanet Velocity Contours (1986 Vesta Opportunity)

SD 67-621-2

2602-01

GRAPH 1

X364C   TAPE REEL NO.   VESTA TO EARTH
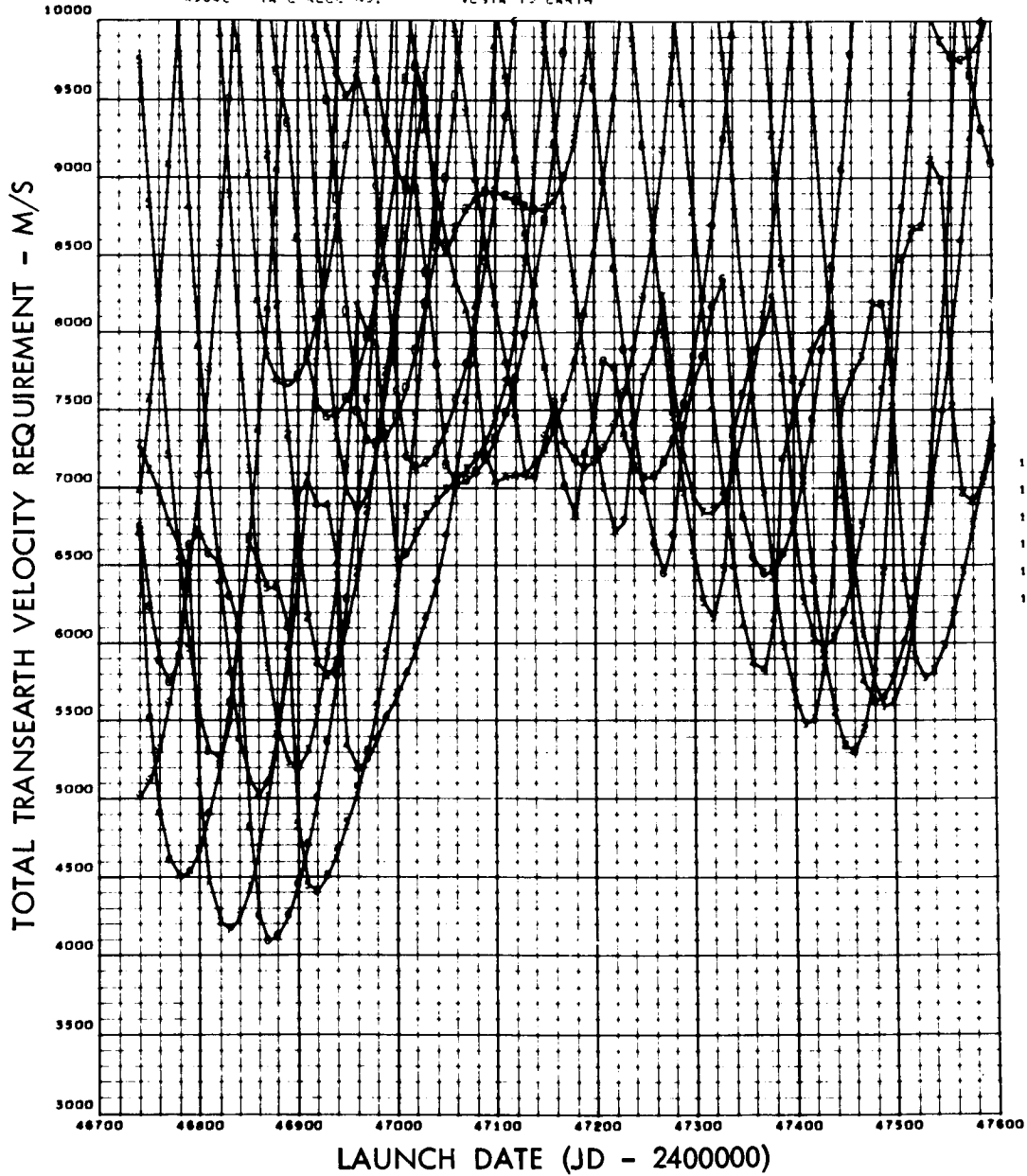
Figure 86.   Total Trans-Earth Velocity Requirements (1986 Vesta
Opportunity)
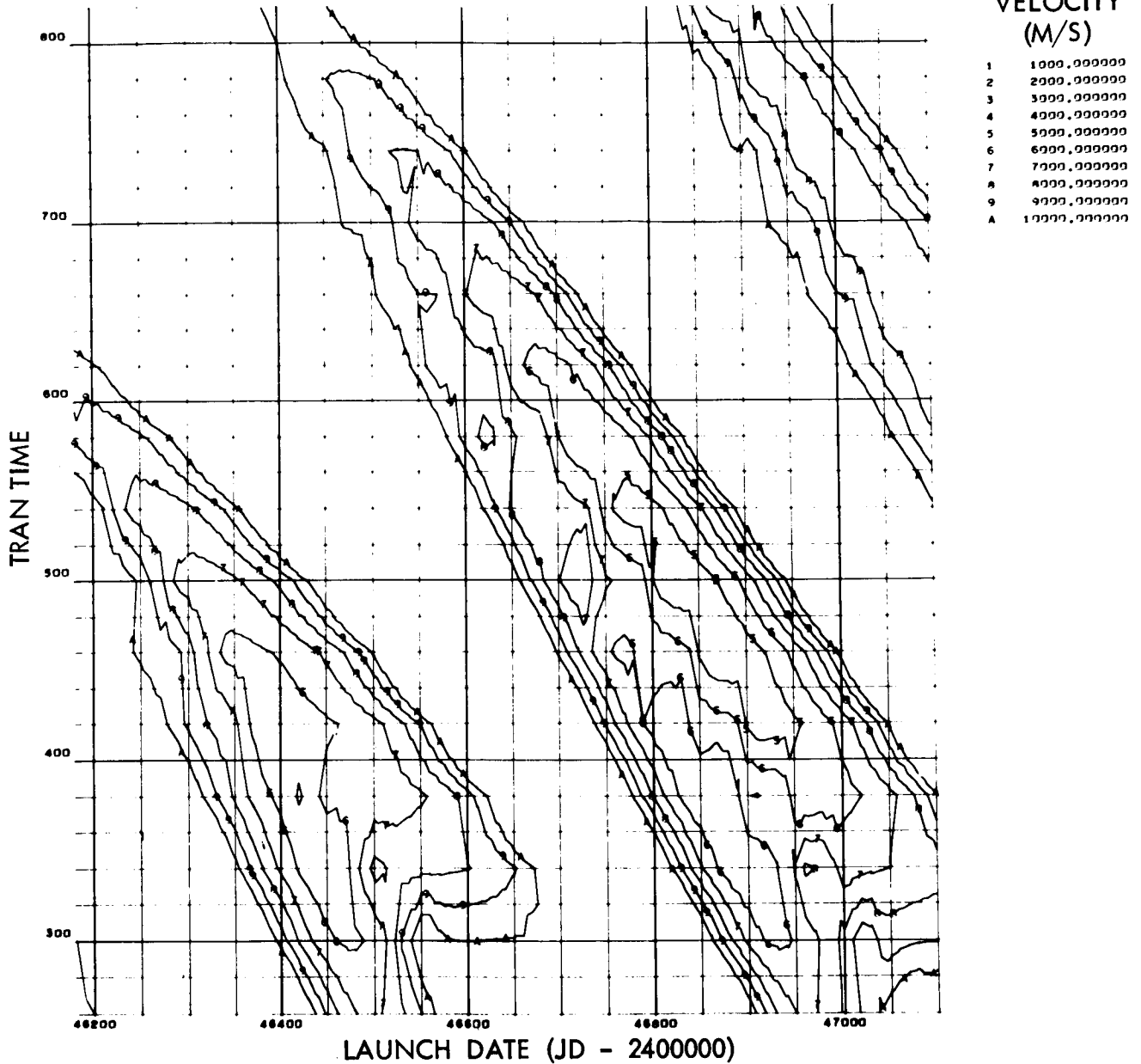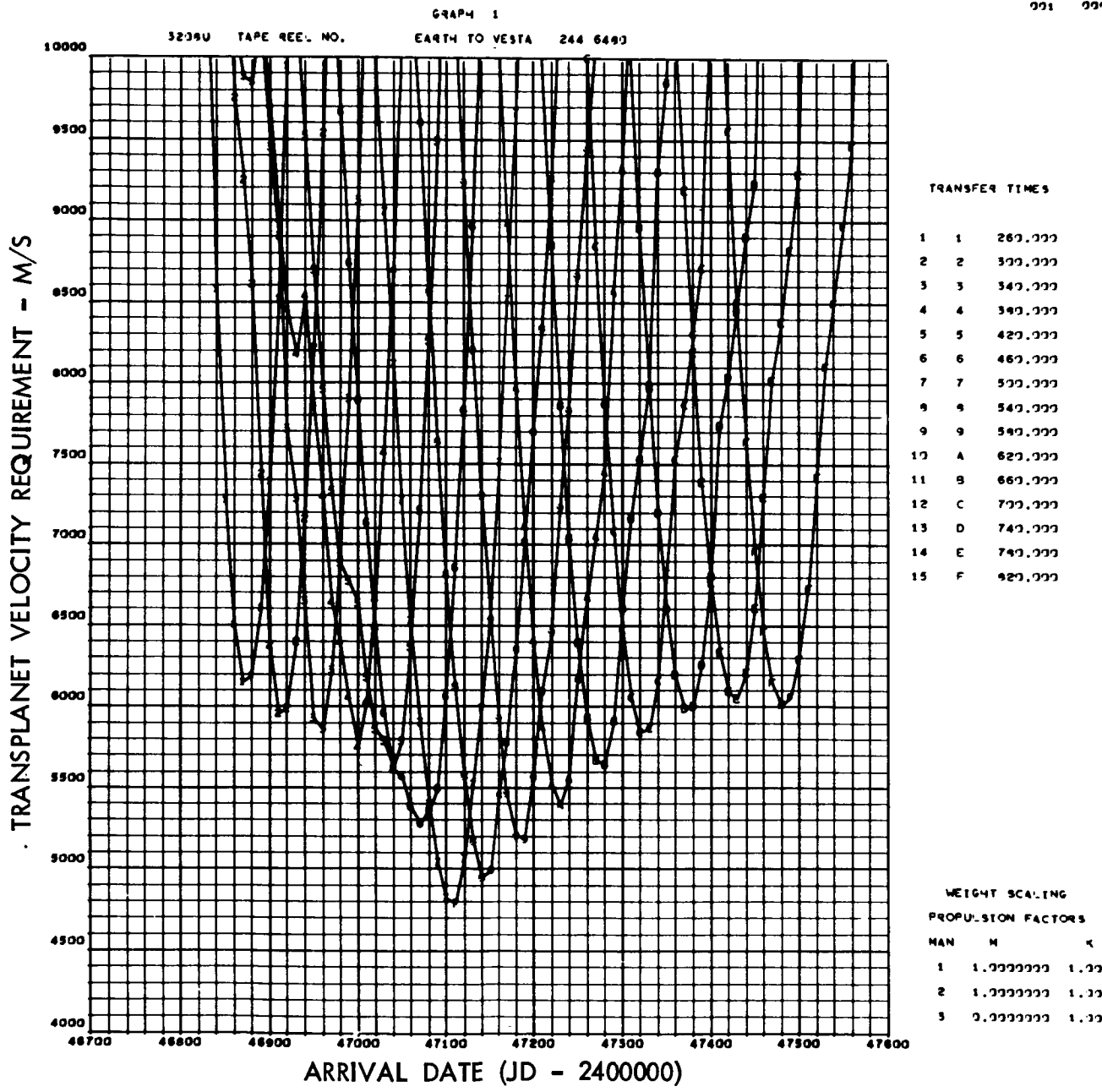
- 128 -

SD 67-621-2
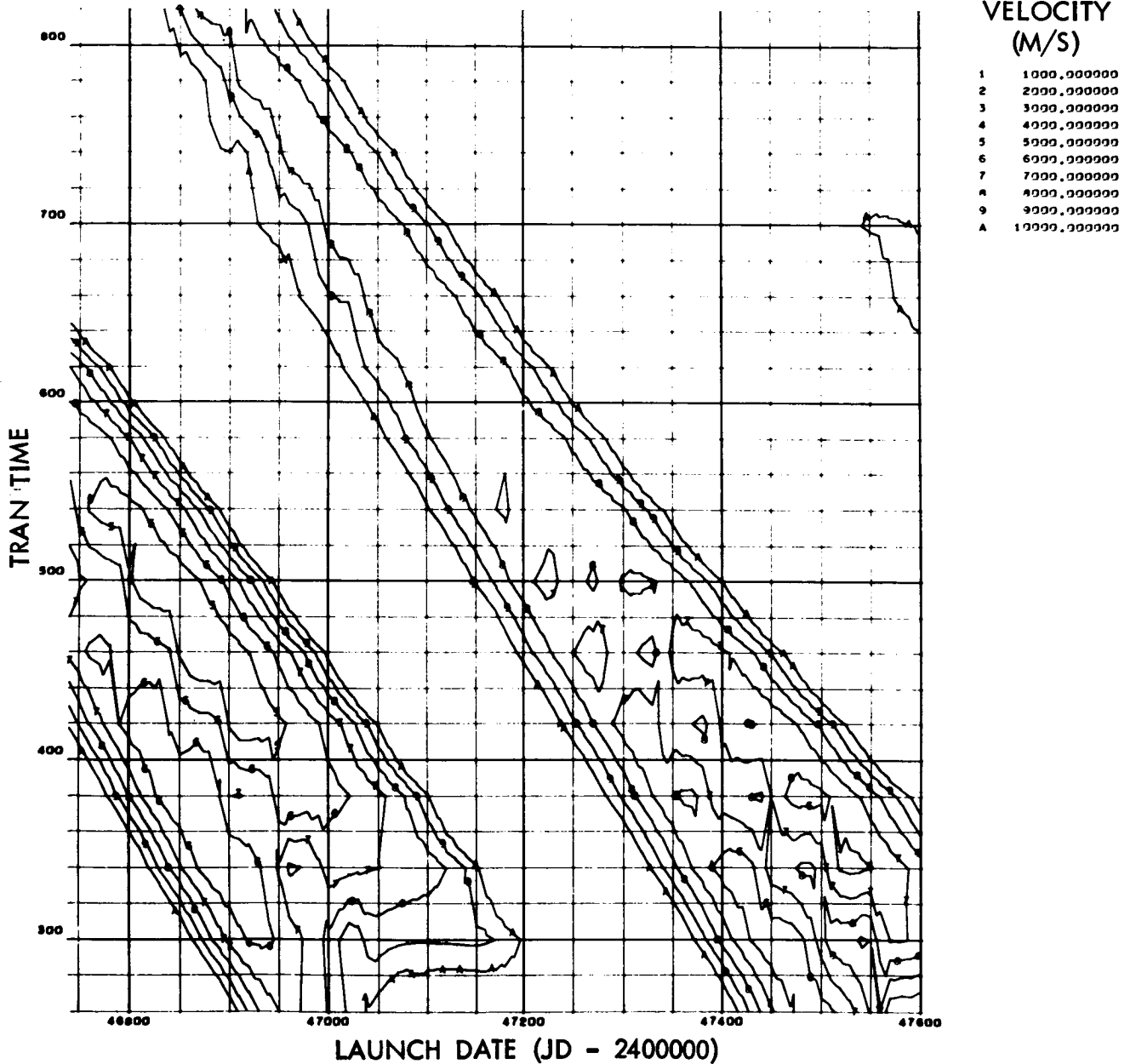
Figure 87. Total Trans-Earth Velocity Contours (1986 Vesta
Opportunity)

- 129 -
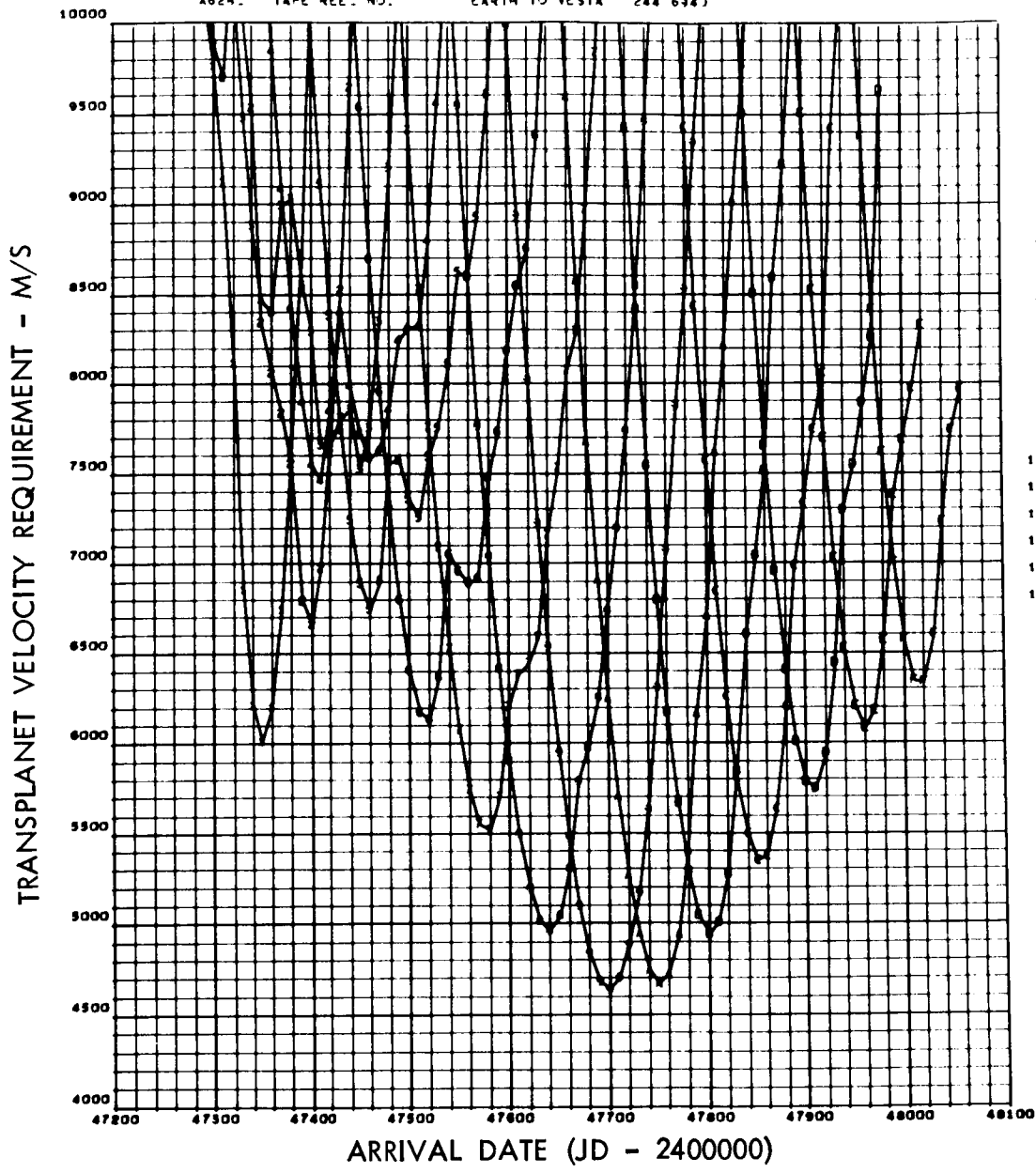
Figure 88. Transplanet Velocity Requirements (1988 Vesta Opportunity)

- 130 -

SD 67-621-2

GRAPH 1

X628L   TAPE REEL NO.   EARTH TO VESTA   244 6940

20000

19000

18000

17000

16000

15000

14000

TOTAL TRANSPLANET VELOCITY REQUIREMENT – M/S

13000

12000

11000

10000

9000

47200   47300   47400   47500   47600   47700   47800   47900   48000   48100

ARRIVAL DATE (JD – 2400000)

TRANSFER TIMES

1	1	260.000
2	2	300.000
3	3	340.000
4	4	380.000
5	5	420.000
6	6	460.000
7	7	500.000
8	8	540.000
9	9	580.000
10	A	620.000
11	B	660.000
12	C	700.000
13	D	740.000
14	E	780.000
15	F	820.000

WEIGHT SCALING
PROPULSION FACTORS

MAN	N	K
1	1.0000000	1.00
2	1.0000000	1.00
3	1.0000000	1.00

Figure 89. Total Transplanet Velocity Requirements (1988 Vesta Opportunity)

- 131 -

SD 67-621-2

Figure 90. Total Transplanet Velocity Contours (1988 Vesta Opportunity)

- 132 -
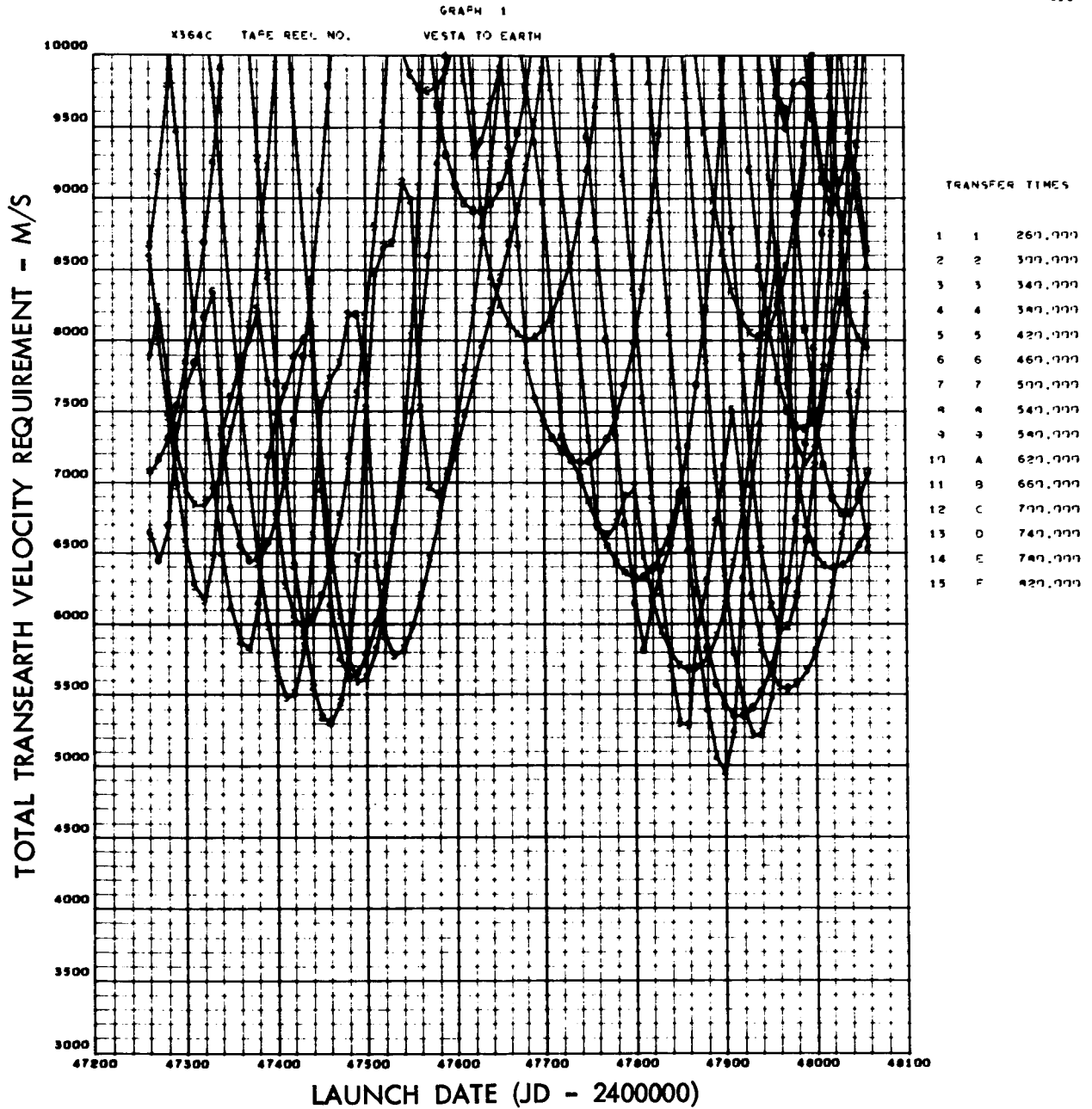
Figure 91. Total Trans-Earth Velocity Requirements (1988 Vesta Opportunity)

GRAPH 1

T713. TAPE REEL NO. EARTH TO VESTA 244 7363

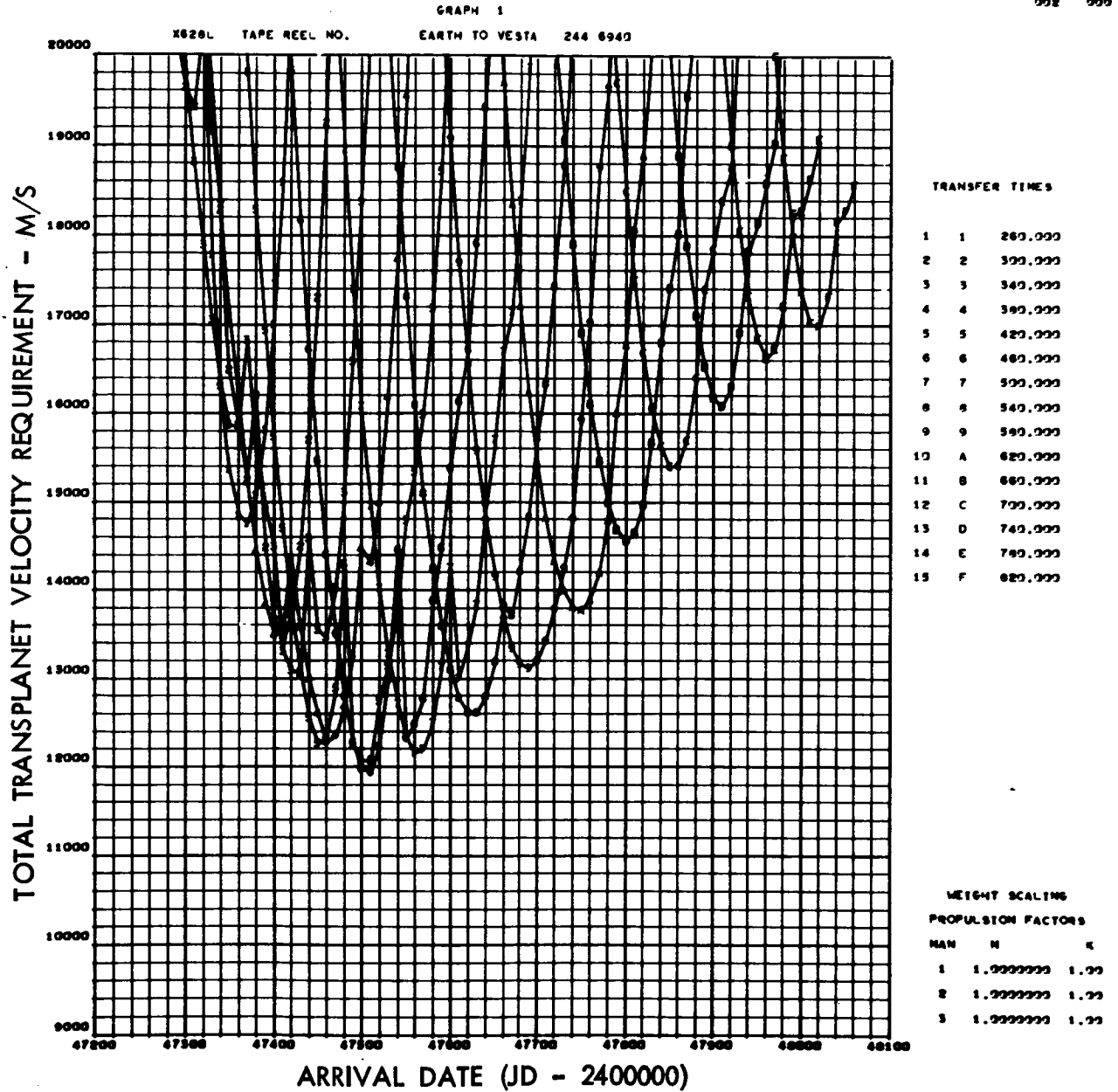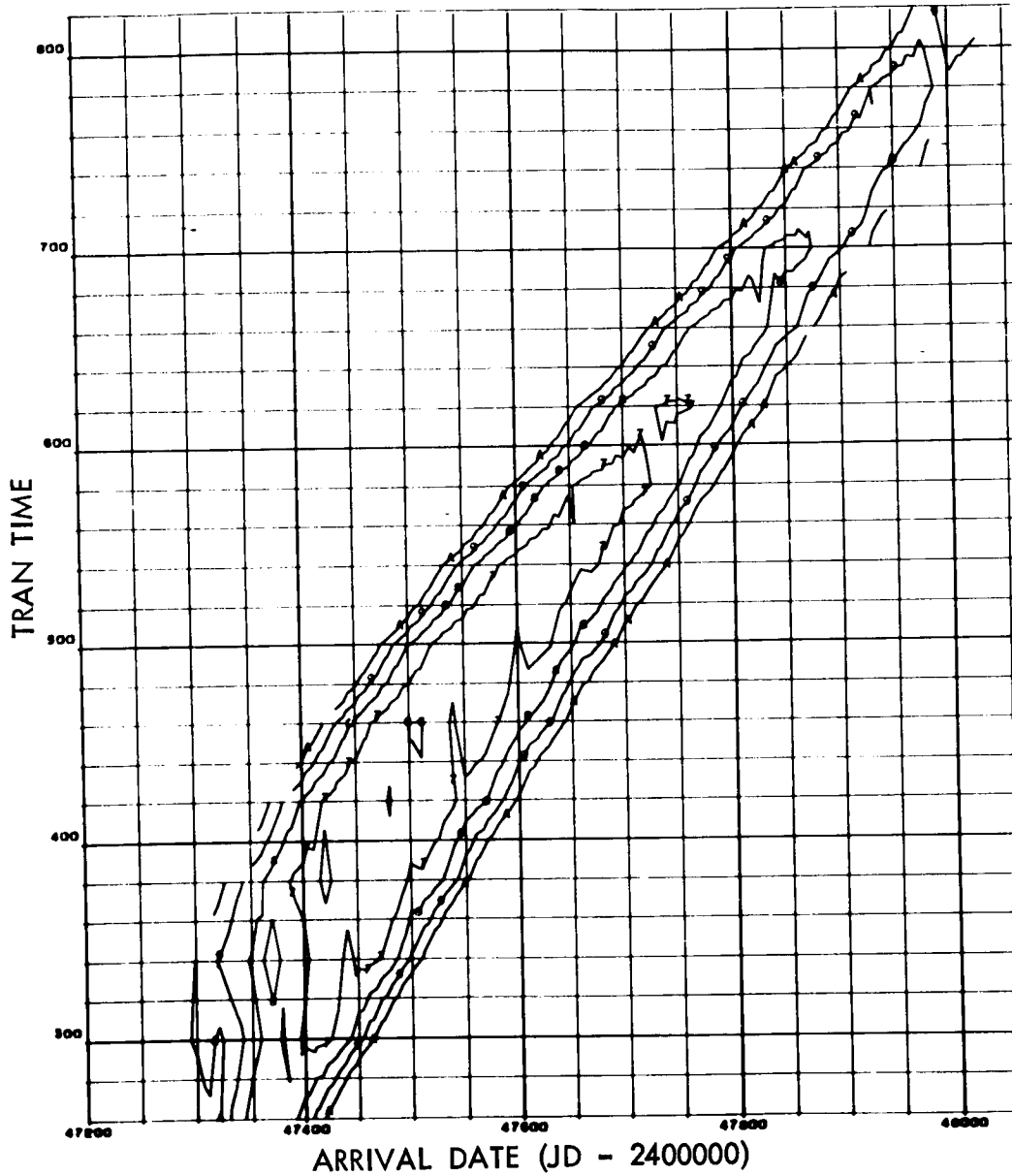Figure 92. Transplanet Velocity Requirements (1991 Vesta Opportunity)
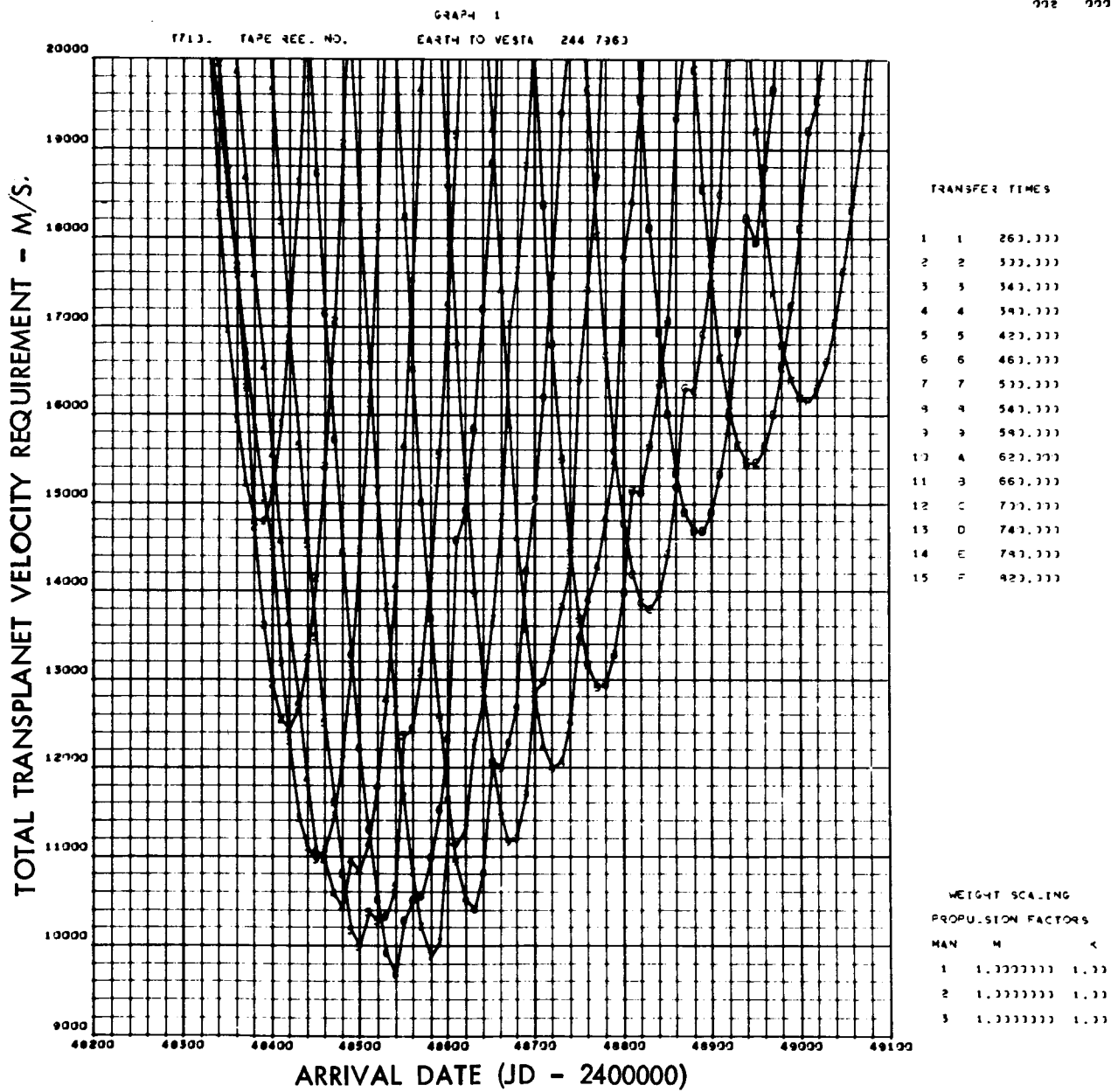
Figure 93. Total Transplanet Velocity Requirements (1991 Vesta Opportunity)
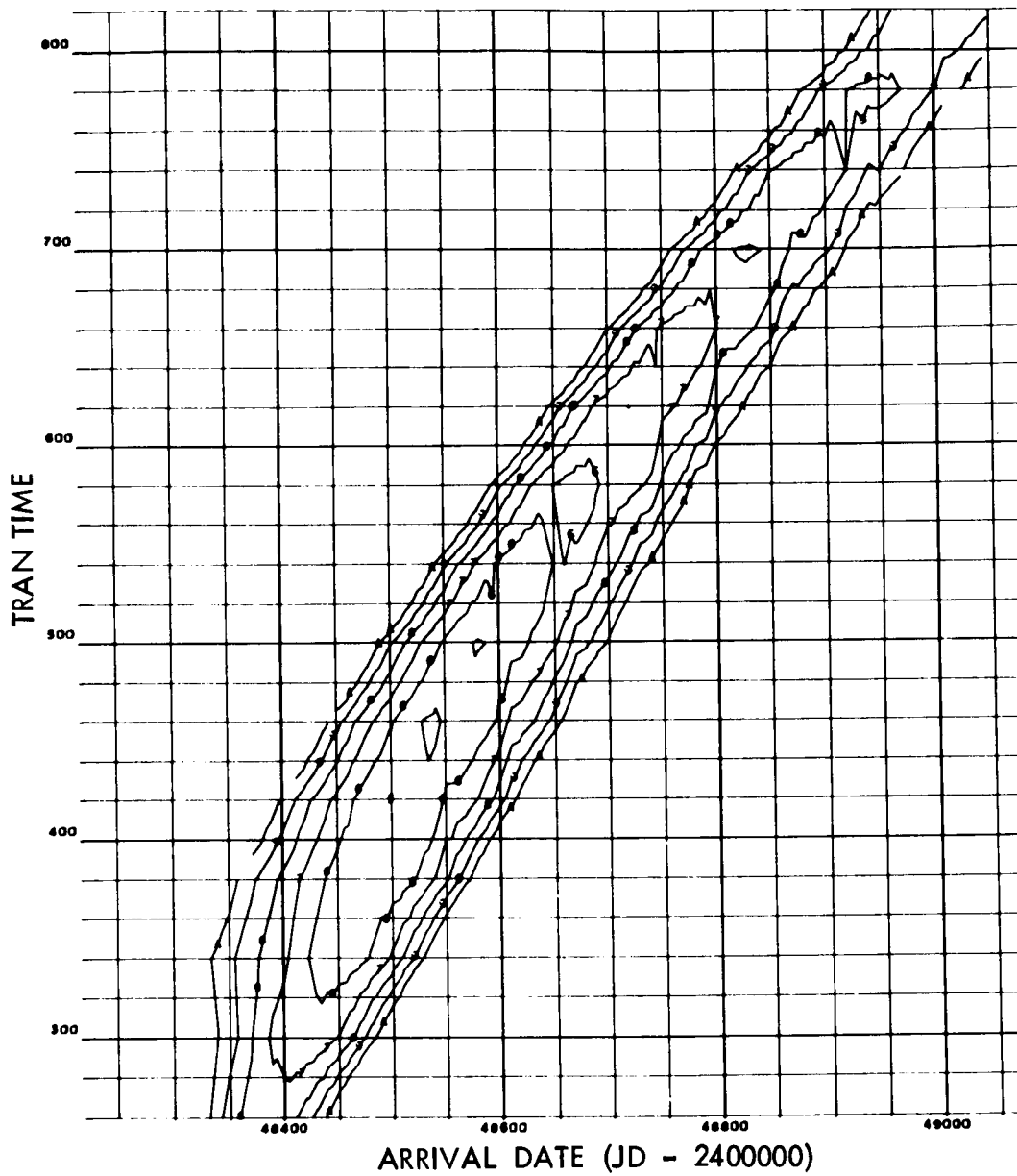
- 135 -

17131.   TAPE REEL NO.   EARTH TO VESTA   244 7360

VELOCITY
(M/S)

1	2000.000000
2	4000.000000
3	6000.000000
4	8000.000000
5	10000.000000
6	12000.000000
7	14000.000000
8	16000.000000
9	18000.000000
A	20000.000000

TRAN TIME

ARRIVAL DATE (JD - 2400000)

WEIGHT SCALING
PROPULSION FACTORS

MAN	M	K
1	1.0000000	1.00
2	1.0000000	1.00
3	1.0000000	1.00

Figure 94. Total Transplanet Velocity Contours (1991 Vesta
Opportunity)

- 136 -

SD 67-621-2

GRAPH 1

K364C   TAPE REEL NO.   VESTA TO EARTH

TRANSFER TIMES

1	1	260.000
2	2	300.000
3	3	340.000
4	4	380.000
5	5	420.000
6	6	460.000
7	7	500.000
8	8	540.000
9	9	580.000
10	A	620.000
11	B	660.000
12	C	700.000
13	D	740.000
14	E	780.000
15	F	820.000
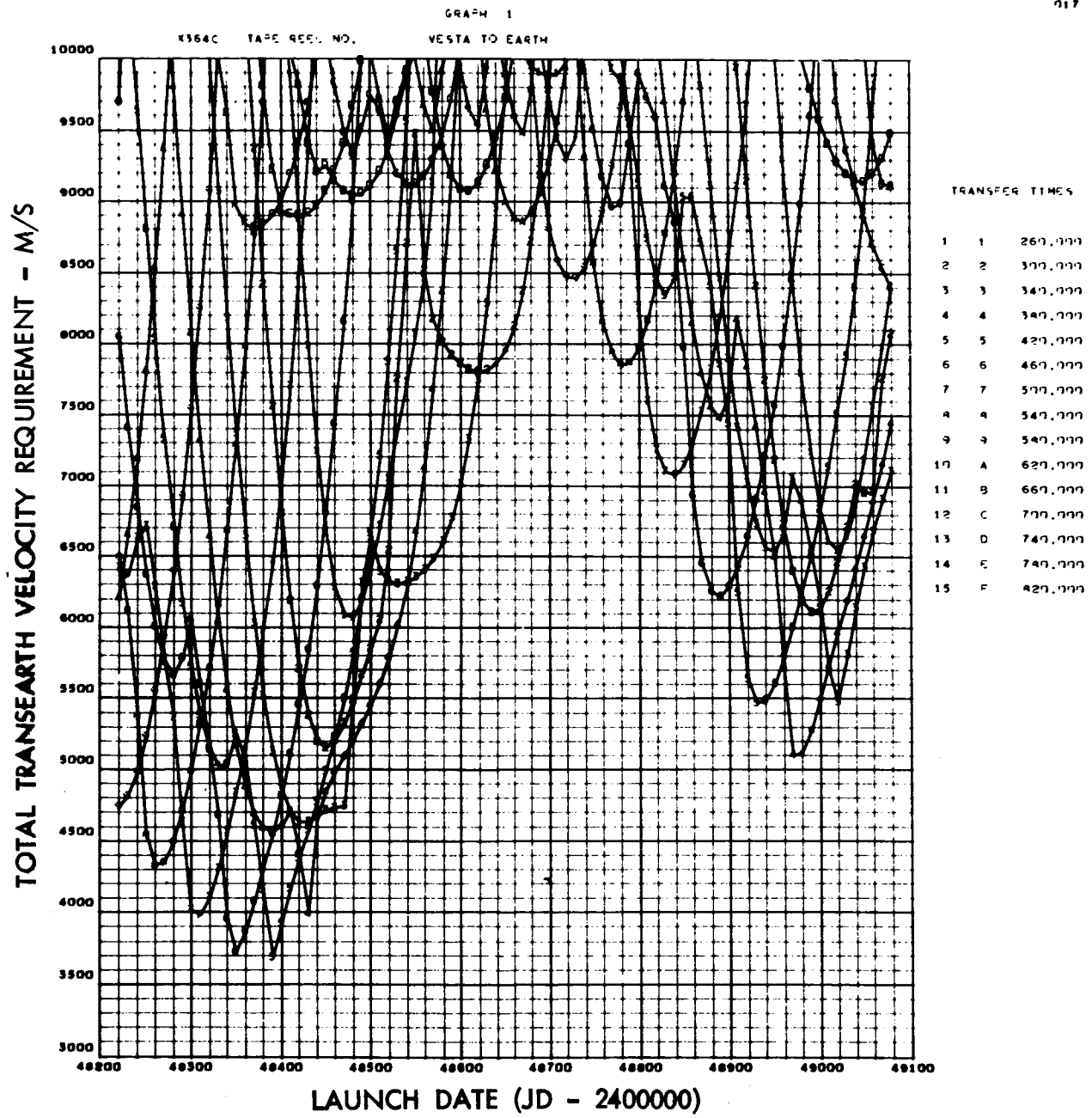
Figure 95.   Total Trans-Earth Velocity Requirements (1991 Vesta
Opportunity)

SD 67-621-2
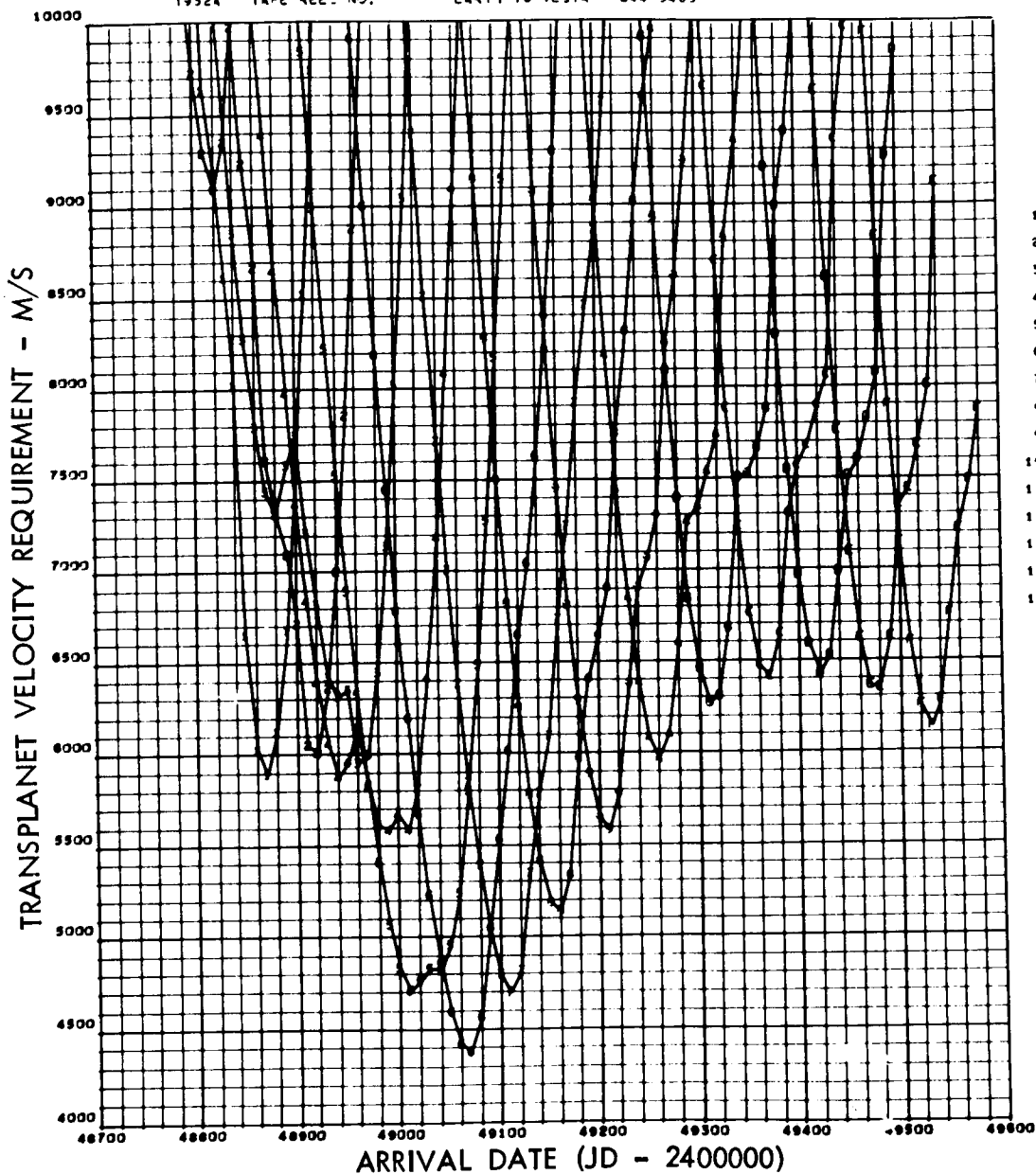
Figure 96. Transplanet Velocity Requirements (1993 Vesta Opportunity)

GRAPH 1

T932A   TAPE REEL NO.   EARTH TO VESTA   244 8469
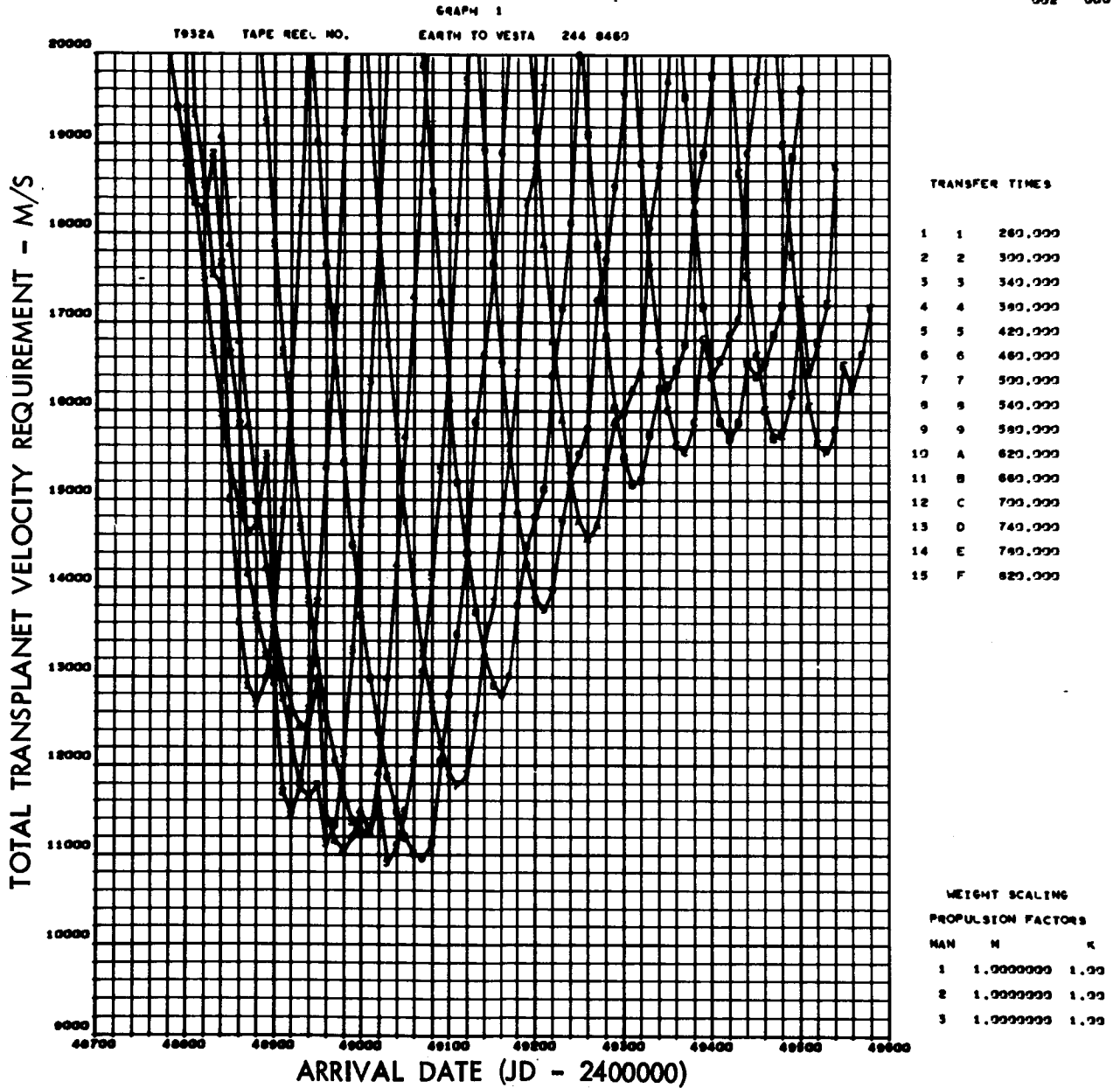
Figure 97.   Total Transplanet Velocity Requirements (1993 Vesta Opportunity)

SD 67-621-2

Figure 98. Total Transplanet Velocity Contours (1993 Vesta Opportunity)

SD 67-621-2

GRAPH 1

X364C   TAPE REEL NO.   VESTA TO EARTH

TRANSFER TIMES

1	1	260.000
2	2	300.000
3	3	340.000
4	4	380.000
5	5	420.000
6	6	460.000
7	7	500.000
8	8	540.000
9	9	580.000
10	A	620.000
11	B	660.000
12	C	700.000
13	D	740.000
14	E	780.000
15	F	820.000

TOTAL TRANSEARTH VELOCITY REQUIREMENT – M/S

LAUNCH DATE (JD - 2400000)
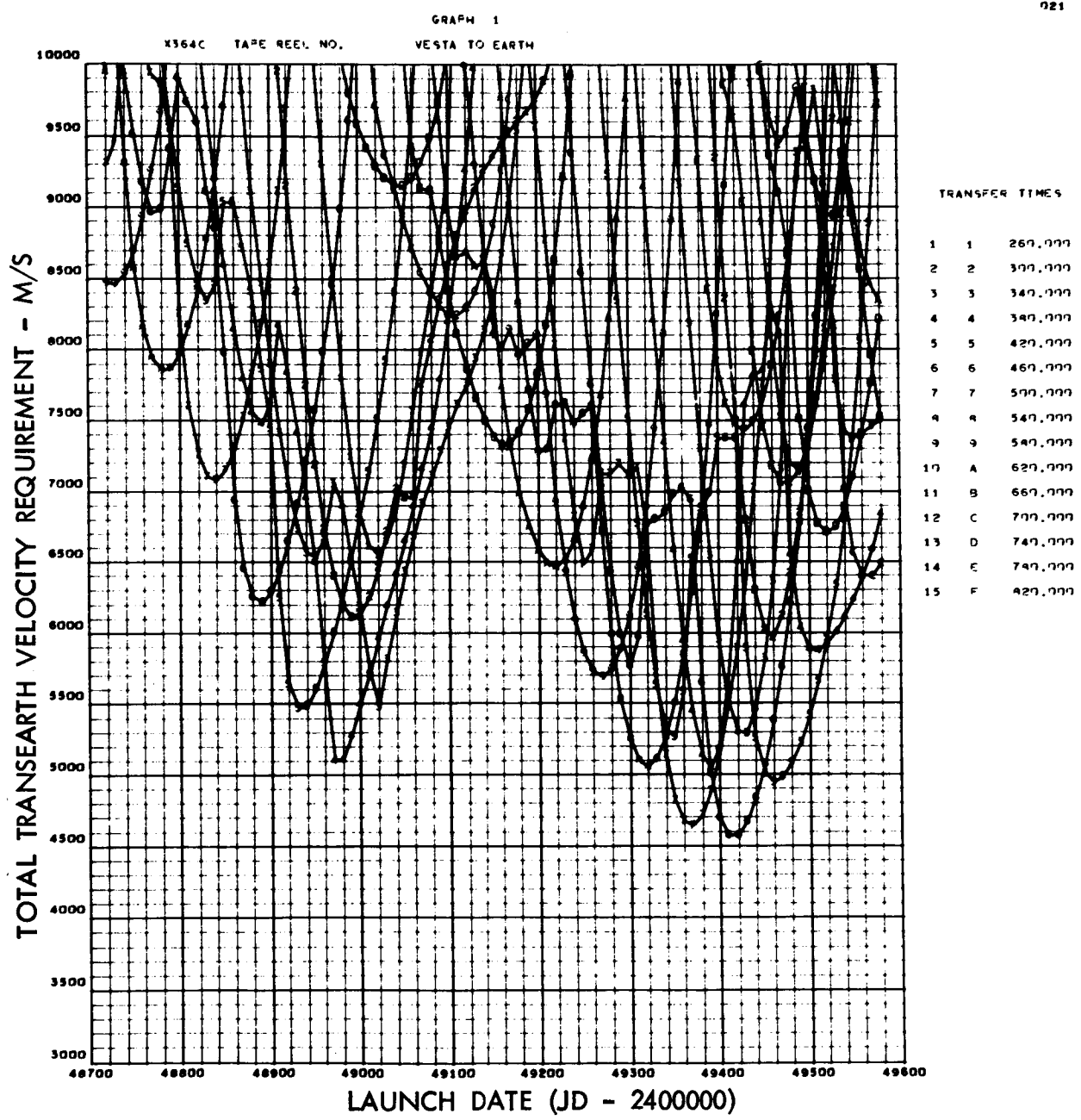
Figure 99. Total Trans-Earth Velocity Requirements (1993 Vesta Opportunity)

- 141 -
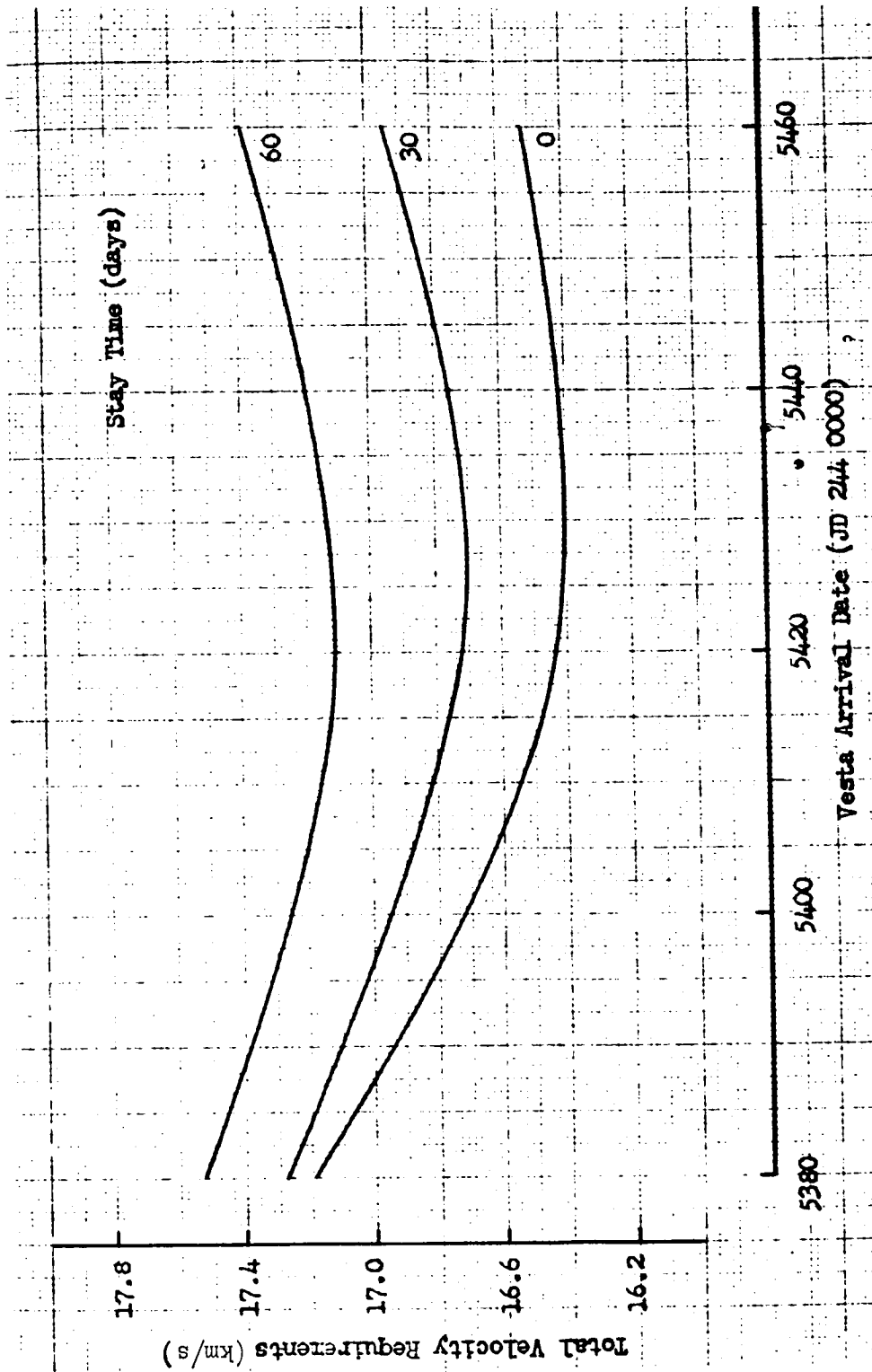
Figure 100. Total Vesta Mission Requirements (1983 Vesta Opportunity)
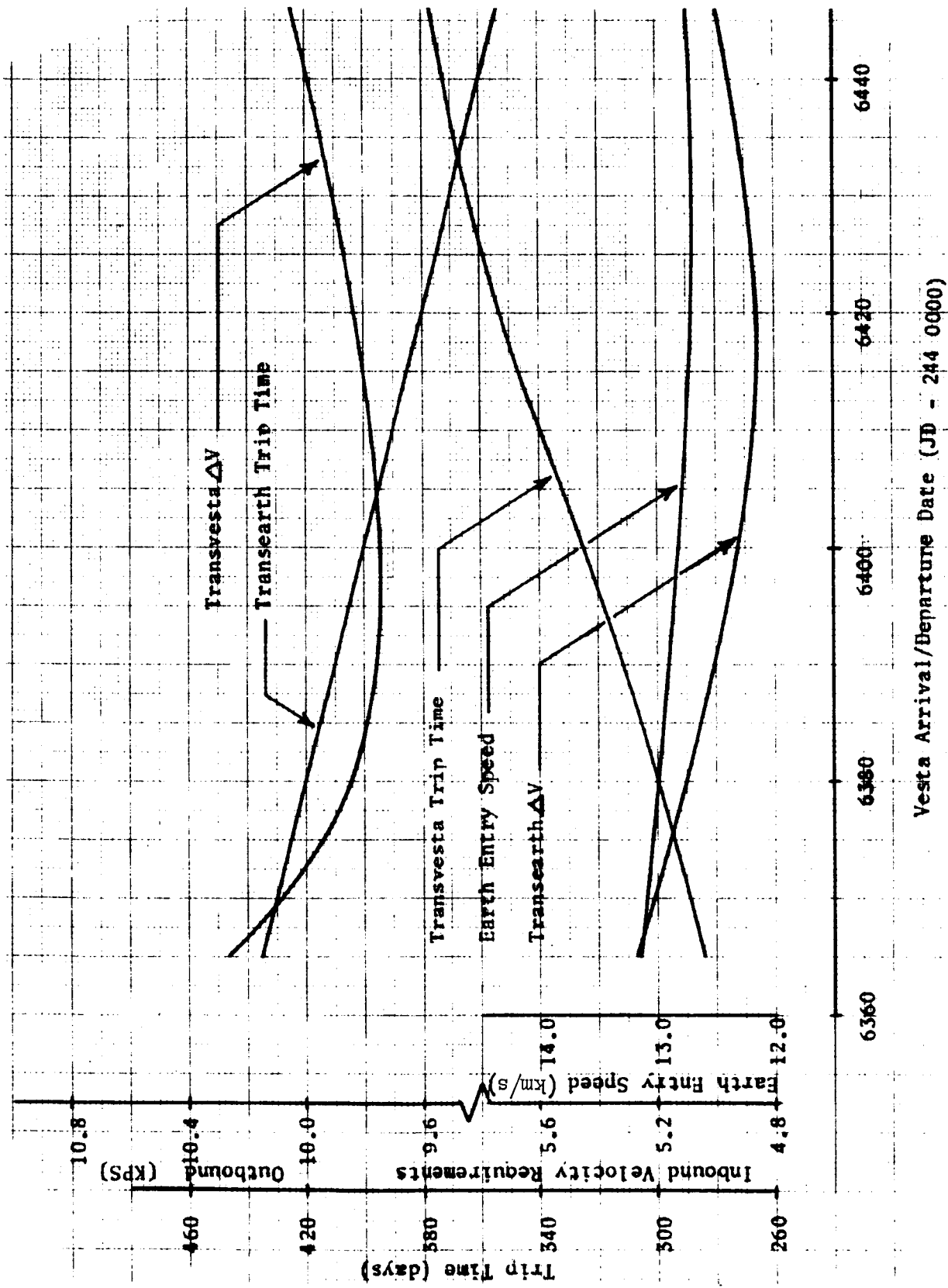
Figure 101. Velocity Requirements Summary
(1985 Vesta Opportunity)
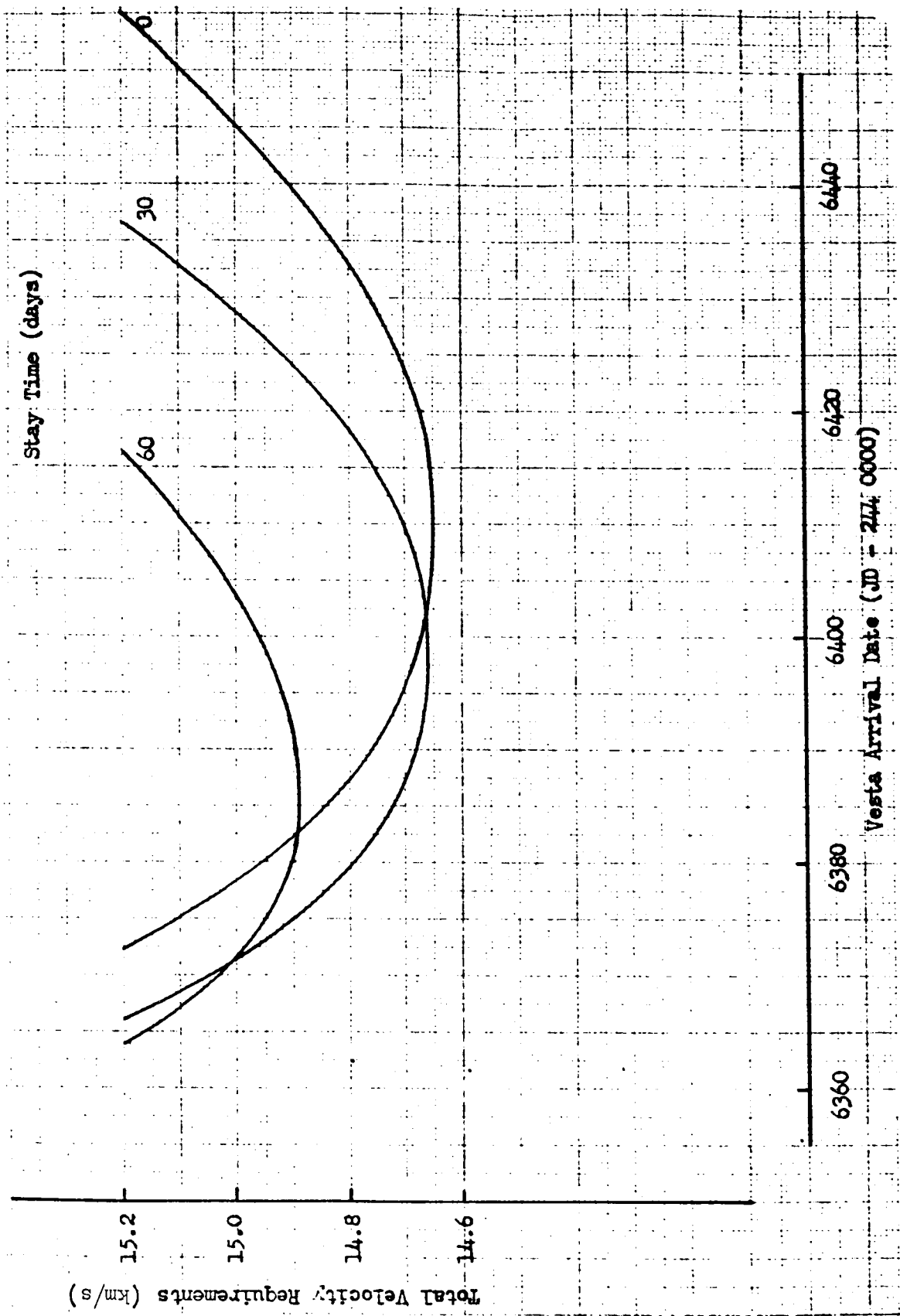
Figure 102. Total Vesta Mission Requirements (1985 Vesta Opportunity)

- 144 -
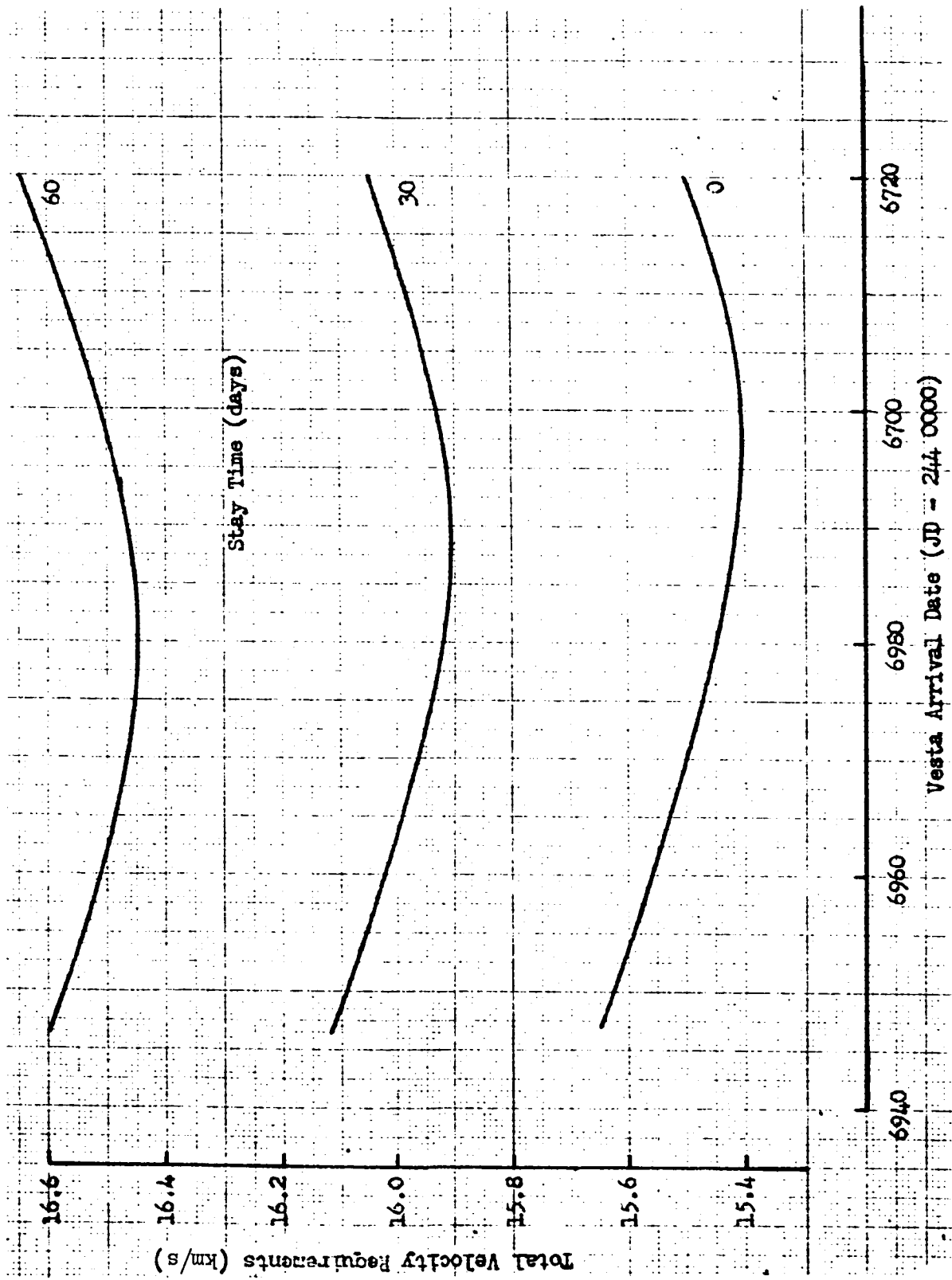
Figure 103. Total Vesta Mission Requirements (1986 Vesta Opportunity)

SD 67-621-2
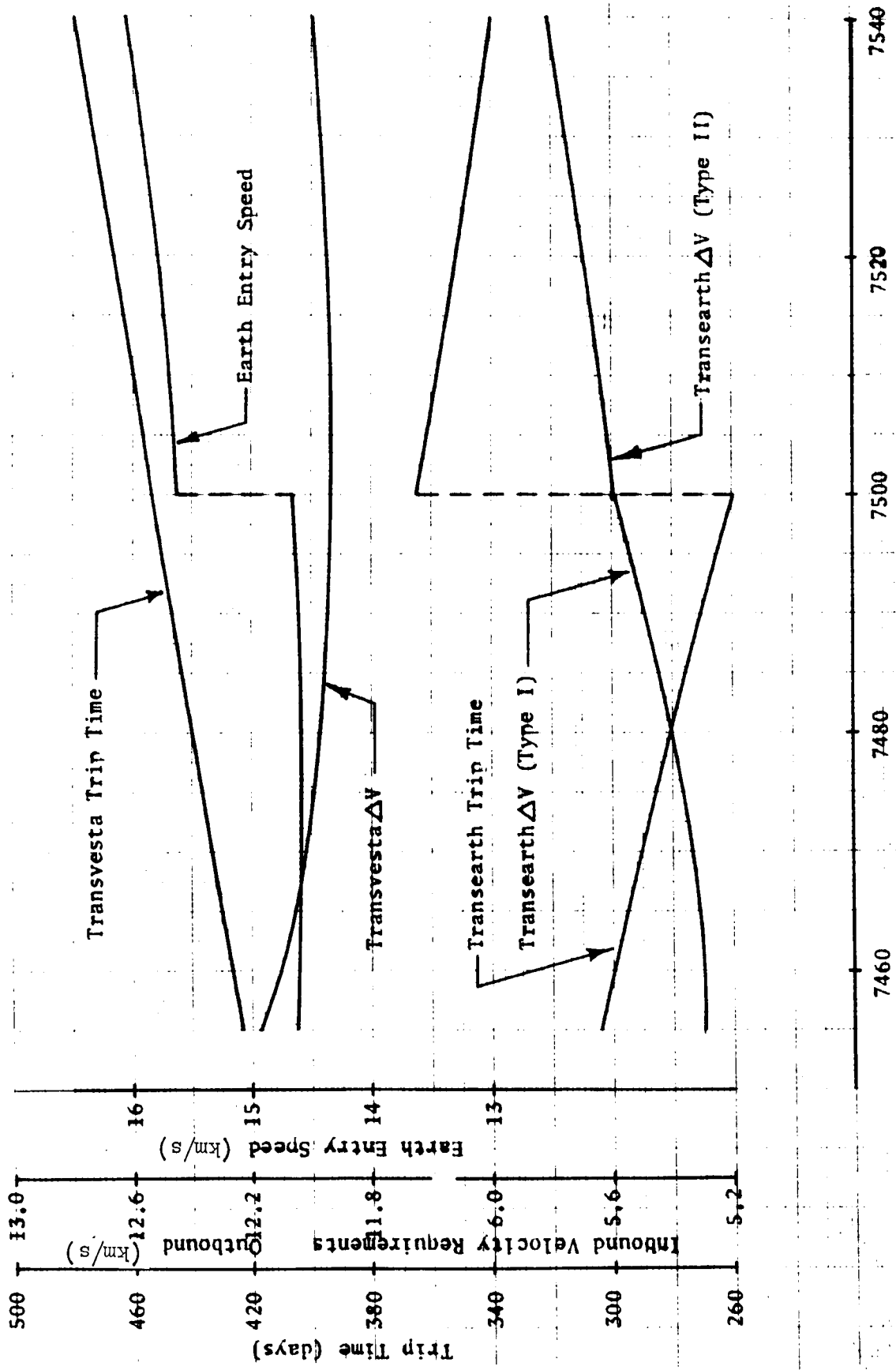
Figure 104. Velocity Requirements Summary
(1987 Vesta Opportunity)

- 146 -
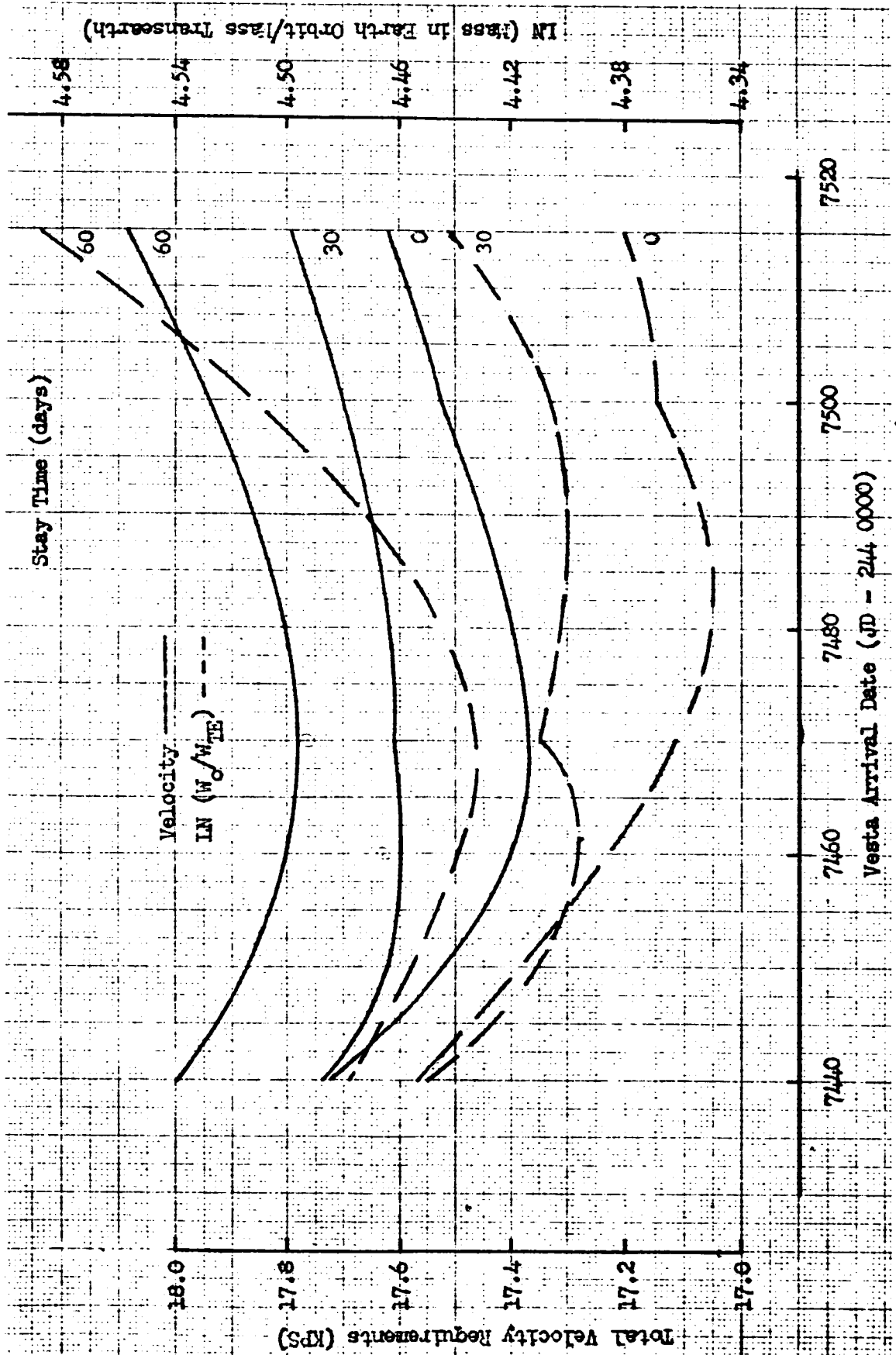
Figure 105.   Total Vesta Mission Requirements (1988 Vesta Opportunity)

SD 67-621-2
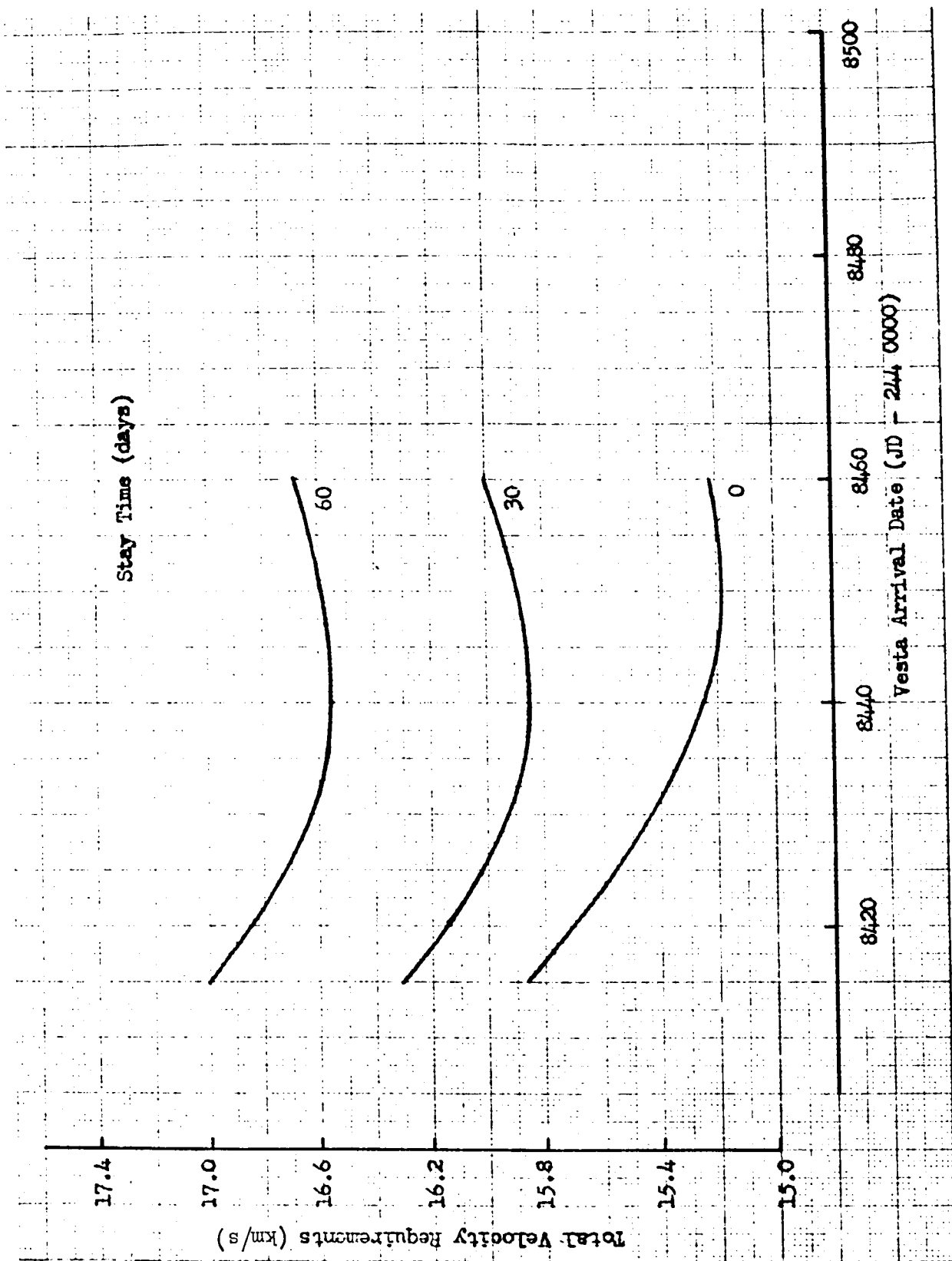
Figure 106. Total Vesta Mission Requirements (1991 Vesta Opportunity)
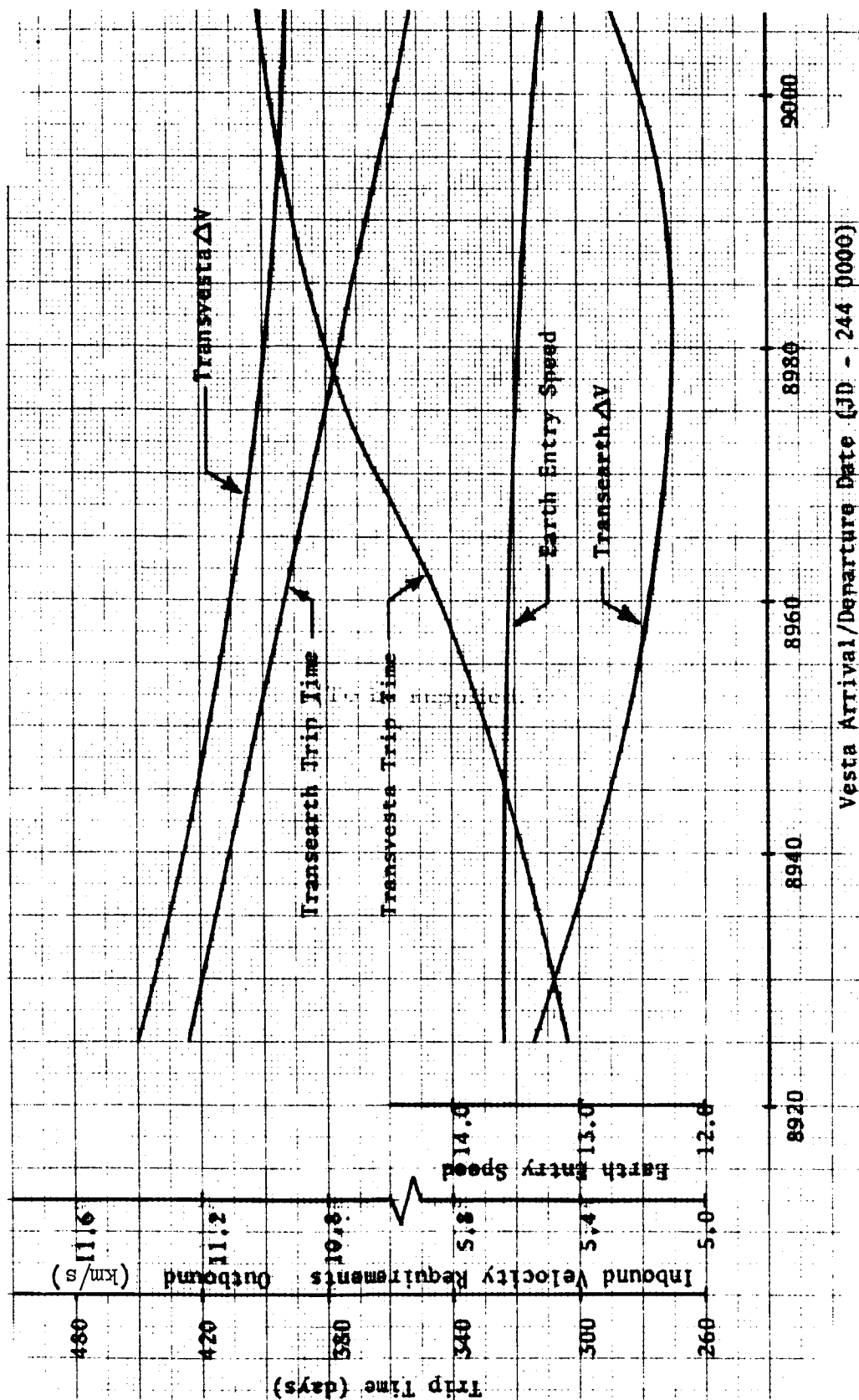
Figure 107. Velocity Requirements Summary
(1991 Vesta Opportunity)

- 149 -
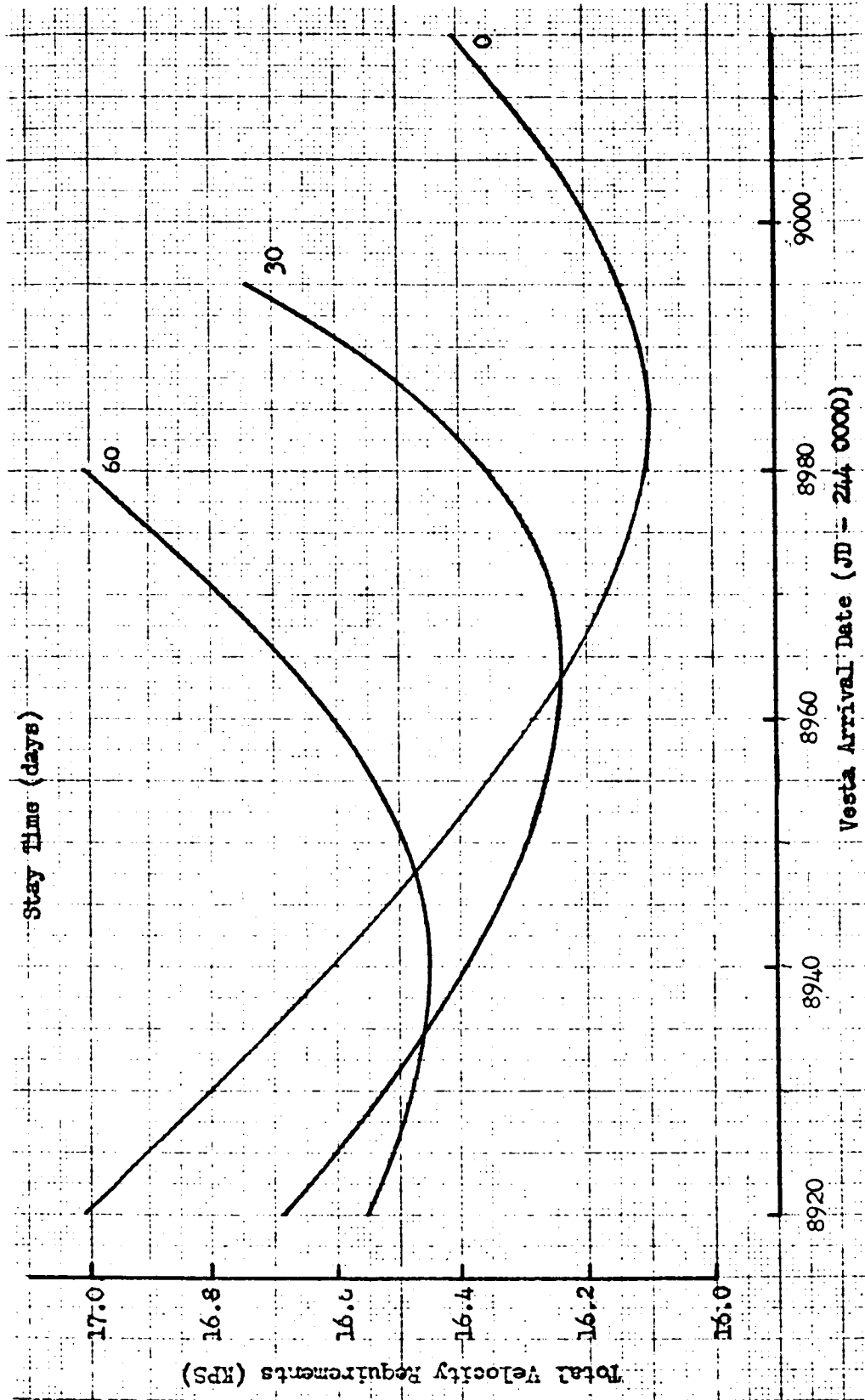
Figure 108. Total Vesta Mission Requirements (1993 Vesta Opportunity)
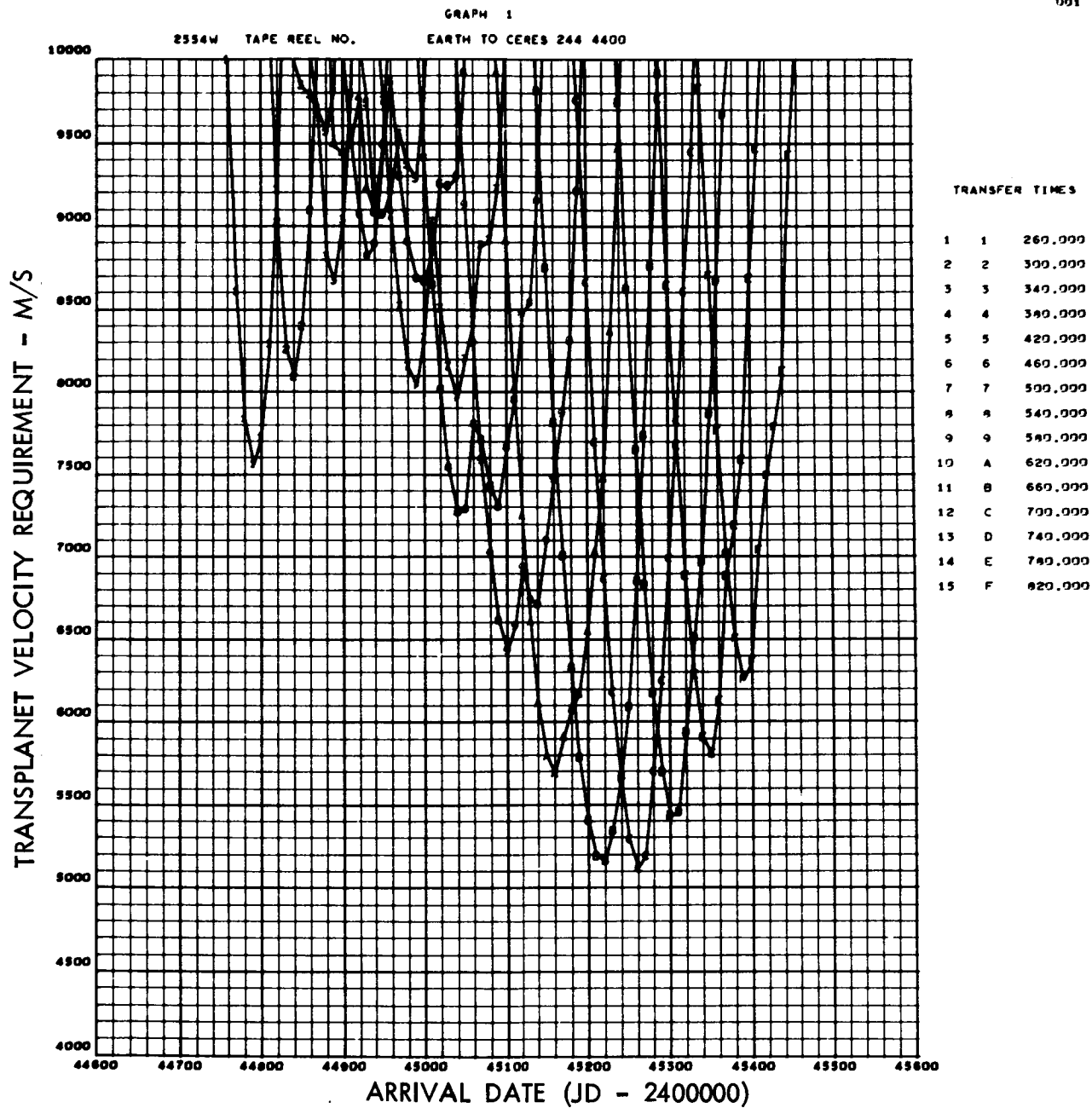
Figure 109.   Transplanet Velocity Requirements (1982 Ceres Opportunity)

SD 67-621-2
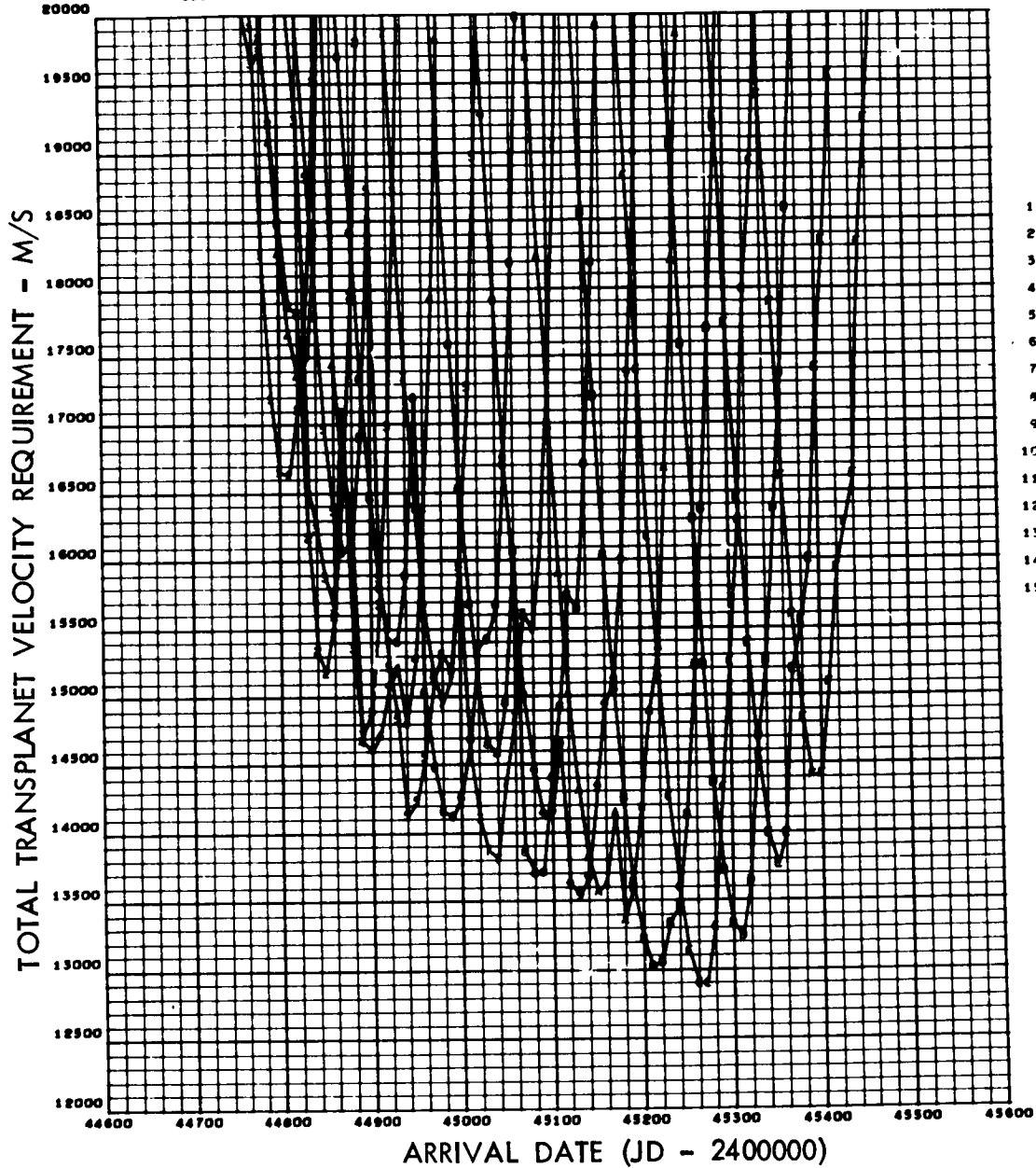
Figure 110.   Total Transplanet Velocity Requirements (1982 Ceres Opportunity)

2602-01
010   000

VELOCITY (M/S)

1	2000.000000
2	4000.000000
3	6000.000000
4	8000.000000
5	10000.000000
6	12000.000000
7	14000.000000
8	16000.000000
9	18000.000000
A	20000.000000

TRAN TIME

800

700

600

500

400

300

44800   45000   45200   45400

ARRIVAL DATE (JD - 2400000)

Figure 111. Total Transplanet Velocity Contours (1982 Ceres Opportunity)

GRAPH 1

J004A   TAPE REEL NO.   CERES TO EARTH 244 4660
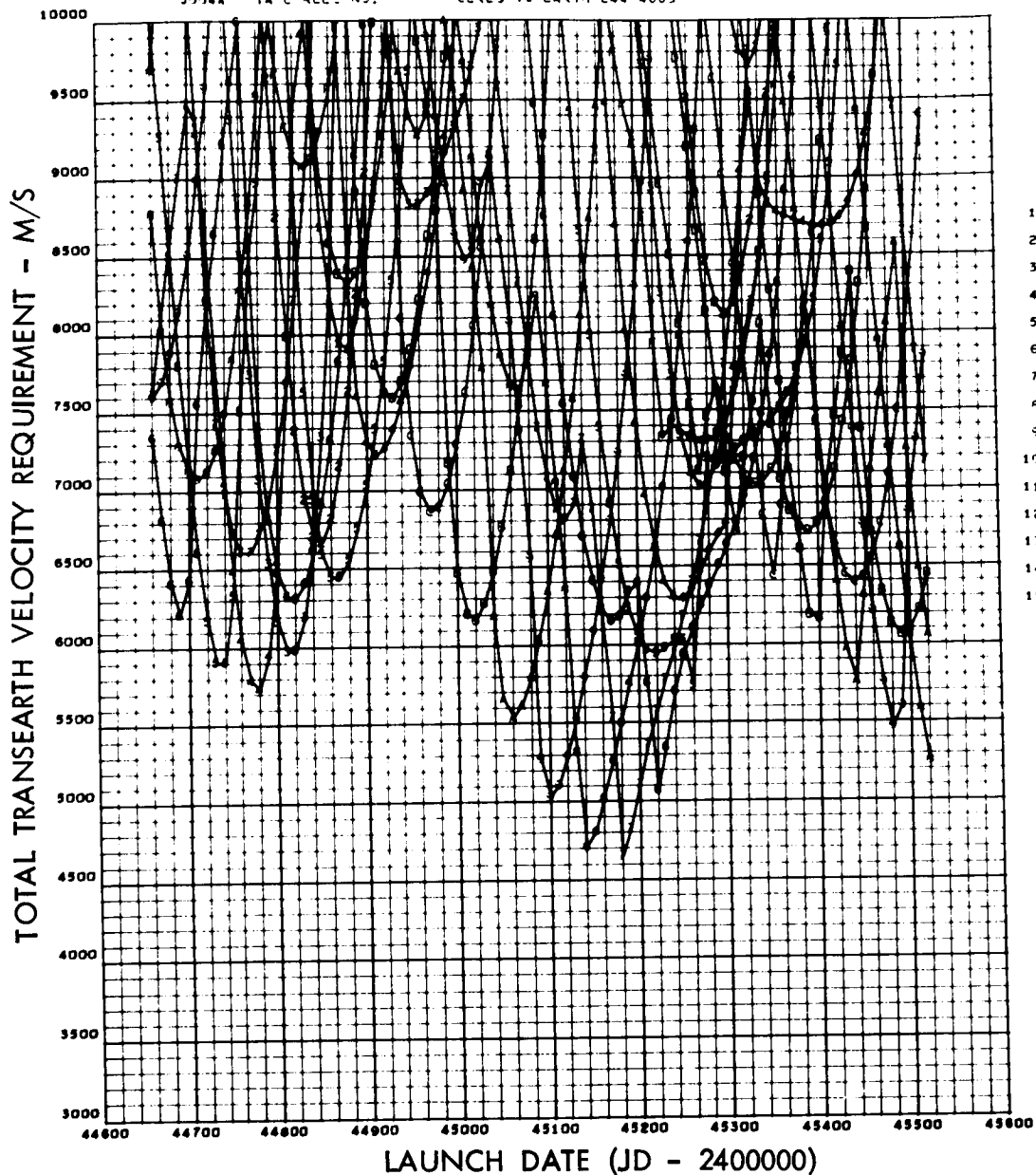
Figure 112.   Total Trans-Earth Velocity Requirements (1982 Ceres
Opportunity)

SD 67-621-2
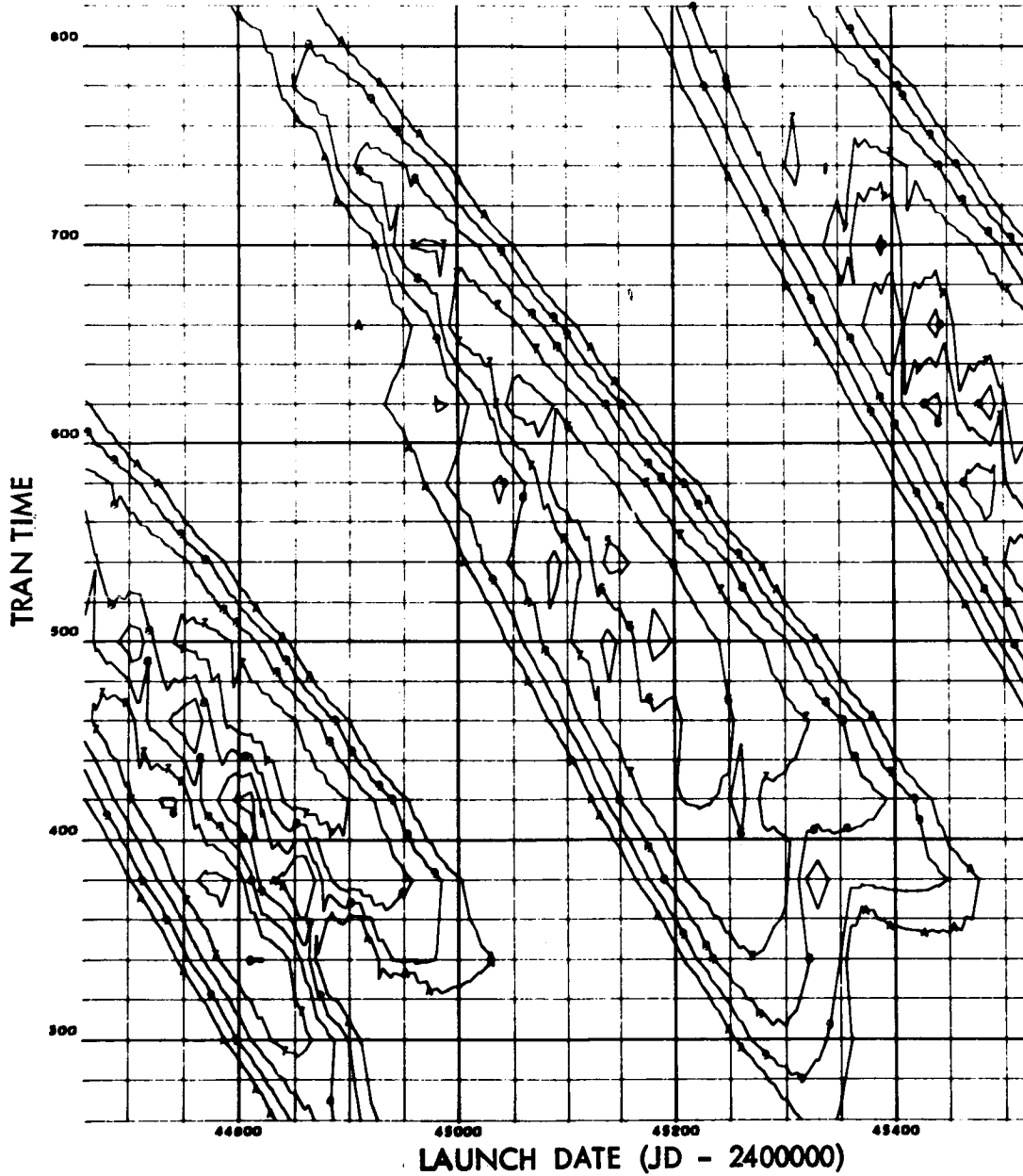
Figure 113. Total Trans-Earth Velocity Contours (1982 Ceres Opportunity)

GRAPH 1

WI33T   TAPE REEL NO.   EARTH TO CERES

TRANSFER TIMES

1	1	260.000
2	2	300.000
3	3	340.000
4	4	340.000
5	5	420.000
6	6	460.000
7	7	500.000
8	8	540.000
9	9	540.000
10	A	620.000
11	B	660.000
12	C	700.000
13	D	740.000
14	E	740.000
15	F	420.000

TRANSPLANET VELOCITY REQUIREMENT – M/S

ARRIVAL DATE (JD – 2400000)
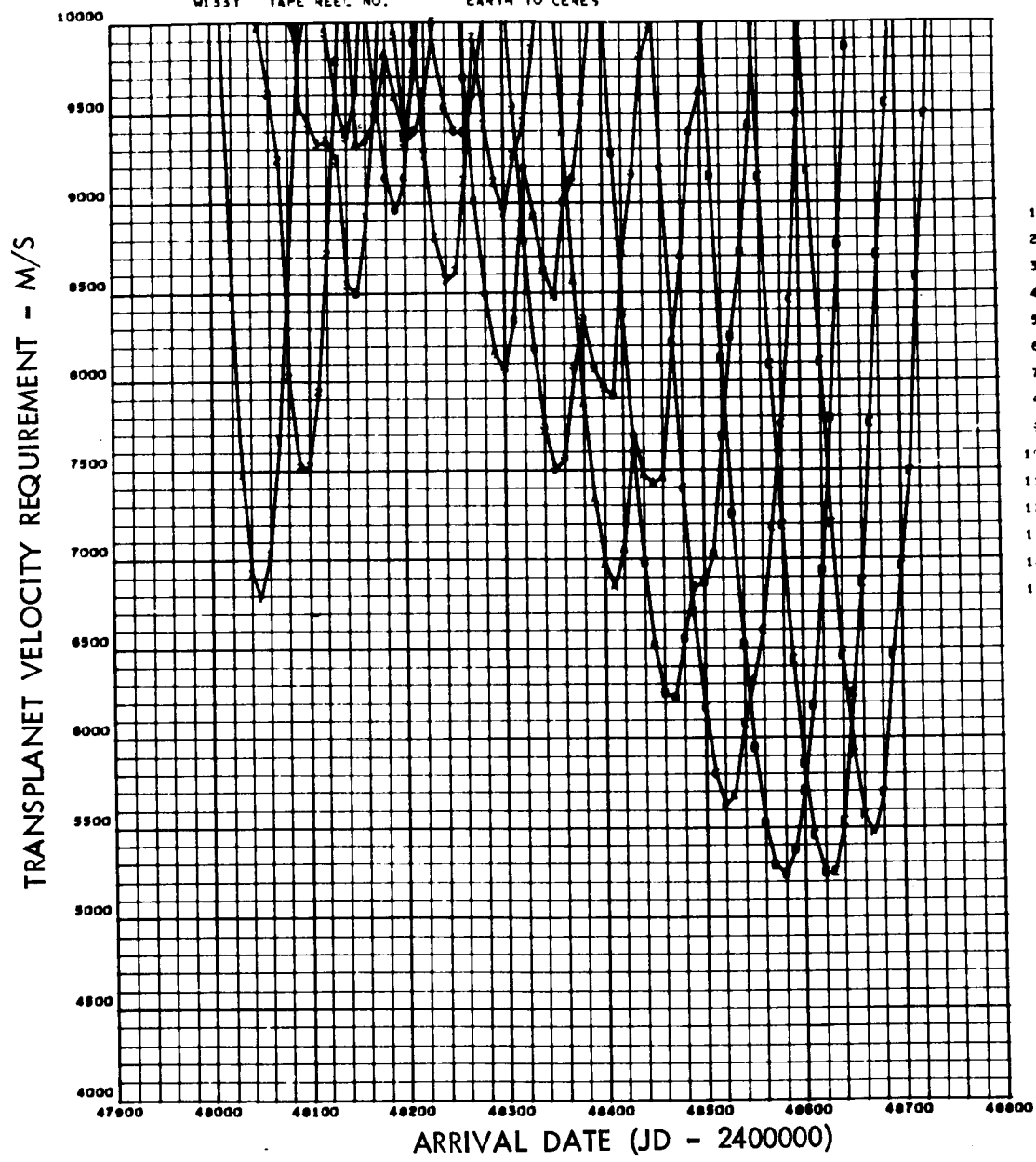
Figure 114. Transplanet Velocity Requirements (1991 Ceres Opportunity)

SD 67-621-2

GRAPH 2

W1337   TAPE REEL NO.   EARTH TO CERES

TRANSFER TIMES

1	1	260.000
2	2	300.000
3	3	340.000
4	4	340.000
5	5	420.000
6	6	460.000
7	7	500.000
4	4	540.000
9	9	540.000
10	A	620.000
11	B	660.000
12	C	700.000
13	D	740.000
14	E	740.000
15	F	820.000
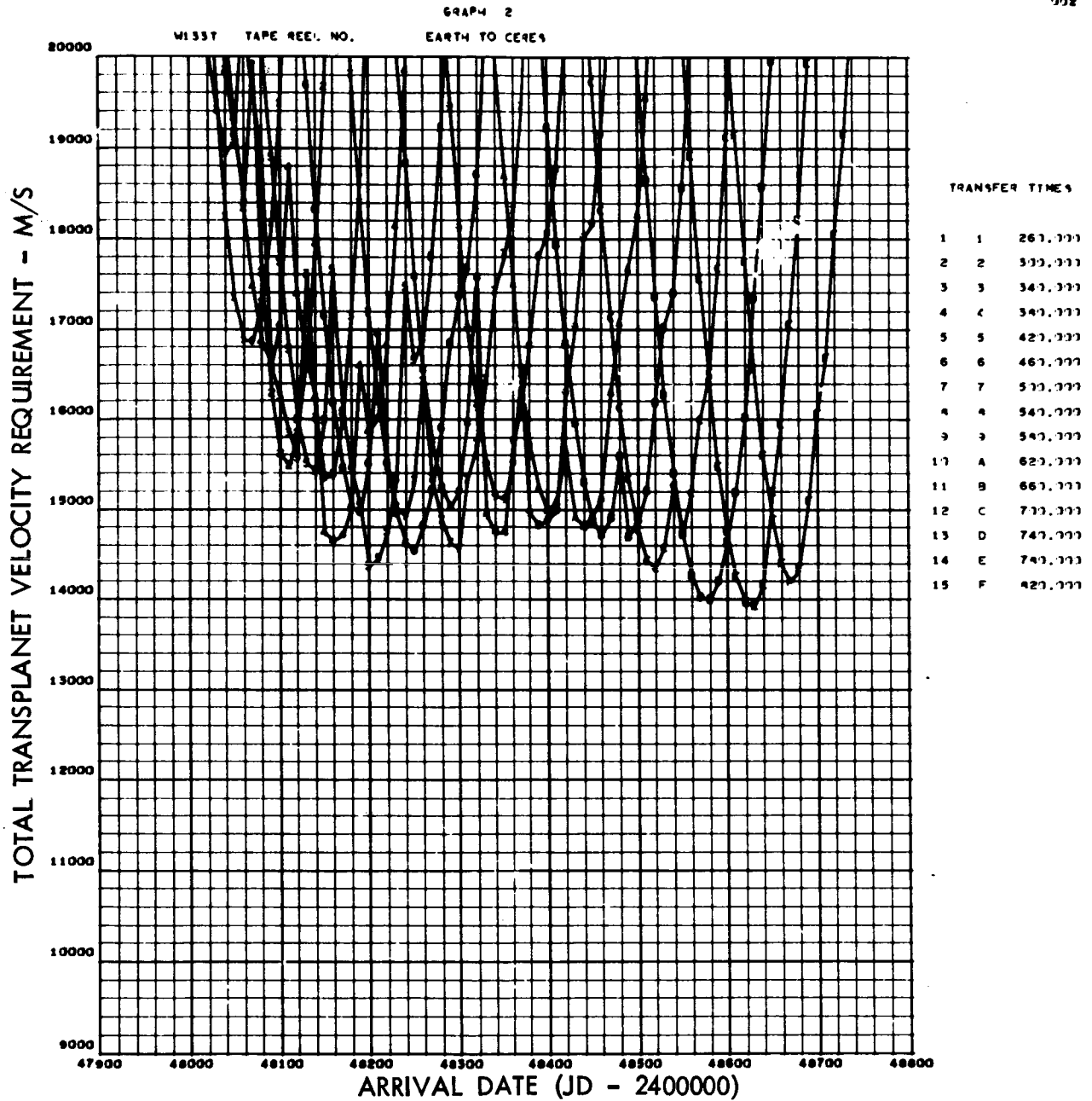
Figure 115.   Total Transplanet Velocity Requirements (1991 Ceres Opportunity)

- 157 -
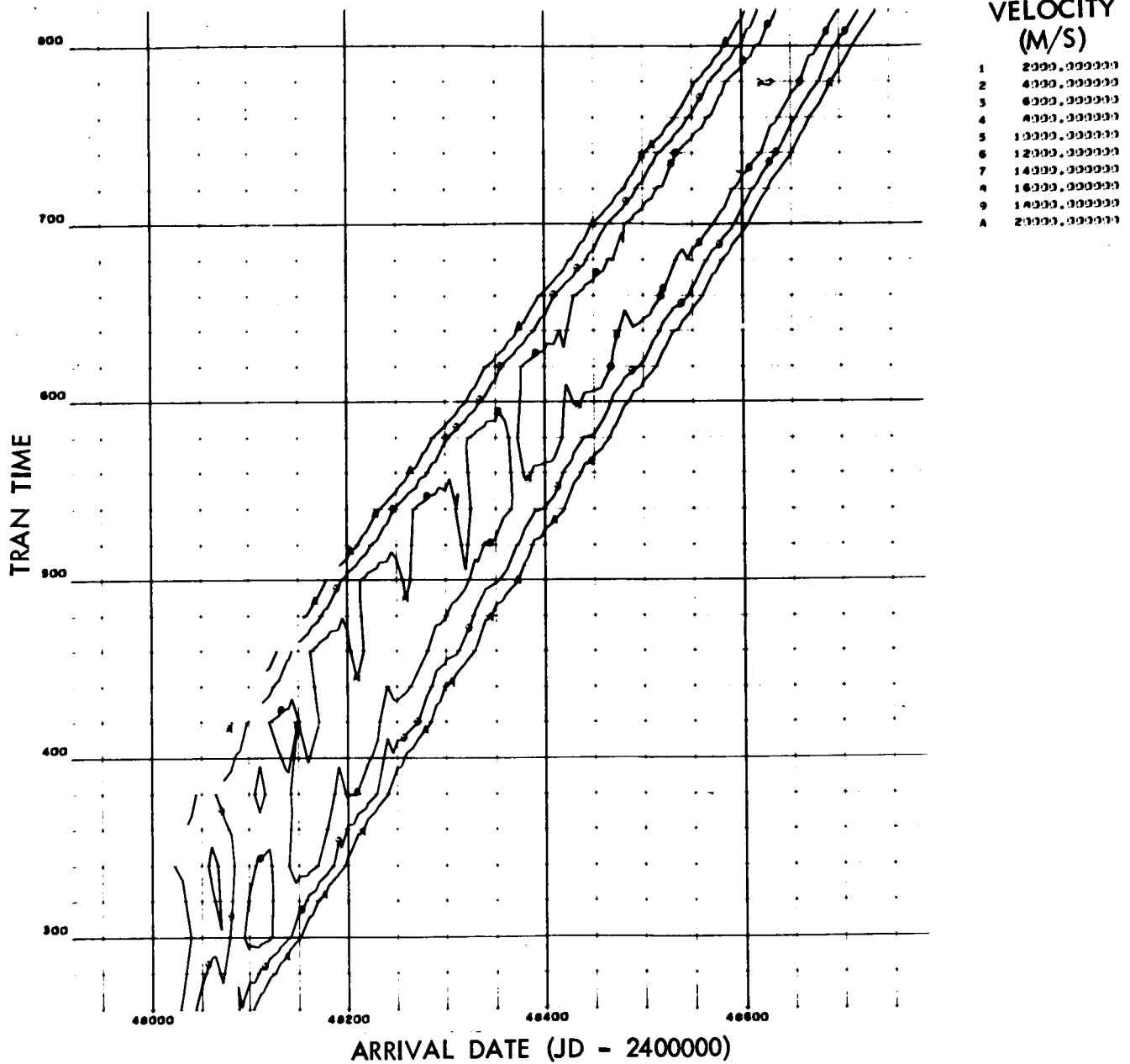
Figure 116.   Total Transplanet Velocity Contours (1991 Ceres
Opportunity)
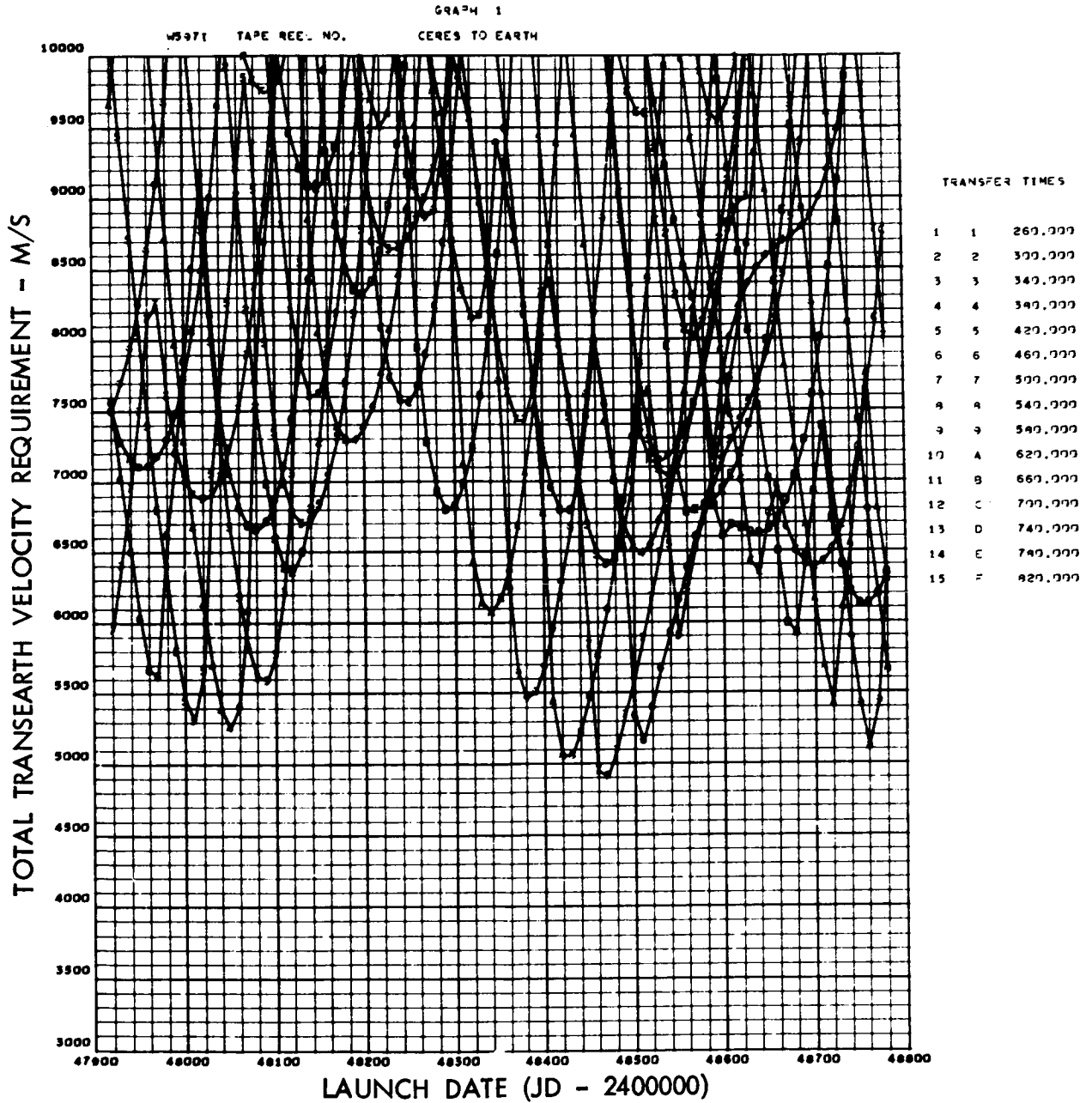
Figure 117. Total Trans-Earth Velocity Requirements (1991 Ceres
Opportunity)
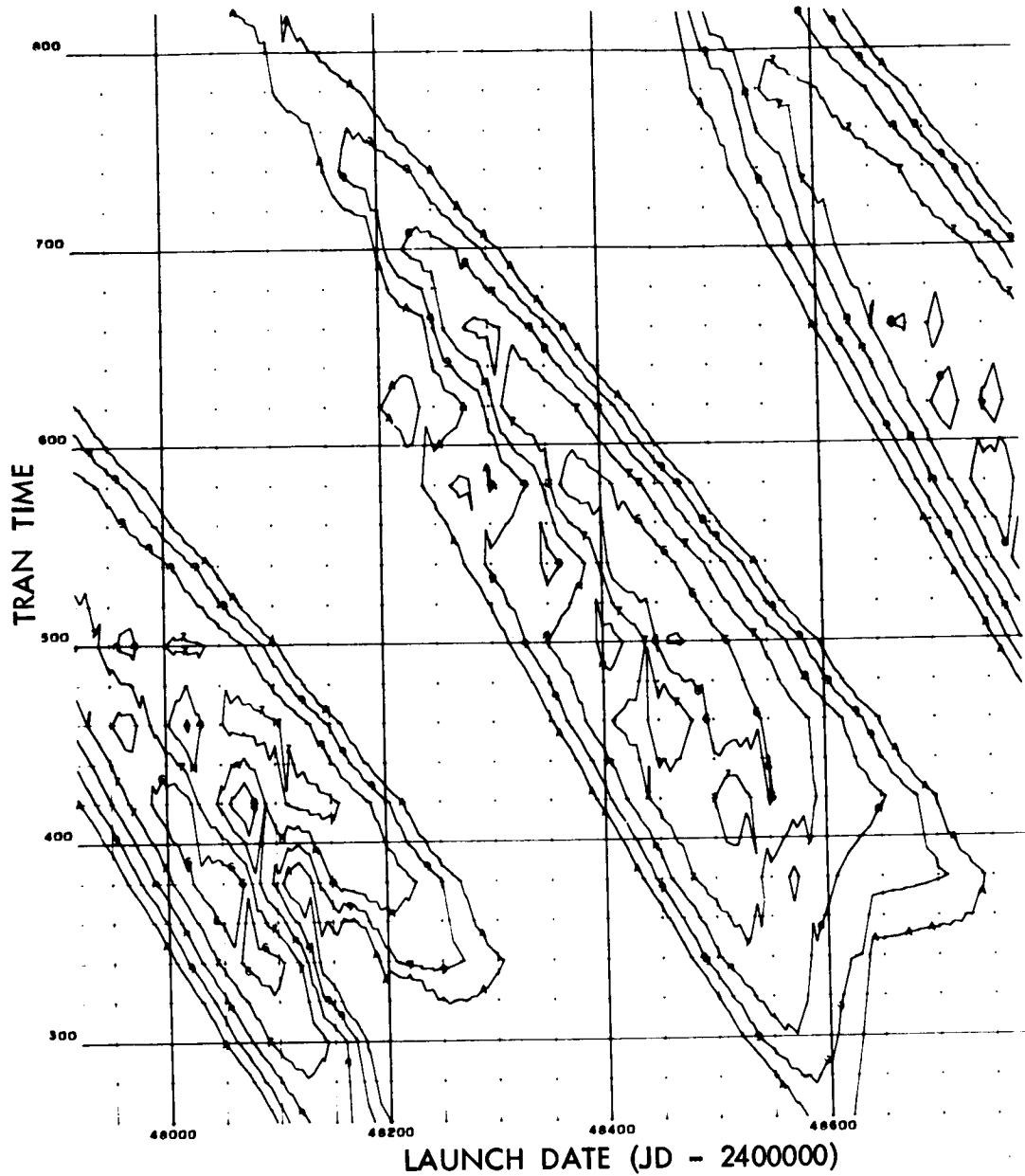
Figure 118. Total Trans-Earth Velocity Contours (1991 Ceres Opportunity)

SD 67-621-2
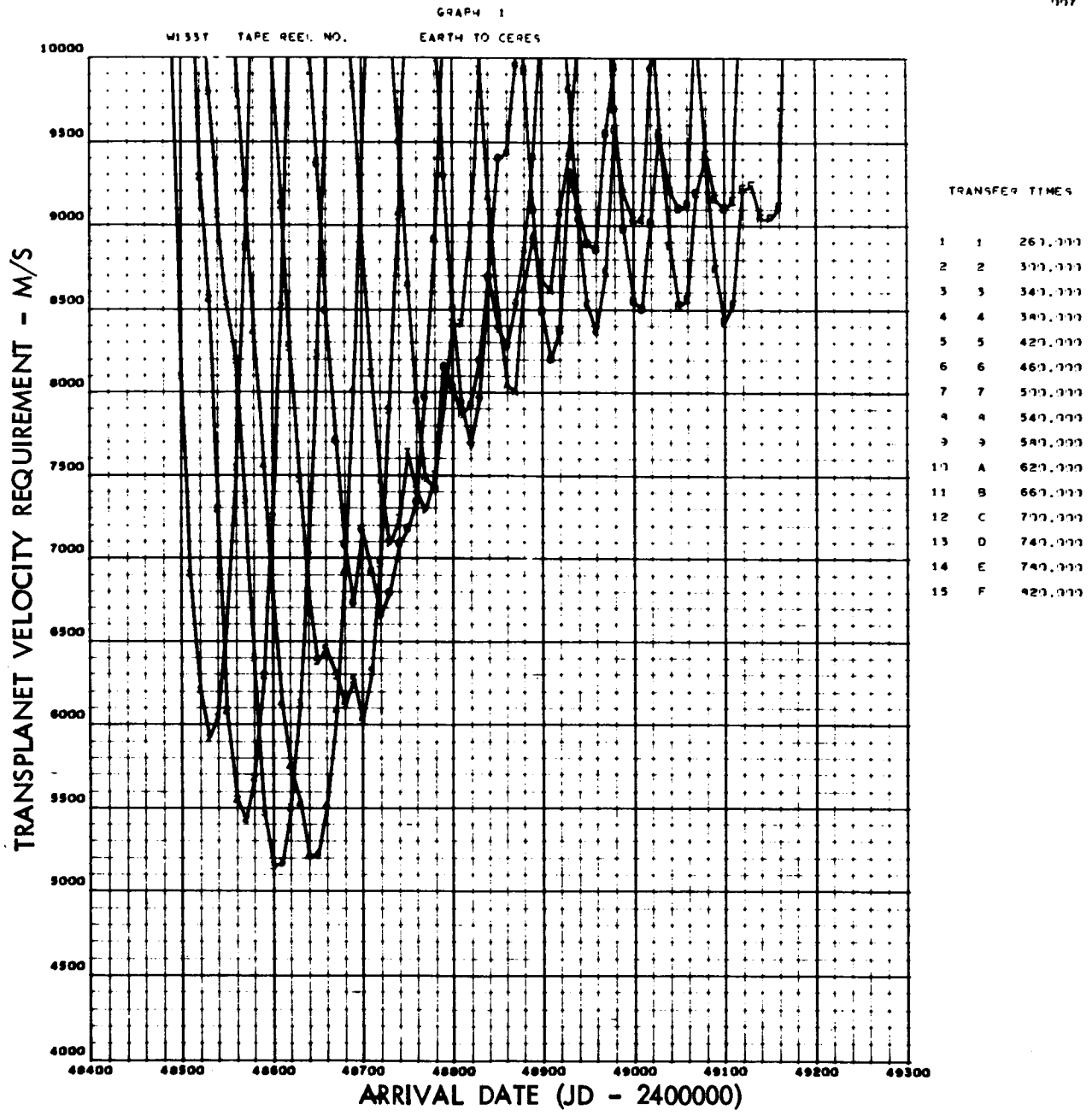
Figure 119. Transplanet Velocity Requirements (1992 Ceres Opportunity)

GRAPH 2

WI55T   TAPE REEL NO.   EARTH TO CERES

TRANSFER TIMES

1	1	260.000
2	2	300.000
3	3	340.000
4	4	340.000
5	5	420.000
6	6	460.000
7	7	500.000
8	8	540.000
9	9	580.000
10	A	620.000
11	B	660.000
12	C	700.000
13	D	740.000
14	E	740.000
15	F	820.000
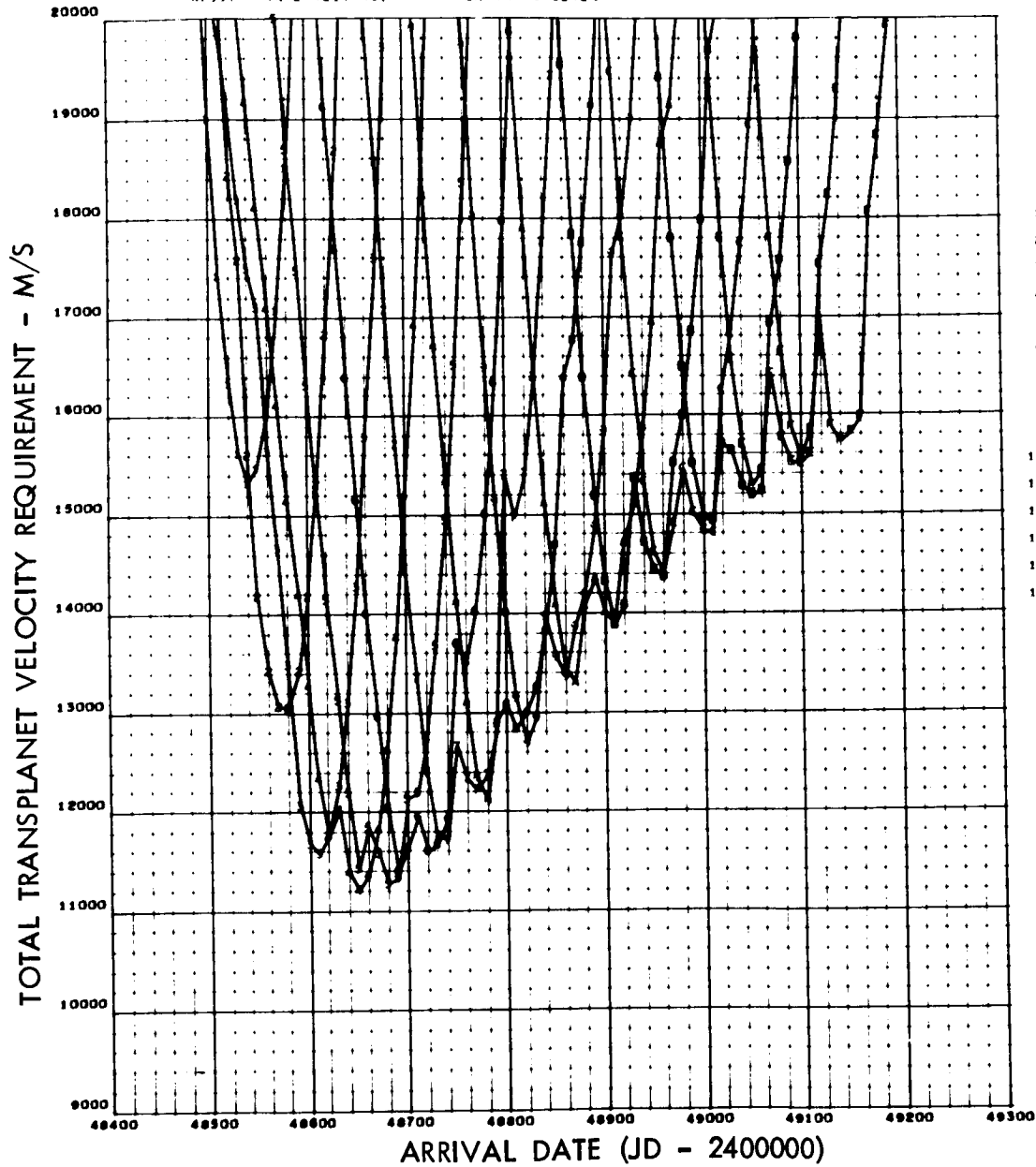
Figure 120.   Total Transplanet Velocity Requirements (1992 Ceres Opportunity)

SD 67-621-2
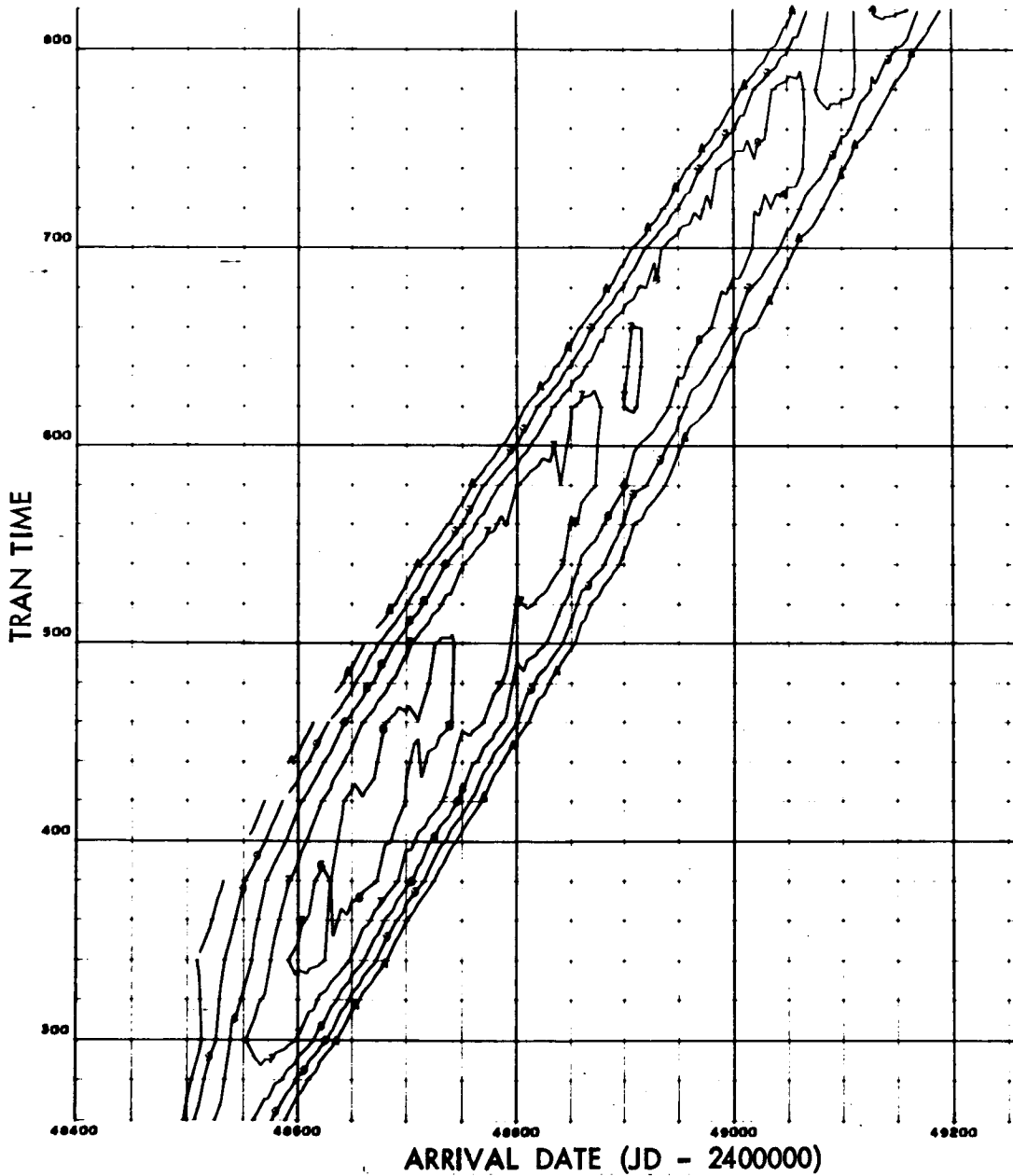
Figure 121. Total Transplanet Velocity Contours (1992 Ceres Opportunity)

SD 67-621-2

GRAPH 1

WS971   TAPE REEL NO.   CERES TO EARTH

TRANSFER TIMES

TOTAL TRANSEARTH VELOCITY REQUIREMENT – M/S

1	1	260.000
2	2	300.000
3	3	340.000
4	4	380.000
5	5	420.000
6	6	460.000
7	7	500.000
8	8	540.000
9	9	580.000
10	A	620.000
11	B	660.000
12	C	700.000
13	D	740.000
14	E	780.000
15	F	820.000

LAUNCH DATE (JD – 2400000)
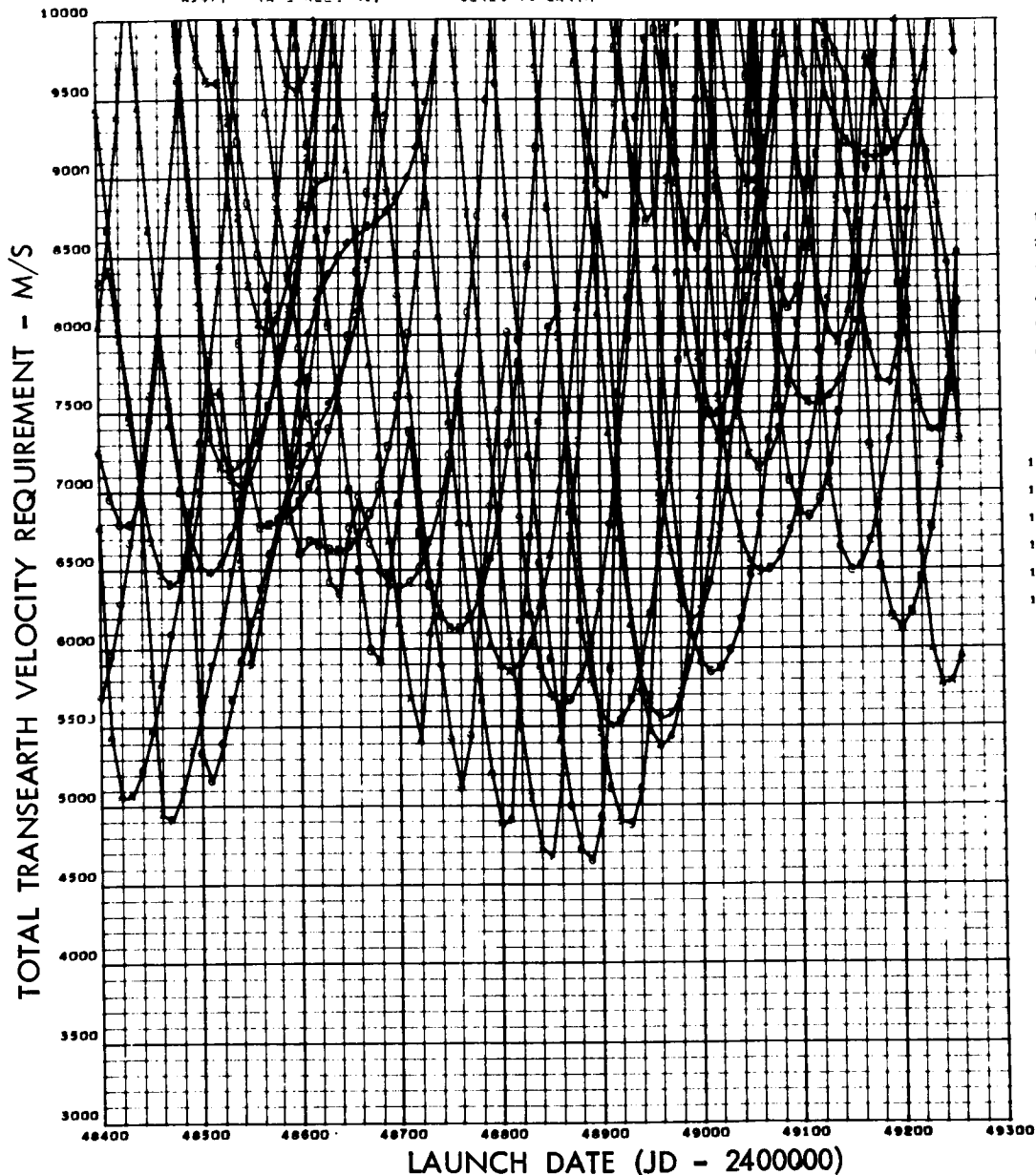
Figure 122.   Total Trans-Earth Velocity Requirements (1992 Ceres Opportunity)

- 164 -

SD 67-621-2
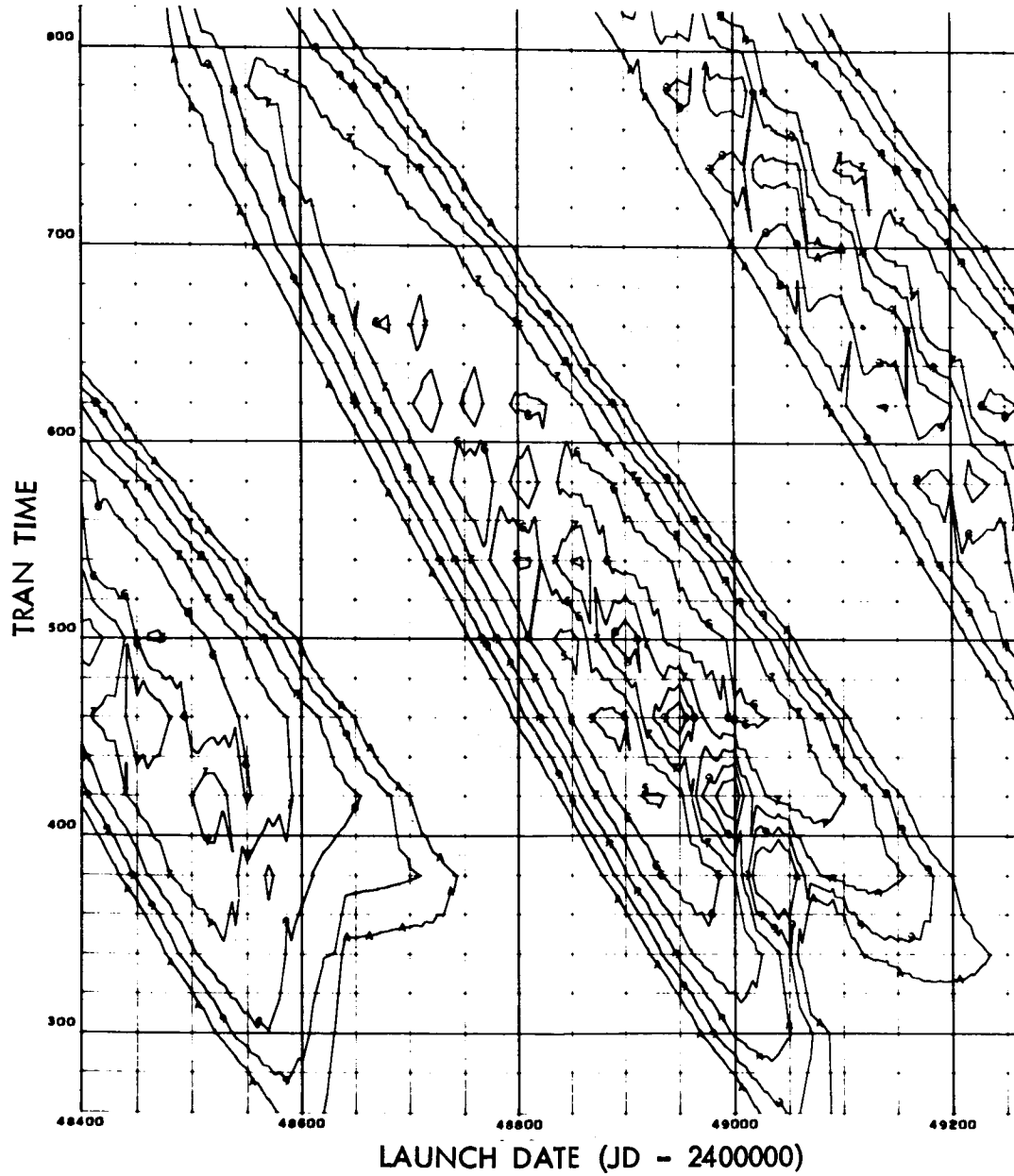
Figure 123. Total Trans-Earth Velocity Contours (1992 Ceres Opportunity)

- 165 -

SD 67-621-2

Figure 124. Transplanet Velocity Requirements (1993 Ceres Opportunity)

SD 67-621-2

GRAPH 2
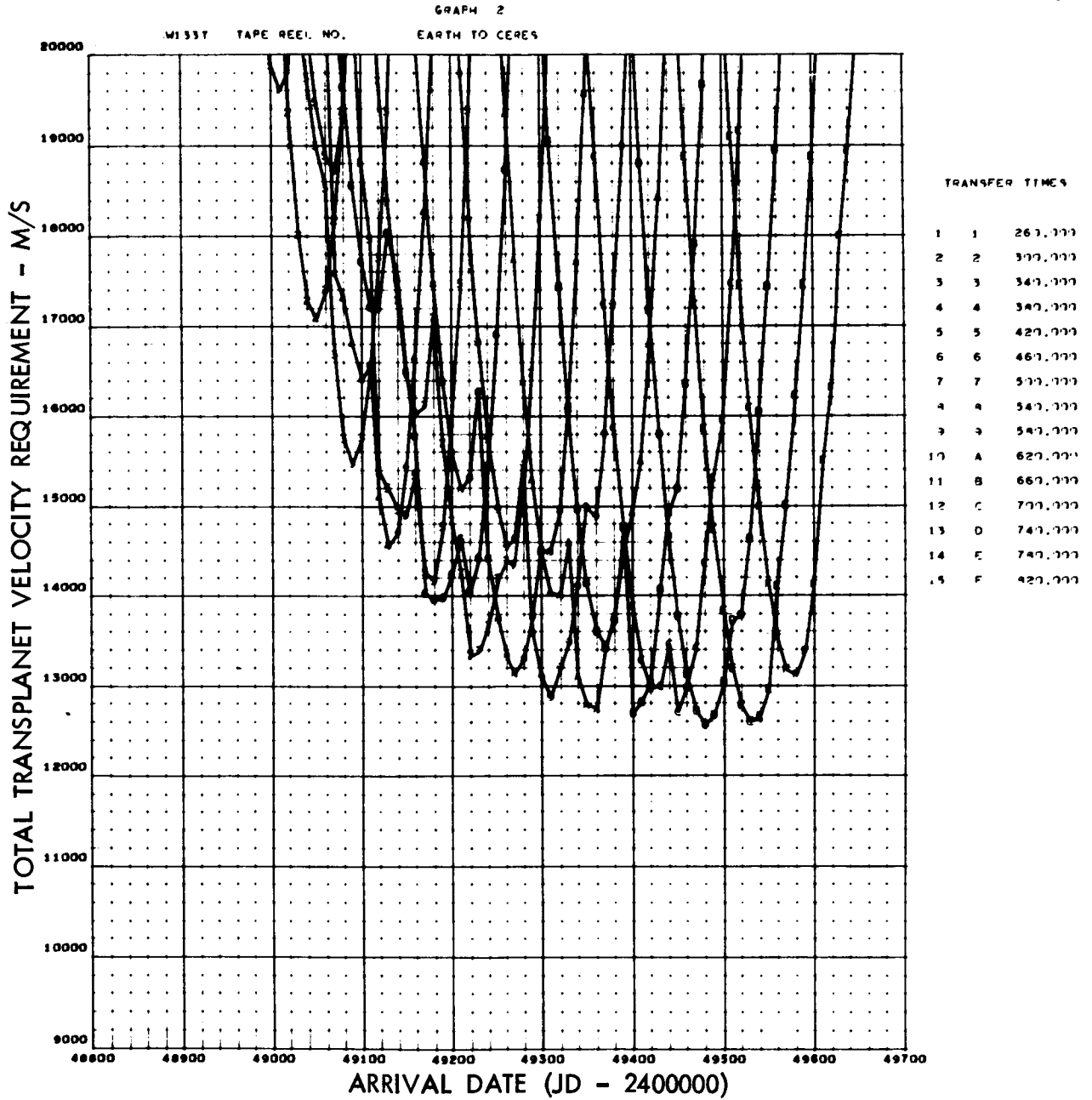
Figure 125.   Total Transplanet Velocity Requirements (1993 Ceres
Opportunity)

SD 67-621-2

VELOCITY
(M/S)

1   2000.000000
2   4000.000000
3   6000.000000
4   8000.000000
5   10000.000000
6   12000.000000
7   14000.000000
8   16000.000000
9   18000.000000
A   20000.000000

TRAN TIME

ARRIVAL DATE (JD - 2400000)

Figure 126. Total Transplanet Velocity Contours (1993 Ceres
Opportunity)

- 168 -

SD 67-621-2

Figure 127. Total Trans-Earth Velocity Requirements (1993 Ceres Opportunity)

Figure 128.   Total Trans-Earth Velocity Contours (1993 Ceres Opportunity)

SD 67-621-2

GRAPH 1

W133T   TAPE REEL NO.   EARTH TO CERES

TRANSFER TIMES

1	1	260.000
2	2	300.000
3	3	340.000
4	4	380.000
5	5	420.000
6	6	460.000
7	7	500.000
8	8	540.000
9	9	580.000
10	A	620.000
11	B	660.000
12	C	700.000
13	D	740.000
14	E	780.000
15	F	820.000

Figure 129.   Transplanet Velocity Requirements (1994 Ceres Opportunity)

GRAPH 2

WI33T   TAPE REEL NO.   EARTH TO CERES

TOTAL TRANSPLANET VELOCITY REQUIREMENT – M/S

ARRIVAL DATE (JD – 2400000)

TRANSFER TIMES

1	1	261.000
2	2	300.000
3	3	340.000
4	4	340.000
5	5	420.000
6	6	460.000
7	7	500.000
8	8	540.000
9	9	540.000
10	A	620.000
11	B	660.000
12	C	700.000
13	D	740.000
14	E	740.000
15	F	820.000

Figure 130. Total Transplanet Velocity Requirements (1994 Ceres
Opportunity)

- 172 -

WISST   TAPE REEL NO.   EARTH TO CERES

VELOCITY
(M/S)

1	2000.000000
2	4000.000000
3	6000.000000
4	8000.000000
5	10000.000000
6	12000.000000
7	14000.000000
8	16000.000000
9	18000.000000
A	20000.000000

Figure 131. Total Transplanet Velocity Contours (1994 Ceres Opportunity)

SD 67-621-2

Figure 132.   Total Trans-Earth Velocity Requirements (1994 Ceres
Opportunity)
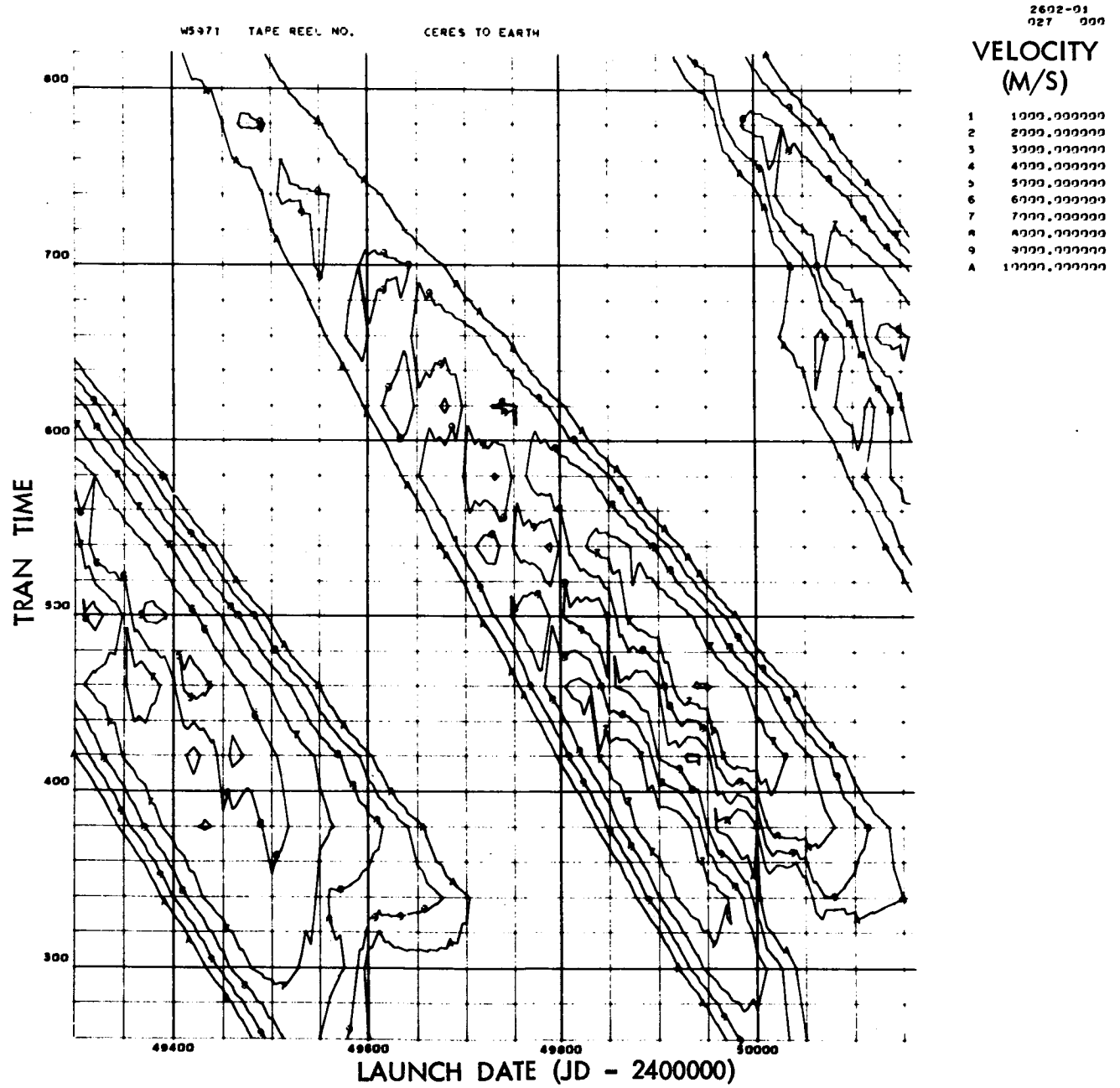
Figure 133. Total Trans-Earth Velocity Contours (1994 Ceres Opportunity)

SD 67-621-2
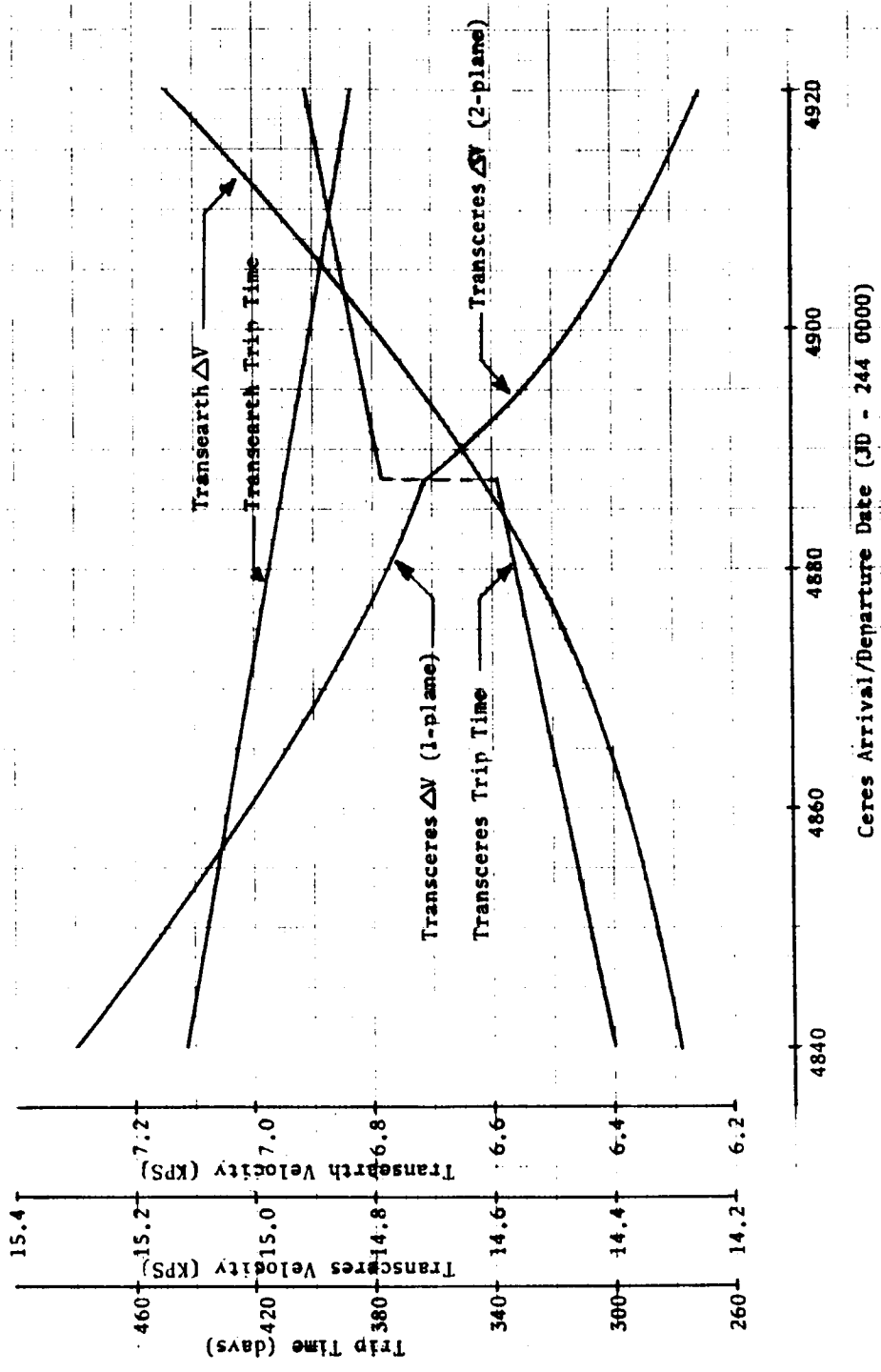
Figure 134. Velocity Requirements Summary (1982 Ceres Opportunity)

- 176 -
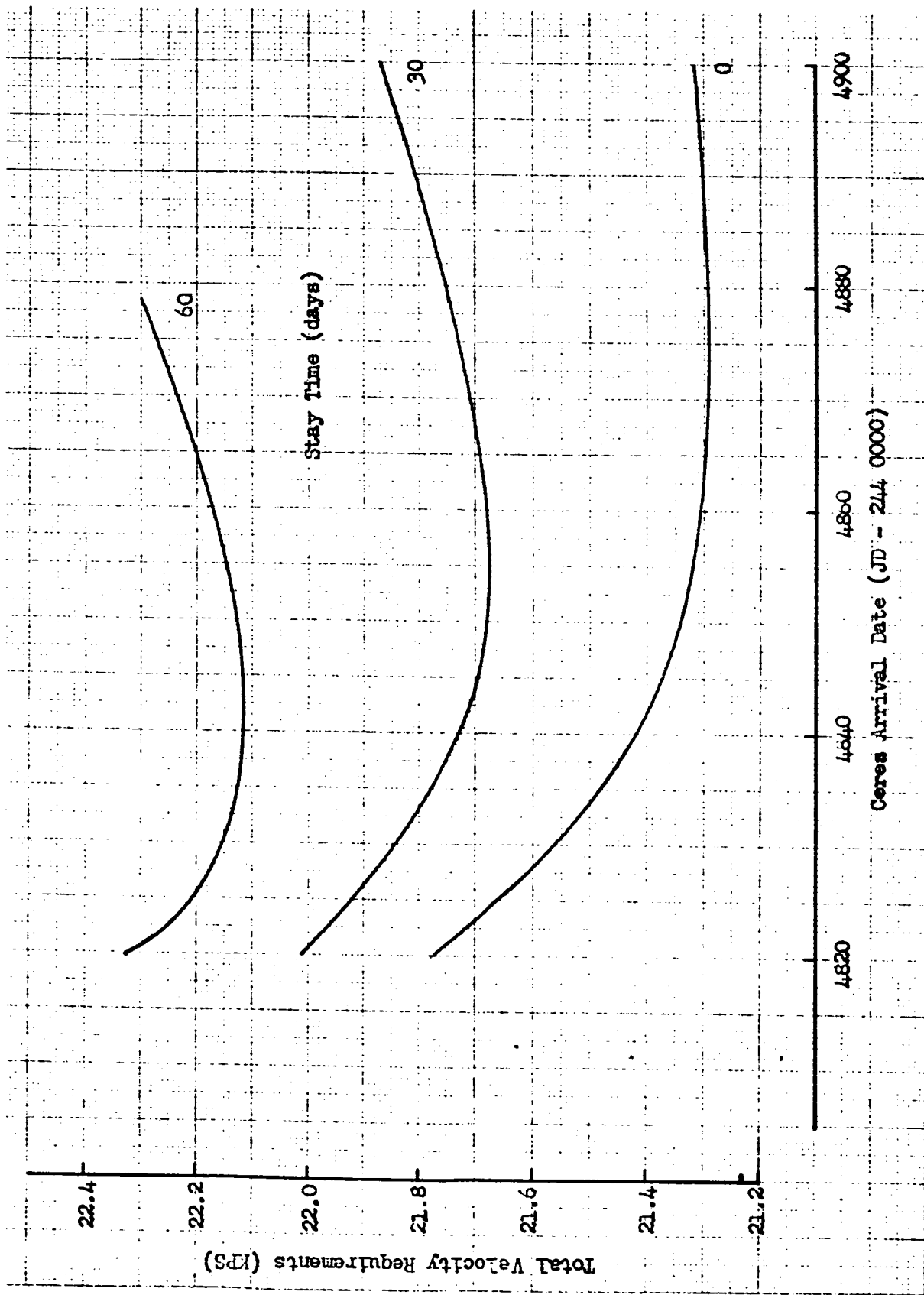
Figure 135. Total Ceres Mission Requirements (1982 Ceres Opportunity)

SD 67-621-2
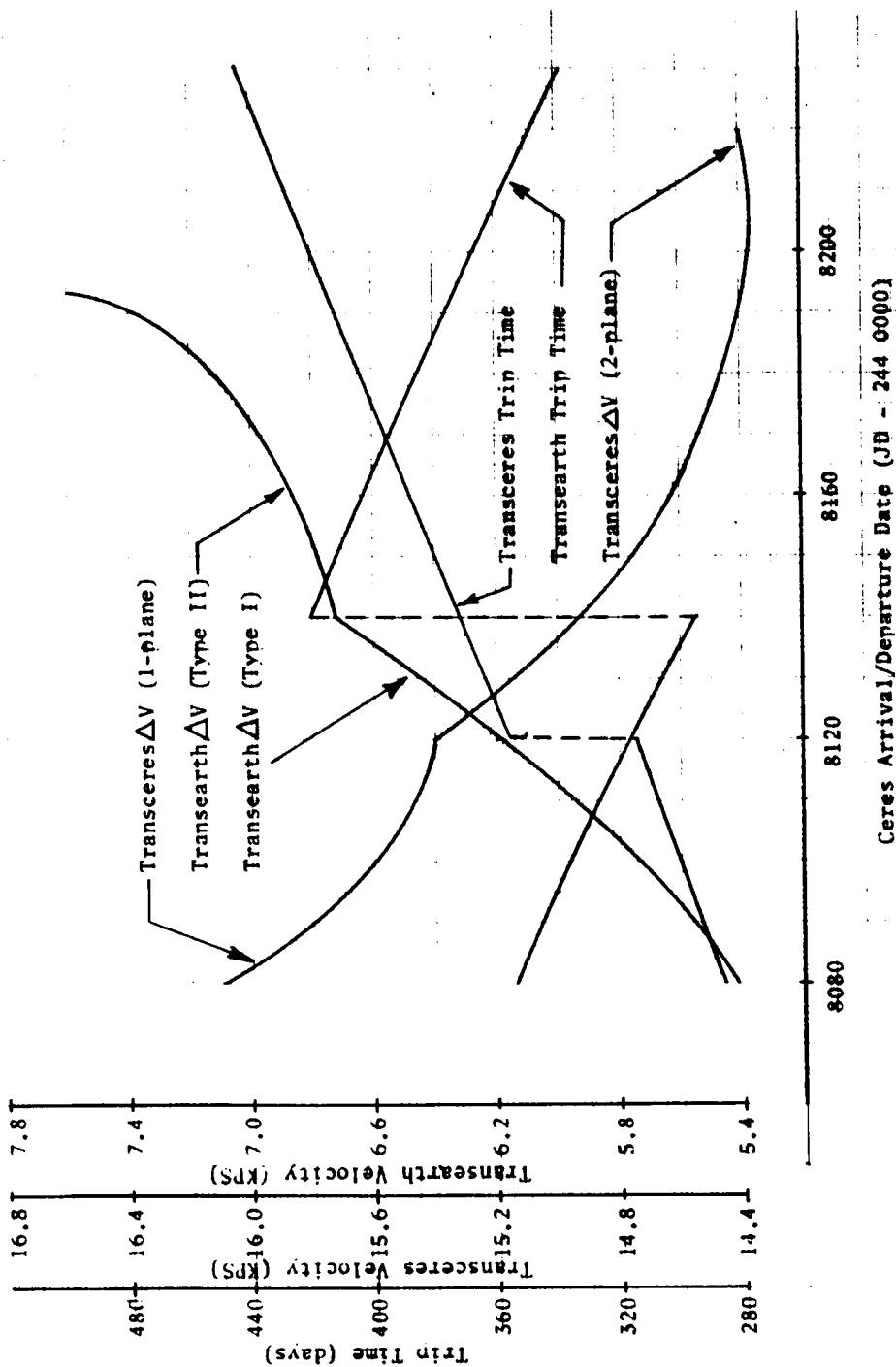
Figure 136. Velocity Requirements Summary (1991 Ceres Opportunity)

SD 67-621-2
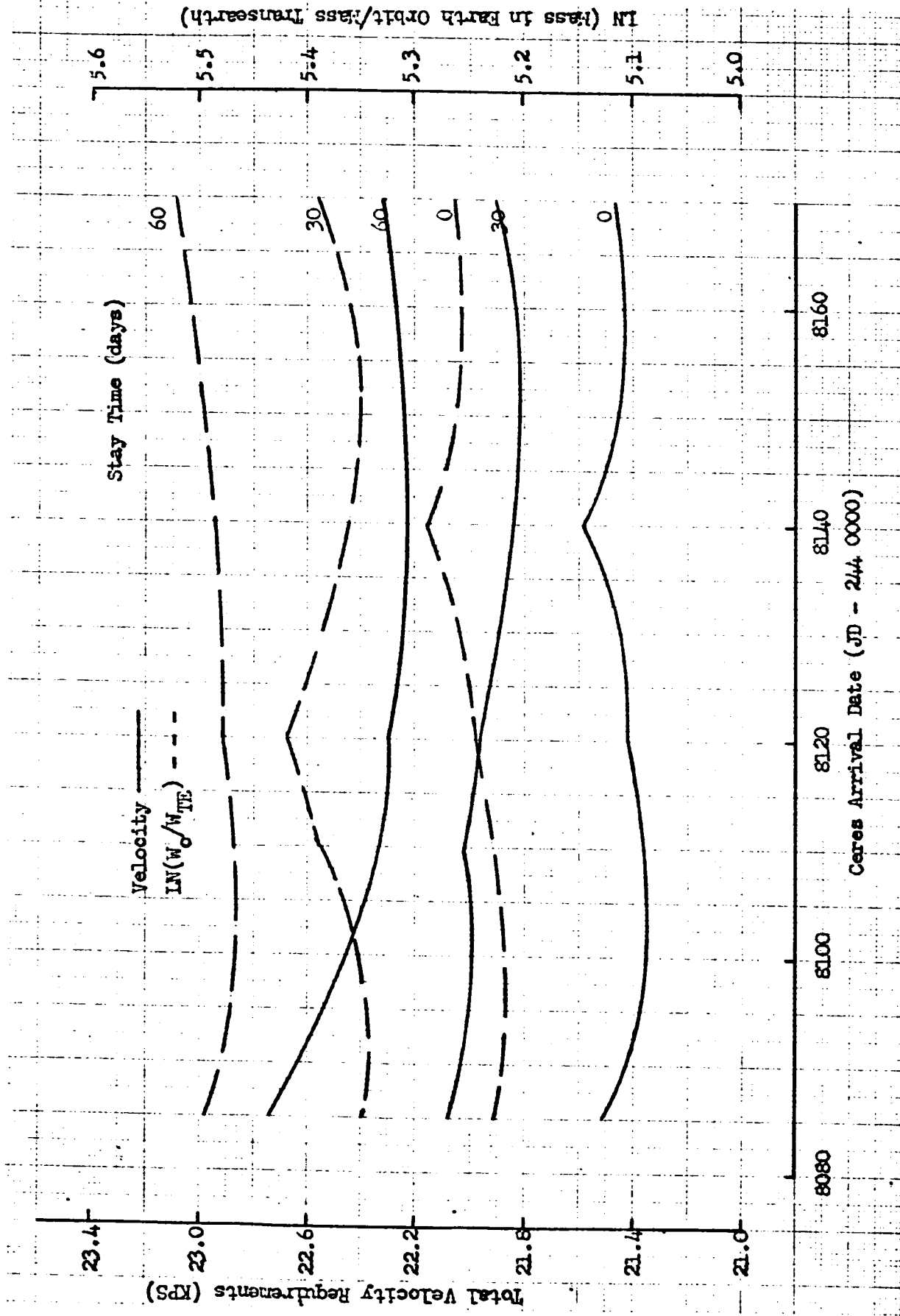
Figure 137. Total Ceres Mission Requirements (1991 Ceres Opportunity)
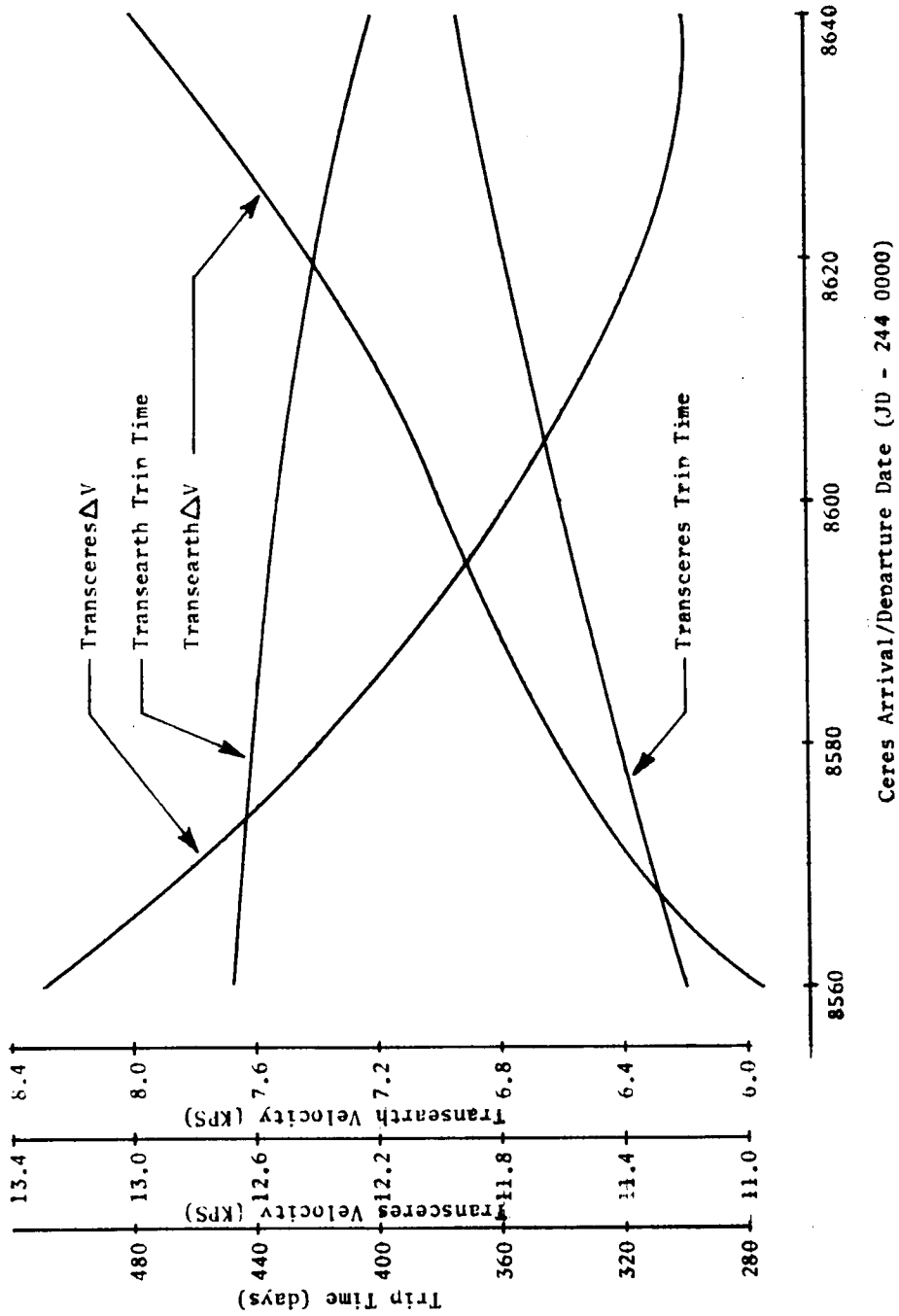
Figure 138. Velocity Requirements Summary (1992 Ceres Opportunity)

SD 67-621-2
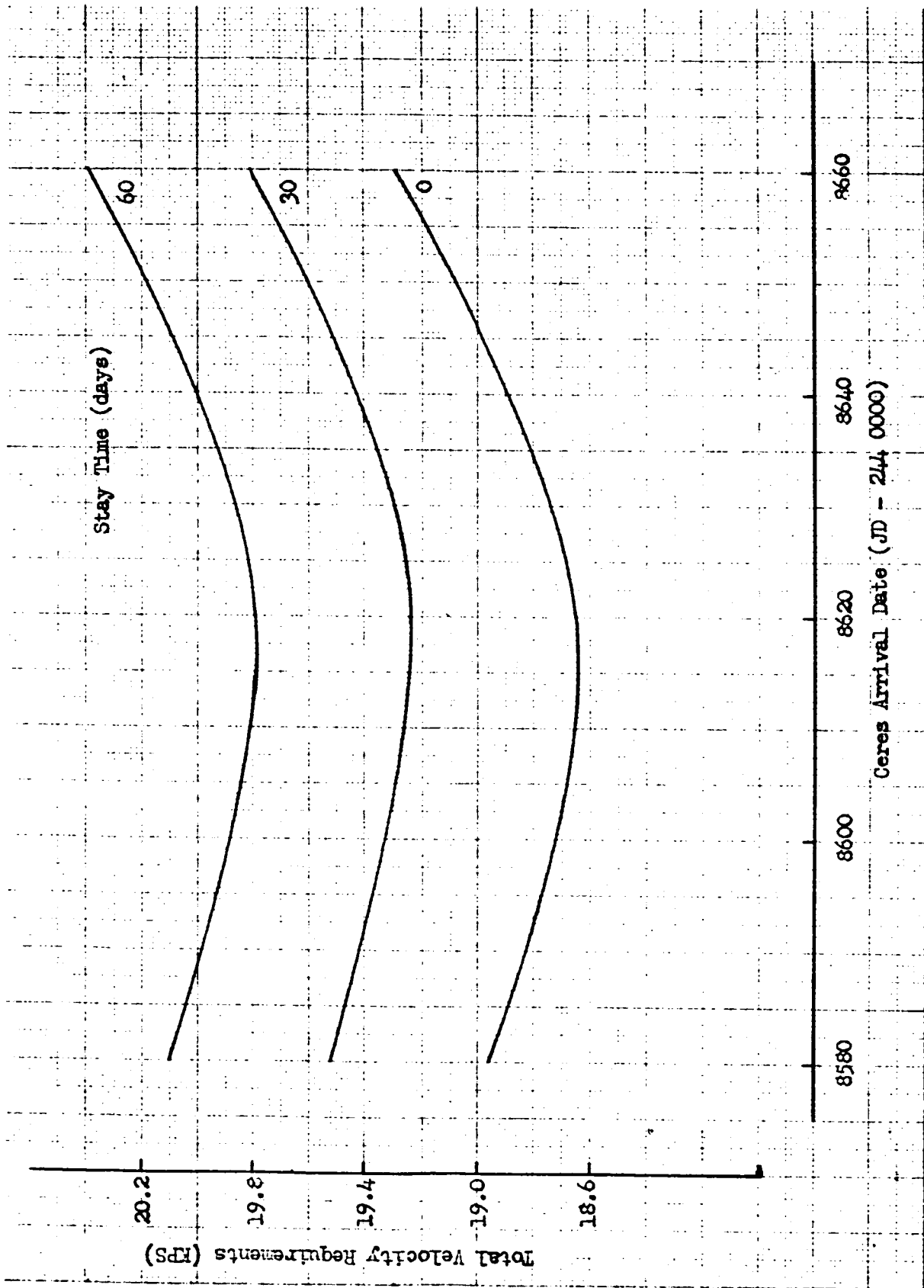
Figure 139. Total Ceres Mission Requirements (1992 Ceres Opportunity)
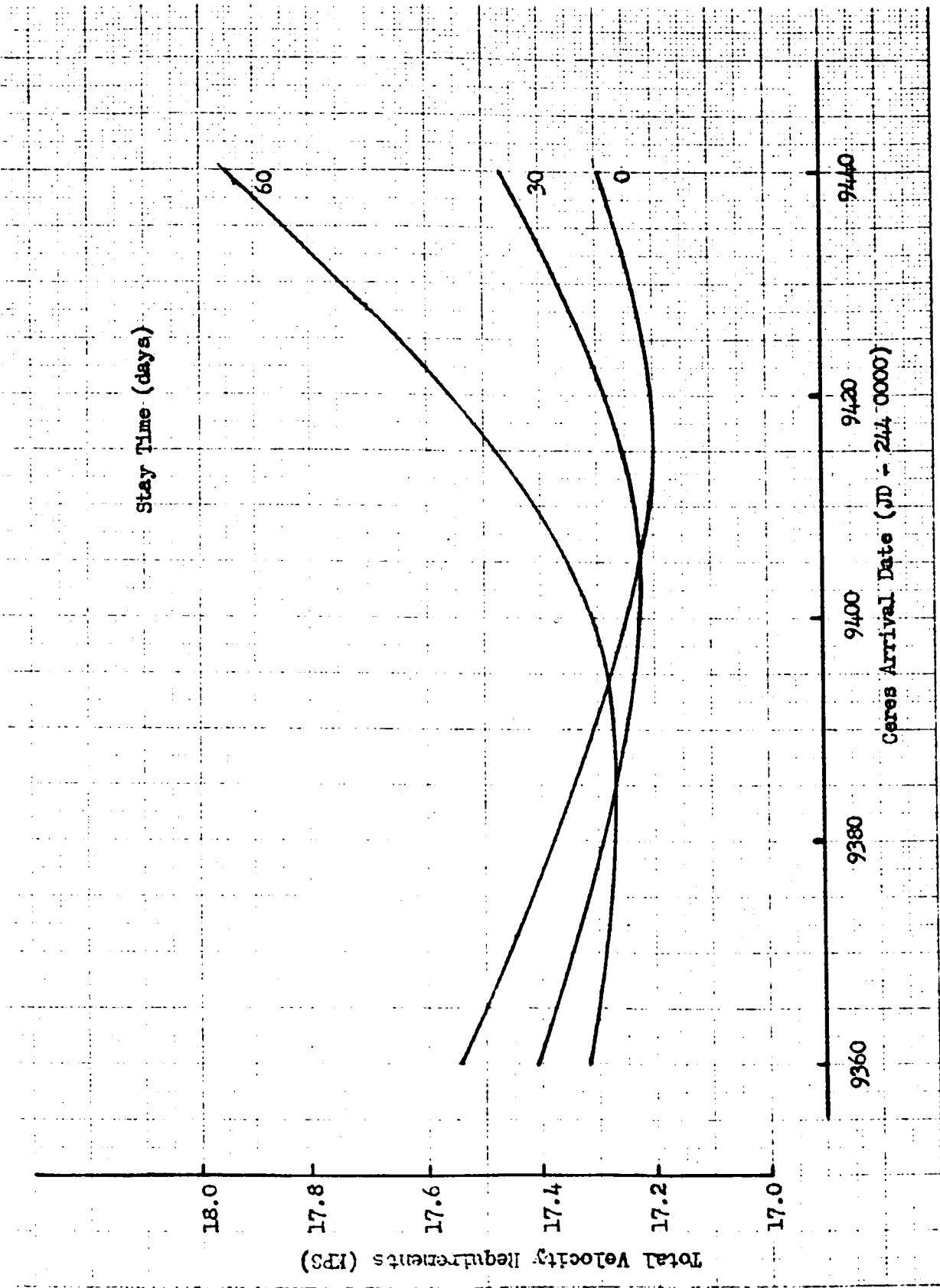
Figure 140. Total Ceres Mission Requirements (1993 Ceres Opportunity)
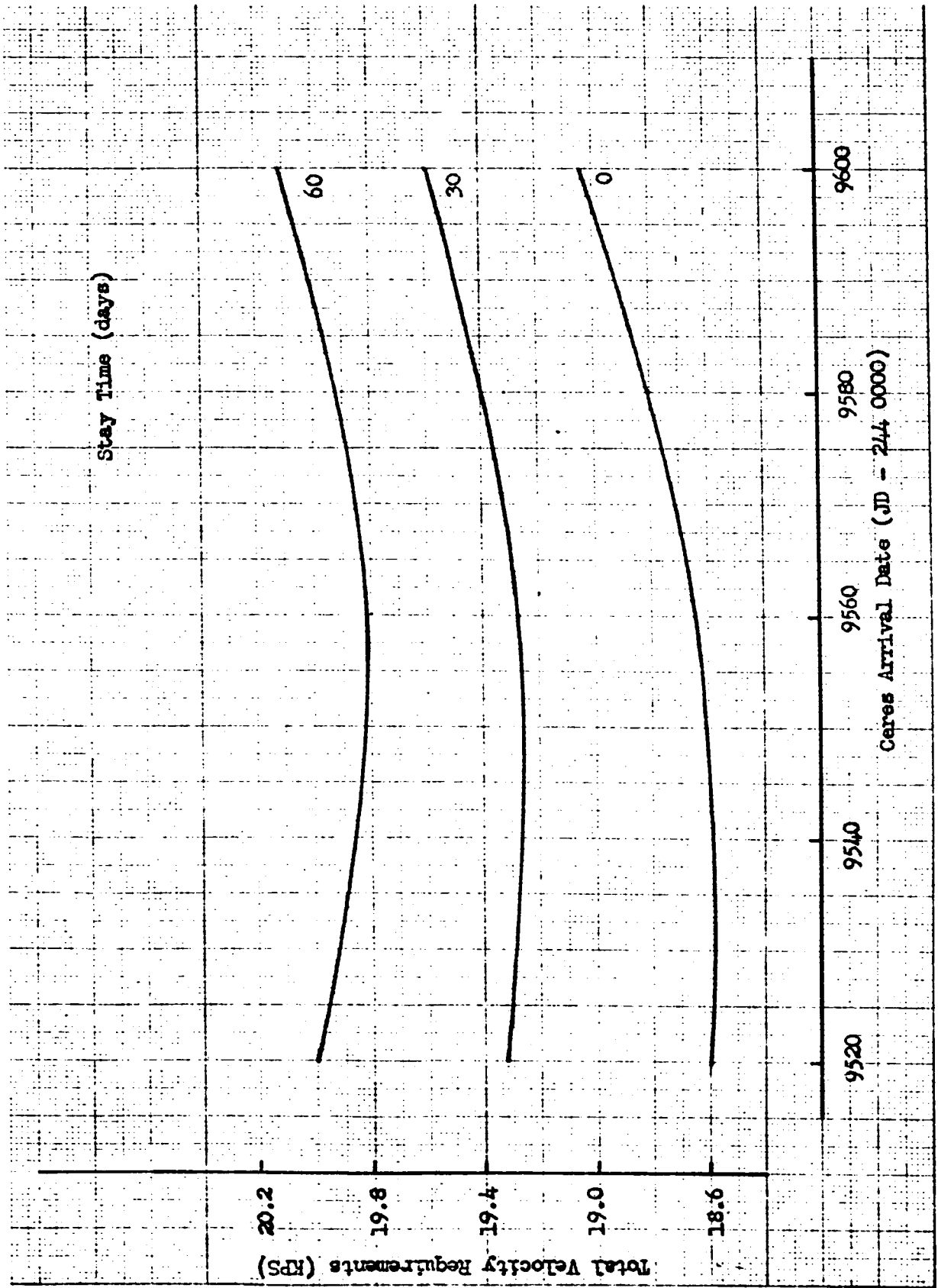
Figure 141. Total Ceres Mission Requirements (1994 Ceres Opportunity)

SD 67-621-2
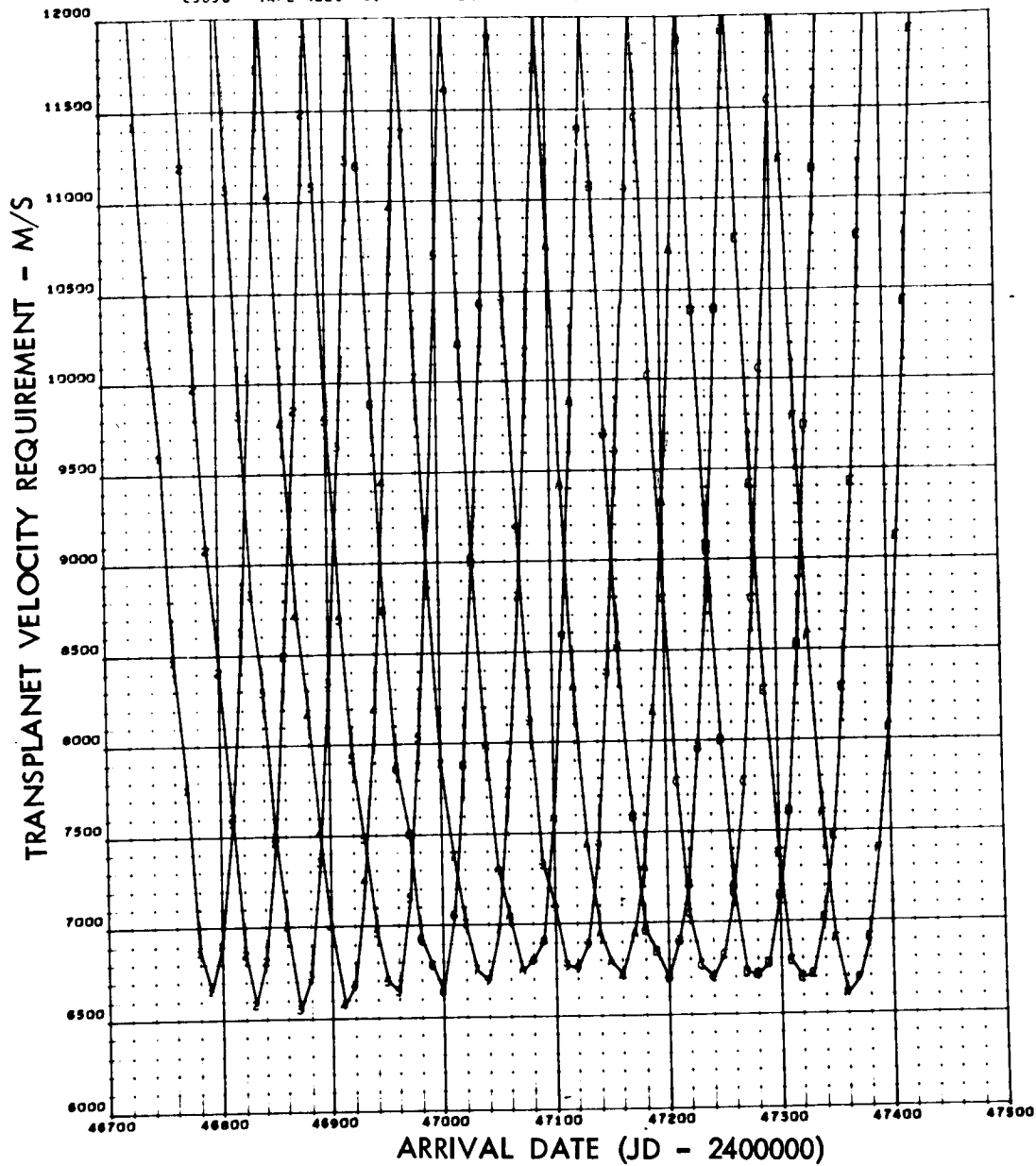
Figure 142. Transplanet Velocity Requirements (1985 Jupiter Opportunity)
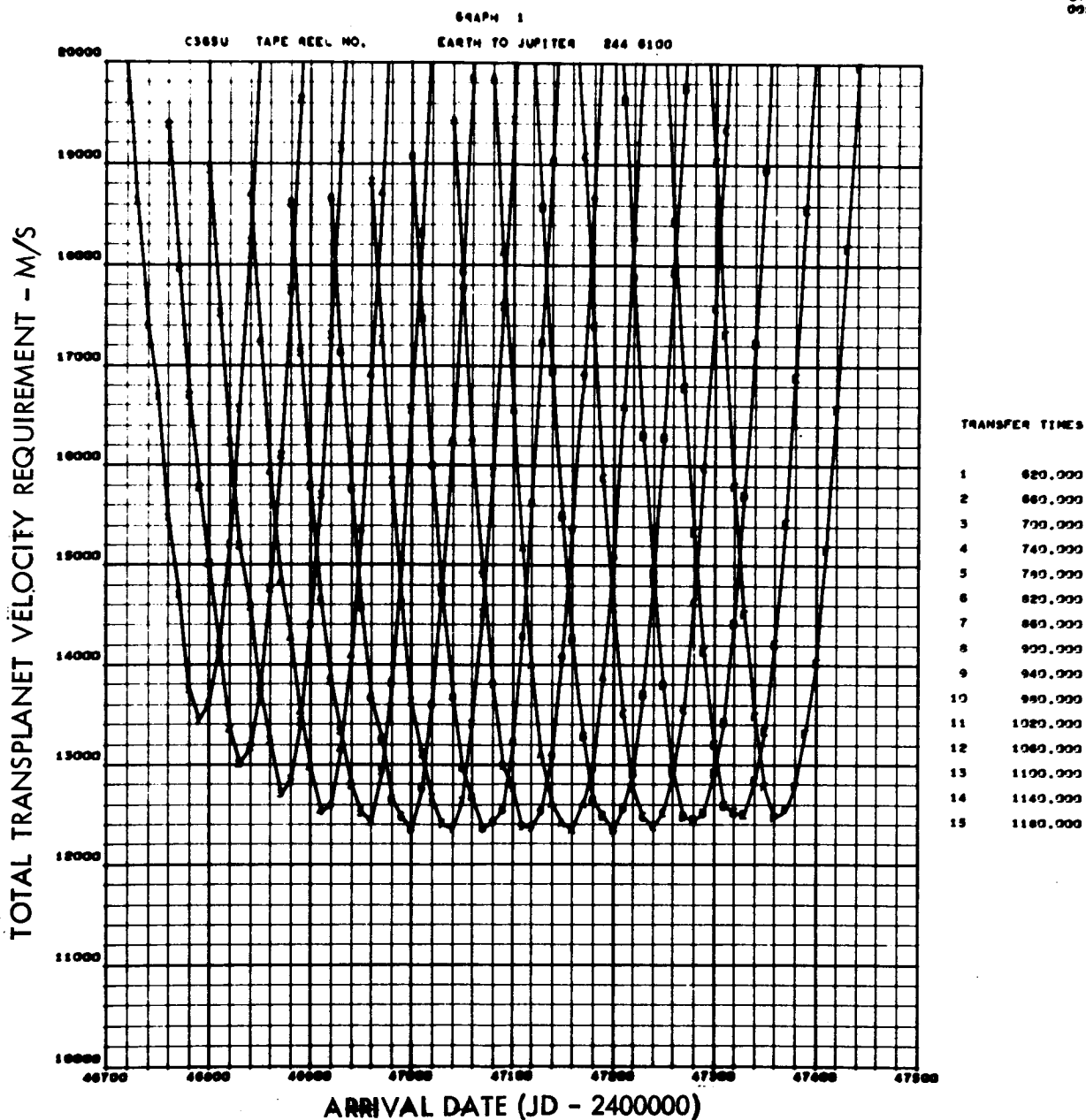
Figure 143. Total Transplanet Velocity Requirements (1985 Jupiter Opportunity)

SD 67-621-2.
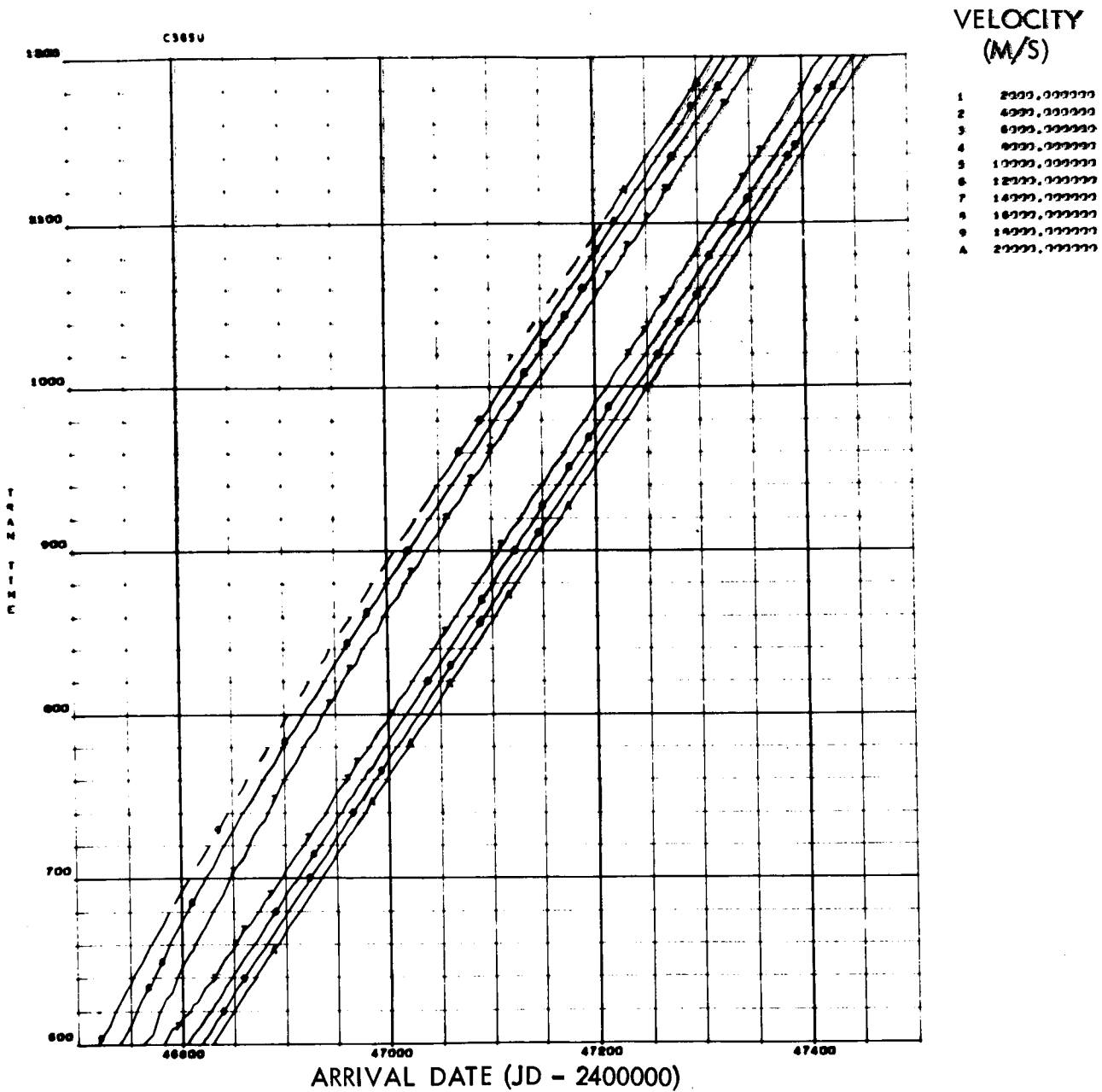
Figure 144. Total Transplanet Velocity Contours (1985 Jupiter Opportunity)

SD 67-621-2
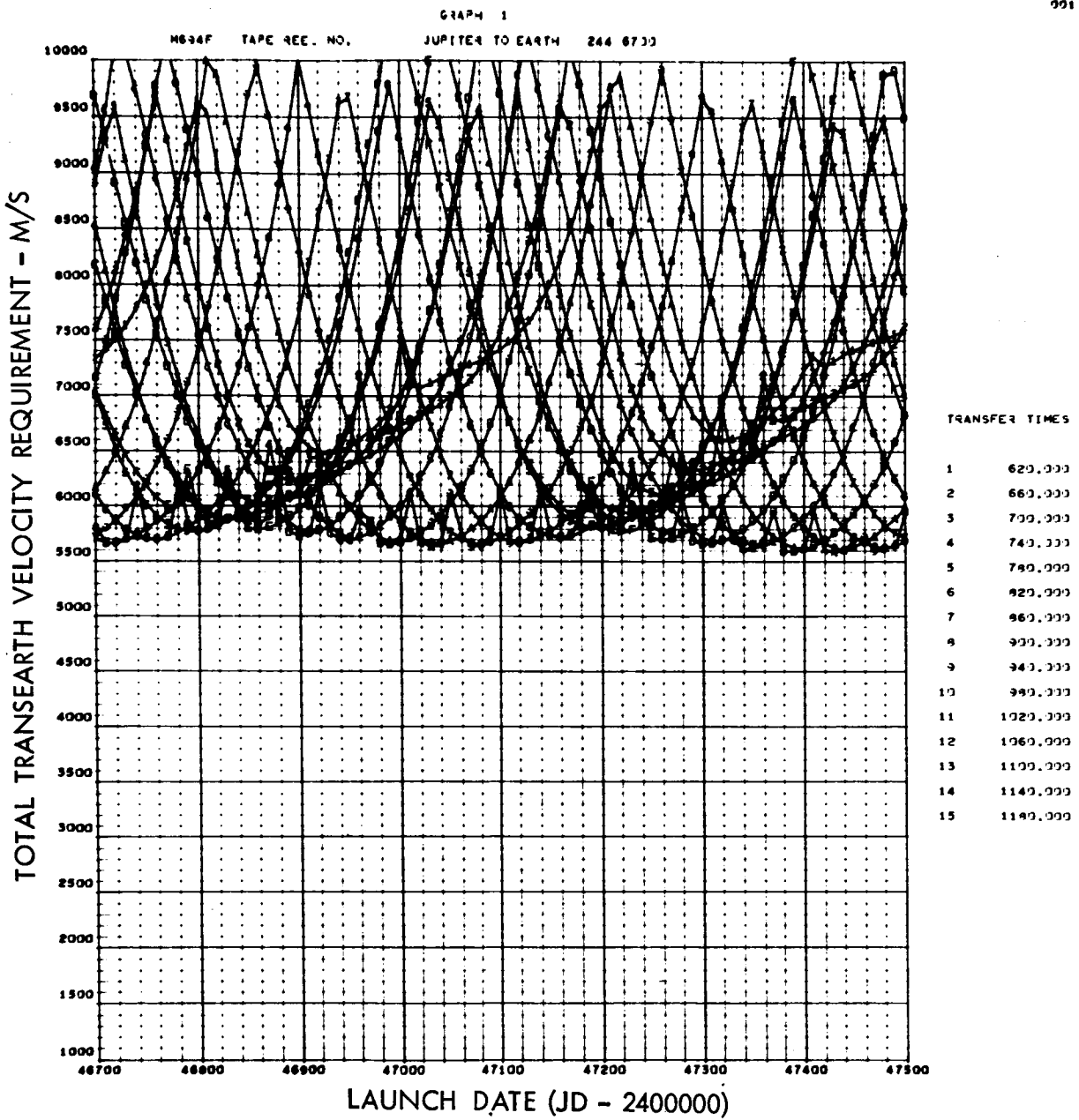
Figure 145. Total Trans-Earth Velocity Requirements (1985 Jupiter
Opportunity)
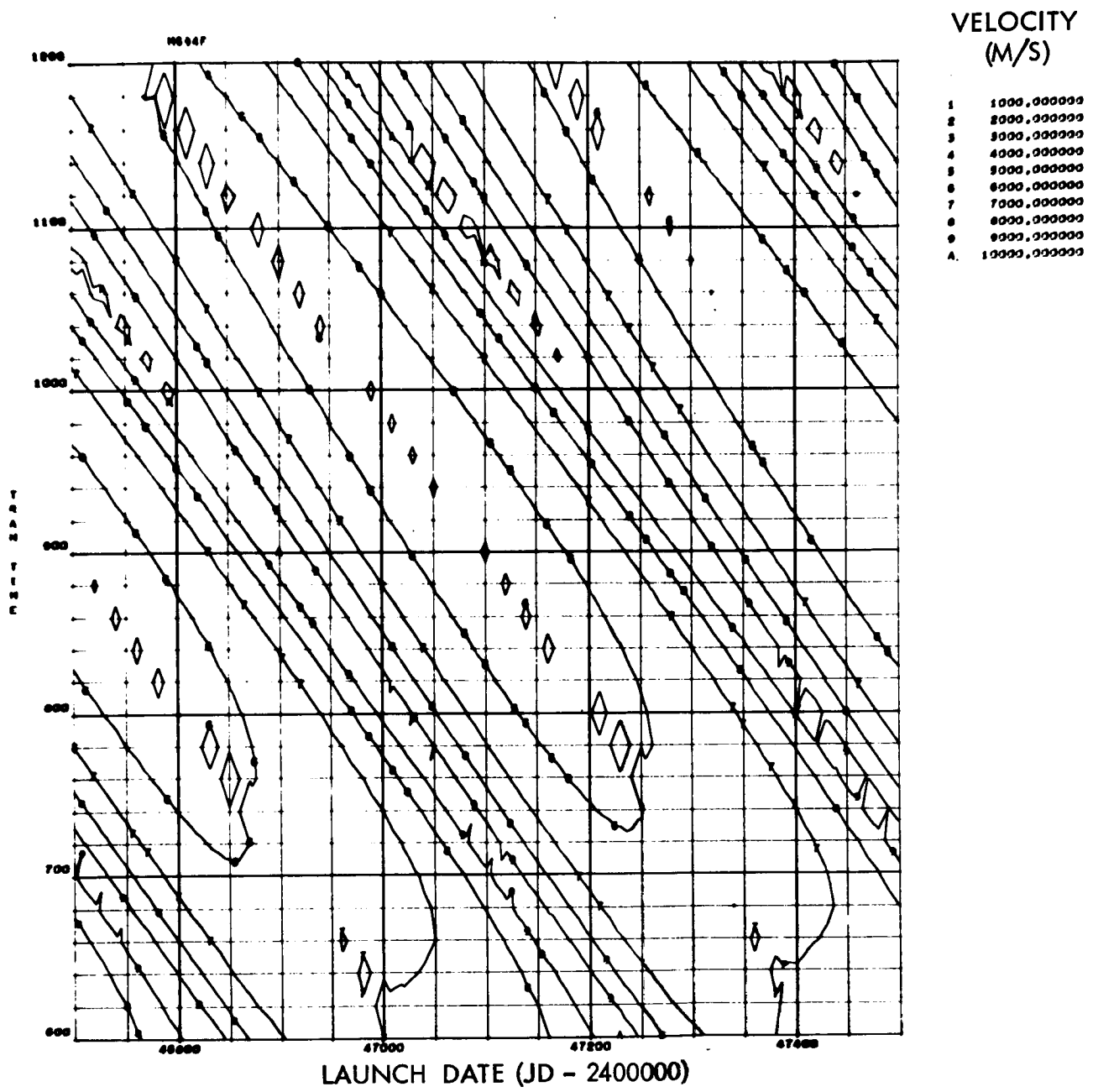
Figure 146. Total Trans-Earth Velocity Contours (1985 Jupiter Opportunity)
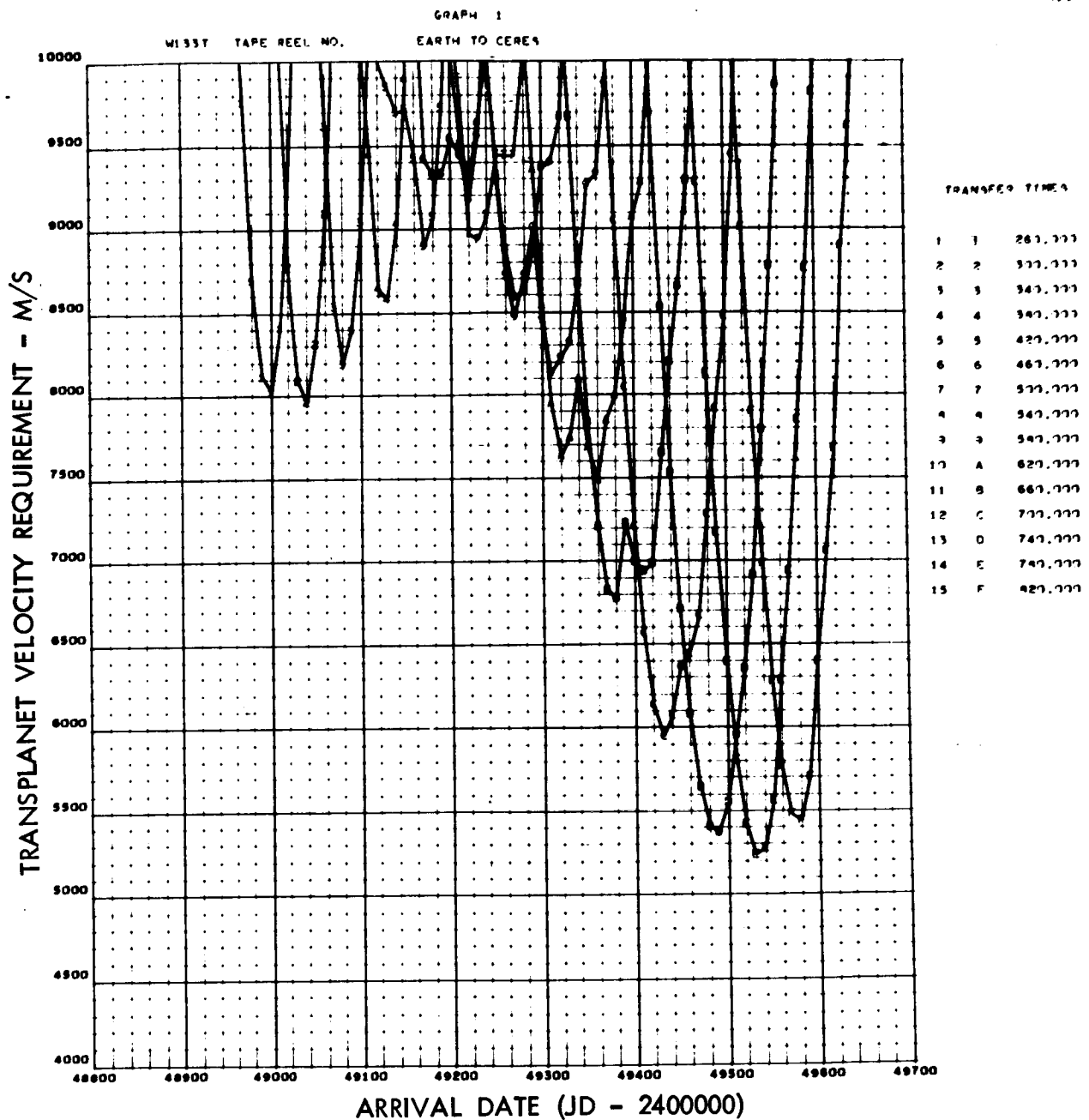
SD 67-621-2
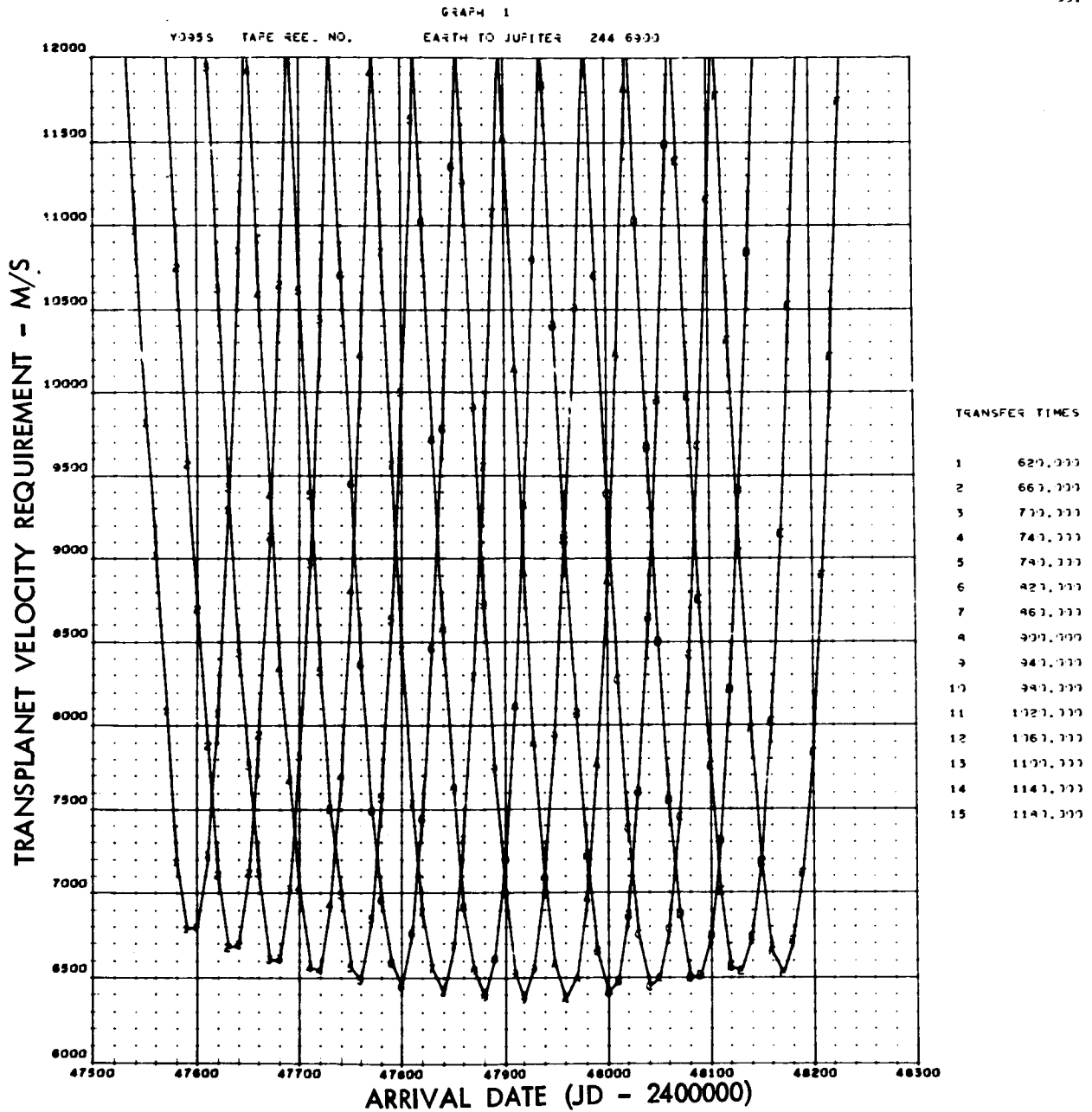
Figure 147. Transplanet Velocity Requirements (1987 Jupiter
Opportunity)
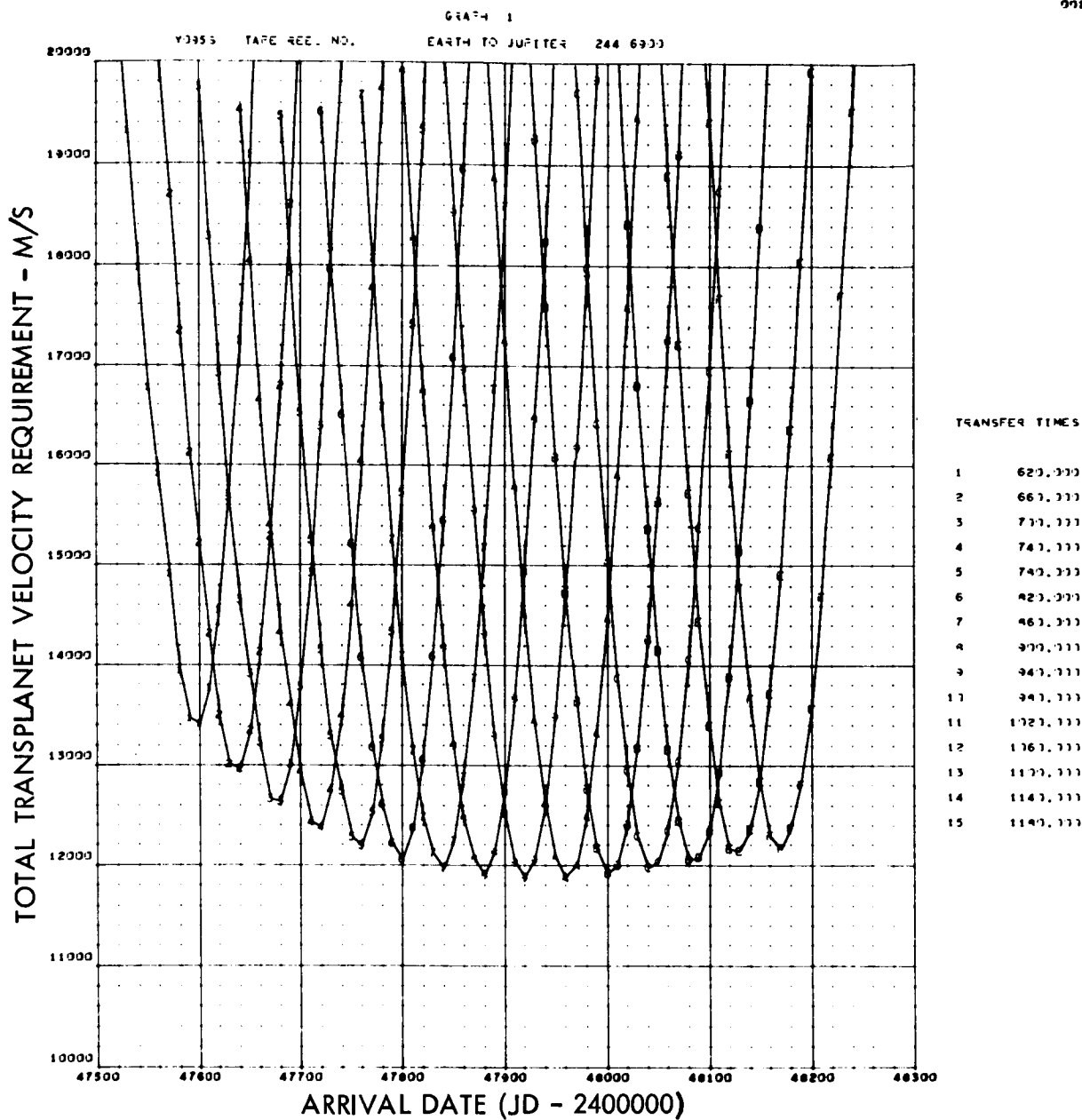
Figure 148.   Total Transplanet Velocity Requirements (1987 Jupiter Opportunity)
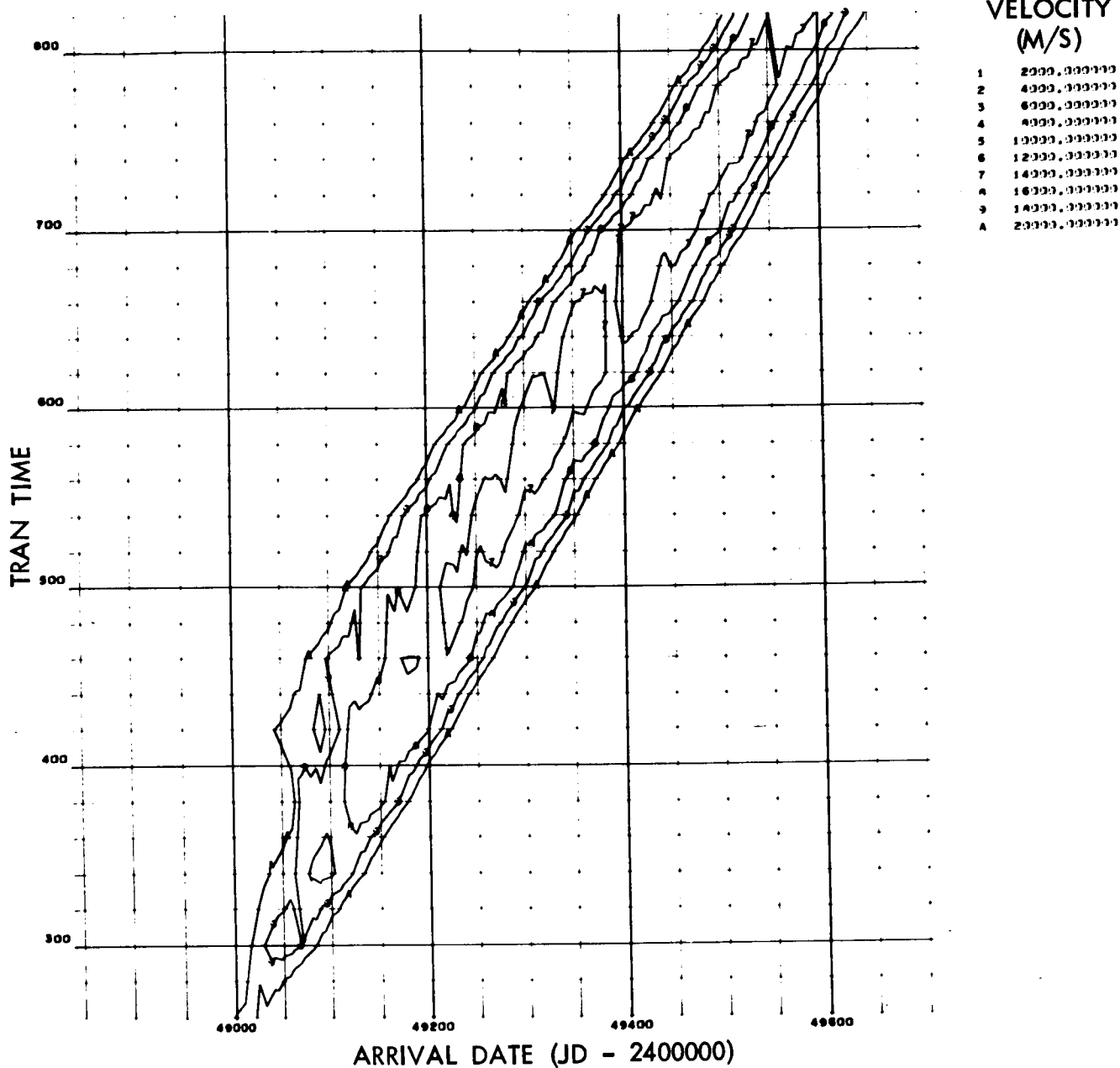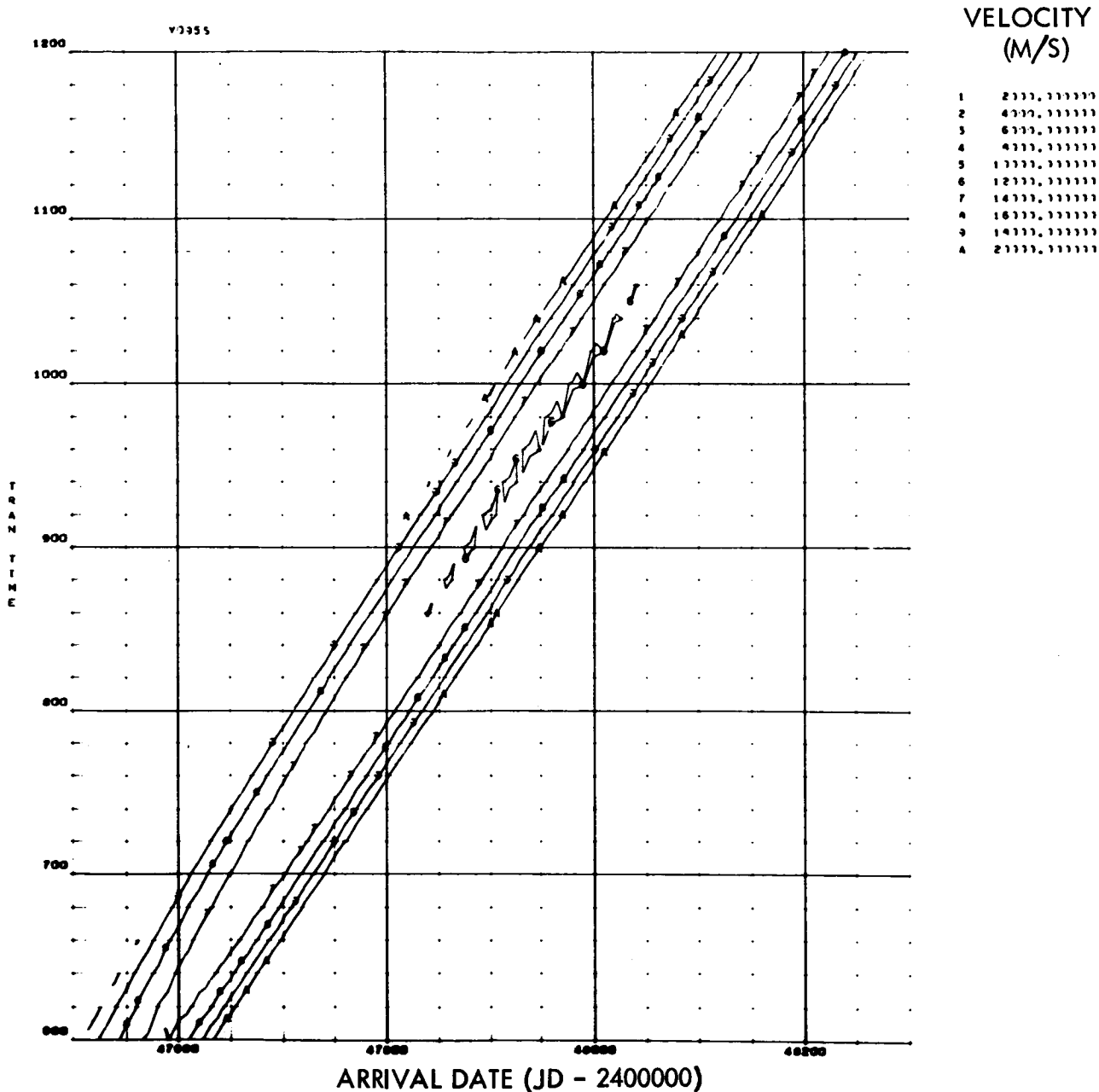
Figure 149.   Total Transplanet Velocity Contours (1987 Jupiter
Opportunity)
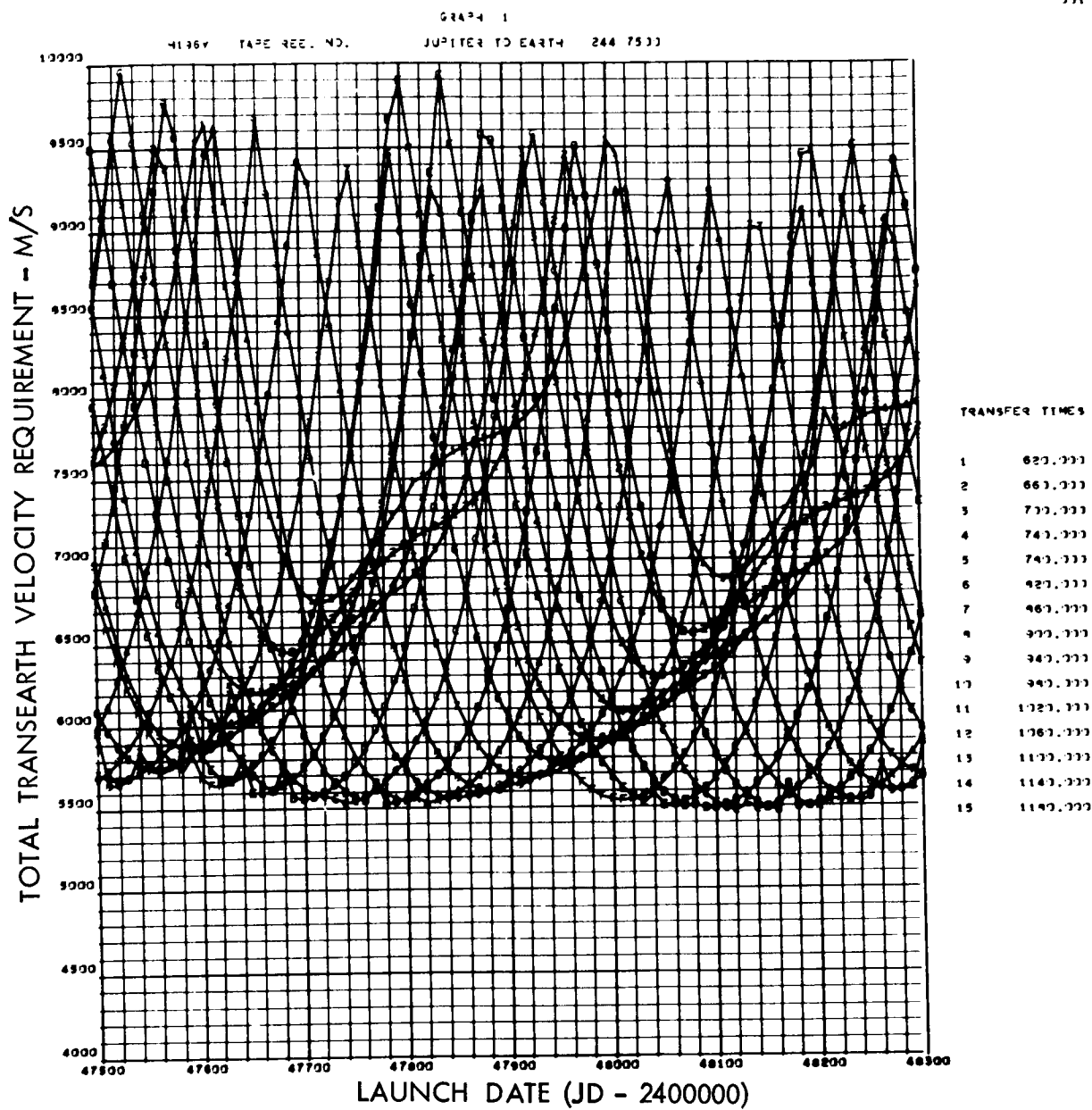
Figure 150. Total Trans-Earth Velocity Requirements (1987 Jupiter
Opportunity)

VELOCITY
(M/S)

1	1000.000000
2	2000.000000
3	3000.000000
4	4000.000000
5	5000.000000
6	6000.000000
7	7000.000000
8	8000.000000
9	9000.000000
A	10000.000000

LAUNCH DATE (JD - 2400000)
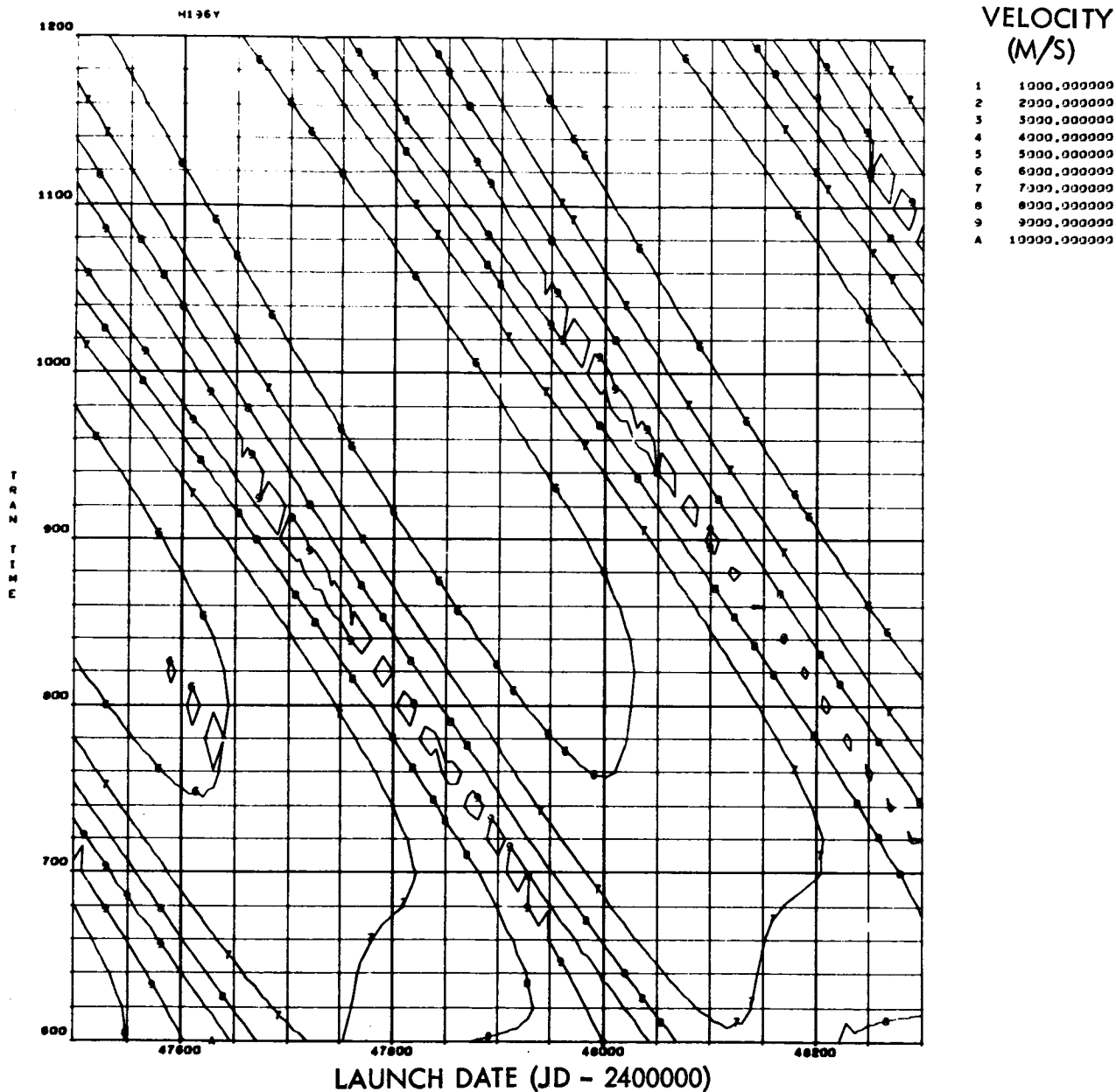
Figure 151. Total Trans-Earth Velocity Contours (1987 Jupiter Opportunity)

- 193 -
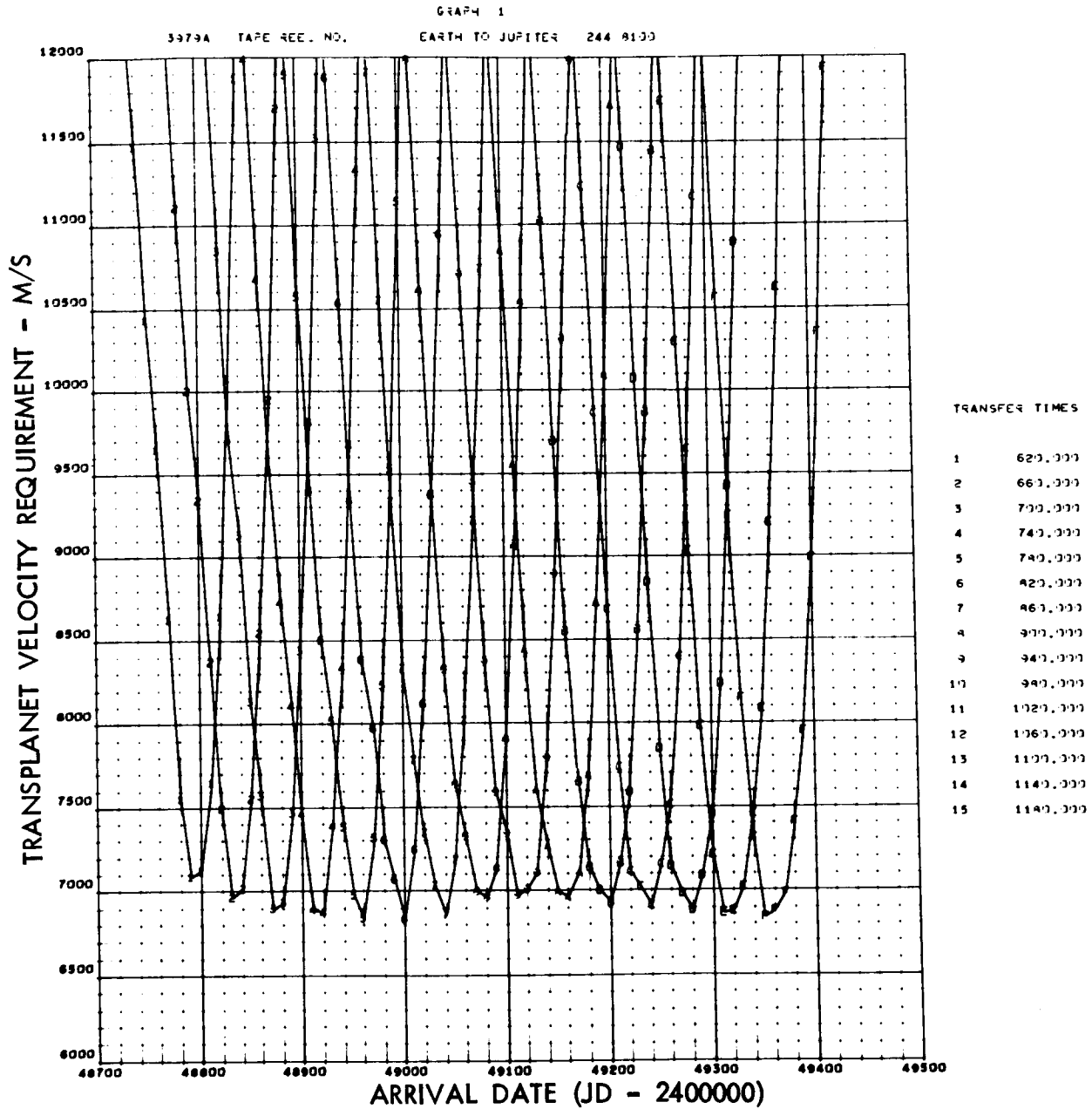
Figure 152. Transplanet Velocity Requirements (1990 Jupiter
Opportunity)
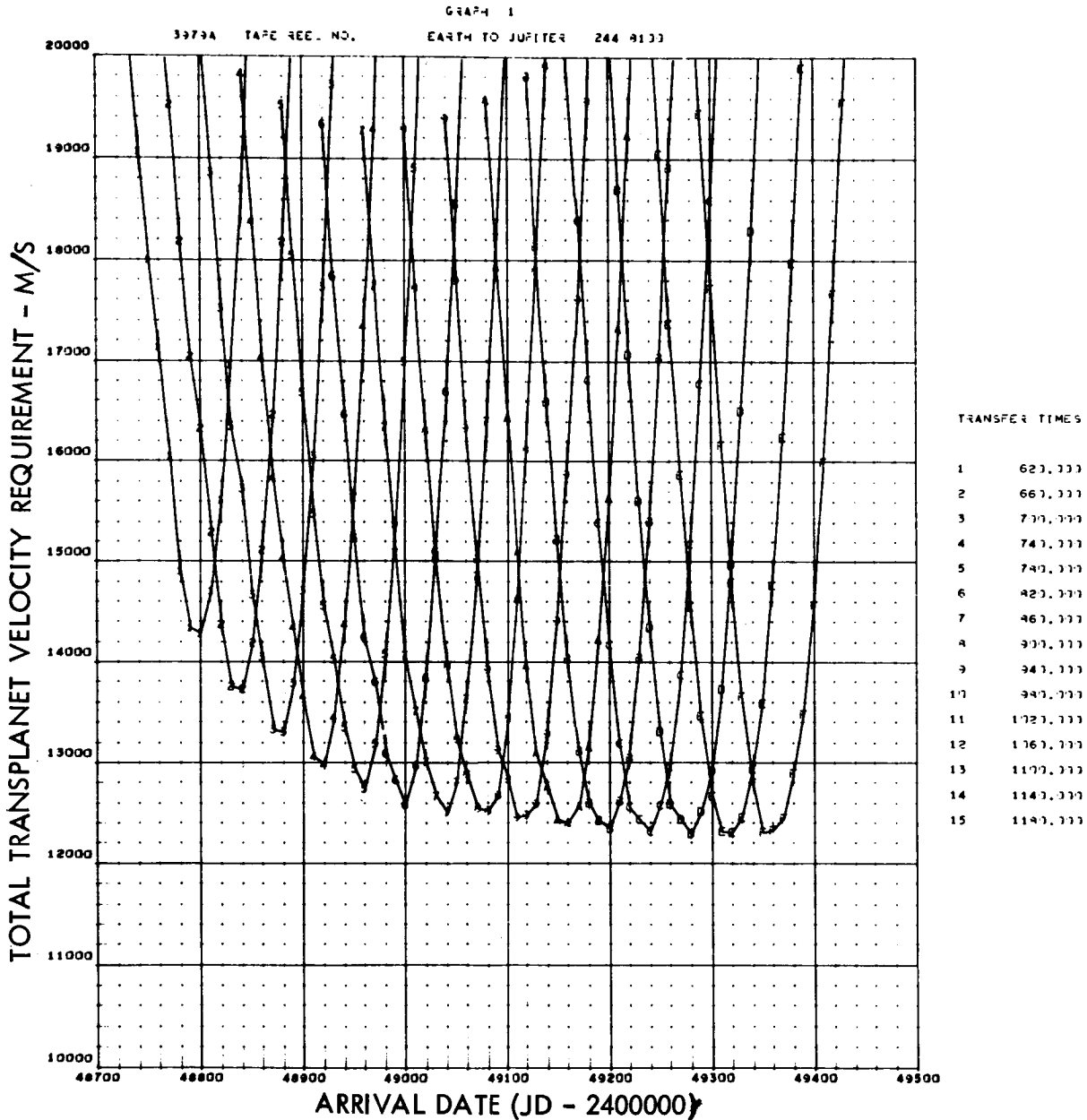
Figure 153. Total Transplanet Velocity Requirements (1990 Jupiter Opportunity)
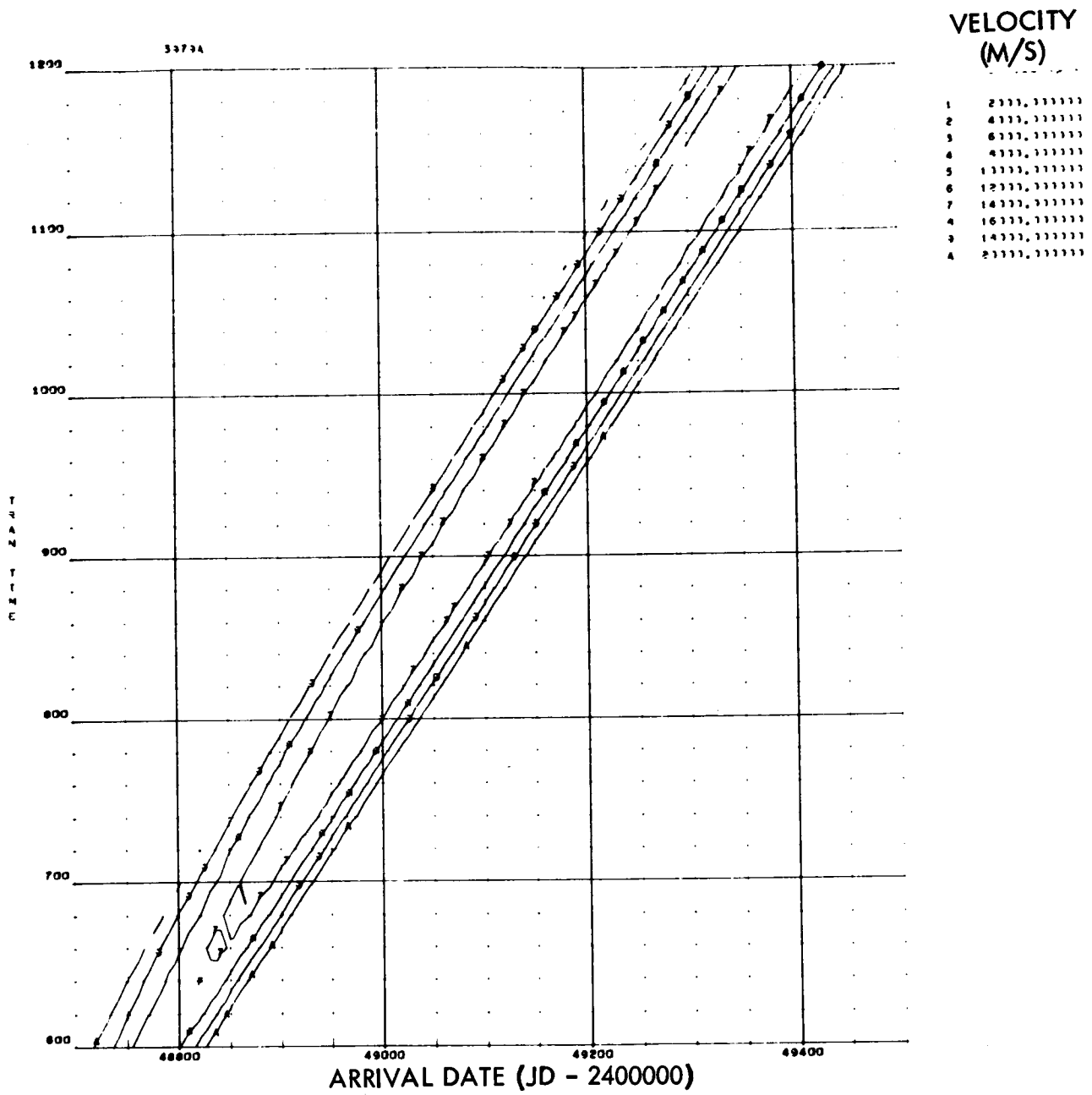
Figure 154. Total Transplanet Velocity Contours (1990 Jupiter Opportunity)
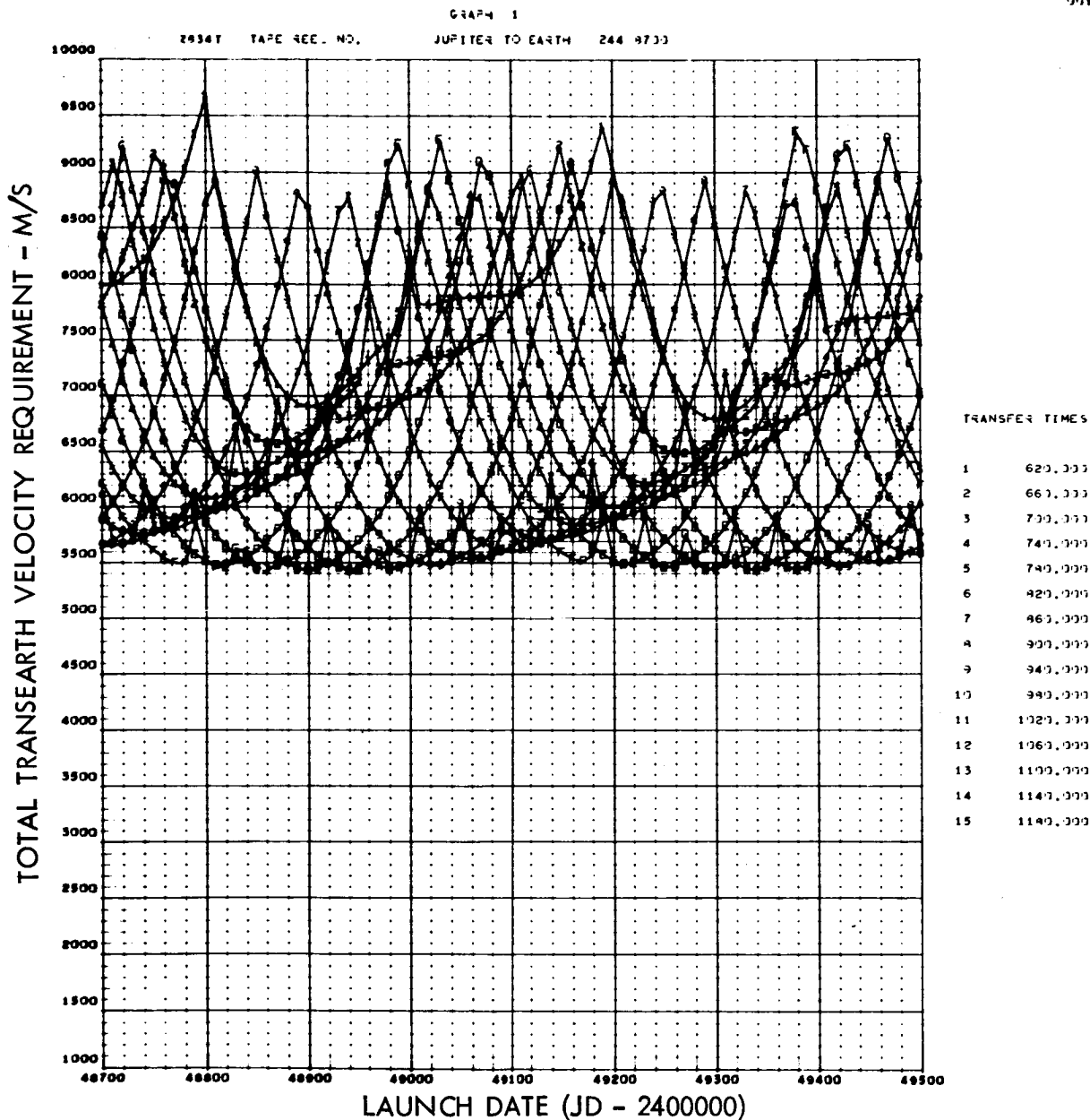
Figure 155.   Total Trans-Earth Velocity Requirements (1990 Jupiter
Opportunity)
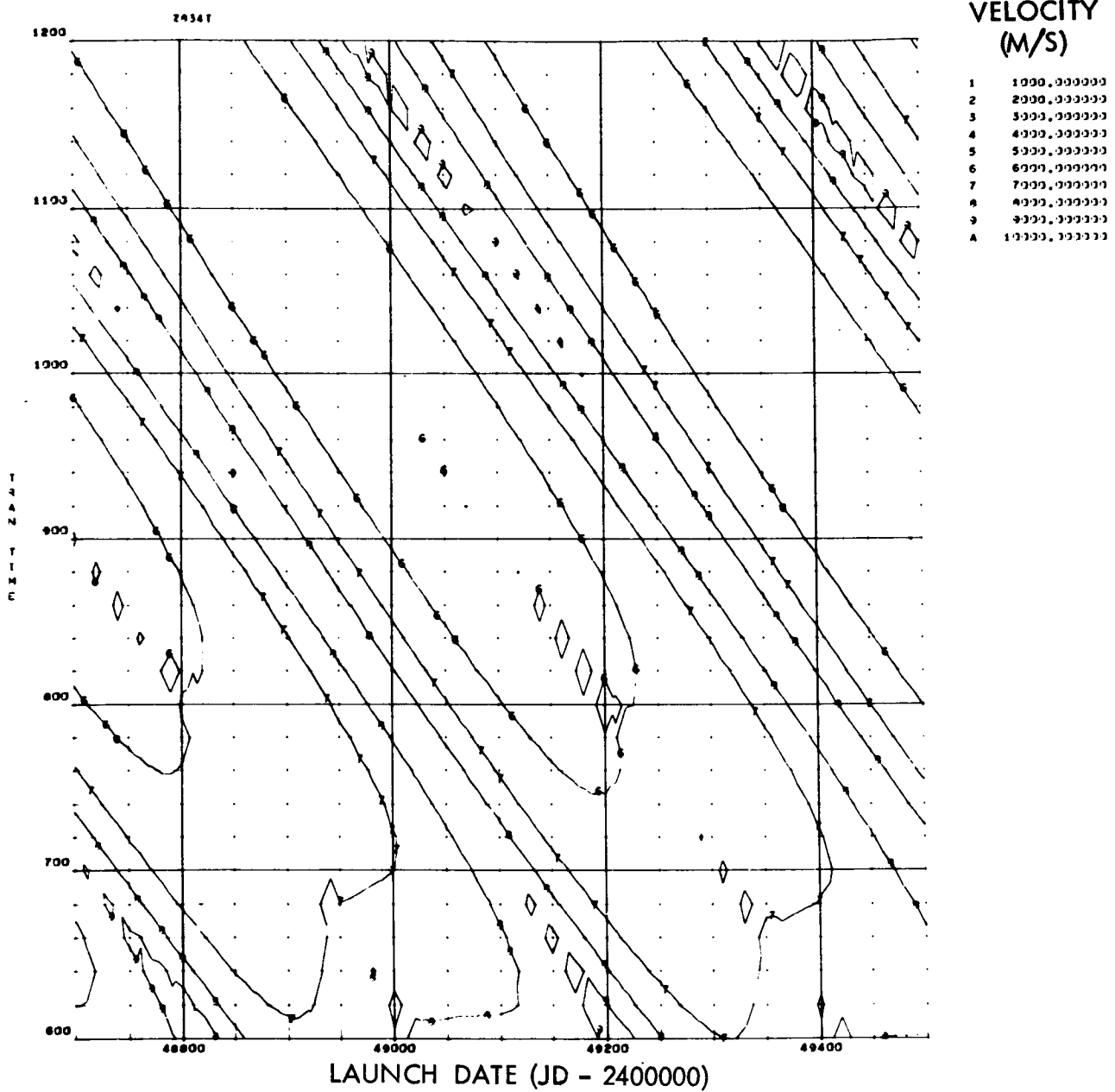
Figure 156. Total Trans-Earth Velocity Contours (1990 Jupiter Opportunity)

SD 67-621-2
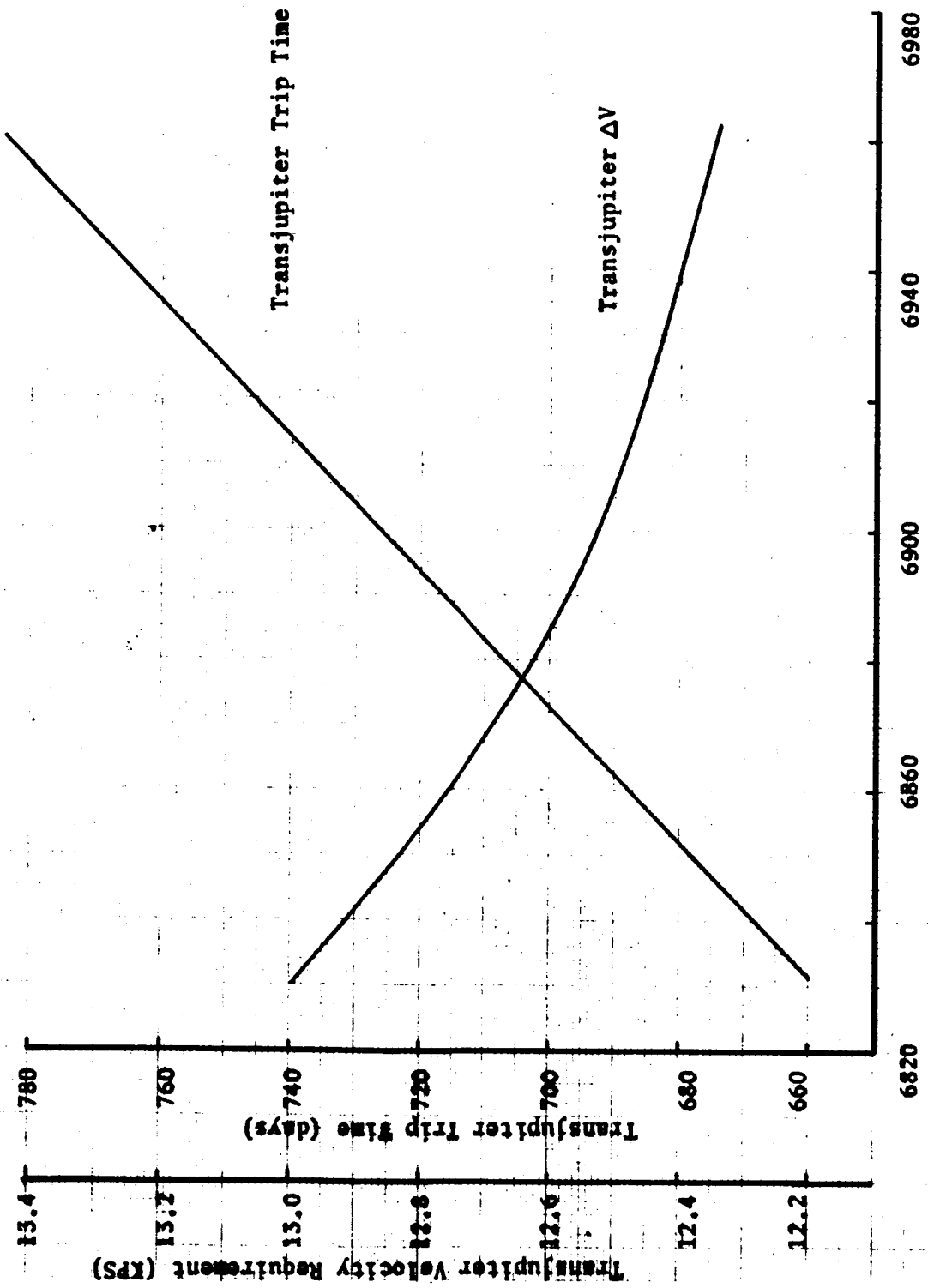
Figure 157. Transplanet Velocity Requirements Summary (1985
Jupiter Opportunity)

- 199 -

SD 67-621-2
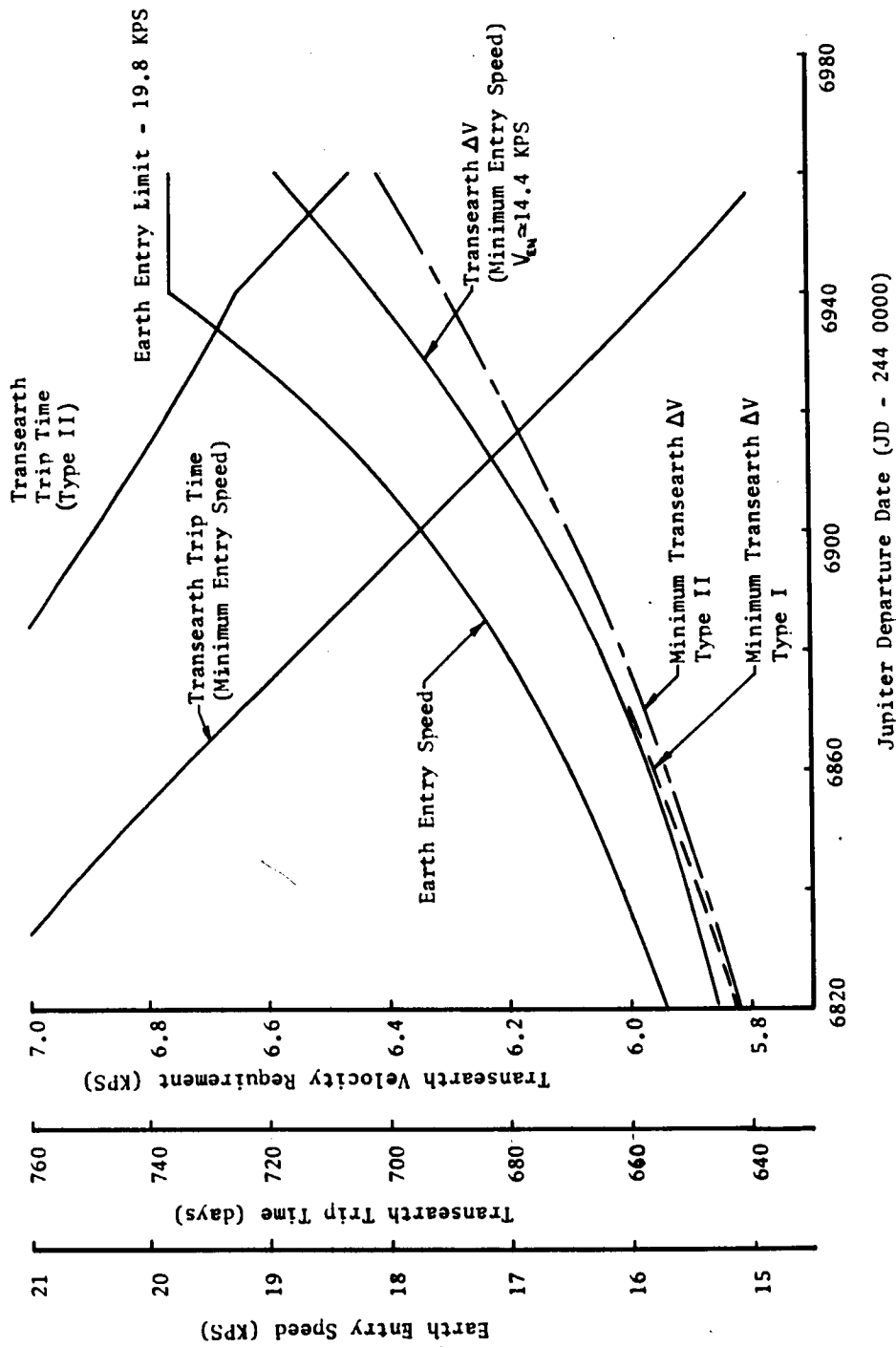
Figure 158. Trans-Earth Velocity Requirements Summary
(1985 Jupiter Opportunity)
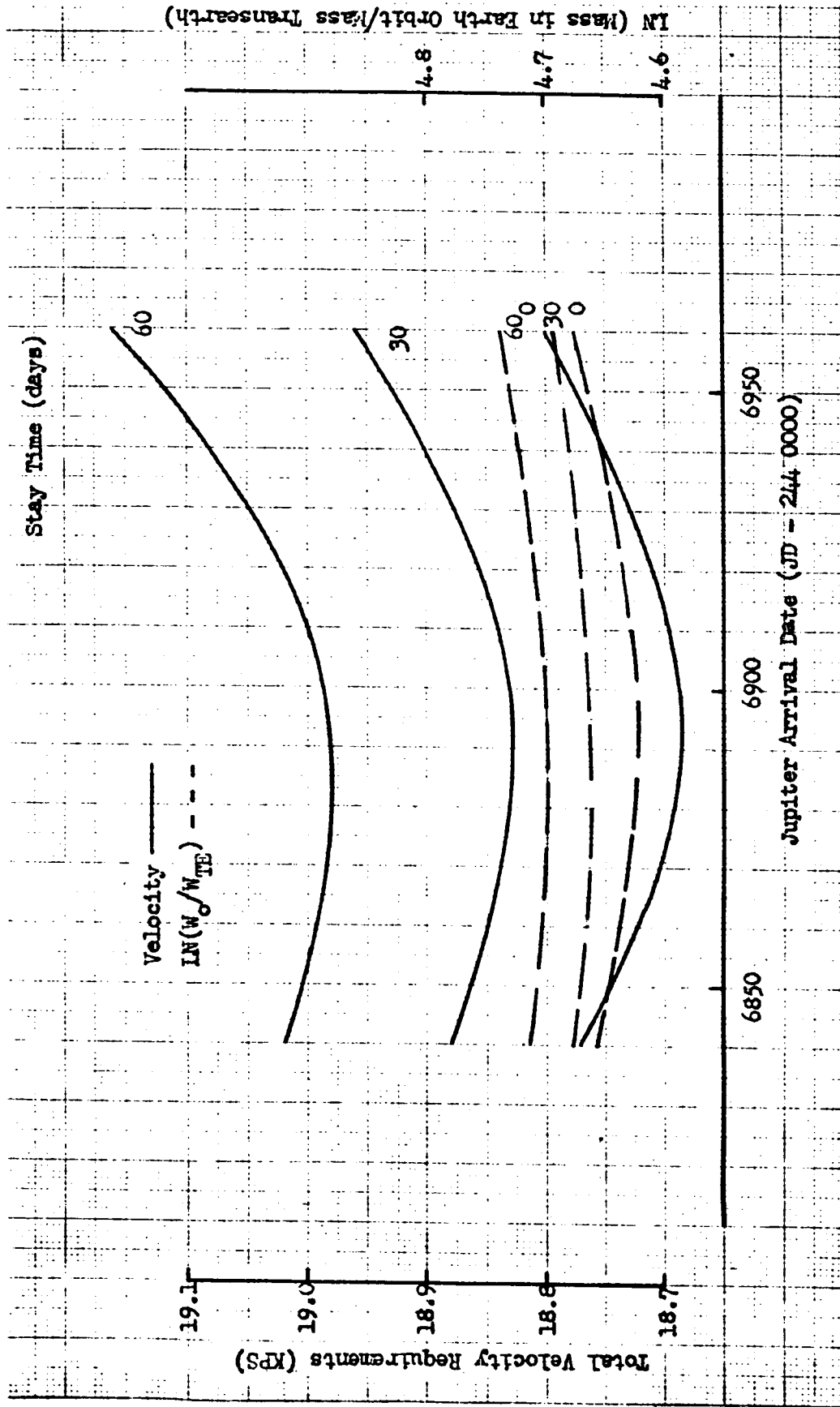
Figure 159. Total Jupiter Mission Requirements (1985 Jupiter Opportunity)

SD 67-621-2
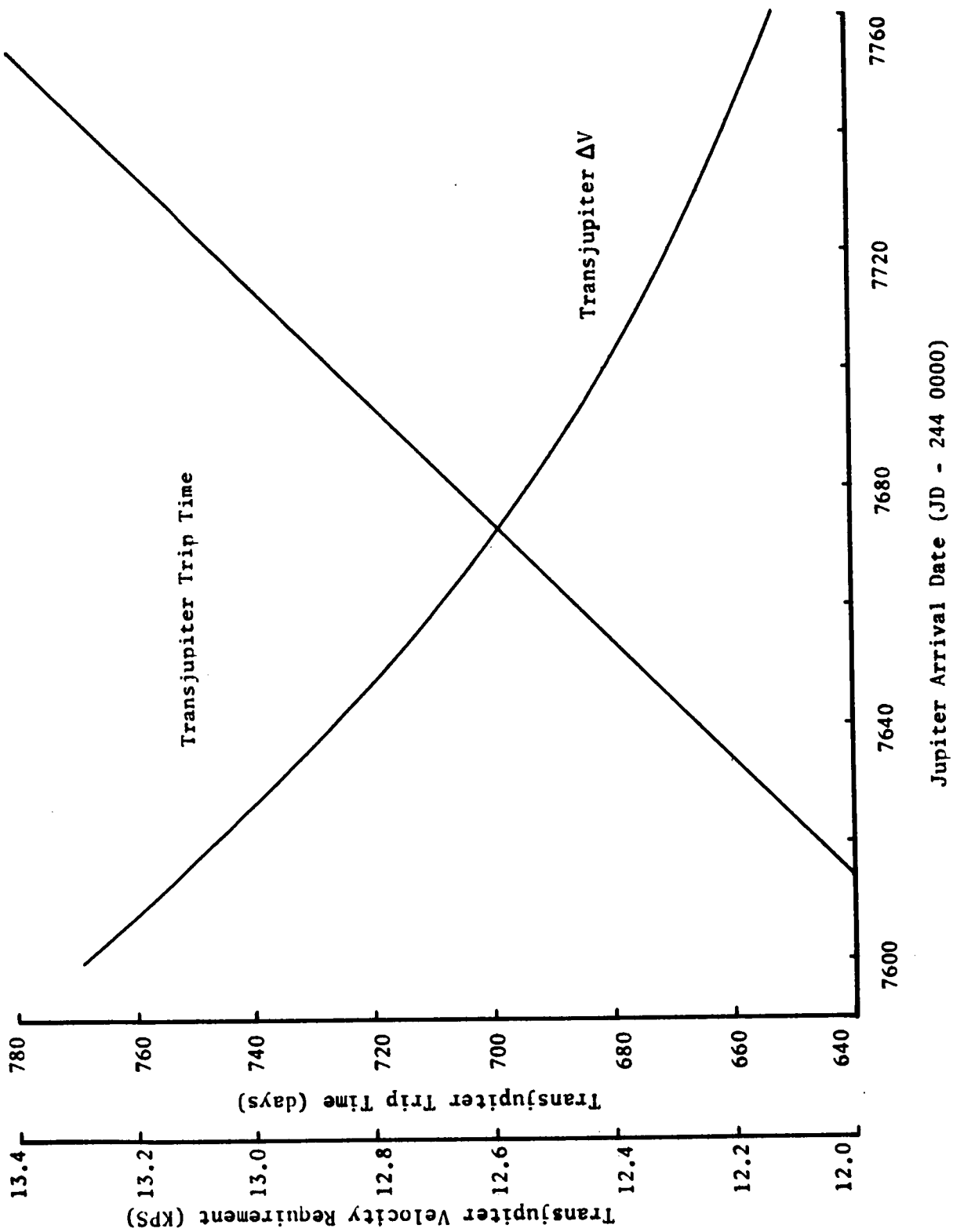
Figure 160. Transplanet Velocity Requirements Summary (1987 Jupiter Opportunity)
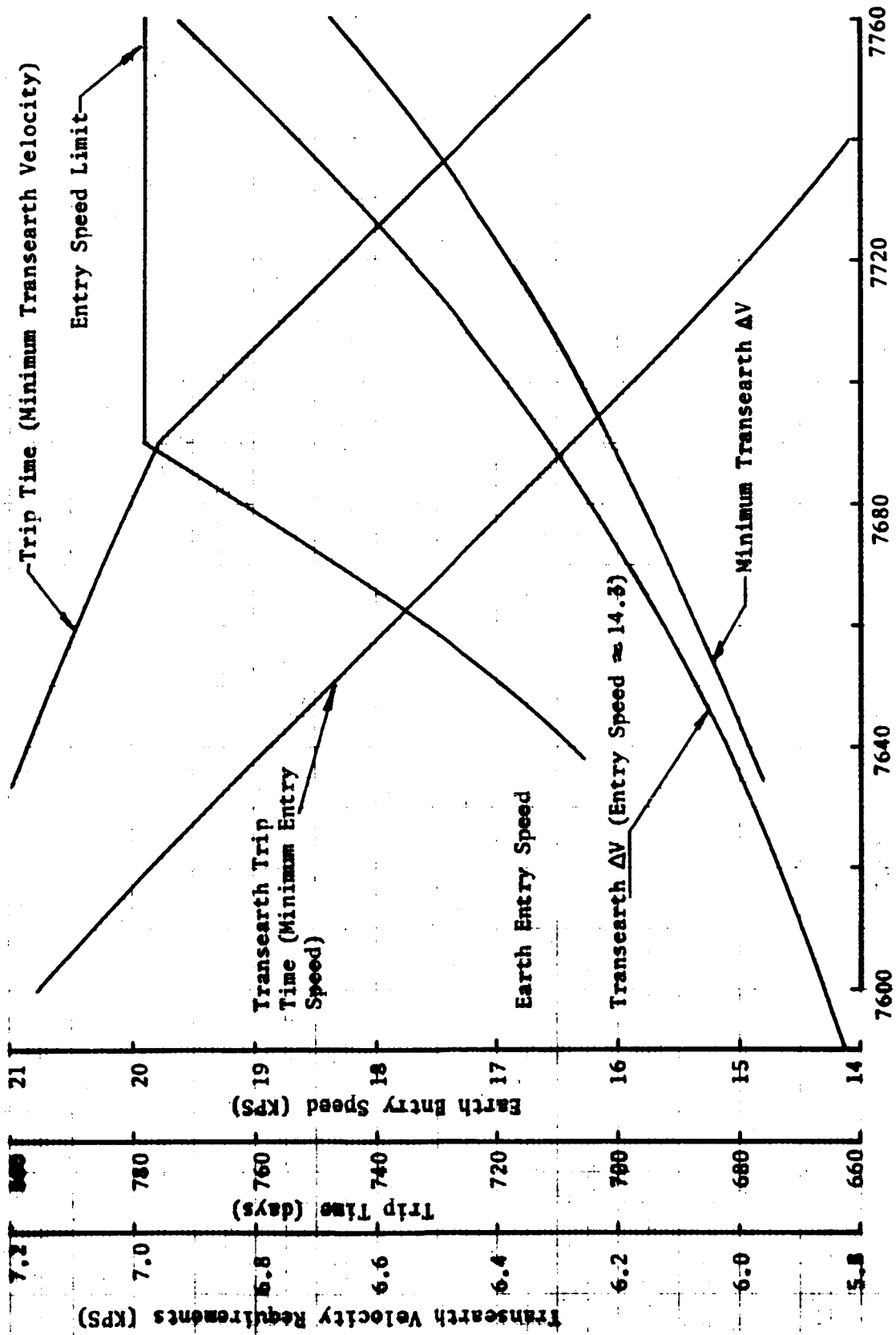
Figure 161. Trans-Earth Velocity Requirements Summary (1987 Jupiter Opportunity)

- 203 -
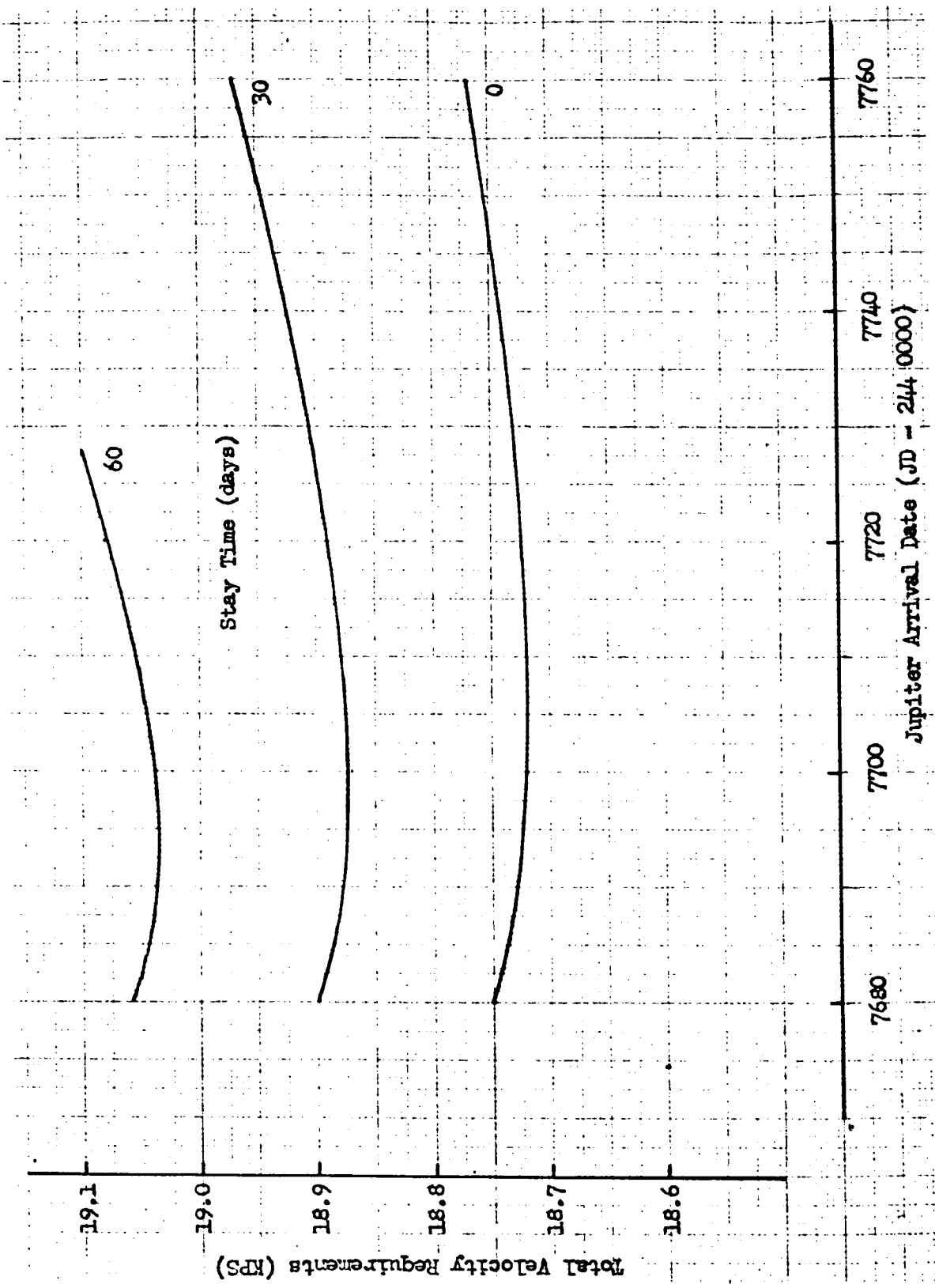
Figure 162. Total Jupiter Mission Requirements (1987 Jupiter Opportunity)
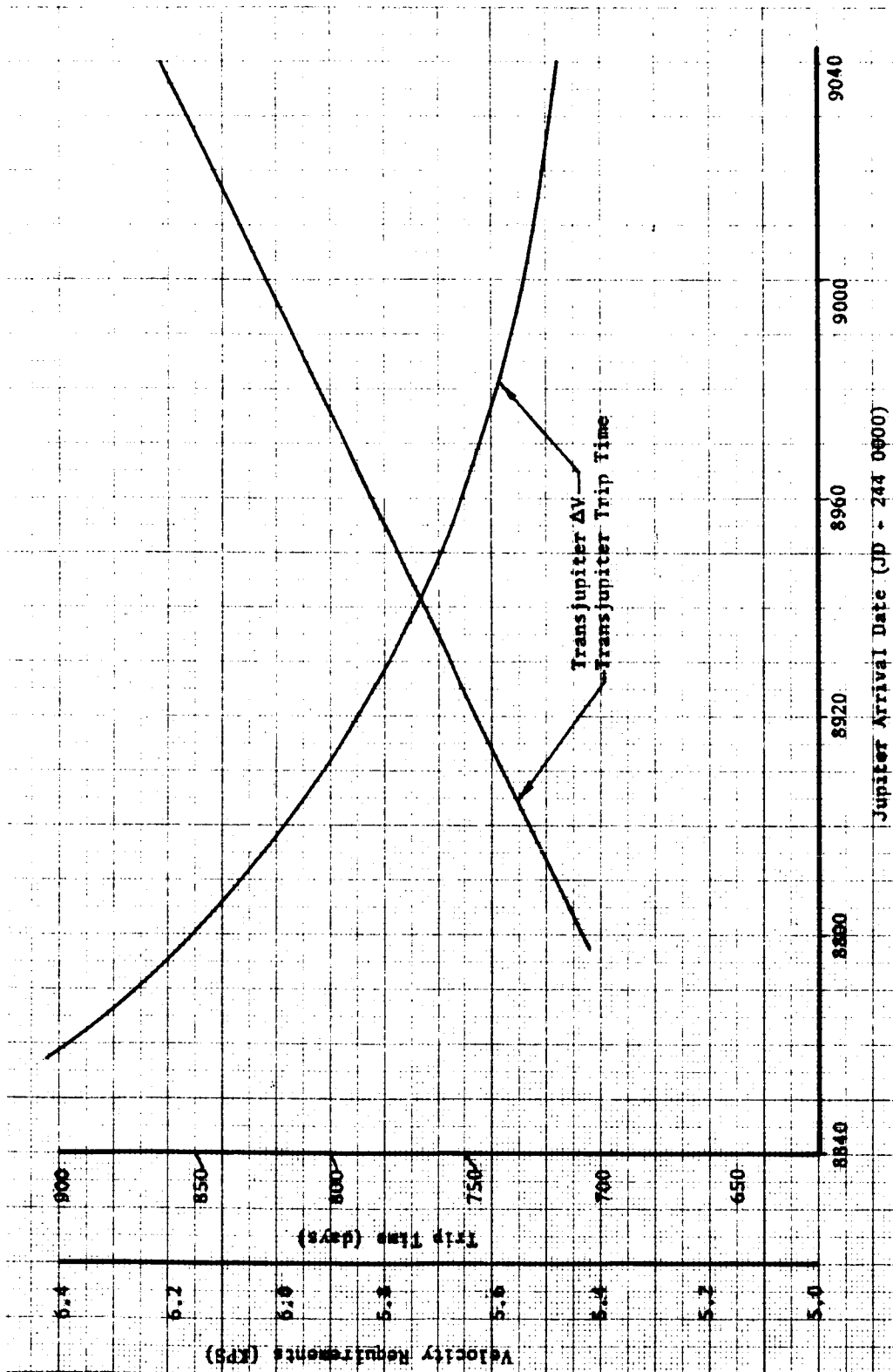
Figure 163. Transplanet Velocity Requirements Summary
(1990 Jupiter Opportunity)

- 205 -
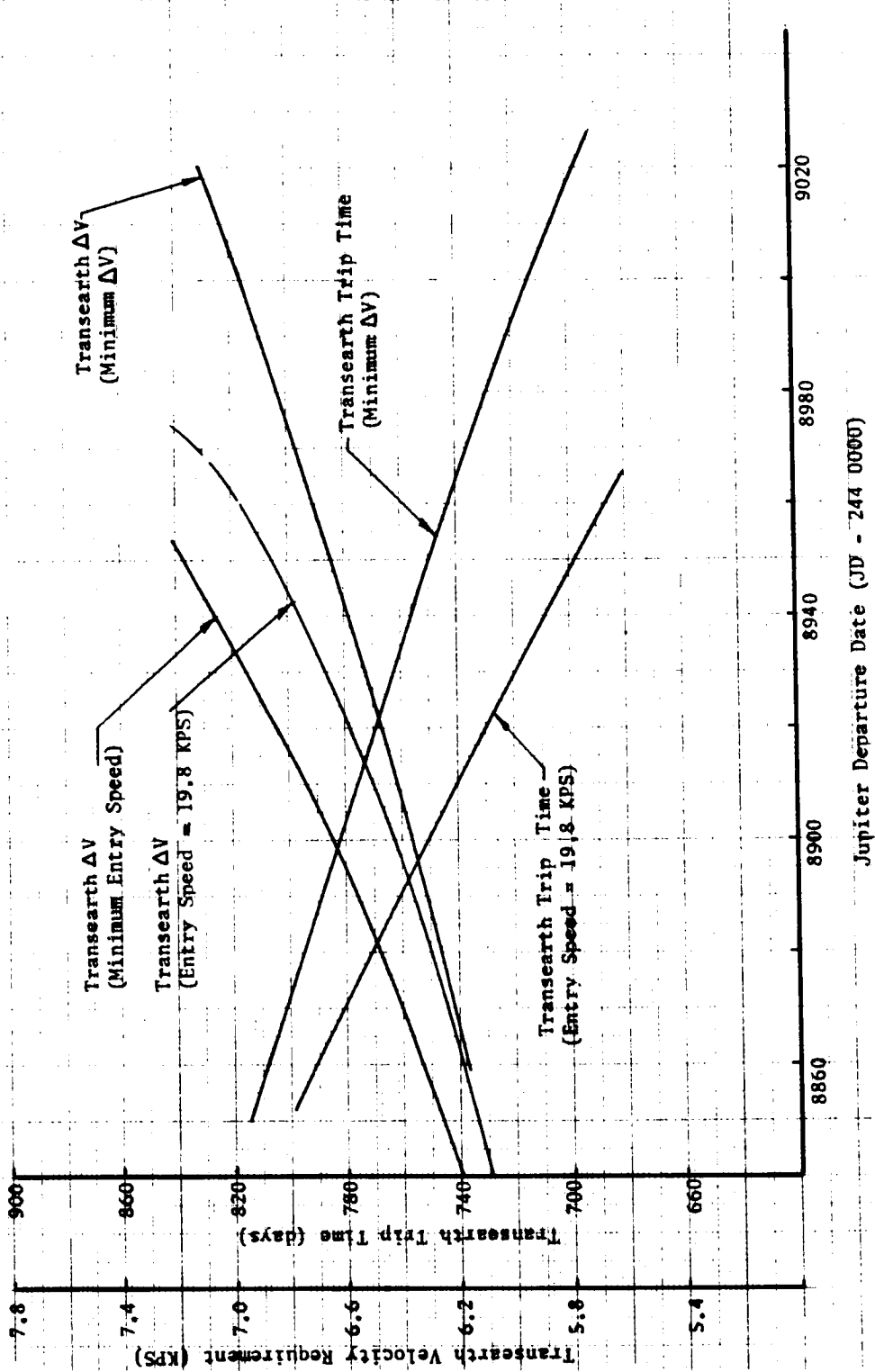
Figure 164. Trans-Earth Velocity Requirements Summary
(1990 Jupiter Opportunity)

SD 67-621-2
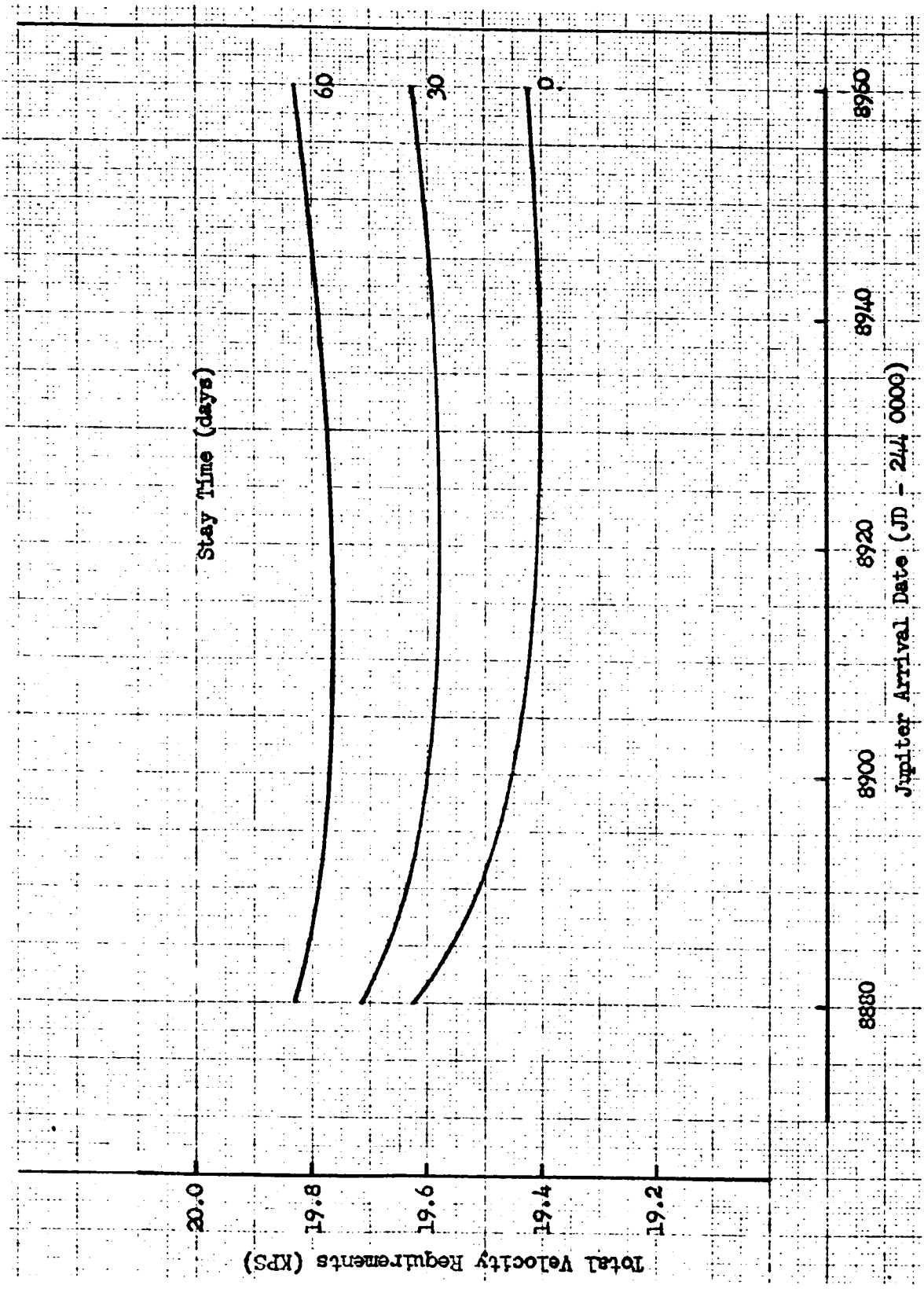
Figure 165. Total Jupiter Mission Requirements (1990 Jupiter Opportunity)

SD 67-621-2
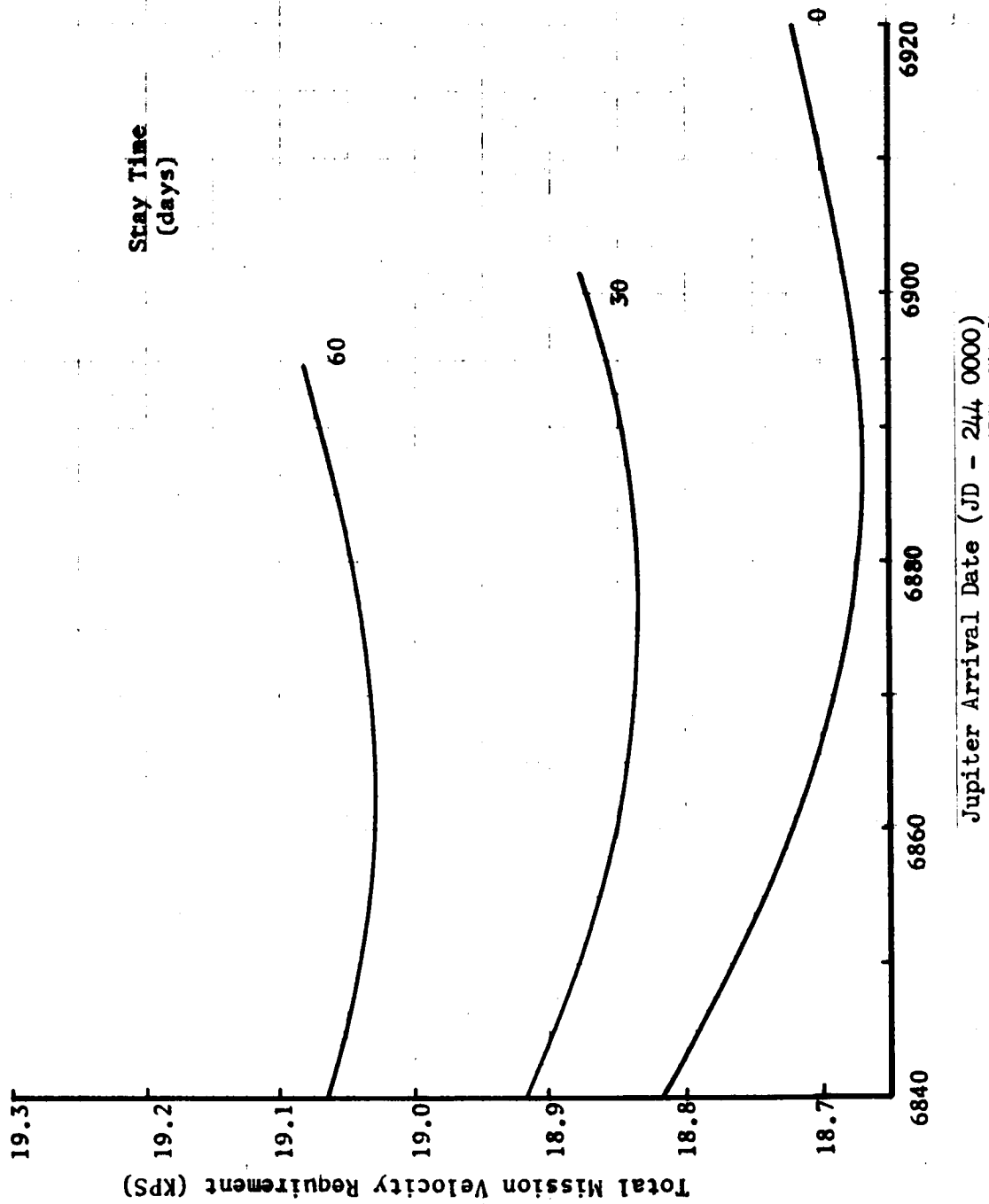
Figure 166. Total Jupiter Mission Requirements (Minimum Entry Speed, 1985 Jupiter Opportunity)
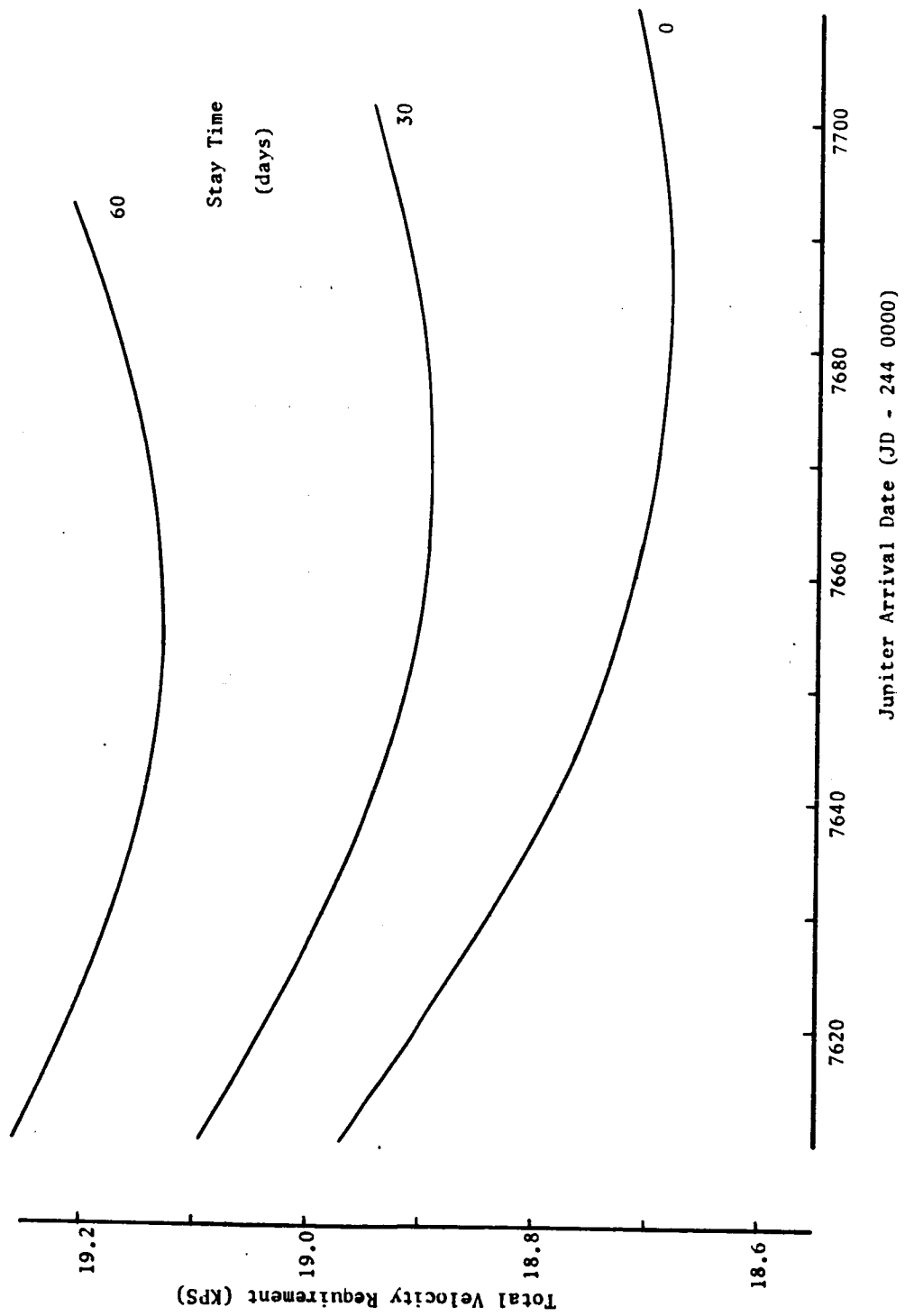
Figure 167. Total Jupiter Mission Requirements (Minimum Entry Speed, 1987 Jupiter Opportunity)

- 209 -
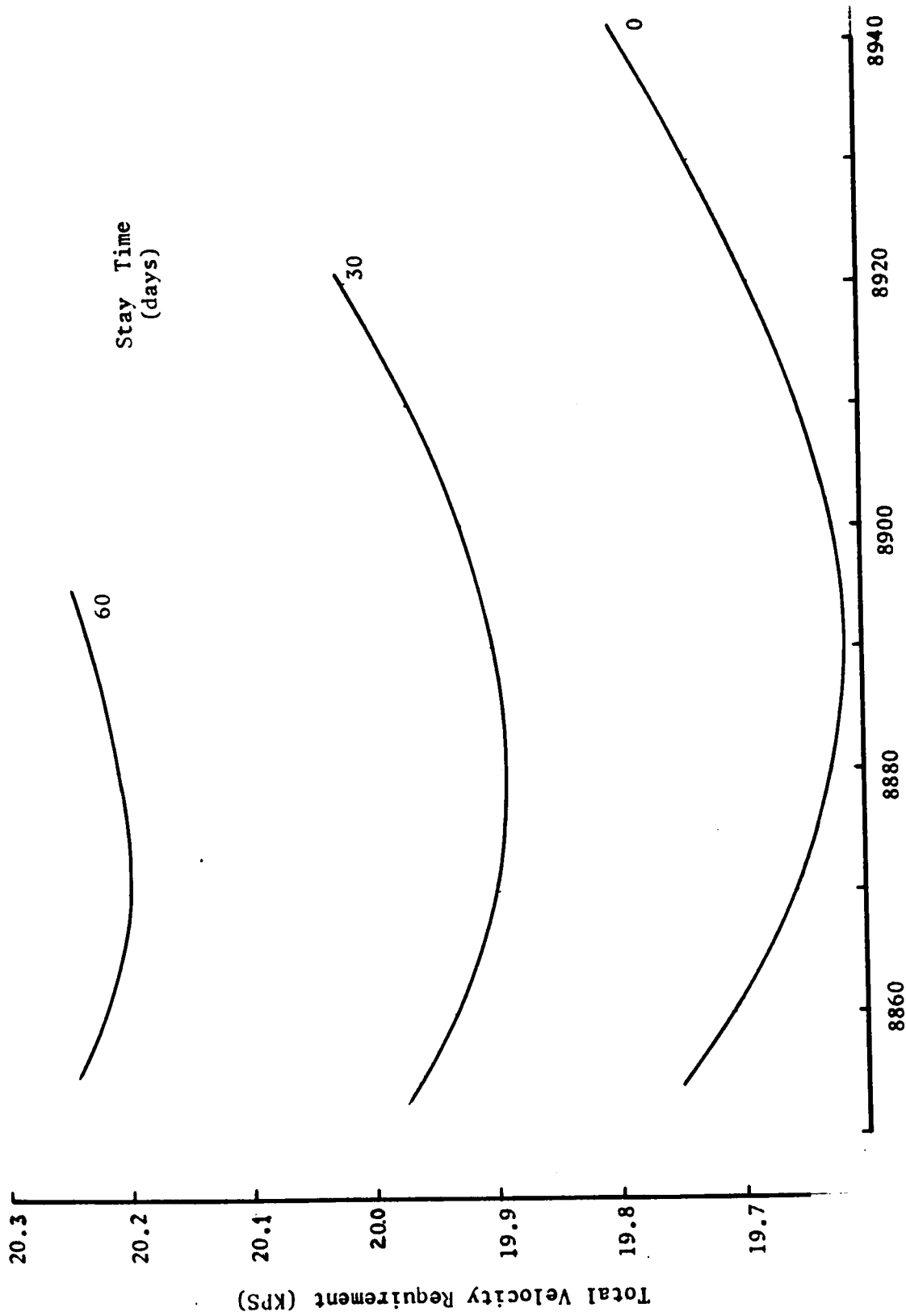
Figure 168. Total Jupiter Mission Requirements (Minimum Entry Speed, 1990 Jupiter Opportunity)

SD 67-621-2
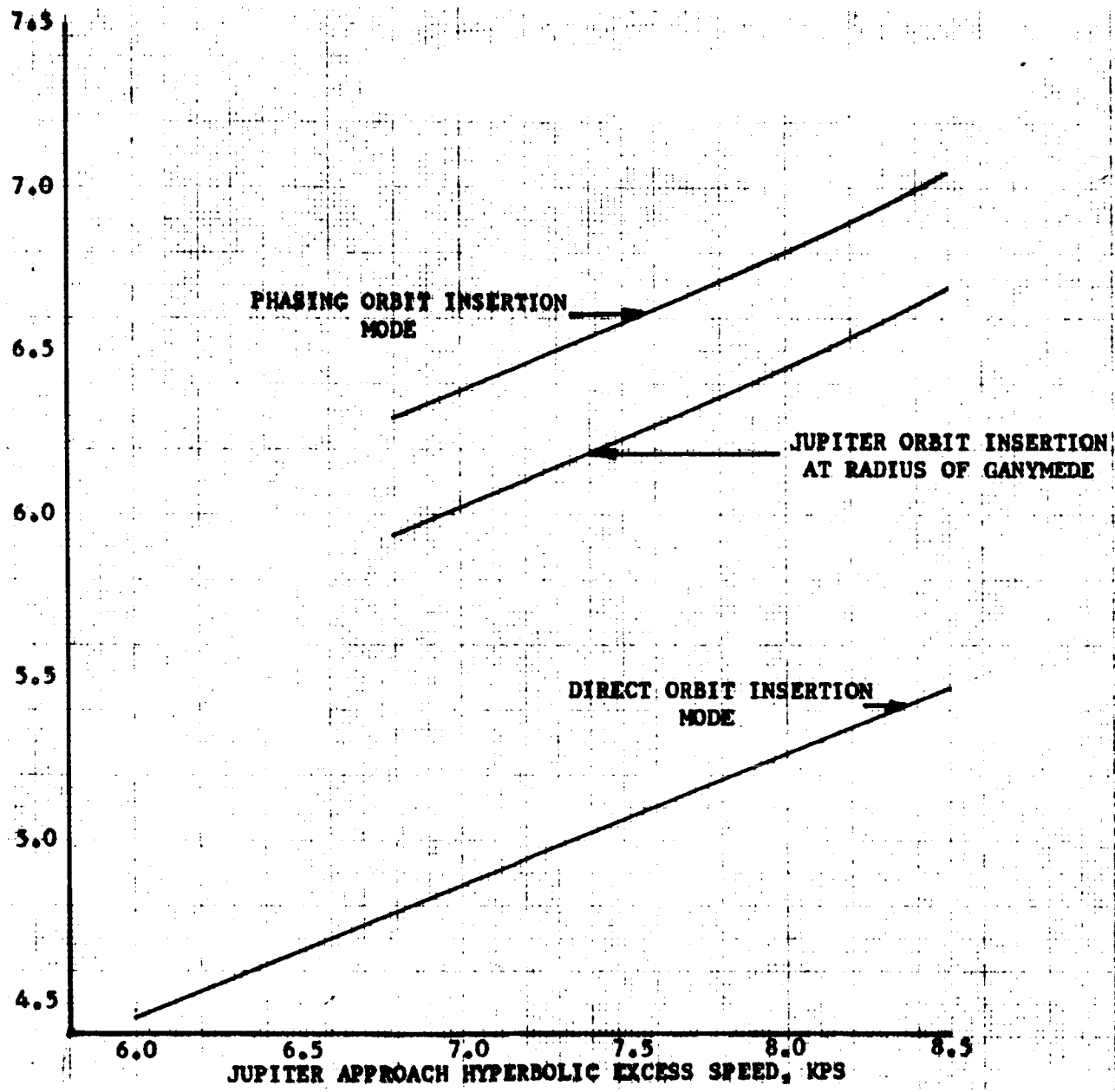
Figure 169. Ganymede Orbit Insertion Requirements

SD 67-621-2
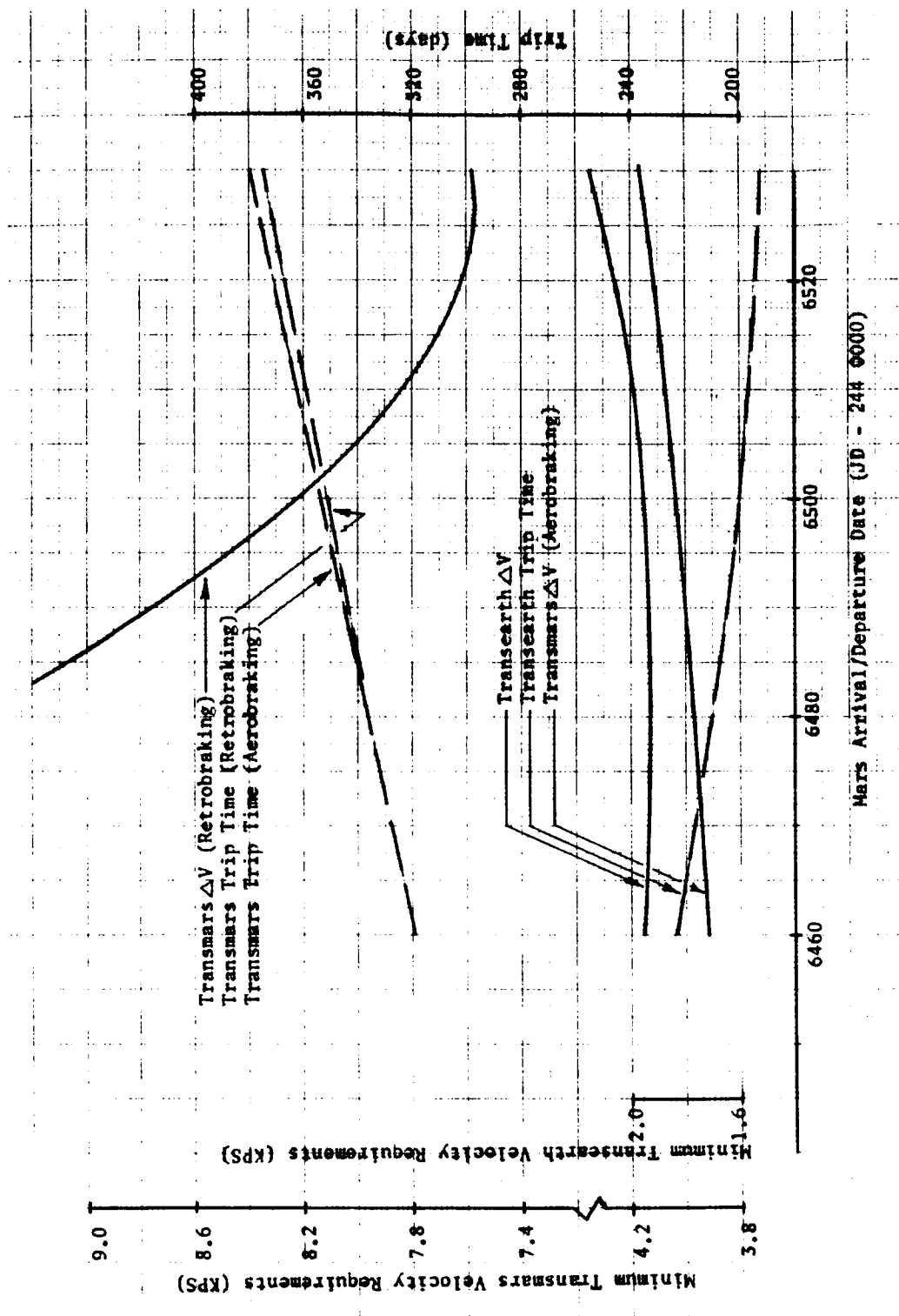
Figure 170.   1986 Mars Mission Summary
(Swingby Outbound - Direct Return)
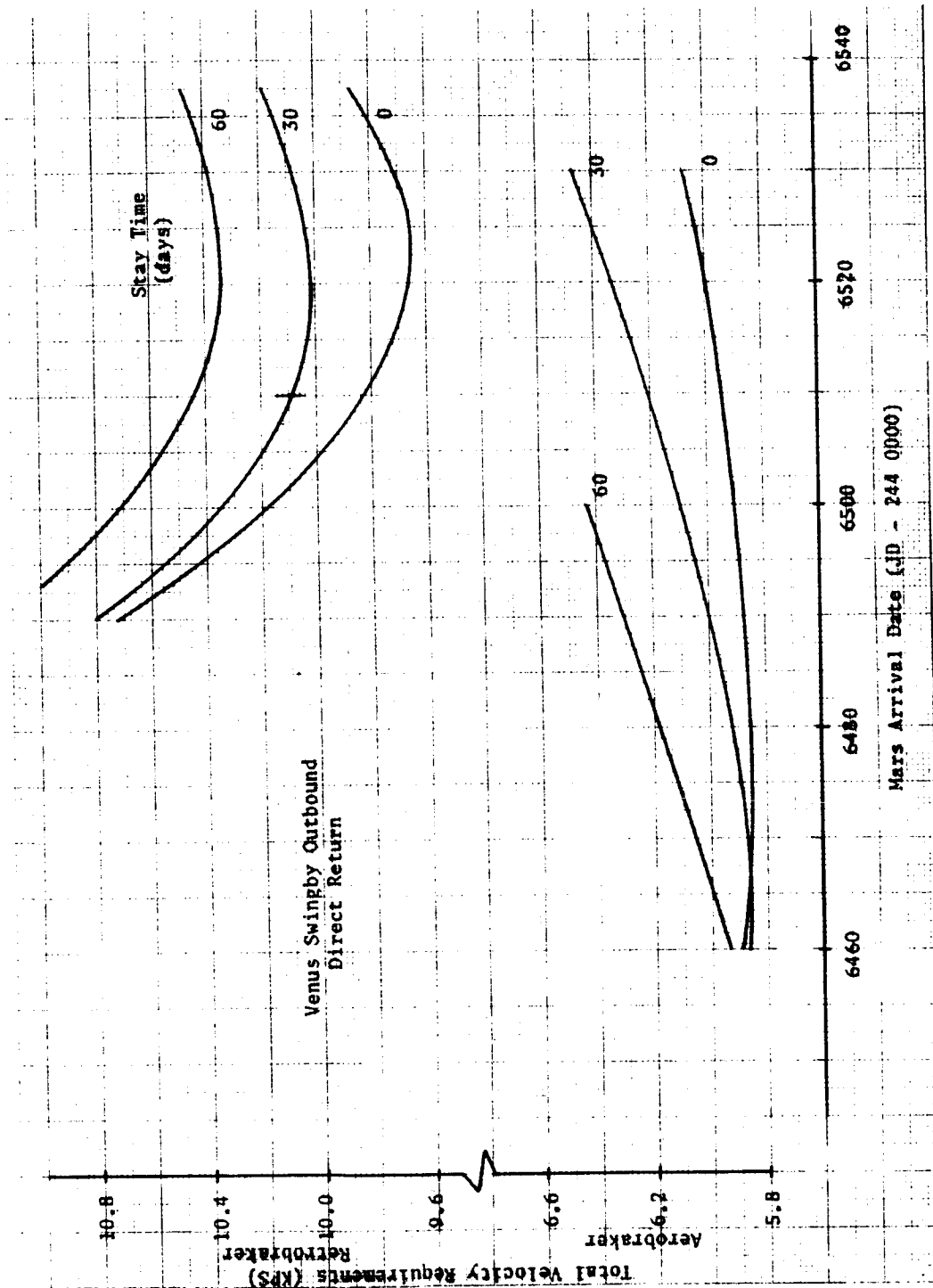
Figure 171. Total Mars Velocity Requirements (1986 Mission)
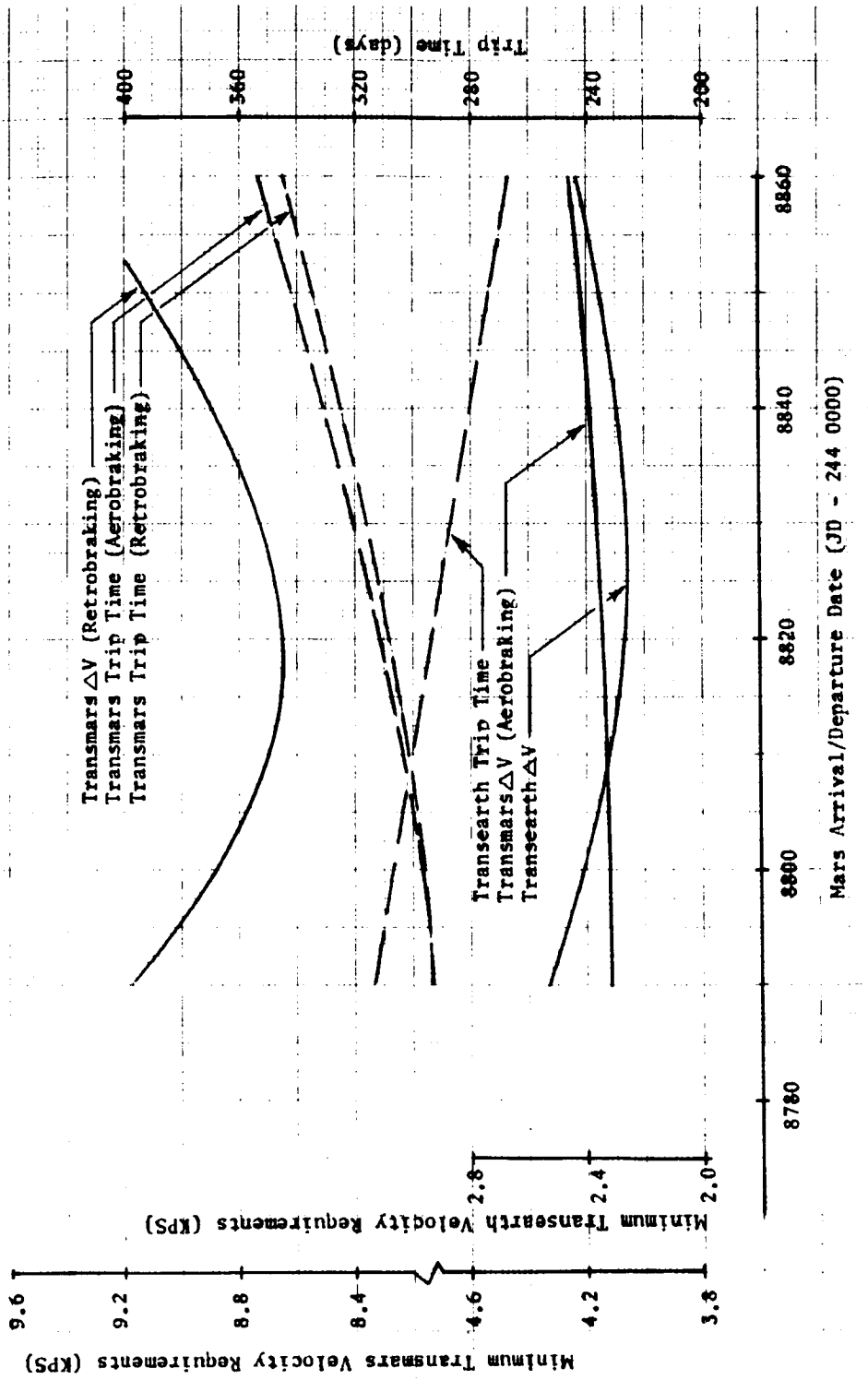
Figure 172. 1993 Mars Mission Summary
(Swingby Outbound - Direct Return)

- 214 -
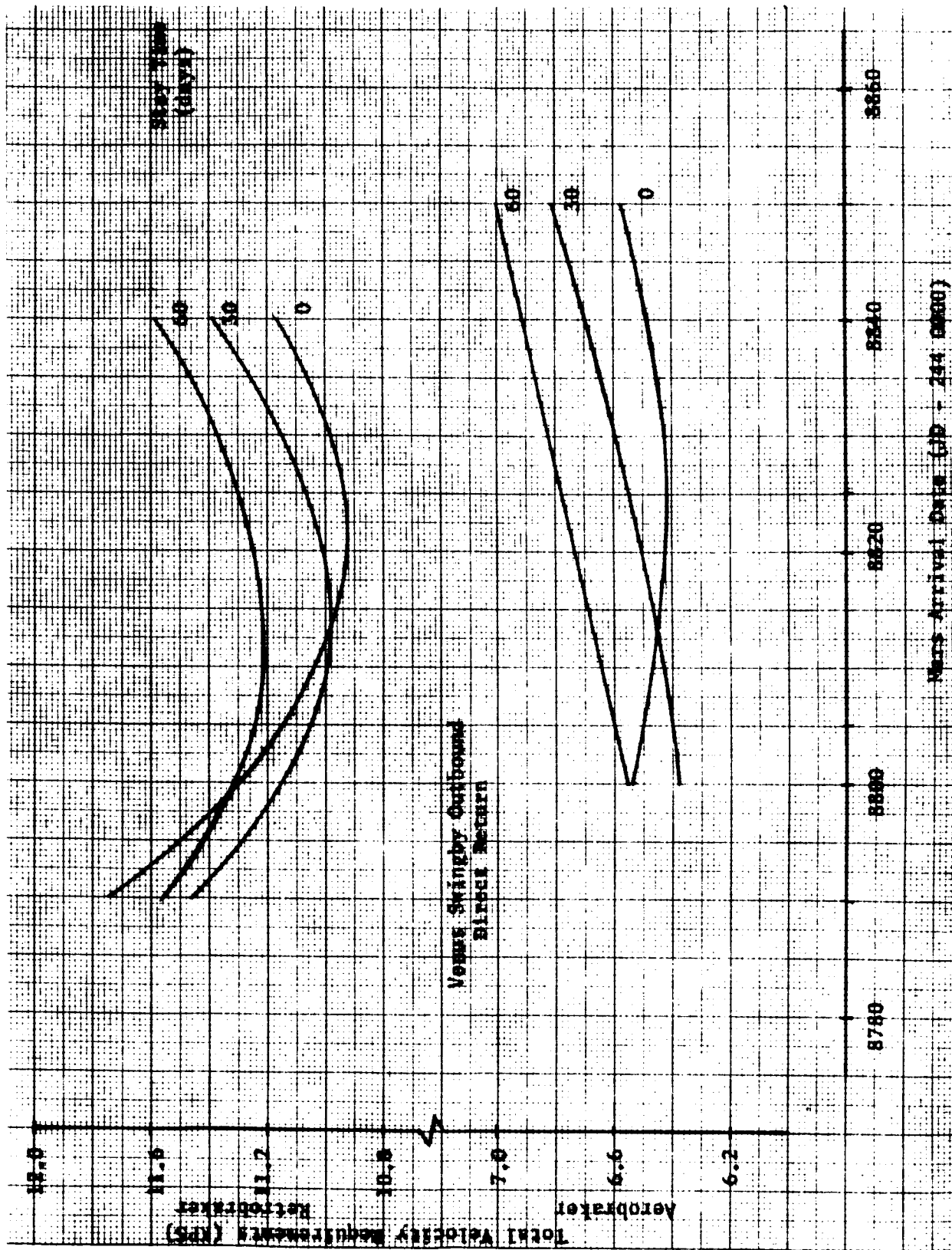
Figure 173. Total Mars Velocity Requirements (1993 Mission)

SD 67-621-2
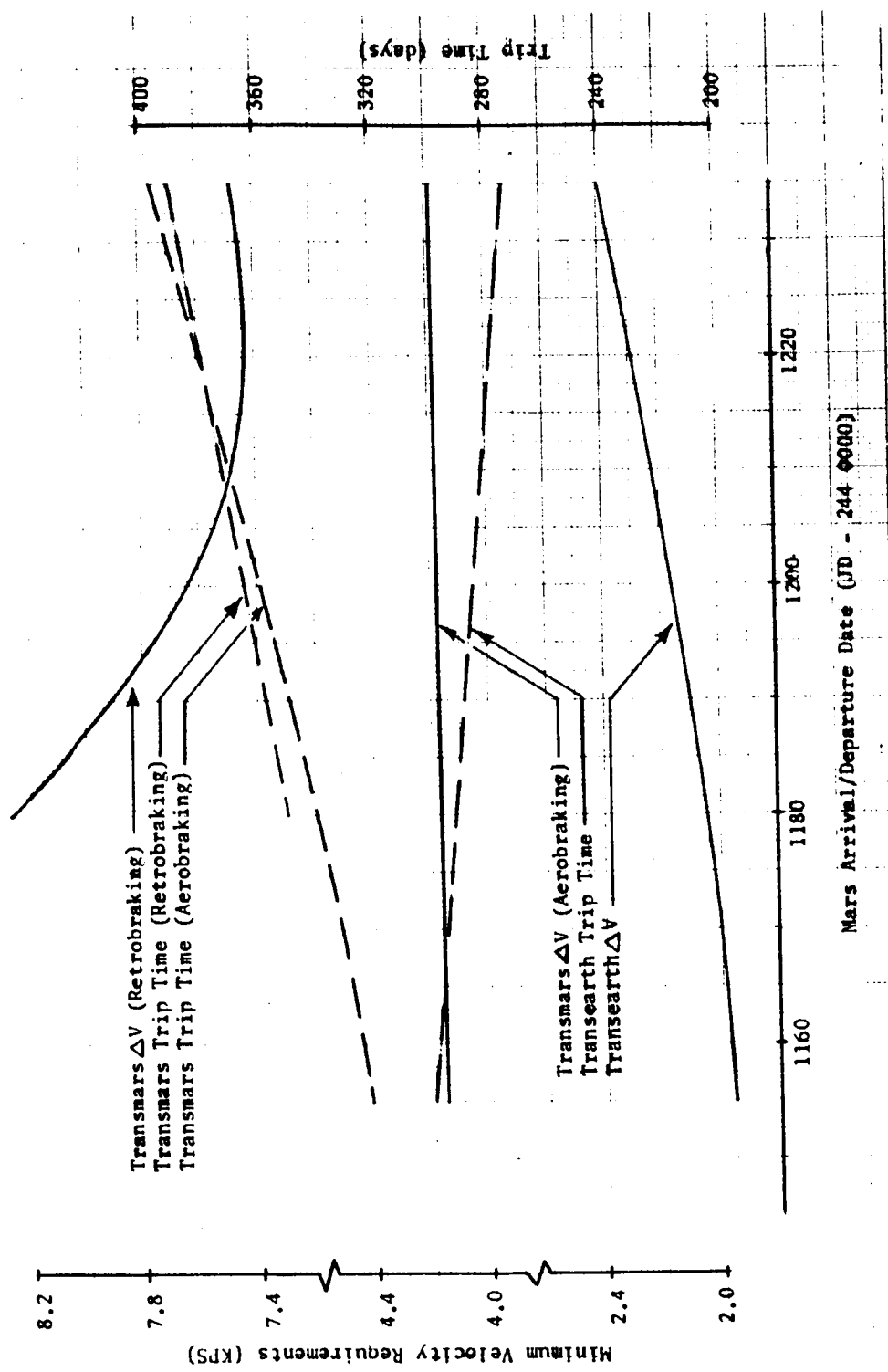
Figure 174.   1999 Mars Mission Summary
(Swingby Outbound – Direct Return)
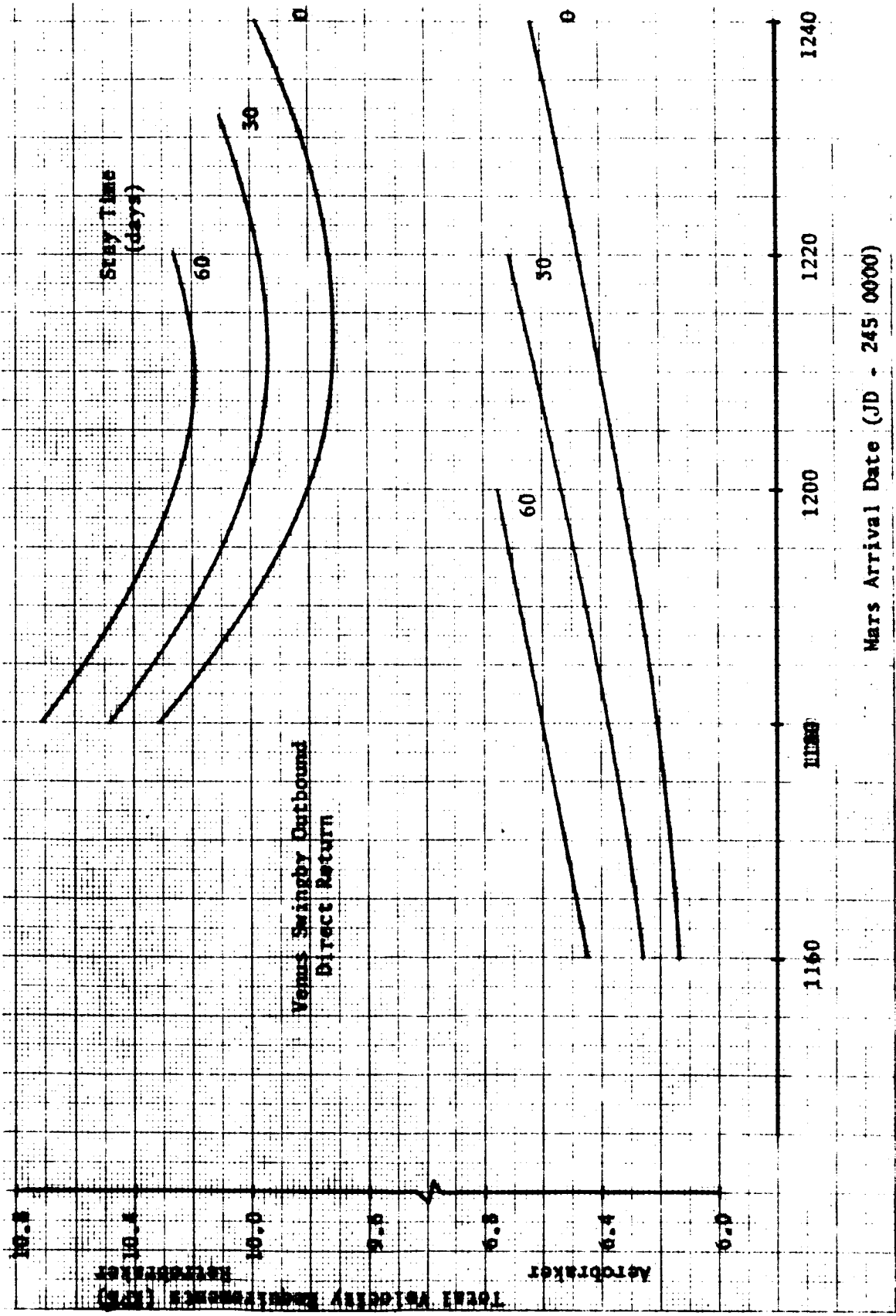
Figure 175. Total Mars Velocity Requirements (1999 Mission)

SD 67-621-2
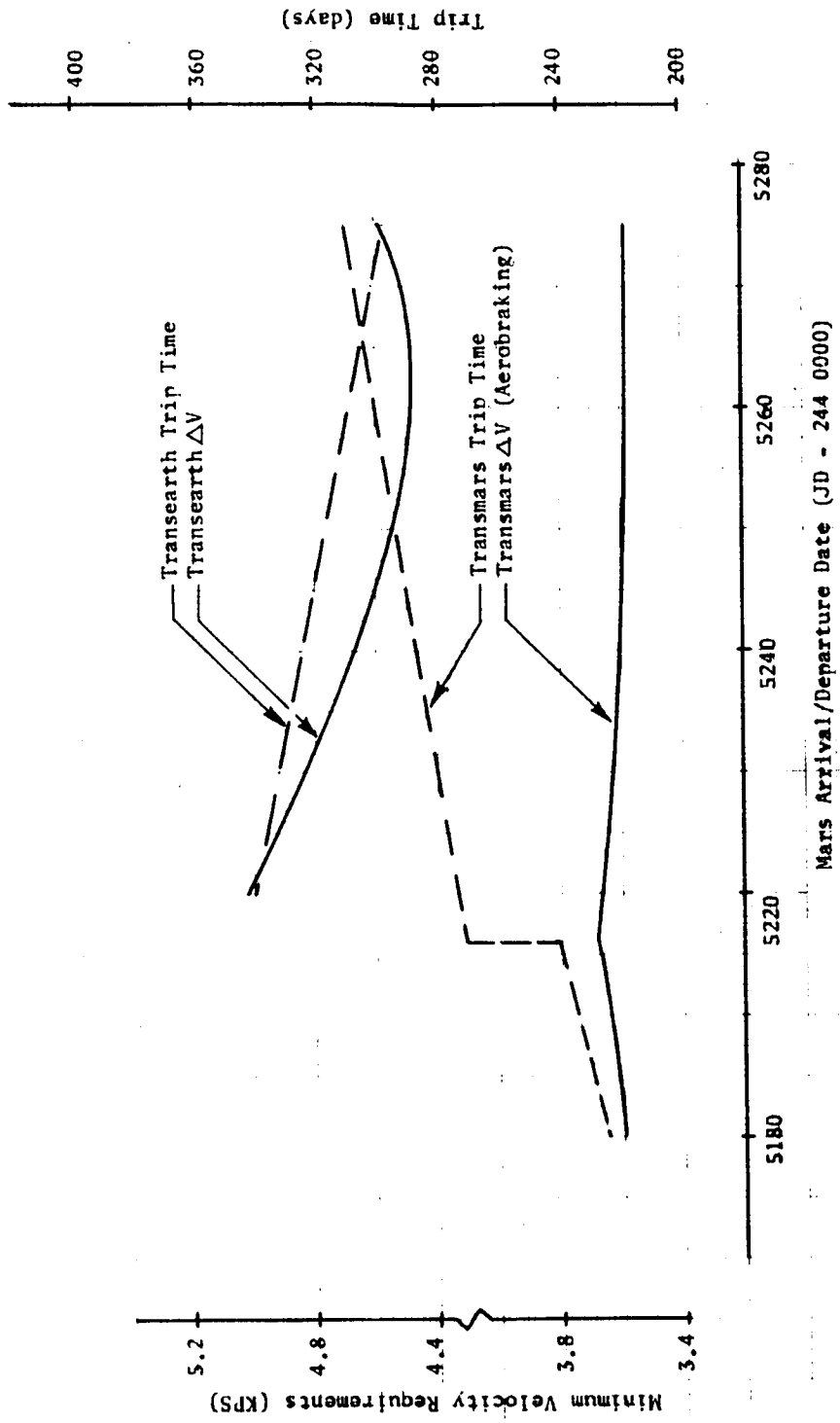
Figure 176. 1982 Mars Aerobraker Mission Summary
(Direct Outbound – Swingby Return)
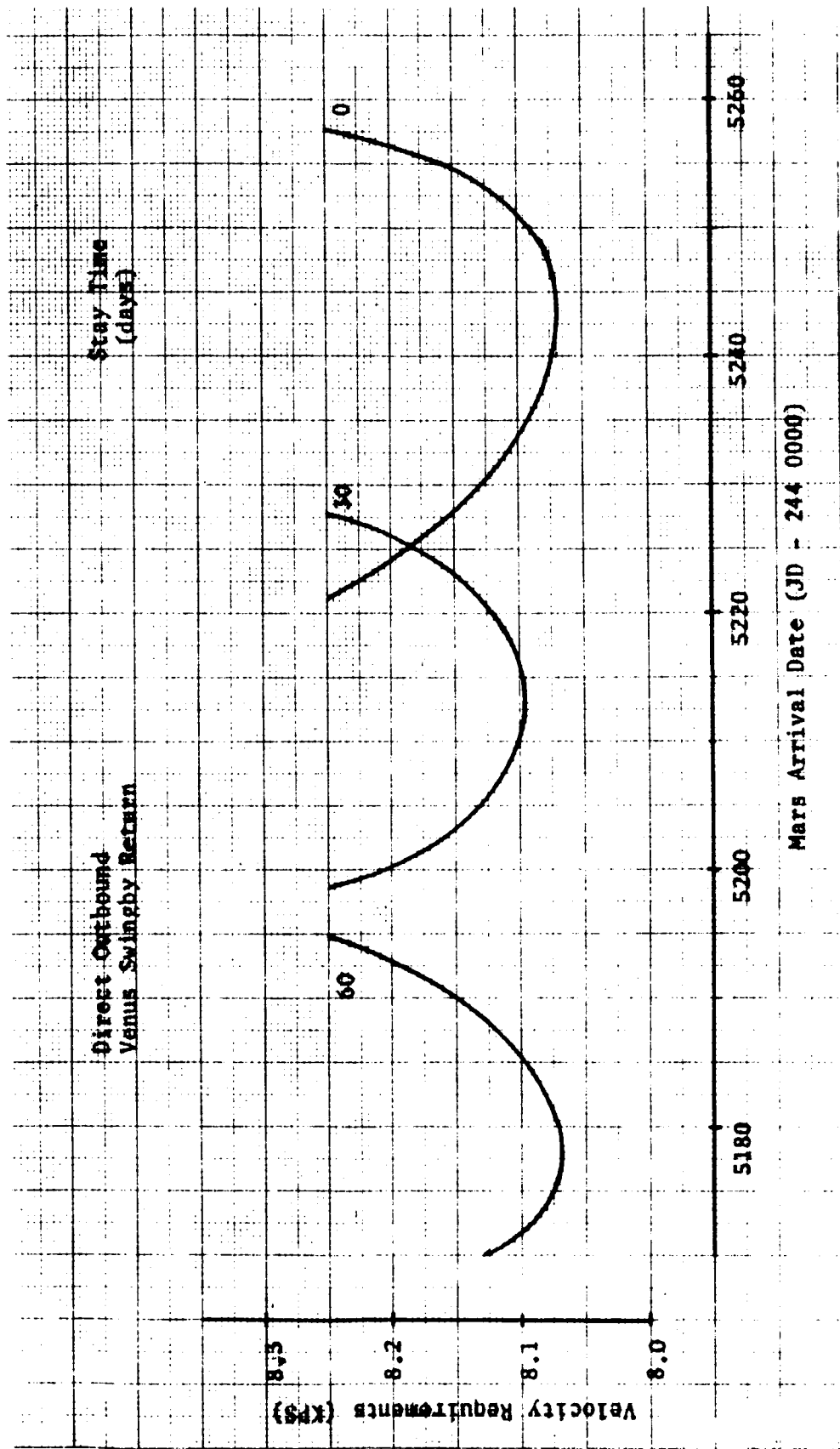
Figure 177. Total Mars Velocity Requirements (1982 Aerobraker Mission)

SD 67-621-2
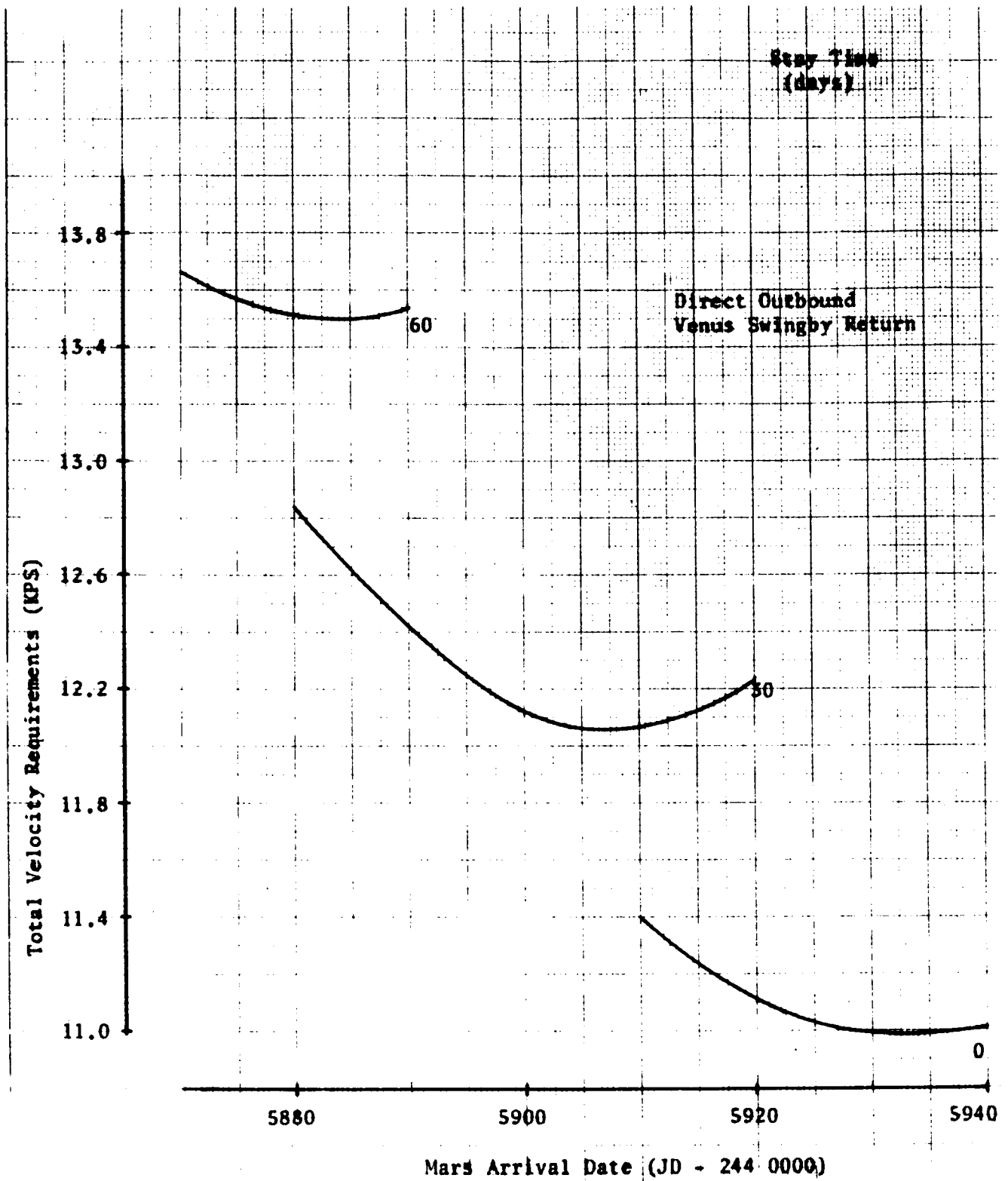
Figure 178.   1984 Mars Retrobraker Mission Summary
(Direct Outbound - Swingby Return)

- 220 -
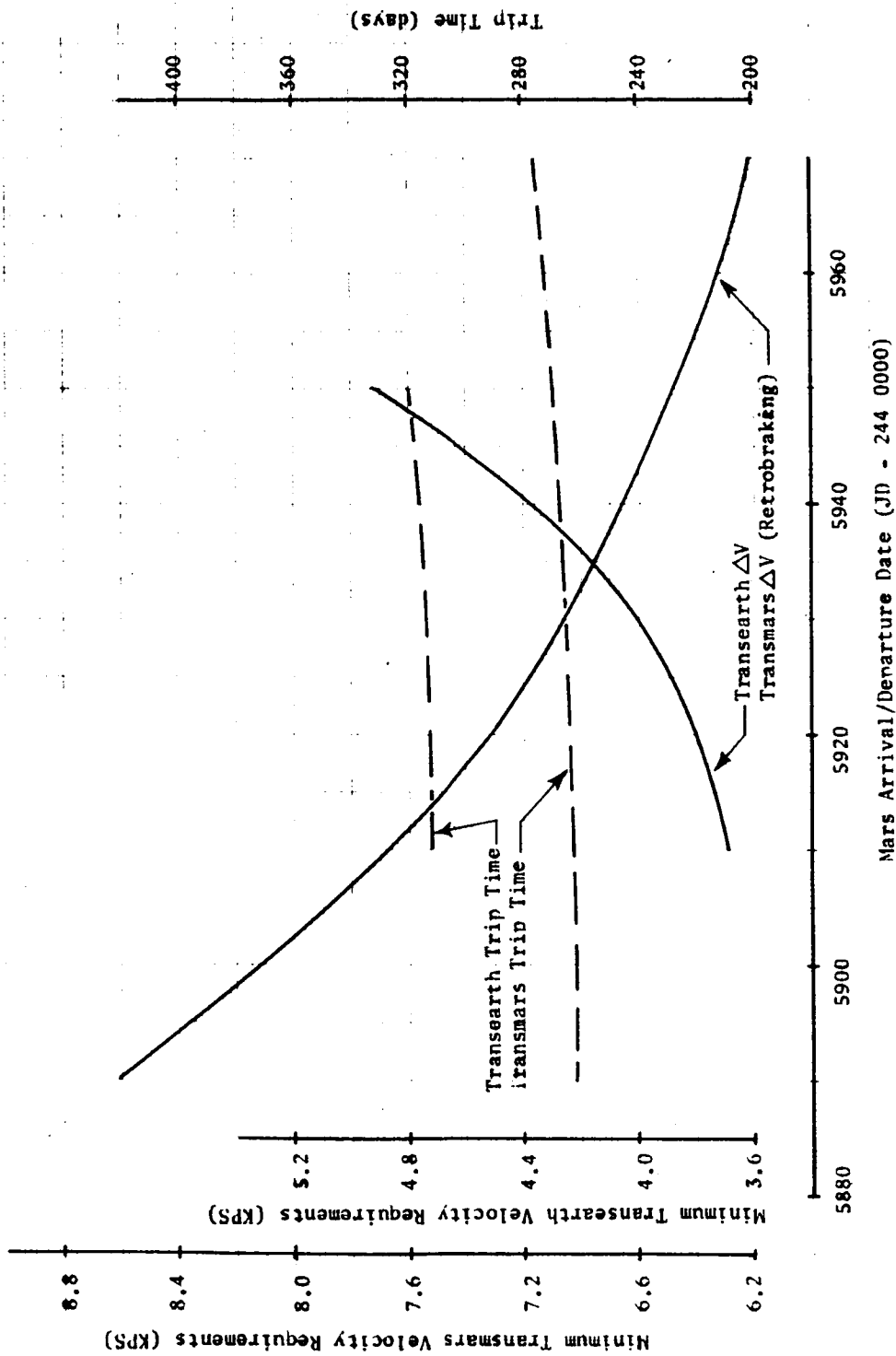
Figure 179. Total Mars Velocity Requirements (1984 Retrobraker Mission)

SD 67-621-2
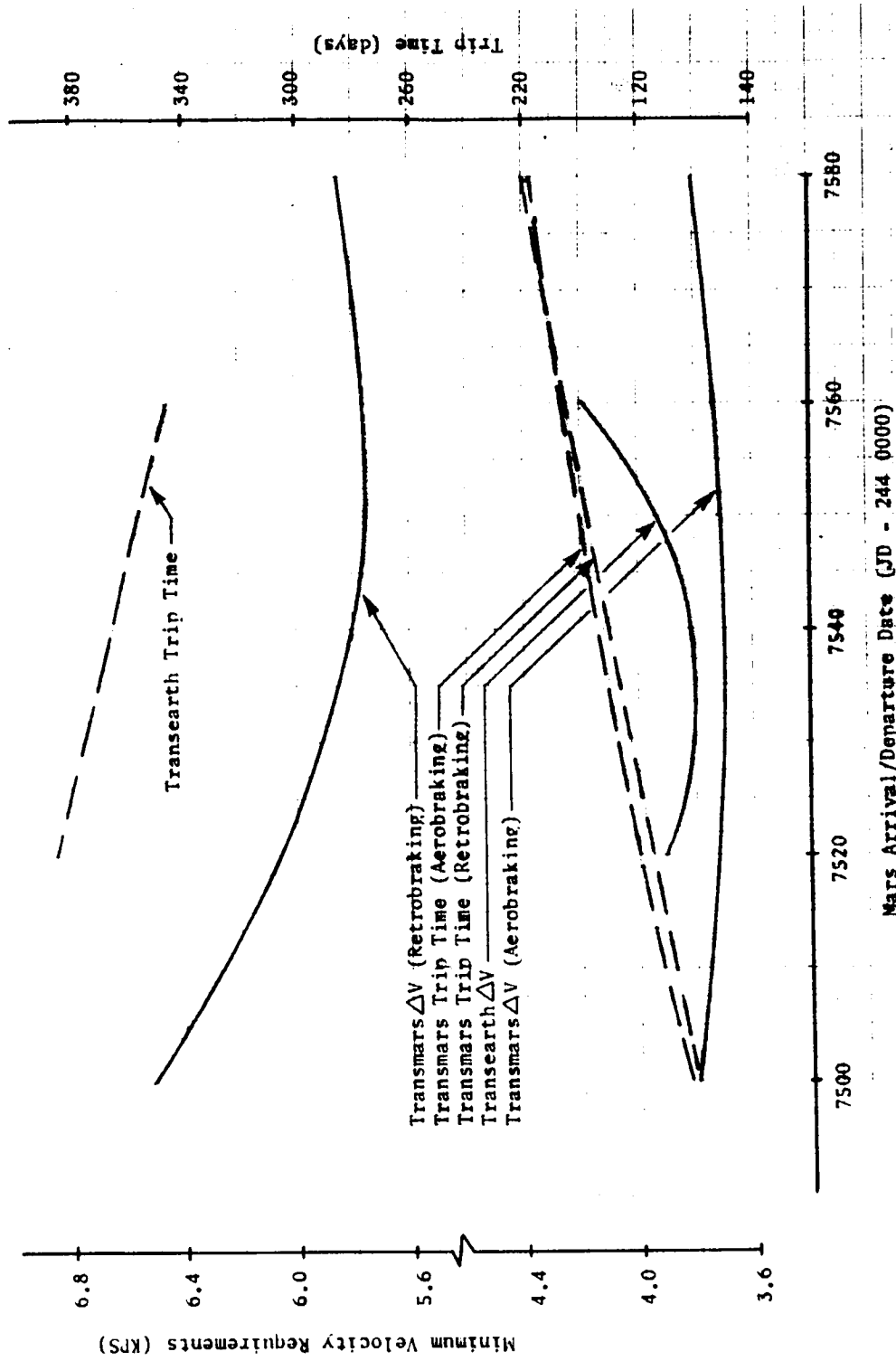
Figure 180.   1988 Mars Mission Summary
(Direct Outbound - Swingby Return)
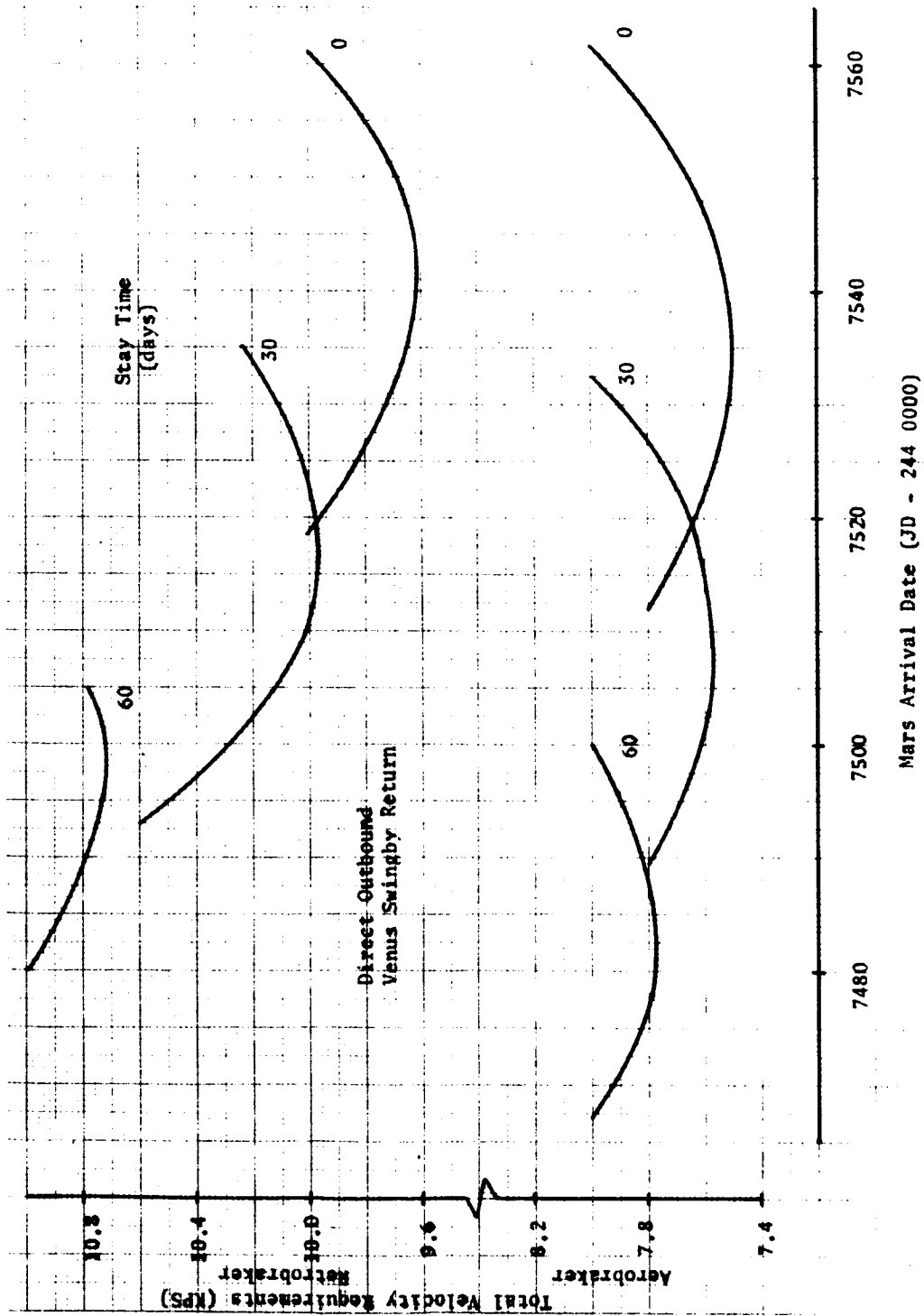
Figure 181. Total Mars Velocity Requirements (1988 Mission)
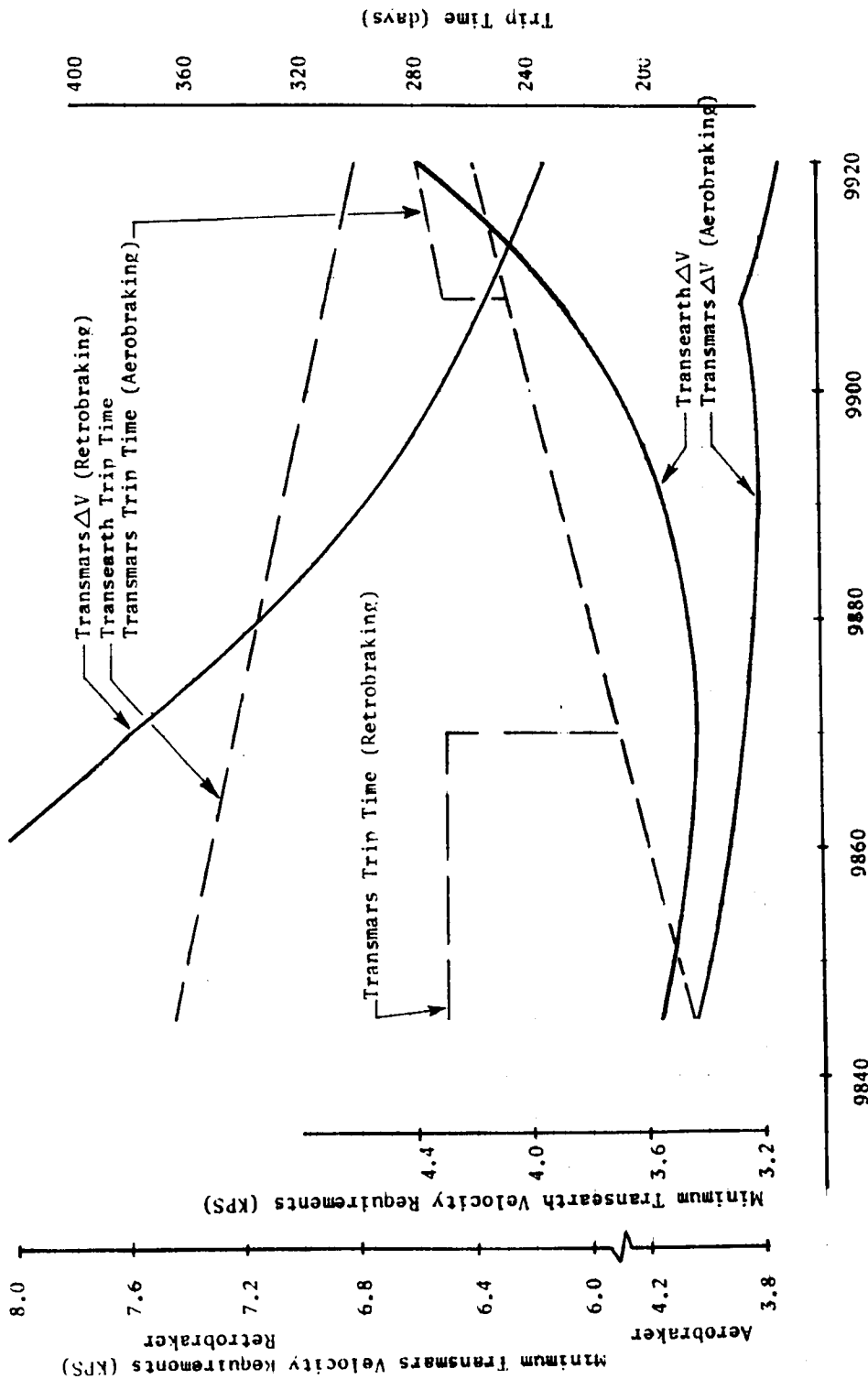
Figure 182. 1995 Mars Mission Summary
(Direct Outbound - Swingby Return)
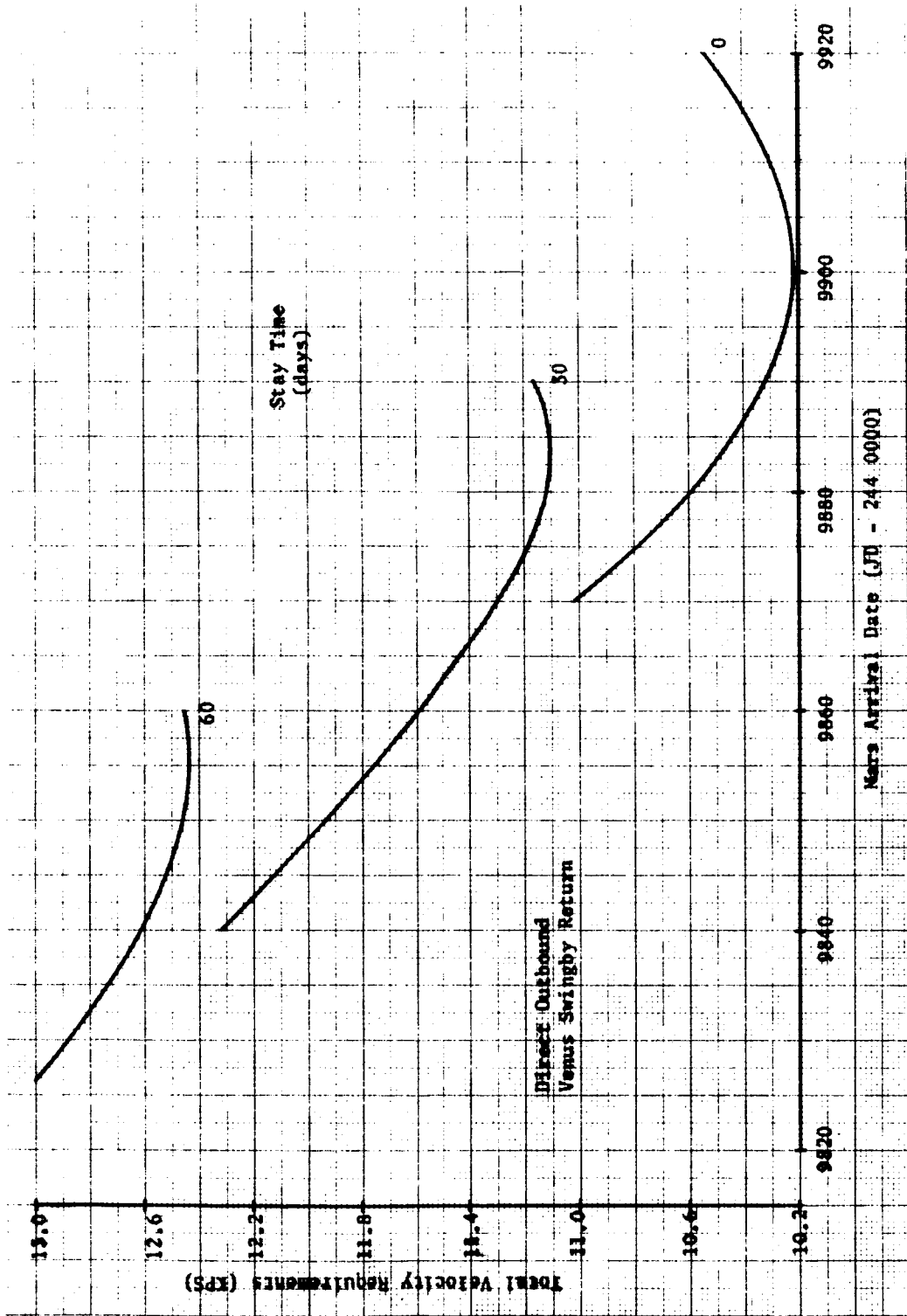
Figure 183. Total Mars Velocity Requirements
(1995 Retrobraker Mission)
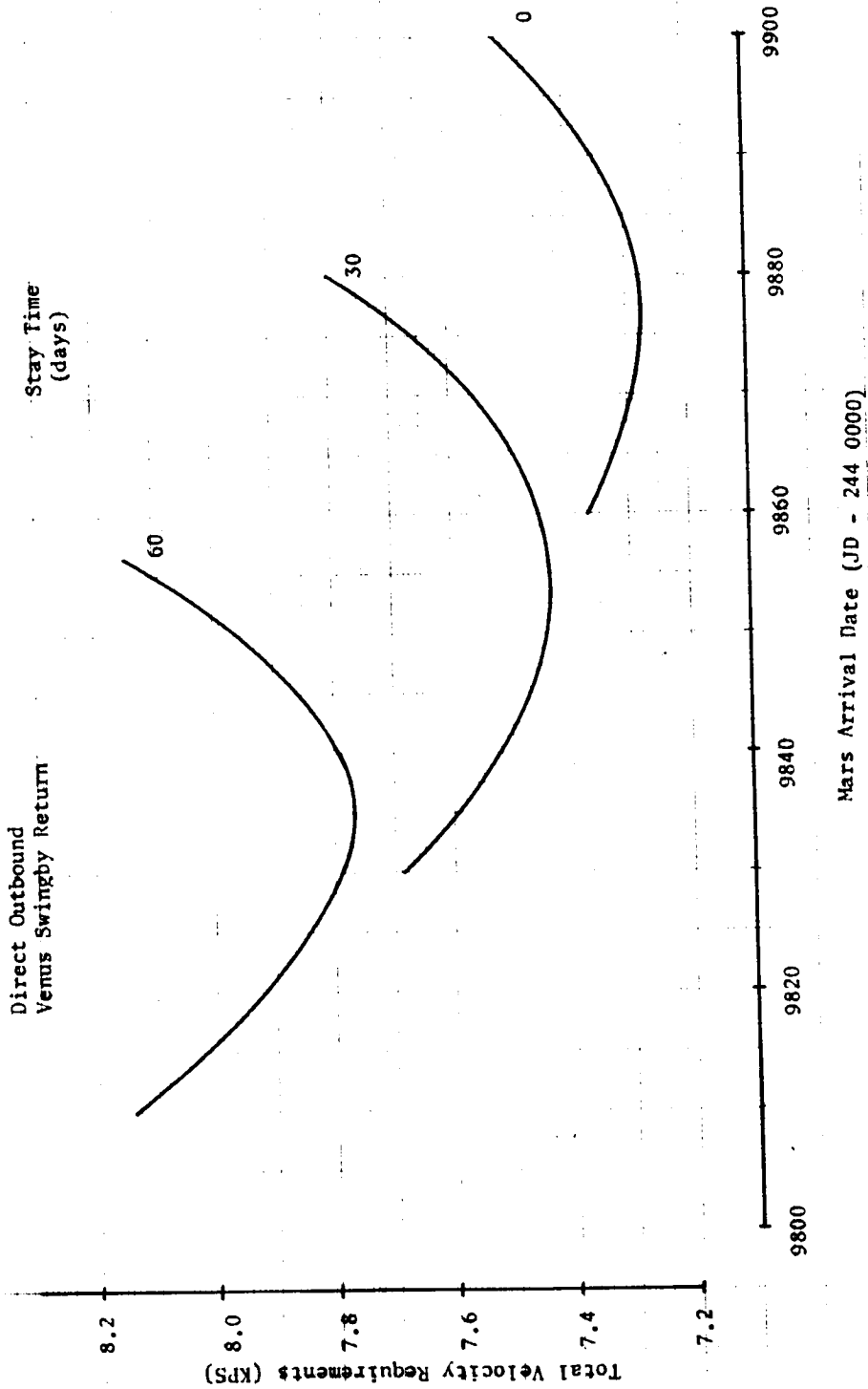
Figure 184. Total Mars Velocity Requirements (1995 Aerobraker Mission)
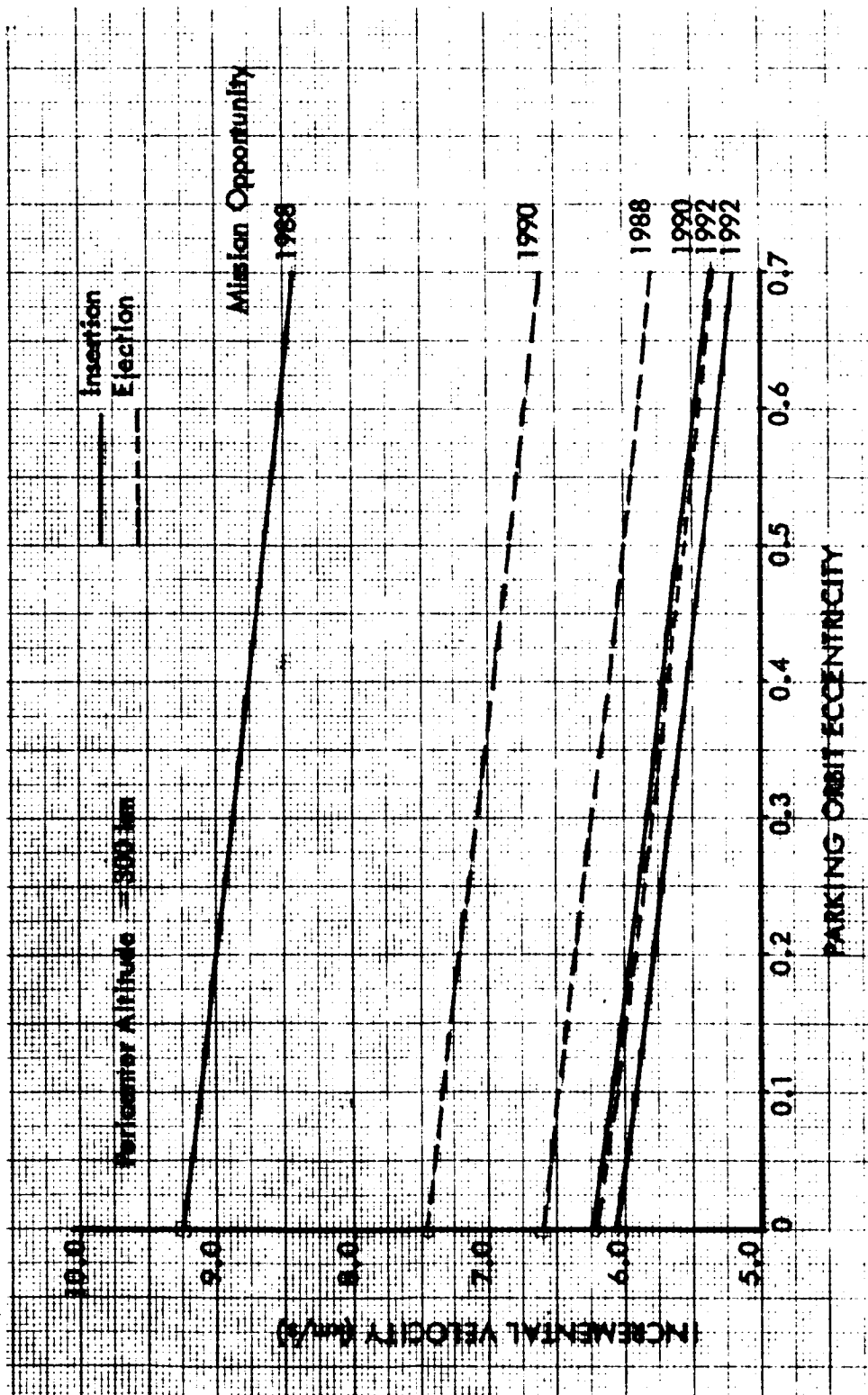
Figure 185. Incremental Velocity Requirements (Mercury Retrobraker)
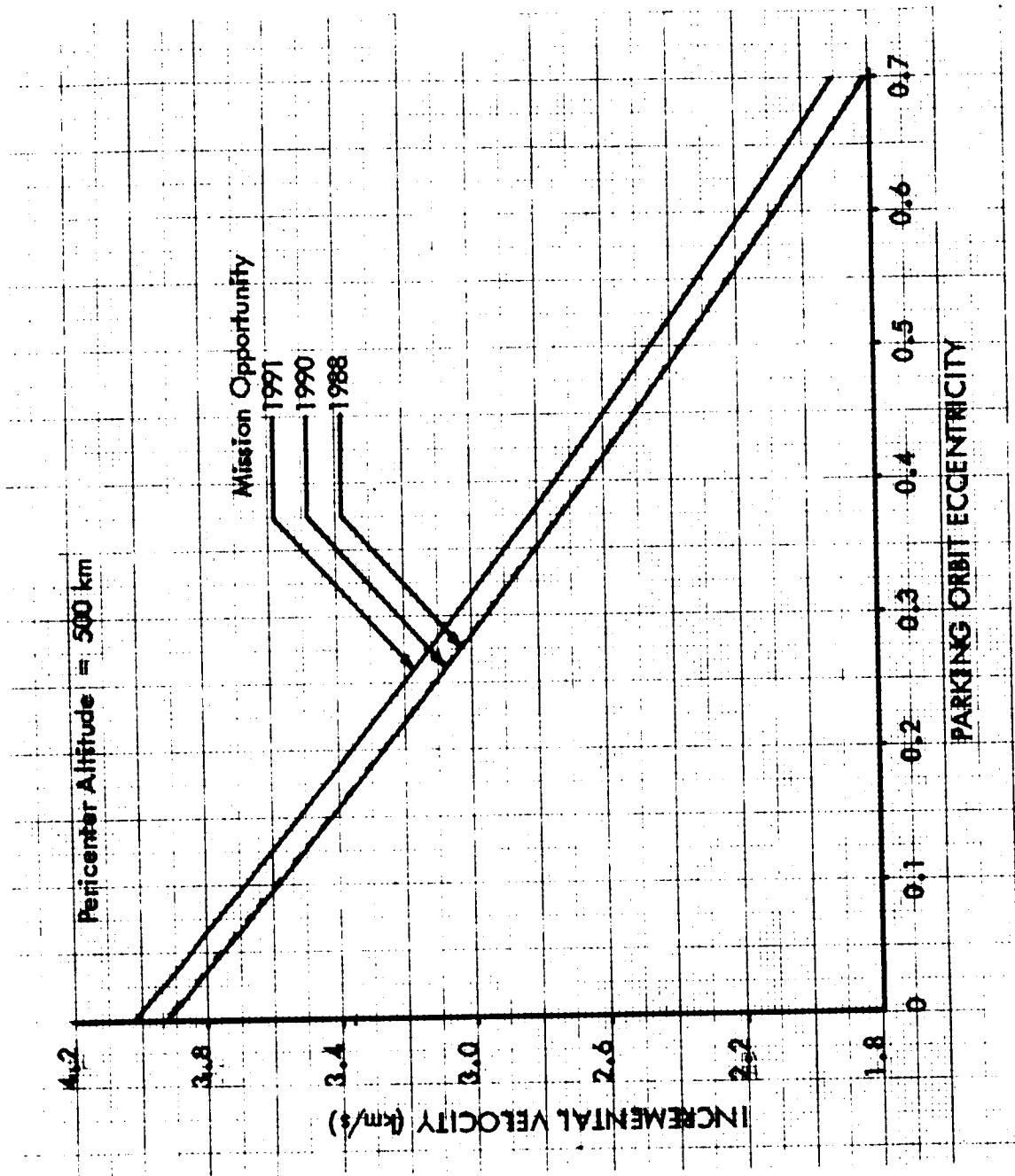
Figure 186. Planetary Orbit Escape Requirements (Venus Aerobraker)
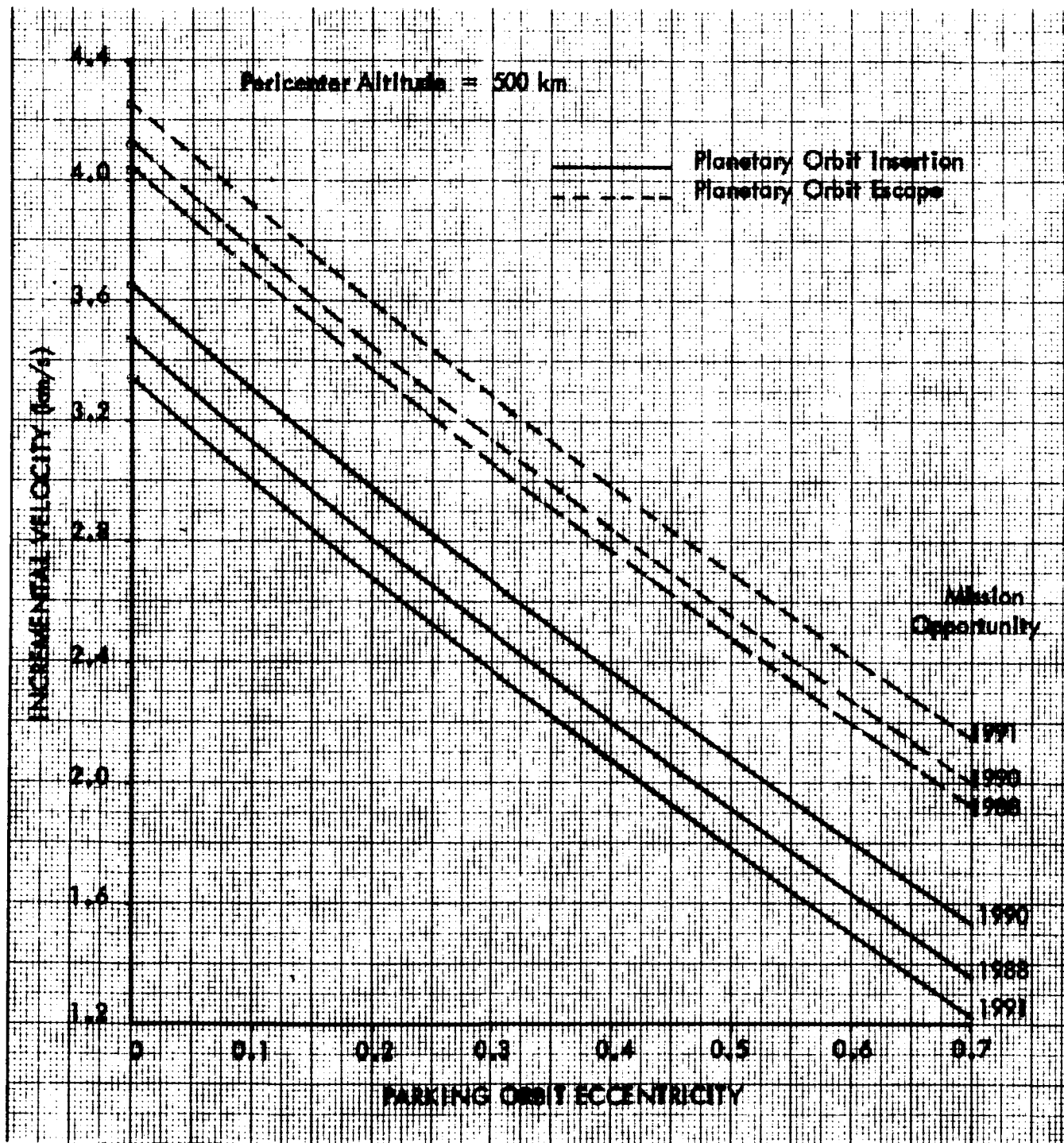
Figure 187. Incremental Velocity Requirements (Venus Retrobraker)

- 229 -
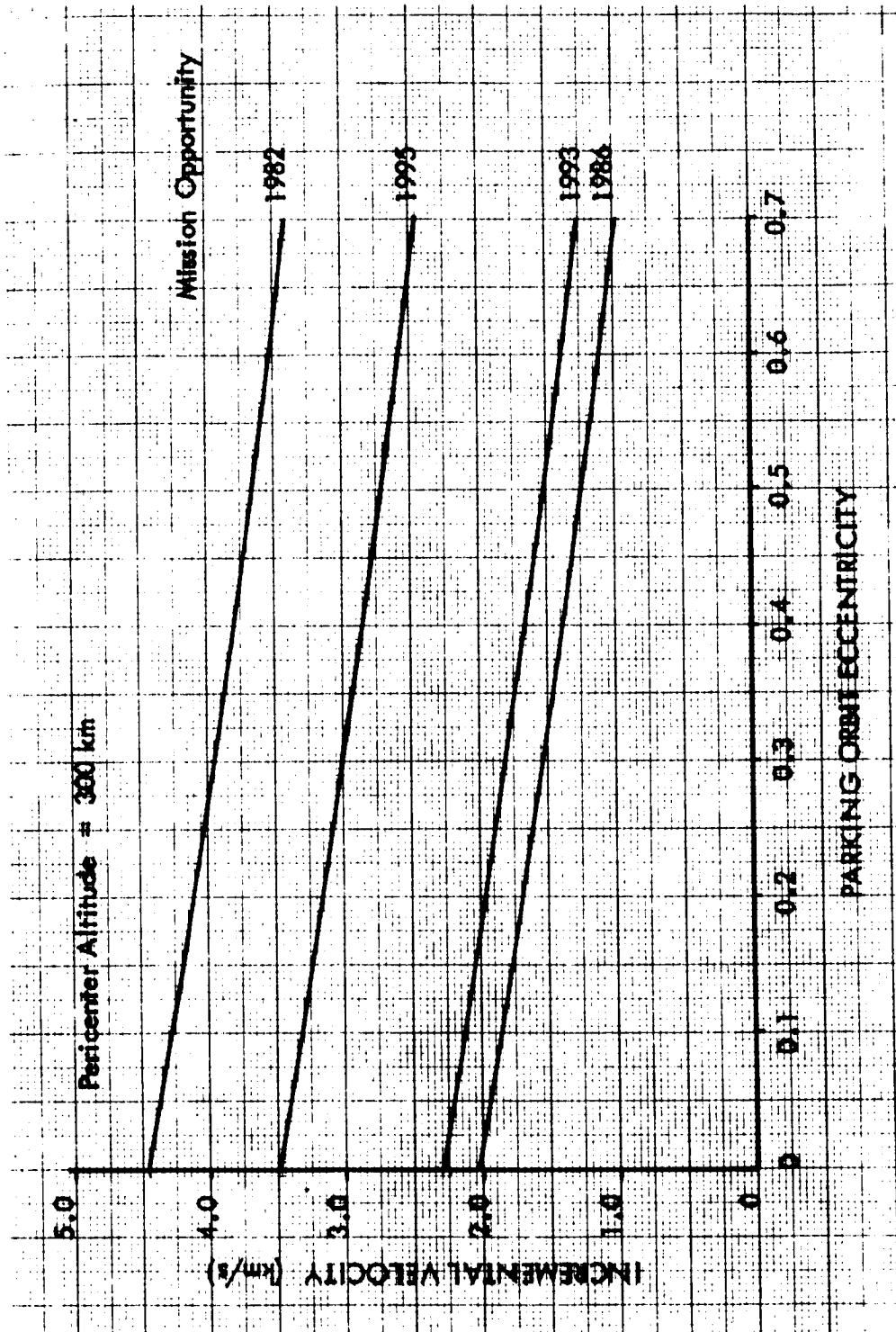
Figure 188. Planetary Orbit Escape Requirements (Mars Aerobraker)
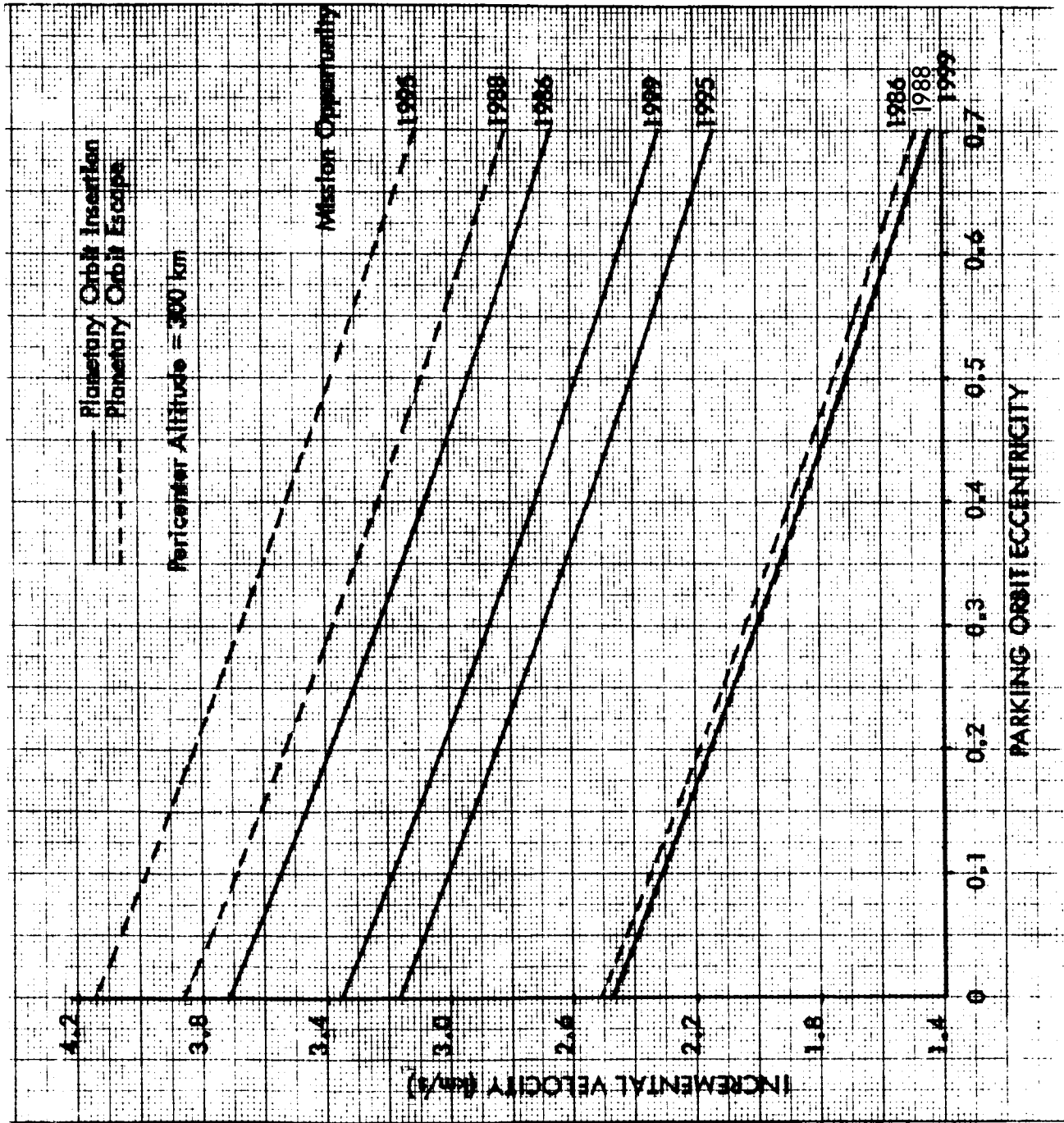
Figure 189. Incremental Velocity Requirements (Mars Retrobraker)

- 231 -
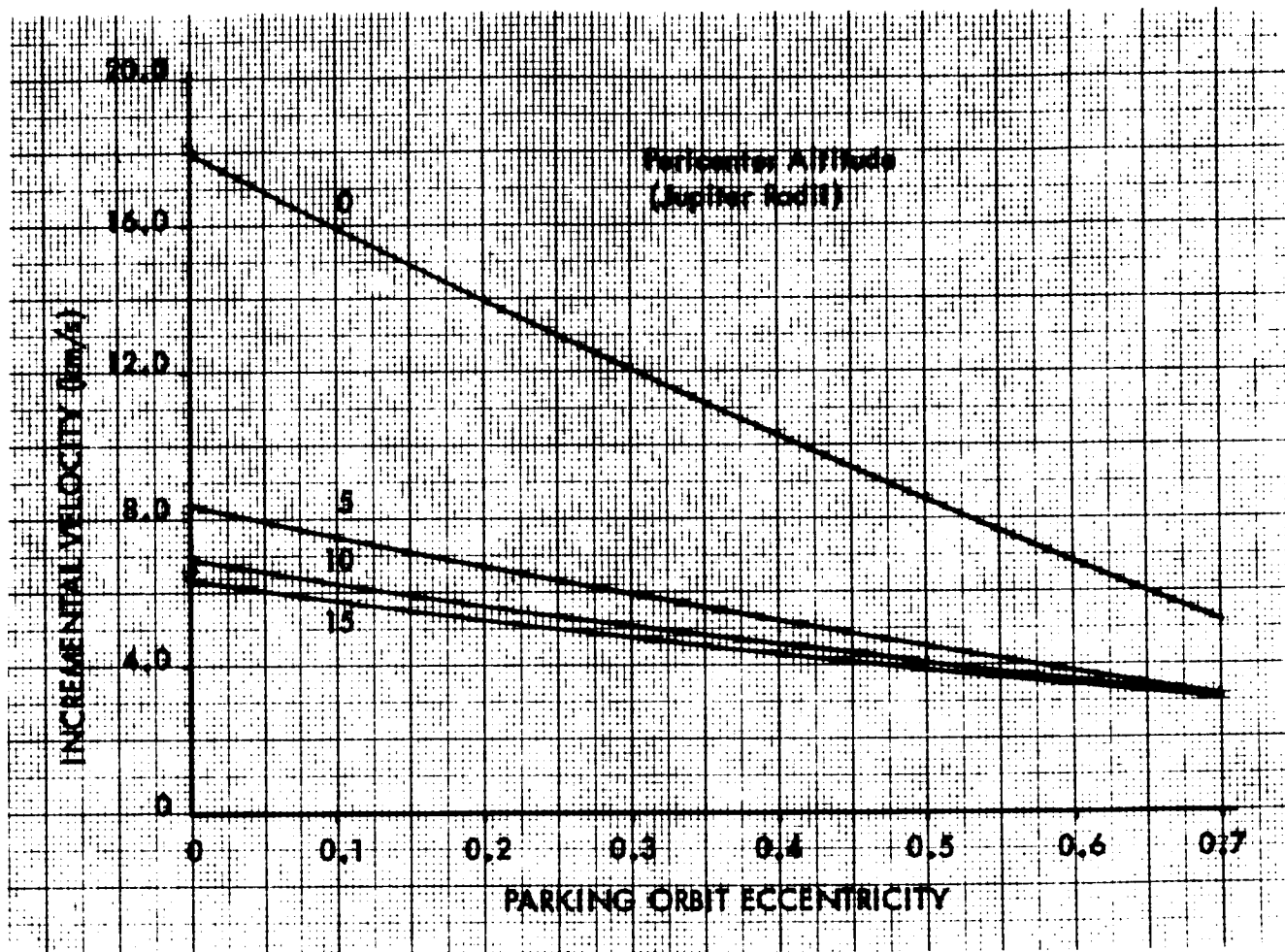
Figure 190. Jupiter Orbit Insertion Requirements (1990 Mission)
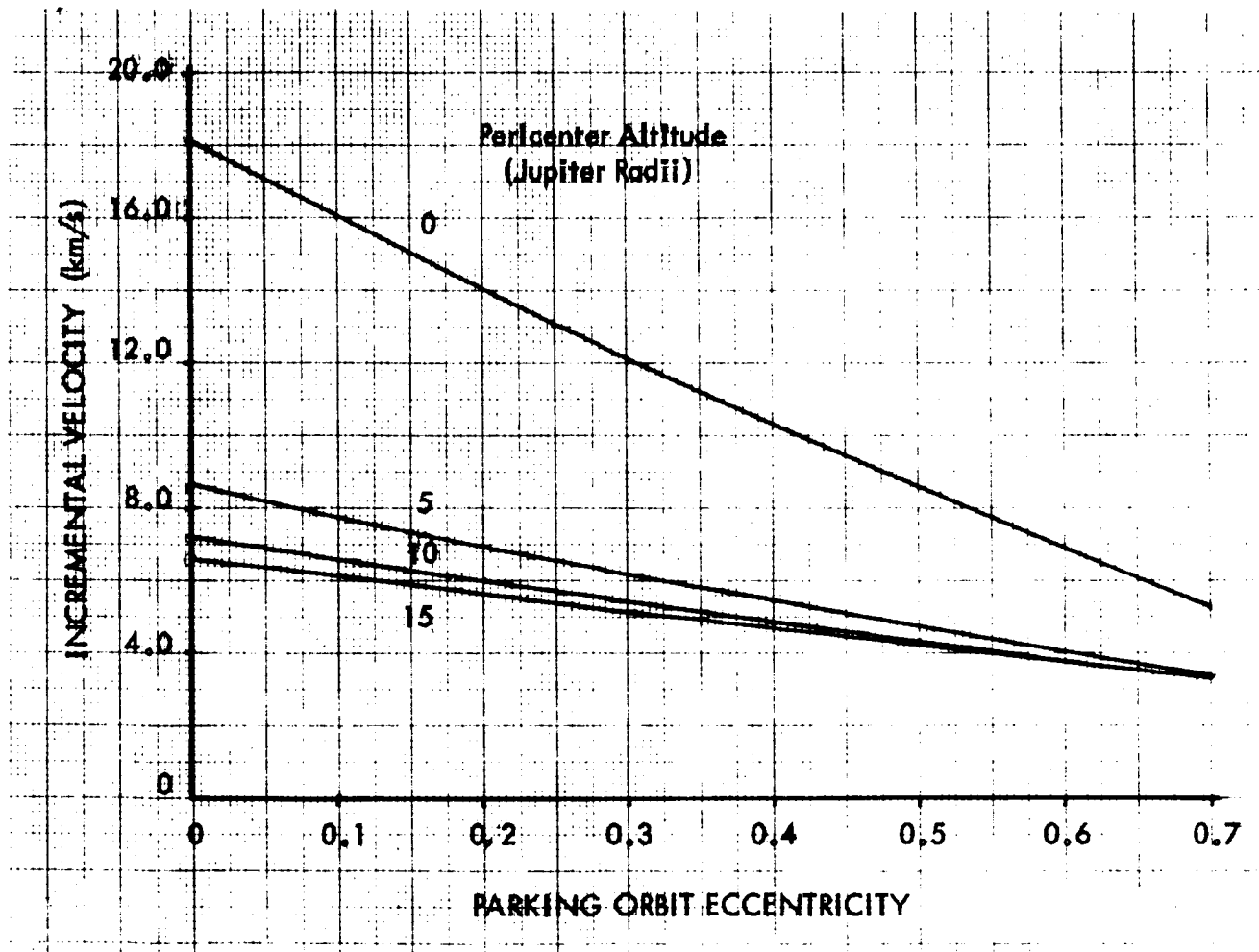
Figure 191. Jupiter Orbit Escape Requirements (1990 Mission)
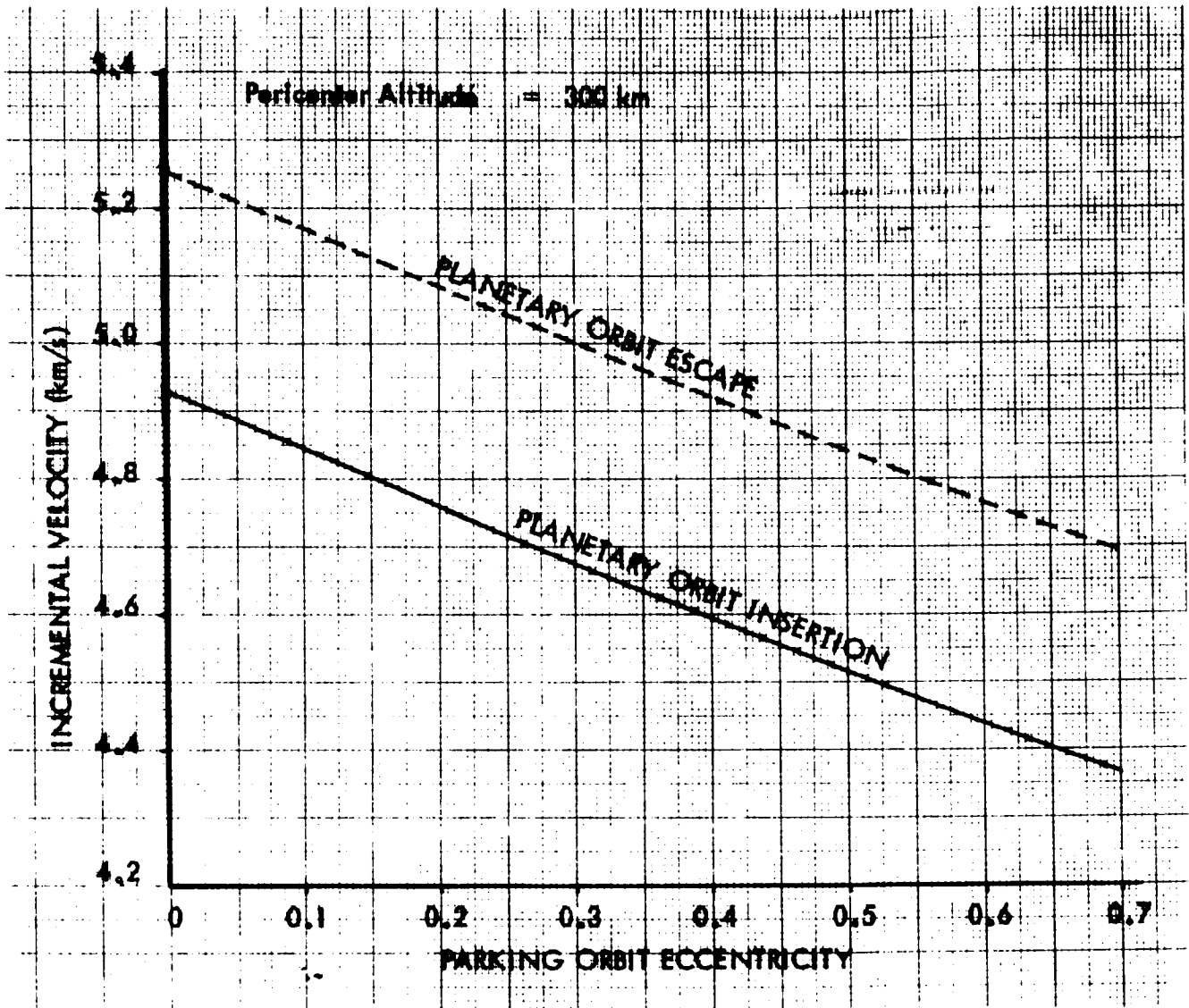
Figure 192. Incremental Velocity Requirements (1990 Ganymede Retrobraker)
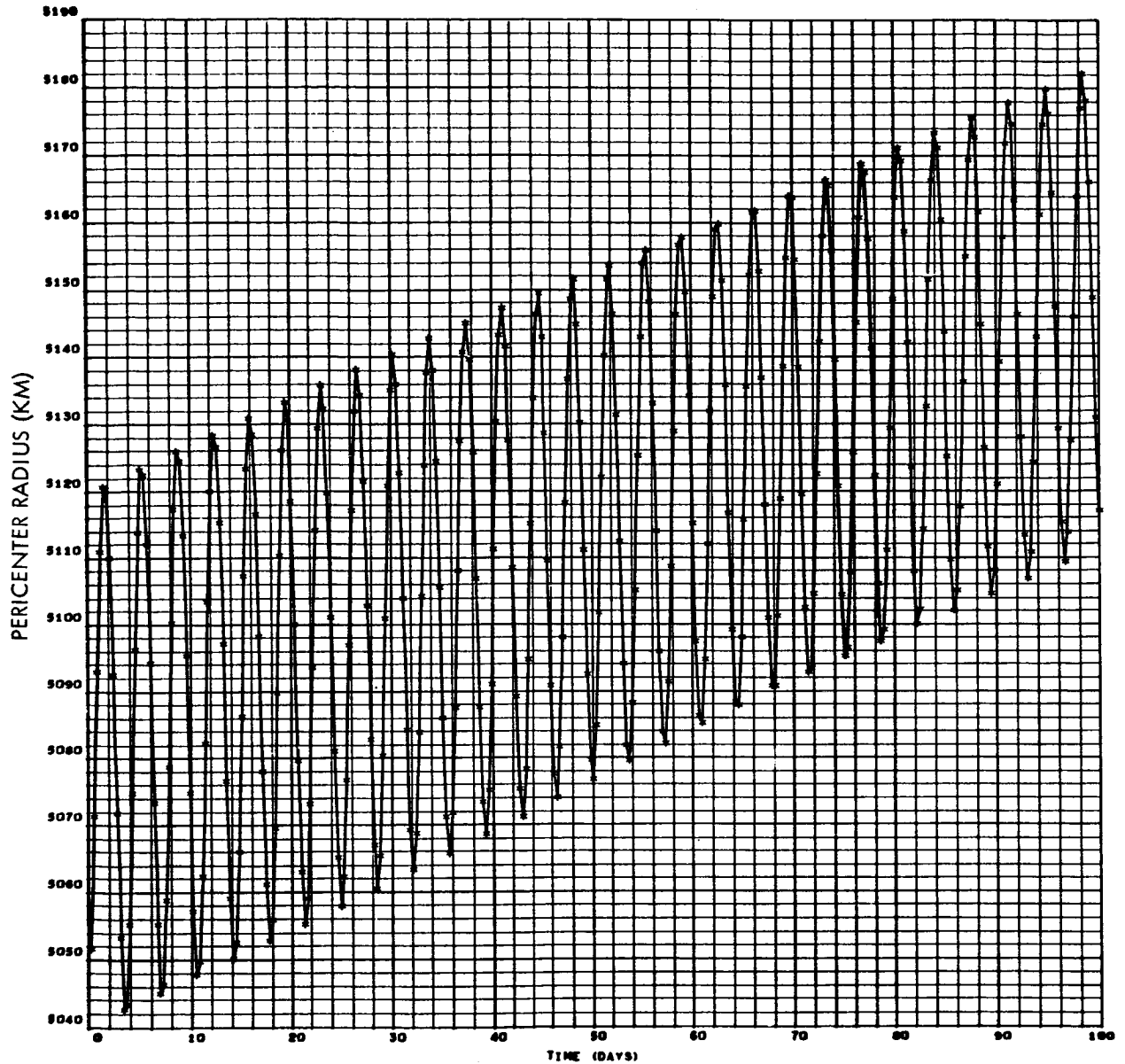
$a_0 = 5600$ KM $\simeq 1$ Radius Alt $i_0 = 0.0$ $\omega_0 = 0.0$

$e_0 = .1$ $\Omega_0 = 0.0$

Julian Date $= 2,436,935.0 +$

Disturbing Bodies: Jupiter (99. + %)
                     Europa
                     Callisto
                     Sun

Figure 193.   Orbit Around Ganymede, Pericenter
              Perturbations, $i_0 = 0.0$
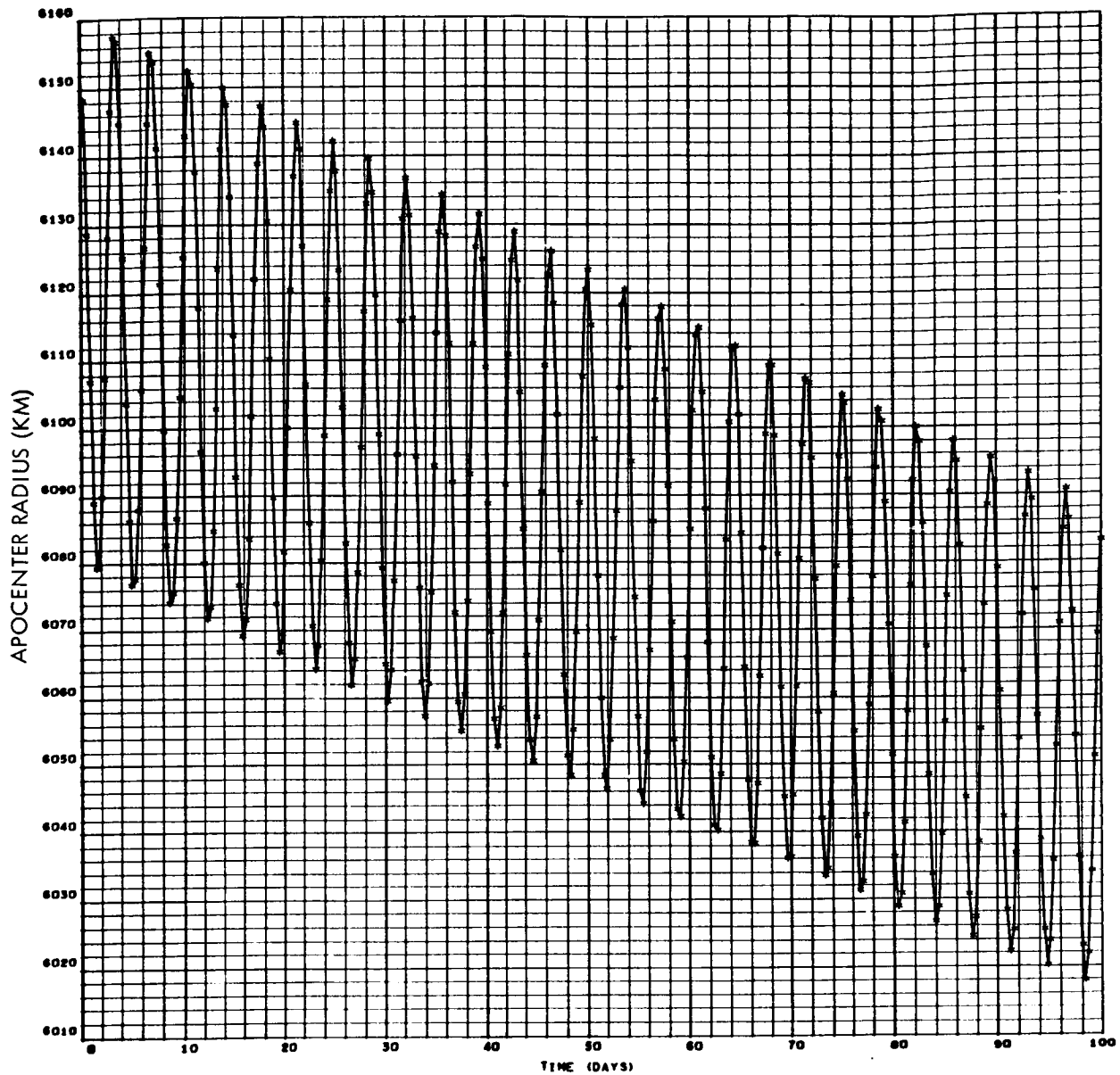
- 235 -

$a_0 = 5600$ KM $\simeq 1$ Radius Alt $i_0 = 0.0$ $\omega_0 = 0.0$

$e_0 = .1$ $\Omega_0 = 0.0$

Julian Date = 2,436,935.0 +

Disturbing Bodies: Jupiter (99. + %)
                        Europa
                        Callisto
                        Sun

Figure 194.   Orbit Around Ganymede, Apocenter Perturbations, $i_0 = 0.0$

- 236 -

PERIFOCUS PERTURBATIONS

Figure 195. Orbit Around Ganymede, Pericenter Perturbations, $i_0 = 90.0$
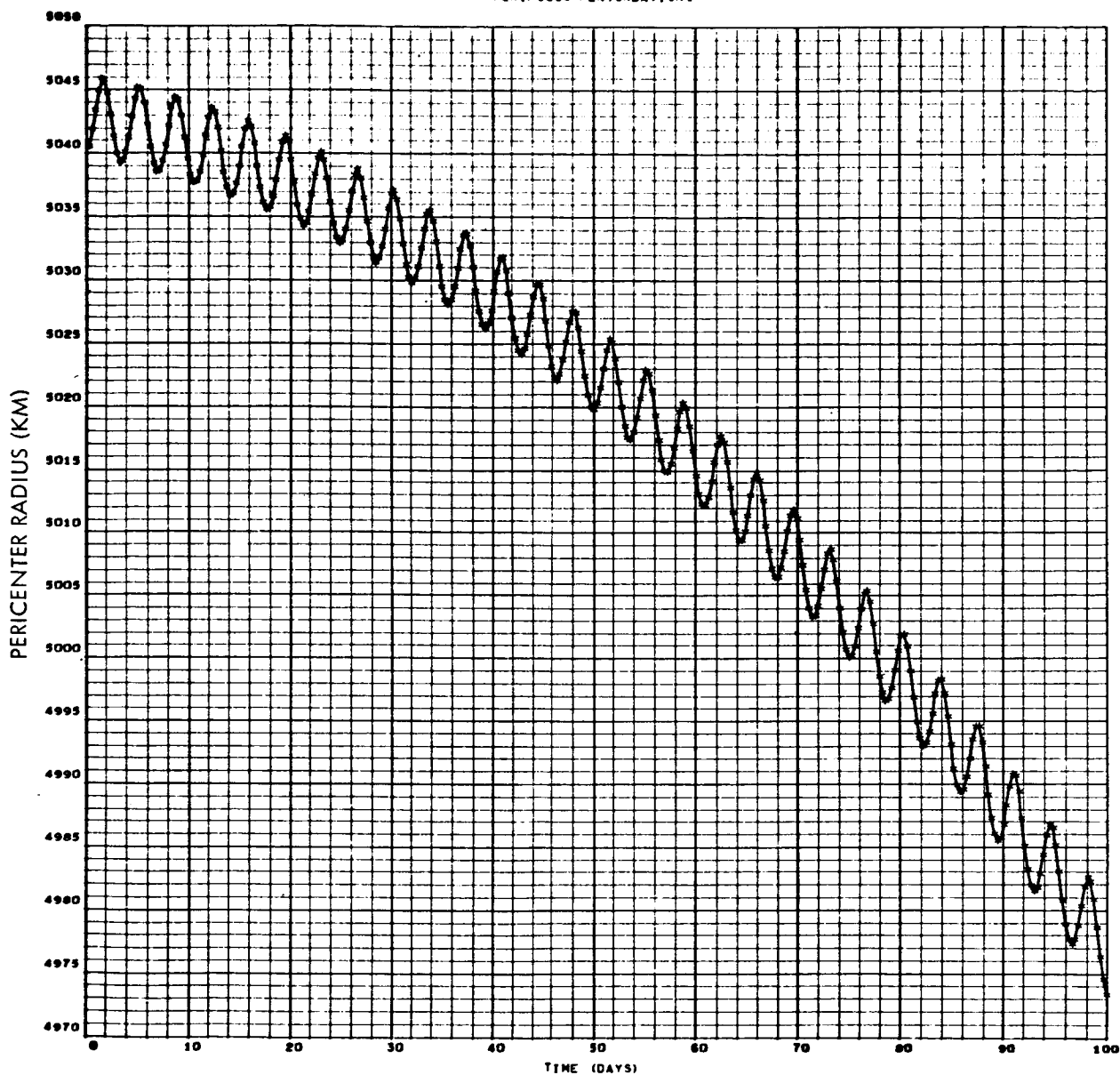
$a_0 = 5600$ KM $i_0 = 90.0$ $\omega_0 = 0.0$

$e_0 = .1$ $\Omega_0 = 0.0$

Julian Date: 2,436,935.0 +

Disturbing Bodies: Jupiter (99. + %)
                    Europa
                    Callisto
                    Sun

- 237 -
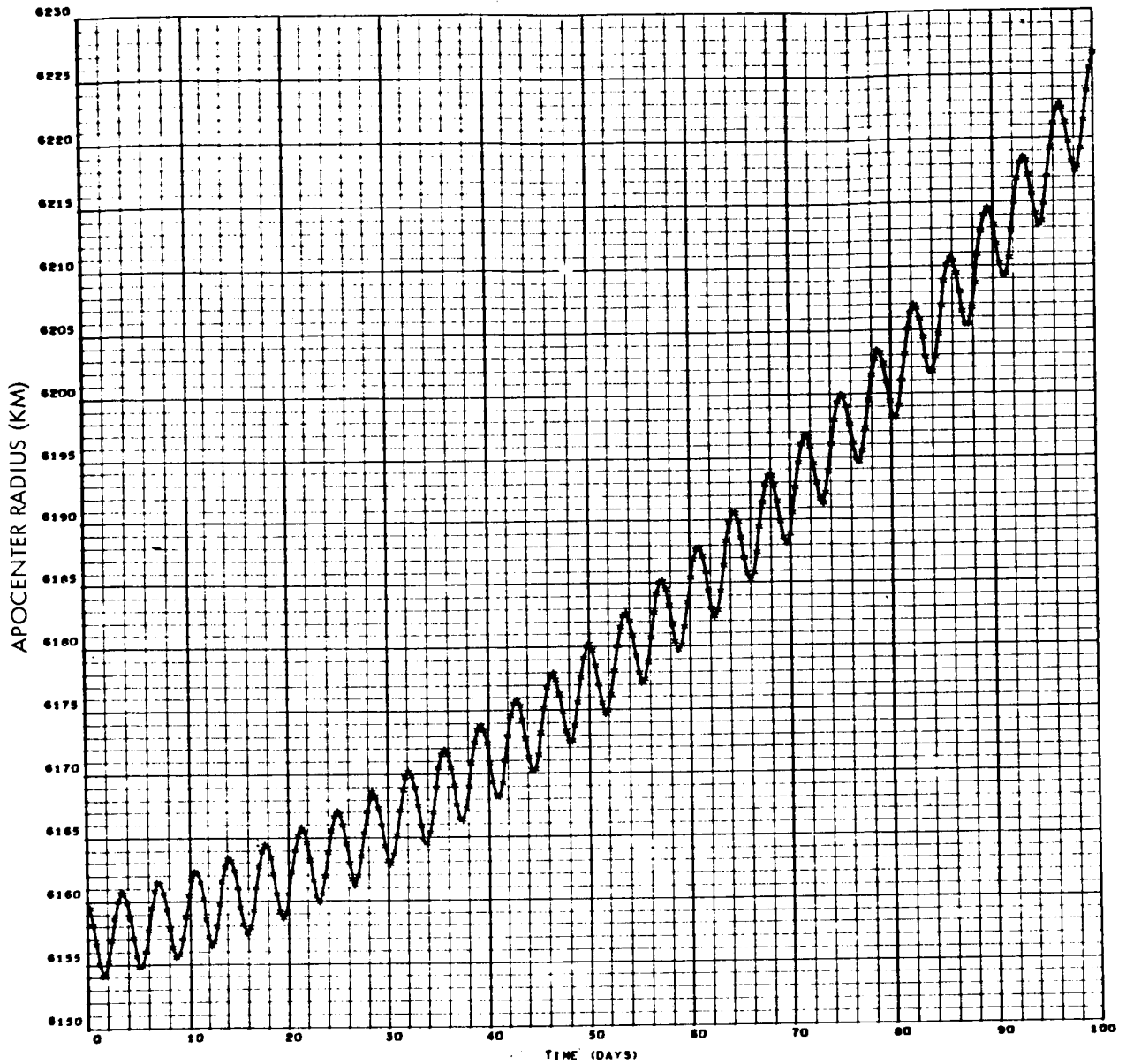
a_o = 5600 KM i_o = 90.0 ω_o = 0.0

e_o = .1 Ω_o = 0.0

Julian Date: 2,436,935.0 +

Disturbing Bodies: Jupiter (99. + %)
                   Europa
                   Callisto
                   Sun

Figure 196. Orbit Around Ganymede, Apocenter Perturbations,
i_o = 90.0

- 238 -

AEROBRAKING TECHNOLOGY REQUIREMENTS

Aerodynamic braking to orbit about Mars and Venus is an attractive mode of decelerating the spacecraft from hyperbolic approach velocities when compared to retrobraking deceleration. This mode, however, results in a much more complex system, which is very sensitive to both the environment and to the vehicle and trajectory parameters. Additional constraints are imposed on the aerobraking vehicle by packaging, tolerable deceleration levels, and achievable navigation accuracy.

Past studies, such as those described in References 5 and 6, have considered some of the complex interactions between the environment and vehicle and trajectory parameters and have developed a feasible vehicle configuration. This configuration, shown in Figure 197, was utilized in the present study as a baseline for the parametric analyses. The configuration was assumed to develop an L/D of 1.0 at a value of C_D of 0.25. Ballistic coefficients ranging from 2400 to 12,200 kg/m^2 were selected for the parametric studies. Entry velocities ranging from 6 to 12 km/sec for Mars and 9 to 15 km/sec for Venus were chosen as representative.

The atmospheres used in this study were obtained from References 7 and 8, and include the VM-8 model from Mars and the NASA/MSFC mean density model for Venus. The analyses were limited to the above atmospheric models since the primary objective of the study was to define the critical spacecraft design sensitivities. Prior to the development of an operational aerobraking spacecraft, the atmospheres will be defined through the use of unmanned spacecraft (e. g., Mariner IV and V) and the actual designs will be based on the resultant atmospheric models.

The results of the study include the aerobraking entry corridors at Mars and Venus as functions of velocity, vehicle $M/C_D A$ and various cut-off criteria, such as maximum deceleration or minimum pull-up altitudes. Heating rates and total heat loads to the vehicle were determined for the critical entry trajectories, and estimates of the required heatshield weights were made. The effects of atmospheric composition were included in the analyses.

EARTH RETURN COURSE CORRECTIC
N₂ O₄ - AEROZINE 50

OPIC-DYNAMIC RADIATORS

ECOLOGICAL RADIATOR

EARTH COMMUNICATION ANTENNA
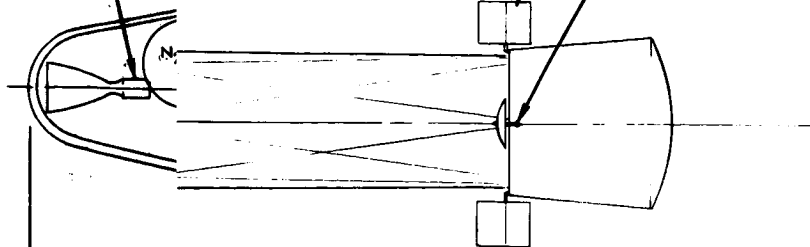
NUS AEROBRAKING CONFIGURATION
ANS-VENUS SPINNING CONFIGURATION)

ALL DIMENSIONS IN METERS

PROBE COMPARTMENT 414 m³

RSE CORRECTION (N₂O₄ - AEROZINE 50)

m³ MISSION MODULE

OUTBOUND COURSE CORRECTION
(OF₂ - MMH)

OF₂/MMH

N₂ O₄

AEROZINE
50

MMH

10.0

OF₂/MMH

1ST & 2ND STA(

5°

VENUS AEROBRAKING CONFIGURATION
(UNMANNED LANDERS/PROBES: OF₂-MMH PLANET DEPARTURE STAGE)
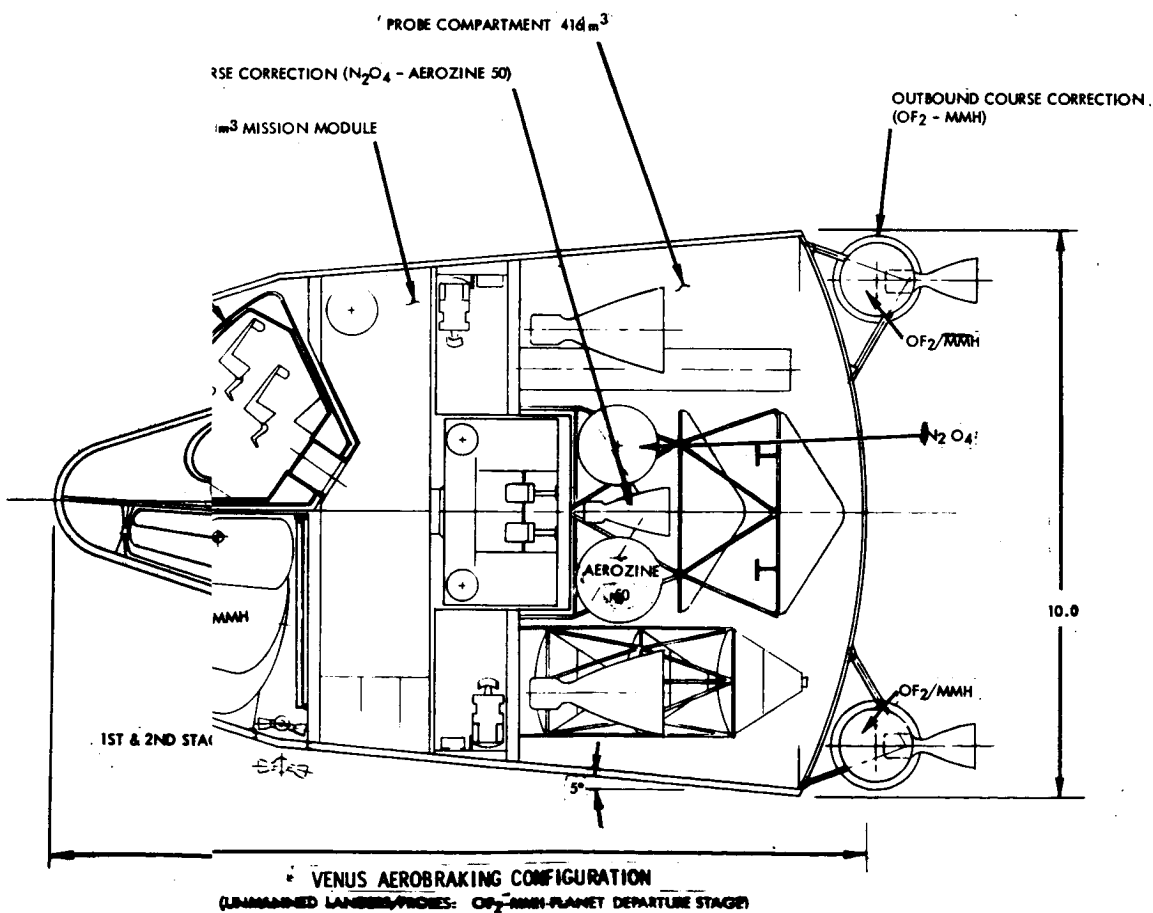
Figure 197. Integrated Spacecraft Concepts

242 -

PLANETARY ATMOSPHERIC MODELS

MARS

The JPL VM series model atmospheres derived from the Mariner IV radio occultation experiments were employed in the Mars aerobraking aerothermodynamic-performance analyses. The new estimates of surface pressure range between 5 and 8 millibar, as compared to previous estimates which were as high as 185 millibars. Figure 198 presents a comparison between post-Mariner atmospheric density profiles and pre-Mariner extreme density profiles. Table 20 presents a tabulation of the JPL Mars atmosphere construction parameters. As indicated by Figure 198, the VM-8 model has values of density considerably below those for the other models and is thus the critical model for aerobraking. The important parameters of the VM-8 atmosphere are tabulated in Table 21 as a function of altitude.

VENUS

The Marshall Space Flight Center (NASA-MSFC) recommended model atmospheres (Reference 7) were employed in the Venus aerobraking aerothermodynamic-performance analyses. These model atmospheres consist of an upper density model (UDM), a mean density model (MDM), and a lower density model (LDM).

The basic construction philosophy of these atmospheres (and other so-called mean and extreme atmospheres) is as follows. Values of construction parameters such as gravity, molecular weight, and surface values of temperature, pressure, and density are combined so as to produce an altitude representation of a selected parameter (usually temperature, but density in these models) which produces a maximum, mean, or minimum profile (Reference 8).

It should be noted that the surface temperatures and pressures associated with the NASA UDM, MDM, and LDM are 750, 700, and 650 K and 40, 10, and 5 atmospheres, respectively. These values bracket the high surface temperature, high surface pressure concept quite well. Construction data for these atmospheres are illustrated in Table 22. The characteristics of these atmospheres are tabulated in Tables 23 through 25.
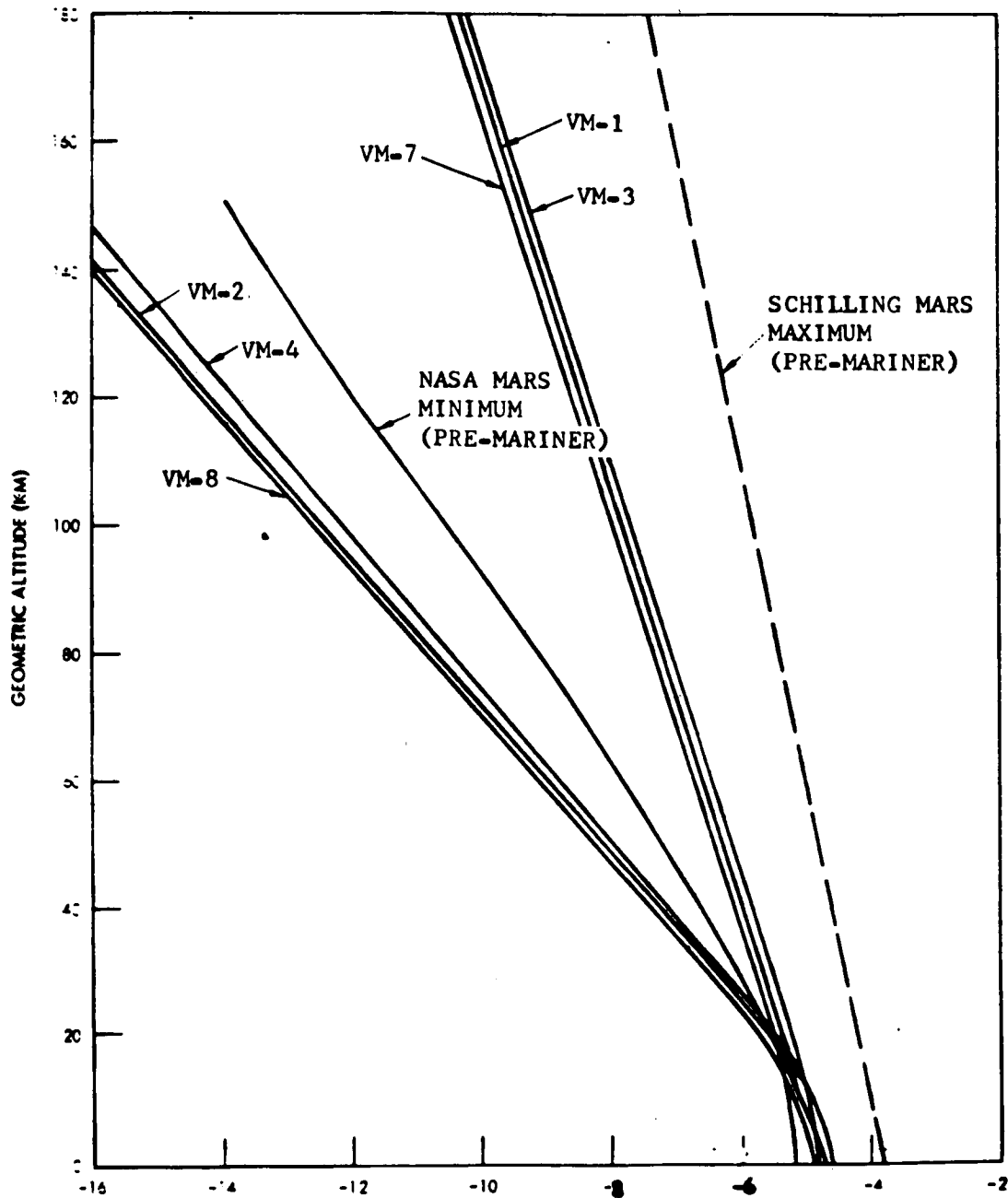
Figure 198. Comparison of Post-Mariner Atmospheric Densities With
Pre-Mariner Extreme Densities

- 244 -

Table 20. Construction Parameters, JPL Mars Atmospheres

Property	Symbol	Dimension	VM-1	VM-2	VM-3	VM-4	VM-7	VM-8
Surface Pressure	P_o	mb	7.0	7.0	10.0	10.0	5.0	5.0
		lb/ft^2	14.6	14.6	20.9	20.9	10.4	10.4
Surface Density	ρ_o	(gm/cm^3)10^5	0.955	1.85	1.365	2.57	0.68	1.32
		(slugs/ft^3)10^5	1.85	3.59	2.65	4.98	1.32	2.56
Surface Temperature	T_o	°K	275	200	275	200	275	200
		°R	495	360	495	360	495	360
Stratospheric Temperature	T_s	°K	200	100	200	100	200	100
		°R	360	180	360	180	360	180
Acceleration of Gravity at Surface	g	cm/sec^2	375	375	375	375	375	375
		ft/sec^2	12.3	12.3	12.3	12.3	12.3	12.3
Composition								
CO_2 (by mass)			28.2	100.0	28.2	70.0	28.2	100.0
CO_2 (by volume)			20.0	100.0	20.0	68.0	20.0	100.0
N_2 (by mass)			71.8	0.0	71.8	0.0	71.8	0.0
N_2 (by volume)			80.0	0.0	80.0	0.0	80.0	0.0
A (by mass)			0.0	0.0	0.0	32.0	0.0	0.0
A (by volume)			0.0	0.0	0.0	32.0	0.0	0.0
Molecular Weight	M	mol^{-1}	31.2	44.0	31.2	42.7	31.2	44.0
Specific Heat of Mixture	C_p	cal/gm°C	0.230	0.166	0.230	0.153	0.230	0.166
Specific Heat Ratio	γ		1.38	1.37	1.38	1.48	1.38	1.37
Adiabatic Lapse Rate	Γ	°K/km	-3.88	-5.39	-3.88	-5.85	-3.88	-5.39
		°R/1000 ft	-2.13	-2.96	-2.13	-3.21	-2.13	-2.96
Tropopause Altitude	h_T	km	19.3	18.6	19.3	17.1	19.3	18.6
		kilo ft	63.3	61.0	63.3	56.1	63.3	61.0
Inverse Scale Height (stratosphere)	β	km^{-1}	0.0705	0.199	0.0705	0.193	0.0705	0.199
		ft^{-1}x10^5	2.15	6.07	2.15	5.89	2.15	6.07

SD 67-621-2

Table 21. Mars Model Atmosphere VM-8

Altitude (ft)	Temperature (°R)	Pressure (lb/ft²)	Density (slug/ft³)	Density Scale Height (ft)	Gravity (ft/sec²)
0	360	1.04×10^1	2.57×10^{-5}	45.7×10^3	1.22×10^1
5×10^3	345	8.95×10^0	2.30	43.8	1.22
10	330	7.63	2.04	42.0	1.22
15	316	6.45	1.81	40.2	1.22
20	301	5.41	1.59	38.3	1.22
30	271	3.71	1.21×10^{-5}	34.6	1.22
40	242	2.44	8.91×10^{-6}	30.9	1.22
50	212	1.51×10^0	6.31	27.2	1.21
60	183	8.79×10^{-1}	4.25	23.5	1.21
61	180	8.29	4.07	23.1	1.21
80	180	2.67×10^{-1}	1.31×10^{-6}	16.8	1.20
100	180	8.18×10^{-2}	4.02×10^{-7}	16.9	1.20
125	180	1.86×10^{-2}	9.17×10^{-8}	17.0	1.20
150	180	4.29×10^{-3}	2.11×10^{-8}	17.0	1.19
175	180	9.93×10^{-4}	4.88×10^{-9}	17.1	1.19
200	180	2.31×10^{-4}	1.14×10^{-9}	17.2	1.18
250	180	1.28×10^{-5}	6.29×10^{-11}	17.4	1.17
300	180	7.27×10^{-7}	3.58×10^{-12}	17.5	1.16
350	180	4.23×10^{-8}	2.08×10^{-13}	17.7	1.15
400	180	2.53×10^{-9}	1.24×10^{-14}	17.8	1.14
500	180	9.68×10^{-12}	4.76×10^{-17}	18.1	1.12
600	180	4.08×10^{-14}	2.01×10^{-19}	18.4	1.10
650×10^3	180	2.75×10^{-15}	1.35×10^{-20}	18.6×10^3	1.09×10^1

SD 67-621-2

Table 22. Construction Parameters, NASA-MSFC Model Atmospheres

Atmospheric Parameter	NASA UDM Atmosphere	NASA MDM Atmosphere	NASA LDM Atmosphere
Surface gravity (centimeters/second^2)	832	886	914
Molecular weight	29.6	32.0	40.0
CO_2 - N_2 (volumetric percent)	10-90	25-75	75-25
Radius (killometers)	6235	6045	5955
Surface temperature (degrees K)	750	700	650
Surface pressure (atmospheres)	40	10	5
Surface pressure (grams/centimeter^3)	19.2×10^{-3}	5.57×10^{-3}	3.75×10^{-3}
Tropopause height (kilometers)	71	56	46
Troposphere lapse rate (degrees K/kilmeter)	-7.84	-8.49	-9.27
Stratosphere temperature (degrees K)	194.2	225.2	224
Stratopause height (kilometers)	126	115	83
Thermosphere lapse rate (degrees K/kilometer)	1.94	2.23	2.89

Table 23. NASA-MSFC Upper Density Model Atmosphere

Altitude (kilometers)	Temperature (degrees K)	Pressure (millibars)	Density (grams/centimeter^3)
0	750.0	4.05 E + 04	1.92 E - 02
5	712.6	3.31 E + 04	1.65 E - 02
10	674.8	2.67 E + 04	1.41 E - 02
20	598.3	1.68 E + 04	1.00 E - 02
30	520.7	9.94 E + 03	6.80 E - 03
40	442.1	5.40 E + 03	4.35 E - 03
50	362.7	2.61 E + 03	2.65 E - 03
75	194.2	1.50 E + 02	2.75 E - 04
100	194.2	3.67 E + 00	6.73 E - 06
150	242.6	3.56 E - 03	5.22 E - 09
200	339.4	2.75 E - 05	2.88 E - 11
300	533.0	4.60 E - 08	3.07 E - 14
400	726.6	6.53 E - 10	3.20 E - 16

Note: 3.56 E - 03 means 3.56×10^{-3}

Table 24. NASA-MSFC Mean Density Model Atmosphere

Altitude (kilometers)	Temperature (degrees K)	Pressure (millibars)	Density (grams/centimeter^3)
0	700.0	1.01 E + 04	5.57 E - 03
5	659.7	7.88 E + 03	4.60 E - 03
10	619.0	6.04 E + 03	3.76 E - 03
20	536.4	3.36 E + 03	2.41 E - 03
30	452.1	1.69 E + 03	1.44 E - 03
40	366.1	7.40 E + 02	7.78 E - 04
50	278.6	2.59 E + 02	3.59 E - 04
75	225.2	6.98 E + 00	1.19 E - 05
100	225.2	1.77 E - 01	3.02 E - 07
150	305.6	2.63 E - 04	3.31 E - 10
200	417.3	2.94 E - 06	2.71 E - 12
300	640.5	6.99 E - 09	4.20 E - 15
400	863.8	1.18 E - 10	5.25 E - 17

SD 67-621-2

Table 25. NASA-MSFC Lower Density Model Atmosphere

Altitude (kilometers)	Temperature (degrees K)	Pressure (millibars)	Density (grams/centimeter^3)
0	650.0	5.07 E + 03	3.75 E - 03
5	608.0	3.57 E + 03	2.83 E - 03
10	565.2	2.46 E + 03	2.09 E - 03
20	477.1	1.06 E + 03	1.07 E - 03
30	384.7	3.84 E + 02	4.81 E - 04
40	286.6	1.05 E + 02	1.76 E - 04
50	224.0	1.74 E + 01	3.73 E - 05
75	224.0	1.42 E - 01	3.05 E - 07
100	273.0	1.65 E - 03	2.90 E - 09
150	417.4	3.33 E - 06	3.84 E - 12
200	561.7	4.66 E - 08	3.99 E - 14
300	850.3	1.38 E - 10	7.78 E - 17
400	1139.0	2.59 E - 12	1.09 E - 18

TRAJECTORY ANALYSIS

The atmospheric flight mechanics is an important factor to be considered in the definition of technological requirements common to the development of systems capable of performing manned exploration of both Mars and Venus. Results of parametric studies of Mars and Venus aerobraking trajectory analyses are presented to show feasible trade-offs. The parametric data identify the limits in which an aerobraking maneuver into Mars and Venus atmospheres can be successfully executed. The results described in the subsequent discussion comprise the definition of aerobraking entry corridors, skip-out operating envelopes and atmospheric exit requirements which can be employed to evaluate vehicle aerothermodynamic characteristics.

ENTRY CORRIDORS

The entry corridor is the region in which the vehicle is required to fly to successfully execute the aerobraking maneuver (i.e., to use the planetary atmosphere as a means of absorbing excess energy above that required for orbital capture). The flight scheme to be employed in the aerobraking maneuver is depicted in Figure 199. At some distance from the planet, the spacecraft retracts all external equipment and assumes the correct attitude to enter the corridor. Entry is accomplished by employing full positive or negative lift until level flight is achieved. Then a constant altitude deceleration is maintained by roll modulation of the lift vector until the velocity is reduced to nearly the planet orbital velocity. Exit from the atmosphere is achieved by removing the negative lift vector and allowing the centrifugal force vector to drive the vehicle back through the atmosphere. During a gravity turn exit, the vehicle would assume a continuous spiral maneuver to cancel out normal aerodynamic forces. When the apoapsis of the exit trajectory is attained, a propulsive velocity increment is applied to the vehicle to establish the orbit.

Boundaries of this aerobraking entry corridor are defined by overshoot and undershoot limits. The overshoot limit is the entry condition at which the normal acceleration at pull-out is zero, while the undershoot limit is defined by a maximum load factor or a pull-out altitude constraint. A modified version of the general purpose two-degree-of-freedom trajectory computer program (AP101) was utilized to determine the corridors. The overshoot limit was

- 251 -
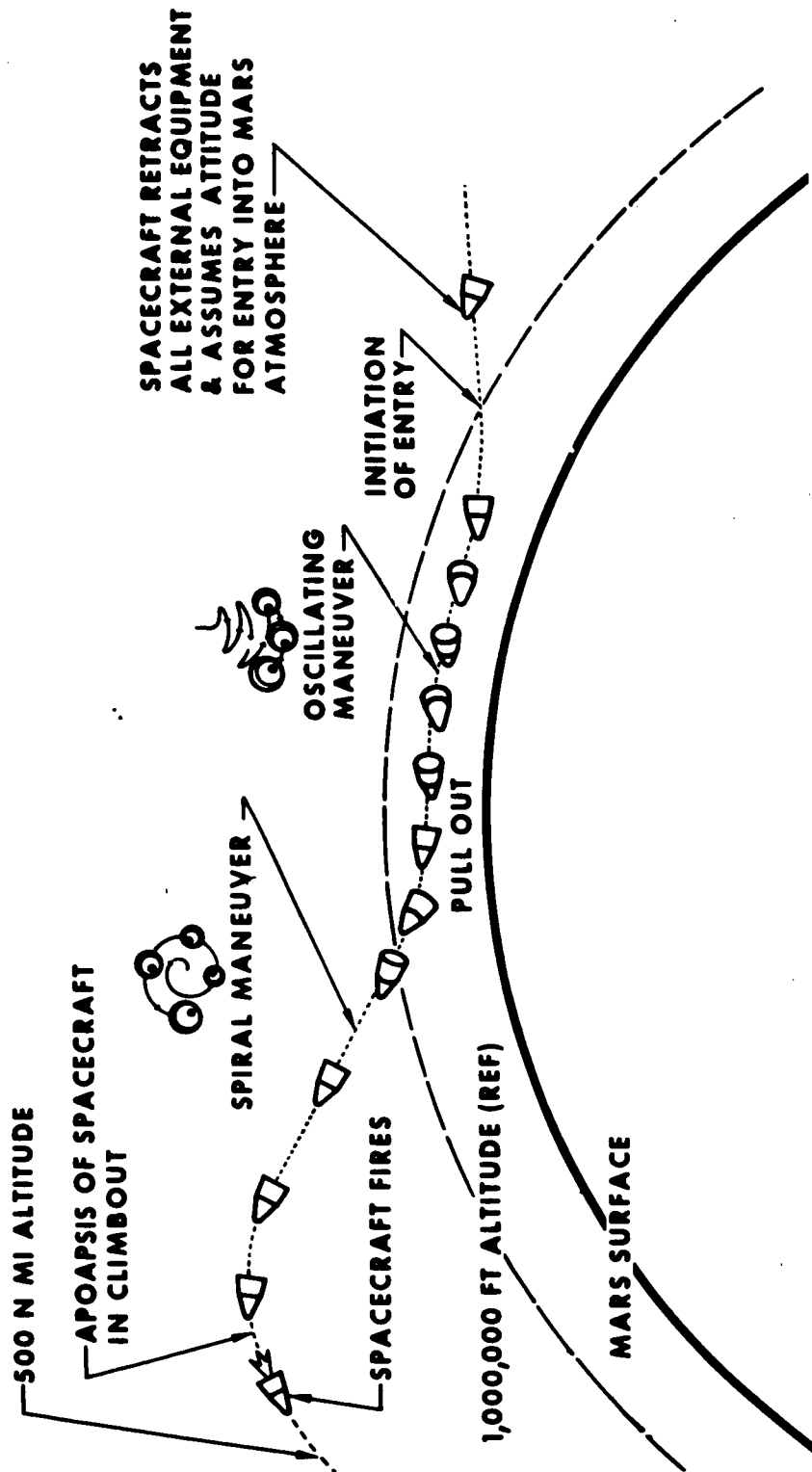
Figure 199. Mars Aerodynamic Braking Maneuver

evaluated by selecting a range of overshoot boundary velocities at the pull-out position and then integrating the equations of motion normal and tangential to the flight path backwards along the trajectory to a specified entry altitude. The resultant entry velocity was then correlated with the entry angle for the particular vehicle L/D and M/C_DA. A similar technique was employed to evaluate the undershoot limit. For a specified maximum load factor the equations of motion normal and tangential to the flight path were numerically integrated backward along the trajectory for a range of pull-out velocities to the entry altitude. Then the entry angle was correlated with the entry velocity. Full negative lift (180-degree roll angle) and full positive lift (0-degree roll angle) were assumed for the overshoot and undershoot limits, respectively. The corridor depths were determined by taking the algebraic difference of the overshoot and undershoot limit periapsis radii derived from propagating the trajectories at the atmospheric interface forwards using vacuum equations. An alternate method of expressing these limits would be the entry angles. This procedure for evaluating corridor boundaries is identical to that employed during previous NR/SD Mars and Venus Aerobraking Technology Studies (References 9, 10, and 11).

The corridor depths for Mars and Venus were evaluated with assumed interface altitudes of 1,000,000 feet (305 kilometers) and 600,000 feet (183 kilometers), respectively, and the atmospheric models already discussed. Entry velocities of 20,000 feet/second (6.1 kilometers/second) to 40,000 feet/second (12.2 kilometers/second), and 30,000 feet/second (9.2 kilometers/sec) to 50,000 feet/second (15.2 kilometers/second) were employed for Mars and Venus to bound a wide range of possible aerobraking missions. For Mars the corridor depths were determined for a representative biconic lifting configuration (Figure 197) with an L/D = 1 and a M/C_DA range of 500 pounds/foot^2 (2400 kilograms/meter^2) to 2500 pounds/foot^2 (12,200 kilograms/meter^2). The corridor depth evaluation for Venus covered an L/D range of 0.5 to 2 and a M/C_DA range of 500 pounds/foot^2 (2440 kilograms/meter^2) to 2500 pounds/foot^2 (12,200 kilograms/meter^2).

Atmospheric models developed from the Mariner IV occultation experiment can place restrictions upon the Mars aerobraking maneuver. The VM-8 model was assumed to be a representative low density atmosphere to depict the entry corridor problems associated with Mars. Figure 200 presents an undershoot pull-out altitude variation with entry velocity, M/C_DA, and maximum load factor. The figure shows that a terrain clearance altitude criteria of 10 kilometers would severely limit the undershoot boundary. For a vehicle with an L/D = 1 and a M/C_DA of 2500 pounds/foot^2 (12,200 kilograms/meter^2) a 5-g undershoot limit is not feasible while a 2-g undershoot limit is practical over an entry velocity range of 25,600 feet/second (7.8 kilometers/second) to 40,000 feet/second (12.2 kilometers/second). The vehicle M/C_DA is shown to have a significant effect upon the
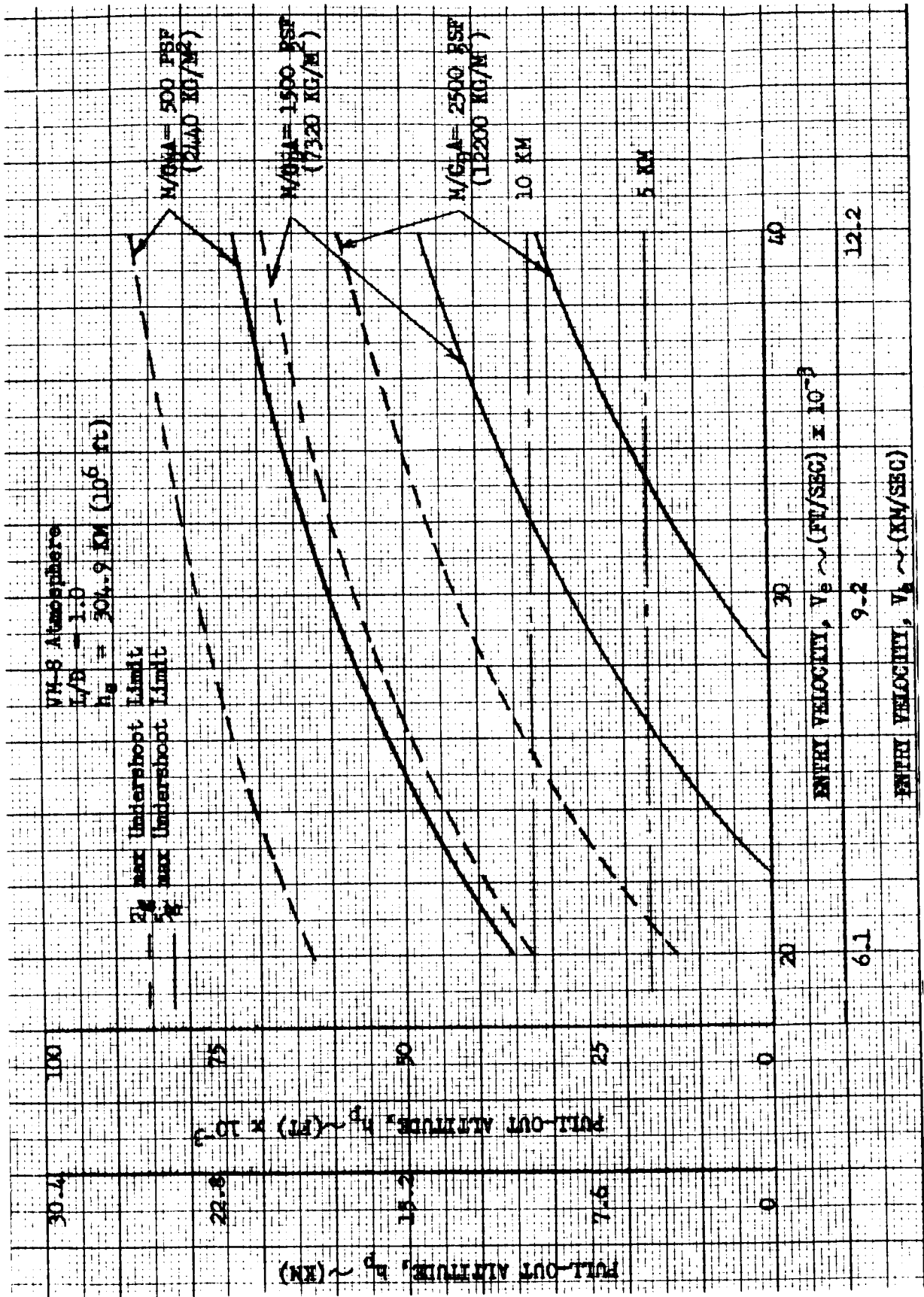
Figure 200. Mars Undershoot Pull-Out Altitude Variation

undershoot boundary. As a consequence of the terrain clearance problem posed by the aerobraking maneuver, the undershoot boundary was constrained to a 10-kilometer pull-out altitude. The undershoot boundary was then determined by a backwards integration of the equations of motion normal and tangential to the flight path from the specified pull-out altitude to the specified entry altitude for a range of pull-out velocities. From a correlation of entry angle with entry velocity the required periapsis radii were determined. Figures 201, 202, and 203 present the corridor depth variation with entry velocity for $M/C_D A$'s of 500 pounds/foot^2 (2400 kilograms/meter^2), 1500 pounds/foot^2 (7320 kilograms/meter^2), and 2500 pounds/foot^2, (12,200 kilograms/meter^2), respectively. The figures show the significant effect of entry velocity and vehicle $M/C_D A$ on corridor depth. If 20 kilometers is the lowest practical corridor depth, the representative VM-8 atmosphere is shown to severely restrict the aerobraking concept with regards to entry velocity and $M/C_D A$. At the lowest $M/C_D A$ (2440 kilograms/meter^2) a maximum load-factor criteria appears to define the undershoot boundary rather than a pull-out altitude constraint and the 20-kilometer corridor depth criteria is satisfied by a 5-g_{max} undershoot boundary for an entry velocity range of 6.1 kilometers per second to approximately 9.2 kilometers per second. Increasing the maximum allowable load factor would extend the aforementioned entry velocity range. For the $M/C_D A$ of 7320 kilograms/meter^2 the 10-kilometer pull-out altitude limit defines the entry corridor over the entire entry velocity range. The total load factor sensed by the vehicle at $V_e = 12.2$ kilometers/second is approximately 7.6. At the upper $M/C_D A$ value of 12,200 kilograms/meter^2, the 20-kilometer corridor depth criteria cannot be achieved with a 10-kilometer pull-out altitude nor by an acceptable load factor limit (Figure 203).

Over the given entry velocity range, a corrodor depth of 20 kilometers can be achieved by reducing the pull-out altitude criteria to 5 kilometers. Figures 204 and 205 present the corridor depth as a function of $M/C_D A$ for entry velocities of 6.1 kilometers/second (20,000 feet/second) and 9.2 kilometers/second (30,000 feet/second), respectively. At $V_e = 6.1$ kilometers/second the 20-kilometer corridor depth criteria can be achieved over the vehicle $M/C_D A$ range of 2440 kilograms/meter^2 to 12,000 kilograms/meter^2, satisfying both maximum load factor and pull-out altitude criteria. At $V_e = 9.2$ kilometers/second the 20-kilometer corridor depth criteria cannot be satisfied over the entire $M/C_D A$ range without relaxing the undershoot pull-out altitude criteria. For a combination of 5-g_{max} and 10-kilometer pull-up altitude, the 20-kilometer corridor depth requirement can be satisfied up to an $M/C_D A$ of approximately 1600 pounds/foot^2 (7800 kilograms/meter^2). The corridor depth evaluation presented herein for a representative critical atmosphere indicate severe limitations exist with regards to defining practical Mars aerobraking missions. Both entry velocity and vehicle $M/C_D A$ are shown to significantly affect the allowable entry corridor. An inproved knowledge of the Martian planet (atmosphere and radius) will be required to refine possible limitations placed upon Mars aerobraking.
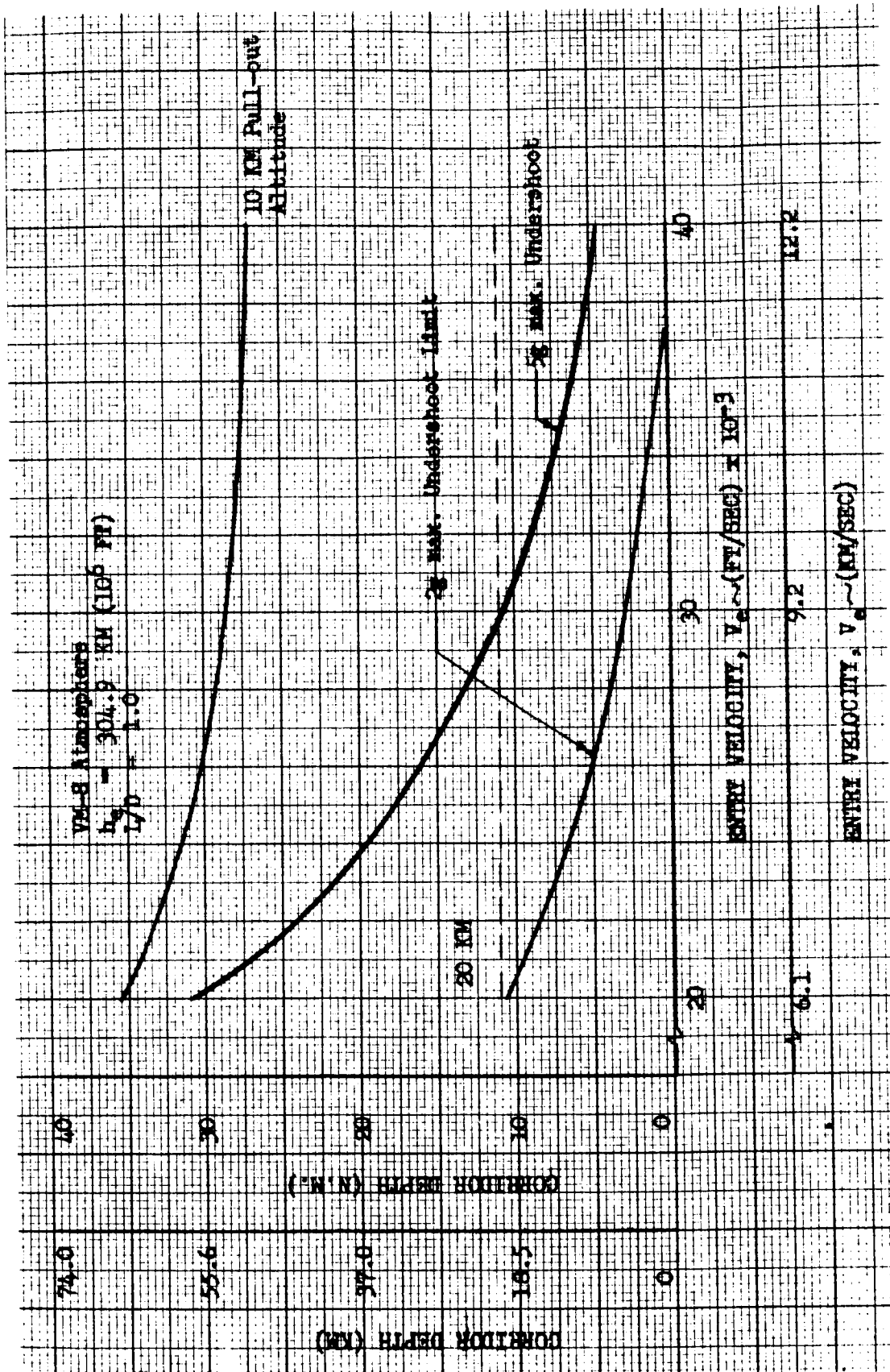
Figure 201. Mars Entry Corridor Depths ($M/C_D A = 2440$ kg/m^2)
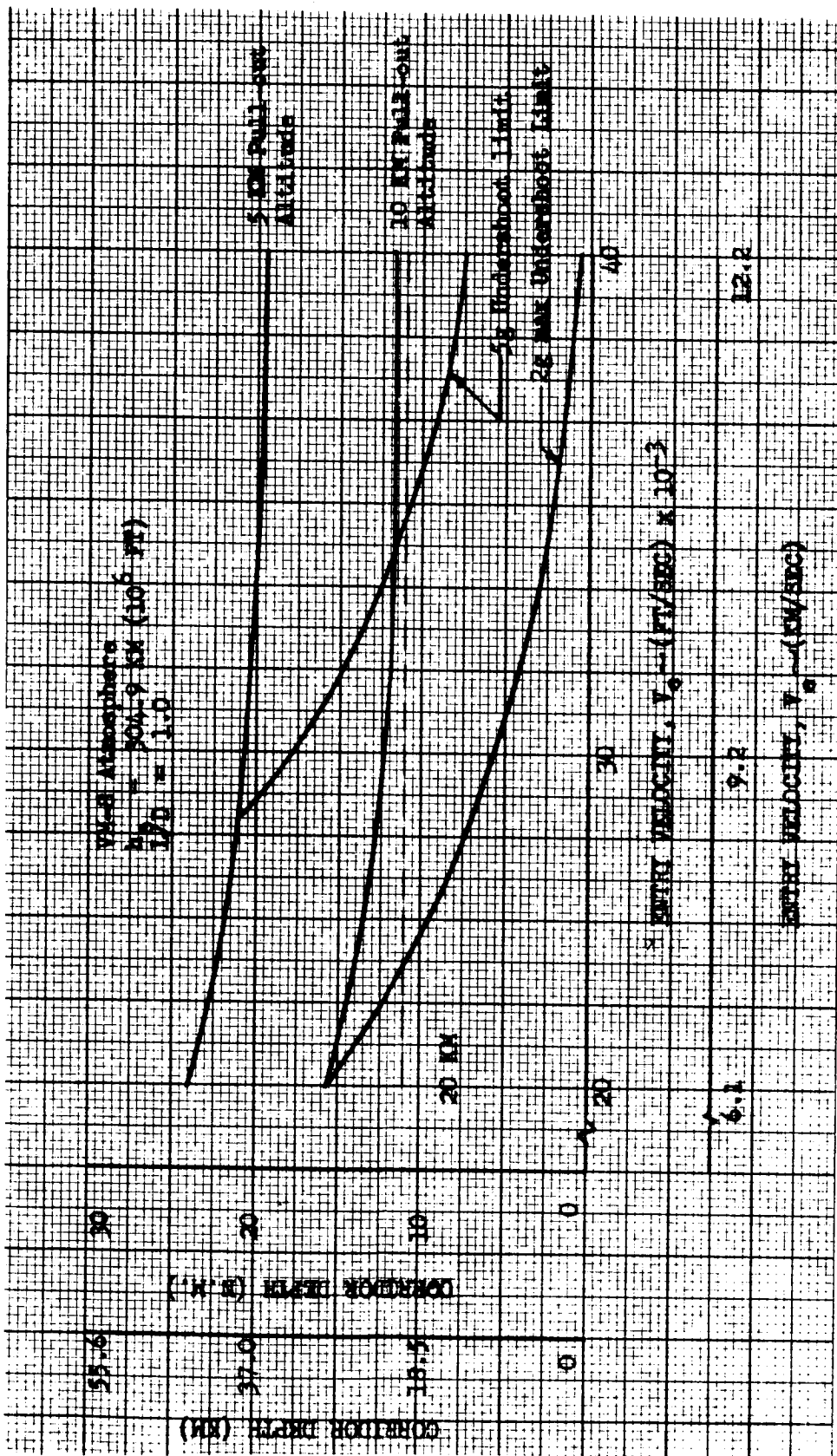
Figure 202. Mars Entry Corridor Depths ($M/C_DA = 7320$ kg/m^2)
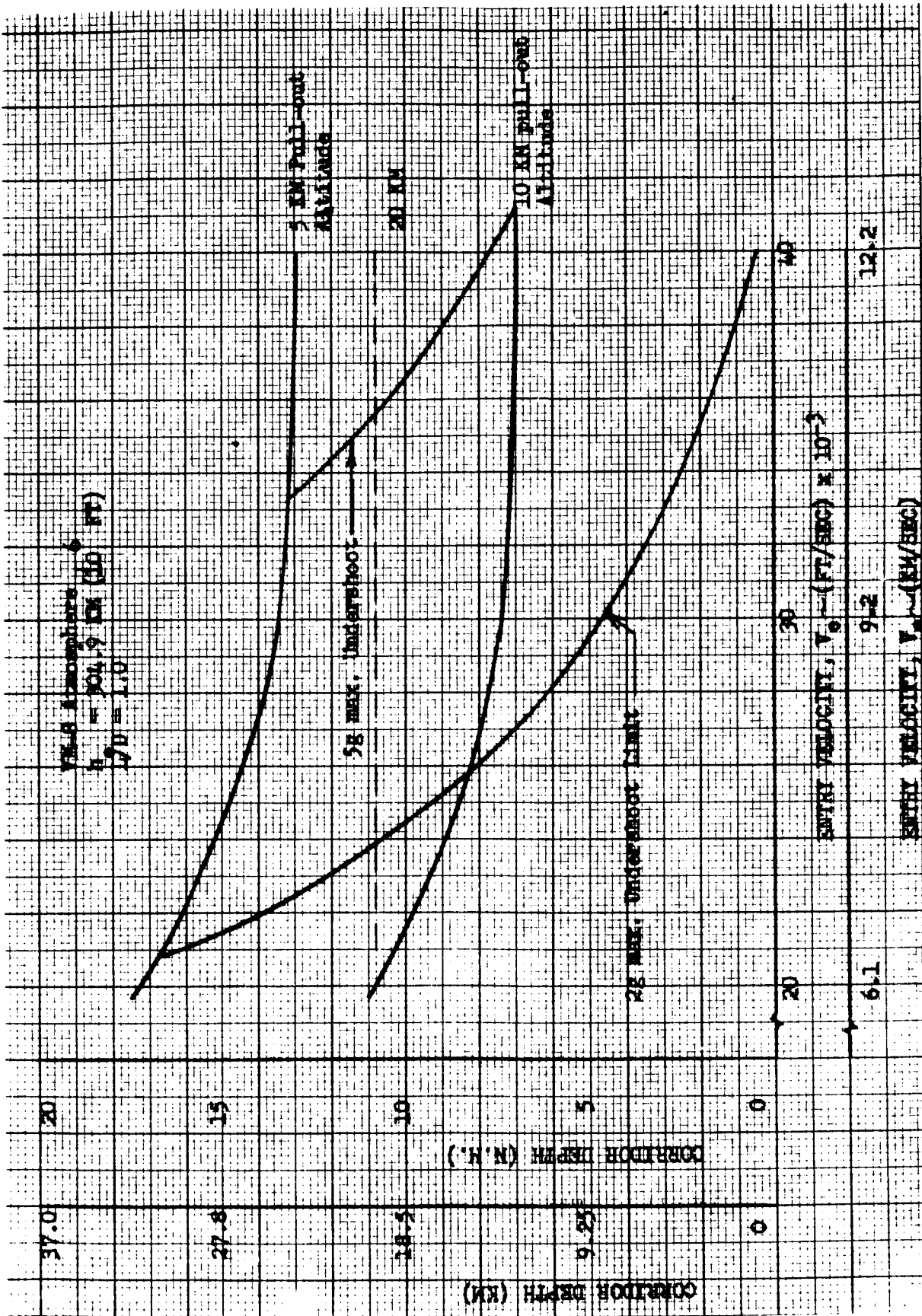
Figure 203. Mars Entry Corridor Depths (M/C_DA = 12,200 kg/m^2)
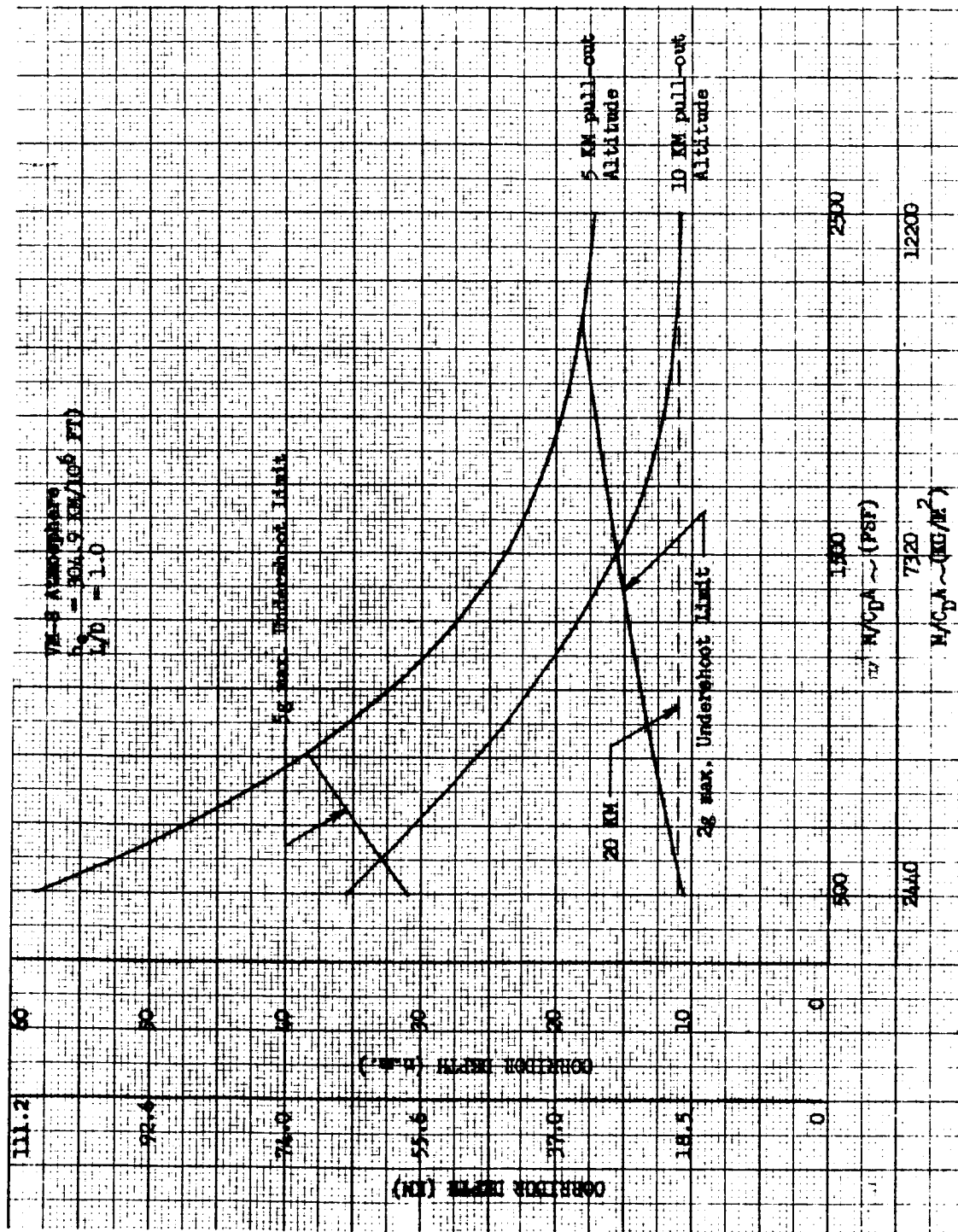
Figure 204. Mars Entry Corridor Depths (V_e = 6.1 km sec)

- 259 -

SD 67-621-2
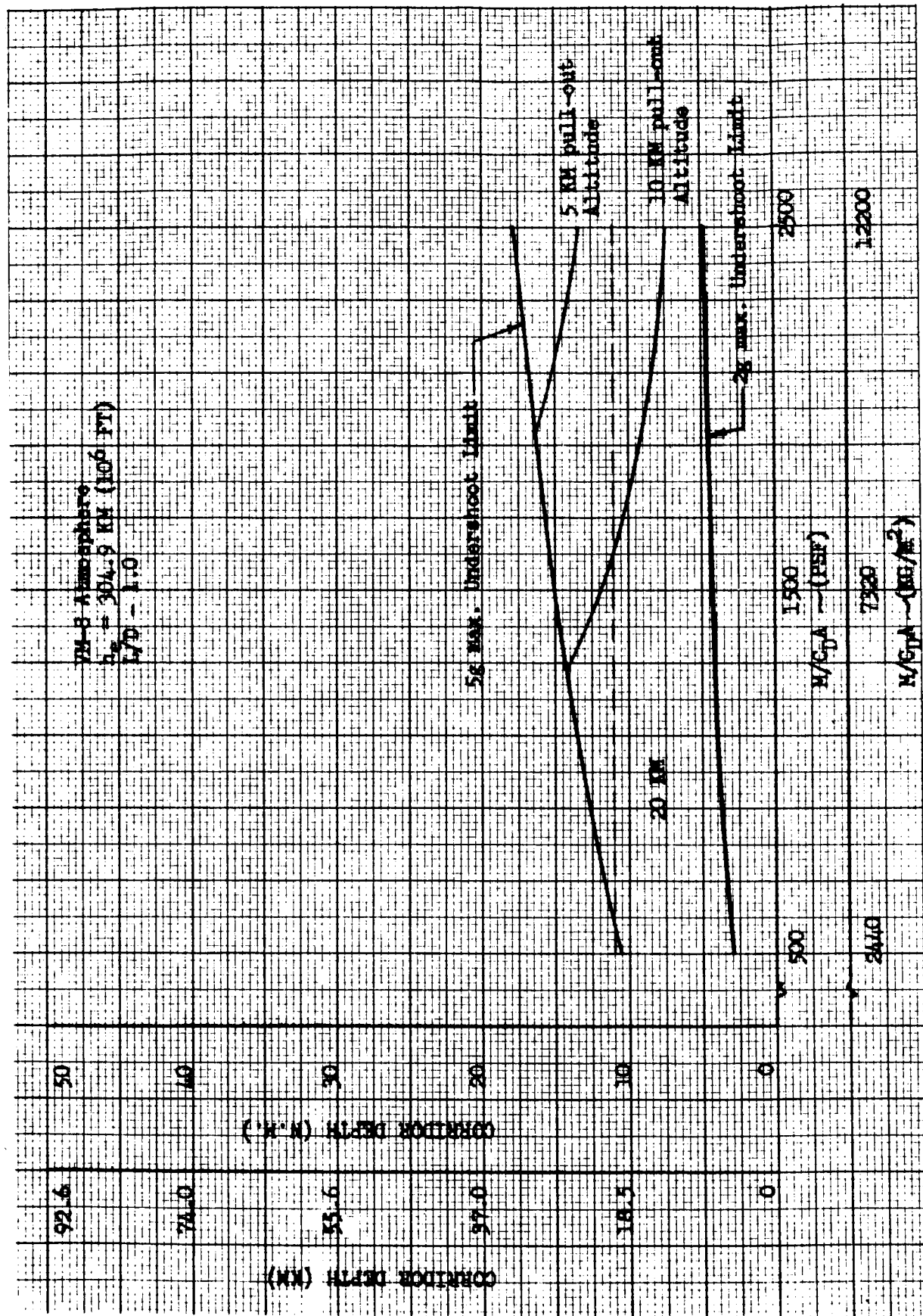
Figure 205. Mars Entry Corridor Depths (V_e = 9.2 km/sec)

5 KM pull-out Altitude

10 KM pull-out Altitude

2g max. Undershoot limit

5g max. Undershoot limit

20 KM

TM-8 Atmosphere
h_s = 304.9 KM (10⁶ FT)
L/D = 1.0

CORRIDOR DEPTH (N.M.)

50 40 30 20 10 0

CORRIDOR DEPTH (KM)

92.6 74.0 55.6 37.0 18.5 0

W/C_DA ~ (PSF)   2500   1500   500

W/C_DA ~ (KG/M²)   1200   7320   2440

The planets Mars and Venus exhibit entirely different aerobraking entry corridor characteristics. The NASA-MSFC recommended mean density profile atmosphere for Venus was employed in the study. Figures 206, 207, and 208 present the corridor depth as a function of entry velocity and vehicle L/D for M/C_DA's of 2440 kilograms/meter^2, 7320 kilograms/meter^2, and 12,200 kilograms/meter^2, respectively. The entry velocity ranged from 9.2 kilometers/ second to 13.7 kilometers/second, and the L/D's investigated were 0.5, 1.0, and 2.0. The corridor depth is shown to decrease with increasing entry velocity and increase with increasing L/D. The undershoot boundary was determined from a 10-g_{max} load factor criteria. All pull-out altitudes were greater than 200,000 feet (61.5 kilometers). Figures 206 and 207 show that the 20-kilometer corridor depth criteria is satisfied for the aforementioned vehicle characteristics and entry conditions.

The effect of L/D on corridor depth is illustrated by Figure 209. As stated previously an increase in L/D will increase the corridor depth. The significant factor depicted by the figure is that when L/D is increased above 1.0 the percentage increase in the corridor depth is less than the increase resulting from varying the L/D from 0.5 to 1. For an entry velocity of 12.2 kilometers/second and M/C_DA = 12,200 kilograms/meter^2, the corridor depth is increased by 36 percent when the L/D is increased from 0.5 to 1, as compared to a 14-percent increase when the L/D is increased from 1 to 1.5. A similar comparison could be shown for other entry velocity and M/C_DA combinations. This indicated that from a corridor aspect little is gained by developing an aerobraking vehicle with an L/D greater than 1.

Figure 210 presents the corridor depth variation with M/C_DA and L/D for an entry velocity of 12.2 kilometers/second. Corridor depth is shown to be a weak function of M/C_DA. This is opposite to what was depicted for Mars aerobraking where the corridor depth was shown to be significantly affected by the M/C_DA because of the pull-up altitude limit. Figure 211 illustrates the effect of atmospheric uncertainties upon the corridor depth. Corridor depths are depicted for the low and high density NASA-MSFC recommended atmospheres as a function of entry velocity. The figure also presents the effect of changing the undershoot boundary maximum load factor from 10 to 5 for an M/C_DA of 12,200 kilograms/meter^2. For an L/D = 1 and a 10-g_{max} undershoot limit the low-density profile atmosphere satisfies the 20-kilometer corridor depth criteria over the entire velocity range. When the undershoot limit is reduced to a 5-g_{max} condition, the corridor depth is observed to fall below the 20-kilometer line at Ve = 12.2 kilometers/second for the low-density atmosphere and at Ve = 14 kilometers/second for the high-density atmosphere. The aerobraking maneuver within the Venus atmosphere is shown to have an adequate entry corridor for a wide range of entry velocities and vehicle characteristics. When considering atmospheric uncertainties the entry corridor appears to fall within allowable bounds except at the upper range of entry velocities and M/C_DA.
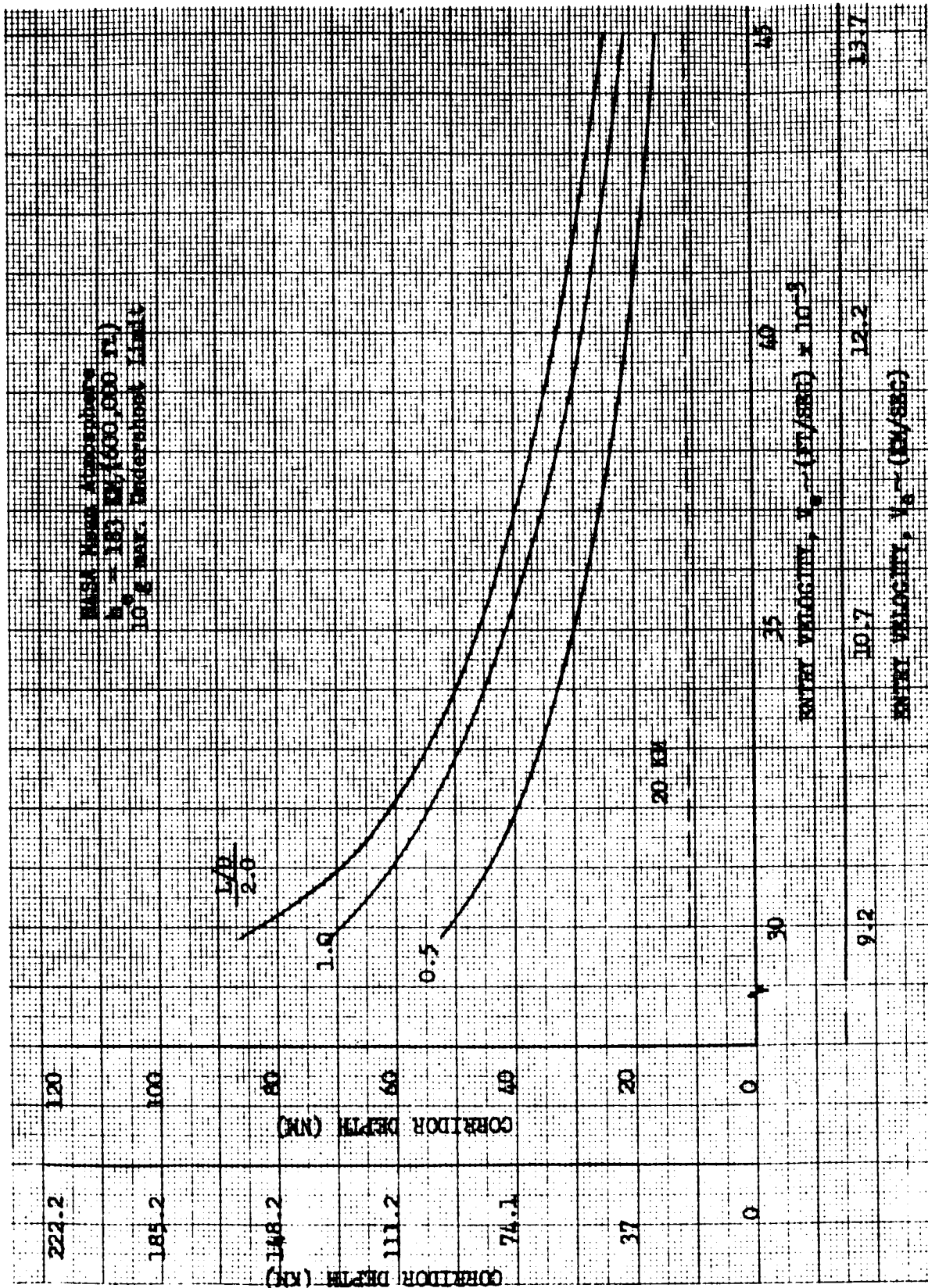
Figure 206. Venus Entry Corridor Depths ($M/C_DA = 2440 \ kg/m^2$)
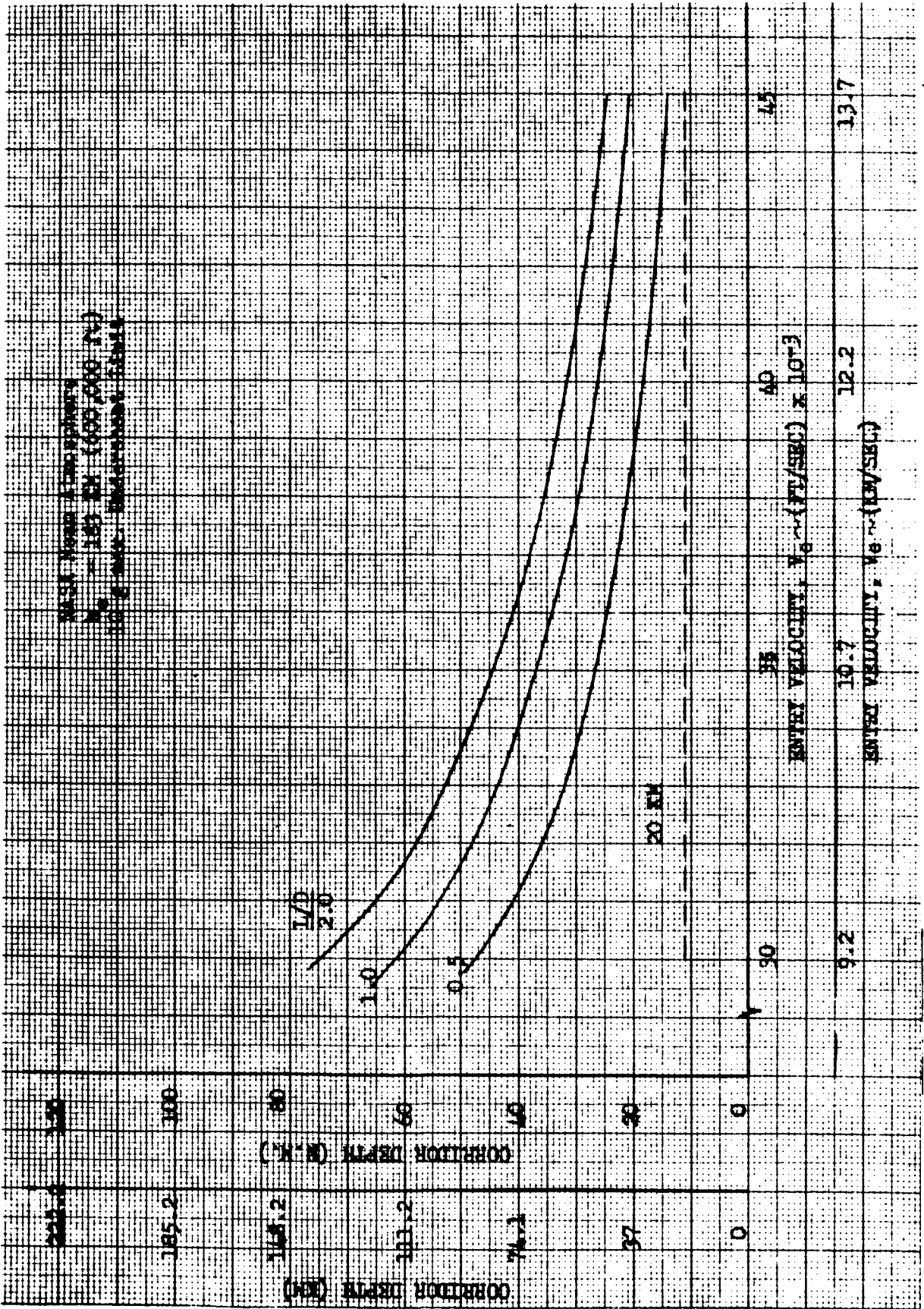
Figure 207. Venus Entry Corridor Depths (M/C_DA = 7320 kg/m²)
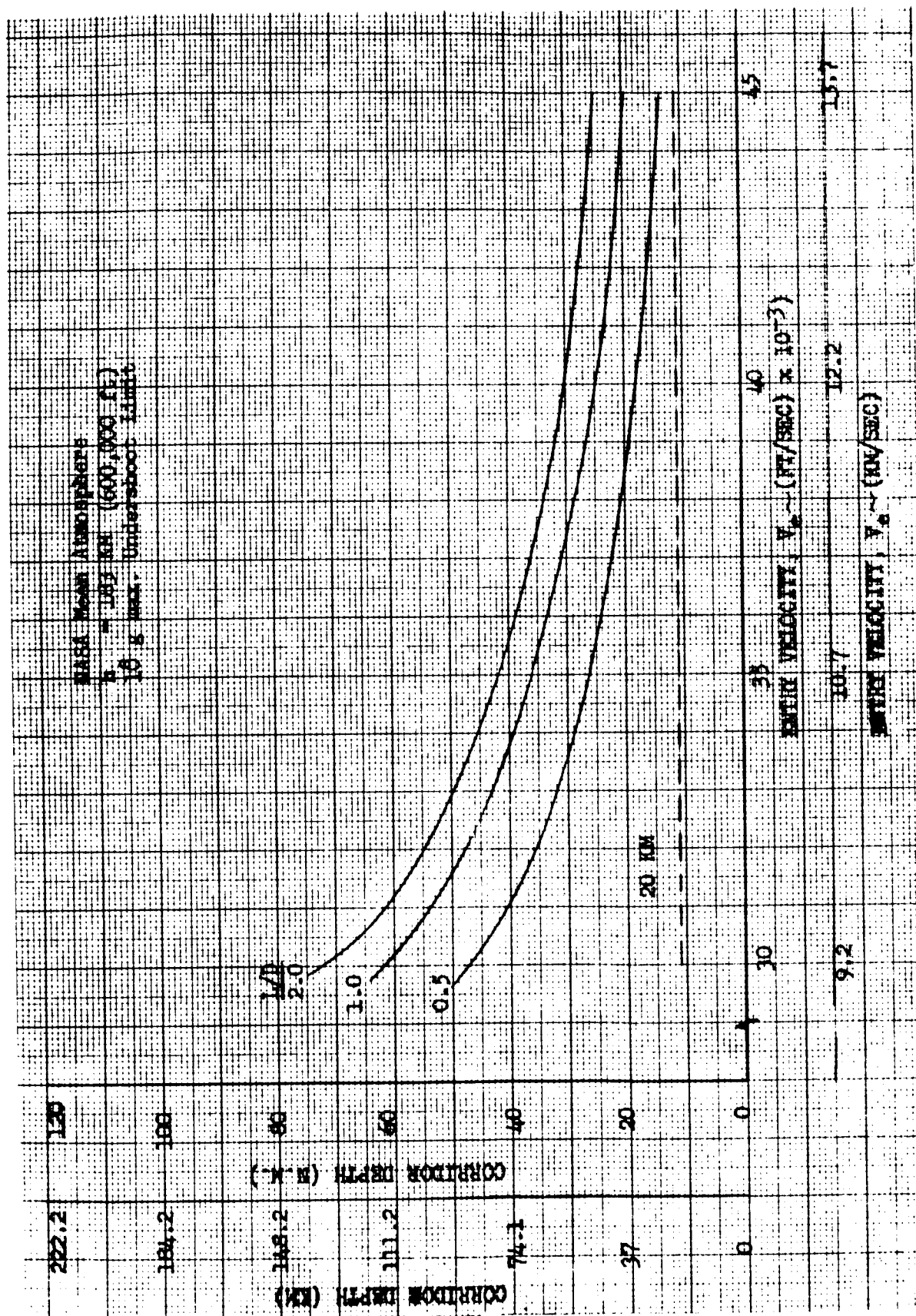
Figure 208. Venus Entry Corridor Depths (M/CDA = 12, 200 kg/m^2)
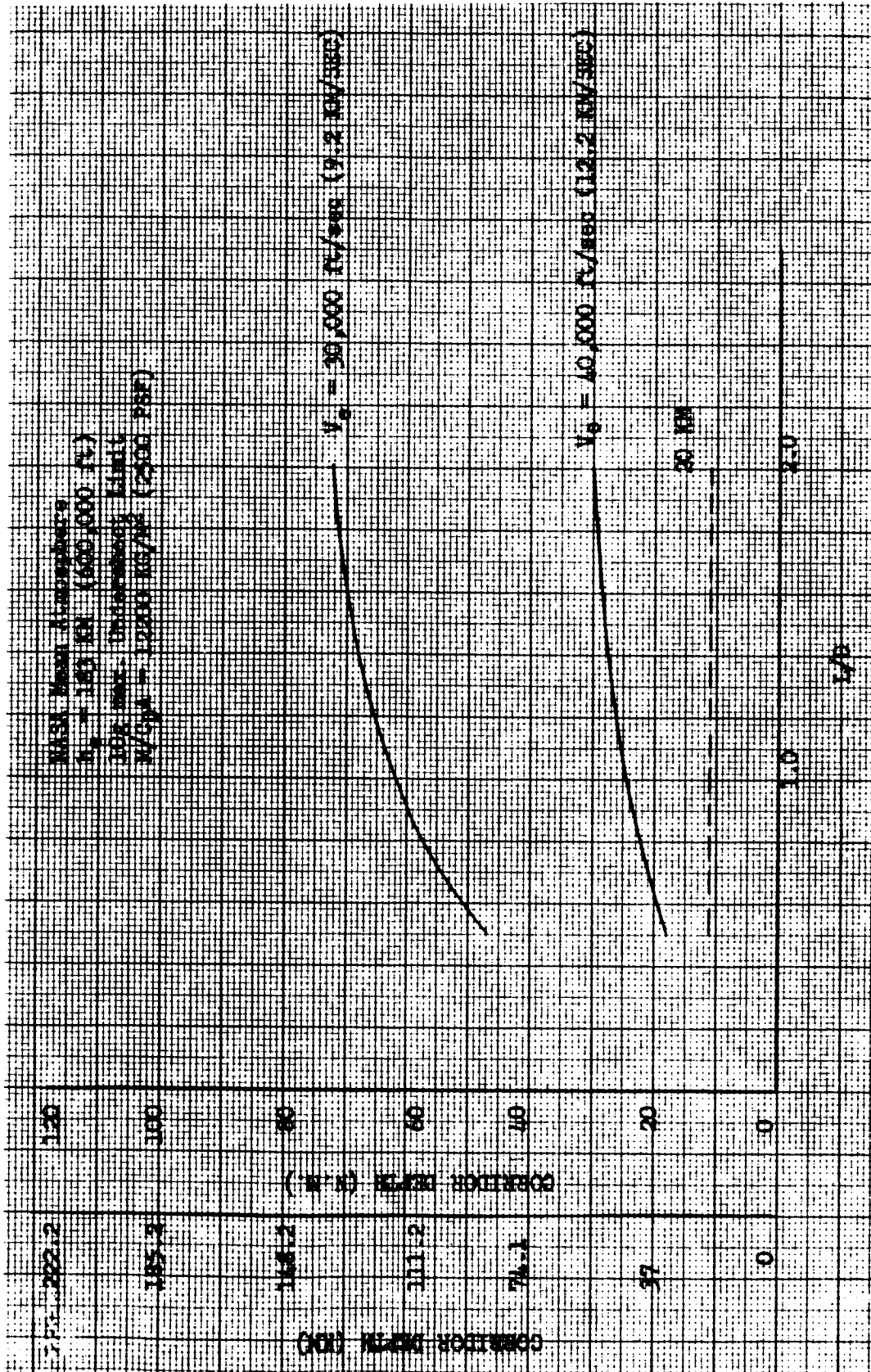
Figure 209.   Venus Entry Corridor Depth Versus L/D

SD 67-621-2
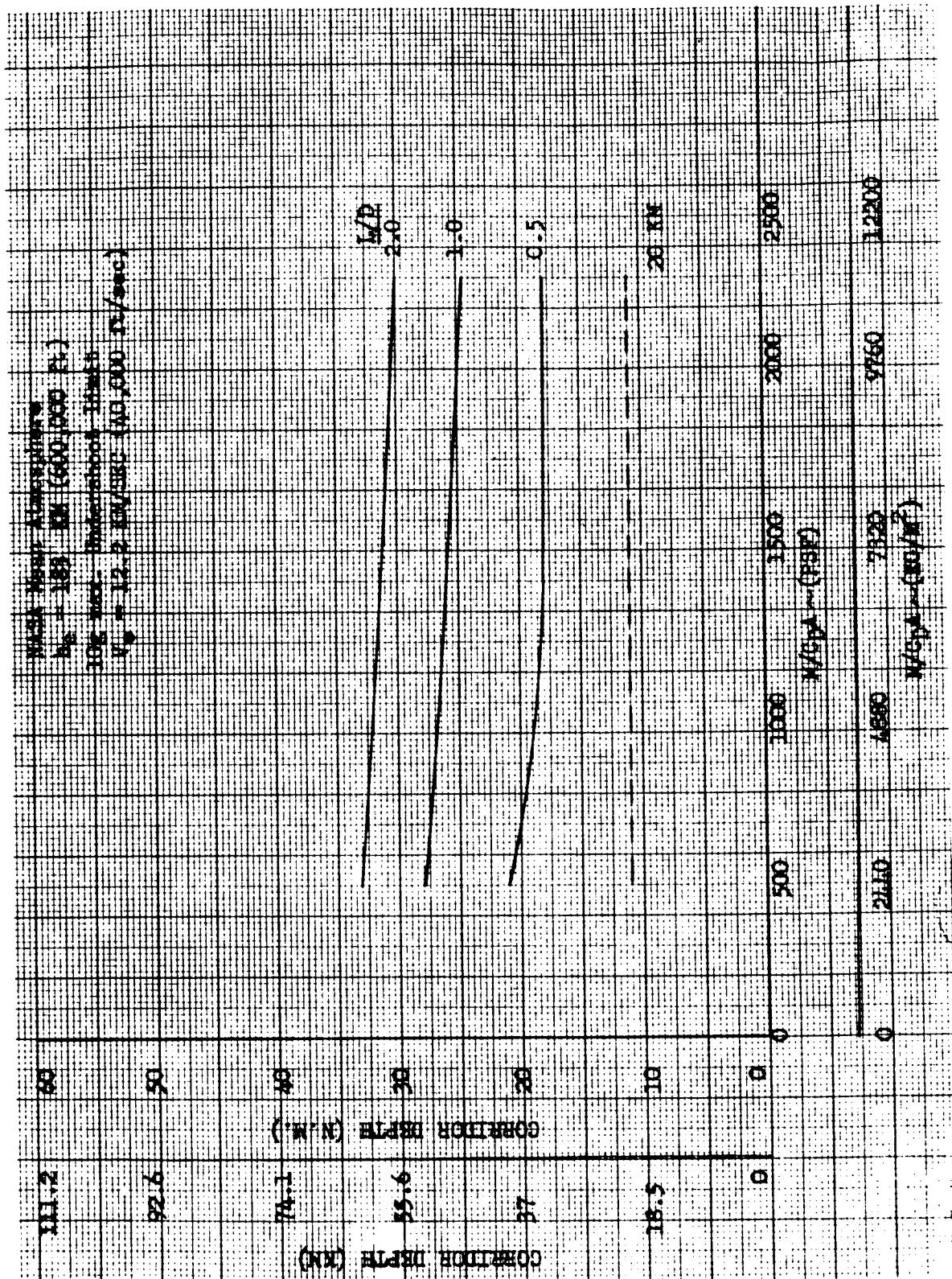
Figure 210. Venus Entry Corridor Versus M/C_DA

SD 67-621-2
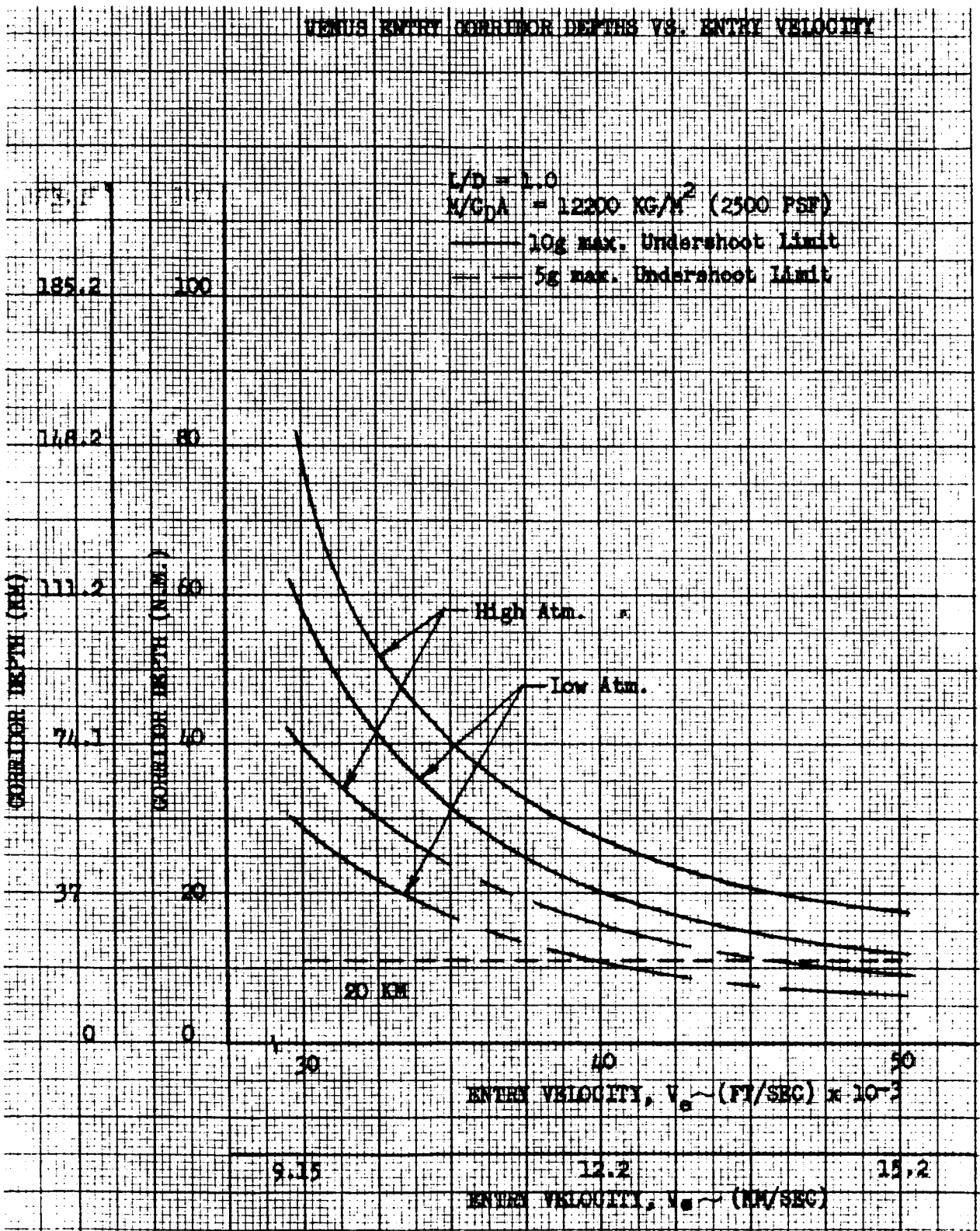
Figure 211. Venus Entry Corridor Depths Versus Entry Velocity

SD 67-621-2

SKIP-OUT TRAJECTORIES

Exit from the planetary atmosphere is initiated at a position along the constant-altitude deceleration flight phase where the velocity is just sufficient to allow the vehicle to follow a gravity turn trajectory back through the atmosphere to a designated apoapsis altitude. At apoapsis, an incremental velocity is applied to establish the orbit. Exit characteristics for an aero-braking maneuver within the Mars VM-8 atmosphere were derived for exit from a 10-kilometer undershoot boundary for a vehicle with an L/D of 1 and an M/C_DA of 12,200 kilograms/meter^2. Figures 212, 213, and 214 present the flight path angle and velocity measured at the atmospheric inter-face altitude of 10^6 feet, and the resultant apoapsis altitude as a function of the initial exit velocity. An initial exit velocity range of 4.05 kilometers/second to 4.45 kilometers/second produced apoapsis altitudes of approximately 300 kilometers to 3000 kilometers, respectively. Figures 215 and 216 depict the flight path angle at the atmospheric interface and the apoapsis altitude as a function of velocity at the atmospheric interface. The apoapsis altitude is shown on Figure 217 as a function of the atmospheric interface flight path angle.

The characteristic operating envelope of the Venus aerobraking and skip-out trajectories have been derived as a function of L/D and M/C_DA for the NASA-MSFC recommended mean density profile atmosphere. Figures 218, 219, and 220 present operating envelopes for M/C_DA's of 2440 kilograms/meter^2, 7320 kilograms/meter^2, and 12,200 kilograms/meter^2, respectively. The undershoot limit lines define the altitude-velocity region for capture without exceeding the desired load factor ($10-g_{max}$). The skip-out line defines the velocity as a function of the altitude at which skip-out to a representative 300-nautical-mile (555 kilometers) altitude can occur when starting from horizontal flight. To initiate skip-out at the peak load factor limit, the space-craft must enter along an undershoot boundary. The skip-out limit lines depicted on Figures 218 to 220 are an approximation at the undershoot boundaries, since horizontal flight was assumed for skip-out initiation, although slightly negative flight-path angles occur when tangent to the under-shoot g_{max} limit (Reference 11). Figure 221 presents the skip-out limit lines. The skip-out initiation velocity is observed to increase with lowering altitude at skip-out initiation and M/C_DA. Operations to the right of each L/D boundary line will result in a flight condition exceeding the undershoot load factor limit. Figure 222 presents the minimum atmospheric exit velocity and impulsive injection velocity variation with the flight-path angle measured at the atmospheric interface. The operating range or band depicted on Figure 222 represents the dispersion in ΔV and V_{EX} due to variations in M/C_DA and skip-out initiation altitude. The dispersions in the operating range produced by variations in M/C_DA and skip-out initiation altitude result in a small ΔV variation to establish a 300-nautical-mile (555 kilometers)

Figure 212. Mars Aerodynamic Braking Exit Conditions Atmopsheric
Interface Flight Path Angle Variation

- 269 -

Figure 213. Mars Aerodynamic Braking Exit Conditions Atmospheric
Interface Velocity Variation

Figure 214. Mars Aerodynamic Braking Exit Conditions (Apoapsis Altitude Variation)

Figure 215. Mars Aerodynamic Braking Exit Conditions
(Atmospheric Interface Flight Path Angle Variation)

- 272 -
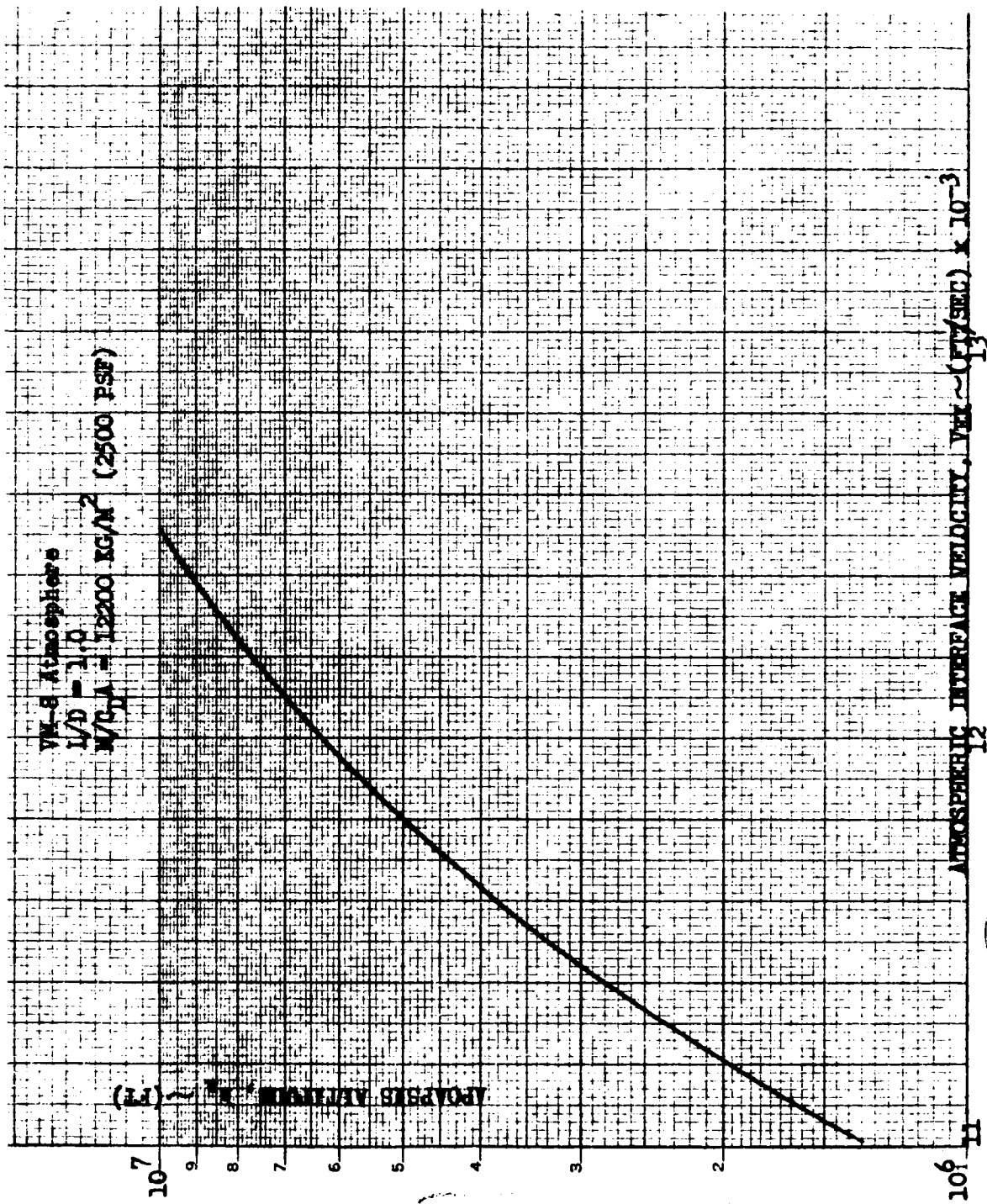
Figure 216. Mars Aerodynamic Braking Exit Conditions (Apoapsis Altitude Variation)

Figure 217. Mars Aerodynamic Braking Exit Conditions (Apoapsis
Altitude Variation)
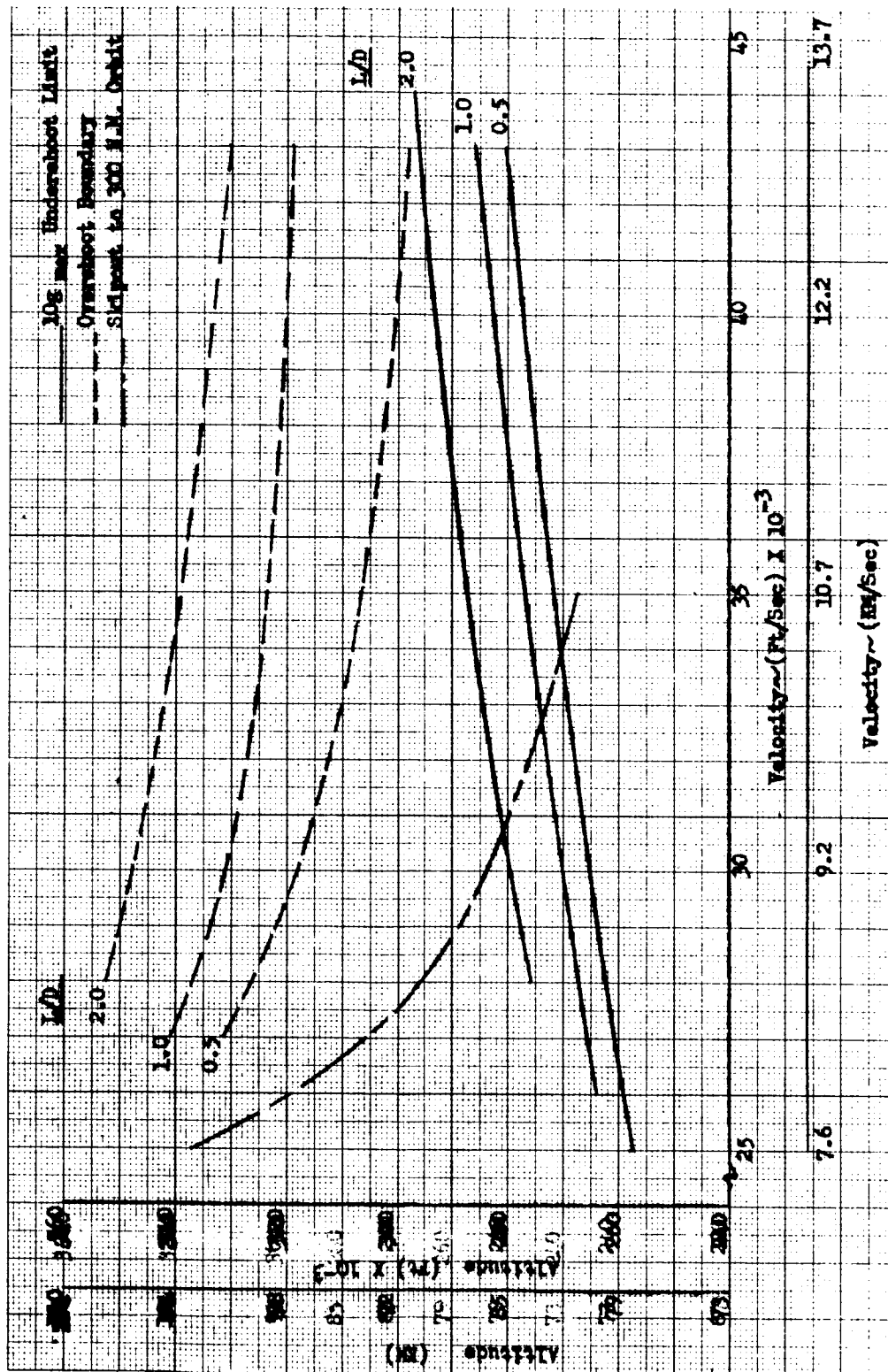
Figure 218. Venus Aerodynamic Braking Operation Envelope
$(M/C_DA = 2440 \text{ kg/m}^2)$

SD 67-621-2
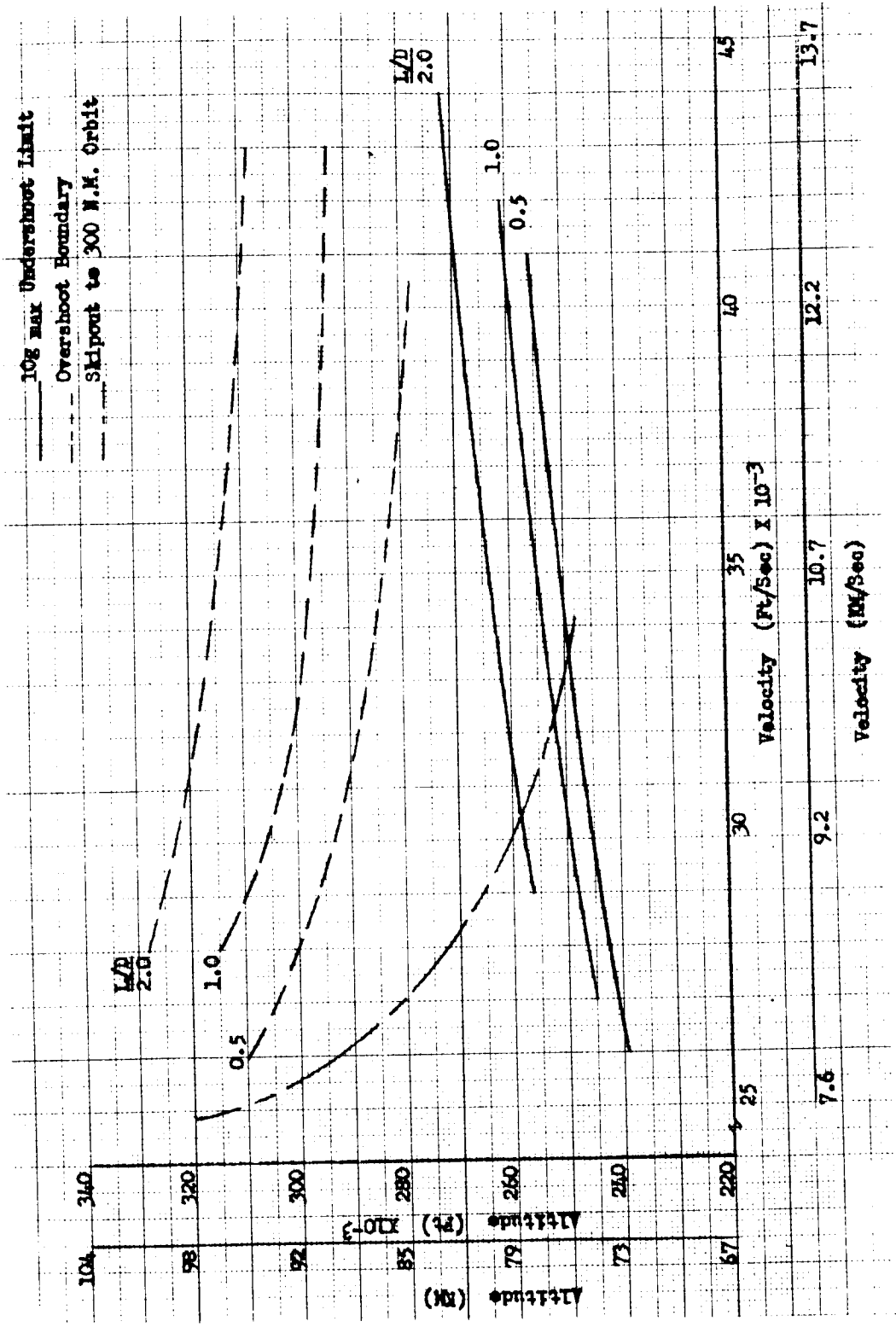
Figure 219. Venus Aerodynamic Braking Operation Envelope
$(M/C_DA = 7320 \text{ kg}/m^2)$
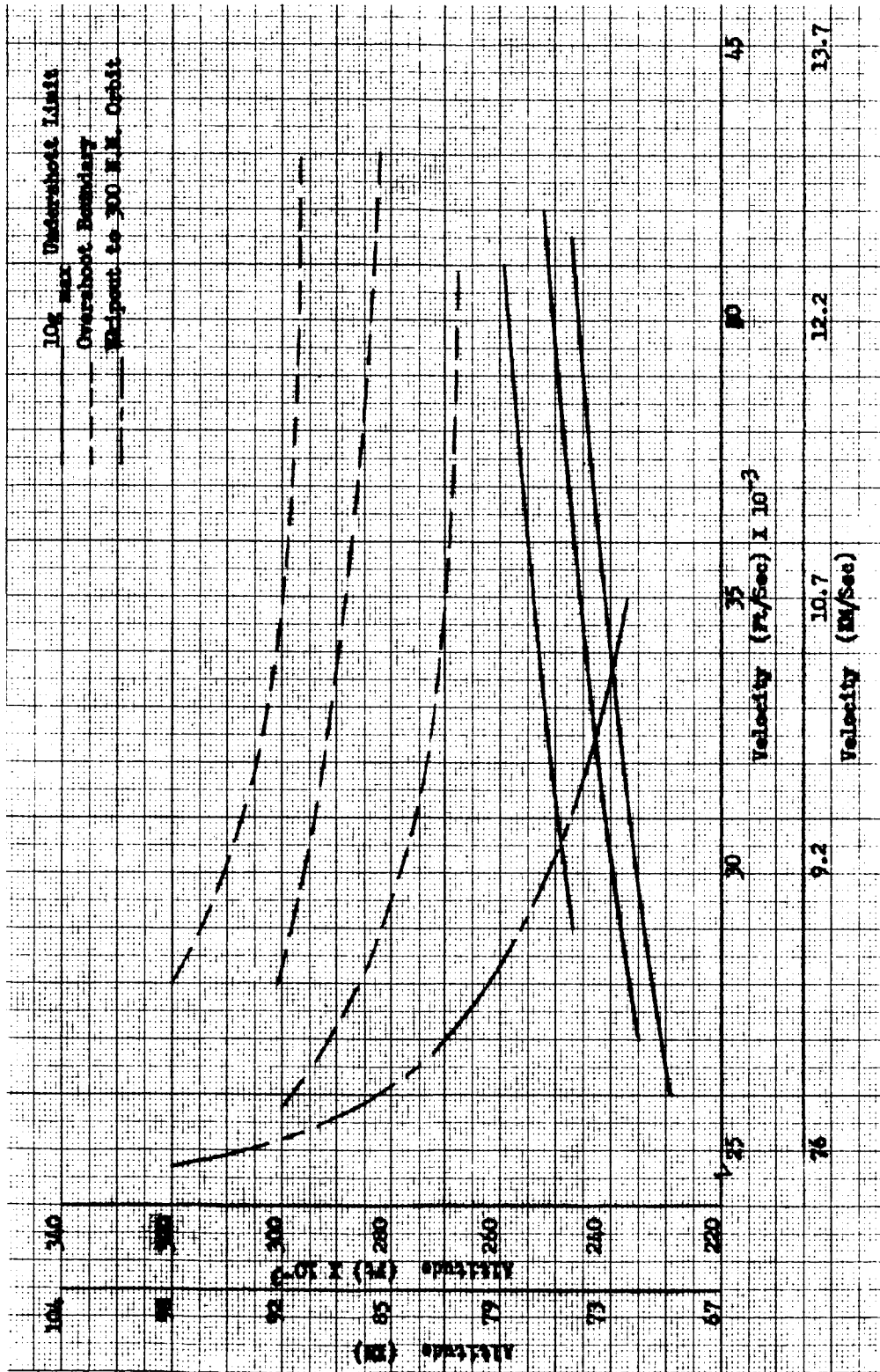
Figure 220. Venus Aerodynamic Braking Operation Envelope
($M/C_D A = 12,200 \ kg/m^2$)
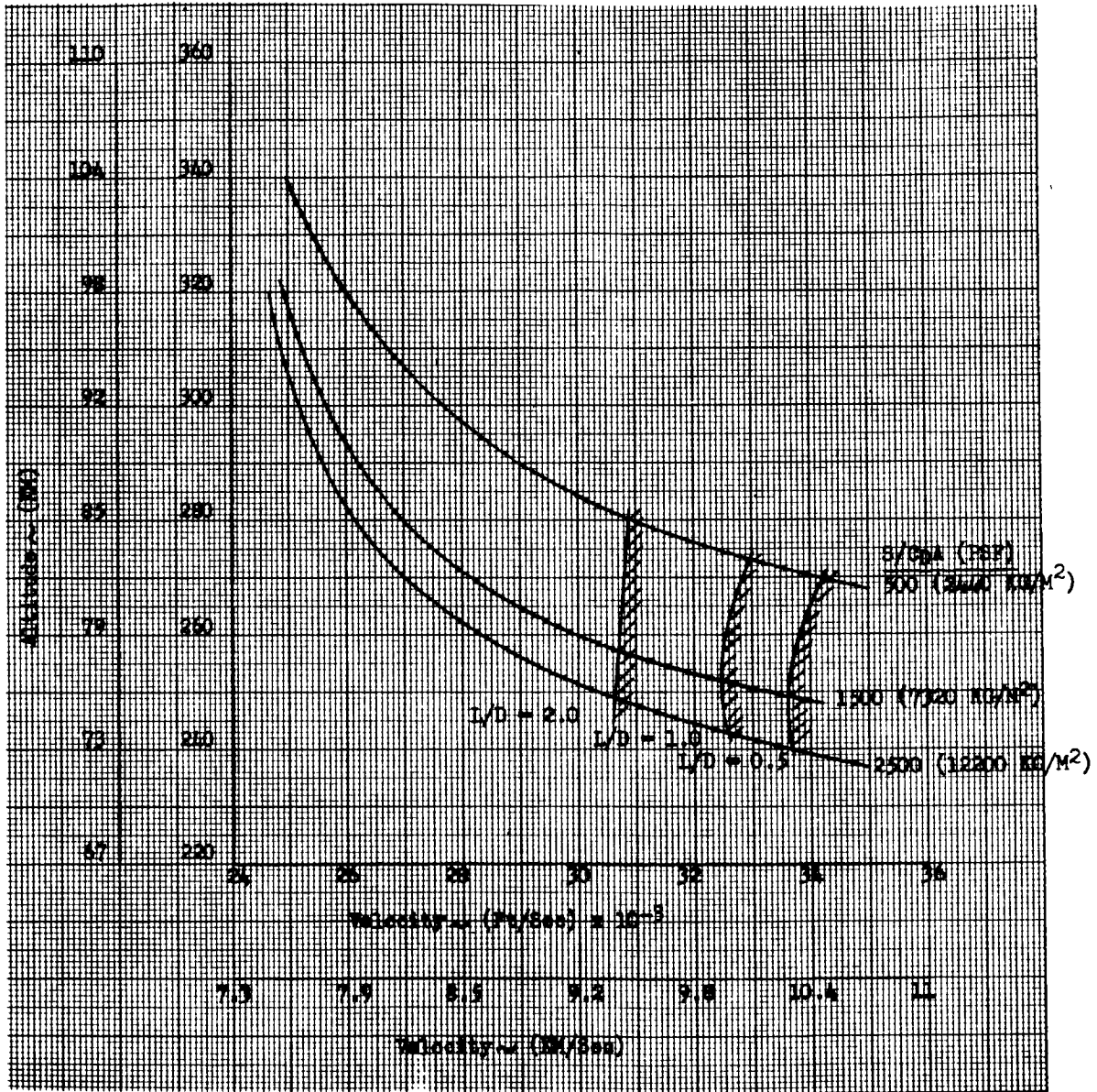
Figure 221. Venus Aerodynamic Braking Skip-out Operating Envelopes
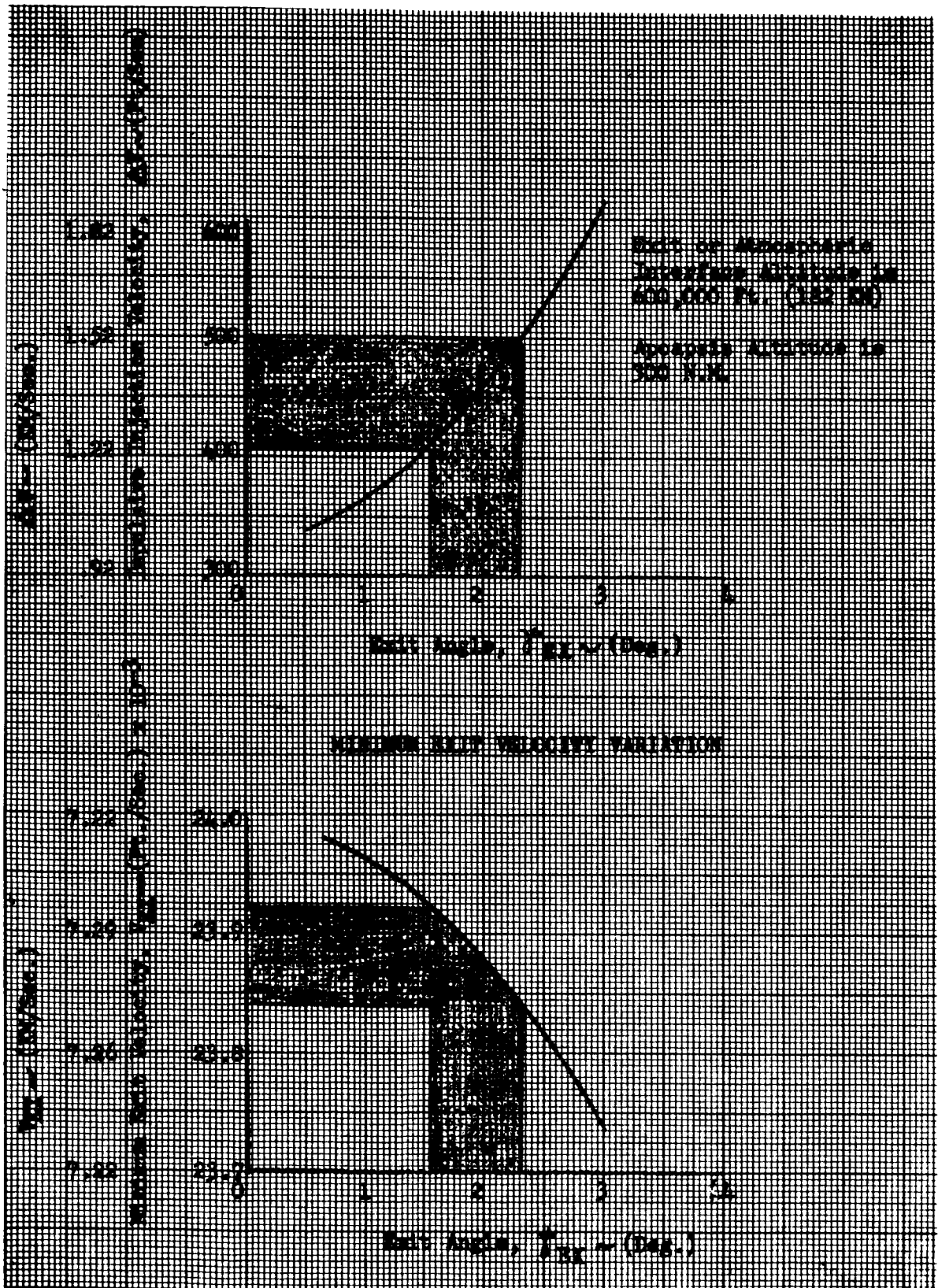
Figure 222.   Impulsive Injection Velocity Variation

SD 67-621-2

circular orbit (Reference 11). This identical conclusion was stated during the previous NR/SD Mars aerodynamic braking study (Reference 9) where a range of orbital altitudes were considered.

The effect of atmospheric uncertainties in the Venus atmosphere upon the exit maneuver have also been investigated. Figures 223, 224, and 225 present the atmospheric interface flight path angle and velocity, and the resultant apoapsis altitude as a function of the initial skip-out velocity for the NASA-MSFC recommended low and high density profile atmospheres.

The aerobraking trajectories consisted of entry along 5-g_{max} under-shoot boundaries at velocities of 12.2 kilometers/second and 15.2 kilometers/ second for an $M/C_D A$ of 12,200 kilograms/meter^2 and an L/D of 1. Exit characteristics depicted by Figures 223 to 225 are not directly comparable to the operating envelope presented in Figures 220 and 221 because of the assumptions regarding the atmospheric models and the undershoot criteria. Measurable differences in the atmospheric interface parameters and the resultant apoapsis altitude are observed for the upper and lower atmospheric models. The atmospheric model is shown to have a more significant affect upon the exit parameters at the lower entry velocity. Additionally, the entry velocity has a greater influence upon the exit parameters than the assumed atmospheric model.

AEROTHERMODYNAMICS

The interaction of the aerobraking vehicle with the planetary atmosphere creates an aerothermodynamic environment which requires special considera-tion in the development of a practical manned spacecraft system. Results of previously conducted aerobraking aerothermodynamic studies compatible with the entry corridor and skip-out trajectory criteria defined in the trajectory analysis are presented herein to indicate the sensitivity of a Mars and Venus aerobraking spacecraft design to the expected thermal environmental condi-tions. The aerothermodynamic environmental and resultant thermal protec-tion characteristics are representative of the class of configurations under consideration for the Mars and Venus aerobraking missions.

VEHICLE CONFIGURATION

The aerothermodynamic environment and the resultant thermal protec-tion requirements were derived for a biconic configuration which is repre-sentative of a class of biconic shapes currently under consideration for Mars/ Venus aerobraking missions (Reference 6). The specific vehicle employed in the current investigation was developed during the previous NR/SD Mars aerobraking study (Reference 9). For the aerothermal analysis, the vehicle was assumed to have a base diameter of 10 meters, a length of 15.8 meters, and a nose radius of 1 meter. The vehicle mass range at entry
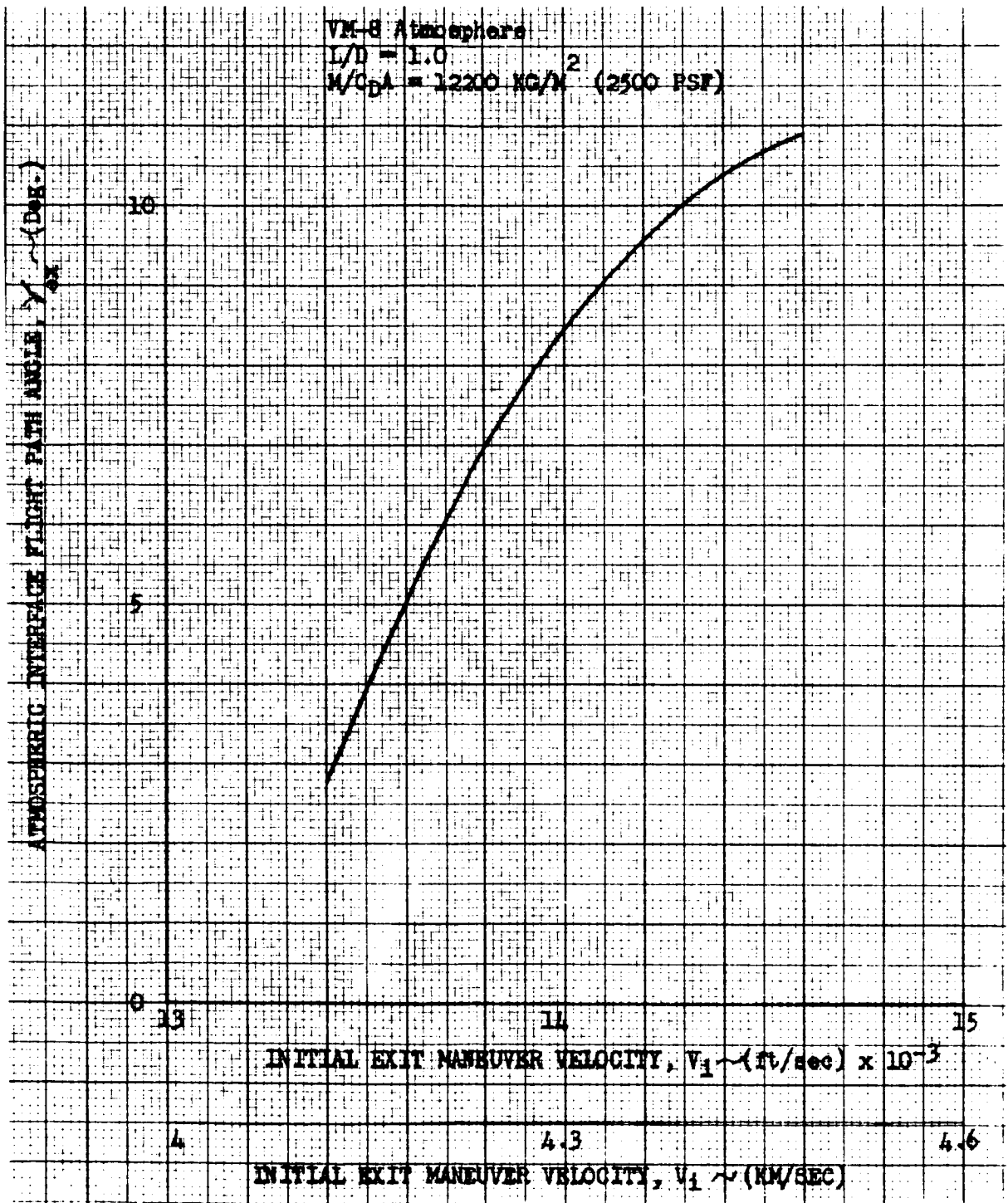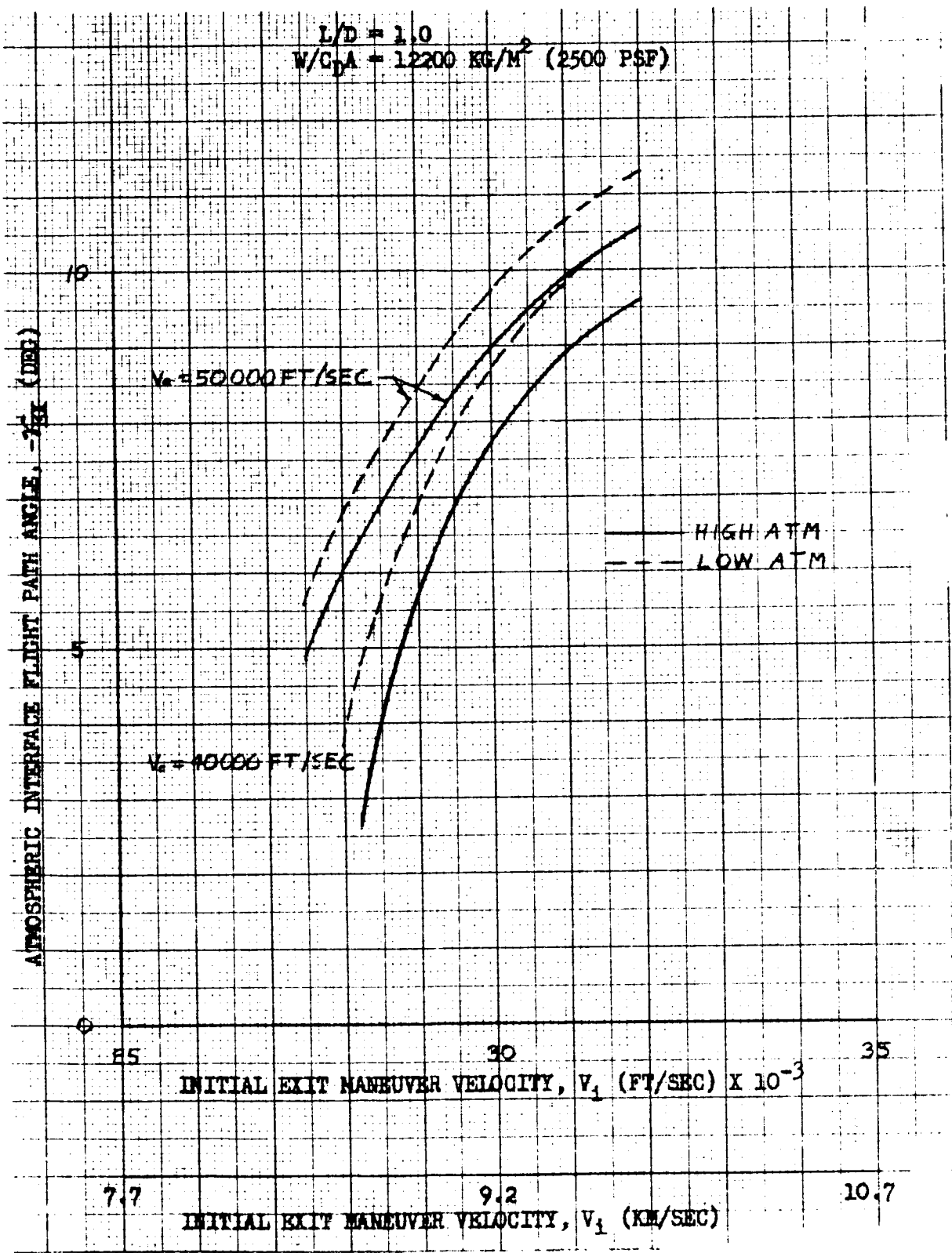
Figure 223. Venus Aerodynamic Braking Exit Conditions (Atmospheric Interface Flight Path Angle Variations)
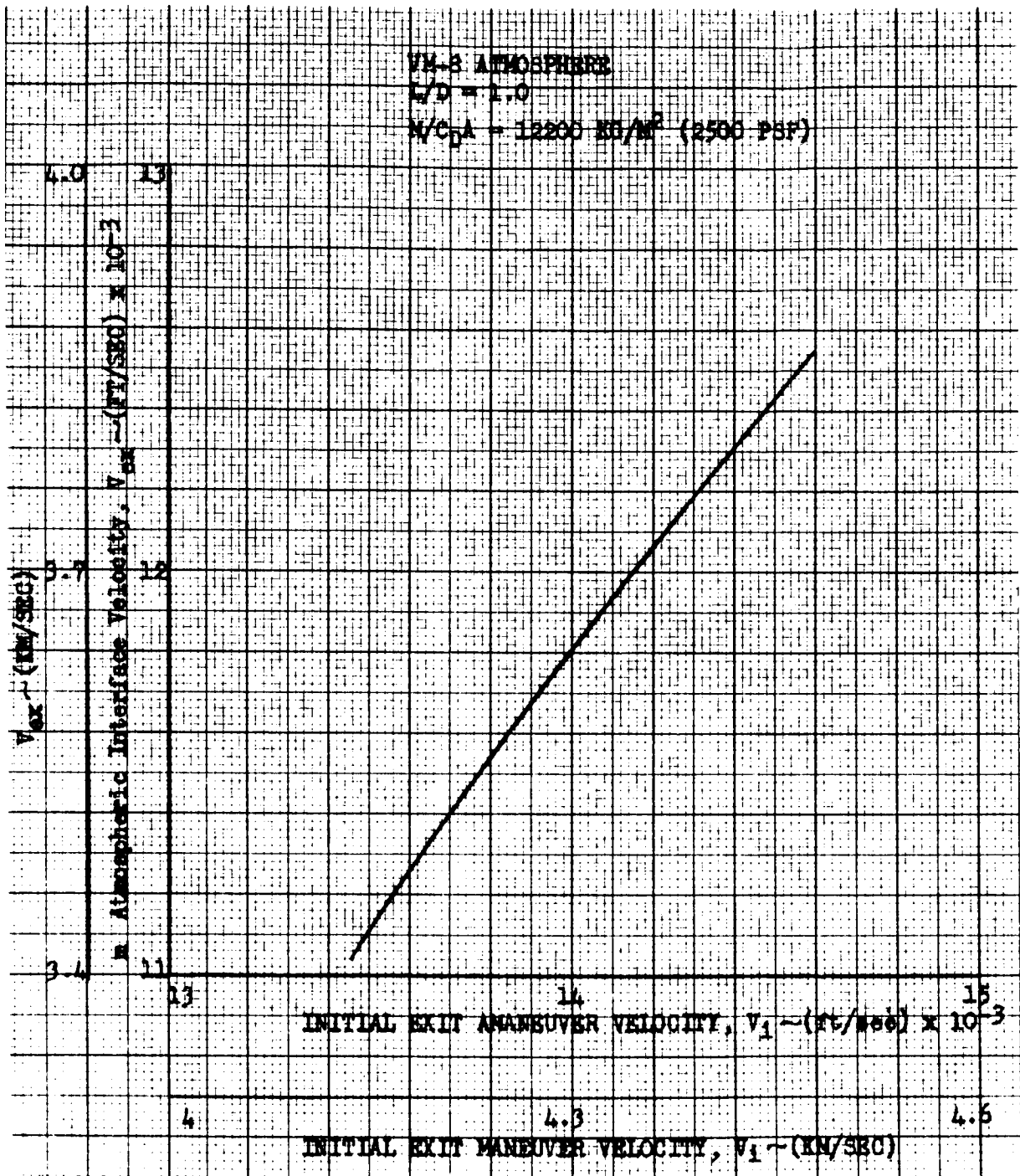
SD 67-621-2
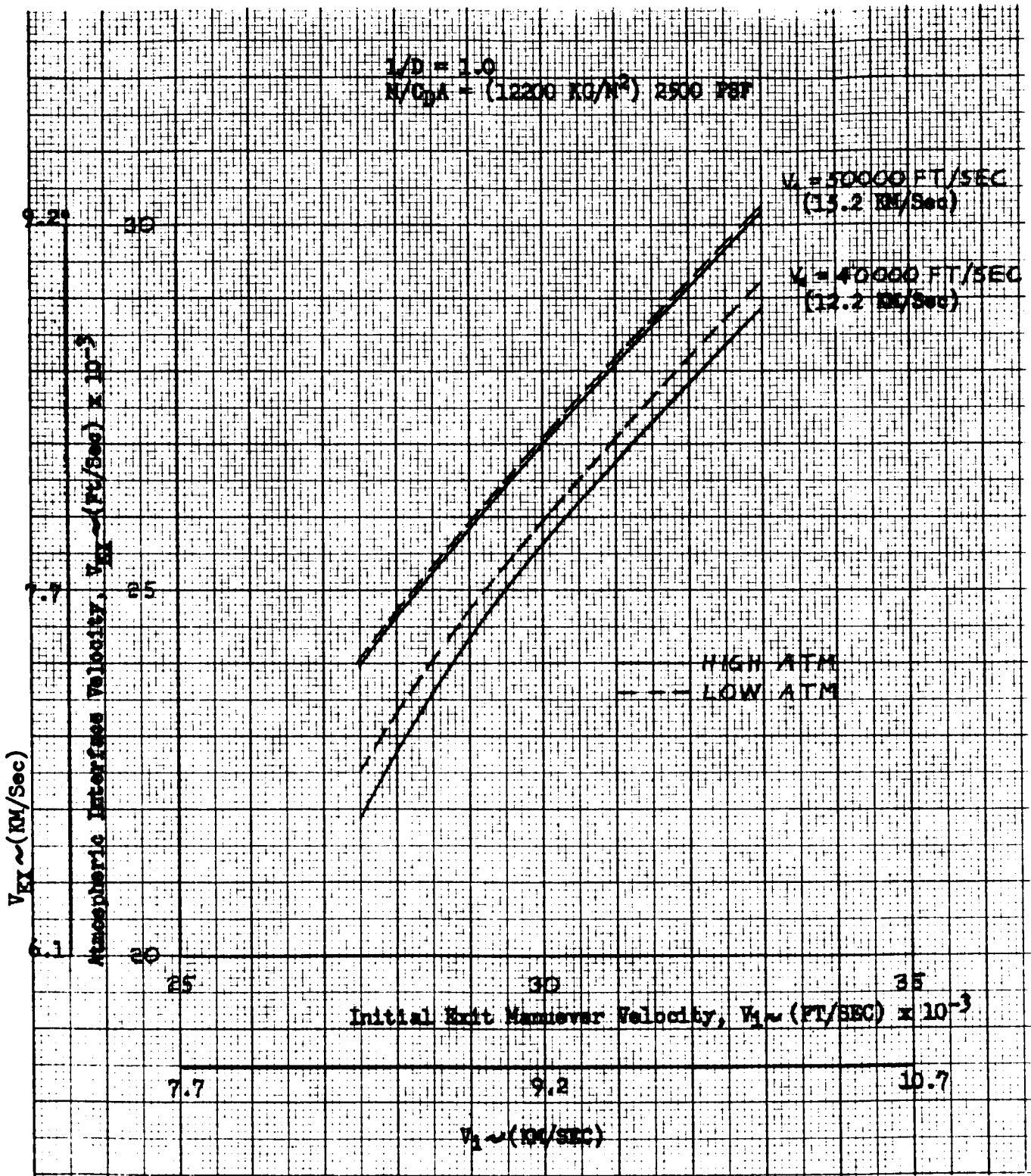
Figure 224. Venus Aerodynamic Braking Exit Conditions
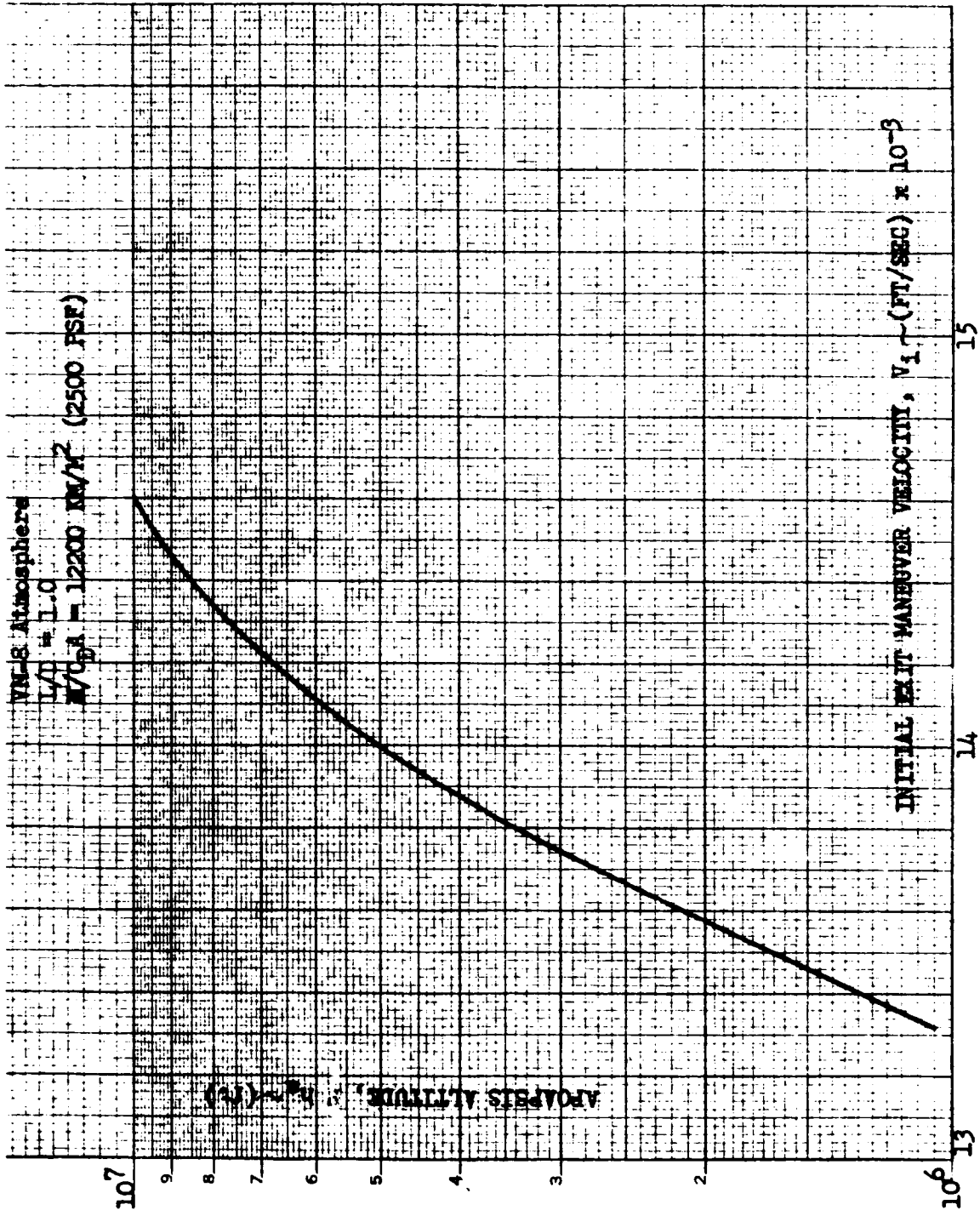(Atmospheric Interface Velocity Variation)

- 282 -

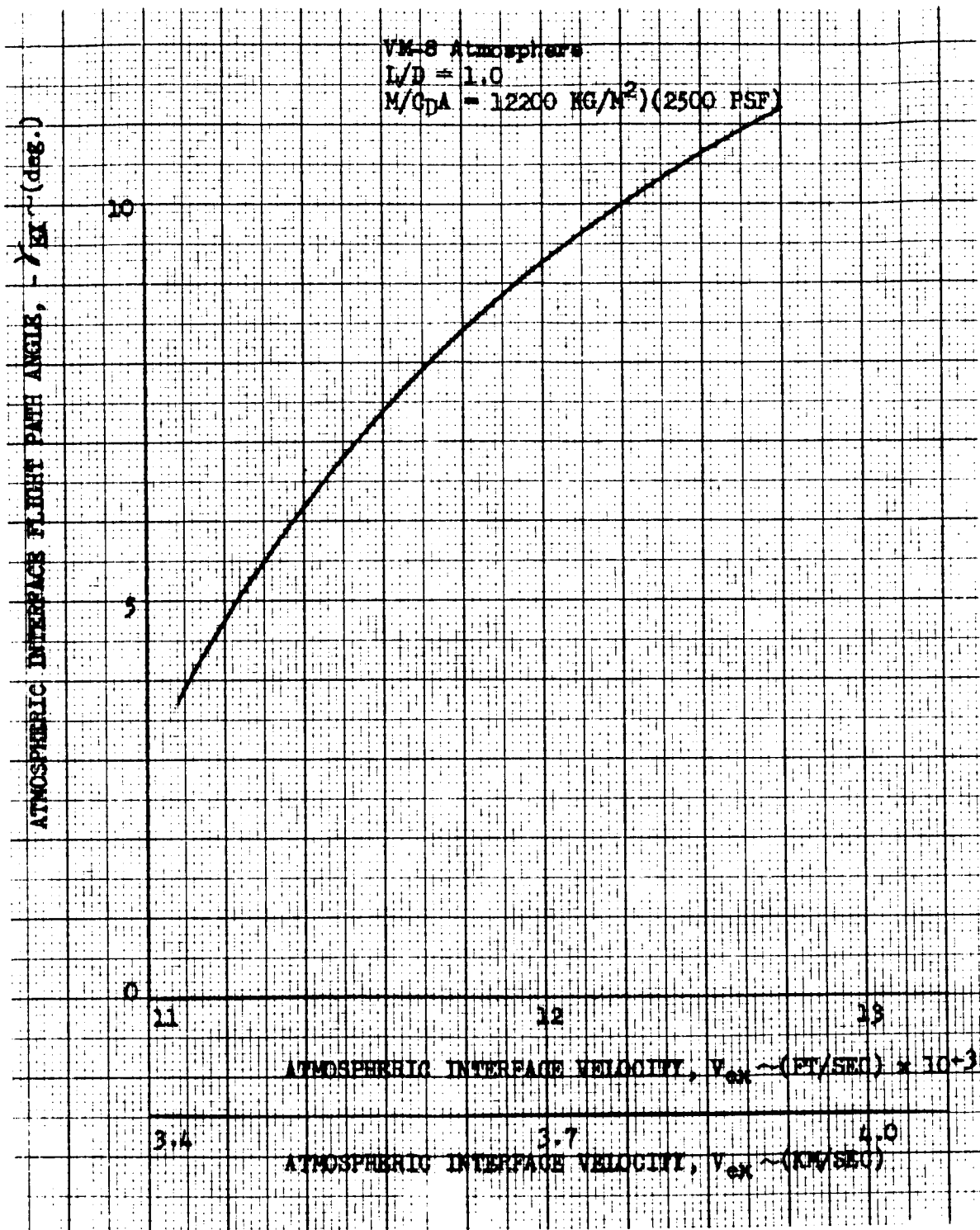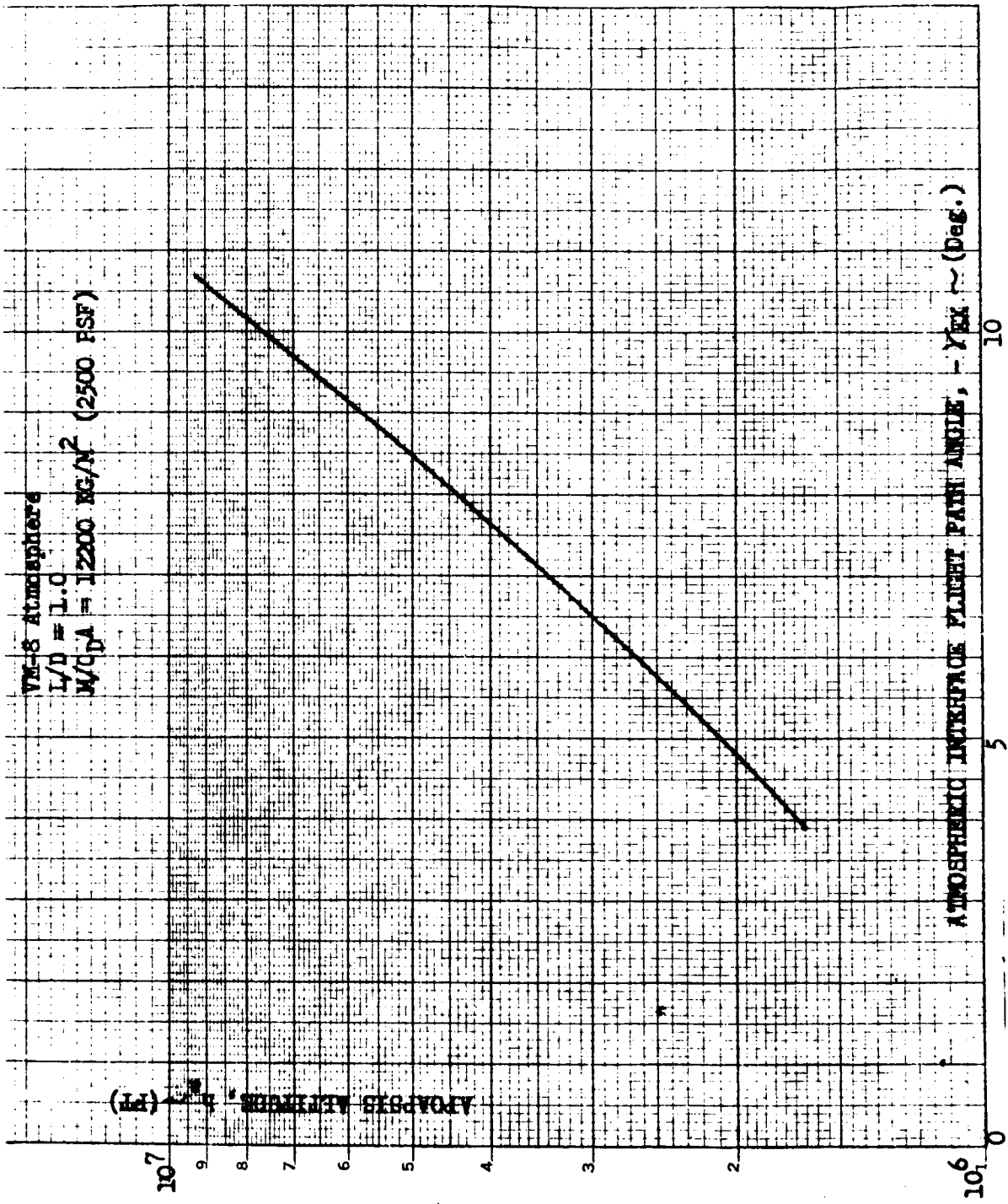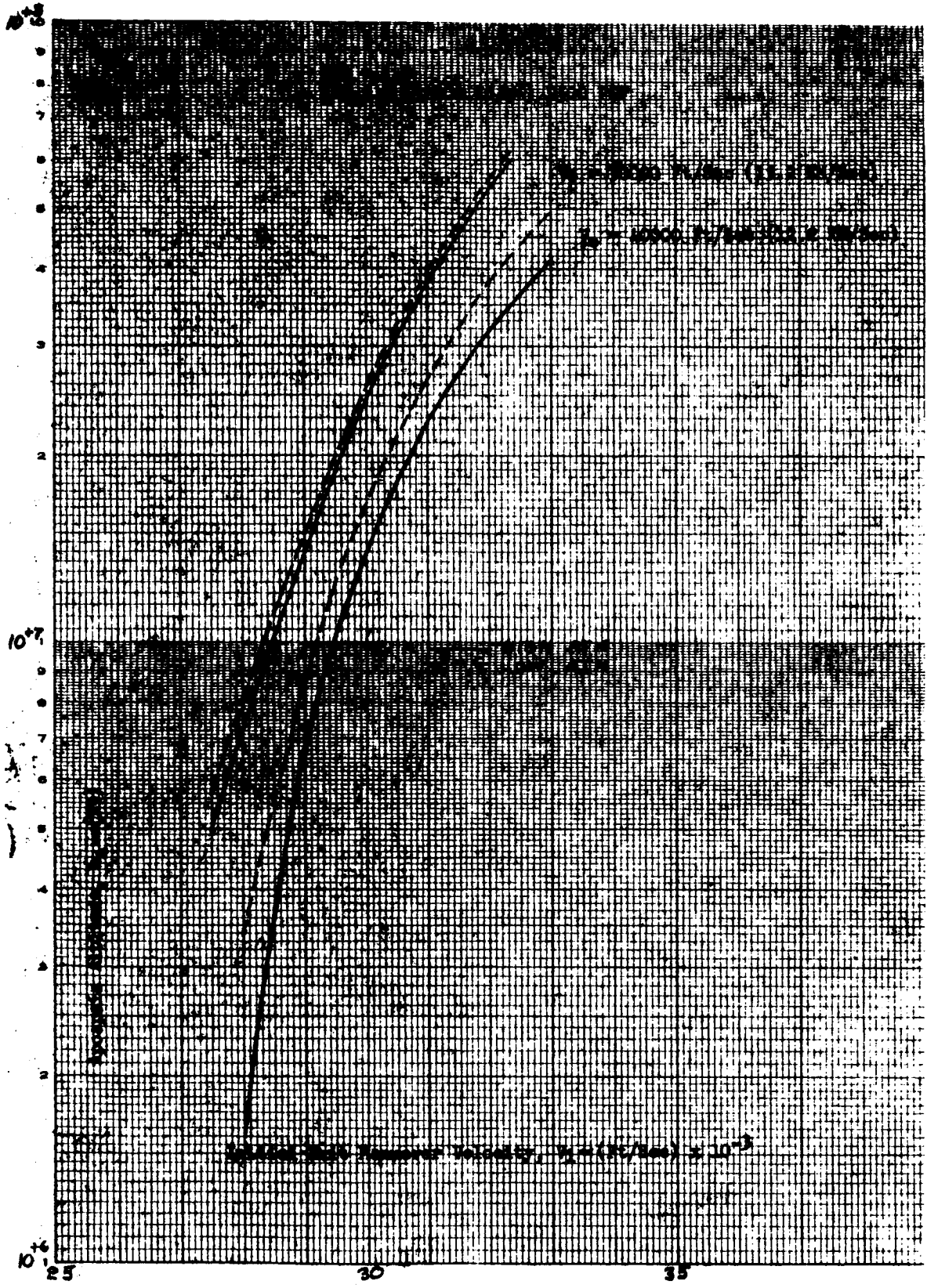Figure 2·25. Venus Aerodynamic Braking Exit Conditions (Apoapsis Altitude Variation)

SD 67-621-2

was selected such that the vehicle ballistic coefficient varied between 2440 kilograms/meter^2 and 12,200 kilograms/meter^2 for an L/D of 1.

GASDYNAMIC HEATING

The prediction of gasdynamic heating is an important factor in the development of a manned system capable of performing Mars and Venus aerobraking maneuvers. An important consideration is the uncertainty associated with evaluating gasdynamic heating in non-air atmospheres. Prediction of convective heat transfer is not considered difficult, while prediction of the radiant transfer mode is complicated by uncertainties in theoretical radiance models, thermodynamic properties, oscillator strengths, and absorption effects. Experimental verification of radiance models are complicated by the limited range of simulated conditions and the wide deviations produced by different experimental facilities attempting to simulate comparable flight conditions (Reference 12).

Three factors which determine the gasdynamic heating are the atmospheric model, the initial entry conditions, and the vehicle configuration characteristics. Of these three factors, the atmospheric model requires special consideration because of its influence upon the vehicle flight profile and the resultant gasdynamic heating and because current estimates of density profiles and constituent volume fractions for Mars and Venus lack adequate verification. The Martian atmosphere is thought to be composed of a mixture of CO_2 and N_2 with possibly substantial fractions of argon (A) and some traces of nitrogen oxides, water vapor and O_2 (Reference 13). For the JPL models the surface pressure and density scale height vary between 5 millibars to 10 millibars, and 15,450 feet to 46,512 feet, respectively. Volume fractions of CO_2, N_2, and A vary between 20 and 100 percent, 0 and 80 percent, and 0 and 32 percent, respectively. The Venusian atmosphere is assumed to be composed of a mixture of CO_2 and N_2. Volume fractions of CO_2 and N_2 for the NASA-MSFC model atmospheres vary between 10 and 75 percent and 25 and 90 percent, respectively.

The effect of simulated Mars and Venus atmospheric gas compositions on convective heating has been investigated theoretically by Hoshizaki (Reference 14) and Scala (Reference 15) and experimentally by a number of investigators (References 16 through 20). Figure 226 presents a summary of heat transfer measurements which cover the assumed atmospheric gas compositions. The results of Hoshizaki's analysis (Reference 14) for air and pure carbon dioxide are also depicted on the figure. The stagnation-point heat transfer rate multiplied by the square root of the nose radius divided by the stagnation pressure is presented as a function of the flight velocity. The summary of experimental data indicates that the effect of gas composition is not clearly defined. Data scatter for the results is observed to be greater than the variations due to changing the composition.
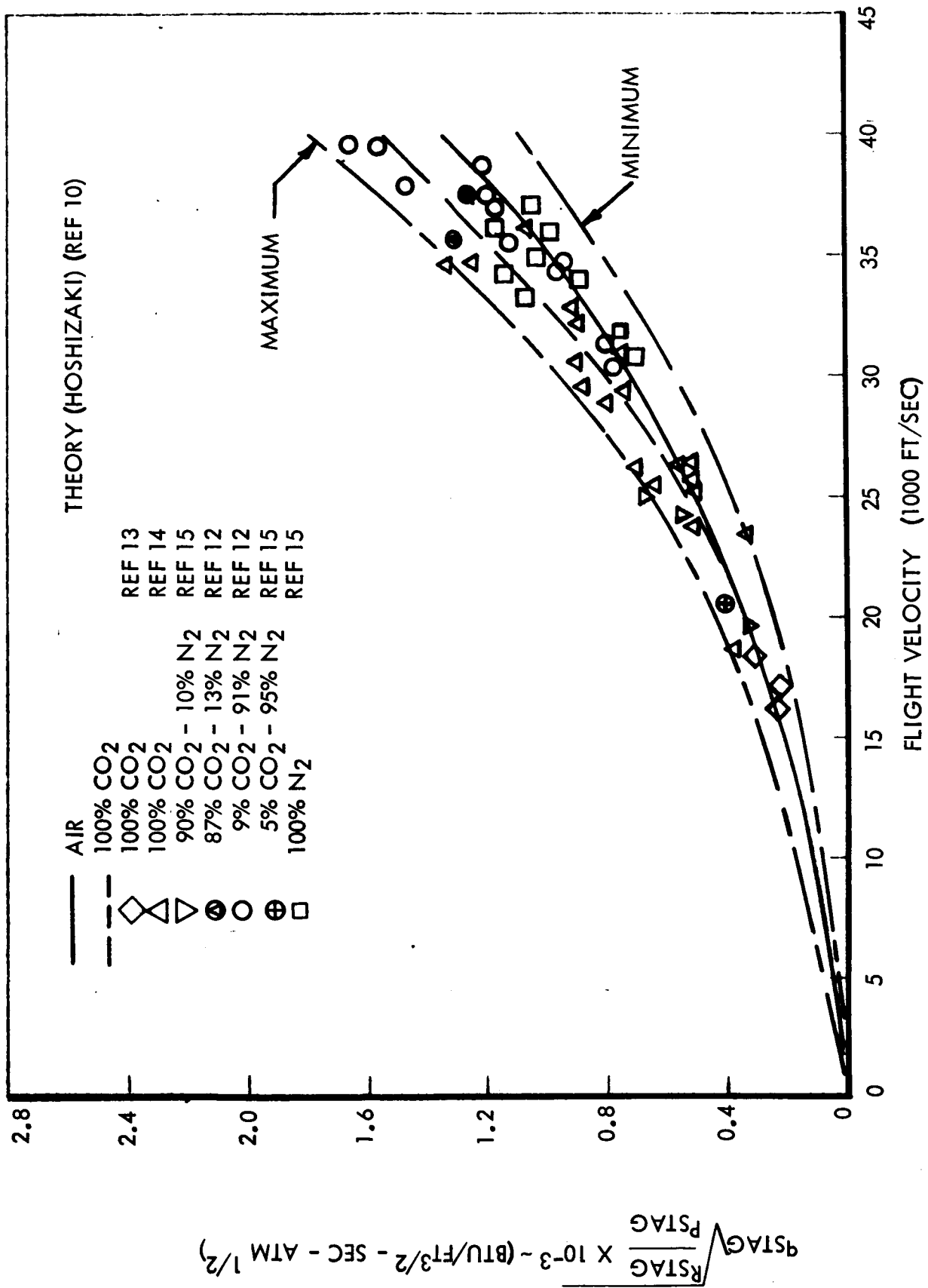
Figure 226. Stagnation Point Convective Heating in Simulated
Planetary Atmospheres

All of the data fall within ±25 percent of a mean derived from Hoshizaki's formulations for air and CO_2. From the given comparison, it could be concluded that the convective stagnation point heating for various combinations of CO_2 and N_2 vary by about ±25 percent from a theoretical mean value for air and CO_2. Gas mixtures containing A, in addition to CO_2 and N_2 have been shown to produce some increases in convective heating (Reference 20). During a recent NR/SD gasdynamic heating study (Reference 10) the effect of the presence of argon upon stagnation-point convective heating was investigated. A comparison was made between two mixtures containing 25 percent CO_2 and 75 percent N_2 and 25 percent CO_2, 50 percent N_2 and 25 percent A volume fractions for a flight velocity of 34,000 feet per second (10.35 km/s) and a stagnation pressure of 3.65 atmospheres. The presence of argon was shown to increase the convective heating by approximately 20 percent (Reference 10). The effect of atmospheric composition on the convective heating to the conical afterbody surfaces is not available. As a consequence of the results derived from theoretical and experimental evaluations of convective heating in simulated planetary atmospheres the current methods developed for air were utilized to determine the Mars/Venus aerobraking convective heating. Hoshizaki's analysis (Reference 14) was employed to evaluate stagnation point heating. Hanley's laminar flat plate analysis (Reference 21) and Eckert's reference enthalpy method (Reference 22) were employed to evaluate laminar and turbulent boundary layer heating on the conical surfaces.

Atmospheric composition has a greater impact upon radiative heating than the convective transfer mode. The influence of gas composition on radiative intensity has been studied theoretically and experimentally by numerous investigators (References 23 through 28). These studies indicate that the magnitude of the radiant intensity can be significantly higher than that for air and varies with composition. A typical example of the influence of gas composition on radiant intensity is shown in Figure 227 in which the radiant intensity behind a normal shock wave is presented as a function of composition and flight velocity. A comparison is presented between Kivel and Bailey's radiant intensity data for air (Reference 29) with experimental and theoretical predictions for selected CO_2 - N_2 combinations (References 16, 23, and 25). As shown by Figure 227, the influence of uncertainties in atmospheric composition would have the greatest effect on Mars aerobraking since the effect of composition is most pronounced within the Martian entry velocity range (Ve = 6 kilometers/second to 10 kilometers/second), while at Venus aerobraking entry velocities, (Ve = 10 kilometers/second to 15.2 kilometers/second), the dependency of radiant heating on composition is reduced significantly. Theoretical predictions of Spiegel (Reference 25) are observed to agree reasonably well with the experimental data. This was found to be the case over the entire range of velocities and compositions reviewed (Reference 30). The figure also presents the
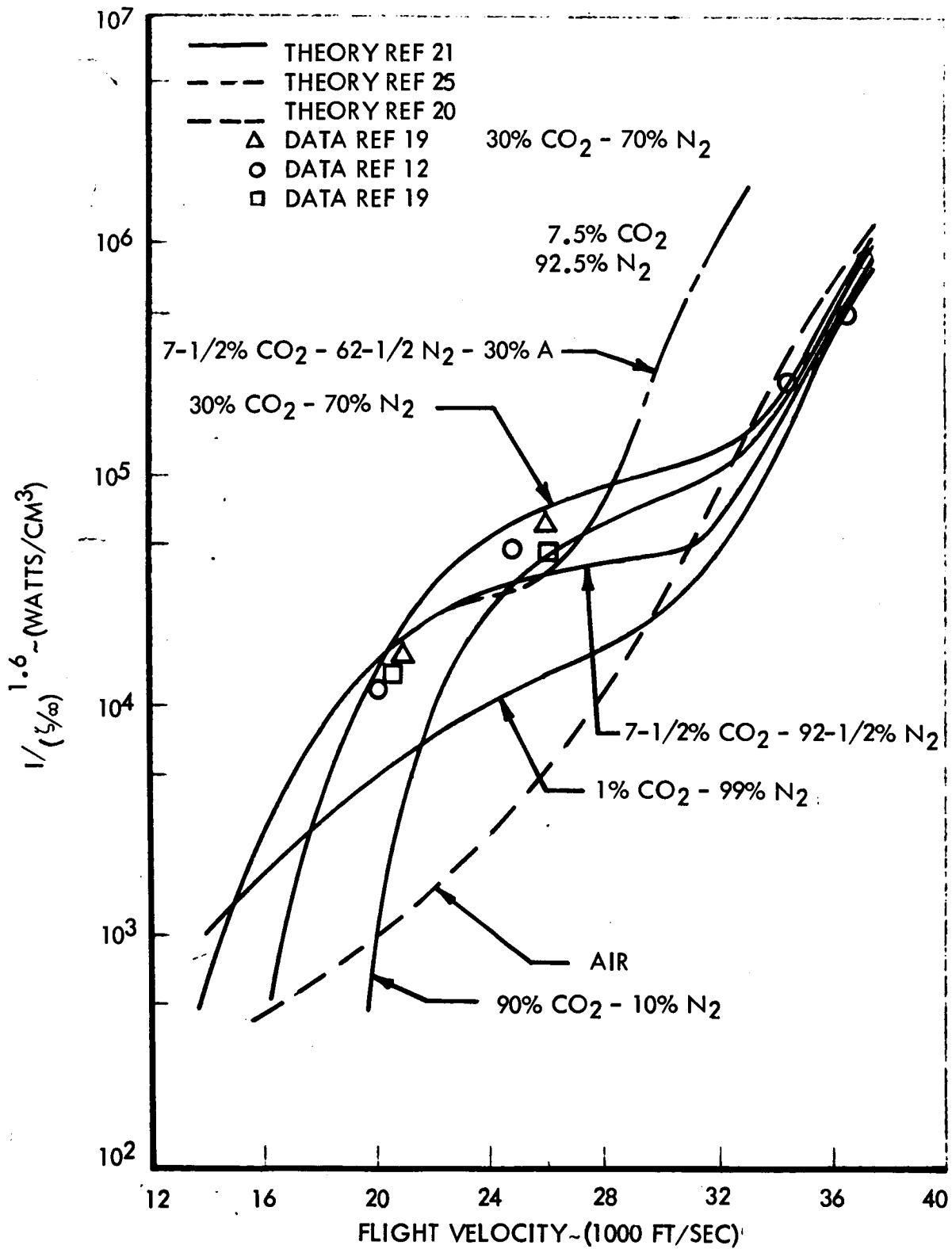
Figure 227. Radiant Intensities in Simulated Planetary Atmospheres

intensity variation of a 7-1/2-percent CO_2 - 62-1/2-percent N_2 - 30-percent A-mixture (Reference 24) which indicates the significant effect of argon on radiant intensity for flight velocities greater than 8 kilometers/second.

Since the scope of the aerothermodynamic analysis was restricted to defining an upper limit to the expected aerobraking thermal environment, a set of empirical equations representing an envelope of maximum equilibrium radiative intensities for all possible combinations of CO_2 - N_2 mixtures was employed in the study to compute equilibrium radiative heating. The empirical curve-fit equations were derived in an unpublished study of CO_2 - N_2 mixtures from a review of available theoretical methods (References 29, 24, and 25) and experimental data (References 16 and 23). The upper boundary of the empirical formulation was 12.2 kilometers/second, which is at the midpoint of the Venus entry-velocity regime considered in the study. A review of recent comparisons of experimental and theoretical evaluation of CO_2 - N_2 gas radiancies (Reference 12) indicate that at the V_e = 15.2 kilometers/second entry, the empirical formulation employed in the study would conservatively overpredict the radiant heating at this flight velocity.

The stagnation point equilibrium radiative heating was evaluated by assuming that all of the radiation to the stagnation point originates from a semiinfinite slab with a thickness equal to the shock detachment distance. The shock detachment distance was computed by a simplification of the Li and Geiger blunt-body, hypersonic-flow analysis (Reference 31). At positions on the windward forebody surfaces, the radiative heating was computed by replacing the free-stream velocity by the component of velocity normal to the oblique shock wave in the radiant intensity expression and then assuming an infinite-plane radiating geometry. Nonadiabatic effects were taken into account by employing a modified form of the nonadiabatic flow-field analyses conducted by Hanley and Korkan (References 32 and 33).

The gasdynamic heating environment for Mars and Venus aerobraking missions were derived for a representative biconic configuration (M/C_DA = 12,200 kilograms/meter^2). Heating rates (convection and radiation) were computed at the nose stagnation point and at four selected points on the upper and lower conical surfaces. Turbulent heating was assumed to exist at the conical surface points over the entire aerobraking trajectory. The analysis was restricted to undershoot boundaries for both Mars and Venus. Previous investigations have indicated that critical thermal protection design conditions are experienced along undershoot boundaries (Reference 5 and 9).

The Mars heating evaluation was based upon a 10-kilometer pull-out altitude undershoot boundary. For the entry velocities considered, the constant altitude deceleration and the subsequent skip-out were executed at the 10-kilometer altitude. An entry velocity range of 20,000 feet per second

SD 67-621-2

(6.15 kilometers/second) to 40,000 feet per second (12.2 kilometers/second) was to be investigated, but at the 10-kilometer pull-out altitude criteria, a constant-altitude deceleration maneuver could not be performed at $V_e = 12.2$ kilometers/second. As a consequence, the Mars heating evaluation was restricted to an entry velocity range of 6.15 kilometers/second to 9.2 kilometers/second. Further entry studies would be required to define a limiting entry velocity for the assumed undershoot boundary. Figure 228 presents a Mars aerobraking trajectory profile for $V_e - 25,000$ feet/second (7.625 kilometers/second) in which altitude, velocity, and dynamic pressure are shown as functions of time. Figure 229 presents the heating rate-time variation at the vehicles's stagnation and lower forward surface positions for the trajectory defined in Figure 228. Radiative heating at the nose is significantly greater than convection, while at the point on the cone, the convective heating is higher than the radiative heating. The static temperatures within the region between the windward conical surfaces and the shock are in a range where the resultant radiative heating is less than the assumed turbulent heating. Along the upper conical surfaces, the radiative heating is negligible as compared to the convective heat transfer mode. The relative magnitudes of the radiative to convective heating on the conical surfaces increased at the higher entry velocities. Figures 230 and 231 present the variation of stagnation-point peak gasdynamic heating rate and integrated heat loads with entry velocity. The relative magnitudes of convection and radiation are indicated. Peak total heating and the integrated heat load increase by approximately a factor of five for the entry velocity range of 6.15 kilometers/second to 9.2 kilometers/second. At $V_e = 6.15$ kilometers/second, the peak stagnation point radiative heating is approximately three times greater than convection, while at $V_e = 9.2$ kilometers/second, this ratio increases to a factor of six. Figures 232 and 233 present peak heating rate and integrated heat-load variations for the stagnation point and three selected conical surface points. The locations of the three points are designated on the figures. For the given entry velocity range, the peak total heating and integrated heat loads experienced by the conical surfaces increase by a factor greater than three. An extension of the upper entry-velocity boundary would increase the relative magnitudes of radiative and convective heating at the stagnation point and the relative increase of conical-surface heating.

The Venus heating evaluation was based upon a 5-g_{max} undershoot boundary and covered an entry velocity range of 30,000 feet per second (9.2 kilometers/second) to 50,000 feet per second (15.2 kilometers/second). Both the NASA-MSFC recommended upper- and lower-density profile atmospheres were considered. Figure 234 presents a Venus aerobraking trajectory derived from the high density-atmospheric model for $V_e = 40,000$ feet/second (12.2 kilometers/second). Altitude, velocity, and dynamic pressure are presented as functions of time. Figure 235 presents the corresponding heating rate-time variation at the vehicle nose and lower forward surface positions for the trajectory defined by Figure 234. The conclusions

concerning the relative importance of radiative to convective heating and the effect of entry velocity upon Venus aerobraking heating are similar to those stated for Mars. At the nose stagnation point, the radiative heating is significantly greater than convection; while along the conical surfaces, turbulent convective heating is greater than radiative heating. Figures 236 and 237 present the peak stagnation-point total heating rate and integrated heat-load variations with entry velocity. Peak total heating and the integrated heat load increased by a factor greater than 16 for the entry velocity range of 9.2 kilometer/second to 15.2 kilometer/second. The ratio of peak stagnation-point radiative to convective heating varies approximately between 10 and 50 for the aforementioned entry-velocity range. The fraction of radiative to total stagnation heating is greater than that predicted for Mars aerobraking. This difference is a result of the higher entry velocity range considered for Venus. Within the stagnation region, the extreme radiative heating would reduce the convective heating to a negligible amount, which is a result of boundary-layer lift-off effects. Figures 238 and 239 present the Venus aerobraking peak heating rate and integrated heat load variations for the stagnation point and three selected conical-surface locations. The heating environment experienced by the conical surfaces are less in magnitude than the stagnation-region heating. The total peak heating and integrated heat loads experienced by the conical surfaces increase in a manner similar to that observed for Mars aerobraking. For the lower forward conical point, the peak total heating rate and the corresponding integrated heat loads vary from 3475 Btu's per $foot^2$-second to 13,180 Btu's per $foot^2$-second and 320,000 Btu's/$foot^2$ to $1.76 \times 10^{+6}$ Btu's/$foot^2$ for the entry range of 9.2 kilometers/second to 15.2 kilometers/second, respectively. At the lower forward conical point, the fraction of peak radiative heating to the peak total heating and the corresponding integrated heat load fraction vary from 6 percent to 28 percent and 2.28 percent to 7 percent for the aforementioned entry velocity range.

These magnitudes of peak radiative heating depicted for the entry velocity range of 12.2 kilometers/second to 15.2 kilometers/second are expected to be extremely conservative. More detailed analyses would yield lower peak conditions. The results presented herein indicate that the radiative heating as the dominant transfer mode is confined to the nose stagnation region, which comprises a small fraction of the total vehicle surface area. As a consequence, the overprediction of the shock-layer radiative heating will not adversely affect the vehicle thermal protection requirements. The dominant factor is the level of the turbulent heating on the conical surfaces.

The Venus aerobraking heating characteristics presented were derived for the NASA-MSFC recommended upper-density-profile atmosphere. Similar results can be presented for the low-density-model atmosphere. Table 26 presents a comparison between peak stagnation point total, convective, and radiative heating rates for Ve = 12.2 kilometers/second.

Figure 228. Mars Aerodynamic Braking Trajectory Profile
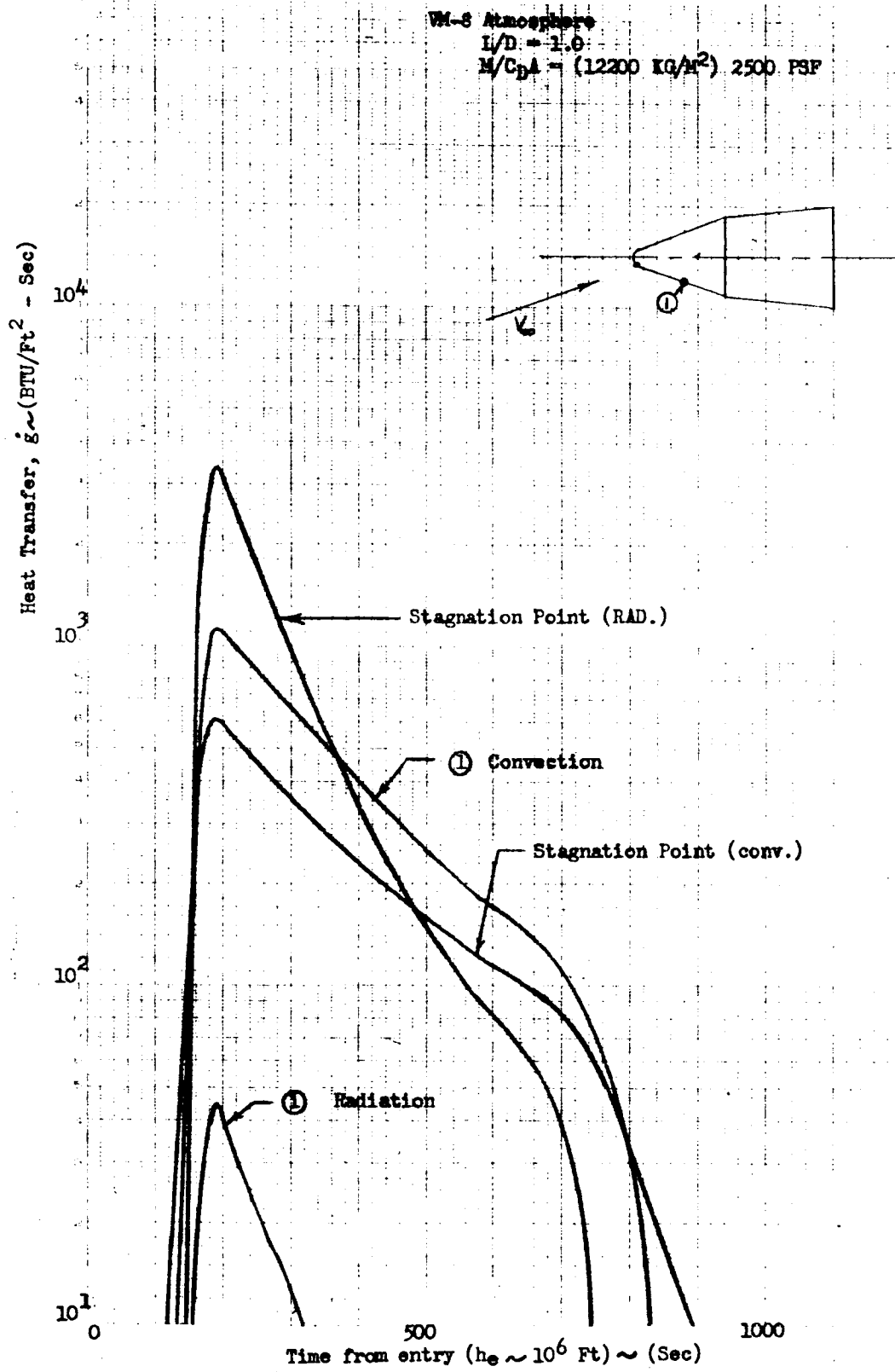
Figure 229. Mars Aerodynamic Braking Gasdynamic Heating Variation

- 293 -
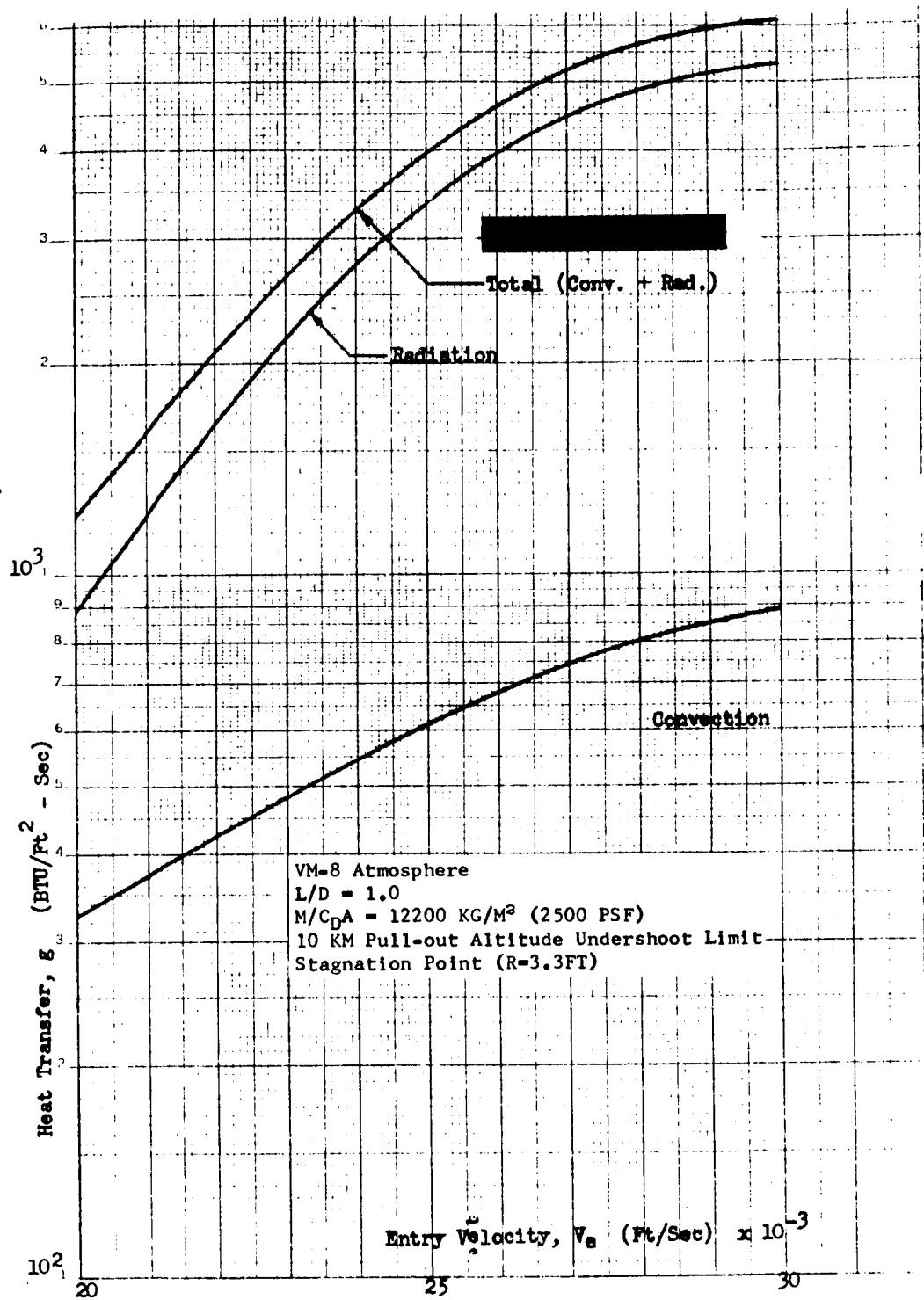
Figure 230. Mars Aerodynamic Braking Peak Gasdynamic Heating Variation
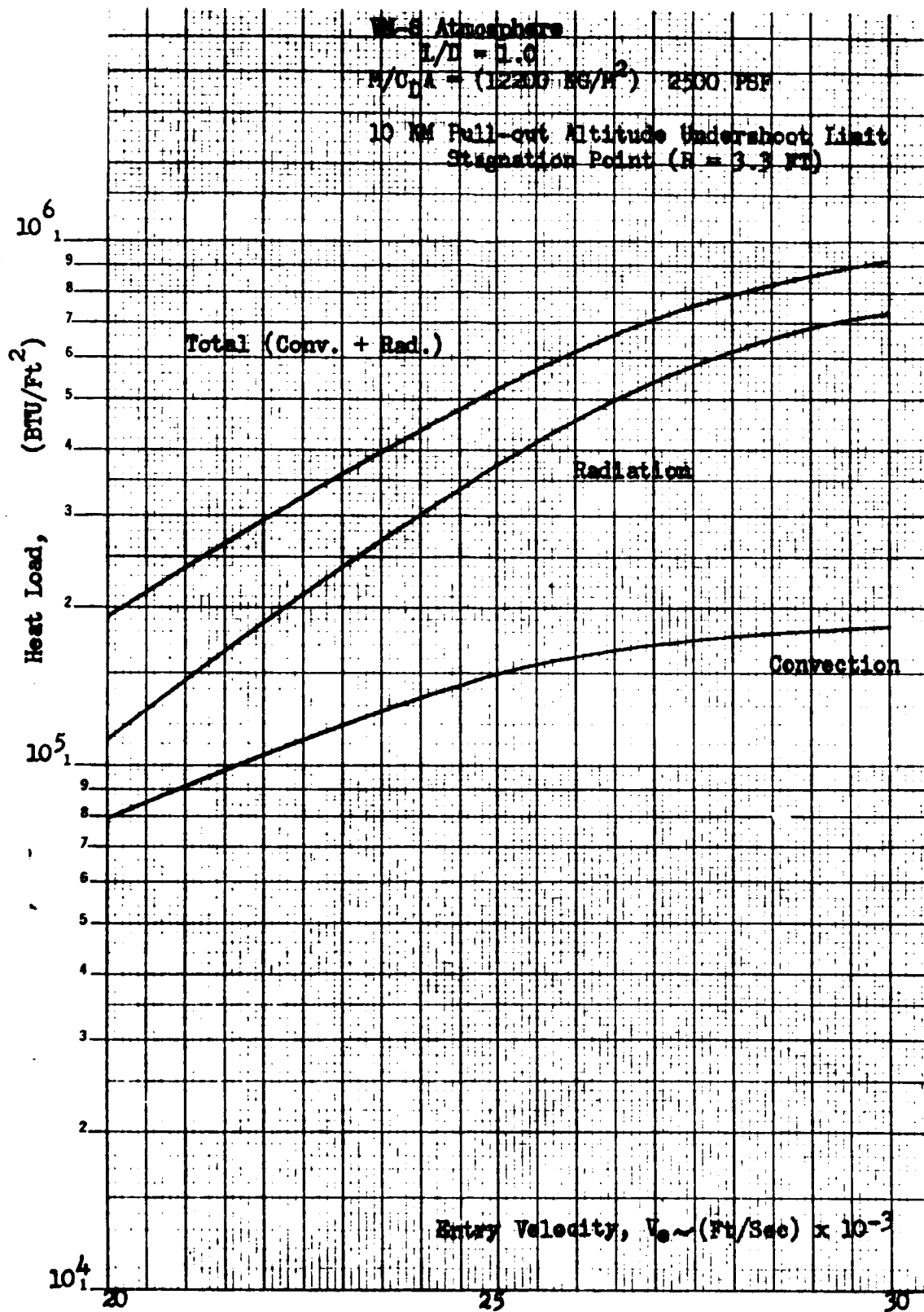
Figure 231. Mars Aerodynamic Braking Integrated Heat Load
Variation

- 295 -
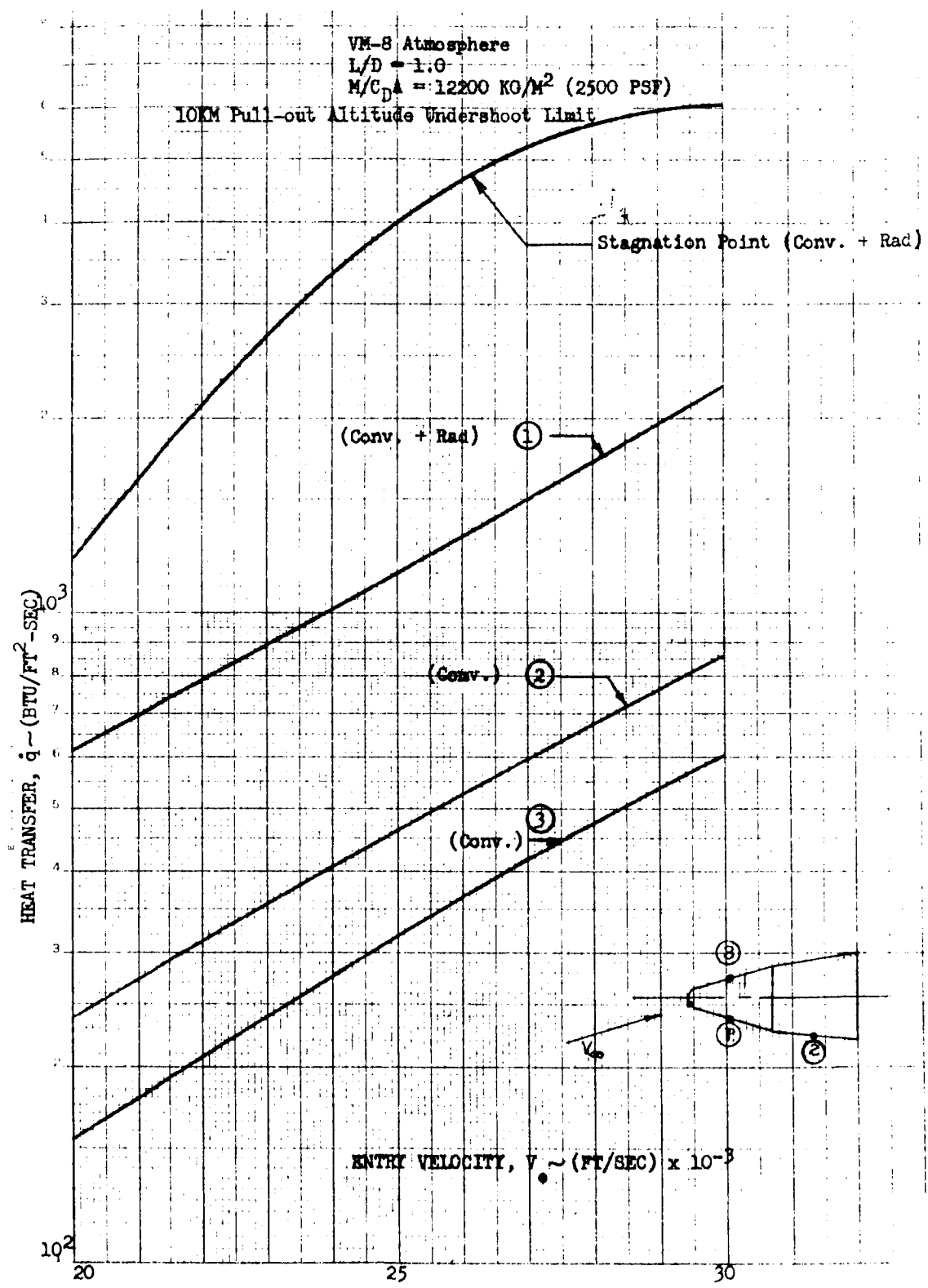
Figure 232. Mars Aerodynamic Braking Total Peak Heating Variation

Stagnation Point (Conv. + Rad)

(CONV. + RAD) ①

(CONV.) ②

10^5

(CONV.) ③

HEAT LOAD, Q ~ (BTU/FT²)

V_∞

VM-8 Atmosphere
L/D = 1.0
M/C_DA = 12200 KG/M² (2500 PSF)
10 KM Pull-out Altitude
Undershoot Limit

10^4

20   25   30

ENTRY VELOCITY, V_e ~ (FT/SEC) x 10^{-3}
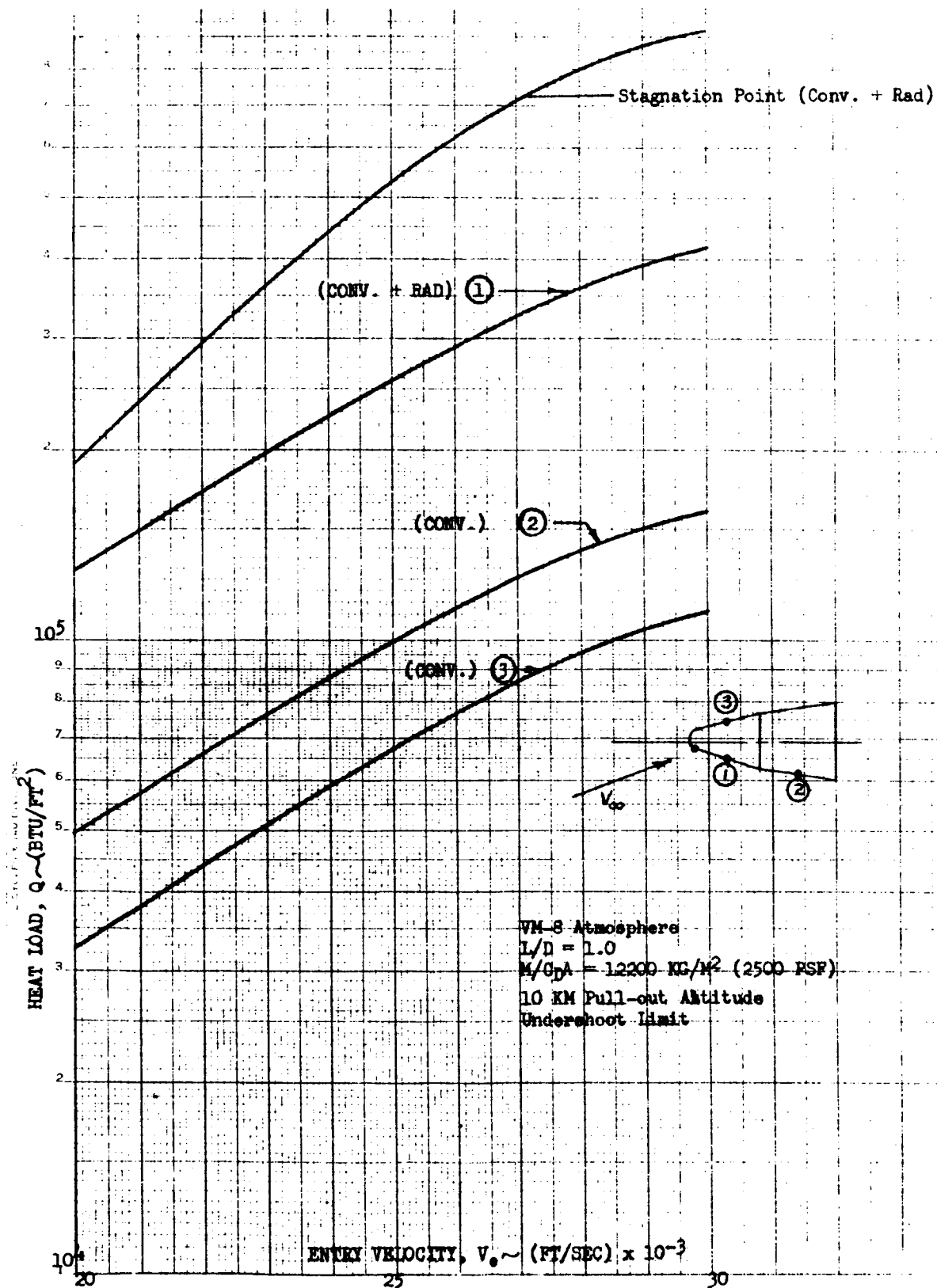
Figure 233. Mars Aerodynamic Braking
Total Integrated Heat Load Variation
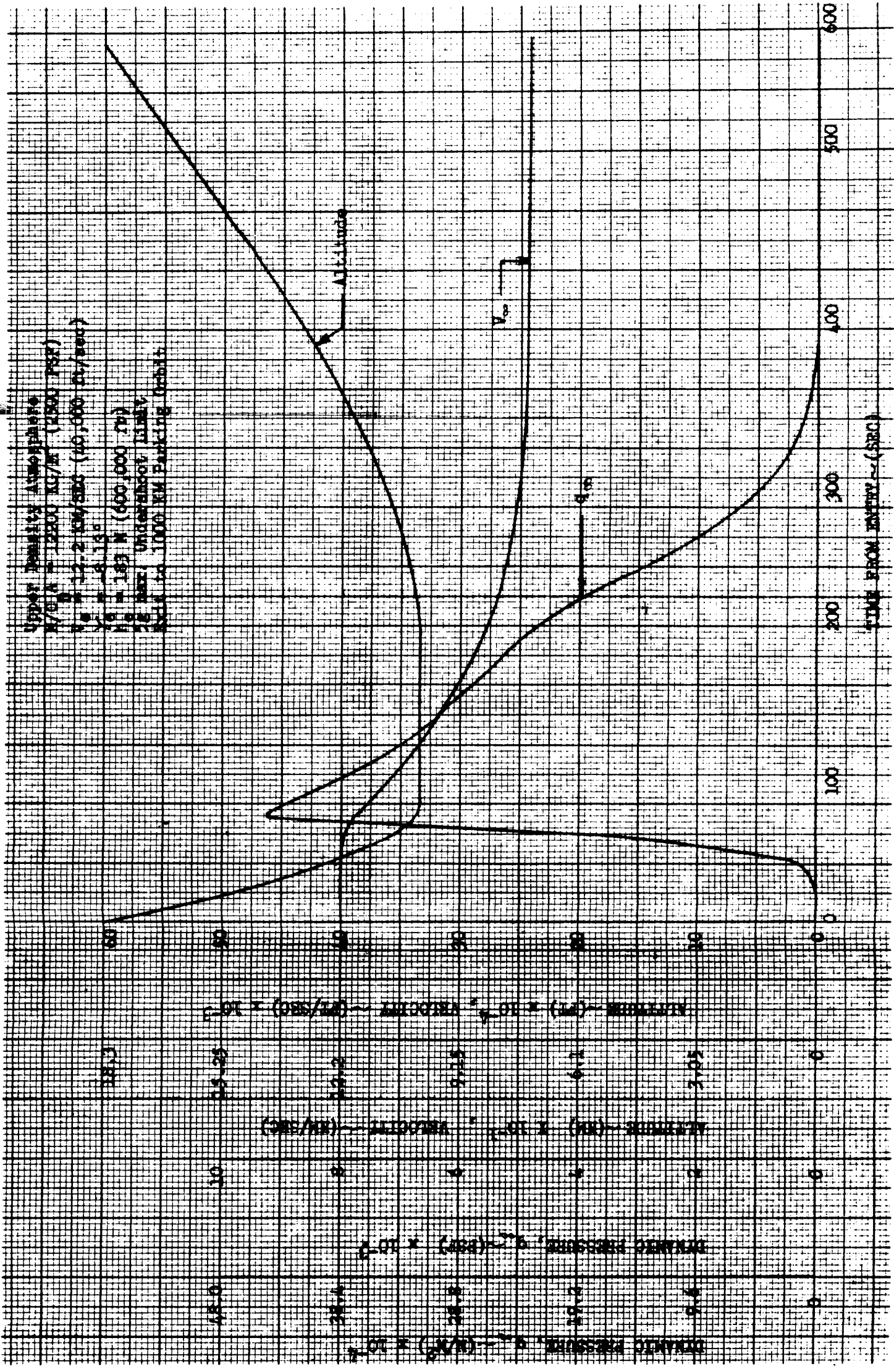
Figure 234. Venus Aerodynamic Braking Trajectory Profile

- 300 -

SD 67-621-2

299
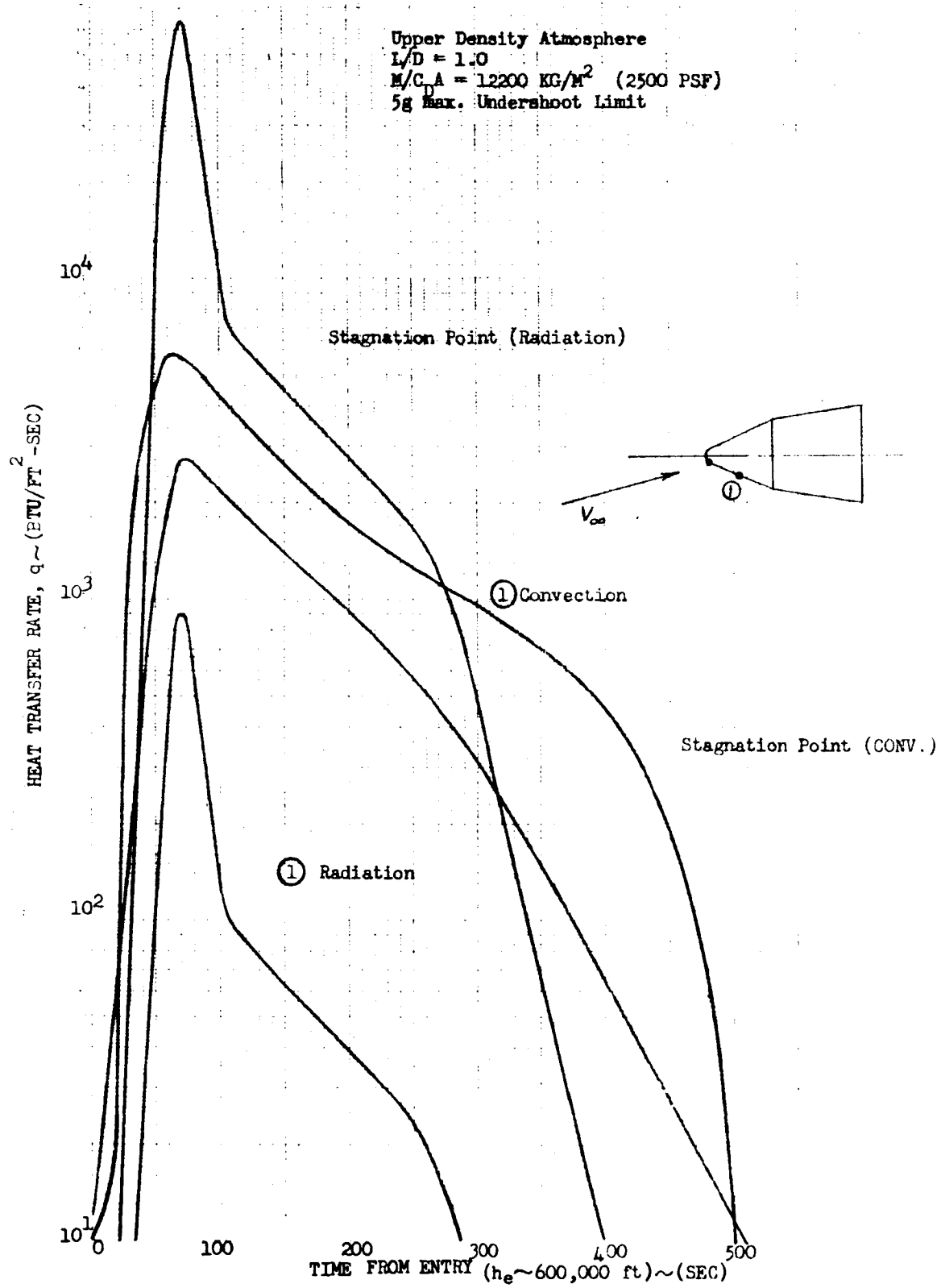
Figure 235. Venus Aerodynamic Braking Gasdynamic Heating Variation

- 301 -
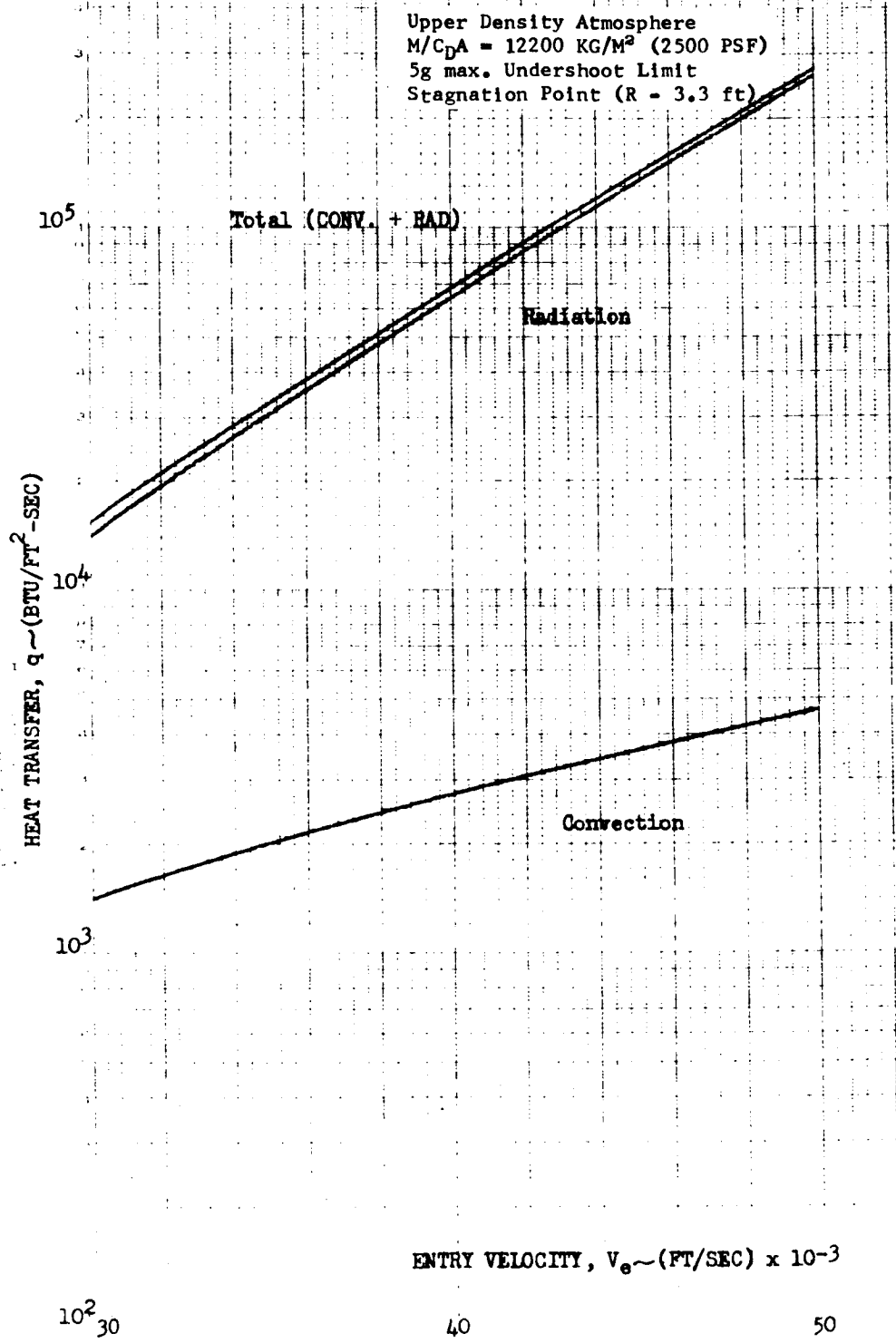
Figure 236. Venus Aerodynamic Braking Peak
Gasdynamic Heating Variation

- 302 -
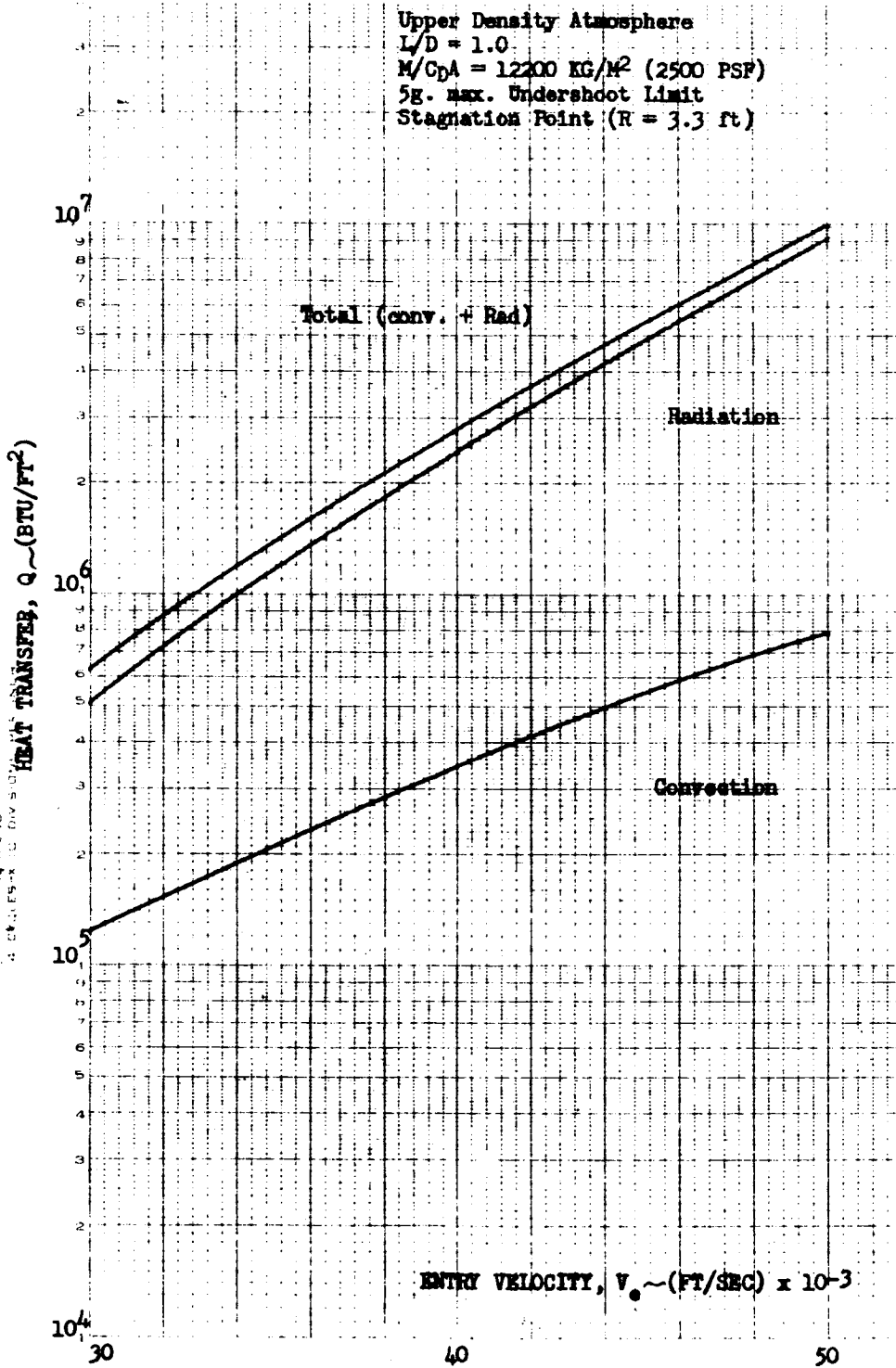
Figure 237. Venus Aerodynamic Braking Integrated Head Load Variation

- 303 -
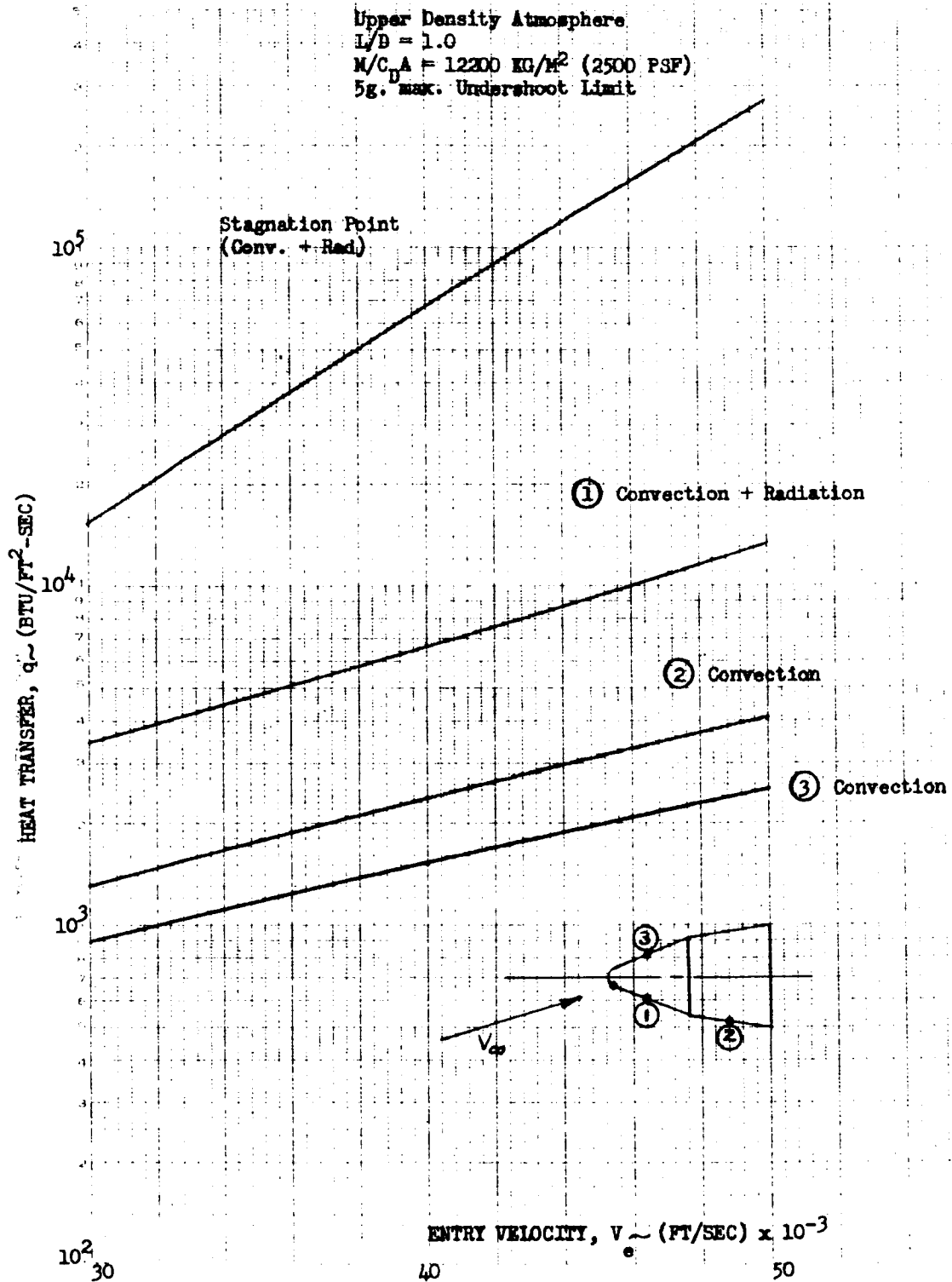
Figure 238. Venus Aerodynamic Braking Total Peak Heating Variation

SD 67-621-2

Figure 239.   Venus Aerodynamic Braking Integrated Heat Load
Variation, Upper Density Atmosphere

SD 67-621-2

Table 26. Peak Stagnation Point Gasdynamic Heating -
Atmospheric Model Comparison

Heating Rate	High-Density Atmosphere	Low Density Atmosphere
$q_{convective}$ (Btu's/feet^2-second)	2,761	2,806
$q_{radiative}$ (Btu's/feet^2-second)	64,409	57,807
q_{total} (Btu's/feet^2-second)	67,170	60,613
Q_{total} (Btu's/feet^2)	2,773,000	2,775,678

The comparison indicates that for the given set of aerobraking characteristics (i.e., L/D, M/C_DA, entry velocity, undershoot limit, and parking-orbit altitude) the total thermal loads are nearly equivalent. If the formulations used to compute the gasdynamic heating were derived for the specific gas composition of each atmosphere, larger differences would be expected as compared to the data identified by Table 26. For convective heat transfer, it has been demonstrated theoretically that for equivalent flight velocities and ambient densities, heating in a pure CO_2 gas will be greater than in a pure N_2 gas. Mixtures of CO_2 and N_2 will yield heating rates between that predicted for pure CO_2 and N_2, but the heating will not necessarily be in a direct proportion to the mixture's mole fraction or molecular weight (Reference 24). Since the lower-density-profile atmosphere is assumed to be composed of a 75 percent CO_2 and 25 percent N_2 by volume mixture, it would be expected to yield convective heating rates greater for equivalent flight conditions than would the high-density atmosphere, which is composed of a 90 percent N_2 and 10 percent CO_2 by volume mixture. Results of Reference 34 indicate that the heating data for the various gas mixtures fall within a band of experimental measurements, which is in agreement with the comparison presented by Figure 226. The high-density atmosphere model would be expected to yield higher radiative heating rates as compared to the low-density atmosphere. Figure 227 shows that the intensity curve for a 30 percent CO_2 - 70 percent N_2 mixture (an approximation to the high-density atmosphere) lies above a curve representing a 90 percent CO_2 - 10 percent N_2 mixture. At the given entry velocity range investigated during the study (Ve ~ 9.2 kilometer/seconds to 15.2 kilometer/seconds), the dependency of radiative heating upon gas composition is shown not to be significant because the radiance of CO_2 - N_2 mixtures approach that predicted for air at these high velocities.

THERMAL PROTECTION

The thermal response of the aerobraking vehicle structure to the attendant gasdynamic heating environment encountered during flight within the sensible planetary atmospheres is a significant factor due to the large vehicle-weight fraction required to protect the vehicle. The scope of this study was to provide the aerobraking vehicle synthesis with a reasonable upper limit to the ablative material requirements expressed in terms of a vehicle-weight fraction. For the broad range of possible aerobraking missions, the most significant design consideration is the entry velocity associated with each specific mission. As a consequence of this, the effect of entry velocity on the ablative-material to vehicle-weight fraction was determined. From these weight fraction evaluations, the design penalties involved with utilizing a common vehicle for off-loaded missions are identified.

The prediction of thermal-protection requirements for Mars and Venus aerobraking missions is complicated by the uncertainties associated with the atmospheric constituents. Atmospheric composition has been shown to produce higher heating environments that what would be experienced for air at equivalent flight conditions. In addition to the increased heating the atmospheric composition can affect the performance of ablative materials. Typical problems identified during a previous NR/SD study (Reference 10) concerning ablation in planetary atmospheres are given as follows:

(1)   Ablative materials like phenolic nylon and Avcoat exhibit different thermal-performance characteristics as compared to that measured for air.

(2)   An increase in the CO_2 content of a gas mixture reduces the thermochemical heat of ablation which results in higher mass loss rate as compared to air.

(3)   Avcoat type materials have been shown to exhibit higher surface recession rates in high-CO_2-concentration mixtures as compared to air.

If the results are applied to the prediction of thermal-protection requirements for Mars and Venus aerobraking, measureable differences in ablator weights could result from differences in the chemical interaction phenomena of the ablator material and the boundary layer constituents for comparable heating environments. An example of this could be the NASA-MSFC recommended upper - and lower-density model atmospheres in which the assumed compositions are 10 percent CO_2 - 90 percent N_2 and 75 percent CO_2 - 25 percent N_2, respectively.

The thermal-protection analysis was based upon predicting the response of an AVCOAT 5026-39-type ablative material to the Mars and Venus aero-braking heating environment discussed under Gasdynamic Heating in the Aerothermodynamics section. Ablative-material requirements were derived under certain restrictive assumptions. The heats of ablation of the Avcoat material were compatible with the values derived for air which are currently employed in the Apollo command module design. The effective heat of ablation variation developed for laminar flow was applied to the nose-region heating. For the conical surfaces, which comprise a major fraction of the vehicle surface, an effective heat of ablation variation derived for a turbulent boundary layer was employed to compute the material mass-loss characteristics. As indicated in the gasdynamic heating discussion, turbulent heating comprised the major heat input to the vehicle. The vehicle heatshield weight fractions derived during the study are based upon a turbulent heating environment, with the nose stagnation region contributing a small fraction of the total thermal-protection weight.

Figures 240 and 241 present the heat shield weight fraction as a function of entry velocity for Mars and Venus aerobraking missions. For the Mars entries, the heatshield weight fraction is observed to vary from approximately 6.8 percent to 14.6 percent of the vehicle gross weight at entry for the entry velocity range of 6.1 kilometer/second to 9.2 kilometer/second. The weight fraction for Venus varies from 12.7 percent to 40 percent for the entry velocity range of 9.2 kilometer/second to 15.2 kilometer/second. Measureable design penalties are indicated if for each planet the vehicle is designed for the highest entry velocity. If an aerobraking vehicle with a design entry velocity of 15.2 kilometer/second is applied to a Venus mission requiring an entry velocity of 12.2 kilometer/second, approximately 20 percent of the vehicle weight consists of excess ablative material. Similar weight penalties are indicated for a vehicle design for a Venus aerobraking mission applied to a lower-velocity Mars mission.

More detailed analyses would be required to refine the weight fractions presented herein. Specific areas which require further investigation are the radiant heating to lower conical-surface regions with regards to gas-composition and flow-field effects, gas-composition effects upon ablative material performance, and the selection of ablative-material concepts to accommodate different vehicle surfaces (nose versus upper - and lower-surface regions).
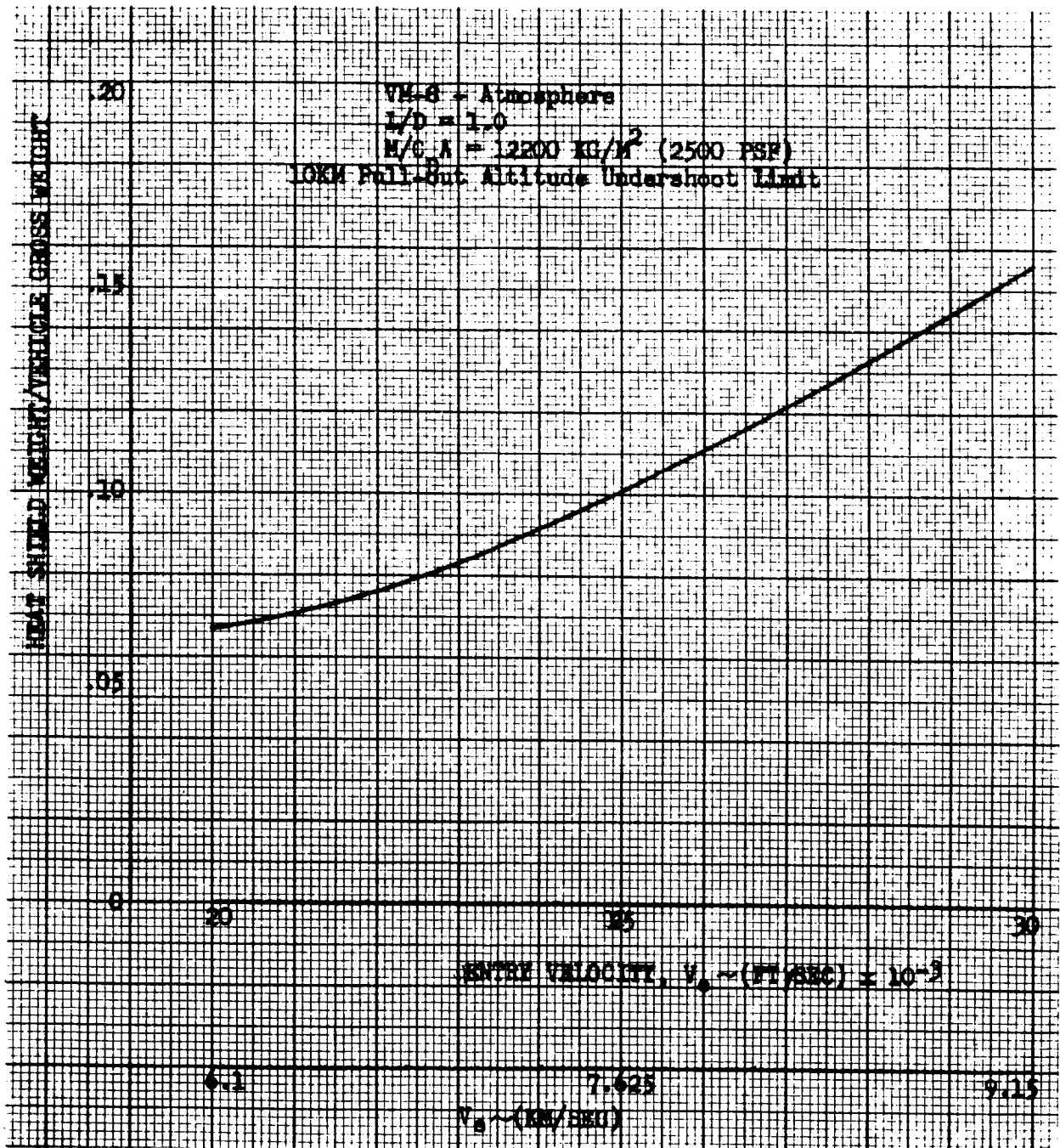
Figure 240.   Mars Aerodynamic Braking Heat Shield Weight
Fraction Variation
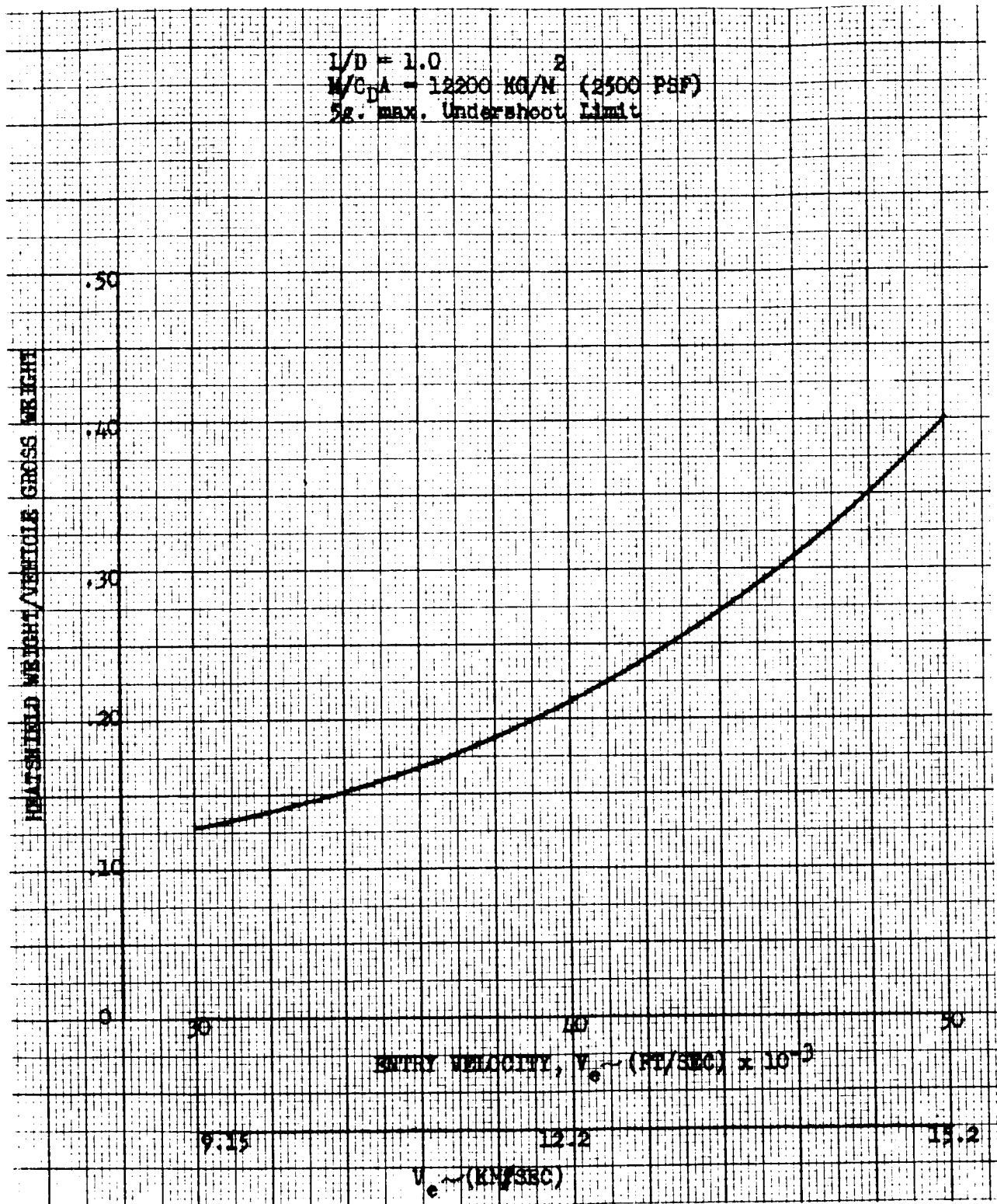
Figure 241. Venus Aerodynamic Braking Heat Shield Weight
Fraction Variation

CHARACTERISTIC VELOCITY REQUIREMENTS

Energy requirements for ascent from the surfaces of the asteroids Vesta and Ceres, the planets Mercury and Mars, and Jupiter's satellite Ganymede are presented in this section. A cursory treatment of descents to the surfaces of all the bodies is also given. Assumptions are included regarding physical characteristics of the attracting bodies.

PHYSICAL CHARACTERISTICS

Planet physical characteristics are summarized in Table 27. Assumed mass properties for Ceres and Vesta were those corresponding to an average density of the asteroid equal to that of the earth. Vacuum flight was assumed for all bodies except Mars, where the VM-7 atmosphere was used. The characteristics of this atmosphere are shown in Table 28.

Table 27. Body Physical Characteristics

Body	Gravitational Parameter, $meters^3/sec^2$ $(feet^3/sec^2)$	Radius, Meters (feet)	Surface Gravity, $meters/sec^2$ $(feet/sec^2)$
Vesta	1.07618×10^{10} (3.8×10^{11})	190,000 (623,359)	0.29811 (0.9780)
Ceres	8.60928×10^{10} (3.04×10^{12})	386,243 (1,267,190)	0.57709 (1.8933)
Mercury	2.16494×10^{13} (7.6444×10^{14})	2,500,000 (8,202,000)	3.4639 (11.3644)
Ganymede	1.03198×10^{13} (3.644×10^{14})	2,575,000 (8,448,060)	1.5564 (5.1062)
Mars	0.429778×10^{14} $(0.15177464 \times 10^{16})$	3,381,000 (11,092,510)	3.7597 (12.335)

SD 67-621-2

Table 28. Mars Model Atmosphere, VM-7

Altitude Geopotential (km)	Altitude Geometrical (km)	Temperature (°K)	Pressure (mb)	Density (gm/cm³)	Density Scale Height (Geop. km)
0	0	275	5.00	6.82×10^{-6}	27.0
2	2.00	267	4.51	6.33	26.2
4	4.00	259	4.05	5.86	25.4
6	6.01	252	3.63	5.41	24.7
8	8.02	244	3.24	4.98	23.9
10	10.03	236	2.88	4.58	23.2
12	12.04	228	2.55	4.19	22.4
14	14.06	221	2.25	3.83	21.6
16	16.08	213	1.98	3.48	20.9
18	18.10	205	1.73	3.16	20.1
19.2	19.31	200	1.59	2.98	19.7
20	20.12	200	1.50	2.81	14.2
24	24.17	200	1.14	2.12	14.2
28	28.23	200	8.57×10^{-1}	1.60	14.2
32	32.30	200	6.47	1.21×10^{-6}	14.2
36	36.38	200	4.89	9.15×10^{-7}	14.2
40	40.48	200	3.69	6.91	14.2
44	44.58	200	2.79	5.22	14.2
48	48.69	200	2.11	3.94	14.2
50	50.75	200	1.83×10^{-1}	3.42	14.2
60	61.08	200	9.07×10^{-2}	1.70×10^{-7}	14.2
70	71.47	200	4.50	8.42×10^{-8}	14.2
80	81.93	200	2.23	4.17	14.2
90	92.45	200	1.10×10^{-2}	2.07	14.2
100	103.03	200	5.48×10^{-3}	1.02×10^{-8}	14.2

Values above this level are based on continuation of isothermal temperature, an arbitrary assumption resulting in P, ρ values progressively lower than more realistic temperature increase values.

150	156.93	200	1.64×10^{-4}	3.07×10^{-10}	14.2
200	212.52	200	4.90×10^{-6}	9.18×10^{-12}	14.2

$P_0 = 5.0$ mb
$\rho_0 = 6.82 \cdot 10^{-6}$ gm/cm³
$T_0 = 275$ °K
$T_{stratosphere} = 200$ °K
$M = 31.2$ (20% CO_2; 80% N_2 by volume)
$H_{stratosphere} = 19.3$ km
$g_0 = 375$ cm/sec²

CHARACTERISTIC VELOCITY REQUIREMENTS FOR VESTA, CERES, MERCURY, AND GANYMEDE

Powered ascent trajectories were computed from the surface to circular orbit conditions at varying altitudes for Vesta, Ceres, Mercury, and Ganymede, assuming no atmosphere. Calculus-of-variations steering was used, except for a five-second initial launch phase utilizing an arbitrarily chosen pitch-over rate of 2.5 degrees per second. A specific impulse of 400 seconds was used during the constant thrust ascent.

Tradeoff data were generated for Vesta, Ganymede, and Mercury. The results of these studies are shown in Figures 242 through 244, which show the variation of velocity requirements with orbit altitude and liftoff acceleration. Only a single case was considered for ascents from Ceres. Table 29 summarizes the ascent velocity requirements to inject into a 20-kilometer orbit for the asteroids and a 50-kilometer orbit for Mercury and Ganymede.

Descent velocity requirements were determined for a selected acceleration level: that which yields a touchdown acceleration 2.5 times the local acceleration due-to-gravity. The powered descent was assumed to begin at 20-km circular orbit conditions for the asteroids and 50-km conditions for Mercury and Ganymede.

Table 29. Ascent and Descent Velocity Requirements

Attracting Body		T/M (newtons/ kilogram)	T/Mgs* (unitless)	Orbit Altitude** (km)	Characteristic Velocity (meters/sec)
Vesta	Ascent	0.55	1.8	20	328
	Descent	0.75	2.5	20	328
Ceres	Ascent	1.44	2.5	20	565
	Descent	1.44	2.5	20	556
Ganymede	Ascent	4.5	2.9	50	2175
	Descent	3.89	2.5	50	2197
Mercury	Ascent	9.0	2.6	50	3220
	Descent	8.66	2.5	50	3277

*gs is acceleration due to gravity at the surface.
**Powered maneuver terminates with or is initiated from this circular orbit altitude.
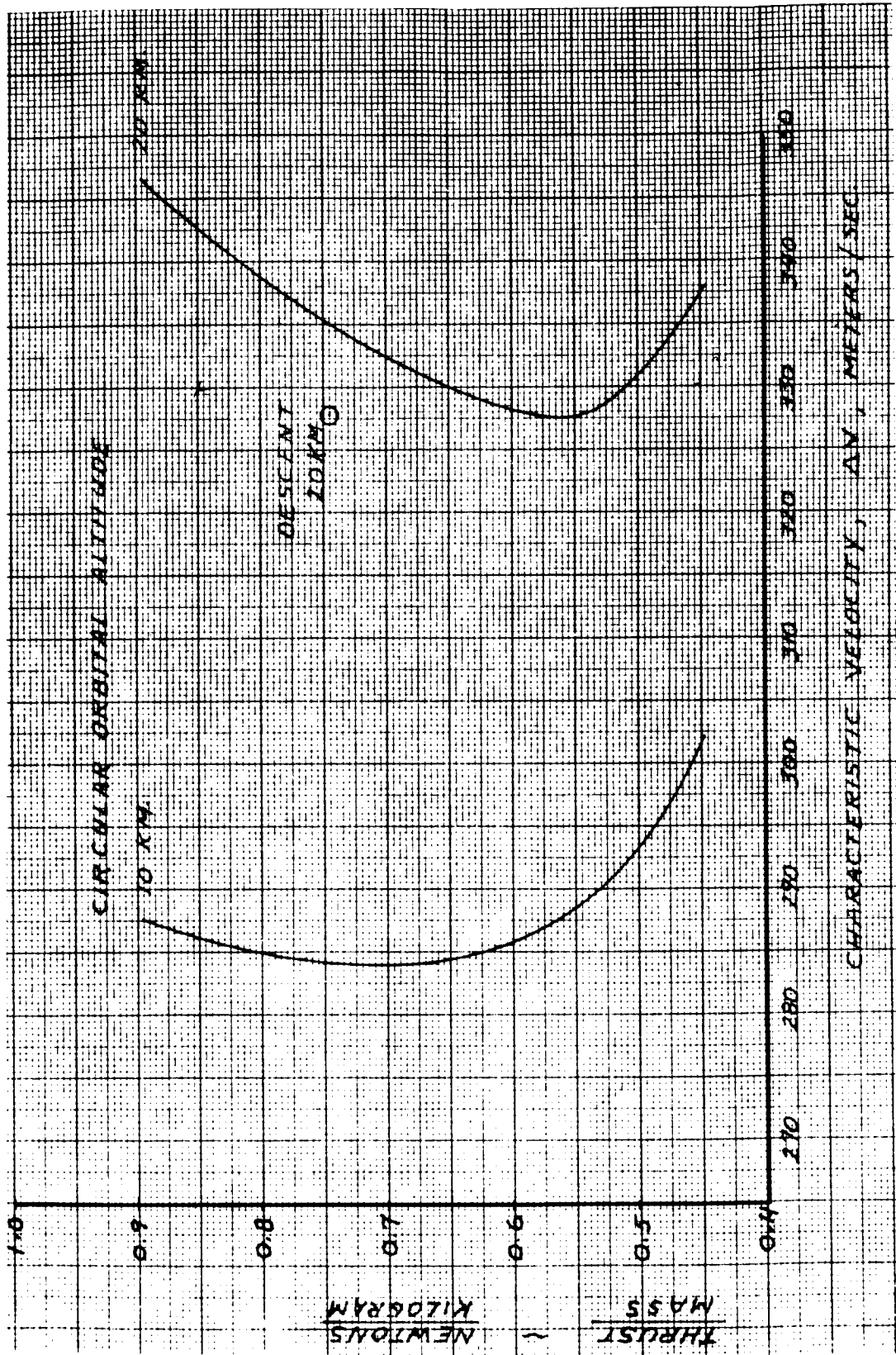
Figure 242. Ascent Velocity Requirements, Vesta
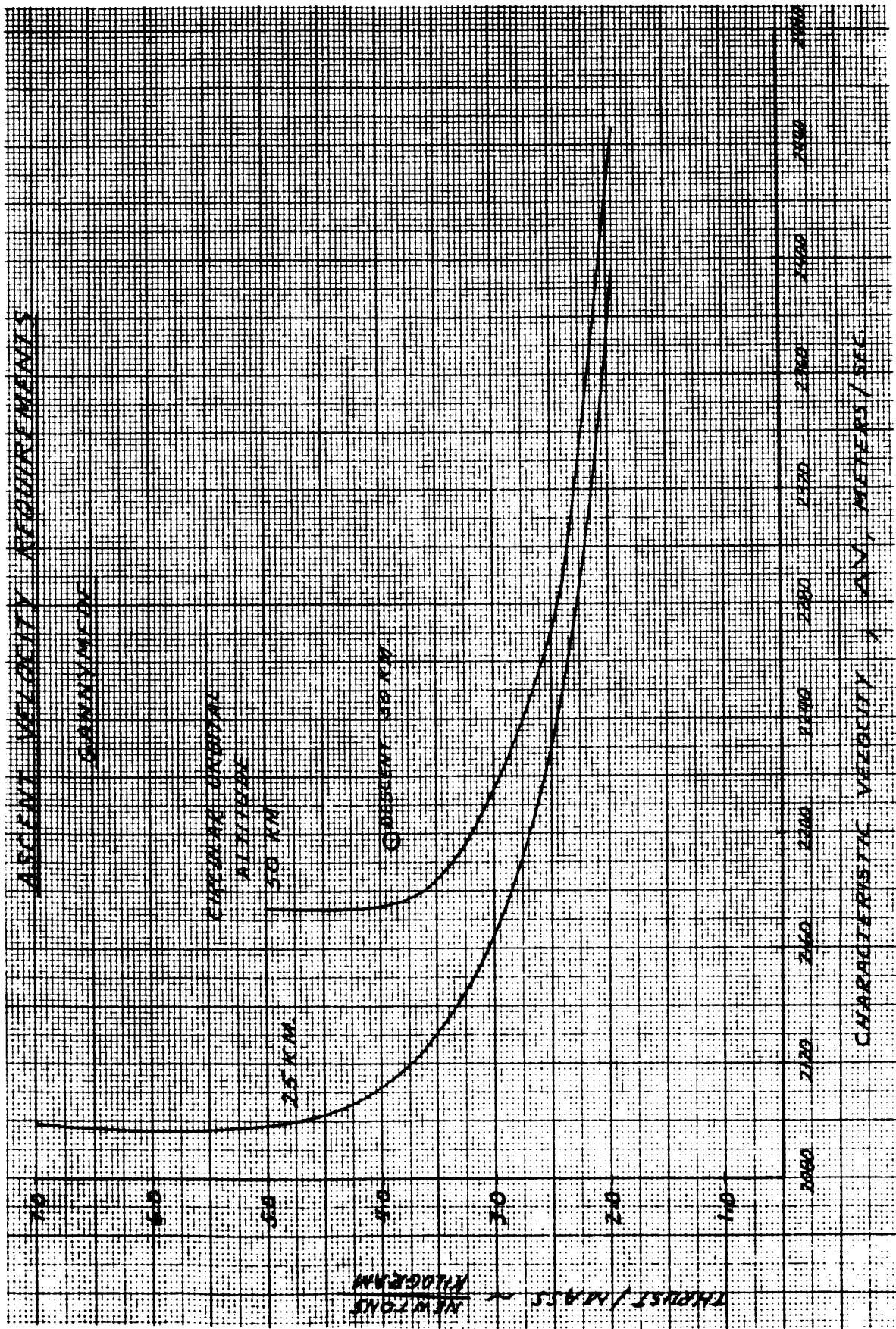
Figure 243. Ascent Velocity Requirements, Ganymede

SD 67-621-2
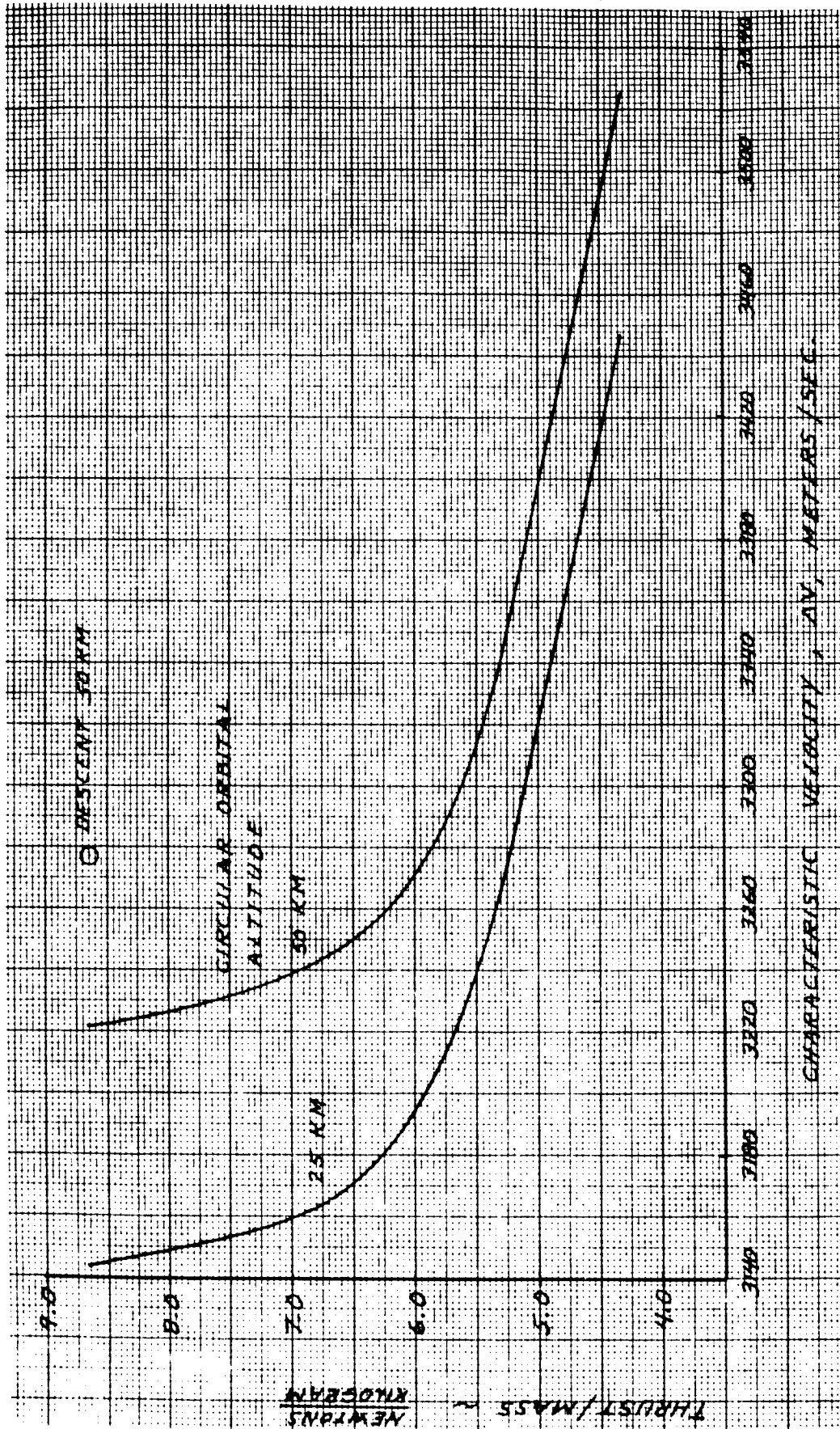
Figure 244. Ascent Velocity Requirements, Mercury

It can be seen from Table 29 and Figures 242 through 244 that the descent requirements do not differ significantly from the ascent requirements if the acceleration level is chosen properly. It should be noted that these characteristic velocity requirements do not include any contingencies such as hover or landing site selection flexibility which must be included in the total descent characteristic velocity. The total descent characteristic velocity must also include the additional requirements for transferring from the initial parking orbit to circular orbit conditions at the altitude at which the final descent maneuver is initiated. Also, the total ascent characteristic velocity must include the additional requirements for the transfer and injection into the parking orbit of the parent spacecraft. The resultant total characteristic velocity requirements (including hover and transfer requirements) for elliptical planetary parking orbits are shown in Figures 245 and 246 for Mercury and Ganymede. The descent profile consists of a Hohmann transfer from apocenter of the elliptical parking orbit to circular orbit speed at an altitude of 50 kilometers. The ascent requirements are based on injecting into an elliptical parking orbit at pericenter. These data are based on a parking orbit pericenter altitude of 300 kilometers.
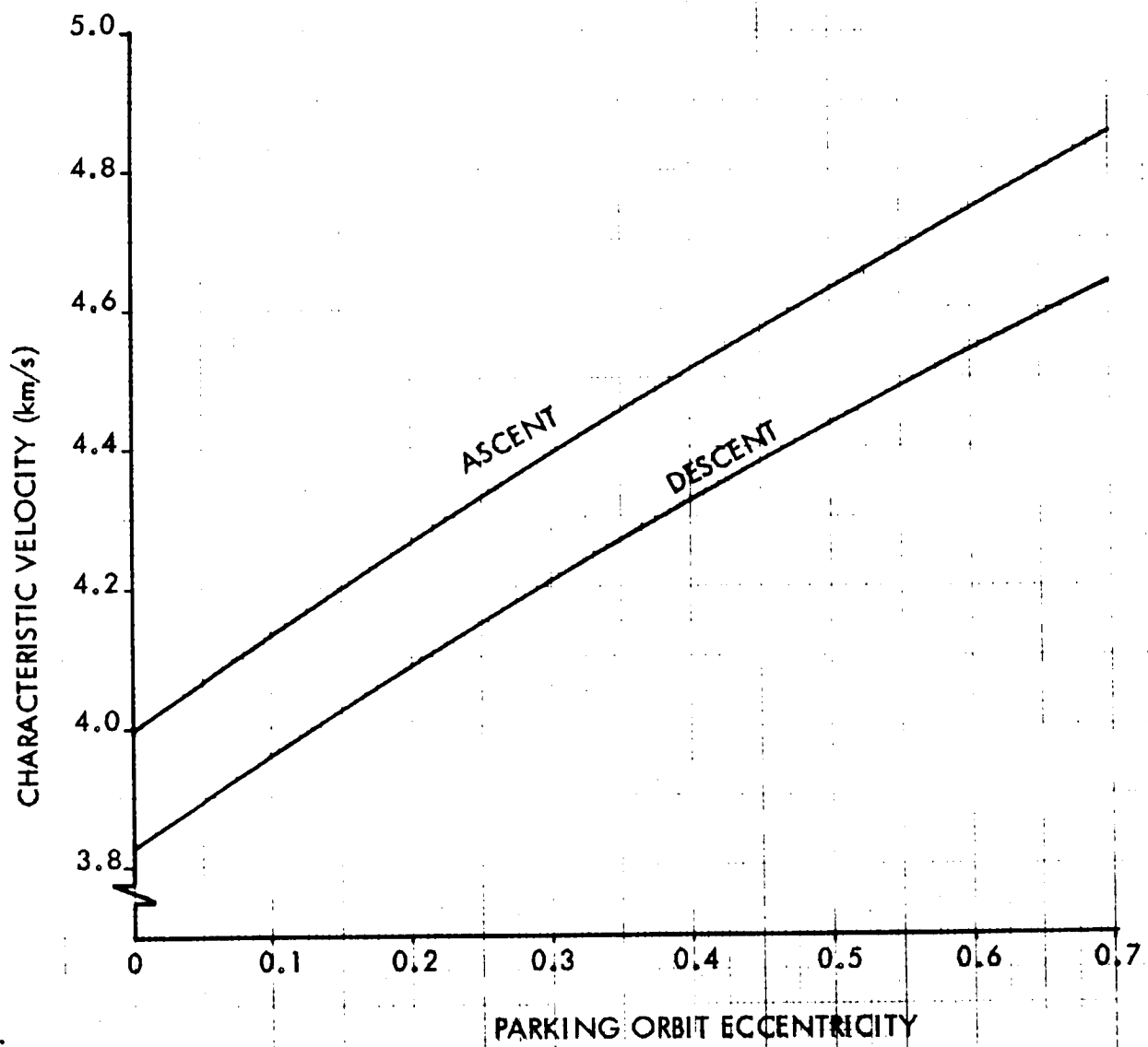
Figure 245. PEM Characteristic Velocity Requirements, Mercury
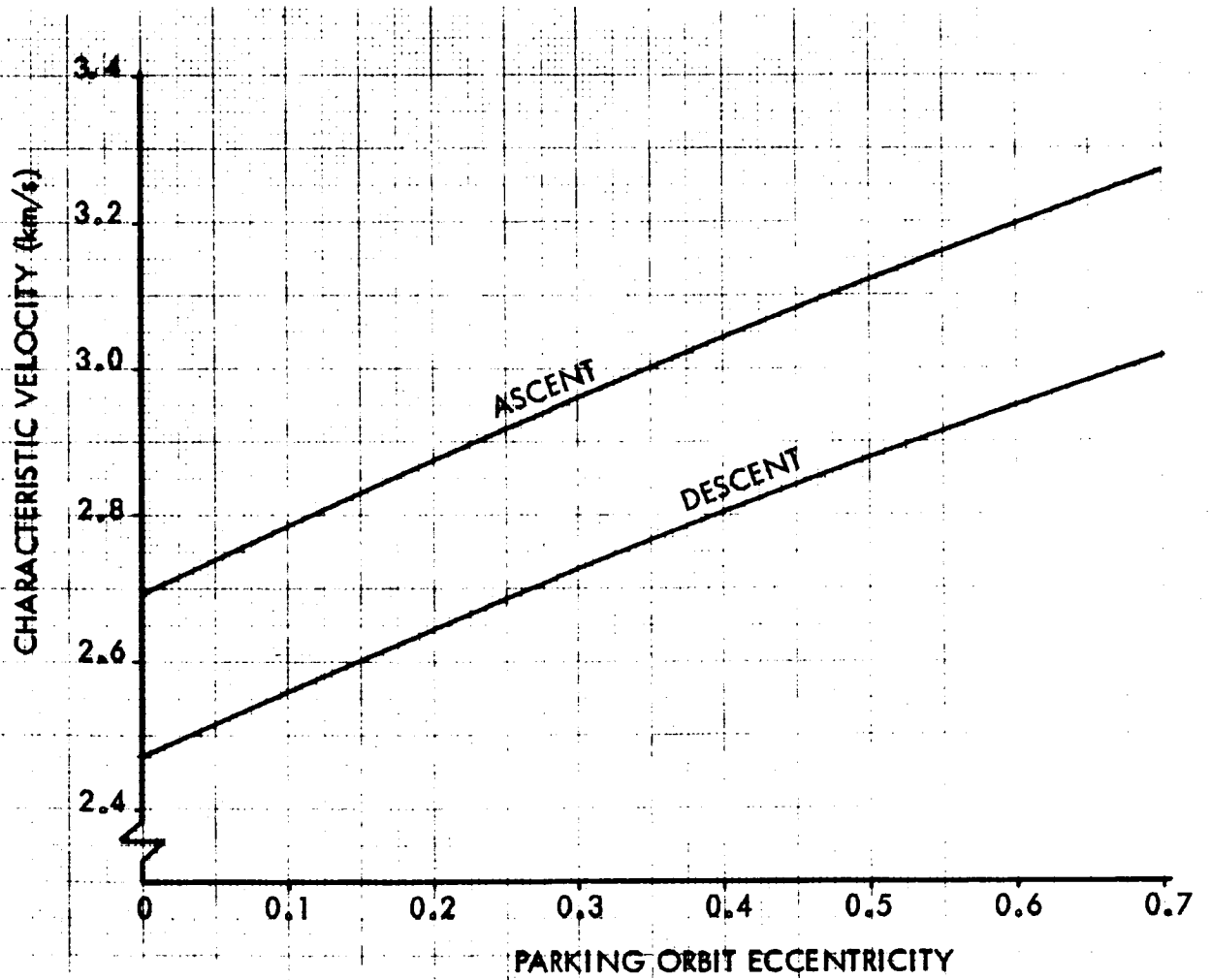
Figure 246. PEM Characteristic Velocity Requirements, Ganymede

CHARACTERISTIC VELOCITY REQUIREMENTS FOR MARS

Ascent trajectories computed from the surface of Mars were initially based on vacuum ascents. The vacuum trajectories utilized calculus-of-variations steering except for a five-second vertical boost used to simulate the initial launch phase. Burnout of the single ascent stage occurred at perifocus of an ellipse having an apofocus altitude of 185 kilometers (100 nautical-mile). Perifocus altitude varied from 30.5 kilometers to 91.4 kilometers. Launch was assumed at an azimuth of 90 degrees east of north and from a latitude of 35 degrees.

The steering profile resulting from the vacuum trajectory simulation was then used in the atmospheric trajectory simulation. It was modified as required to effect the same ending conditions that were obtained in the vacuum trajectory simulation. The basic shape was retained, thereby assuring a near-optimum ascent under the influence of drag forces.

The atmosphere model used was VM-7 as shown in Table 28. Vehicle characteristics assumed were as follows:

Mass = 27,600 kilograms (61,000 pounds mass)

Diameter = 5.08 meters (200 inches)

Specific impulse = 386 seconds

Apollo nose drag at relevant Mach numbers is shown in Table 30.

The following simplifying assumptions were made:

1. No aerodynamic forces normal to the wind axis

2. No change in effective specific impulse due to atmospheric pressure

3. No change in drag characteristics due to power on

The resultant velocity requirements are shown in Figure 247 as a function of perifocus altitude and liftoff acceleration. The total characteristic velocity requirements for ascent and descent are shown in Figure 248 for elliptical planetary parking orbits. The descent to the planetary surface is initiated at apocenter of the elliptical parking orbit. The ascent maneuver terminates at injection in the elliptical parking orbit at pericenter.

Table 30. Apollo Nose Drag

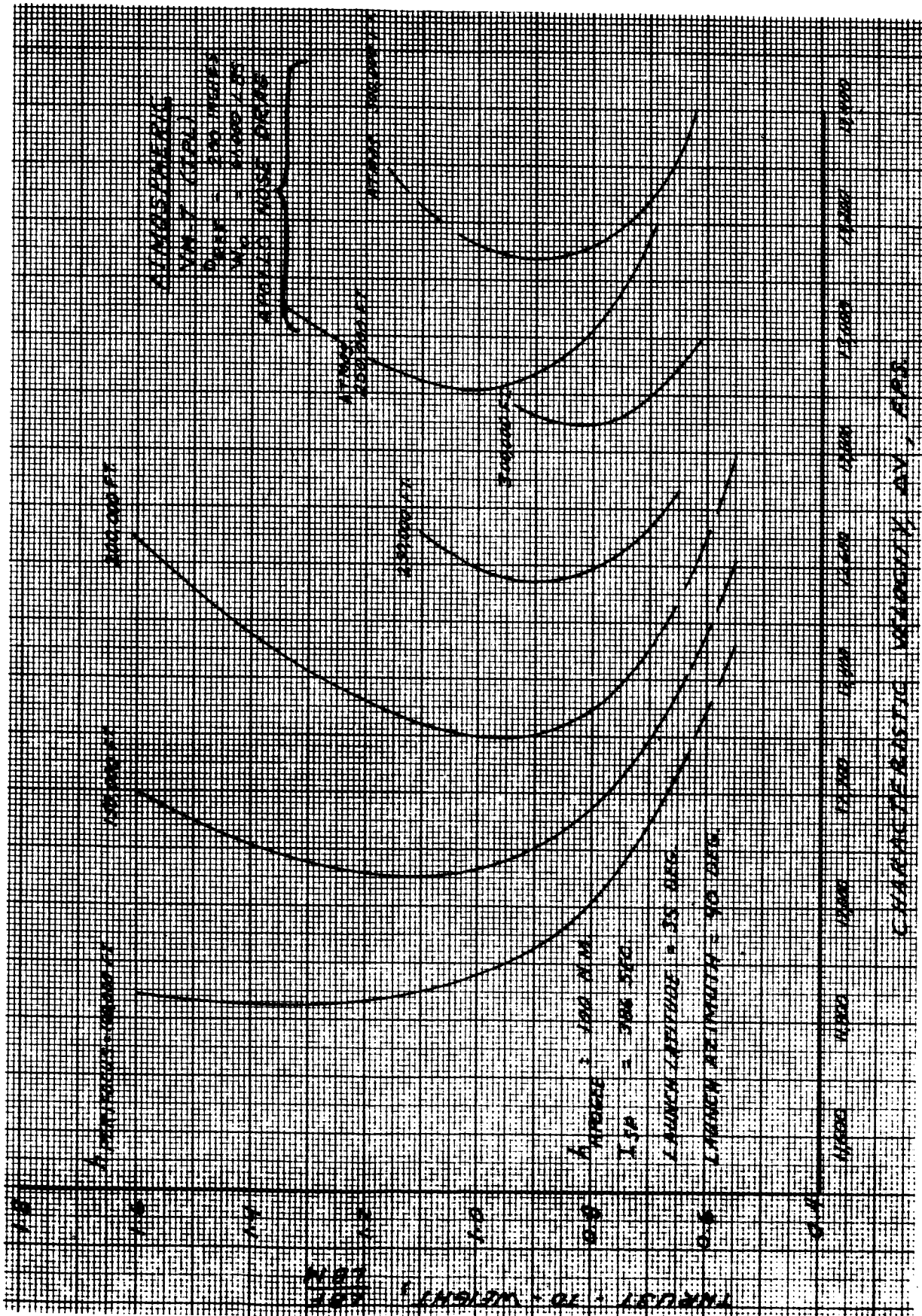| Mach Number	C_D	Mach Number	C_D
0.0	0.548	2.0	0.95
0.4	0.548	2.4	0.86
0.7	0.646	3.0	0.767
0.9	0.719	4.0	0.70
1.1	1.015	6.0	0.65
1.2	1.05	10.0	0.644
1.35	1.09		
1.65	1.09		

Figure 247. Performance for Launch to Martian Orbit, Single Stage
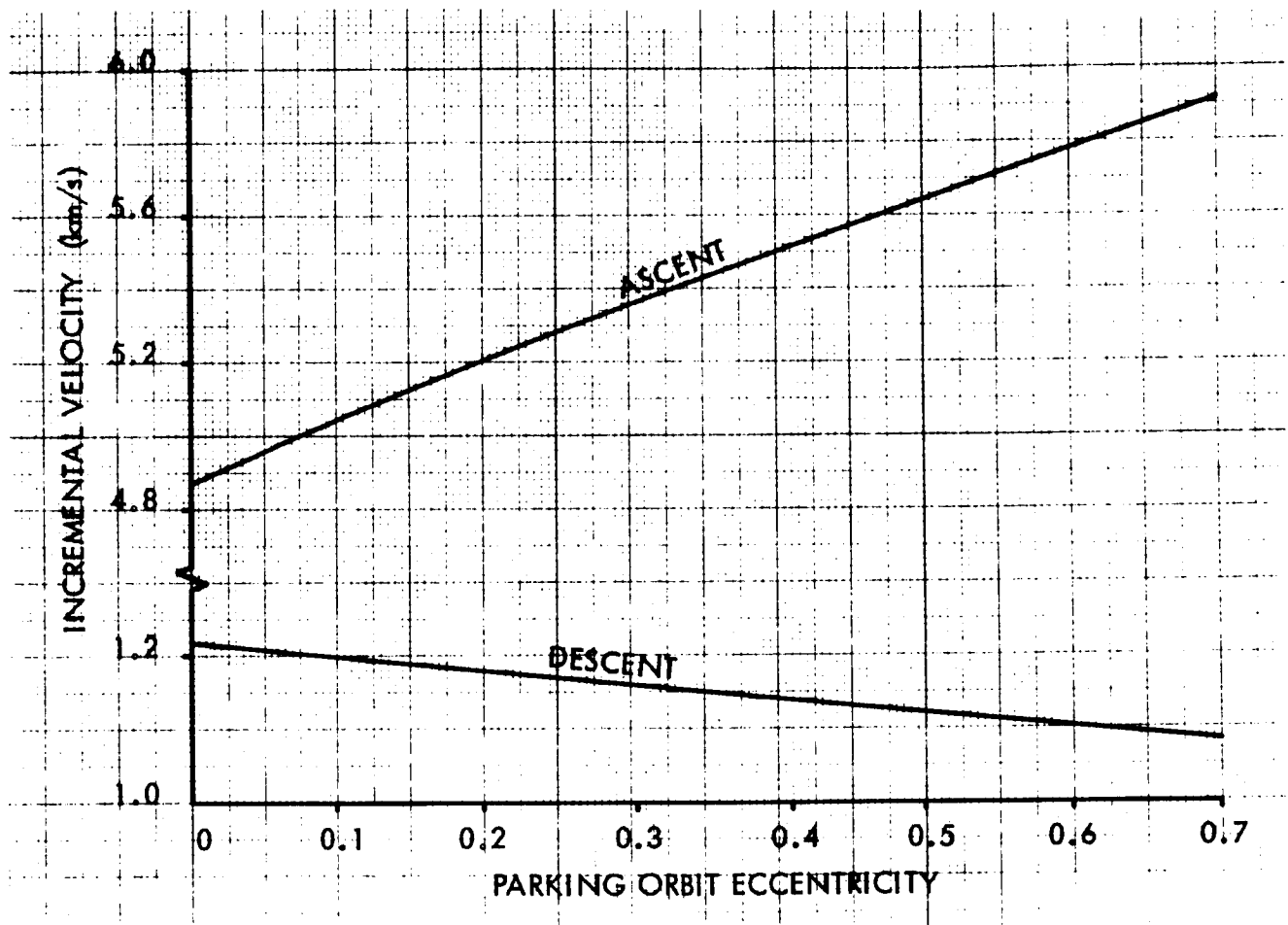
- 323 -

SD 67-621-2

Figure 248. PEM Characteristic Velocity Requirements, Mars

MIDCOURSE GUIDANCE REQUIREMENTS

A limited study was conducted to determine the effects of the midcourse guidance requirements on the selection of the mission profile for Ganymede orbiter and lander missions. It has been shown in the Performance Requirements section that the direct Ganymede orbit insertion mode minimizes the total incremental velocity requirements if only the major propulsive maneuvers are considered. The objective of the midcourse guidance investigation was to determine whether or not the midcourse correction requirements for the direct Ganymede orbit insertion mode would exceed the savings in the nominal mission performance requirements and thus invalidate the premise that the direct insertion mode minimizes the total mission incremental velocity requirements.

The midcourse guidance problem for the Ganymede rendezvous is determined by (1) the errors in the trajectory relative to Jupiter after the heliocentric correction process has been completed; (2) the ability to predict the trajectory of Ganymede and of the spacecraft relative to Ganymede during the final approach; (3) the concept imposed in regard to the choice of state variables, the time of rendezvous (whether variable or fixed), the cost function to be optimized in the guidance process and constraints on the problem; and (4) the ability to control the orbit of the spacecraft (application errors for the midcourse corrections).

The first of these problems was investigated in Reference 35, where it was shown, even with a relatively crude guidance concept, the correction magnitude need not exceed the order of 15 to 30 m/s (3σ). When Jupiter's sphere of influence was reached, 3σ errors in position and velocity of approximately 50,000 km (relative to a radius of 48×10^6 km) and approximately 2 m/s were shown to be obtainable before the process of navigating with respect to Jupiter was begun. These requirements and errors were predicated on using a contemporary Earth launch vehicle inertial guidance system and the assumption that an earlier correction has occurred to null as many of the Earth departure errors as possible. The early correction was within the Earth's sphere of influence and was approximately 10 to 15 m/s (3σ).

The second aspect of the problem has probably also been investigated although no specific reference could be found as to the probable accuracies associated with the orbit of Ganymede. Thus, no detailed knowledge as to

the effects of these uncertainties on the approach navigation problem has been prepared. Estimates of these errors, however, can be obtained by considering the equations for elliptic motion:

$$\Delta r = \left[\frac{r}{a} - \frac{3}{2} \frac{a}{r} e M \sin E \right] \Delta a + \left[-a \cos E + \frac{a^2 e}{r} \sin E \right] \Delta e$$

$$+ \left[-\frac{a^2 e}{r} \eta \sin E \Delta t_p \right]$$

$$r\Delta \phi = - \left[\frac{3pM}{2r \sqrt{1-e^2}} \right] \Delta a + \frac{a \sin E}{1 - e^2} \left(1 - \frac{p}{r} \right) \Delta e - \frac{pa\eta}{r \sqrt{1-e^2}} \Delta t_p + r \Delta \omega$$

(where the notation is standard), and the following assumptions:

1. The eccentricity of Ganymede's orbit can be neglected.

2. The time elapsed since the last fix on Ganymede is less than one period (M = 2π). Since this error has a secular nature, only the secular part will be considered.

Under these assumptions

$$\Delta r_{max} \approx \Delta a + a \Delta e$$

$$r \Delta \phi_{max} \approx - 3 \pi \Delta a - r \sqrt{\frac{u}{a^3}} \Delta t_p + r \Delta \omega$$

Thus, errors no larger than approximately 5000 km in r and 10,000 km in the plane longitudinal position are expected.

The third problem and the effect of the fourth are discussed in Reference 36. The reference establishes the theory for the optimal correction sequence and defines the effects of all of the error sources on the gain structure for the problem. If applied, this theory would yield the control policy to be mechanized for the spacecraft. This step is felt to be premature for the present study since the primary objective is to define the extent to which the midcourse energy requirements determine the concept for producing rendezvous with Ganymede. Thus, attention should be turned to the simplified

guidance logic discussed in Reference 35. By using this logic and the errors occurring during the heliocentric mission phase, it can be shown that the midcourse correction requirements within the sphere of influence of Jupiter are of the order of 50 to 200 m/s provided a reasonable accurate navigation process is utilized. Sextant measurements of 3- to 10-second error are achievable (and adequate) particularly if augmented with stadiametric data during the final approach. The above midcourse correction requirements include the effects of both spacecraft and Ganymede trajectory errors.

Corrections required prior to encounter are necessary for all Jupiter missions and the corrections within Jupiter's frame of reference are small compared to the energy differences which can be achieved by utilizing the direct rendezvous mission mode. Thus, the direct rendezvous mission mode for Ganymede orbiter and lander missions appears to be a promising mission concept.

SD 67-621-2

REFERENCES

1. Nautical Almanac Officers of the United Kingdom and the United States of America, Explanatory Supplement to the Astronomical Ephemeris and the American Ephemeris and Nautical Almanac. London: Her Majesty's Stationery Office (1961).

2. Deerwester, J. M., and D'Haem, S. M. Systematic Comparison of Venus Swingby Mode with Standard Mode of Mars Round Trips. AIAA Paper 67-27 (January 1967)

3. Manning, L. A. Minimal Energy Ballistic Trajectories for Manned and Unmanned Missions to Mercury. AIAA Paper 67-28 (January 1967)

4. Manned Mars Landing and Return Mission Study. NAA/S&ID, SID 64-619-4 (April 1964).

5. Hanley, G. M. and Lyon, F. J. "The Feasibility of Spacecraft Deceleration by Aerodynamic Braking at the Planet Mars." AIAA Paper 64-479 (June 1964).

6   Proposal for a Study of Technology Requirements for Atmosphere Braking to Orbit About Mars and Venus - Volume I: Technical. NAA/S&ID, SID 66-1396-1 (19 September 1966).

7. Mars and Venus Nominal Natural Environment for Application to Advanced Manned Planetary Mission Program Studies. NASA, SP-3016 (1964).

8. Physical Characteristics and Atmospheric Data for Venus. NAA/S&ID, SID 65-1316 (30 September 1965).

9. Study of Subsystems Required for a Mars Mission Module - Volume No. 4 Aerobraking. NAA/S&ID, SID 64-1-4 (2 January 1964).

10. Study of Unmanned Systems to Evaluate the Martian Environment - Final Report. NAA/S&ID, SID 65-1172 (September 1965).

11. Research Study Report - Manned Interplanetary Spacecraft Systems R. A. 6506. NAA/S&ID, SID 65-1278.

SD 67-621-2

12. Wolf, F. and J.M. Spiegel. "Status of Basic Shock Layer Radiation Information for Inner Planet Atmospheric Entry." AIAA paper 66-421, presented at the AIAA 4th Aerospace Science Meeting, Los Angeles, California (June 27-29, 1966).

13. Physical Characteristics and Atmospheric Data for Mars. NAA/S&ID, SID 65-1684.

14. Hoshizaki, H. "Heat Transfer in Planetary Atmospheres at Super-Satellite Speeds, ARS Journal. Volume 32, No. 10 (October 1962).

15. Scala, S.M. Heating Problems of Entry Into Planetary Atmospheres from Supercircular Orbiting Velocities. Proc. of Symposium on Aerothermoelasticity. USAF, ASD TR 61-645 (October 1961).

16. Gruszcynaski, J.S. and W.R. Warren Jr. "Experimental Heat Transfer Studies of Hypervelocity Flight in Planetary Atmosphere." AIAA Paper 63-450, presented at the AIAA Conference on Physics of Entry into Planetary Atmospheres, Cambridge, Massachusetts (August 26-28, 1963).

17. Yee, L., H.E. Bailey, and H.T. Woodward. Ballistic Range Measurements of Stagnation Point Heating in Air and Carbon Dioxide at Velocities up to 18,000 Feet Per Second. NASA TN D-777 (1961).

18. Nerem, R.M., C.J. Morgan, and B.C. Graber. "Hypervelocity Stagnation Point Heat Transfer in a Carbon Dioxide Atmosphere." AIAA Journal, Volume 1, No. 9 (September 1963).

19. Rutowski, R.W. and K.K. Chan. Shock Tube Experiments Simulating Entry into Planetary Atmospheres. Lockheed Missiles and Space Division, 288139 (January 1960).

20. Horton, T.E. and T.L. Rabineaux. "Experimental Assessment of the Effect of Large Amounts of Argon in a Planetary Atmosphere on Stagnation Point Convective Heating." AIAA Paper No. 66-29 (1966).

21. Hanley, G.M. "Hypervelocity Laminar Flat-Plate Heating." ARS Journal, Volume 32, No. 11 (November 1962).

22. Eckert, E.R.G. Survey on Heat Transfer at High Speeds. WADC TR 54-70, U.S. Air Force (April 1954).

23. James, C.S. "Experimental Study of Radiative Transport from Hot Gases Simulating in Composition the Atmospheres of Mars and Venus." AIAA Journal Volume 2, No. 3 (March 1964).

24. Wolf, F. and T. Horton. "Effect of Argon on Shock-Layer Radiance of CO_2-N_2 Mixtures." AIAA Journal, Volume 2, No. 8 (August 1964).

25. Spiegel, J.M., et al. Aerothermodynamics of Planetary Entry. Jet Propulsion Laboratory, SPS 37-22, Vol. IV, Section 354.

26. Breene, R.G., Jr. and M.C. Nordone. Radiant Emission in the Atmospheres of the Terrestrial Planets. Dynamics of Manned Lifting Planetary Entry. New York: John Wiley and Sons, Inc. (1963).

27. Thomas, G.M. and W.A. Menard. Experimental Measurements of Non-Equilibrium and Equilibrium Radiation from Planetary Atmospheres, proceedings of AIAA Entry Technology Conference (October 1964).

28. Arnold, J.C., V.H. Reis and H.T. Woodward. "Theoretical and Experimental Studies of Equilibrium and Non-Equilibrium Radiation to Bodies Entering Postulated Martian and Venusian Atmospheres at High Speeds." AIAA Paper 65-116 (January 1965).

29. Kivel, B. and K. Bailey. Tables of Radiation from High Temperature Air. AVCO, Research Report 21 (December 1957).

30. Repic, E.M., G.M. Hanley, and C.D. Martin. "Mars Atmospheric Uncertainties and Resulting Entry Considerations." paper presented to the Space Sciences Board of the National Academy of Sciences, Woods Hole, Massachusetts, (July 5-16, 1965).

31. Li, T.Y., and Geiger, R.E., "Stagnation Point of a Blunt Body in Hypersonic Flow." Journal of the Aeronautical Sciences, Volume 24, No. 1, pp 25-32 (January 1957).

32. Hanley, G.M. and K.D. Korkan. "Inviscid, Non-Adiabatic Flow in the Stagnation Region of Blunt Bodies." Proceedings of the XVth International Astronautical Congress. Vol. III, pp 213-245, Warsaw, Poland (1964).

33. Hanley, G.M. and K.D. Korken. "Approximate Inviscid, Non-Adiabatic Stagnation Region Flow Field Solution." AIAA Journal, Vol. 3, No. 8, pp 1537-1538 (August 1965).

34. Marvin, J. G. and R. B. Pope. "Laminar Connective Heating and Ablation in the Mass Atmosphere," presented at the AIAA/AAS Stepping Stones to Mars Meeting, Baltimore, Maryland (March 28-30, 1966).

35. Grier, D. R. Guidance and Navigation Analyses for a Jupiter Flyby Mission. NAA/SD IL, FC/FCA-66-66 (20 May 1966).

36. Townsend, G. E. Guidance Equations for Orbital Operations. NAA/SD, SID 66-1678-3 (February 1967).